Al-Kitab Journal for Pure Sciences

KJPS

ISSN: 2617-1260 (print), 2617-8141(online)
DOI: http://10.32441/kjps
https://isnra.net/index.php/kjps

An Academic Semi-Annual Journal

Volume: 10 Issue: 02 Nov. 2026

Editor-In-Chief
Prof. Dr. Ayad Ghani Ismaeel
(President of Al-Kitab University)

Managing Editor
Prof. Dr. Ali Ismail Al- Juboury

The Journal English Proofreading
Dr. Imad Rifat Madhat

The Journal's Final Review Before Publication
Prof. Dr. Bilal Abdullah Nasir

Design and Publication Requirements Implementation
Mr. Aziz Qarany Abdulla

Iraqi Academic Scientific Journals IASJ: **https://iasj.rdd.edu.iq/journals/journal/view/103**
Journal Website: **https://isnra.net/index.php/kjps**
E-mail: **kjps@uoalkitab.edu.iq**

Editorial Board for Al-Kitab Journal for Pure Sciences

Professor	Dr.	Ayad Ghany Ismaeel / Editor in Chief - Iraq
Professor	Dr.	Prof. Dr. Ali Ismail Al- Juboury / Managing Editor - Iraq
Professor	Dr.	Ahmed Rifaat Mohamed Mahmoud Gardouh - Jordan
Professor	Dr.	Mostafa El-Sheekh – Egypt
Professor	Dr.	Mohammad A. M. Aljaradin - Sweden
Professor	Dr.	Fathy Ahmed Abeed - Iraq
Professor	Dr.	Othman Saad Saeed Al-Hawshabi - Yemen
Professor	Dr.	Aziz Ibrahim Abdulla – Iraq
Assis. Professor	Dr.	Sufyan Abaas Wuhaib- Iraq
Professor	Dr.	Ahed Elias Abouyounes - Syria
Assis. Professor	Dr.	Burhan Ahmed Mohammed - Iraq
Professor	Dr.	Eda M. A. Alshailabi - Libya
Professor	Dr.	Manal Mohamed Adel Ahmed Hassanein - Egypt
Professor	Dr.	Shaymaa Hadi Khudhair - Iraq
Assis. Professor	Dr.	Huda Saad Azzawi - iraq
Professor	Dr.	Mamdouh Mohammed Salem Siraj - Egypt
Professor	Dr.	Zakaria Yahya Al-Gamal - Iraq
Professor	Dr.	Khalid A. Ahmad - Iraq
Professor	Dr.	Hala Sobhi Wattar – Syria
Professor	Dr.	Adel Mohammed Ali Al-Qashbari - Yemen
Professor	Dr.	Wael Al Abdulla – Australia
Professor	Dr.	Mira Ausama Ahmed Al-Katib - Iraq
Assistant Professor	Dr.	Nouara Emrajae Elazirg Elammari - Libya
Assistant Professor	Dr.	Omaima Abdul aal Zaree Alessawi -Kingdom of Saudi Arabia
Assistant Professor	Dr.	Mohamed Effendi – Tukey
Assistant Professor	Dr.	Yasmina Khan – Algeria
Assistant Professor	Dr.	Naseem Alwahishi – Tunisia
Assistant Professor	Dr.	Kadri Nabih Alsayed Abdul Khaliq - Egypt
Lecturer	Dr.	Hagar Fathy Saad Abdellatif Mohamed Forsan - Egypt
Lecturer	**Dr.**	Eman Abdelazem Abelrhaman Ahmad - Egypt
Lecturer	**Dr.**	Cinaria Tarik Albadri - Ireland
Lecturer	**Dr.**	Dunia Tahseen Nema Al-Aridhi - Iraq

Aims and Scope

The Al-Kitab Journal for Pure Sciences aims to provide an international forum for the publication and dissemination of original work that contributes to the understanding of the principal and related disciplines of science. Al-Kitab Journal for Pure Sciences publishes two peer-reviewed issues per year, an online and print journal, which publishes innovative research papers, literature reviews, and **technical notes on the fields of Biology, Computer Sciences, Chemistry, Physics, Geology and Mathematics.**

Authors Guidelines

Rules and Instructions for Publication in Al-Kitab Journal for Pure Sciences

First: General requirements

1. The paper is submitted to the Editorial Secretariat directly in four copies with CD-ROM or E-mail of the magazine in MS Word and PDF files.
2. Research before being sent to scientific evaluators is subject to the quotation Turnitin program.
3. Research shall be accepted for publication after being judged by scientific evaluators and according to the rules.
4. The publication fee is (100,000 ID) for researchers from Iraqi Universities and (free of charge) for foreign researchers.

Second: To prepare research for publication, authors are recommended to follow the following procedures.

1. **The article:**

   The article needs to be typed on one side of A4 paper (Right margin =2.5 cm, left margin =2.5 cm, and 2cm for the top and bottom) with 1.5 space, and the pages must be numbered.

2. **The content organization:**

   MS Word is to be used as follows: "Simplified Arabic" font for the Arabic articles, and "Times New Roman" for the English articles. The Size of the title must be 18 bold. The names of the authors must be typed in 11 bold in Arabic and 11 bold in English. Abbreviations, keywords, the main headings, the reference, and the acknowledgment should be typed in 14. Subheadings must be in 12 bold. The abstract is usually size 12. The body of the article/paper is in size 12. The organization of the content should be as follows: **The article heading, the names of authors and their**

addresses, and the abstract (Both in Arabic and English).

3. **Research paper title:**

The title must be as short as possible and indicate the content of the subject together with the name (names) of the authors. The names of the authors to whom correspondence is to be made should be indicated with (*) and show his / her email.

4. **The size:**

The paper should contain no more than 25 pages of journal pages including charts and diagrams.

5. **Abstract:**

The abstract should include the purpose and the means of the founding results and the conclusions. It should also contain the knowledge values of the subject of research. It is meant to be no more than 250 words. It should also emphasize the content of the subject and include the keywords used throughout the paper.

6. **Diagrams:**

Figures and diagrams must be given following the explanation referring to the diagram. Each diagram must contain its title below the diagram at the first size of 12. The diagram should be editable in terms of enlargement or reduction within the margins of the paper size. The parts of each diagram must be grouped into drawing parts.

7. **Tables:**

The tables should follow the parts of the main body and should be located below the indicated part of the text. Tables must have titles with a text size of 12. The text used inside the tables should be of size 12 and kept within the cells of the table.

8. **References:**

The references used in the paper must be given in order and their numbers given inside the square bracket [ ]. The following instructions are to be followed:

If the reference is a book, the First name of the reference must be given first followed by the other names. Then the title (bold and Italic) of the book, edition, year of publication, the publisher, and place of publication (year of publication).

Example: [1] P. Ring and P. Schuck, "**The Nuclear Many-Body Problem**", First Edition, Springer-Verlag, New York (1980).

(b) If the reference is a research paper or an article in a journal: The name of the author must be given first, the title of the article, the name of the journal, the volume (issue), page (Year). **Example:** [1] Ali H. Taqi, R. A. Radhi, and Adil M. Hussein,

"Electroexcitation of Low-lying Particle-Hole RPA States of ^{16}O with WBP Interaction", Communication Theoretical Physics, 62(6), 839 (2014).

c) If the reference is an M.Sc. or Ph.D. thesis, the name of the anther must be written with the first name first followed by the surname, title of the thesis, the name of the university, and Country (Year).

Example: [1] R. A. Radhi, **"Calculations of Elastic and Inelastic Electron Scattering in Light Nuclei with Shell-Model Wave Functions"**, Ph.D. Thesis, Michigan State University, USA (1983).

(d) If the reference is from the conference. Authors Name, "**Paper Title**", Conference, Country, Publisher, volume, page (Year).

Example: [1] Ali H. Taqi and Sarah S. Darwesh, **"Charge-Changing Particle-Hole Excitation of ^{16}N and ^{16}F Nuclei"**, 3rdInternational Advances in Applied Physics and Materials Science Congress, Turkey, AIP Conf. Proc., 1569, 27 (2013)

Third: Privacy Statement

1. The names and e-mail addresses entered into the journal's website will be used exclusively for the purposes stated in this journal and will not be provided for any other purpose or to any other party.
2. The editor of the journal has the right to change any statement or phrase of the research content he may find necessary to express the work suitable to the general style of the journal.
3. After publishing the paper and its presentation on the journal page, the editors' team will destroy all the scrap papers. The author has no right to ask for them in any case.

Fourth: Modernity of sources:

The percentage of modern references used in the research should not be less than 50% of the total references used in the research. Modernity is measured within the last ten years of the year of submission of the research. For example, when submitting the research in 2018, the references should be from 2008 upwards and not less than 50%. The journal prefers to have at least one of the reference types of research published in the previous journal issues.

Note: For more information, please visit:

Iraqi Academic Scientific Journals IASJ: **https://iasj.rdd.edu.iq/journals/journal/view/103**
Or Journal Website: https://isnra.net/index.php/kjps
The Journal can also be e-mailed to kjps@uoalkitab.edu.iq

Table of Contents

Volume: 10 Issue: 02 Nov. 2026

No.	Research Title	Researcher Name	Pages
01	**Using bioinformatics tools to analyze the effect of Steviol Glycosides on the C-Glucan binding protein of bacteria Streptococcus mutans compared to Eugenol** استخدام أدوات المعلوماتية الحيوية لتحليل تأثير ستيفيول جليكوسيدات على بروتين ربط سي-جلوكان للبكتيريا العقدية الطافرة مقارنة بالأوجينول	• Baydaa Hamad Obaid Selah	1-12
02	**The Isolation and Characterization of Indigenous Rhizobacteria from Rhizosphere of Phaseolus vulgaris L. and their Potential Applications in Sustainable Agriculture** عزل وتشخيص الرايزوبكتريا المحلية من المنطقة الجذرية لنبات الفاصوليا Phaseolus vugaris L.	• Noor Azez Aref • Raad Hassani Sultan • Vineetha Edavana	13-23
03	**Computational Study of the Properties of the Medicinal Compound Tromantadine** دراسة حسابية لخصائص المركب الطبي ترومانتادين	• Zeena R. Katoof • Athra G. Sager • Jawad Kadhim Abaies	24-40
04	**A Brief review of the role of microalgal communities in reduce climate change** مراجعة مختصرة لدور مجتمع الطحالب في تقليل التغييرات المناخية	• Ebtehal Mussa Jaffer • Najlaa Hashem Adlan	41-51
05	**The Impact of Varying Plasticizers on Coated Graphite Electrodes Performance for Doxycycline Hyclate Estimation** تأثير تغيير الملدنات على أداء أقطاب الجرافيت المطلية لتقدير هيكلات الدوكسيسيكلين	• Aveen Kh. Mohammed • Muthana S. Ali	52-66
06	**Review: Efficiency of Helianthus annuus L. Plant Tissues in phytoremediation of nano Pollutants** كفاءة أنسجة نبات زهرة الشمس *Helianthus annuus L* في المعالجة النباتية للملوثات النانوية	• Rana TariqYahya • Sara Nazar Ghanem • Hala Muzher Yaqub	67-86
07	**The Effect of Tacrolimus and Triticum Aestivum Germ Oil on the Intrinsic Pathway of Apoptosis in the Liver of Male Albino Mice: An Immunohistochemical and Molecular Study** تأثير التاكرولميس وزيت جنين القمح في المسار الداخلي للموت المبرمج في الكبد لذكور الفئران البيض: دراسة كيميائية مناعية نسجية وجزيئية	• Thamer Ahmed Mohamed • Baidaa Abdulaziz Mohamed Salah	87-103
08	**Chemical and Bacteriological Evaluation of Water Quality in some Water Treatment Units in Diyala Governorate** التقييم الكيميائي والبكتريولوجي لنوعية المياه في بعض وحدات معالجة المياه في محافظة ديالى	• Zainab Esmail Sadeq • Hiba Shihab Ahmed • Hawraa Hussein Khudhayer	104-115
09	**Isolation and Antibiotic Resistance Profiling of Gram-Negative Bacteria Recovered from Wound and Burn Infections** عزل وتحديد مقاومة المضادات الحيوية للبكتيريا السالبة لغرام المعزولة من الجروح والحروق	• Iman Abdulrazzaq Aljuraisy • Reem Z. Shakir	116-131
10	**The Role of Folic Acid in Avoiding Congenital Disabilities: A Review** مراجعة: دور حامض الفوليك في منع التشوهات الخلقية	• Nawras Ali Hussein Al-Jubouri • Huda Saad Azzawi • zahraa hussein abdulateef	132-142
11	**Secondary Metabolites as a Nonenzymatic Antioxidant System in Plants: A Brief Review** مركبات الايض الثانوي كنظام مضاد للأكسدة غير انزيمي في النباتات	• Faten khaleel Ibrahim	143-154

12	**Antimicrobial Resistance Patterns of Acinetobacter haemolyticus from Urinary Tract Infections and Hospital Wastewater** أنماط المقاومة المضادة للميكروبات للبكتيريا *Acinetobacter haemolyticus* المعزولة من التهابات المسالك البولية ومياه الصرف الصحي في المستشفيات	• Jilan Ahmed Shakur • Alaa R. Nadim • Wael Adil Obaid • Rafeef A. Yass	155-167
13	**Bacterial Interactions and Cancer Prognosis: A Review of Their Role in Tumor Progression and Theapy** التفاعلات البكتيرية وتشخيص السرطان: مراجعة لدورها في تطور الورم السرطاني	• Mohammed S. Abbas	168-183
14	**The Barberry Fruit Extract and Metformin as a protective effect on the embryonic development and kidney tissues functioning in a rat model of experimental gestational diabetes** مستخلص ثمار البرباريس والميتفورمين كعامل وقائي على نمو الجنين ووظائف أنسجة الكلى في نموذج جرذ مصاب بسكري الحمل التجريبي	• Zainab Hasan Majeed	184-202
15	**Alterations in Serum Lactate Dehydrogenase and Creatine Kinase Levels in Relation to Physical Activity Intensity** التغيرات في مستويات إنزيم لاكتات ديهيدروجيناز (LDH) وكرياتين كيناز (CK) في المصل تبعًا لشدة النشاط البدني	• Nuha Hamza Khedhir • Muntaha Mezhir Abbas • Galawesh Norri Taher	203-220
16	**Synthesis And Characterization and Anti-Cancer Activity of Nickel (II) Complexes Containing a Mixture of Benzotriazole Derivative, Phenanthroline, And Bipridine, And Evaluation of Their Bioavailability** تحضير وتشخيص ودراسة النشاط المضاد للسرطان لمعقدات النيكل (II) الحاوية على مزيج من مشتق البنزاترايازول والفينونثرولين والبايبريدين وتقييم فعاليتها الحيوية	• Alaa H. Ali	221-241
17	**Using Laplace transforms and their inverses as a graph-based data structure** استخدام تحويلات لابلاس ومعكوساتها كبنية بيانات قائمة على الرسم البياني	• Ali Farhan Hashoosh • Hasan Ramadhan Musa • Omar Osama Dawood	242-254
18	**On Ideals and α-Sets in Topological Spaces with Types of I-Continuity** حول المثاليّات ومجموعات α في الفضاءات الطوبولوجية وأنواع الاستمرارية I	• Ahmed T Mohammed	255-266
19	**Synthesis, Characterization, and Biological Evaluation of Mixed-Ligand Cadmium Cd (II) Complexes Containing 5-Benzylthio-1H-Tetrazole and Phosphine Ligands** تحضير , تشخيص , و تقييم الفعالية الحيوية لمعقدات الكادميوم ثنائي التكافؤ *[Cd(II)]* المتحدة مع الليكاندات المحتوية على-*5)* بنزيل ثيو -١– *H*تيترازول *(* و الفوسفينات.	• Riyad. D. Salman	267-278
20	**Petrography, Microfacies, Depositional Environment and Diagenetic Evolution of the Upper Triassic Kurra Chine and Baluti Formations, Northern Iraq** بتروغرافية، سحنات الدقيقة، بيئة الترسيبية، والتطور التحويري لترياسي الاعلى لتكويني قوراجين وبلوطي، شمال العراق	• Eman W. Al-Berzanje • Hassan A. Al-Jumaily • Ali I.Al-Juboury	279-298
21	**Calcareous Nannofossils Biostratigraphy of Chia Gara Formation in Banik village, Northern Iraq** الطباقية الحياتية لمتحجرات النانو الكلسية لتكوين جياكارا في قرية بانيك شمالي العراق	• Alaa Mahmood Al-Wazan • Enas Hazim Al-Khafaf • Omar Ahmed Al-Badrani	299-314
22	**Heavy Metal Contamination in Drinking Water, Groundwater, and Industrial Water Sources in Kirkuk and Selected Iraqi Cities: A Structured Evidence Synthesis and Evaluation of Treatment Technologies** تلوث المعادن الثقيلة في مياه الشرب والمياه الجوفية والمياه الصناعية في كركوك ومدن عراقية مختارة: توليف منظم للأدلة المنشورة وتقييم تقنيات المعالجة	• Noor N. Abdulqader • Hayder M. Jasim	315-333

Al-Kitab Journal for Pure Sciences (2026); 10(2):01-12.
https://doi.org/10.32441/kjps.10.2.p1

Al-Kitab Journal for Pure Sciences
ISSN: 2617-1260 (print), 2617-8141(online)

https://isnra.net/index.php/kjps

Using bioinformatics tools to analyze the effect of Steviol Glycosides on the C-Glucan binding protein of bacteria *Streptococcus mutans* compared to Eugenol

Baydaa Hamad Obaid Selah [1]

[1]Ministry of Higher Education and Scientific Research / Scientific Research commission

Corresponding Author: baidaa.hamad1105a@csw.uobaghdad.edu.iq

Citation: *Baydaa Hamad Obaid Selah*[1]. **Using bioinformatics tools to analyze the effect of Steviol Glycosides on the C-Glucan binding protein of bacteria *Streptococcus mutans* compared to Eugenol.**
Al-Kitab J. Pure Sci. [Internet]. 2025 Jan 11; 10(2):01-12
DOI:
https://isnra.net/index.php/kjps/article/view/2026.
https://doi.org/10.32441/kjps.10.02.p1.

©20--. THIS IS AN OPEN-ACCESS ARTICLE UNDER THE CC BY LICENSE
http://creativecommons.org/licenses/by/4.0/

Keywords: Bioinformatics Tool, Steviol Glycosides, *Streptococcus Mutans,* Eugenol, docking accuracy, PyRx

Article History

Received	18 Oct. 2024
Accepted	11 Jan. 2025
Available online	01 Nov. 2026

Abstract:

Dental caries is a common and chronic condition caused by bacterial activity that erodes the tooth structure. *Streptococcus mutans* is the main causative bacteria, which adheres to tooth surfaces and breaks down carbohydrates to produce acids. These acids demineralize tooth enamel, leading to caries. In the current research, the focus was on eugenol and steviol glycosides, which have medicinal properties. Eugenol is a natural compound with analgesic, antibacterial, antiviral, and antioxidant properties, making it a promising option in caries prevention. Steviol glycosides are substances extracted from the stevia plant, and have a wide range of health benefits, including their ability to prevent caries, but their mechanism of action is still under investigation. The aim of the study was to evaluate the efficacy of steviol glycosides compared to eugenol in their interaction with GbpC protein in Streptococcus mutans, and to provide evidence for the potential use of steviol glycosides as a natural option for the prevention of dental caries. In this research used an in-silico approach to investigate complexes of 5UQZ (Glucan Binding Protein C) in chain A with eugenol as a control and Steviol glycosides. A virtual screening experiment was performed using PyRx software to improve the accuracy of the association between the compounds and the target protein. The results showed that eugenol achieved a binding degree of -5.9 kcal/mol, while steviol glycosides recorded a

higher binding degree of -9.8 kcal/mol. These results indicate that steviol glycosides have a higher efficacy in interacting with the target protein than eugenol. This research highlights the promising potential of steviol glycosides as a natural option for combating dental caries, and lays the foundation for future studies aimed at developing effective and sustainable oral health products.

Keywords: Bioinformatics Tool, Steviol Glycosides, *Streptococcus Mutans,* Eugenol, docking accuracy, PyRx

استخدام أدوات المعلوماتية الحيوية لتحليل تأثير ستيفيول جليكوسيدات على بروتين ربط سي-جلوكان للبكتيريا العقدية الطافرة مقارنة بالأوجينول

بيداء حمد عبيد صالح [1]

وزارة التعليم العالي والبحث العلمي / هيئة البحث العلمي[1]

الايميل الرسمي: baidaa.hamad1105a@csw.uobaghdad.edu.iq

الخلاصة:

تسوس الأسنان هو حالة شائعة ومزمنة ناجمة عن نشاط بكتيري يؤدي إلى تآكل بنية الأسنان. تعد *Streptococcus mutans* هي البكتيريا المسببة الرئيسية، والتي تلتصق بأسطح الأسنان وتحلل الكربوهيدرات لإنتاج الأحماض. تعمل هذه الأحماض على إزالة المعادن من مينا الأسنان، مما يؤدي إلى تسوس الأسنان. في البحث الحالي، كان التركيز على الأوجينول وجليكوسيدات ستيفيول، والتي لها خصائص طبية. الأوجينول هو مركب طبيعي له خصائص مسكنة ومضادة للبكتيريا ومضادة للفيروسات ومضادة للأكسدة، مما يجعله خيارًا واعدًا في الوقاية من تسوس الأسنان. جليكوسيدات ستيفيول هي مواد مستخرجة من نبات ستيفيا، ولها مجموعة واسعة من الفوائد الصحية، بما في ذلك قدرتها على منع تسوس الأسنان، ولكن آلية عملها لا تزال قيد التحقيق. هدفت الدراسة إلى تقييم فعالية جليكوسيدات ستيفيول مقارنة بالأوجينول في تفاعلهما مع بروتين GbpC في *Streptococcus mutans*، وتقديم دليل على الاستخدام المحتمل لجليكوسيدات ستيفيول كخيار طبيعي للوقاية من تسوس الأسنان. في هذا البحث، استخدمنا نهجًا حسابيًا للتحقيق في معقدات 5UQZ (بروتين رابط الجلوكان C) في السلسلة A مع الأوجينول كعنصر تحكم وجليكوسيدات ستيفيول. تم إجراء تجربة فحص افتراضية باستخدام برنامج PyRx لتحسين دقة الارتباط بين المركبات والبروتين المستهدف. أظهرت النتائج أن الأوجينول حقق درجة ارتباط ٥,٩- كيلو كالوري / مول، في حين سجلت جليكوسيدات ستيفيول درجة ارتباط أعلى٩,٨ - كيلو كالوري / مول. تشير هذه النتائج إلى أن جليكوسيدات ستيفيول لها فعالية أعلى في التفاعل مع البروتين المستهدف من الأوجينول. يسلط هذا البحث الضوء على الإمكانات الواعدة لجليكوسيدات ستيفيول كخيار طبيعي لمكافحة تسوس الأسنان، ويضع الأساس لدراسات مستقبلية تهدف إلى تطوير منتجات صحة الفم الفعالة والمستدامة.

الكلمات المفتاحية: أداة المعلوماتية الحيوية، جليكوسيدات ستيفيول، العقدية الطافرة، الأوجينول، دقة الالتحام، PyRx.

1. Introduction:

Dental caries are a major dental and public health hazard worldwide, particularly among low-income people. Frequent consumption of dietary carbohydrates, particularly sweets, raises the risk of dental caries by generating acidity and upsetting the symbiotic diverse and complex microbial population of the mouth [1, 2]. Excessive acid production alters the nature of the bacterial biofilm, demineralizes tooth structure, and produces cavities.Acidic and acid-tolerant bacteria that bind to cavities include Streptococcus mutans, Lactobacillus, Actinomyces, Bifidobacterium, and Scardovia. The microbiota composition varies based on the tooth site, severity of carious lesions, and the rate of disease progression [1].

Streptococcus mutans, a pathogenic bacteria, is regarded as the primary factor agent of dental caries; it is assumed to be the most cariogenic bacteria. When it comes in contact with sweet or sucrose-containing products, it multiplies and secretes acids and other substances that damage the enamel of teeth [3, 4]

Streptococcus mutans, a gram-positive, facultative anaerobic coccus (round bacterium) commonly found in the human oral cavity, is a primary cause of tooth decay [5]. S. mutans' natural habitat is the human oral cavity, specifically dental plaque, a multispecies biofilm that forms on the hard surfaces of teeth [6].

Streptococcus mutans has been identified as the major bacterium causing dental caries in people. The bacteria create numerous glucan-binding proteins (GBPs), one of which is Glucan Binding Protein C (GbpC). When stressed, GbpC, a member of the streptococcal protein family PAc, is expressed. [7].

Streptococcus mutans are large cariogenic organisms—the result of their ability to manufacture huge volumes of glucans and acid, exceeding the salivary buffering capacities, which gives the bacteria an advantage to outcompete noncariogenic commensal species at low pH circumstances [8].

Eugenol is an allyl-substituted guaiacol from the allylbenzene family. It is a colorless to pale yellow, aromatic oily liquid made from essential oils, most notably clove, nutmeg, cinnamon, basil, and bay leaf. It is found in levels of 82-88% in clove leaf oil and 80-90% in clove bud oil [9].

Eugenol, also known as 4-allyl-2-methoxyphenol, is an aromatic chemical. It is an organic chemical compound belonging to the phenols category. Its chemical formula is $C_{10}H_{12}O_2$. It consists of a benzene ring linked to a methoxyl group ($-OCH_3$) and also to a hydroxyl group (-OH). According to numerous studies, this molecule has analgesic, antiviral, antioxidant,

antibacterial, and anti-inflammatory characteristics; it is also used in dentistry to treat pulpitis and toothaches [9]. Some research suggests that eugenol has an antimicrobial effect on S. mutans. Eugenol may be a useful therapeutic agent for dental caries since it has a better effect than the chemical Eugenol [10, 11, 12].

Stevia rebaudiana (Asteraceae) is a natural plant native to South America. Steviol glycosides are the chemical components that give the leaves their sweet taste [13]. Steviol glycosides show superior sweetening efficiency to sucrose and are calorie-free, non-cariogenic and do not cause side effects [14]. Steviol is the main compound in stevioside, and it contains a structure consisting of 20 carbon atoms (C20H30O3), with a hydroxyl group (-OH) and a ring consisting of carbon. Stevia rebaudiana bertoni has numerous health benefits, including antihyperglycemic, antihypertensive, antioxidant, renal protection, antitumor, antidiarrheal, diuretic, antiviral, immunomodulatory, and dental caries prevention [15]. Stevioside also helps reduce the risk of tooth decay, with some research showing it has anti-caries properties. However, more research is needed to discover how it works and the ideal concentration [16, 17, 18].

2. Material and methods:

Protein preparation and Ligands

Streptococcus mutans' Glucan Binding Protein C (GbpC), a primary target for Eugenol and Steviol glycosides, was acquired from the human PDB database using the PDB ID 5UQZ (URL: https://www.rcsb.org). Furthermore, the target proteins for the docking experiment are chosen based on their X-ray diffraction profiles. Proteins should be in PDB format. All heteroatoms, including ions and water, were removed from Streptococcus mutans' X-ray crystallographic structure in preparation for molecular docking. Use the Chimera tool and Discovery Studio 2021 Client. Certain protein-binding sites in the chain are selected, while others are avoided.

Preparation of Ligands

Open Babel software was used to obtain SDF format for three-dimensional chemical structures, which were then translated to PDB format by Pubchem (https://pubchem.ncbi.nlm.nih.gov). Throughout the docking study, steviol glycosides were utilized as the reference molecule, with Eugenol serving as a control to assess correlation strength. Both of these compounds were obtained via Pubchem.

The process of docking molecules

The structural interactions between the (target protein) 5UQZ and the (ligand molecules) Steviol glycosides and Eugenol (ligand molecules (control)) have been investigated using an in

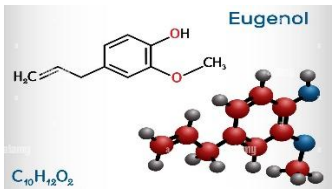
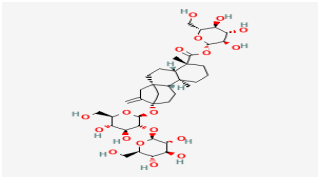
silico approach for analyzing ligand and receptor docking to display the conformation of this protein target selectivity. Used PyRx, a virtual screening tool, to increase docking accuracy by applying an algorithm as a scoring mechanism and integrating Vina and Auto Dock. [7]. the target protein included 583 amino acid atoms. X-ray crystallography was used to precisely establish the chemical makeup of the macromolecule at 1.14 Å. The work continues with the UCSF Chimera software, which removes the bonds and accompanying water molecules to prepare the target. In addition, we eliminate all chains except Chain A, which solely shows a ligand-binding site chain. Then we added it to the PyRx tool by marking it as a macromolecule in the PyRx workflow. Using auto dock techniques, the protein and ligand molecules were transformed to their suitable readable file format (pdbqt). All investigations of docking were carried out as blind docking in a grid box, which included all possible ligand-receptor complexes, and its dimensions were to Eugenol, as control and Steviol glycosides [(X = 100.54, Y =57.5798, and Z = 71.5732) and (X=92.5157, Y = 54.1111, and Z =67.8058)] respectively. All ligand bindings were allowed to freely rotate, and all other software parameters remained fixed while the receptor was considered as rigid. . The final visualization of the docked structure was done using Discovery Studio Visualizer 3.0. Prior to assessing the efficiency of the compounds from Urtica dioica against 5UQZ [7].

3. Results:

Molecular docking studies were carried out between The Glucan Binding Protein C (GbpC) of *Streptococcus mutans* (receptor) and (Eugenol and steviol glycosides), as seen in table (1). As the negative value of affinity binding increases, so does the precision of the receptor-ligand connection. The RMSD (Root Mean Square Deviation) number, which is used to confirm docking tests, represents the average difference between two proteins' corresponding atoms. [19].Each atom in one conformation is matched with itself in the opposite conformation by the RMSD upper bound, which ignores any symmetry. The RMSD lower bound is used to compare each atom in one conformation to the closest atom of the same element type in the other conformation [19].

Table 1. Diagnosis of ligands using Glucan Binding Protein C (GbpC) of *Streptococcus mutans*

docking term for ligands	Binding Affinity kcal/mol	RMSD/ UB	RMSD/LB	substance name

5uqz_3314uff_E=169.59	-5.9	0.0	0.0 	Eugenol: 4-Allyl-2-methoxyphenol
5uqz_442089uff_E=2828.21	-9.8	0.0	0.0 	Steviol glycosides

Eugenol:4-Allyl-2-methoxyphenol as a Control Ligand

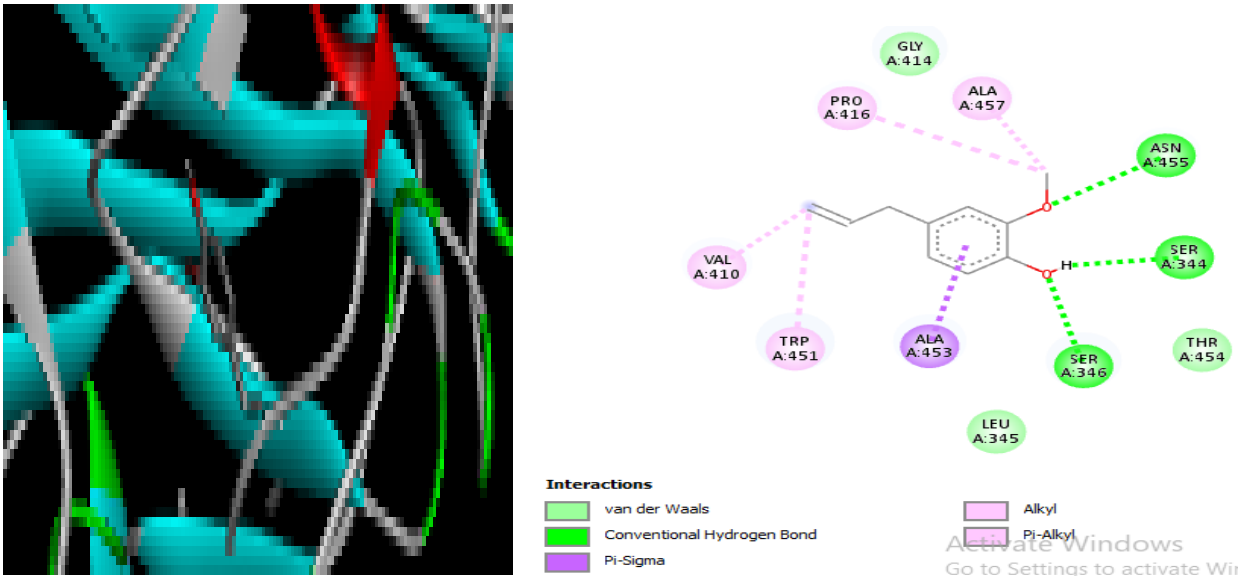
Eugenol (4-Allyl-2-methoxyphenol) was the standard molecule used in the docking analysis, and it was retrieved from PubChem using Pubchem CID-3314. Eugenol serves as a control in this investigation. Figure 1 shows the interaction state of the experimental control ligand. Table (2) depicts the interaction of the ligand with chain A of *Streptococcus mutans'* Glucan Binding Protein C (GbpC), which contains eleven amino acids, as well as the five different types of interactions formed between the ligand and receptor. Van der Waals, Carbon hydrogen bond, Alkyle, Pi-Alkyle, and Pi-Sigma score binding energy (-5.9) increased the affinity between the two chemicals as the binding strength was good. Usually, docking experiments are verified using the RMSD value.

Eugenol's docked ligand and the experimental ligand shared an acceptable RMSD of 0.0 angstrom. Table (2) depicts the interaction of amino acids and the type of bonds between ligands for Eugenol and chain A of Streptococcus mutans' Glucan Binding Protein C (GbpC). Use the PyRx tool to do virtual screening by docking in a target protein's active region. The study's findings also revealed that Eugenol had a good interaction with the A chain of Glucan Binding Protein C receptors, as illustrated in Figure (1).

Table 2. Streptococcus mutans and Eugenol's glucan binding protein C (GbpC) with amino acid position inside chain A

Amino acids	Location inside the chain	Bonds Type
THR	454	Van der -waals
LEU	345	
GLY	414	
ASN	455	Carbon hydrogen bond
SER	344	

SER	346	
PRO	416	Alkyle
ALA	457	
VAL	410	Pi- Alkyle
TRP	451	
ALA	453	Pi-Sigma



(a) (b)

FIGURE 1. (a) Interactions between Glucan Binding Protein C (GbpC) of *Streptococcus mutans* and Eugenol at the active site (**A**) 3D representation
(b) 2D representation. Van der Waals, Carbon hydrogen bond, Alkyle, Pi- Alkyle and Pi-Sigma are shown in the figure

Steviol Glycosides

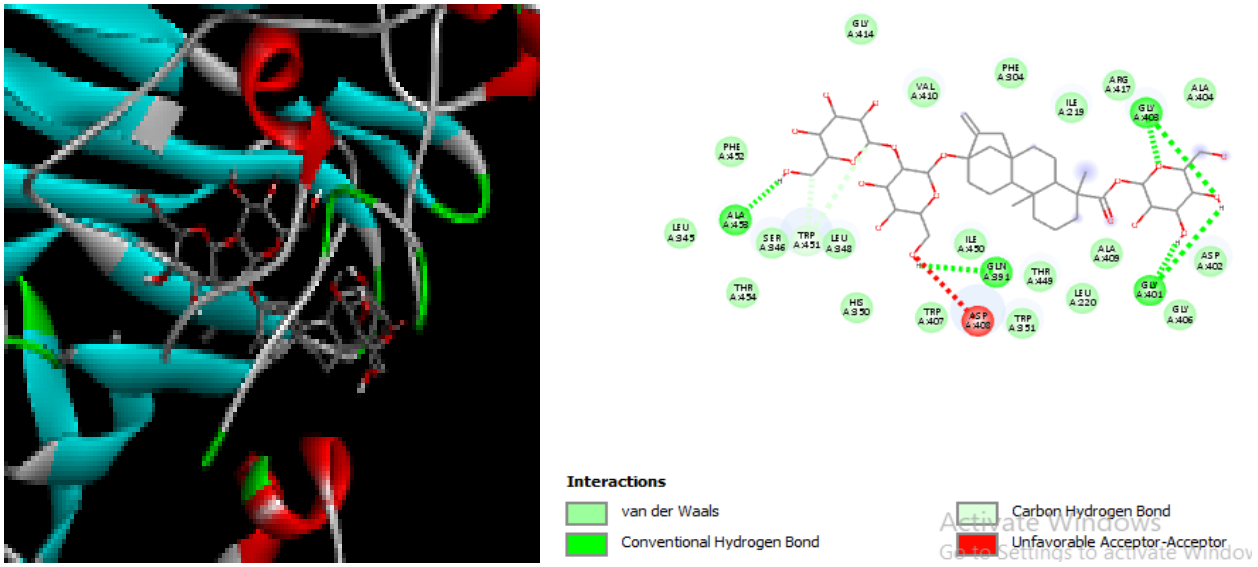
The ligand interacts with chain A of *Streptococcus mutans*. Table (3) shows Glucan Binding Protein C (GbpC), which has twenty-two amino acids. There are four types of unfavorable acceptor-acceptor interactions: conventional hydrogen bonds, carbon hydrogen bonds, and Van der Waals between ligand and receptor. The binding energy (-9.8) improved the affinity between the two compounds since the binding strength was excellent. Typically, docking experiments are validated using RMSD values.

Steviol Glycosides docked with experimental ligands had RMSD differences of 0.0 angstrom, which was acceptable. The steviol glycosides and chain A of *Streptococcus mutans'* Glucan Binding Protein C (GbpC) were represented by amino acid interactions and the type of bonds between ligands, as shown in Table 3. The docking approach was employed with the PyRx program to perform a virtual screening of Steviol Glycosides in a target protein's active regions. The results of this investigation demonstrated that the bind had an excellent interaction

with the A chain of the receptor *Streptococcus mutans* GbpC (Glucan Binding Protein C) with Steviol Glycosides, as shown in Figure (2).

Table 3. *Streptococcus mutans* Glucan Binding Protein C (GbpC) and Steviol Glycosides have amino acid locations within chain A.

Amino acids	Location inside the chain	Bonds Type
ASP	408	Unfavorable Acceptor-Acceptor
GLY	401	Conventional hydrogen bond
GLY	408	
GLN	391	
ALA	458	
TRP	451	Carbon hydrogen bond
GLY	414	Van der- waals
VAL	410	
PHE	304	
IEL	219	
APG	417	
ALA	404	
PHE	452	
LEU	345	
SER	346	
LEU	348	
THR	454	
HIS	350	
TRP	407	
ILE	450	
THR	449	
TRP	351	
LEU	220	
ALA	409	
ASP	402	
GLY	406	



(a) (b)

FIGURE 2. (a) Interactions between Glucan Binding Protein C (GbpC) of *Streptococcus mutans* and Steviol Glycosides at the active site (**A**) 3D representation
(b) 2D representation. Unfavorable Acceptor-Acceptor, Conventional hydrogen bonds, carbon-hydrogen bonds and Van der waals are shown in the figure

4. Discussion

Eugenol (4-allyl-2-methoxyphenol) is the main component of the essential oil of this plant, and it is a natural compound with broad biological activity, as it has proven to be effective as an antibacterial and antifungal, including its effect on microbial biofilms. In addition, eugenol is non-toxic and safe for human use, making it a promising option in medical applications. Numerous studies have shown its ability to combat dental caries and this is consistent with the results obtained, as the binding strength was good -5.9 kcal/mol [20, 21,22], as this activity is linked to its strong interaction with caries-causing bacteria, which enhances its feasibility as a natural treatment.

On the other hand, the stevia plant stands out as a rich source of natural compounds with multiple health benefits, as studies indicate that it has anti-cancer and anti-inflammatory properties, in addition to its role in modifying the immune response and its diuretic effect. It is noteworthy that stevia also has a distinct role in oral and dental health, as its non-carbohydrate compounds prevent the growth of *Streptococcus mutans*, the bacteria associated with dental caries and cavity formation. Furthermore, research has shown that the use of Stevia rebaudiana Bertoni leaf extracts as an herbal mouthwash shows clear efficacy in preventing caries [23].

The alcoholic extract of stevia also shows strong antibacterial activity caries and this is agree with the results obtained, as the binding strength was excellent -9.8 kcal/mol

Based on the available scientific results, steviol glycosides, the active ingredient in stevia, appear as a promising option with antimicrobial properties that are superior in some aspects to eugenol. Studies have shown a strong affinity of steviol glycosides for the target bacteria, which opens up prospects for their use as a potential alternative to eugenol in the future. However, in-depth research is still needed to understand the exact mechanism of action of these glycosides, as well as to evaluate their efficacy in clinical settings, with a focus on the effect of crude extracts to maximize the benefit [24, 25].

5. Conclusions

According to the study's findings, the degree of binding for eugenol was -5.9 kcal/mol, whereas the degree of binding for Steviol Glycosides was -9.8 kcal/mol. Some research have discovered that stevioside has anti-mutagenic qualities and may help reduce the incidence of tooth decay; this confirms the results obtained, as steviol glycosides have a higher binding strength than eugenol. However, additional research is needed to determine the mechanism of action and appropriate concentration of this substance, and raw Steviol Glycosides extract is preferred.

6. References

[1] Simón-Soro A, Mira A. Solving the etiology of dental caries. Trends in microbiology. 2015 Feb 1;23(2):76-82. . https://doi.org/10.1016/j.tim.2014.10.010

[2] Spatafora G, Li Y, He X, Cowan A, Tanner AC. The evolving microbiome of dental caries. Microorganisms. 2024 Jan 7;12(1):121. https://doi.org/10.3390/microorganisms12010121

[3] Kouidhi B, Al Qurashi YM, Chaieb K. Drug resistance of bacterial dental biofilm and the potential use of natural compounds as alternative for prevention and treatment. Microbial pathogenesis. 2015 Mar 1;80:39-49. https://doi.org/10.1016/j.micpath.2015.02.007

[4] Flayyih AS, Hassani HH, Wali MH. Identification of Streptococcus mutans from human dental plaque and dental caries using 16srrna gene. Iraqi Journal of Science. 2016:552-7.

[5] Ryan, K. J., Ray, C. G., & Sherris, J. C. (2004). Sherris medical microbiology: an introduction to infectious diseases.

[6] Lemos JA, Palmer SR, Zeng L, Wen ZT, Kajfasz JK, Freires IA, Abranches J, Brady LJ. The biology of Streptococcus mutans. Microbiology spectrum. 2019 Feb 27;7(1):10-128. . https://doi.org/10.1128/microbiolspec.gpp3-0051-2018.

[7] Mieher JL, Larson MR, Schormann N, Purushotham S, Wu R, Rajashankar KR, Wu H, Deivanayagam C. Glucan binding protein C of Streptococcus mutans mediates both sucrose-independent and sucrose-dependent adherence. Infection and Immunity. 2018 Jul;86(7):10-128 . https://doi.org/10.1128/iai.00146-18

[8] Metwalli KH, Khan SA, Krom BP, Jabra-Rizk MA. Streptococcus mutans, Candida albicans, and the human mouth: a sticky situation. PLoS pathogens. 2013 Oct 17;9(10):e1003616. https://doi.org/10.1371/journal.ppat.1003616.

[9] Heinrich M, Barnes J, Prieto-Garcia J, Gibbons S, Williamson EM. Fundamentals of Pharmacognosy and Phytotherapy: Fundamentals of Pharmacognosy and Phytotherapy E-Book. Elsevier Health Sciences; 2017 Nov 24.

[10] Xu JS, Li YA, Cao XU, Cui YU. The effect of eugenol on the cariogenic properties of Streptococcus mutans and dental caries development in rats. Experimental and Therapeutic Medicine. 2013 Jun 1;5(6):1667-70. . https://doi.org/10.3892/etm.2013.1066.

[11] Firyanto R, Azizah N. Effectiveness of Eugenol as An Antibacterial Toward Staphylococcus epidermidis. InJournal of Physics: Conference Series 2019 Sep 1 (Vol. 1295, No. 1, p. 012034). IOP Publishing. DOI 10.1088/1742-6596/1295/1/012034.

[12] Fatene N, Mounaji K, Soukri A. Effect of Eugenol on Streptococcus mutans Adhesion on NiTi Orthodontic Wires: In Vitro and In Vivo Conditions. European Journal of General Dentistry. 2021 Sep; 10(03):151-7. DOI: 10.1055/s-0041-1736372

[13] Brandle JE, Telmer PG. Steviol glycoside biosynthesis. Phytochemistry. 2007 Jul 1; 68(14):1855-63. https://doi.org/10.1016/j.phytochem.2007.02.010.

[14] Orellana-Paucar AM. Steviol glycosides from Stevia rebaudiana: an updated overview of their sweetening activity, pharmacological properties, and safety aspects. Molecules. 2023 Jan 27; 28(3):1258. https://doi.org/10.3390/molecules28031258

[15] Escobar E, Piedrahita M, Gregory RL. Growth and viability of Streptococcus mutans in sucrose with different concentrations of Stevia rebaudiana Bertoni. Clinical oral investigations. 2020 Sep; 24:3237-42. https://doi.org/10.1007/s00784-020-03197-5

[16] Abbas Momtazi-Borojeni A, Esmaeili SA, Abdollahi E, Sahebkar A. A review on the pharmacology and toxicology of steviol glycosides extracted from Stevia rebaudiana. Current Pharmaceutical Design. 2017 Mar 1;23(11):1616-22.

[17] Frentzen M, Besrukow P, Ackermann A, Pierog S, Schiermeyer B, Winter J, Wölwer-Rieck U, Kraus D. Steviol Glycosides in Dentistry. https://doi.org/10.1039/9781788010559-00162

[18] Guo M, Yang K, Zhou Z, Chen Y, Zhou Z, Chen P, Huang R, Wang X. Inhibitory effects of Stevioside on Streptococcus mutans and Candida albicans dual-species biofilm. Frontiers in Microbiology. 2023 Apr 5;14:1128668. https://doi.org/10.3389/fmicb.2023.1128668

[19] Bell EW, Zhang Y. DockRMSD: an open-source tool for atom mapping and RMSD calculation of symmetric molecules through graph isomorphism. Journal of cheminformatics. 2019 Dec;11:1-9.https://doi.org/10.1186/s13321-019-0362-7

[20] Adil M, Singh K, Verma PK, Khan AU. Eugenol-induced suppression of biofilm-forming genes in Streptococcus mutans: An approach to inhibit biofilms. Journal of global antimicrobial resistance. 2014 Dec 1;2(4):286-92.https://doi.org/10.1016/j.jgar.2014.05.006

[21] Rodriguez OE, Sánchez RM, Verde MJ, Núñez MA, Castro R, Montes AC. Obtaining of the essential oil of Syzygium aromaticum, identification of eugenol and its effect on Streptococcus mutans. Journal of oral research. 2014;3(4):218-24. https://doi.org/10.3390/molecules28031258

[22] Jafri H, Khan MS, Ahmad I. In vitro efficacy of eugenol in inhibiting single and mixed-biofilms of drug-resistant strains of Candida albicans and Streptococcus mutans. Phytomedicine. 2019 Feb 15;54:206-13. https://doi.org/10.1016/j.phymed.2018.10.005

[23] Sharangi AB, Bhutia PH. Stevia: Medicinal Miracles and therapeutic magic. International Journal of Crop Science and Technology. 2016;2(2).

[24] Ajagannanavar SL, Shamarao S, Battur H, Tikare S, Al-Kheraif AA, Al Sayed MS. Effect of aqueous and alcoholic Stevia (Stevia rebaudiana) extracts against Streptococcus mutans and Lactobacillus acidophilus in comparison to chlorhexidine: An: in vitro: study. Journal of International Society of Preventive and Community Dentistry. 2014 Dec 1;4(Suppl 2):S116-21.*DOI:* 10.4103/2231-0762.146215

[25] Deviyanti S, Herawati M, Ferhad A. ANTIMICROBIAL POTENCY of Stevia rebaudiana Bertoni as HERBAL MOUTHWASHES AGAINST CARIOGENIC BACTERIAL Streptococcus mutans. InICCD 2019 Nov 27 (Vol. 2, No. 1, pp. 317-321).https://doi.org/10.33068/iccd.Vol2.Iss1.207

Al-Kitab Journal for Pure Sciences (2026); 10(2):13-23.
https://doi.org/10.32441/kjps.10.2.p2

Al-Kitab Journal for Pure Sciences
ISSN: 2617-1260 (print), 2617-8141(online)

https://isnra.net/index.php/kjps

The Isolation and Characterization of Indigenous Rhizobacteria from Rhizosphere of *Phaseolus vulgaris* L. and their Potential Applications in Sustainable Agriculture

Noor Azez Aref [1], Raad Hassani Sultan[2],Vineetha Edavana[3]

[1,2]Department of Biology, College of Education for Pure Sciences, University of Mosul, Mosul, Iraq.

[3] Director, Clinical Development, Replimune, Woburn, MA, U.S.A.

*Corresponding Author: noor.23esp34@student.uomosul.edu.iq,dr.raadsultan@uomosul.edu.iq

Citation: *Noor Azez Aref [1], Raad Hassani Sultan[2],Vineetha Edavana[3]*. **The Isolation and Characterization of Indigenous Rhizobacteria from Rhizosphere of Phaseolus vulgaris L. and their Potential Applications in Sustainable Agriculture. Al-Kitab J. Pure Sci. [Internet]. 2025 Aug 07; 10(2):13-23 DOI:** https://isnra.net/index.php/kjps/article/view/2026. https://doi.org/10.32441/kjps.10.02.p2.

Keywords: Rhizobacteria, Biochemical, Antibiotics sensitivity, NaCl tolerance.

Article History

Received	23 June.	2025
Accepted	07 Aug.	2025
Available online	01 Nov.	2026

©20--. THIS IS AN OPEN-ACCESS ARTICLE UNDER THE CC BY LICENSE
http://creativecommons.org/licenses/by/4.0/

Abstract:

This study aimed to isolate plant growth-promoting bacteria (PGPB) and characterize the isolates. A collection of soil from root rhizosphere of *Phaseolus vulgaris* L. cultured in Hawi Al-Kanissa region on the right bank of Tigris and Al-Qubba region on the left bank of Tigris River of Mosul City-Iraq was done. Eighteen rhizobacterial isolates were obtained, nine from each bank. Purification of rhizobacterial isolates was done and subjected to cultural and microscopic examination. Results revealed that the shape of the cells varied from short bacilli to bacilli and spherical. All the isolates were Gram-positive, with the exception of NR6 and NR7 which were negative for Gram stain. Results showed that all the isolates were motile except NR1, NR8, NR12 and NR16. Cultural emphasis showed extreme production of exopolysaccharide by the isolates NR9, NR12, NR13 and NR15. Biochemical test results revealed positive results for catalase, whereas negative results for oxidase, triple sugar iron, starch hydrolysis and citrate utilization. All the isolates were negative for urea test with the exception to NR8 and NR9. All the rhizobacterial isolates were positive for the indole test with the exception of NR11, NR12

and NR14. Sensitivity and resistance tests for the eight studied antibiotics revealed that three rhizobacterial isolates had resistance to three antibiotics or more. Test of tolerance of rhizobacterial isolates to different concentrations of sodium chloride revealed that these isolates were tolerant to this salt and the maximum tolerance reached 10 % (w/v) by the isolate NR3. It was concluded that the isolates varied in their cultural and biochemical characteristics as well as for antibiotic resistance and sodium chloride tolerance.

Keywords: Rhizobacteria, Biochemical, Antibiotic sensitivity, NaCl tolerance.

عزل وتشخيص الرايزوبكتريا المحلية من المنطقة الجذرية لنبات *Phaseolus vugaris* L. الفاصوليا

نور عزيز عارف[1], رعد حساني سلطان[2], Vineetha Edavana[3]

[2,1] قسم علوم الحياة, كلية التربية للعلوم الصرفة, جامعة الموصل, العراق.

[3] Director, Clinical Development, Replimune, Woburn, MA, U.S.A.

الايميل الرسمي: noor.23esp34@student.uomosul.edu.iq,dr.raadsultan@uomosul.edu.iq

الخلاصة:

تهدف هذه الدراسة الى عزل البكتريا المشجعّة على نمو النبات وتشخيص العزلات, حيث تم جمع تربة من المنطقة الجذرية لنبات الفاصوليا المزروعة في منطقة حاوي الكنيسة في الساحل الايمن وكذلك من منطقة القبة في الساحل الايسر من نهر دجلة من مدينة الموصل-العراق. تم الحصول على ١٨ عزلة رايزوبكتريا بواقع تسعة عزلات من كل ساحل. تم تنقية عزلات الرايزوبكتريا والقيام بالفحص الزرعي والمجهري واظهرت النتائج ان شكلها تراوح ما بين العصوي القصير الى العصوي والكروي وإنها موجبة لصبغة كرام ماعدا العزلتين NR6 وNR7 حيث كانتا سالبتين لصبغة كرام. كما أظهرت النتائج ان جميع العزلات متحركة ما عدا أربعة عزلات وهي: NR1 وNR8 وNR12 وNR16 حيث كانت غير متحركة. واظهرت نتائج الفحص الزرعي ان أربعة عزلات وهي: NR9 وNR12 وNR13 وNR15 كانت غزيرة انتاج السكر المتعدد الخارجي. وكما اظهرت نتائج الاختبارات الكيموحيوية انها موجبة للكاتاليز وتباينت نتائج اختبارات الاوكسيديز وثلاثي السكر والحديد وتحلل النشأ واستهلاك السترات. جميع العزلات كانت سالبة لاختبار اليوريا ما عدا العزلتين NR8 وNR9 وجميع العزلات سالبة لاختبار الاندول. أظهرت تجربة الحساسية والمقاومة لثمانية مضادات حيوية ان ثلاثة عزلات كانت مقاومة لثلاثة مضادات حيوية او أكثر. واظهرت تجربة تحمّل كلوريد الصوديوم لتراكيز مختلفة ان هذه العزلات كانت متحمّلة لهذا الملح ووصل اقصى التحمّل الى ١٠ % (وزن/حجم) في العزلة NR3. استنتجنا ان العزلات متنوعة في صفاتها المزرعية والكيموحيوية كما في الحساسية للمضادات الحيوية وتحمّلها لمح كلوريد الصوديوم.

الكلمات المفتاحية: رايزوبكتريا, الكيموحيوية, الحساسية للمضادات الحيوية, تحمّل كلوريد الصوديوم.

1. Introduction:

The microbiome-rhizosphere of leguminous plants constitutes a critical interface for nutrient exchange, disease suppression, and plant-microbe interactions. Research works indicate that legume roots selectively recruit beneficial bacteria through the secretion of

phenolic compounds, flavonoids, as well as organic acids, which act as chemoattractant for symbiotic. Rhizobia and other plant-growth-promoting rhizobacteria (PGPR) [1]. The microbial diversity within this area is shaped by plant, soil characteristics, and agricultural nutrients, making it a key factor in sustainable crop yield [2].

The mutualistic relationships between legumes and rhizobacterial rhizosphere extend beyond nitrogen fixation, encompassing induced systemic resistance (ISR) against any pathogens and improved biotic and abiotic stress tolerance [3]. Advances in metagenomics and microbial ecology have deepened our understanding of these interactions, paving the way for microbiome-based agricultural innovations [4]. Thus, studying the bacterial communities in the legume rhizosphere not only enhances our knowledge of plant-rhizobacterial symbiosis, but also offers practical solutions for eco-friendly cultures.

Plant Growth-Promoting Bacteria (PGPB) play a pivotal role in enhancing the productivity of leguminous crops, including green beans (*Phaseolus vulgaris* L.), through mechanisms such as biological nitrogen fixation, phytohormone production, and phosphate solubilization. These bacteria colonize the rhizosphere, forming symbiotic relationships that improve nutrient uptake and stress tolerance [5].

The rhizosphere rhizobacteria found in rhizosphere of *Phaseolus vulgaris* L. are highly dynamic, influenced by soil type, climatic conditions, and agricultural practices. Metagenomic studies reveal that some genera like *Rhizobium* and *Pseudomonas* spp. dominates this niche, contributing to nitrogen fixation and pathogen suppression [6].

2. Materials and methods:

2.1 Isolation of rhizobacteria:

Isolation of rhizobacterial bacteria was done according to Liu *et al.* [7] The field where the leguminous plant green beans is grown was selected, as this plant has been grown in the field on the right side for 48 years in the Hawi Al-Kanisa area and for a period of up to 50 years on the left side in the Al-Qubba area, taking into account that the soil is moist and not dry, as the plant was gently uprooted and shaken to exclude soil with weak adhesion to the root group, as the remaining soil attached to the root was chosen for isolation of rhizobacteria.

An amount of 1-2 grams of soil was taken from the upper root zone and 1-2 grams from the lower zone of the root of leguminous plant. The serial decimal dilution method is a core technique for assessing microbial density in soil. A 1-gram soil sample is mixed with 9 mL of

distilled water to achieve a 10^{-1} dilution. Subsequent dilutions were 10^{-2} to 10^{-6} are prepared by transferring 1 mL of the prior dilution into 9 mL of distilled water. Each dilution was then cultured on the appropriate medium and incubated [8] .

2.2 Cultural and microscopical emphasis:

Colony colour appearance and ability for the production of exopolysaccharide were recorded after culturing the 18 purified colonies on suitable solid medium and incubation for 1-3 days in an incubator at 30 °C. Cell shape and Gram staining were examined under a microscope with 1000x power.

2.3 Biochemical tests for rhizobacterial isolates:

Biochemical tests for isolating soil isolated rhizobacteria from rhizosphere of common bean were conducted and included the following tests: motility [9], urease [10], starch hydrolysis [11], catalase [12], Kovacs (indole) [13], citrate utilization [14], oxidase [15], triple sugar and iron test [16].

2.4 Intrinsic antibiotic resistance of rhizobacteria:

Antibiotic resistance testing of soil bacterial isolates was performed to determine the growth of plant growth-promoting bacterial isolates in the presence of the following antibiotics (µg/ml): Nitrofurantoin (N), 100; Ciprofloxacin (Cip), 10; Erythromycin (E), 10; Lincomycin (L), 10; Chloramphenicol (C), 10; Ampicillin (Am), 25; Clindamycin (Da), 10 and Amikacin (Ak), 10.

These antibiotics were produced by Turkey Bioanalysis. Using a cotton swab, the tested rhizobacterial isolates were spread onto Mueller-Hinton (M.H.A.) agar medium before introducing antibiotic discs. Using sterile forceps, liquid fresh growth was spread onto the medium, and cultured for 24 hours at 30 °C. The presence of a transparent halo surrounding the antibiotic discs was used to identify rhizobacterial isolates for sensitivity and resistance against different studied antibiotics [17,18].

2.5 Tolerance of rhizobacterial isolates to different concentrations of sodium chloride:

To emphasize the ability of isolated rhizobacteria for tolerance, the following concentrations of sodium chloride: 2.0, 4.0, 6.0, 8.0 and 10 % (w/v), a nutrient agar plate was supplanted the mentioned concentrations of sodium chloride inoculated with the same concentration of inoculum which equal 0.5 value on O.D. 600. [19]

3. Results:

The isolation and characterization of rhizobacteria from rhizosphere of roots of common bean (*Phaseolus vulgaris* L.) cultured in right bank (Hawi Al-Kanissa) and left bank (Al-Qubba) of the Tigris river in Mosul city of Iraq. A total of six rhizobacterial isolates were isolated and purified. Table (1) below shows microscopic and cultural characteristics of the isolated rhizobacteria. All the isolates with exception with NR6 were Gram-positive and positive for the motility test with exception to NR8 which were non-motile. Cell shape was varied from spherical to short rod to rod (Table 1). Colony colour was different for the six isolates as follows: yellow, orange, white and milky white.

Table 1: Cultural and microscopical examination of rhizobacterial isolates.

Isolate No.	Gram stain	Motility	Cell shape	Colony colour	EPS production
NR4	+	+	Spherical	Yellow	-
NR6	-	+	Short rod	Orange	-
NR8	+	-	Spherical	White	-
NR9	+	+	Short rod	Milky white	+
NR13	+	+	Rod	Orange	+
NR14	+	+	Rod	Orange	-

EPS: Exopolysaccharide.

Biochemical characterization tests (Table 2) revealed that all the isolates were positive for catalase and negative for indole tests. Oxidase test result revealed that NR4, NR6 and NR9 isolates were positive for this test and the rest isolates were negative for oxidase test. Triple sugar iron results were positive with the exception with NR13 which was negative for this test. Only two rhizobacterial isolates were positive for the urea test, i. e., NR8 and NR9 isolates, whereas the other isolates were negative for this test. Five of the six isolates were able to hydrolyze the starch and the rest isolate was negative for this test. Two isolates NR1 and NR14 showed the ability to utilize citrate, whereas other isolates were unable to utilize citrate as sole carbon source.

Table 2: Biochemical tests of rhizobacterial isolates.

Isolate No.	Catalase	Oxidase	TSI	Urea	Strach hydrolysis	Indole	Citrate utilization
NR4	+	+	+	-	+	-	+
NR6	+	+	+	-	+	-	-

NR8	+	-	+	+	+	-	-
NR9	+	+	+	+	+	-	-
NR13	+	-	-	-	+	-	-
NR14	+	-	+	-	-	-	+

TSI: Triple sugar iron test.

Results of resistance and sensitivity to the eight different studied antibiotics revealed that the isolates NR4 and NR8 were resistant to Nitrofurantoin 100 µg/ mL. All six isolates were sensitive to Ciprofloxacin 10 µg/ mL. The maximum average inhibition zone was 43 cm with NR9 isolate and minimum of average inhibition zone was 25 cm with NR4 isolate. Only one isolate (NR4) was resistant to Erythromycin 10 µg/ mL, whereas the other isolates showed different average inhibition zones and a maximum reached to 30 cm by NR9 isolate and minimum 18 cm by the isolates NR6 (Table 3).

Isolates NR9 and NR12 were resistant to Lincomycin 10 µg/ mL. The maximum average inhibition zone was 30 cm by NR8 isolate and minimum average inhibition zone was 10 cm by NR6 isolate. All the isolates were sensitive to chloramphenicol 10 µg/ mL with the exception of NR4 which was resistant to this antibiotic. The maximum average inhibition zone was 42 cm by NR8 isolate and minimum was 10 cm by NR6 isolate. NR9 rhizobacterial isolate was resistant to Ampicillin 25 µg/ mL, and the rest of the isolates were sensitive to this studied antibiotic. A maximum average inhibition zone was 32 cm by the NR13 isolate and minimum average inhibition zone was 17 cm by the isolate NR8.

NR9 was resistant to Clindamycin 10 µg/ mL, the other five isolates were sensitive to this antibiotic. Maximum sensitivity was by the NR4 isolate which was 34 cm and the minimum sensitivity was 9 cm by the NR13 isolate. None any of the isolates showed ability for resistance against the antibiotic Amikacin 10 µg/ mL, i.e. all the isolates were sensitive to this antibiotic and the maximum of average of inhibition zone was 29 cm by the isolate NR13 and the minimum average inhibition zone was 20 cm by the isolates NR4 and NR8.

Table 3:Resistance and sensitivity of rhizobacterial isolates to different studied antibiotics (µ/mL).

Isolate No.	F 100	Cip 10	E 10	L 10	C 10	Am 25	Da 10	Ak 10
NR4	R	25	R	28	R	23	34	20

NR6	16	35	18	10	10	20	27	25
NR8	R	33	29	30	42	17	27	20
NR9	15	43	30	R	33	R	R	23
NR13	30	40	24	R	37	32	9	29
NR14	20	29	18	15	20	20	22	18

Each value is mean of triplicates.

Abbreviations: F: Nitrofurantoin; Cip: Ciprofloxacin; E: Erythromycin; L: Lincomycin; C: Chloramphenicol; Am: Ampicillin; Da: Clindamycin; Ak: Amikacin.

Tolerance of the rhizobacterial isolates against different studied concentrations of sodium chloride revealed high ability of the isolated rhizobacteria to tolerate this salt (Table 4). From this table it is clear that the isolates have extreme tolerance to 2.0 % (w/v) concentration sodium chloride. With 4.0 % (w/v) concentration isolates NR8 and NR9 showed less ability to tolerate this concentration. Most of the isolates revealed varied growth from weak to good to very good growth on 6.0 % (w/v) concentration and the isolate NR9 showed no signals of growth. With 8.0 % (w/v) concentration three isolates NR6, NR8 and NR9 showed no growth and three isolates were able to grow viz., NR4, NR13 and NR14. All the six isolates were not able to grow on 10 % (w/v) which considered high concentration. (Table 4).

Table 4: Tolerance of rhizobacterial isolates to different NaCl concentrations % (w/v).

Isolate No.	**Concentration of NaCl % (w/v)**				
	2.0	**4.0**	**6.0**	**8.0**	**10.0**
NR4	+++	+++	++	+	-
NR6	+++	+++	++	-	-
NR8	+++	++	+	-	-
NR9	+++	++	-	-	-
NR13	+++	+++	++	+	-
NR14	+++	+++	+++	++	-

+++: very good growth; ++: Good growth; + moderate to weak growth; -: no growth.

4. Discussion

Two rhizobacterial isolates (NR9 and NR13) were high exopolysaccharide producers. [20] isolated polysaccharide producer and heavy metal-tolerant local rhizobial isolates. [21] isolated and identified rhizobacteria and they concluded that the Tigris and Euphrates rivers are

important for habitat developments as they provide water for agriculture and then support a variety of ecosystem. Their results on phenotypic examination revealed differences in Gram staining, motility and cell morphology as well as colony characteristics among isolated rhizobacteria. The positive catalase activity in all isolates suggests their potential for oxidative stress mitigation in plants. [22] reviewed antibiotic resistance in plant growth-promoting bacteria and their introduction into the soil could serve as antibiotic resistance gens and the invasion may enter into the food chain. Understanding the antibiotic resistance in plant agricultural systems, particularly those that use biofertilizers, is crucial because we must determine whether applying these fertilizers to the soil has the potential to select ARGs that could have an adverse effect on human health [22]. Therefore, it is essential to comprehend the antibiotic resistance profiles of PGPR in order to assess potential dangers that could affect the health of humans and animals, such as the transfer of resistance traits to dangerous bacteria [17]. Antibiotic resistance is evidenced through general different mechanisms such as decreased permeability then preventing penetration of antibiotics. The other method is Efflux system pump, the antibiotic pushed out of the cell before reaching the target. Target evasion and antibiotic metabolism, i. e., alter the structure of antibiotic targets [23]. [19] tested 20 rhizobacterial isolates and screened them for their salt tolerance potential and they found they showed halotolence to sodium chloride. Osmolyte compounds such proline, trehalose and total soluble sugars are biosynthesized in response to osmotic stress which and then accumulated in the cytoplasm as known as compatible solutes play a potential role in tolerance of salts [24]. [25] pointed out such these bacteria can be introduced into the root plant system to augment their stress-tolerant potential without compromising their productivity and lead to safeguarding the ecosystem.

5. Conclusions

Plant Growth Promoting Bacteria (PGPB) play a vital role in life sustainability as long as the rhizobacteria improve soil mixture as well as many positive roles in nature generally. This study succeeded in isolating and characterizing the isolates from soil in rhizosphere of *Phaseolus vulgaris* L. in both banks of Tigris river in Mosul city of Iraq. These isolates have a genetic marker such as antibiotic resistance genes as well as genes of tolerance of sodium chloride. Another feature of some of these isolates is their ability to produce high of exopolysaccharide which is considered signal of interaction between two partners leguminous plant and microorganism. Recent studies revealed that bacterial exopolysaccharides have industrial and medical applications, so these four isolates have immense potential in the future.

Acknowledgement

The Department of Biology/ College of Education for Pure Sciences/ University of Mosul/ Mosul-Iraq, is acknowledged by the authors for its valuable contribution to the enhancement and support of the quality of this research effort.

6. References

[1] Dakora F D, Phillips D. A. Root exudates as mediators of mineral acquisition in low-nutrient environments. Plant Soil. 2002; 245(1), 35-47.

[2] Sasse J, Martinoia E, Northen T. Feed your friends: do plant exudates shape the root microbiome. Trends in Plant Science. 2018; 23(1), 25-41.

[3] Compant S, Clément C, Sessitsch A. Plant growth-promoting bacteria in the rhizo- and endosphere of plants: their role, colonization, mechanisms involved and prospects for utilization. Soil Biology Biochemistry. 2010; 42(5), 669-678.

[4] Philippot L, Raaijmakers J M, Lemanceau P, van der Putten W H. Going back to the roots: the microbial ecology of the rhizosphere. Nature Reviews Microbiology. 2013; 11(11), 789-799.

[5] Santos M S, Nogueira M A, Hungria M. Plant growth promotion by *Rhizobium* and *Bacillus* strains in common bean (*Phaseolus vulgaris* L.). Applied Soil Ecology. 2019; 144, 134-142. https://doi.org/10.1016/j.apsoil.2019.07.010

[6] Martínez-Hidalgo P, Hirsch A M. The *Rhizobium*-legume symbiosis in the rhizosphere: Insights from genomic and metagenomic approaches. Frontiers in Microbiology 2017; 8: 2204. https://doi.org/10.3389/fmicb.2017.02204.

[7] Liu F, Hewezi T, Lebeis S L, Pantalone V R, Grewal P S. Rhizosphere sampling protocols for microbiome analysis in common bean (Phaseolus vulgaris L.): A comparative evaluation of different collection methods. Applied Soil Ecology. 2023; 182: 104712. https://doi.org/10.1016/j.apsoil.2022.104712

[8] Johnson K L, Brown M A, Lee S. Microbial diversity in extreme environments: Insights from metagenomic analysis. Applied Environmental Microbiology. 2015; 81(12), 3205-3212.

[9] Collee J G, Fraser A G, Marmiom B P, Simmon A. Mackie and McCarteny, Practical Medical Microbiology. 1996; 4 (USA: Churchill Livingstone inc.).

[10] Tille P M. Baily and Scott's Diagnostic Microbiology. 41thed. Elsevier, Inc. China. 2017; 1115pp

[11] Cowan, S T Cowan, Steel's. Manual for the Identification of Medical Bacteria, 2nd ed, Cambridge University Press, Cambridge, England. 1974; 67-83.

[12] Procop G W, Church D L, Hall G S, Janda W M, Koneman E W, Schreckenberger P C, Wods G L. Koneman's Color Atlas and Textbook of Diagnostic Microbiology. 7th ed Wolters Kluwer Health, Philadelphia, U.S.A., 2017.

[13] Baron E J, Peterson L R, Finegold S M. Baily and Scotts's Diagnostic Microbiol. 9th ed. Mosby. St. Louis, U. S. A, 1994.

[14] Somasegaran P, Hoben H J. Handbook for Rhizobia: Methods in Legume-*Rhizobium* Technology. Springer. 2020.

https://doi.org/10.1007/978-1-4419-3876-3

[15] Ribeiro R A, Ormeño-Orrillo E, Dall'Agnol R F, Graham P H, Martinez-Romero E, Hungria M. Phenotypic and genetic diversity of rhizobia nodulating common bean in different agroecological regions. Frontiers in Microbiology. 2022; 13: 789542.

https://doi.org/10.3389/fmicb.2022.789542

[16] Martínez-Romero E, García-Fraile P, López-López A. Biochemical and molecular characterization of rhizobia isolated from *Phaseolus vulgaris* nodules. Applied and Environmental Microbiology. 2021; 87(15): e01234-21.

https://doi.org/10.1128/AEM.01234-21

[17] Taoufiq K, Aberchane L, Amri O, Oufdou K, El Biari K, Talbi A, Fghire R, Ouachtak H, Faghire M. Antibiotics resistance and PGPR traits of endophytic bacteria isolated in arid region of Morocco. 2024. International Journal of Plant Biology. 2024; 15: 1063-1076. https://doi.org/10.3390/ijpb15040075.

[18] Smith J, Patel R. Evaluation of antibiotic resistance profiles in PGPR isolates using disc diffusion assay. Journal of Applied Microbiology. 2022; 133(4), 2456-2468. https://doi.org/10.1111/jam.15678.

[19] Pallavi, Mishra R K, Sahu P K, Mishra V, Jamal H, Tripathi. Isolation and characterization of halotolerant plant growth promoting rhizobacteria from mangrove region of Sundarbans, India for enhanced crop productivity. Frontiers in Plant Sciences. 2023; 20: 1-15. Doi: 10.3389/fpls.2023.1122347.

[20] Jasim M H, Sultan R H. Isolation of polysaccharide producer and heavy metal tolerant local rhizobial isolates. Advanced Life Science. 2023; 10: 657-662.

[21] Hussein S N, Safaie N, Shams-bakhsh M, Al-Juboory H H. Harnessing rhizobacteria: Isolation, identification, and antifungal potential against soil pathogens. Heliyon. 2024; 10: 1-17.

[22] Mahdi I, Fahsi N, Hijri M, Sobeh M. Antibiotic resistance in plant growth promoting bacteria: A comprehensive review and future perspectives to mitigate potential gene invasion risks. Frontiers Microbiology. 2022; 20: 1-22. Doi:10.3389/fmicb2022.999988.

[23] Abbas A, Barkhouse A., Hackenberger D and Wright G D. Antibiotic resistance: A key microbial survival mechanism that threatens public health. Cell Host & Microbe. 2024; 32(12): 837-851. Doi: org/10.1016/j.chom.2024.05.015.

[24] Gosh U, Kjosavik D J, Bose S. The certainty of uncertainty: climate change realities of the Indian Sundarbans. In: The Politics of Climate Change and Uncertainty in India. Eds. I. Mehta, H. N. Adam and S. Srivastava (Routledge). 2021; 107-133. Doi: 10.4324/9781003257585-5.

[25] Sati, D.; Pande, V. and Samant, M. Isolation, and characterization of indigenous rhizobacteria from wheat (*Triticum aestivum* L.) and determining their drought tolerance. Advances in Zoology and Botany. 2023; 11(1): 59-66. DOI: 10.13189/azb.2023.110106

Al-Kitab Journal for Pure Sciences (2026); 10(2):24-40.
https://doi.org/10.32441/kjps.10.2.p3

Al-Kitab Journal for Pure Sciences
ISSN: 2617-1260 (print), 2617-8141(online)

https://isnra.net/index.php/kjps

Computational Study of the Properties of the Medicinal Compound Tromantadine

Zeena R. Katoof[1], Athra G. Sager[2], Jawad Kadhim Abaies[3]

[1,2,3]Department of Chemistry, College of Science, University of Wasit, Wasit, Iraq.

Corresponding Author: asaker@uowasit.edu.iq

Citation: *Zeena R. Katoof[1], Athra G. Sager[2], Jawad Kadhim Abaies[3]*. **Computational Study of the Properties of the Medicinal Compound Tromantadine.**
Al-Kitab J. Pure Sci. [Internet]. 2025 Aug. 17 ;10(2):24-40
DOI.
https://isnra.net/index.php/kjps/article/view/2026.
https://doi.org/10.32441/kjps.10.2.p3.

Keywords: DFT, Gaussin, Herpes,Virus, Tromantadine.

Article History

Received	19 Jun.	2025
Accepted	17 Aug.	2025
Available online	01 Nov.	2026

©20--. THIS IS AN OPEN-ACCESS ARTICLE UNDER THE CC BY LICENSE
http://creativecommons.org/licenses/by/4.0/

Abstract:

Tromantadine is a medicine commonly prescribed for treating the herpes simplex virus. In this work, computational methods, including density functional theory (DFT) and molecular docking simulations, were utilized to investigate the antiviral potential activity of Tromantadine. The structural optimization and quantum chemical analysis were performed via Density Functional Theory (DFT) at the B3LYP/6-311^{++}G (d,p) level using GAUSSIAN 09, while molecular docking against Herpes Simplex Virus (HSV) proteins-DNA polymerase (PDB ID: 8OJA) and glycoprotein (PDB ID: 3SKU) was conducted using MOE 2019. Electronic descriptors, energy gap, Mulliken charges, and Fukui functions were evaluated to identify the key reactive sites of the targeted proteins. The molecular docking results revealed a favorable binding affinity of Tromantadine with both viral targets, suggesting its potential effectiveness as an inhibitor for HSV replication and entry. These findings warrant further in vitro and in vivo experimental validation.

Keywords: DFT, Gaussin, Herpes,Virus, Tromantadine.

دراسة حسابية لخصائص المركب الطبي ترومانتادين

زينه رزاق كطوف[1]، عذراء كطامي صكر[2]، جواد كاظم عبيس[3]

[1,2,3]قسم علوم الكيمياء ، كلية العلوم، جامعة واسط، واسط، العراق

الايميل الرسمي: zeenarazaq22@gmail.com , asaker@uowasit.edu.iq, jabaies@uowasit.edu.iq

الخلاصة:

يُوصف دواء الترومانتادين عادةً لعلاج فيروس الهربس البسيط. في هذا البحث، استُخدمت أساليب حسابية، بما في ذلك نظرية الكثافة الوظيفية (*DFT*) ومحاكاة الالتحام الجزيئي، لدراسة النشاط المحتمل للترومانتادين كمضاد للفيروسات. أُجري التحسين الهيكلي والتحليل الكيميائي الكمي باستخدام نظرية الكثافة الوظيفية (*DFT*) عند مستوى *B3LYP/6-311^{++}G (d,p)* باستخدام *GAUSSIAN 09*، بينما أُجرِيَ الالتحام الجزيئي ضد بروتينات فيروس الهربس البسيط (*HSV*) - بوليميراز الحمض النووي (معرف قاعدة بيانات البروتين: *OJA٨*) والبروتين السكري (معرف قاعدة بيانات البروتين: *SKU٣*) باستخدام *MOE 2019*، قُيِّمت الواصفات الإلكترونية، وفجوة طاقة، وشحنات موليكن، ووظائف فوكوي لتحديد المواقع التفاعلية الرئيسة للبروتينات المستهدفة، وأظهرت نتائج الالتحام الجزيئي تقاربًا إيجابيًا لترابط ترومانتادين مع كلا الهدفين الفيروسيين، مما يشير إلى فعاليته المحتملة كمثبط لتكاثر فيروس الهربس البسيط واختراقه، وتستدعي هذه النتائج مزيدًا من التحقق التجريبي في المختبر وفي الجسم الحي.

الكلمات المفتاحية: *DFT* , برنامج الغاوسين ، فيروس الهربس ، ترومانتادين

1. Introduction:

Antiviral medicines, Tromantadine, was utilized for therapy of herpes simplex virus. Commercially, this medicine is known as Viru-Merz and Viru-Merz Serol. Tromantadine's IUPAC name is N-(1-adamantyl)-2-[1] (dimethylamino)ethoxy]acetamide see Figure 1. Tromantadine is obtainable in a local gel, and its performance is very close to acyclovir action [2,3]. Similar to rimantadine, and amantadine, Tromantadine is an adamantine derivative. It was established that the early and late processes in the virus DNA duplication cycle are inhibited by Tromantadine[4]. This medicine targets the glycoproteins of the host cells through variations, resulting in obstruction of the virus absorption. It inhibits the penetration of the virus. As Tromantadine obstructs the uncoating of the virions, virus penetration is inhibited [5-7]. As a category of antimicrobials, antivirals are a broad range of medicines. On the basis of monoclonal antibodies, this category also comprises antibiotics, antifungals and antiviral drugs. To some extent, the majority of these antivirals drugs are regarded as safe medications, so they are prescribed for treating diversity of infections [8]. Nowadays, the computational techniques are considered dependable theoretical methods and promising

approaches in medical industries to discover new drugs with potential activities and applications [9-11].

This study aims to examine the antiviral efficacy of Tromantadine against Herpes Simplex Virus (HSV) using computational techniques, including density functional theory (DFT) analysis and molecular docking, and assess its binding affinity and identify its potential inhibitory effects.

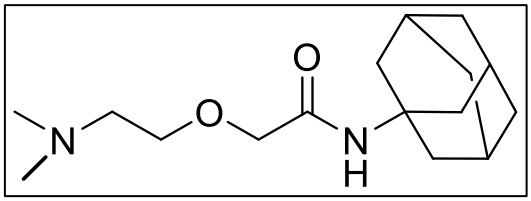


Figure 1. Structure of Tromantadine

2. Materials and Methods :

2.1 Computational methods.

The computational study was carried out using the GAUSSIAN 09W software package [12,13]. All calculations were accomplished utilizing a personal computer with an Intel Core i7 processor (HP). Density Functional Theory (DFT) calculations were performed using the B3LYP functional and the 6-311^{++}G basis set [14,15]. The antiviral medicine, Tromantadine, was chosen as the subject of the analysis. The docking simulations were performed using two protein targets: DNA polymerase (8OJA) and Glycoprotein (3SKU), which were obtained from web the Protein Data Bank.

2.2 Excretion, and toxicity (ADMET)

Several drugs failed in clinical trials and further development stages due to unpleasant pharmacological properties and other unfavourable results. In this study, Tromantadine was investigated using the Swiss ADME website. In silico toxicity testing was performed using the website ProTox-II, which is provided a projected oral toxicity, cytotoxicity, mutagenicity, carcinogenicity, hepatotoxicity, and immune toxicity values for the compound.

3. Results and Discussion:

3.1 Energy band gaps

Computational study process started with finding out the optimized molecular structure of the molecule under study (Figure 2). The optimized molecular structure of tromantadine was ascertained utilizing DFT(6-311^{++}G basis set) at a vacuum. In this step, numbering of the atoms and the molecule orientation were established. Table 1 below illustrates the definite

geometrical parameters of the medicine molecule. The length of the bond between C(17)-C(19) in the ring is 1.556 Å and it is1.427 Å for N(4)-C(11) in the side. Nevertheless, the bond length of C(6)-C(7)in the chain = 1.528 Å. Furthermore, the C(17)-C(18) bond length in the ring = 1.540 Å, and is 1.045 Å of the N(4)-H(23) out of the chain, while for O(5)-C(6) = 1.414 Å. The bond length of C(1)-O(3) in C=O and C(14)-H(38) in N-H =1.225, and 1.427. Å, respectively. which it was confirmed that the tromantadine possesses a good activity as the atom angles in its arrangement were typical.

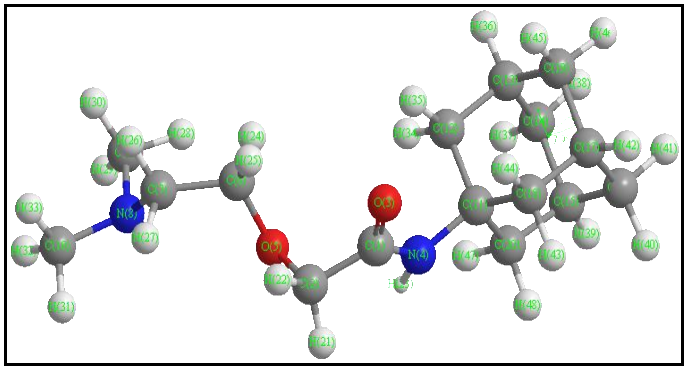


Figure 2. Tromantadine structure with symbols of Atoms

Table 1. Geometrical parameters of Tromantadine medicine

Atoms	*bond length* (Å)	*Atoms*	*Bond angles(Å)*	*Atoms*	*Dihedral(Å)*
C(20)-H(48)	1.104	H(42)-C(17)-C(19)	109.39	C(16)-C(17) C(19)-C(13)	55.576
C(20)-H(47)	1.092	H(42)-C(17)-C(18)	109.39	C(16)-C(17)-C(19)-H(45)	172.685
C(19)-H(46)	1.103	H(42)-C(17)-C(16)	109.39	C(16)-C(17)-C(19)-H(46)	-66. 053
C(19)-H(45)	1.079	C(19)-C(17)-C(18)	109.51	C(18)-C(17)-C(19)-C(13)	-65. 791
C(18)-H(44)	1.077	C(19)-C(17)-C(16)	109.51	C(18)-C(17)-C(19)-H(45)	51.318
C(18)-H(43)	1.074	C(18)-C(17)-C(16)	109.51	C(18)-C(17)-C(19)-H(46)	172.580
C(17)-H(42)	1.128	H(41)-C(16)-H(40)	109.4	H(42)-C(17)-C(19)-C(13)	172.178
C(17)-C(19)	1.558	H(41)-C(16)-C(17)	109.410	H(42)-C(17)-C(19)-H(45)	-70. 713
C(17)-C(18)	1.525	H(41)-C(16)-C(15)	109.410	H(42)-C(17)-C(19)-H(46)	50.549
C(16)-H(41)	1.097	H(40)-C(16)-C(17)	109.410	C(16)-C(17)-C(18)-C(11)	-58. 130
C(16)-H(40)	1.077	H(40)-C(16)-C(15)	109.410	C(16)-C(17)-C(18)-H(43)	64.822
C(16)-C(17)	1.563	C(17)-C(16)-C(15)	109.500	C(16)-C(17)-C(18)-H(44)	-17 6.77
C(15)-H(39)	1.129	H(39)-C(15)-C(20)	109.390	C(19)-C(17)-C(18)-C(11)	61.447
C(15)-C(20)	1.595	H(39)-C(15)-C(16)	109.390	C(19)-C(17)-C(18)-H(43)	-17 5.60
C(15)-C(16)	1.514	H(39)-C(15)-C(14)	109.390	C(19)-C(17)-C(18)-H(44)	-57. 201
C(14)-H(38)	1.146	C(20)-C(15)-C(16)	109.510	H(42)-C(17)-C(18)-C(11)	-17 7.80
C(14)-H(37)	1.154	C(20)-C(15)-C(14)	109.510	H(42)-C(17)-C(18)-H(43)	-54.8
C(14)-C(15)	1.552	C(16)-C(15)-C(14)	109.510	H(42)-C(17)-C(18)-H(44)	63.545

C(13)-H(36)	1.123	H(46)-C(19)-H(45)	109.400	C(15)-C(16)-C(17)-C(18)	62.329
C(13)-C(19)	1.498	H(46)-C(19)-C(17)	109.410	C(15)-C(16)-C(17)-C(19)	-5 6.38
C(13)-C(14)	1.538	H(46)-C(19)-C(13)	109.410	C(15)-C(16)-C(17)-H(42)	-17 4.98
C(12)-H(35)	1.121	H(45)-C(19)-C(17)	109.410	H(40)-C(16)-C(17)-C(18)	-54. 780
C(12)-H(34)	1.120	H(45)-C(19)-C(13)	109.410	H(40)-C(16)-C(17)-C(19)	-17 3.49
C(12)-C(13)	1.531	C(17)-C(19)-C(13)	109.500	H(40)-C(16)-C(17)-H(42)	67.91
C(11)-C(20)	1.576	H(38)-C(14)-H(37)	109.400	H(41)-C(16)-C(17)-C(18)	-17 5.92
C(11)-C(18)	1.616	H(38)-C(14)-C(15)	109.410	H(41)-C(16)-C(17)-C(19)	65.356
C(11)-C(12)	1.613	H(38)-C(14)-C(13)	109.410	H(41)-C(16)-C(17)-H(42)	-53. 235
C(10)-H(33)	1.080	H(37)-C(14)-C(15)	109.410	C(14)-C(15)-C(20)-C(11)	-59. 743
C(10)-H(32)	1.097	H(37)-C(14)-C(13)	109.410	C(14)-C(15)-C(20)-H(47)	65.338
C(10)-H(31)	1.098	C(15)-C(14) C(13)	109.500	C(14)-C(15)-C(20)-H(48)	-17 9.57
C(9)-H(30)	1.069	H(36)-C(13) -C(19)	109.390	C(16)-C(15)-C(20)-C(11)	59.882
C(9)-H(29)	1.079	H(36)-C(13)-C(14)	109.390	C(16)-C(15)-C(20)-H(47)	-17 5.03
C(9)-H(28)	1.068	H(36)-C(13)-C(12)	109.390	C(16)-C(15)-C(20)-H(48)	-59. 949
N(8)-C(10)	1.467	C(19)-C(13)-C(14)	109.510	H(39)-C(15)-C(20)-C(11)	-17 8.18
N(8)-C(9)	1.502	C(19)-C(13)-C(12)	109.510	H(39)-C(15)-C(20)-H(47)	-53. 103
C(7)-H(27)	1.063	C(14)-C(13)-C(12)	109.510	H(39)-C(15)-C(20)-H(48)	61.985
C(7)-H(26)	1.114	H(48)-C(20)-H(47)	109.400	C(14)-C(15)-C(16)-C(17)	60.658
C(7)-N(8)	1.514	H(48)-C(20)-C(15)	109.410	C(14)-C(15)-C(16)-H(40)	-17 9.70
C(6)-H(25)	1.145	H(48)-C(20)-C(11)	109.410	C(14)-C(15)-C(16)-H(41)	-57. 806
C(6)-H(24)	1.081	H(47)-C(20)-C(15)	109.410	C(20)-C(15)-C(16)-C(17)	-60. 289
C(6)-C(7)	1.527	H(47)-C(20)-C(11)	109.410	C(20)-C(15)-C(16)-H(40)	59. 350
O(5)-C(6)	1.427	C(15)-C(20)-C(11)	109.500	C(20)-C(15)-C(16)-H(41)	-17 8.75
N(4)-H(23)	1.007	H(44)-C(18)-H(43)	109.400	H(39)-C(15)-C(16)-C(17)	179.886

3.2 Study of Mulliken charge and correlation with quantum chemical distribution of Tromantadine

To decide the major reactive spots in the arrangement and to differentiate between types of reactions, Frontier Molecular Orbitals (FMOs) have been employed. The energy of the lowest unoccupied molecular orbital (LUMO) and the highest occupied molecular orbital (HOMO), and their energy difference (ΔE) were utilized to evaluate the molecule reactivity. For Tromantadine medicine, the level B3LYP/6-31^{++}G (d, p) was utilized to calculate HOMO and LOMO energies as shown in Figure 3. The minimal electronic energy that required for the electron transition n–π* is represented by the (HOMO – LUMO) energy difference gab. The HOMO energy average at 77th was calculated at -0.23179 eV and LOMO slightest energy at

78th was calculated at -0.01571 eV for the molecule under test, Tromantadine. Upon the optimization of the current molecule arrangement, the (HOMO – LUMO) energy band gab was calculated from MOs and found = 2.0324638 eV. Although this value indicates that the energy band gap of Tromantadine is high, the stability of its structure is significant. Parameters for Tromantadine, including chemical hardness, electronegativity, electronic chemical potential, and electro-philicity index were measured utilizing DFT and the results were listed in Table 2. The following are parameters for Tromantadine molecule [16-18]:

- The HOMO energy (EHOMO).
- The LUMO energy (ELUMO).
- The energy gap between EHOMO and ELUMO (ΔE=HOMO-LUMO) .
- Electronegativity(χ).
- Dipole moment (μ).
- Electron affinity(A).
- Ionization energy (IP).
- Softness(s),global hardness(η).
- Global electrophilicity (ω).

Based on molecular gas-phase of Tromantadine molecule, the distribution of density for LUMO and HOMO is displayed in Figure 3. In the medicine structure, the highes electronic density is specified by the red color area, which represented by C6, C7, and N8 atoms, wherese, the lesser electron density is specified by the green color site. Due to the double bond and aromatic ring moities of the inhibitor structure, it possesses a significant electronic density. It can be noticed that, the greatest electronic density focused over atom N8 atom in $N(CH_3)_2$ segment of Tromantadine structure.

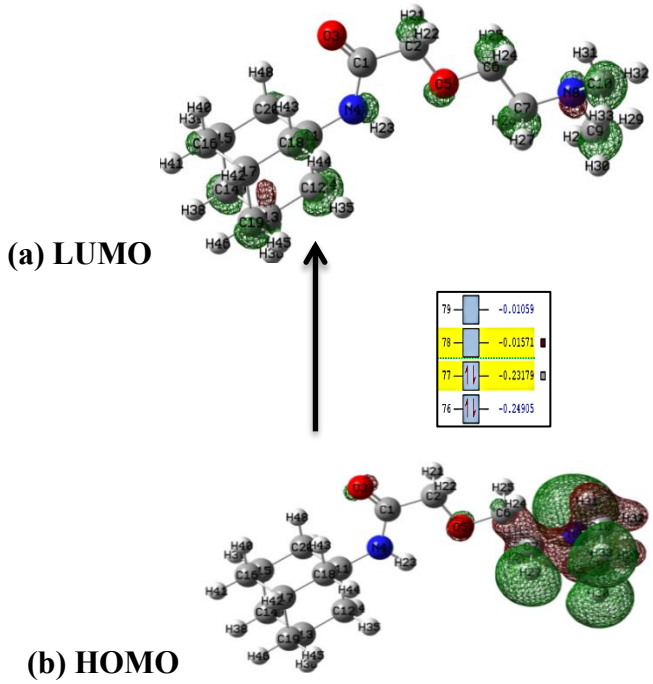


Figure 3. Frontier surfaces for Tromantadine(a)LUMO and (b) HOMO

Fukui functions calculation determine the active atoms in the molecule. This calculation is related to the electronic density variations. To calculate of Fukui functions, Equations (1,2 and 3) f+(r) , f-(r) and f0(r) were employed [19-21]:

$$f^{+} = [q(N+1) - q(N)] \quad \ldots \quad (1) \text{ nucleophilic species}$$

$$f^{-} = [q(N) - q(N-1)] \quad \ldots \quad (2) \text{ electrophilic species}$$

$$f^{0} = [q(N+1) - q(N-1)]/2 \quad \ldots \quad (3) \text{ free radicals species}$$

Where: the charge located on atoms in neutral classes is represented by q(N), the atomic positive charges in cationic species are implied by q(N+1), and the atomic anionic charges are signified by q (N-1) [22]. Table. 3 illustrates the descriptor values that were calculated by Mulliken charges over the atom of the molecule structure. As shown in Figure 3, the distribution of the charges on the atom was evaluated via Mulliken equation. The calculated Fukui functions provide additional information about the molecule reactive sites. Carbon atoms (9C and 10C) have the highest dual reactivity for both nucleophilic (f^{+1} = 0.173, 0.174) and electrophilic (f^{-1} = 0.236, 0.159) attacks, making them the most chemically active centres. Remarkably, Carbon atom (13C) showed an exceptionally high electrophilic reactivity (f^{-} = 1.569), indicating a potential site for strong electron donation. Conversely, other atoms such as 5O and 6C showed minimal or even negative Fukui values, suggesting low or negligible participation in chemical reactions. The carbon atom (13C) exhibited a high electrophilic reactivity (f^{1}=1.569), suggesting a potential site for strong electron donation. In contrast,

atoms such as 5O and 6C had minimum or even negative Fukui values, indicating a little or no participation in the chemical reactions. Furthermore, the carbon atoms (13C and C17) showed an exceptionally high free radical reactivity (f^0=0.778876,0.374119). The atoms (8N and 9C) have the greatest exposure to electrophilic species reactions. These calculations were performed to investigate the electronic structure of Tromantadine and assess its bioactivity.

The Mulliken charge analysis revealed a significant variations in electronic distribution throughout the molecule, which denotes concentrated areas with high electron density. Thus, these sites are expected to serve as nucleophilic centres, enabling of generating hydrogen bonds and coordinating interactions with electrophilic sites on viral proteins. Conversely, electron-deficient regions are more likely to interact with electron-rich (nucleophilic) groups found in viral components such as glycoproteins and nucleic acids. This intramolecular polarity distribution identifies possible active areas through which Teromatin can interact with viral targets. The HOMO energy was computed at -6.307 eV and the LUMO energy at -4.275 eV, yielding an energy gap(ΔE)of 2.03 eV (Table 2). This moderate band gap indicates an appropriate chemical reactivity for biological interactions. The chemical hardness (η = 2.94eV) and electronegativity (χ =3.37eV) values show the molecule resistance to charge deformation and its ability to attract electrons. The softness (S=0.34eV) indicates the flexibility of the electron cloud. Tromantadine has a high electrophilicity index (ω=1.93 eV), indicating its ability to accept electrons and interact with electron-rich active sites in the virus. The dipole moment (3.67 Debye) emphasises the molecule polarity, increasing its water solubility and enabling contact with polar viral surfaces. Collectively, these electronic and structural properties demonstrate that Tromantadine is well-suited to interact with HSVtargets via hydrogen bonding and electrostatic interactions with viral proteins or genetic material. Cosequenyely, it potentially inhibiting the viral replication cycle Figure 4.

Table 2. Quantum chemical parameters for Tromantadine in vacuum medium

Parameter	Value	Parameter	Value
EHOMO (a.u)	-6.307469 (eV)	ELUMO (a.u)	-4.2750052 (eV)
IE= -EHOMO	6.037469(eV)	ΔE =HOMO - LOMO	-2.0324638(eV)
EA= -ELUMO	4.2750052(eV)	S =[1/2η]	0.340134(eV)
CP	-3.36749(eV)	$\omega = \left(\frac{\mu 2}{2\eta}\right)$	1.928574(eV)
Nmax	1.14540 (eV)	X =[(IP+EA)/2]	3.367485(eV)
So	0.17006 (eV)	Ŋ=[ELOMO-EHOMO]/2	2.939984(eV)
(μ)	3.66722*(Debye)*	EA	0.427501(eV)

Table 3. Mulliken atomic charges distribution.

Atoms	*n*	*n+1*	*n-1*	f^{+1}	f^{-1}	f^{0}
1C	0.38	0.415501	0.287376	0.035501	0.092624	0.064063
2C	0.014871	0.094837	-0.05378	0.079966	0.068653	0.07431
3O	-0.38577	-0.24308	-0.40192	**0.142695**	0.016153	0.079424
4N	0.670015	0.739273	1.022085	0.069258	-0.35207	-0.14141
5O	-0.30051	-0.30028	-0.2966	0.000231	-0.00391	-0.00184
6C	0.052123	0.049837	0.216372	-0.00229	-0.16425	-0.08327
7C	-0.10067	0.0401	0.007068	0.14077	-0.10774	0.016516
8N	0.001455	0.024892	-0.17317	0.023437	**0.174623**	0.09903
9C	0.149082	0.321834	-0.08691	**0.172752**	**0.235991**	0.204372
10C	0.078181	0.251909	-0.08039	**0.173728**	0.158571	0.16615
11C	-1.84057	-2.10509	-1.39697	-0.26452	-0.4436	-0.35406
12C	-0.14539	-0.06631	-0.11369	0.079079	-0.0317	0.023688
13C	0.476269	0.464657	-1.09309	-0.01161	**1.569363**	**0.778876**
14C	-0.32702	-0.26338	0.343588	0.063645	-0.67061	-0.30348
15C	0.4619	0.432179	-0.24903	-0.02972	0.710933	0.340606
16C	-0.21634	-0.1473	0.259176	0.069044	-0.47552	-0.20324
17C	0.453838	0.420594	-0.32764	-0.03324	0.781481	**0.374119**
18C	0.461948	0.580397	0.425512	0.118449	0.036436	0.077443
19C	-0.32661	-0.26387	0.337688	0.062742	-0.6643	-0.30078
20C	0.440801	0.553289	0.374338	0.112488	0.066463	0.089476

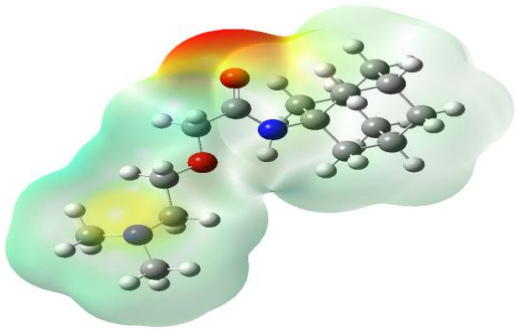


Figure 4. Electrostatic Potential Map

3.3 Molucular docking analysis

Herpes simplex virus (HSV-1), a double-stranded DNA virus, replicates with seven essential proteins encoded in its genome. Among these protiens, the UL30 DNA polymerase, in conjunction with the UL42 processivity factor, coordinates leading and lagging strand replication of the 152 kb viral genome 23]. Docking of Tromantidine (T) was performed to investigate the compound stabilising interactions within the protein pockets of the chosen

target. This research was carried out utilising MOE-2019 software. DNA polymerase (PDBID:8OJA(A)) and Glycoprotein (PDBID:3SKU(D)) were downloaded from an internet data bank server at https://www.rcsb.org/pdb and stored in Pdb format [24]. Tromantadine three-dimensional structure was created using the Gaussian 09W software. This was done by standard protocols for ligand and protein preparation, which include energy minimization and the active site identification (see Table 4). The docking results demonstrated a favourable interaction between Tromantadine and the target Glycoprotein (see Table 5 and Figure 5) . While they did not show any interaction between Tromantadines and the DNA polymerase. In the case of 3SKU, Tromantadine exhibited a modrate binding affinity, forming one key hydrogen bond (H-acceptor) within the active site pocket, particularly with the residue LYS190(A). The binding energy was estimated to be (-4.741 kcal/mol), indicating a stable complex formation(see Figure 5 . Similarly, the docking of Acyclovi (conterol) with DNA polymerase (8OJA) revealed notable interactions through hydrogen bonding. Thymotadine was observed to engage with crucial surface residues, possibly interfering with the virus-host cell attachment mechanism. The calculated binding energy for this complex was (-5.248 kcal/mol). These results suggest that Tromantadine could potentially inhibit HSV replication through once targeting mechanism through preventing viral entry through glycoprotein interference. While the acyclovir results suggest that acyclovir could potentially inhibit HSV replication through dual targeting mechanisms. Firstly, obstructing DNA synthesis via polymerase inhibition, and secondly by preventing viral entry through glycoprotein interference(see Table 5 and Figure 5). The docking outcomes provide a theoretical basis for further in vitro and in vivo antiviral evaluations of Tromantadine as a favourable therapeutic candidate against HSV infection.

Table 4. Binding site residues as input for receptor grid generation throughout docking

Receptor	PLB	Hyd	Side	Residues
8OJA	2.95	24	41	1:(HIS148 VAL311 PHE313 GLY314 TRP315 ILE352 GLY355 MET356 SER357 ASP358 LEU359 HIS595 LEU596 SER59ALA600 ARG603 LEU802 LYS805 GLN806)
3SKU	5.00	56	90	1:(ASP368 ILE369 GLU370 CYS371 LYS372 ALA373 GLU378 LEU379 ALA380 PRO382 GLU426 TYR465 ASN466 PHE470 ASP471 LYS539 LEU540 ASN541 LYS552 LYS553 ASP554 LEU555 SER556 TYR557 ARG558 ILE560 PRO561 ILE574 GLU576 TYR577 CYS578 GLN580 ASP581

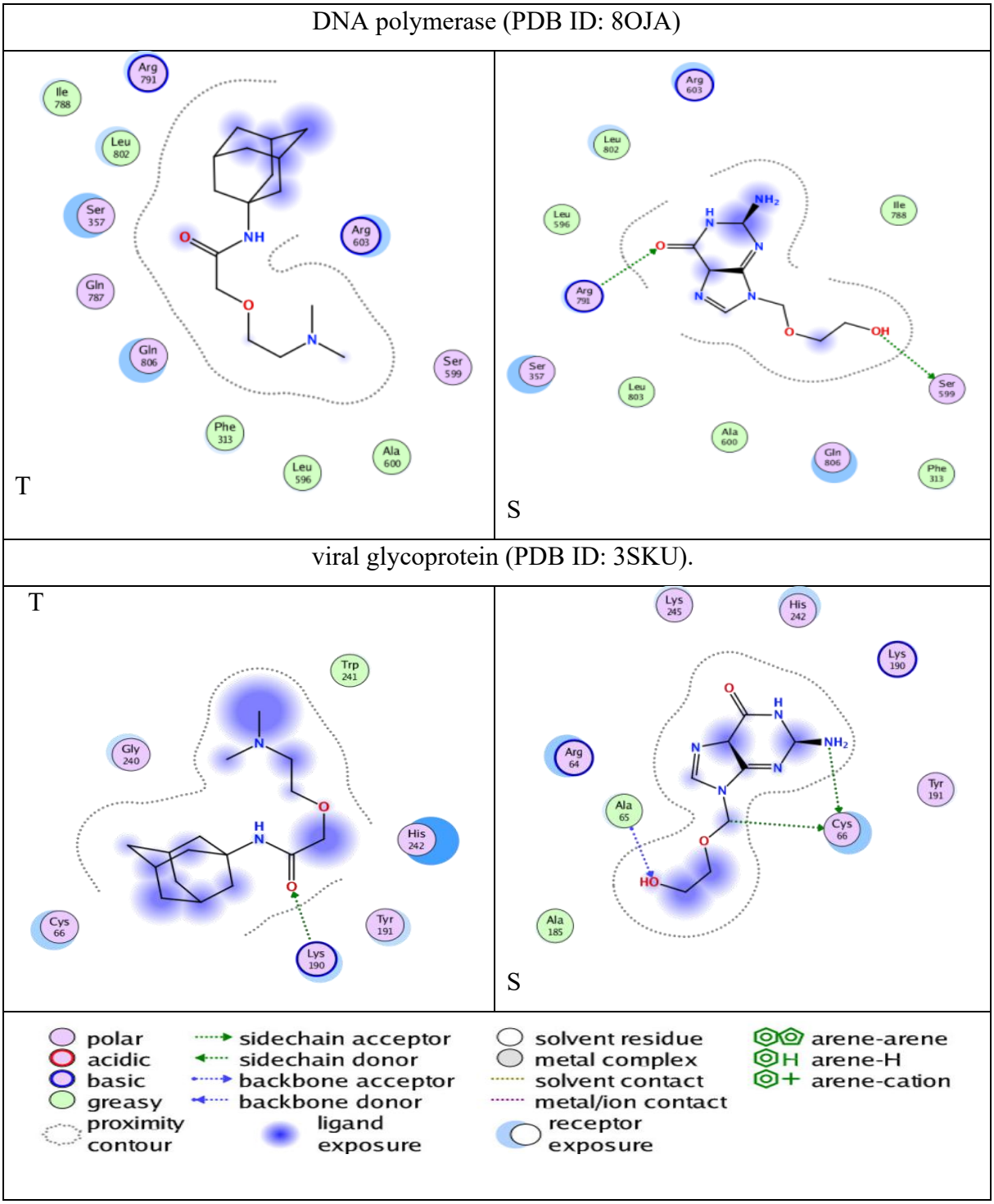


Figure 5. 2D Binding site interaction of Tromantadine (T) and Acyclovi (S) a with DNA polymerase (PDB ID: 8OJA) and the viral glycoprotein (PDB ID: 3SKU).

Table 5 . Docking findings of compounds (Tromantadine and Acyclovi)with(8OJA &3SKU) in site (1)

Code Drug	Receptor	S-score (kcal/ mol)	RMSD (Å)	Bonding between atoms of compounds and residues of the active site 1 in 3OG7					
				Atom of compound	Atom of receptor	Involved receptor residues	Interaction bond	Distance (Å)	E(Kcal /mol)
T	8OJA	-5.6217	2.358	-	-	-	-	-	-
Acy	8OJA	-5.248	1.501	O 16 O8	OG NH2	SER599(A) AGR791(A)	H-donor H-acceptor	3.03 3.4	-0.5 -0.8
T	3SKU	-4.741	2.158	O12	NZ	LYS190(A)	H-acceptor	2.59	-0.9
Acy	3SKU	-4.491	1.750	N7 C 12 O 16	SG SG N	CYS 66 (A) CYS 66 (A) ALA 65 (A)	H-donor H-donor H-acceptor	3.55 3.62 3.23	-0.5 -0.5 -1.4

3.4 Study analysis of ADMET and toxicity Properties.

Table 6 shows Tromantadine under study has the molecular formula of $C_{16}H_{28}N_2O_2$ with a molecular mass of 280.41 g/mol. Tromantadine displays favorable drug-like characteristics as outlined by sundry key parameters obtained via web SwissADME.

The physicochemical properties display the molecular weight within the drug-likeness scale(<500). While The topological polar surface area (TPSA) of Tromantadine was 41.57 Å², indicating a good potential for membrane permeability**.** The value (Log P) was within a range =2, suggesting a moderate lipophilicity, which is beneficial for oral absorption. The number of rotatable bonds was seven, indicating a moderate molecular flexibility**.**

Tromantadine is soluble in aqueous solution, so it is appropriate for oral preparations. GI absorption was high, indicating a good absorption in the gastrointestinal system. while the blood-brain barrier (BBB) demonstrates a permeant ability to cross the BBB, which is useful in medications that target the CNS. Table 6 shows there is no inhibition to CYP1A2, CYP2C19, CYP2C9, CYP2D6, CYP3A4 which suggests low potential for drug-drug interactions involving these metabolic enzymes**.** The drug-likeness and medicinal chemistry results indicated a good oral bioavailability, moderate probability of oral bioavailability, and moderate ease of synthesis (from 1(easy)to 10 (difficult**)**. These findings indicate that tromantadine has a promising oral bioavailability, drug-likeness, and low toxicity potential, as well as strong gastrointestinal absorption and BBB permeability. It is not expected to inhibit key CYP450 enzymes, reducing the possibility of metabolic interactions. Its moderate water

solubility and acceptable physicochemical qualities make it a promising option for further development as an orally active medicinal drug, particularly for CNS indications due to BBB permeability (see Figure 6).

Table 6 . Predicted absorption and distribution parameters of Tromantadine

Physicochemical Properties							
Formula	**Mwt (g/mol)**	**TPAS Å²**	**HBA**	**HBD**	**Rotatable Bonds**	**Fraction Csp³**	**Mola Refractivity**
$C_{16}H_{28}N_2O_2$	280.4	41.57	3	1	7	0.25	79.70
Lipophilicity		**Water Solubility**					
Log Po/w =2.02		Log $S_{(ESOL)}$= -2.46	Soluble	Solubility9.62e-01 mg/ml		Soluble	Log $S_{(SILICOS-IT)}$ -3.01
Pharmacokinetics							
GI absorption	BBB	P-gp	CYP1A2	CYP2C19	CYP2C9	CYP2D6	Log Kp
Yes	Yes	No	No	No	No	No	-6.49 cm/s
Druglikeness						Medicinal Chemistry	
Lipinski	Ghose	Veber	Egan	Muegge	Bioavailability Score	Synthetic accessibility	
Yes	Yes	Yes	Yes	Yes	0.55	4.48	

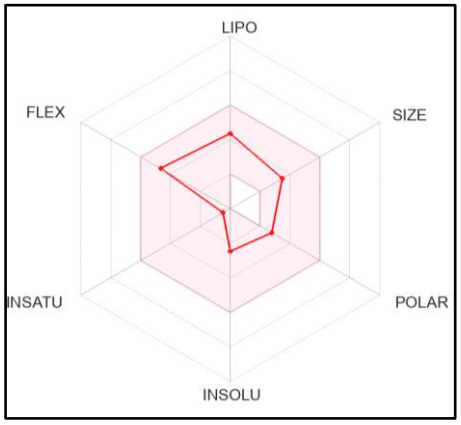


Figure 6. A spider shape of Tromantadine.

The toxicity of Tromantadine was determined using ProTox-II (website). It was expected to be non-toxic based on organ toxicity (hepatotoxicity). The toxicity-endpoint results indicated that the compound was expected to be non-mutagenic, non-cytotoxic, and non-carcinogenic. The toxicity class for the chemical was (4). Notes: Class I: lethal if eaten (LD50 ≤ 5); Class II: fatal if swallowed (5<LD50≤50). Class III is hazardous if swallowed (50< LD50≤ 300). Class IV: hazardous if swallowed (300<LD50<2000). Class V may be dangerous if eaten (LD50 <

2000), but Class VI is non-toxic (LD50>5000)[25]. The projected LD50 value suggests that the chemical is hazardous if eaten and falls into class IV (see Table 7).

Table 7. Insilco toxicity evaluation of Tromantadine.

Organ Toxicity	Toxicity - endpoints				Predicted LD50(mg/kg)	Predicted Toxicity
Hepatotoxicity	**Carcinogenicity**	**Immunotoxicity**	**Mutagenicity**	**cytotoxicity**	800	4
Inactive	inactive	inactive	Inactive	Inactive		

4. Conclusions

In this study, activity of the medicinal compound, Tromantadine, was evaluated utilizing DFT methods at B3LYP/6-31^{++}G basis. The comprehensive DFT and Fukui functions analysis of Tromantadine revealed distinct electronic features that underpin its potential biological activity. The identification of nucleophilic and electrophilic centers within the molecule, alongside a moderate HOMO-LUMO gap, indicating a balanced chemical reactivity favorable for interaction with viral targets. The calculated quantum chemical descriptors, including chemical hardness, electronegativity, softness, and electrophilicity, collectively suggest that Tromantadine possesses an electronic flexibility and polarity necessary for effective binding and interfering with viral proteins and genetic material.

These insights support the hypothesis that Teromatin could serve as a promising candidate for antiviral applications against herpes simplex virus by disrupting critical molecular interactions within the viral replication cycle. Molecular docking studies of herpes virus proteins DNA polymerase(8OJA) andGlycoprotein (3SKU) have demonstrated a complete mechanism of action, thereby confirming computational predictions of the molecule. We strongly support the need for experimental validation through laboratory-based assays based on these data.

5. Acknowledgments

The authors are thankful for the College of Science, University of Wasit for the help in doing this study.

6. Conflict of Interest

The author declares no conflict of interest. The author declares no conflict of interest.

7. References

[1] Ostheimer KE, Busch T, Görtelmeyer R, Hahn KD. Randomized double-blind trial of tromantadine versus aciclovir in recurrent herpes orofacialis. Arzneimittel-Forschung. September. 1989;39 (9):1152–1155. https://api.semanticscholar.org/CorpusID:26354703.

[2] Diezel W, Michel G, Görtelmeyer R, Ostheimer KE. Efficacy of tromantadine and aciclovir in the topical treatment of recurrent herpes orofacialis. Comparison in a clinical trial. Arzneimittel-Forschung.1993;43(4):491–496. PMID: 8494582.

[3] Rosenthal KS, Sokol MS, Ingram R L, Subramanian R, Fort RC. Tromantadine: inhibitor of early and late events in herpes simplex virus replication. Antimicrobial Agents and Chemotherapy.,December.1982;22(6):1031–1036. https://dx.doi.org/10.1128/aac.22.6.1031.

[4] Sager AG, Abaies, JK, Katoof ZR. Design, Molecular Docking, ADMET Studies, Synthesis, Characterization, and Antimicrobial of Nicotinamide Derivatives via Mannich reaction. Iraqi Journal of Science. 2025;66(3):1-17. https://dx.doi.org/10.24996/ijs.2025.66.3.2.

[5] Sager AG, Salah AS, Mekky AH. Microwave Synthesis, Characterization of Some Novel Curcumin Compound and its Metal Complexes with Antimicrobial, Antioxidant Studies. International Journal of Medical Research and Pharmaceutical. 2020;12(1):429-448.https:// doi.org/10.31838/ijpr/2020.12.01.200.

[6] Zhu XY, Li QX, Kong Y. A novel human single-domain antibody-drug conjugate targeting CEACAM5 exhibits potent in vitro and in vivo antitumor activity. Acta Pharmacologica Sinica - Natu 2024; 45(3):609-618. https://10.1038/s41401-023-01200-9.

[7] Rossmann MG. The structure of antiviral agents that inhibit uncoating when complexed with viral capsids. Antiviral Research.1989;1(1):3-13. https://10.1016/0166-3542(89)90016-8.

[8] Sundareswaran T, Jagan R, Karthikeya N, Boaz BM. Rational analysis of hydrogen bonding interaction in phenazine, 2-hydroxynaphthalene (1:1) cocrystal: from molecular modeling to photophysical properties. Ournal of Molecular Modeling. 2024;30(10): 351. https://doi.org/10.1007/s00894-024-06128-3.

[9] Bakker MJ, Mládek A, Semrád H, Zapleta V, Pavlíková Přecechtělová J. Improving IDP theoretical chemical shift accuracy and efficiency through a combined

MD/ADMA/DFT and machine learning approach. Physical Chemistry Chemical Physics. 2022;24(45):27678-27692. https://doi.org/10.1002/ardp.202400423.

[10] Prajapati P, Pandey J, Tandon P, Sinha K, Shimpi MR. Molecular structural, hydrogen bonding interactions, and chemical reactivity studies of ezetimibe-L-proline cocrystal using spectroscopic and quantum chemical approach. Frontiers in Chemistry. 2022;10:848014. https://doi.org/10.3389/fchem.2022.848014.

[11] Zayed EM, Zayed MA, Abd El Salam HA, Noamaan MA. Novel triazole thiole ligand and some of its metal chelates: synthesis, structure charactertization, thermal behavior in comparison with computational caculations and biological activities. Computational Biology and Chemistry. 2019;78:260-272. https://doi.org/10.1016/j.compbiolchem.2018.12.008.

[12] Arulaabaranam K, Muthu S, Mani G, Ben Geoffrey AS. Speculative assessment,molecular composition, PDOS, topology exploration (ELF, LOL, RDG), ligand-protein interactions, on 5-bromo-3-nitropyridine-2-carbonitrile. Heliyon. 2021; 7(5): 07061. https://doi.10.1016/j.heliyon.2021.e07061.

[13] Pinzi L, Rastelli G. Molecular docking: shifting paradigms in drug discovery. International Journal of Molecular Sciences. 2019;20(18):4331. https://doi.10.3390/ijms20184331.

[14] Morales-Bayuelo A, Sánchez-Márquez J. Receptor-based pharmacophore modelling of a series of ligands used as inhibitors of the SARS-CoV-2 virus by complementary theoretical approaches, molecular docking, an reactivity descriptors. F1000Researchs. 2023;12:749. https://doi.10.12688/f1000research.133426.1.

[15] Razooqi MS, Al-Ani HN.Quantum me chanical calculations and electrochemical study of vibrational frequencies, energies in some flavonoids molecules. Iraqi Journal Sceince. 2022;63(6):2331-2344. https://doi.10.24996/ijs.2022.63.6.2

[16] Obayes H R, Al-Amiery AA, Alwan HG, Abdullah TA, Kadhum AAH, Mohamad AB. Sulphonamides as corrosion inhibitor: experimental and DFT studies. Journal Molecular. Structure . 2017;1138:27–34. https://doi.org/10.1016/j.molstruc.2017.02.100.

[17] Stephens PJ, Devlin F, Chabalowski C, Frisch MJ. An initio calculation of vibrational absorption and circular dichroism spectra using density functional force

fields. Journal. Physical Chemical B .1994;98:11623– 11627. https://doi.org/10.1021/j100096a001.

[18] Aquino AAJ , Borges I, Nieman, R., Köhn A, Lischka H. Intermolecular interactions and charge transfer transitions in aromatic hydrocarbon-tetracyanoethylene complexes.Journals Physical Chemistry Chemical Physics. 2021;16:20586-20597.https://doi.org/10.1039/C4CP02900.

[19] Echegaray E, Cárdenas C, Rabi S, Rabi N, Lee S, Zadeh FH. In pursuit of negative fukui functions: examples where the highest occupied molecular orbital fails to dominate the chemical reactivity. Journal of Molecular Graphics and Modelling. 2019;19: 2779–2783. https://doi.10.1007/s00894-012-1637-3.

[20] Balachandar S, Dhandapani M. Biological action of molecular adduct pyrazole: trichloroacetic acid on Candida albicans and ct DNA - a combined experimental, Fukui functions calculation and molecular docking analysis. Journal of Molecular Structure. 2019; 1184:129-138. https://doi.org/10.1016/j.molstruc.2019.02.006.

[21] Parr RG, Yang W. Density functional approach to the frontier-electron theory of chemical Reactivity. Journal of the American Chemical Society. 1989;106:4049-4050. https://doi.org/10.1021/ja00326a036.

[22] Gazquez JL, Mendez F. The hard and soft acids and bases principle: an atoms in molecules Viewpoint. Journal of Physical Chemistry. 1994;984:591-4593. https://doi.org/10.1021/j100068a018.

[23] Mulliken R S. Electronic population analysis on LCAO-MO molecular wave functions.Journal of Chemical Physics. 1955;23:1833-1840. https://doi.org/10.1063/1.1740588.

[24] Laplaza R, Peccati, F, Boto RA, Quan C, Carbone A, Piquemal J-P. NCIPLOT and the analysis of noncovalent interactions using the reduced density gradient. Wiley Interdisciplinary Reviews:Computational Molecular Scienc. 2021;11(2):1-37. https://doi.org/10.1002/wcms.1497

[25] Sager A, Abbood A F, Abaies J K, Khazal F A. A design, molecular docking, ADMET studies, synthesis, characterization, and Invitro pharmacological evaluation of tetrazole derivatives. Iraqi Journal of Pharmaceutical Sciences.2025;34:10-25. https://doi.org/10.31351/vol34iss1pp10-25.

Al-Kitab Journal for Pure Sciences (2026); 10(2):41-51.
https://doi.org/10.32441/kjps.10.2.p4

Al-Kitab Journal for Pure Sciences
ISSN: 2617-1260 (print), 2617-8141(online)

https://isnra.net/index.php/kjps

A Brief Review of the Role of Microalgae Communities in Reducing Climate Change

Ebtehal Mussa Jaffer[1], Najlaa Hashem Adlan[2]

[1,2]Department of Ecology, College of Science, University of Basrah, Iraq

Corresponding Author: ebtehal.jaffer@uobasrah.edu.iq, najla.adlane@uobasrah.edu.iq

Citation: *Ebtehal Mussa Jaffer[1], Najlaa Hashem Adlan[2]*. **A Brief review of the role of microalgal communities in reduce climate change**.
Al-Kitab J. Pure Sci. [Internet]. 2025 Aug. 28 ;10(2):41-51
DOI.
https://isnra.net/index.php/kjps/article/view/2026.
https://doi.org/10.32441/kjps.10.2.p4.

Keywords: Algal biomass, Climate Change, CO2 Emissions, greenhouse gas.

Article History

Received	24 Jun.	2025
Accepted	28 Aug.	2025
Available online	01 Nov.	2026

©20--. THIS IS AN OPEN-ACCESS ARTICLE UNDER THE CC BY LICENSE
http://creativecommons.org/licenses/by/4.0/

Abstract

Over the past few decades, there has been a global focus on the threat posed by pollution and climate change brought on by diverse human activities. Although carbon capture and storage (CCS) techniques were originally seen to be a potential technological solution to lessen this concerning situation, they are now regarded as economically Stressful, and it is yet unknown how they would affect the environment in the long run. An alternative method for recycling the surplus CO_2 (produced by power stations, cars, volcanic explosions, and the breakdown of organic matter) is the biological capture of CO_2 using microalgae. Algae offer a promising method for sequestration carbon as global CO_2 emissions rise. They effectively collect CO_2 from the atmosphere through photosynthesis, turning it into biomass at rates that are noticeably higher than those of ordinary plant systems. Microalgae are considered as a feasible substitute for reducing climate change due to this natural process. This essay examines the ecological significance of algae in absorbing CO_2 and converting CO_2 into biomass by microalgae, like *Chlorella* sp. and its conversion into bioenergy goods, such as biohydrogen.

key words: Algal biomass, Climate Change, CO2 Emissions, greenhouse gas.

مراجعة مختصرة لدور مجتمع الطحالب في تقليل التغييرات المناخية

ابتهال موسى جعفر[1], نجلاء هاشم عدلان[2]

[1,2]قسم علوم البيئة، كلية العلوم، جامعة البصرة- العراق

الايميل الرسمي: ebtehal.jaffer@uobasrah.edu.iq, najla.adlane@uobasrah.edu.iq

الخلاصة:

على مدى العقود الماضية، كان هناك تركيز عالمي على التهديد الذي يشكله التلوث وتغير المناخ الناجم عن الأنشطة البشرية المتنوعة، وعلى الرغم من أن تقنيات احتجاز الكربون وتخزينه (CCS) كانت تُعدُّ في الأصل حلاً تكنولوجيًا محتملاً للحدّ من هذا الوضع المقلق، إلا أنها فضلا عن ذلك تُعدُّ الآن عبئًا اقتصاديًا، ولا يزال مجهولا تاثيره على البيئة على المدى الطويل. تتمثل إحدى الطرق البديلة لإعادة تدوير فائض ثاني أكسيد الكربون الناتج عن محطات الطاقة والسيارات والانفجارات البركانية وتحلل المواد العضوية في الاحتجاز البيولوجي لثاني أكسيد الكربون باستخدام الطحالب الدقيقة. توفر الطحالب طريقة واعدة لعزل الكربون مع ارتفاع انبعاثات ثاني أكسيد الكربون العالمية. فهي تجمع ثاني أكسيد الكربون بفعالية من الغلاف الجوي من خلال عملية التمثيل الضوئي، وتحوله إلى كتلة حيوية بمعدلات أعلى بشكل ملحوظ من فعالية النباتات التقليدية. وتعدُّ الطحالب الدقيقة بديلاً عمليًا للحد من تغير المناخ بفضل هذه العملية الطبيعية. تبحث هذه المقالة في الأهمية البيئية للطحالب في امتصاص ثاني أكسيد الكربون وتحويله إلى كتلة حيوية بواسطة الطحالب الدقيقة، مثل *Chlorella* sp. وتحويلها إلى طاقة حيوية، مثل الهيدروجين الحيوي.

الكلمات المفتاحية: الكتلة الطحلبية، التغييرات المناخية ، انبعاثات CO_2، الغازات الدفيئة.

1. Introduction:

NASA defines climate change as the ongoing alteration of the earth's climate brought on by human activities (industrialization, the burning of, deforestation, fossil fuels etc.), which produce greenhouse gases (GHGs) and ultimately lead to global warming. The rise in greenhouse gases, primarily CO2 (418 ppm at the moment), is blamed for climate change. This trend is increasing and contributes to an increase in our planet's surface temperature of roughly 33.81°F [1]. In addition, this phenomenon causes the oceans to warm by more than 0.4°F since the early 1970s, Antarctica's ice mass to rapidly diminish (by roughly 147 gigatons annually), the sea level to rise (by 3.4 mm annually), and ultimately, various natural disasters such as drought, heavy precipitation, or ocean acidification [2]. There are global efforts made to reduce the negative consequences of climate change and lower greenhouse gas emissions like CO_2. Certain microorganisms, like microalgae and photosynthetic bacteria, have the ability to absorb CO_2 and use it as a

source of carbon for growth. Microalgae are excellent options for lowering atmospheric CO_2 in cities due to their exceptional CO_2 bio-capture or CO_2 capacity [3].

Many people agree that one of the important concerns confronting the world today is climate change, which has broad implications like increasing sea levels, biodiversity loss, increased atmospheric GHG concentrations, and longer heat waves that occur more frequently [4,5]. Unfortunately, human health has also suffered as a result of these resulting changes in natural phenomena, these detrimental effects are constantly made worse by the ozone layer's thinning and also the rise in temperature, which raises the number of illnesses and fatalities related to heat [6,7,8].

The ability of algae to fix CO_2 higher than terrestrial plant up to 50 times, one of the primary advantages of employing them to reduce CO_2 [9] and store solar energy as chemical fuels through the photosynthetic process [10] **Figure 1** [11].

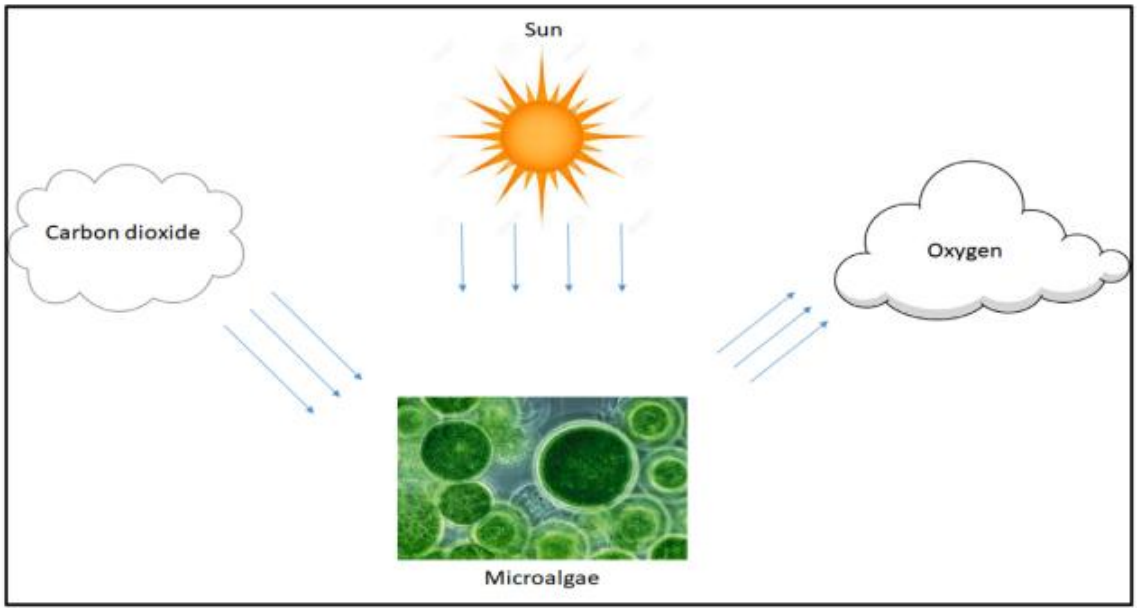


Figure 1: Minimizing carbon footprint via microalgae as a biological capture [11].

According to the mechanism of photosynthesis, microalgal species may thrive at high levels of CO_2 (40%). It is proven to facilitate in reducing greenhouse gas emissions, which eventually benefits the Blue Economy [12] **Figure 2** [13]. To estimate, half of the biomass of microalgae is made up of carbon (w/w), and they can convert inorganic air carbon into organic carbon biomass [14]. Algae biomass can transform into different biofuels (like bioethanol, biodiesel, and biogas). By producing liquid fuels, biogas, these procedures help remedy environmental worries related to fossil fuels [15].

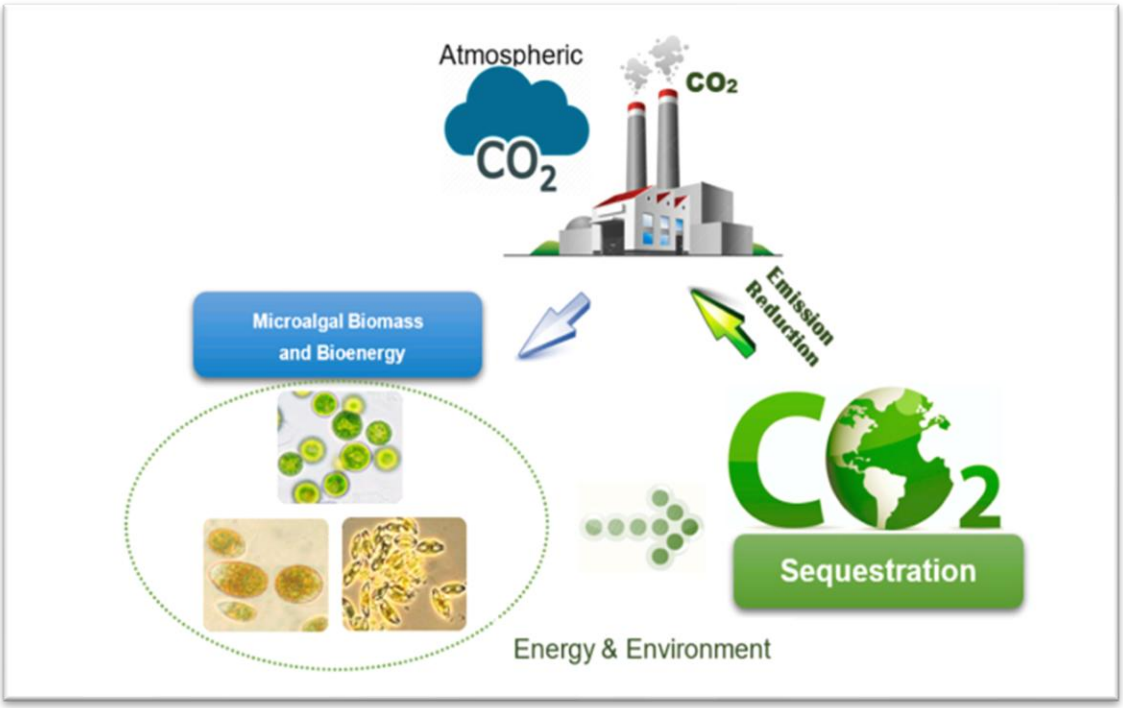


Figure 2: Macro assessment of microalgae-based CO_2sequestration: Environmental and energy effects **[13].**

The microscopic, free-drifting microalgae, also known as phytoplankton, are the most abundant plant life found in the waters.

Photosynthesis is how these single-celled organisms like Chlorella use solar energy to stay alive, and algae stay suspended in water bodies [16]. Phytoplankton contribute over 50% of the world's primary production and oxygen, as well as other supporting services. Furthermore, phytoplankton significantly influences nutrient recycling and biogeochemical cycles in both terrestrial and aquatic environments. So, it makes a substantial contribution to climate regulation [17]. In contrast to numerous other species, algae are characteristically very adjustable and lack the need for arable land for cultivation, making them a suitable biomass alternative [18].

The role of CO_2 in algal growth and biocomponent-1.2

production

CO_2 is a basic substrate for photosynthetic processes undertaken by algae, acting as the main source of carbon for the production of biomass and bioproducts. During photosynthesis, microalgae use CO_2 to transform sunlight and inorganic carbon for

organic compounds, including proteins, lipids, carbohydrates, and other useful biochemicals. CO_2 is a basic substrate for photosynthetic processes undertaken by algae, acting as the main source of carbon for the production of biomass and bioproducts. During photosynthesis, microalgae use CO_2 to transform sunlight and inorganic carbon for organic compounds, including proteins, lipids, carbohydrates, and other useful biochemical according to studies, adding CO_2 to cultures often increases biomass yield and microalgal development while also the synthesis of important biochemical components, including pigments, lipids, and fatty acids [١٩]. Increased synthesis of these chemicals results from improved carbon flow through metabolic pathways brought about by elevated CO2 levels. Lipid production is a crucial component in biofuel applications, so this result is very significant. While some species may tolerate concentrations as high as 30%, the ideal CO_2 concentrations for different species usually fall between 0.1% and 15%. For instance, when CO_2 concentration is raised from ambient levels (~0.04%) to roughly 15%, Chlorella vulgaris shows improved growth and higher lipid accumulation[20].

Excessively elevated amounts may be harmful. Elevated CO_2 lowers pH, which can inhibit photosynthetic efficiency and interfere with the activity of enzymes like carbonic anhydrase. Also, by competing for the activity of Rubisco and producing oxidative stress, the buildup of dissolved oxygen during photosynthesis can prevent CO_2 fixation [21].

Microalgae are crucial to the carbon cycle because they are thought to absorb about 50 gigatons of CO_2 a year, which is more than half of all photosynthetic activity worldwide. In addition to reducing human-caused CO_2 emissions, using microalgae for CO_2 bio-fixation offers prospective avenues for carbon capture and use carbon capture and utilization for the production of renewable biofuels and bioproducts. The economic viability and environmental advantages of scaling up CO_2-enriched cultivation of algae in conjunction with treatment of wastewater and industrial sources of carbon dioxide could be enhanced [22].

1.3-Sources of CO2 Emissions

The Earth heats as a result of greenhouse gases catching heat. Nearly every increase in greenhouse gases during the past 150 years in the atmosphere is attributable to human activity, also Fossil fuel combustion for electricity, transportation, and heating is the major cause of greenhouse gas emissions linked to human activities [23] **Figure 3**[24]. Carbon

dioxide occurs as part of the Earth's carbon cycle in the atmosphere, which is the natural flow of the element carbon between the atmosphere, seas, soil, animals, and plants. Anthropogenic activity is changing the carbon cycle by raising the atmospheric concentration of CO_2 and influencing the ability of natural ecology, like soils and forests, to absorb and hold onto CO_2. Human activity is the main driver of the rise in the atmosphere through the industrial upheaval, despite the fact that there are other natural sources of CO2 emissions [25].

Approximately 45 percent of Iraq's domestic product is derived from industrial production. Recognizing that energy significantly increases carbon emissions is essential. The International Energy Agency estimates that the energy industry in Iraq is responsible for 90% of the country's carbon emissions. Carbon emissions, produced by industry, are detrimental to the environment, public health, economic sustainability [26]. Since many industrial processes require electricity, the generation of electricity indirectly increases CO_2 emissions [24].

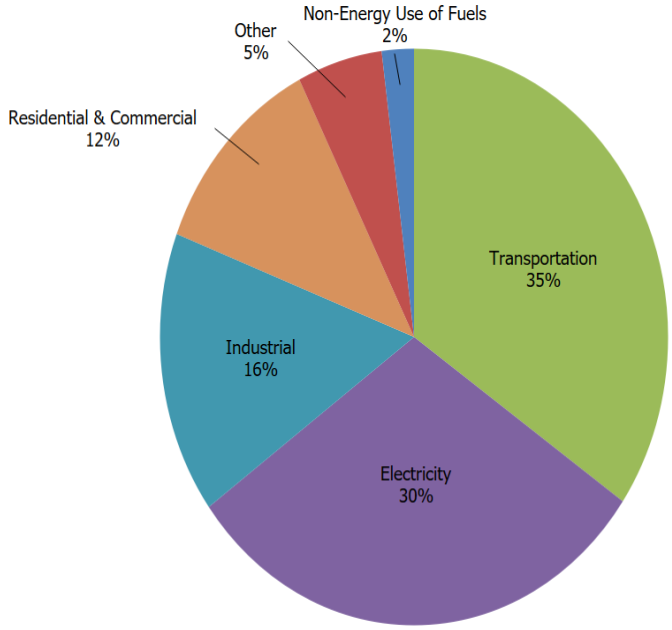


Figure 3: United States Environmental Protection Agency (EPA). Carbon Dioxide Emissions [24]

1.4- The mechanism of CO2 phyco-capture

The technique known as "phyco-capture" allows microalgae to fixate CO2 through photosynthesis, which is the mechanism used by most kinds of carbon capture. In this mechanism, photoautotrophs transform light energy and inorganic molecules into organic matter [27]. Energy is produced by microalgae through both light-dependent and light-independent processes. Both reactions take place inside the chloroplasts, the first in the stroma and the second in the thylakoid membranes Figure 4[3]. During photosystems 1 and 2 (light-reliant processes), which are composed of protein and pigment complexes that absorb light and carry out the reactions to produce NADPH and ATP, electrons are transported from water out of non-cyclic photophosphorylation. Following energy collection, the Calvin cycle (including light-non-reliant processes) uses it to create glucose (C6H12O6) and other carbohydrates [28,29].

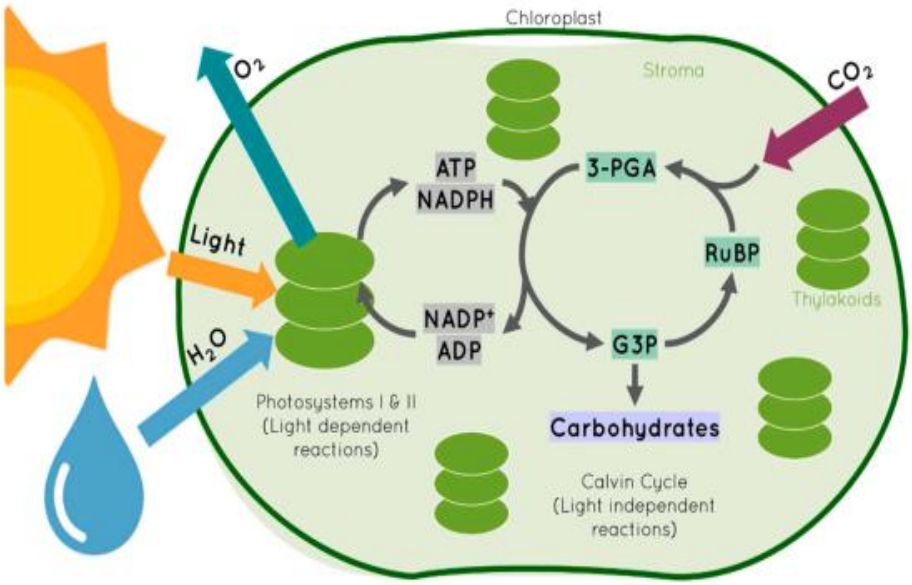


Figure 4: Phycocapture of CO2 as an option to reduce greenhouse gases in cities: Carbon sinks in urban spaces [3]

Due to its effects, climate change has become The main topic on international agendas. Finding ways to trap greenhouse gases is crucial for both the environment and our way of life. One promising option for global implementation is the biocapture of CO2 by microalgae. These systems can operate on a large scale similarly to the carbon credits currently in place in forest zones, In the broadcast area, they capture CO2 comparable to emissions from human activities that are not exactly carried out. Because the algae system

can take in more than 15 times as much data as a typical tree, this form of capture can ensure a higher capture rate than that utilized with taller plants [20].

2. Conclusions

Biological CO_2 capture using rapidly growing microalgae during photosynthesis is one of the key elements that can eventually aid in decarbonization and turn it into biomass. Microalgae biomass can be converted into renewable biofuels, providing sustainable energy alternatives that lower reliance on fossil fuels and decrease carbon emissions, thus reducing global warming. Additionally, by taking the place of feed and chemical fertilizers, microalgae provide a multifaceted strategy to mitigate climate change and improve sustainable agriculture. Microalgae also support ecosystem health by lowering nutrient pollution and treating wastewater. Although several studies on the bio-capture of carbon dioxide by algae have been published, additional study is demanded to decrease the greenhouse effect.

3. References

[1] Ferdous UT, Yusof ZNB. Climate Change and Algal Communities. In: Progress in Microalgae Research - A Path for Shaping Sustainable Futures. 2022.https://doi.org/10.5772/intechopen.104710

[2] NASA. Evidence | Facts – Climate Change: Vital Signs of the Planet [Internet]. 2024 Available from: https://science.nasa.gov/climate-change/evidence

[3] Lopez-Pacheco, IY., Rodas-Zuluaga, L. I., Fuentes-Tristan, S., Castillo-Zacarías, C., Sosa-Hernandez, J. E., Barcelo, D., Iqbal, H. M. N., & Parra-Saldívar, R. Phycocapture of CO_2 as an option to reduce greenhouse gases in cities: Carbon sinks in urban spaces. Journal of CO_2 Utilization.2021;53:101704. https://doi.org/10.1016/j.jcou.2021.101704

[4] Dawson TP, Jackson ST, House JI, Prentice IC, Mace GM. Beyond predictions: biodiversity conservation in a changing climate. Science. 2011;332(6025):53-58. https://doi.org/10.1126/science.1200303

[5] Biermann F, Kim RE. The boundaries of the planetary boundary framework: a critical appraisal of approaches to define a “safe operating space” for humanity. Annu Rev Environ Resour. 2020;45:497–521. https://doi.org/10.1146/annurev-environ-012320-080337

[6] Xu X, Gu X, Wang Z, Shatner W, Wang Z. Progress, challenges and solutions of research on photosynthetic carbon sequestration efficiency of microalgae. Renew Sustain Energy Rev. 2019;110:65–82. https://doi.org/10.1016/j.rser.2019.04.050

[7] Arun S, Sinharoy A, Pakshirajan K, Lens PN. Algae based microbial fuel cells for wastewater treatment and recovery of value-added products. Renew Sustain Energy Rev. 2020;132:110041. https://doi.org/10.1016/j.rser.2020.110041

[8] Ekwebelem OC, Ofielu ES, Nnorom-Dike OV, Aleke JC, Nwachukwu GA. Towards Sustainable Energy: The Requisite Role of Microorganisms in the Production of Biogas and Bioethanol. J Energy Res Rev. 2020;6(2):20–32. https://doi.org/10.9734/JENRR/2020/v6i230164

[9] Cheng J, Huang Y, Feng J, Sun J, Zhou J, Cen K. Improving CO2 fixation efficiency by optimizing Chlorella PY-ZU1. Bioresource Technology. 2013;144:321-327. https://doi.org/10.1016/j.biortech.2013.06.122

[10] Mussgnug, J. H., Thomas-Hall, S., Rupprecht, J., Foo, A., Klassen, V., McDowall, A., Schenk, P. M., Kruse, O., & Hankamer, B. Engineering photosynthetic light capture: Impacts on improved solar energy to biomass conversion. Plant Biotechnology Journal, 2007; 5(6):802-814. https://doi.org/10.1111/j.1467-7652.2007.00285.x

[11] Onyeaka H., Miri T., Obileke K., Hart A., Anumudu C., Al-Sharify Z. T. Minimizing carbon footprint via microalgae as a biological capture. Carbon Capture Science & Technology. 2021;1: Article 100007. https://doi.org/10.1016/j.ccst.2021.100007

[12] Costa JAV, de Freitas BCB, Lisboa CR, Santos TD, de Fraga Brusch LR, de Morais MG. Microalgal biorefinery from CO2 and the effects under the blue economy. Renew Sustain Energy Rev. 2019;99:58–65 https://doi.org/10.1016/j.rser.2018.08.009

[13] Zhao B, Su Y. Macro assessment of microalgae-based CO2 sequestration: Environmental and energy effects. Algal Research, 2020: 51, 102066. https://doi.org/10.1016/j.algal.2020.102066

[14] Yen HW, Chen Hu I, Chen CY, Ho SH, Lee DJ, Chang JS. Microalgae-based biorefinery: From biofuels to natural products. Bioresour Technol. 2013;135:166–174. https://doi.org/10.1016/j.biortech.2012.10.099

[15] Rony Z I, Mofijur M., Hasan M M, Ahmed, S F, Badruddin I A, & Khan T M Y. Conversion of algal biomass into renewable fuel: A mini review of chemical and

biochemical processes. Frontiers in Energy Research 2023. https://doi.org/10.3389/fenrg.2023.1124302

[16] Reynolds CS. The Ecology of Phytoplankton. Cambridge University Press, Cambridge; 2006.

[17] Naselli-Flores L, Padisák J. Ecosystem services provided by marine and freshwater phytoplankton. Hydrobiologia. 2023;850:2691–2706 . https://doi.org/10.1007/s10750-022-04795-y

[18] Fernandez LAG, Ramos VC, Polo MS, Castillo NAM. Fundamentals in applications of algae biomass: a review. Journal of Environmental Management. 2023;338:117830. https://doi.org/10.1016/j.jenvman.2023.117830

[19] Ashour M., Mansour A. T., Alkhamis Y. A., Elshobary M. Usage of Chlorella and diverse microalgae for CO_2 capture - towards a bioenergy revolution. Frontiers in Bioengineering and Biotechnology. 2024; 12: Article 1387519.https://doi.org/10.3389/fbioe.2024.1387519

[20] Zheng H., Gao Z., Yin F., Ji X., Huang H. Effect of CO_2 supply conditions on lipid production of Chlorella vulgaris from enzymatic hydrolysates of lipid-extracted microalgal biomass residues. Bioresource Technology. 2012;126:24-30. https://doi.org/10.1016/j.biortech.2012.09.048

[21] Mackinder L. C. M., Chen C., Leib R. D., Patena W., Blum S. R., Rodman M., Ramundo S., Adams C. M., Jonikas M. C. A spatial interactome reveals the protein organization of the algal CO2-concentrating mechanism. 2017, 21;171(1):133-147.e14.doi: https://doi.org/10.1016/j.cell.2017.08.044.

[22] Molazadeh M., Ahmadzadeh H., Pourianfar H. R., Lyon S., Rampelotto P. H.The Use of Microalgae for Coupling Wastewater Treatment With CO2 Biofixation.Frontiers in Bioengineering and Biotechnology. 2019; 7: Article 42.https://doi.org/10.3389/fbioe.2019.00042

[23] IPCC. Climate Change. The Physical Science Basis. Contribution of Working Group I to the Fifth Assessment Report of the Intergovernmental Panel on Climate Change. Cambridge University Press, Cambridge, United Kingdom and New York, NY, USA; 2013.

[24] United States Environmental Protection Agency (EPA). Carbon Dioxide Emissions [Internet]. 2025 [cited 2025 Jul 23]. Available from: https://www.epa.gov/ghgemissions/carbon-dioxide-emissions

[25] IPCC. Climate Change. The Physical Science Basis. Contribution of Working Group I to the Sixth Assessment Report of the Intergovernmental Panel on Climate Change. Cambridge University Press, Cambridge, United Kingdom and New York, NY, USA; 2021.

[26] Algashamy, H. A. A., Abbas, S. Q., Ghassan, A., and Chornomordenko, I. The carbon footprint of Iraqi industry :Navigating the path to sustainability. Investigacion Operacional.2024; 45(2): 181-202.

[27] Masojídek J, Torzillo G, Koblízek M. Photosynthesis in Microalgae, in: Handb. Microalgal Cult. Appl. Phycol. Biotechnol. Second Ed., John Wiley & Sons, Ltd, Oxford, UK, 2013: pp. 21–36. https://doi.org/10.1002/9781118567166.ch2.

[28] Petrova EV, Kukarskikh GP, Krendeleva TE, Antal TK. The mechanisms and role of photosynthetic hydrogen production by green microalgae. Microbiol (Russian Fed). 2020;89:251–265. https://doi.org/10.1134/S0026261720030169

[29] Singh UB, Ahluwalia AS. Microalgae: A promising tool for carbon sequestration. Mitig Adapt Strateg Glob Chang. 2013;18:73–95. https://doi.org/10.1007/s11027-012-9393-3

Al-Kitab Journal for Pure Sciences (2026); 10(2):52-66.
https://doi.org/10.32441/kjps.10.2.p5

Al-Kitab Journal for Pure Sciences
ISSN: 2617-1260 (print), 2617-8141(online)

https://isnra.net/index.php/kjps

The Impact of Varying Plasticizers on Coated Graphite Electrodes Performance for Doxycycline Hyclate Estimation

Aveen Kh. Mohammed[1], Muthana S. Ali[2]

[1]Kirkuk General Education Directorate, Ministry of Education, Iraq.

[2]Department of Science, College of Basic Education, Diyala University, Iraq.

Corresponding Author: Aveen@tu..edu.iq,basicsci18@uodiyala.edu.iq

Citation: ***Aveen Kh. Mohammed[1], Muthana S. Ali[2].*** **Impact of Varying Plasticizers on Coated Graphite Electrodes Performance for Doxycycline Hyclate Estimation.**
Al-Kitab J. Pure Sci. [Internet]. 2025 Aug. 28 ;10(2):52-66
DOI.
https://isnra.net/index.php/kjps/article/view/2026.
https://doi.org/10.32441/kjps.10.2.p5.

©20--. THIS IS AN OPEN-ACCESS ARTICLE UNDER THE CC BY LICENSE
http://creativecommons.org/licenses/by/4.0/

Keywords: Coated graphite electrode, Doxycycline hyclate, Di butyl phthalate, Graphite rode, Monodoks capsules.

Article History

Received	03 Aug.	2025
Accepted	28 Aug.	2025
Available online	01 Nov.	2026

Abstract:

Coated graphite electrodes (CGE) are used in this study. Doxycycline hyclate (DOX) has been successfully detected using the manufactured electrodes DOX-DBP, DOX-TBP, and DOX-NB in pure, pharmaceutical (monodoks 100 mg/capsules), and biological formulations. With a low percentage of RSD (1.18-2.16) %, the percentage of recoveries was found to be within the range of (96.99-103.68) %, indicating the accuracy of the drug estimation method at optimum conditions pH (2-6) and temperature (10-45). Additionally, it was discovered to have a long life, low detection limit, broad linearity and a good slope as compared to the construction electrodes. Also this method is rapid, economical and has excellent potential stability. Employing the t-test and F-test to assess the validity and efficacy of using the manufactured electrodes, the results demonstrate that the electrodes were successful and that there was no discernible difference between the technique suggested and the standard method.

Keywords*:* Coated graphite electrode, Di butyl phthalate, Doxycycline hyclate, Graphite rode, Monodoks capsules.

تأثير تغيير الملدنات على أداء أقطاب الجرافيت المطلية لتقدير هيكلات الدوكسيسيكلين

أفين خيرالله محمد [١]، مثنى سعيد علي [٢]

المديرية العامة لتربية كركوك، وزارة التربية، العراق ١

قسم العلوم، كلية التربية الاساسية، جامعة ديالى، العراق٢

الايميل الرسمي: Aveen@tu..edu.iq,basicsci18@uodiyala.edu.iq

الخلاصة:

تستعمل في هذه الدراسة أقطاب الجرافيت المطلية (CGE). حيث تم تقدير هيكلات الدوكسيسيكلين (DOX) بنجاح في شكله النقي والمستحضر الصيدلاني (مونودوكس ١٠٠ ملغ/كبسولات) والسوائل البيولوجية باستخدام الأقطاب المصنعة DOX-DBP و DOX-TBP و DOX-NB , حيث كانت (RSD)% نسبته منخفضة %(1.18-2.16)، ونسبة الاسترجاعية كانت تتراوح بين (٩٦,٩٩-١٠٣,٦٨)%، وتدل هذه النتائج على دقة الطريقة لتقدير الدواء في الظروف المثلى من درجة الحامضية (٢-٦) ودرجة الحرارة (١٠-٤٥) °م. فضلا عن ذلك، وُجد أن هذه الطريقة تتميز بعمر طويل للاقطاب، وحد كشف منخفض، وخطية واسعة، وميل جيد عندما قرن مع اقطاب محضرة بطرق اخرى. كما تتميز هذه الطريقة بالسرعة والاقتصادية وبثباتية عالية للجهد. وباستمال اختبار t واختبار F لتقييم صحة وفعالية استخدام الأقطاب الكهربائية المصنعة، أظهرت النتائج أن الأقطاب الكهربائية كانت ناجحة وأنه لا يوجد فرق واضح بين التقنية المقترحة والطريقة القياسية.

الكلمات المفتاحية: قطب الجرافيت المطلي، ثنائي بيوتيل الفثالات، هيكلات الدوكسيسيكلين، قضيب الجرافيت، كبسولات المونودوكس.

1. Introduction:

Doxycycline hyclate (DOX) chemically it is Hydrochloride hemiethanol hemihydrate of (4S,4aR,5S,5aR,6R,12aS)-4-(dimethylamino)-3,5,10,12,12a-pentahydroxy-6-methyl-1,11-dioxo-1,4,4a,5,5a,6,11, 12a-octahydrotetracene-2-carboxamide. has chemical structure showed in **Figure 1** in pharmaceutical samples, doxycycline hyclate is utilized more frequently. because it is significantly more soluble in water than another form of doxycycline. [1,2]. A broad-spectrum antibiotic that is classified as part of the tetracycline class, doxycycline can find use in medicine for both humans and animals [3]. In order to treat pulmonary illnesses DOX has been used extensively during the COVID surge [4]. Additionally, DOX has been shown to be effective against microorganisms, inflammation, urinary tract infections, and some bacterial sexually transmitted diseases [5]. has antitumor effects as well [6]. The examination of DOX in different biological and pharmacological formulations has been studied in many of published articles using a variety of analysis techniques, including spectrophotometry [7-13], RP-HPLC [14] HPLC [15-17], HPLC-mass [18], HPTLC [19], ratiometric probe [20], flow injection [21], Fluorometric [22-24], glassy carbon [25], potentiometric sensor [26,27] and voltammetry [28].

The purpose of this work is to use coated graphite electrodes (CGE) with three types of plasticizers (DOX-DBP, DOX-TBP and DOX-NB) to develop a simple, inexpensive, and widely linear range analytical method for determining DOX in pharmaceutical and pure formulations. The basic analytical measures were calculated and compared and attracted a lot of attention due to their exceptional properties, which include good chemical stability, accurate and sensitivity.

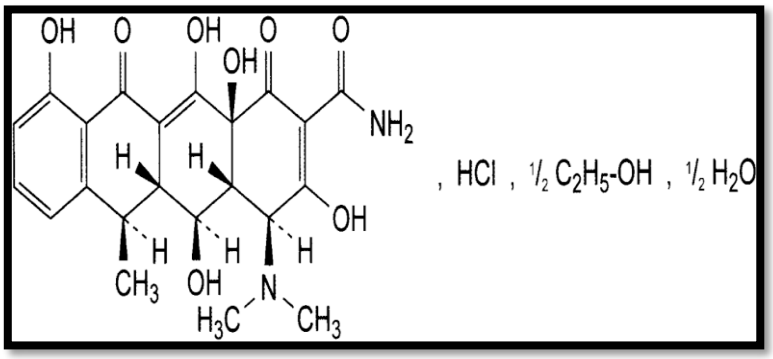


Figure 1: Chemical Structure of Doxycycline Hyclate

2. Material and methods:

2-1- Instrumentation

Potentiometric measurements were performed using a HANNA instruments pH301 and a Jenway 3310 pH-meter, equipped with calomel reference electrodes (Swiss supplier). Elemental analysis (CHN) was carried out using a PerkinElmer USA 2400 Series II analyzer.

2-2-Materials

Deionized distilled water (DDW) was used throughout all experiments. Doxycycline (DOX) was kindly provided as a gift from SDI (Samara, Iraq). Poly (vinyl chloride) (PVC), dibutyl phthalate (DBP), nitrobenzene (NB), tetrahydrofuran (THF), graphite rods, phosphomolybdic acid (PMA), and tributyl phosphate (TBP) were purchased from Sigma-Aldrich. Pharmaceutical-grade doxycycline monohydrate capsules (Monodoks, 100 mg) were purchased from a local pharmacy.

2-3- Preparation of stock solutions

A precisely weighed quantity of DOX (5.129 g) was transferred to a 100 mL volumetric flask and dissolved in deionized distilled water to prepare a 0.1 M (1.0×10^{-1} M) stock solution. The volume was then made up to the mark with DDW. Subsequent working solutions in the concentration range of 10 nM to 10 mM (1.0×10^{-8} M to 1.0×10^{-2} M) were prepared by appropriate serial dilution of the stock solution with deionized distilled water.

2-4- Pharmaceutical sample preparation (monodoks100 mg/ capsules)

A suitable quantity of powdered capsules of (monodoks) was dissolved in 50 mL of deionized distilled water to create (1.0×10^{-1}) M in order to prepare this sample. Deionized distilled water was used to properly dilute the other diluted solutions.

2-5- Ion pair preparation (DOX-PMA)

50 mL of PMA and 50 mL of DOX at (1.0×10^{-2}) M were combined to create the ion-pair DOX-PMA precipitate. After filtering, the precipitate was repeatedly washed with deionized water and left to dry at room temp for some days. The supposed ion-pair complex composition, with a molar ratio of 1:1 for DOX-PMA, was determined by elemental analysis; the results are shown in **Table 1 below.**

Table (1): C.H.N. for the (DOX-PMA) ion pair

DOX-PMA			
Element	***%C***	***%H***	***%N***
Found	9.99	2.90	1.00
Calculated	9.97	2.91	1.01
Formula	$[C_{23}H_{29}N_2O_9Cl][H_3PO_{40}Mo_{12}].24H_2O$		

2-7- Construction of electrodes (DOX-DBP, DOX-TBP and DOX-NB)

The process described previously [29] is used to prepare PVC membranes and assemble them into the sensor. These membranes employed three different kinds of plasticizers [DBP, TBP, and NB] to prepare coated graphite electrodes (CGE).

3. Results and Discussion:

3-1- Linearity, slope and detection limit

Potentiometric measurements were performed using a Calomel reference electrode immersed in DOX drug solutions (1.0×10^{-8} - 1.0×10^{-1}) M. E (mV) was measured for every solution, and a calibration curve was plotted, as seen in **Figure 2** , E(mV) versus –log [DOX]. DBP plasticizer is renowned for its superior plasticizing effectiveness and PVC compatibility the electrodes' parameters can be seen in **Table 2** where it is obvious that the electrode made with DBP plasticizer has wider liner range than the electrode made with TBP and NB and All prepared electrodes demonstrated a near-Nernstian slope and a low detection limit. Furthermore, when compared to other reported electrodes for doxycycline detection, the proposed electrodes were found to possess a superior combination of a wide linear range and a low detection limit. A

comparative summary of the performance characteristics between the suggested electrodes and previously published ones is provided in Table 2.

Table (2): Analytical parameters for the DOX-DBP, DOX-TBP and DOX-NB electrodes and comparison with those previously published in the literature

Electrode type	*Liner range M*	*Slopes (mV decade-1*	*Upper detection limit M*	*Lower detection limit M*
present study				
DOX -DBP	1.0×10^{-6} - 1.0×10^{-1}	58.64	0.2019	4.76×10^{-7}
DOX-TBP	5.0×10^{-6} - 1.0×10^{-2}	58.13	0.0207	2.37×10^{-6}
DOX -NB	1.0×10^{-5} - 1.0×10^{-2}	57.93	0.0203	5.00×10^{-6}
previously published electrodes				
[26]	1.0×10^{-5} - 1.0×10^{-2}	54.4	Not cited	4.0×10^{-6}
[27]	1.99×10^{-5} - 3.19×10^{-3}	62.30	Not cited	1.33×10^{-5}

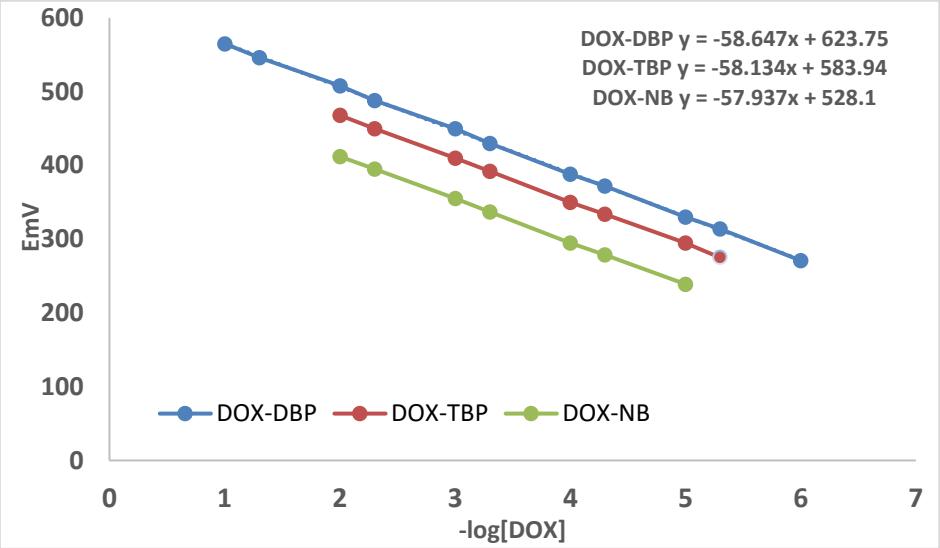


Figure 2 : calibration curve of DOX for the manufactured electrodes

3-2- Effect of pH

The ideal pH range was determined, within which the electrode potential is constant independent of the pH of the sample. The electrode potential was measured in a DOX solution (1.0×10^{-4}) M with a pH range of 1–8 for this purpose. Using KOH and/or HCl solutions, the pH

was adjusted. **Figure 3** illustrates how the electrode potential and solution pH relate to one another. It is clear that the DOX-DBP, DOX-TBP, and DOX-NB sensors have a pH range of (2–6). Potential measurements decrease at pH values below 2 and above 6 because the efficacy of doxycycline hyclate is diminished in solutions with a pH below 2, and it is quickly destroyed in alkali hydroxide solutions [2].

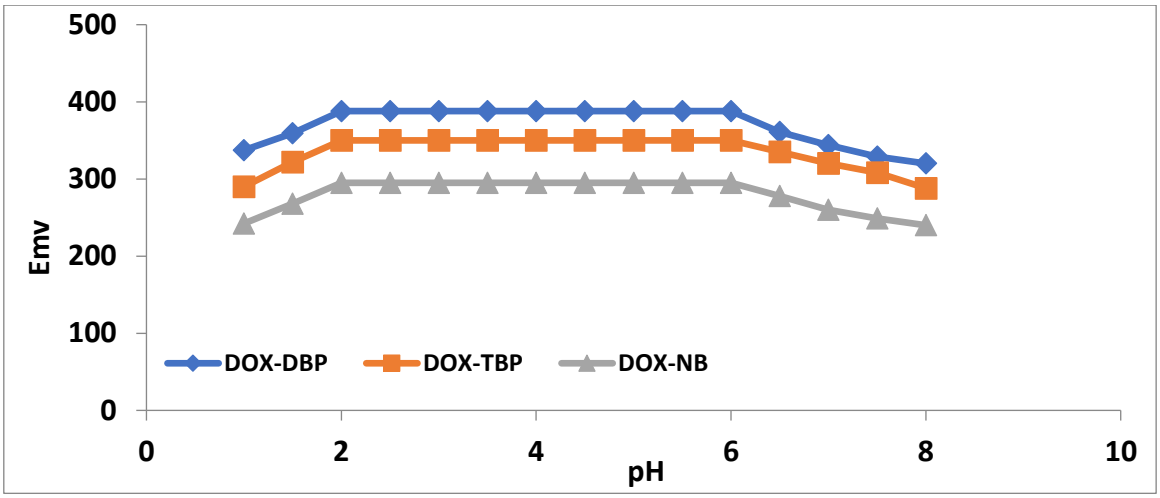


Figure 3: Effect of pH for (DOX-DBP, DOX-TBP, and DOX-NB) electrodes

3-3- Temperature's impact

Using a range of temperature values (5–70) °C, the impact of temperature was investigated. The electrode potential was measured in a DOX solution (1.0×10^{-3}) M with a temperature range (5-70) °C. The results displayed in **Figure 4** showed that the DOX-DBP, DOX-TBP, and DOX-NB electrodes work best at temperatures between 10 and 45 °C. Without appreciably changing its Nernstian slope, the results indicate that each fabrication electrode has a high degree of thermal stability.

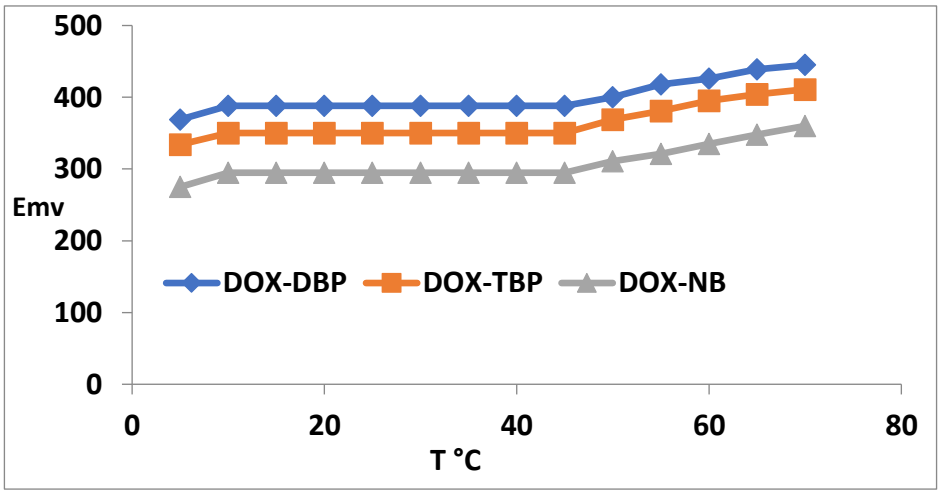


Figure (4): Temperature's impact on manufactured electrode response

3-4- Life time

The stability of the construction electrodes was assessed by by performing potentiometric analyses three times a week in the various DOX drug solutions. The results showed that the potential value and Nernstian slope could be maintained without significantly altering the use of the (DOX-DBP, DOX-TBP, and DOX-NB) electrodes for (27, 32, and 40) days, respectively. The electrodes' potential was gradually observed to be decreasing, and the Nernstian slope was gradually drifting. This may be due to the formation of a water layer between the solid contact (graphite rod) and membrane phase [30].

3-5- Interference studied

The selectivity coefficients for the manufactured electrodes (DOX-DBP, DOX-TBP, and DOX-NB) were determined using the separate solution method (SSM) [31]. The coefficients were calculated using the following equation:

$$\text{Log } K = (E_j - E_i) / S$$

as described previously [32]. The results, presented in Table 3, reveal high selectivity of the sensors towards doxycycline (DOX). The very low values of the selectivity coefficient (K) for each electrode indicate that the electrode potential was unaffected by interfering ions, demonstrating excellent selectivity for the target analyte.

Table 3: K values of the constructed sensors

Interfering ion	***Selectivity coefficient values*** $K_{i,j}^{pot}$		
	DOX-DBP	***DOX-TBP***	***DOX-NB***
Na^{1+}	5.84×10^{-2}	6.55×10^{-2}	7.09×10^{-2}
K^{1+}	5.10×10^{-1}	5.92×10^{-1}	6.67×10^{-1}
Ca^{2+}	9.53×10^{-2}	9.96×10^{-2}	4.71×10^{-1}
Cl^{1-}	3.43×10^{-1}	6.06×10^{-1}	6.59×10^{-1}
Br^{1-}	2.98×10^{-1}	3.71×10^{-1}	6.92×10^{-2}
CO_3^{1-}	2.17×10^{-1}	2.88×10^{-1}	4.81×10^{-1}
NO_3^{1-}	3.44×10^{-1}	6.01×10^{-1}	6.50×10^{-1}
SO_4^{2-}	4.00×10^{-2}	7.60×10^{-2}	1.25×10^{-1}
Glucose	8.33×10^{-3}	9.78×10^{-3}	2.00×10^{-2}
Fructose	1.30×10^{-2}	3.69×10^{-2}	8.99×10^{-2}

Starch	3.48×10^{-2}	3.77×10^{-2}	5.51×10^{-2}

3-6- Accuracy and precision

The accuracy and precision of the procedure were assessed by examining the pure drug and repeating each solution multiple times. Precision and accuracy were evaluated utilizing recovery% and relative standard deviation% (RSD%). The RSD% ranged from 1.1873% to 2.1691%, while recovery percentages ranged from 96.99% to 102.86%. These techniques have respectable accuracy and precision, as shown by the results **Table 4**.

Table 4: Statistics for measuring pure DOX with manufactured sensors.

Electrodes	***Taken [DOX] M***	***Found [DOX] M***	***%Recovery***	***%RE***
DOX-DBP	1×10^{-1}	1.0064×10^{-1}	100.64	0.64
	1×10^{-2}	9.8537×10^{-3}	98.54	1.46
	1×10^{-3}	1.0035×10^{-3}	100.35	0.35
	1×10^{-4}	9.8251×10^{-5}	98.25	1.75
	1×10^{-5}	1.0006×10^{-5}	100.06	0.06
	1×10^{-6}	9.7965×10^{-7}	97.96	2.04
%Mean ± SD	99.30 ± 1.17			
n	6			
Variance	1.39			
%RE	-0.69			
%RSD	1.18			
DOX -TBP	1×10^{-2}	1.0130×10^{-2}	101.30	1.30
	1×10^{-3}	1.0184×10^{-3}	101.84	1.84
	1×10^{-4}	9.8413×10^{-5}	98.41	−1.59
	1×10^{-5}	9.8936×10^{-6}	98.93	−1.07
	5×10^{-6}	4.8498×10^{-6}	96.99	−3.01
%Mean ± SD	99.499±2.03			
N	5			
Variance	4.13			
%RE	-0.50			
%RSD	2.04			

DOX-NB	1×10^{-2}	9.9105×10^{-3}	99.10	−0.90
	1×10^{-3}	1.0286×10^{-3}	102.86	2.86
	1×10^{-4}	9.8611×10^{-5}	98.61	−1.39
	1×10^{-5}	1.0235×10^{-5}	102.35	2.35
%Mean ± SD	100.73±2.18			
n	4			
Variance	4.77			
%RE	0.73			
%RSD	2.16			

3-8- Application of the method

Under optimal conditions for working, the proposed technique could be used to determine DOX in biological formulations and pharmaceutical formulations (Monodoks 100 mg/capsules) using the direct method and the standard addition method. **Table 5** provides a summary of the results that were obtained. The findings presented in Table 5 suggest that the method has good efficiency and estimation accuracy because the recovery percentages for the pharmaceutical form analysis ranged from 98.55 % to 103.6808 %, while the recovery percentages for biological formulations ranged from 98.19 % to 101.08 %.

Table 5: Manufactured electrodes for determinations of DOX in pharmaceutical and biological samples

Electrode	***Sample***	***Taken [DOX] M***	***Found [DOX] M***	***%Recovery***	***%RE***
Direct method					
DOX-DBP	Monodoks	7×10^{-3}	6.8986×10^{-3}	98.55	-1.45
DOX-TBP		7×10^{-3}	7.0930×10^{-3}	101.32	1.32
DOX-NB		7×10^{-3}	6.9304×10^{-3}	99.00	-0.99
Standard addition method					
DOX-DBP	Monodoks	2×10^{-4}	2.0225×10^{-4}	101.12	1.12
DOX-TBP		2×10^{-4}	2.0325×10^{-4}	101.62	1.62
DOX-NB		2×10^{-4}	2.0736×10^{-4}	103.68	3.68
biological forms					

DOX-DBP	Urine	2×10^{-3}	1.9639×10^{-3}	98.19	-1.81
DOX-TBP		2×10^{-3}	1.997×10^{-3}	99.85	-0.15
DOX-NB		2×10^{-3}	2.0216×10^{-3}	101.08	1.08
DOX-DBP	Plasma	2×10^{-3}	2.0028×10^{-3}	100.14	0.14
DOX-TBP		2×10^{-3}	2.0128×10^{-3}	100.14	0.64
DOX-NB		2×10^{-3}	1.9818×10^{-3}	99.09	-0.91

3-9- Robustness and ruggedness

The process of evaluating a method's robustness involved changing the aqueous solution to ethanol and seeing how it held up against small changes in standard operating parameters Results are displayed in the **Figure 5**. Ruggedness was assessed in this study using a different pH meter and was derived from the analysis of the same drug under various conditions (pH meter Jenway 3310). Results are displayed in the **Figure 6.** [32,33]

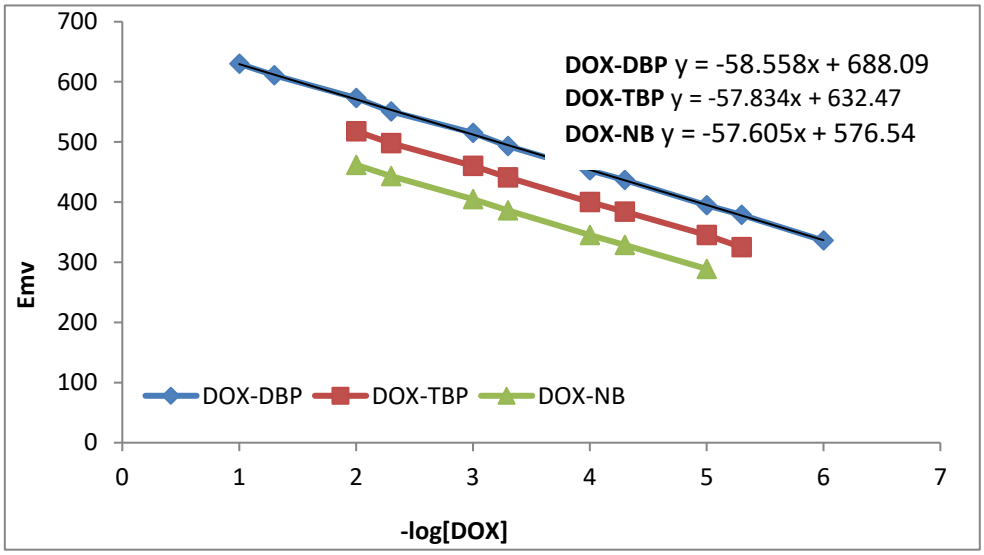


Figure 5: The robustness of the manufactured electrodes

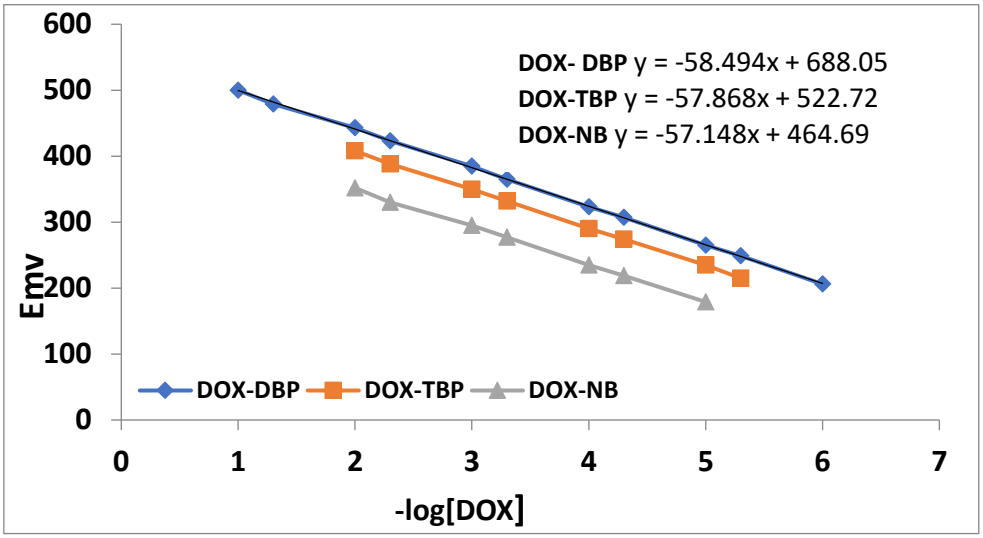


Figure 6: Ruggedness of the manufactured electrodes

3-10- Assessment of results

Employing the t-test and F-test to assess the validity and efficacy of using the manufactured electrodes for determining (Monodoks 100 mg/capsules), the results in Table 6 demonstrate that the electrodes were successful and that there was no discernible difference between the technique suggested and the standard method.

Table 6: The t-test and F-test are used to assess the results.

Electrode	*%Mean ±SD*	*n*	*Calculated t-test*	*Tabulated t-test for %95*	*Calculated F-test*	*Tabulated F-test for %95*
DOX-DBP	99.30 ± 1.17	6	0.78	2.57	0.80	5.19
DOX-TBP	99.49 ± 2.03	5	-1.92	2.78	0.26	6.39
DOX-NB	100.73±2.18	4	1.80	3.18	0.23	9.12
Standard method* (HPLC)	100.28± 1.05	5	0.00	0.00	0.00	0.00

*The constitutional method (USP41) for Wadi Al-Rafidain Pharmaceutical Industries using HPLC

4. Conclusions

The present method uses construction electrodes (DOX-DBP, DOX-TBP, and DOX-NB) to measure DOX in biological formulation (urine and plasma) and pharmaceutical forms. The manufactured electrodes had a long life time, a low detection limit, broad linearity, a good slope, and very good potential stability. Statistical analyses indicate that the accuracy and precision of all electrodes are respectable. The constructed sensors were unaffected by to foreign ions and highly sensitive to DOX drugs.

5. References

[1] Sweetman S C. Martindale: The complete drug reference, 40th Ed., Pharmaceutical Press. London. 2020.p.130.

[2] U.S. pharmacopeia on CD-ROM", 44th Ed. NF 25, by system simulation ltd. The stationary office, America, 2021:1965.

[3] Luo D, Gould D J, Sukhorukov G B, Local and sustained activity of doxycycline delivered with layer-by-layer microcapsules. Biomacromolecules. 2016;17(4):76-1466. 10.1021/acs.biomac.6b00070

[4] Malek AE, Granwehr BP, Kontoyiannis DP. Doxycycline as a potential partner of COVID-19 therapies. ID Cases. 2020; 21: e00864, 10.1016/j.idcr.2020.e00864

[5] Grant JS, Stafylis C, Celum C, Grennan T, Haire B, Kaldor J, Luetkemeyer AF, Saunders JM, Molina JM, Klausner JD., Doxycycline prophylaxis for bacterial sexually transmitted infections. Clin Infect Dis. 2020;70(6):1247-1253. 10.1093/cid/ciz866

[6] Markowska A, Kaysiewicz J., Markowska J., Huczy nski, "A. Doxycycline, Salinomycin, Monensin and Ivermectin Repositioned as Cancer Drugs" ,Bioorg. Med. Chem. Lett. 2019;29: 1549-1554.

[7] Pradyumna KS, Padmabhusana S, Jagannath M, Debadash P, Anup KP, Amiyakanta M. Development and Validation of Stability Indicating Assay Method of Doxycycline Hyclate by using UV-Spectrophotometer. Journal of Drug Delivery & Therapeutics. 2023; 13(6):89-94.

[8] Nameer MK, Nabeel SO. Diazo-coupling reaction in spectrophotometric determination of doxycycline in pure and its dosage form. Egypt J Chem. 2023;66(6):171-177. https://doi.org/10.21608/ejchem.2022.152883.6619

[9] Awad FH, Taki A G. Spectrophotometric Determination of Doxycycline Via Oxidation Reduction Reactions. Egyptian Journal of Chemistry. 2021;64(11):6621-6651. https://doi.org/10.21608/ejchem.2021.77684.3791

[10] Gholse YN, Chaple DR, Kasliwal RH. Development and Validation of Novel Analytical Simultaneous Estimation Based UV Spectrophotometric Method for Doxycycline and Levofloxacin Determination. Biointerface Res.In Appl. Chem. 2021;12(4):5458-5478.

[11] Patil MS, Khatal ST, Ranpise AS, Thorve JP, Naik SS, Jain AS. Development and validation of UV spectrometeric method for estimation of doxycycline hyclate. World J Pharm Res.2020; 9:2050-2037.

[12] Sabreen SM, Dalia MJ, Fahad J H, Ala'a RS, Zamzam A, Sohad AA, Zainab SA, Mohammed HAl-M. Spectroscopic Determination of Doxycycline by its Reaction with Schiff Base by Ion Pairing Method.2024; 7: 5085–5071. https://doi.org/10.1007/s42250-024-01086-y

[13] Khalaf NM, Othman NS. Determination of doxycycline as pure and in pharmaceutical preparation (capsule) using 4-aminoantipyrine in presence of potassium periodate. Rafidain J Sci. 2022; 31(4):15-28.

[14] Mashru R, Koshti N. Development and validation of UV-Spectrophotometric and RP-HPLC method for simultaneous estimation of Metformin and Doxycycline in bulk and synthetic mixture. Journal of Drug Delivery and Therapeutics, 2021;11(4-S): 26-35.

[15] Dil EA, Ghaedi M, Asfaram A, Tayebi L, Mehrabi F. A ferrofluidic hydrophobic deep eutectic solvent for the extraction of doxycycline from urine, blood plasma and milk samples prior to its determination by high-performance liquid chromatography-ultraviolet. Journal of Chromatography a, 2020; 22(1613):460695. 10.1016/j.chroma.2019.460695

[16] Becze A, Resz MA, Ilea A, Cadar O. A validated HPLC multichannel DAD method for the simultaneous determination of Amoxicillin and doxycycline in pharmaceutical formulations and wastewater samples. Appl. Sci. 2022; 12(9789);2-13. https://doi.org/10.3390/app12199789

[17] Mahmoud OA , Omran AA , Gomaa HA , Mohamed MA . Stability indicating high-performance liquid chromatography method for determining doxycycline hyclate and ***r***elated substances in their various dosage forms: Utilizing Six Sigma tools, uniformity testing, and in-vitro dissolution approaches. 2023;7(2): 2300173. https://doi.org/10.1002/sscp.202300173

[18] Sancho E, Granados-Chinchilla F, Calvo EB. Determination of streptomycin and doxycycline using LC/MS towards an effective treatment against an experimental Brucella abortus infection in mice. Journal of Microbiological Methods. 2022;194,106436. https://doi.org/10.1016/j.mimet.2022.106436

[19] Kumssa L, Layloff T, Hymete A, Ashenef A. High performance thin layer chromatography (HPTLC) method development and validation for determination of doxycycline hyclate in capsule and tablet formulations. Acta Chromatographica, 2021; 34(3):287-295. https://doi.org/10.1556/1326.2021.00926

[20] Tian X , Fan Z. Novel ratiometric probe based on the use of rare earth-carbon dots nanocomposite for the visual determination of doxycycline. Spectrochimica Acta Part A: Molecular and Biomolecular Spectroscopy.2021; 260 .10.1016/j.saa.2021.119925

[21] Tawfeeq AH, Qassim BB. A green method for assay of doxycycline hyclate using continuous flow injection/merging zones technique via coupling with azo metol in aqueous medium. Voprosy khimii i khimicheskoi tekhnologii. 2020;4: 31-37.

[22] Mei C, Li L, Zhang J, Pan L, Yang F, Wang Z, Yang L. Ion-induced enhanced fluorescence colorimetric hydrogel sensor for visual quantization of doxycycline. Sens Actuators B Chem. 2023; 380(0925-4005):133359. https://doi.org/10.1016/j.snb.2023.133359

[23] Xu X, Huang L, Wu Y, Li Z, Huang L. A novel nanostructured organic framework sensor for selective and sensitive detection of doxycycline based on fluorescence enhancement. Spectrochim Acta A Mol Biomol Spectrosc. 2023; 5(288):122143.
https:// doi. org/ 10. 1016/j. saa. 2022. 122143

[24] Sun Y. Fluorometric determination of doxycycline based on the use of carbon quantum dots incorporated into a molecularly imprinted polymer.Microchimica Acta.2028;185(11):1-9.

[25] Mulu G, Adane K, Molla T, Meareg A, Belete AA. Sensitive and selective electrochemical determination of doxycycline in pharmaceutical formulations using poly(dipicrylamine) modified glassy carbon electrode. Sensing and Bio-Sensing Research, 2022; 37:1-21. https://doi.org/10.1016/j.sbsr.2022.100507

[26] Sun XX , Aboul-Enein HY .Internal solid contact sensor for the determination of doxycycline hydrochloride in pharmaceutical formulation. Talanta. 2002;58(2): 387-396.

[27] Issa YM, Abdel-Fattah HM, Abdel-Moniem NB. Chemically Modified Carbon Paste Sensor for Potentiometric Determination of Doxycycline Hydrochloride in Batch and FIA

Conditions. International Journal of ELECTROCHEMICAL SCIENCE. 2013;8: 9578-9592. https://doi.org/10.1016/S1452-3981(23)12995-6

[28] Han S, Zhang X, Sun H, Wei J, Wang H, Wang S, Jin J, Zhang Z. Electrochemical Behavior and Voltammetric Determination of Chloramphenicol and doxycycline using a glassy Carbon Electrode modified with single-walled Carbon Nanohorns. Electroanalysis. 2022; 34(4):735-742. https://doi.org/10.1002/elan.202100354

[29] Mohammed AK, Ali MS , Haidar OI, Coated Wire, Coated Graphite and modified carbon paste Electrodes for Potentiometric Determination of Azithromycin, Academic Science Journal. 2024; 2(1): 37-53. https://doi.org/10.24237/ASJ.02.01.826C

[30] Frag EYZ, Mohamed AMK, Mohamed GG,Alrahmony EE, Construction and Performance Characterization of Ion Selective Electrodes for Potentiometric Determination of Ranitidine Hydrochloride in Pharmaceutical Preparations and Biological Fluids. International Journal of Electrochemical Science. 2011; 6: 3508-3524.

[31] Umezawa U, Buhlmann P, Umezawa K, Tohda K, Ameiya S. Potentiometric Selectivity Coefficients of IonSelective Electrodes. Part I. Inorganic Cations. Pure and Applied Chemistry. 2000; 72(10): 1851-2082. 10.1351/pac200072101851.

[32] Ali MS. Construction of Modified Carbon Paste Electrodes for Determination of Tramadol in Very Trace Amounts. Al-Kitab Journal for Pure Sciences. 2025; 9(1):91-102. https://doi.org/10.32441/kjps.09.01.p6.

[33] Mohammed AK, Khaleel AI, Ahmed NN. New Modified Electrodes of Graphite paste with Nano Silicon dioxide For Determination of Sildenafil citrate Drug. Tikrit Journal of Pure Science. 2019; 24(6): 57-64. https://doi.org/10.25130/tjps.v24i6.436

.

Al-Kitab Journal for Pure Sciences (2026); 10(2):67-86.
https://doi.org/10.32441/kjps.10.2.p6

Al-Kitab Journal for Pure Sciences
ISSN: 2617-1260 (print), 2617-8141(online)

https://isnra.net/index.php/kjps

Review: Efficiency of *Helianthus Annuus* L. Plant Tissues in Phytoremediation of Nano Pollutants

Rana TariqYahya[1], Sara Nazar Ghanem[2], Hala Muzher Yaqub[3]

[1]Department of Medical Physics, College of Science, University of Mosul, Mosul, Iraq.

[2]Medical research center, University of Mosul, Mosul, Iraq.

[3] Department of Biology, College of Science, University of Mosul, Mosul, Iraq.

*Corresponding Author: drranaaltaee@uomosul.edu.iq

Citation: *Rana TariqYahya[1], Sara Nazar Ghanem[2], Hala Muzher Yaqub[3]*. **Review: Efficiency of *Helianthus annuus* L. Plant Tissues in phytoremediation of nano Pollutants**. **Al-Kitab J. Pure Sci. [Internet]. 2025 Aug. 30 ;10(2):67-86 DOI.**
https://isnra.net/index.php/kjps/article/view/2026.
https://doi.org/10.32441/kjps.10.2.p6

Keywords: Environmental, Sunflowers, Nano pollutants, Phytoremediation, Pollution.

Article History

Received	27 May.	2025
Accepted	30 Aug.	2025
Available online	01 Nov.	2026

©20--. THIS IS AN OPEN-ACCESS ARTICLE UNDER THE CC BY LICENSE
http://creativecommons.org/licenses/by/4.0/

Abstract:

Nanoparticles (NPs) are a high throughput, multiflexible material and have transformed nearly every part of human life in the last decade by possessing immense commercial applications all over the world. Nevertheless, these particles have found their way into the environment in many ways, causing unintended effects to the environment and risking the health of human beings and ecosystems. Conventional remediation methods often involve expensive chemical treatments that can disrupt ecosystems. In contrast, phytoremediation—the use of plants to treat polluted environments—offers an environmentally friendly and cost-effective solution. The sunflower (*Helianthus annuus* L.) stands out as an excellent candidate thanks to its rapid growth, resilience against challenging environmental conditions like high temperatures, adaptability to varying soil types, and its remarkable capacity to extract heavy metals that accumulate in its roots. This article explores nanomaterials, their environmental implications, and the innovative use of sunflower plants for their treatment. It further delves into converting the treated biomass into sustainable biofuel. Additionally, the study examines the mechanisms that improve phytoremediation efficiency, addresses the challenges encountered in the process, and discusses recent advancements designed to enhance its effectiveness.

Keywords: Environmental, Sunflowers, Nano pollutants, Phytoremediation, Pollution.

Helianthus annuus L كفاءة أنسجة نبات زهرة الشمس في المعالجة النباتية للملوثات النانوية

رنا طارق يحيى[1]، سارة نزار غانم[2]، حلا مزهر يعقوب[3]

[1]قسم الفيزياء الطبية، كلية العلوم، جامعة الموصل، الموصل، العراق.
[2]مركز البحوث الطبية، جامعة الموصل، الموصل، العراق.
[3]قسم علوم الحياة، كلية العلوم، جامعة الموصل، الموصل، العراق.
الايميل الرسمي: drranaaltaee@uomosul.edu.iq

الخلاصة:

تعدُّ المواد الناناوية مواد متطورة وعالية الإنتاجية أحدثت ثورةً في كل جانب من جوانب الحياة البشرية تقريبًا خلال العقود الماضية بتطبيقاتها التجارية العديدة حول العالم، ومع ذلك فقد شقت هذه الجسيمات طريقها إلى البيئة عبر مسارات مختلفة مُسببةً عواقب بيئية غير مقصودة، ومُعرِّضةً الأنظمةً البيئية المُختلفة وصحة الانسان للخطر. غالبًا ما تتضمن طرق المعالجة التقليدية مُعالجات كيميائية مُكلفة قد تُخلّ بالأنظمة البيئية. وعلى النقيض، تُقدم المعالجة النباتية - استخدام النباتات لمعالجة البيئات المُلوثة - حلاً صديقًا للبيئة وفعّالاً من حيث التكلفة. وتعدُّ نباتات زهرة الشمس مرشحا واعدا بفضل نموها السريع، وتحملها للظروف البيئية كارتفاع درجات الحرارة، وقدرتها على التكيف مع تقلبات التربة، وازالة المعادن الثقيلة المتراكمة في جذوره وتضمين المواد النانوية داخل انسجتها . تهدف هذه المقالة إلى تسليط الضوء على المواد النانوية وتأثيرها على البيئة ومعالجتها باستخدام نباتات زهرة الشمس وكيفية تحويل الكتلة الحيوية المعالجة الى وقود حيوي صديق للبيئة، ودراسة الآليات التي تعزز فعالية المعالجة النباتية، وتسليط الضوء على التحديات التي تواجهها في المعالجة النباتية والتطورات الحديثة الهادفة إلى تحسين كفاءتها.

الكلمات المفتاحية: البيئة، زهرة الشمس، ملوثات نانوية، المعالجة النباتية، التلوث.

1. Introduction:

Nanomaterial pollution has become a prevalent environmental issue, presenting serious threats to both ecosystems and human health [1]. Industrial and agricultural activities have contributed to the extensive release of nanomaterials like zinc and silver into soil and water systems [2]. These metals are highly toxic and non-biodegradable, which means they leads to long-term pollution if it remains in the environment for a long time. As these substances accumulate in the food chain, they expose humans and animals to significant health risks, including neurological damage, cancer, and organ toxicity [3].

Traditional approaches to environmental remediation, such as excavation, chemical treatments, and incineration, are undoubtedly effective but come with significant drawbacks. They are costly, consume large amounts of energy, and often result in additional ecological disruption Excavation, for instance, can strip away vital topsoil, while chemical treatments

risk introducing secondary pollutants or harmful toxins. Furthermore, the long-term sustainability of these methods is questionable, highlighting the growing demand for more eco-conscious solutions. In response to this challenge, phytoremediation has gained recognition as a viable, environmentally sustainable, and cost-efficient alternative to conventional techniques [4].

Phytoremediation stands out as an innovative and eco-friendly approach to mitigating the impact of environmental pollutants. By harnessing the natural abilities of plants, particularly hyperaccumulators, and fine-tuning environmental conditions, this method offers an effective solution for pollution control across various sites, aiding in ecosystem recovery [5]. Its reliance on plants as self-sustaining agents minimizes the need for expensive infrastructure and energy-heavy remediation efforts. The adaptability of phytoremediation to address diverse contaminants—ranging from heavy metals and organic compounds to emerging pollutants—highlights its potential across a broad spectrum of environmental challenges. Aligned with the principles of ecological balance and conservation, this strategy reduces dependence on chemical interventions while lowering the likelihood of unintended adverse effects. Moreover, phytoremediation supports ecological health by fostering biodiversity and bolstering ecosystem resilience [6].

Sunflower (*Helianthus annuus* L.) has emerged as one of the most effective plant species for phytoremediation, largely due to its rapid growth, substantial biomass production, and remarkable ability to absorb diverse heavy metals [7]. Originally native to North America, this annual species thrives across various environments, ranging from farmlands to industrial areas polluted by metals. Its distinct advantages over other phytoremediation plants include superior biomass yield and highly efficient metal uptake, positioning it as a prime choice for large-scale remediation efforts [8]. Whether addressing contaminated soils or polluted water bodies, sunflowers excel in extracting pollutants. Their extensive root system enhances the absorption of contaminants, making them equally suited for both land-based and aquatic remediation projects. Sunflowers stand out as an appealing option due to their low cultivation costs and ease of handling, making them accessible for various applications [9]. While their potential for pollutant treatment shows promise, there are significant challenges that need resolution to fully capitalize on their effectiveness. These challenges primarily involve concerns such as metal toxicity, environmental fluctuations, and the disposal or management of metal-rich biomass post-phytoremediation. This review seeks to offer a detailed exploration of nanotechnology, emphasizing its ecological impact and the mechanisms

driving its role in phytoremediation. Particular attention will be given to sunflower's capability in removing nano-pollutants and the feasibility of repurposing treated biomass for biofuel production. Additionally, it will delve into the existing obstacles and suggest future research directions aimed at optimizing the use of sunflowers for pollutant remediation efforts.

2. Pollution

Adding pollutants to the natural environment causes harmful changes. Pollution can come from a variety of sources: chemicals or energy, such as noise, heat, and light. However, when these levels exceed normal levels, they are classified as pollution. Environmental pollution is one of the worst emerging problems in our world today, negatively impacting humanity and other living organisms, "Environmental pollution is defined as pollution of the physical and biological components of the Earth's atmospheric system to the extent that normal environmental processes are negatively affected" [10].

In recent decades, factories and means of transportation have developed whose waste destroys the environment and overuses pesticides, which are toxic substances and fuel materials [11]. As well as a significant increase in heavy metals, which are a group of common metallic chemicals such as cadmium (Cd), mercury (Hg), lead (Pb), arsenic (As), zinc (Zn), copper (Cu), nickel (Ni) and chromium (Cr) that originate either from natural or industrial sources including wastewater released from the oil and gas industries [12], as well as the use of phosphate fertilizers in agriculture sanitation, pesticide use, and fossil fuel burning which pose a significant threat to human health [13]. The widespread use of NPs in various products and applications further escalates environmental contamination, released into the air, water, and soil, these nanoscale particles present a grave threat; their minuscule size allows them to float in the atmosphere, spread via water systems into soil, and eventually enter the food chain through plant absorption. This accumulation in plants leads to transmission into humans, ultimately causing harmful impacts; therefore, it is necessary to find therapeutic methods to rid the environment of heavy metals or reduce their quantities [14]. Biological techniques to address the problem of pollution are one of the most used and safe methods for the environment, known collectively as biological remediation, and include the use of living organisms (plant, microorganisms, genetically modified organisms with the ability to reduce pollution levels through metabolic biological processes to reduce or prevent pollution [15].

3.Nanotechnology

Nanotechnology is the science, engineering, and technology of materials at a nanoscale ranging from 1 to 100 nm [16], which is the study and application of extremely small objects and is used in all other fields of science, such as chemistry, biology, physics, materials science, and engineering. Nanomaterials manifest in the environment through several pathways, including (i) intentionally crafted man-made nanomaterials, which afford precise control over size and properties. There are two types of methods to synthesize nanoparticles: The top-down process involves taking raw materials in bulk and reducing their dimensions using various techniques, such as grinding and lithography. The bottom-up method is a chemical and biological approach in which atoms or chemical compounds, along with a reducing agent (such as leaf extract), are used for cost-effective nanoparticle synthesis, allowing for the rapid formation of nanoparticles [17] (**Fig.1**). (ii) unintentional nanomaterials generated by industrial processes like combustion in heat engines, and natural phenomena such as fires, and (iii) naturally occurring nanomaterials. Recent years have witnessed an upsurge in nanoparticle production [18], exemplified in their use as antibacterial agents, where they mitigate bacterial proliferation and enhance the efficacy of antibacterial treatments. In drug delivery systems, nanoparticles offer physiochemical properties that selectively target cancer cells while minimizing side effects, albeit higher concentrations may induce toxicity [19]. Nanoparticles also serve as protective shields in food preservation, feature in sunscreens to shield against ultraviolet radiation, contribute to diagnostic procedures [20], and aid in pathogen elimination. Furthermore, their applications extend to the purification of water sources, removal of heavy metals from water, and augmentation of fertilizers for agricultural purposes. The electronics industry also harnesses the potential of nanoparticles [21]. Nanoparticles are integral to our daily lives, thanks to their unique physical, chemical, and biological properties. Their behavior and characteristics shift based on factors such as size, shape, acidity, and concentration. While these transformations can lead to environmental harm through specific reactions, nanoparticles also offer significant benefits. They contribute to enhanced plant growth, support advancements in renewable energy, and are essential in pharmaceutical treatments. Their influence spans multiple fields, bringing both advantages and challenges. To ensure the well-being of living organisms, it is crucial to adopt environmentally responsible practices that maintain a balanced ecosystem.

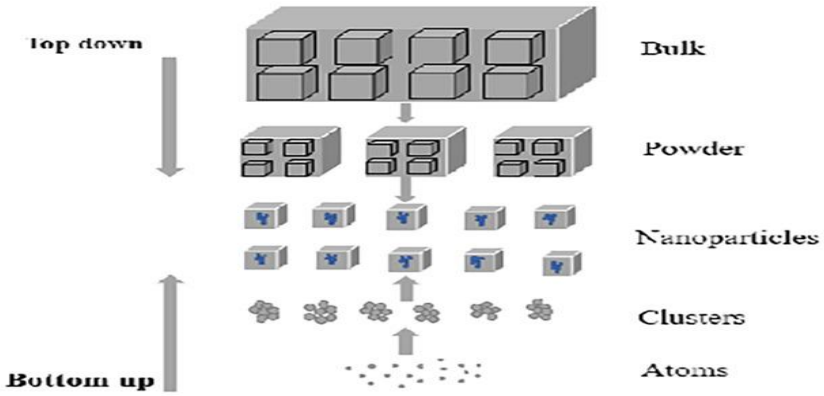


Figure 1: Top-down and bottom-up approach to the synthesis of nanoparticles [17]

4. Impact of Nanoparticles on Environmental

In today's world, numerous human activities contribute to the release of nanoparticles into the environment, leading to contamination in essential elements such as soil, air, and water. Among the key sources of these emissions is the disposal of unwanted nanomaterial waste, which often involves burning, releasing nanoparticles in the form of ashes. Construction sites, as well as gas, petroleum, and water pipelines, also contribute to environmental emissions. Cement industries release small particles into the environment during their processes, and even different fields like agriculture, roadside traffic, and the polymer industry experience toxic emissions of nanoparticles. Workers are particularly susceptible to this nanoparticle exposure, which may increase the risk of health problems such as skin issues, damage to the respiratory system, and harm to certain cells in the body. Nanoparticles' behavior changes depending on their size, shape, and other factors, leading to changes in their chemical and physical properties. Nano fertilizers are responsible for soil toxicity, climate changes, soil deficiency, and other issues [22] . Zinc nanoparticles can induce cellular toxicity in plants, leading to growth retardation, reduced photosynthesis, and altered gene expression in all affected plants. Higher nanoparticle concentrations are primarily responsible for the reduction in photosynthesis. AgNP can also inhibit plant growth [23]. Nanoparticles represent a double-edged sword, offering immense potential while demanding caution to mitigate their negative impact. Often described as "invisible pollution," nanoparticle contamination is among the most critical environmental issues to address [24]. Due to their extremely small size, these particles pose significant risks by infiltrating plant and animal cells and even penetrating human skin, potentially causing severe adverse effects. The widespread use of nanoparticles

in numerous products and applications has led to substantial environmental pollution. Once released into the air, water, and soil, nanoparticles present serious concerns due to their ability to disperse through these mediums and accumulate within plants. These contaminated plants eventually enter the human food chain, leading to harmful and sometimes long-term consequences [25] [26]. Nanoparticles can directly interact with plants through their foliar parts, affecting growth, development, biochemical processes, and physiological functions [27]. For example, copper nanoparticles (CuNPs), widely used as bactericides and fungicides in agriculture, are highly toxic to aquatic ecosystems [28]. The effects of nanoparticle pollution are far-reaching, disrupting environmental balance, destabilizing ecosystems, and contributing to a range of human health disorders. Prolonged exposure to nanoparticles elevates the risk of severe cardiovascular and respiratory diseases and can also result in premature death [29]. Inhaling air laden with nanoparticles triggers pulmonary inflammation and worsens respiratory conditions in humans [30]. As the production of nanoparticles continues to surge across various sectors, it exerts an undeniable influence on both the environment and living organisms, impacting health and well-being (Fig. 2).

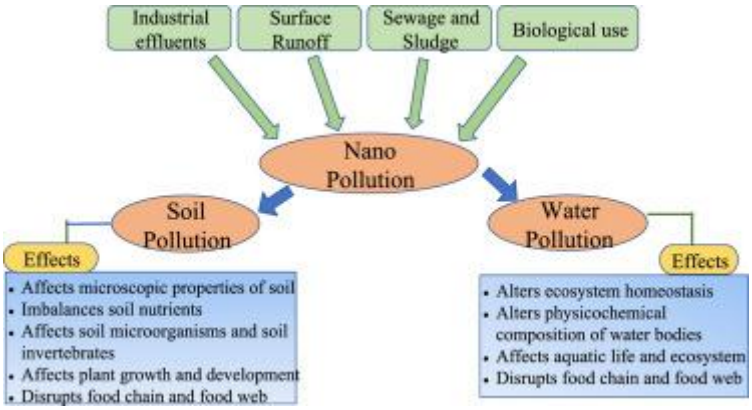


Figure 2: Impact of nanoparticles on environmental [24]

5. Phytoremediation

The origin of the word phytoremediation from the prefix "Phyto" means plant and remediation means treatment or reversal of damage, Phytoremediation is the practical application of plants to clean up or sequester (fix) contaminants in a growing medium (soil, water, or sediment) through natural biological processes and/or plants, which is one of the important means ensure in cleaning the environmental pollutants and usually plant species with the ability to attract those pollutants and convert them into forms less harmful to the environment or useful in its growth, and depends on the plant type and its ability on the

absorption of pollutants [31], scientists have tended to use methods that can treat these pollutants by less harmful means through bioremediation techniques, in particular plant treatment to clean sites contaminated with plants, this treatment is often a better option than traditional methods of soil cleaning, such as digging the soil or treating it with chemicals, as it is less expensive and more aesthetically pleasing than those methods, but it is important to use plants that are usually found naturally that can break down a specific contaminant from a specific source, such as lead from a nearby plant, for example when using a plant to absorb contaminated water, it will be necessary to choose a plant with a comprehensive root system, including willow, Indian mustard, poplar and sunflower, and phytotherapy can be used to clean pollutants such as metals, pesticides, solvents, explosives, multiple aromatic hydrocarbons, and sediments from the environment [32].

Phytoremediation is a green strategy that uses highly accumulated plants to stabilize pollutants in the soil, decompose them in water or transfer them to the environment [33], and this technique is highly efficient, cheap and adaptable to the environment, and there are many technologies used in phytoprocessing (Fig. 3): including the following:

- **Phytostabilization**

In phytostabilization, plants are used to reduce metal mobility and bioavailability in soils by a process of stabilization [35]. It is vital to mention that this process does not lead to a decreased concentration of metals in the contaminated places; it only renders metals immobile and reduce metal movement off sites making it less harmful. This is because the metals are restricted to the vadose zone of the plants there by means of this process, it is inhibited to be mobile [36].

- **Phytovolatilization**

Plants take in and break down the pollutants of heavy metals in the soil and release them as less harmful vapors through transpiration. During this process, heavy metals are taken up into volatile organic compounds but released as the biomolecules [37]. The phytoremediation process is only applicable to very few elements of the metals, which can come in the gaseous state in the environment. Such as Hg [38].

- **Phytoextraction**

This takes the form of phytoremediation where plants are used to hyper-accumulate metal. This is a solar-based technology that greatly relies on the ability of plant roots to absorb the metals, translocate them to parts above the ground so that it can accumulate there. The effect of the process is the reduction of metal concentration in soil and increasing the metal contaminants concentration that are above the grounds of plants, although this technology will ensure that the metals in the soils are eliminated, it is not suitable at high level of metal contamination because plants cannot withhold metal contaminants in the soils over long periods of time. Plants capable of accumulating high concentration of metal contamination into their shoot tissues with little to no visible toxicity consequence are generally referred to as hyperaccumulators [39].

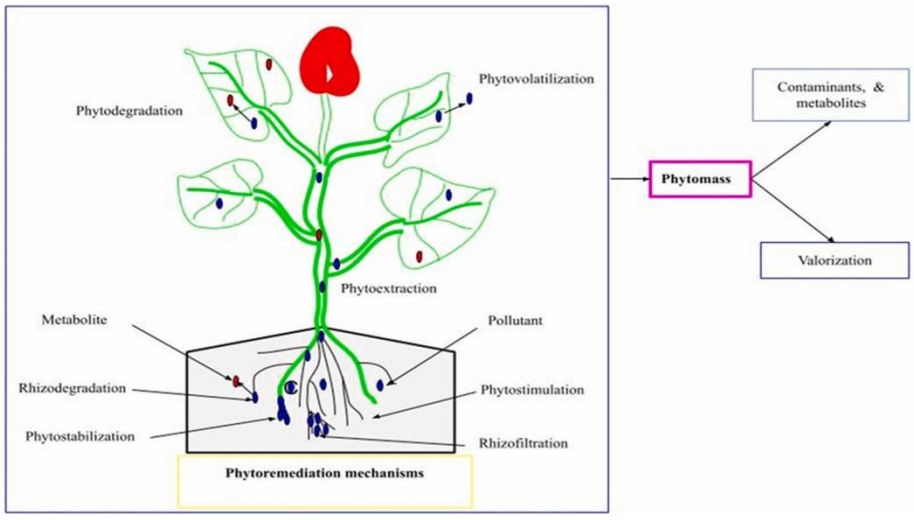


Figure 3: Phytoprocessing Technologies [34]

Advantages of plant processing [40, 41]

- Maintain the natural balance of the ecosystem using organisms that already exist.
- The possibility of companies specialized in mining from the plant recovering and reusing heavy metals.
- Ease of procedure and low cost.
- Prevents corrosion and leaching of metals by fixing metals, which reduces the risk of contaminant spread.

Disadvantages of plant treatment [42, 43]

- Determined by the land area and rooting depth the roots take up.

- Heavy metals in large proportions are difficult to process.
- Processed vegetative growth requires a long time and the need to increase biomass.\
- The leakage of pollutants into groundwater cannot be prevented entirely without removing contaminated groundwater, which is an essential aspect of the pollution problem.

6. Factors Effecting on Phytoremediation

Plant types, root region, environmental conditions, root composition and elemental species, as well as the soil physio-chemical and biological properties, all have an effect on HM buildup and distribution in plants. The remediation process can also be improved by applying agricultural practices (such as pH correction, the use of chelators, and fertilizers). Other factors to consider include soil pH, organic matter, and phosphorus content. In addition, the uptake of HMs by plants depends on various aspects, as described below [1].

7. Sunflower plants as a phytoremediation for Nano pollutants

The sunflower stands out as one of the most significant oilseed crops, serving as an abundant source of biomass and vegetable oil for energy production and industrial applications. The plant is a very adaptable species that is remarkable with regard to its resistance to heavy metal levels that are not much higher than concentrated levels [44]. Its resilience to extreme temperature ranges and adaptability to varied climatic and soil conditions are key agronomic traits. Sunflowers are recognized for their tolerance to heavy metals, attributed to their rapid growth, substantial biomass, high translocation capacity, and ability to accumulate heavy metals, particularly in their fatty tissues. This characteristic makes them effective for heavy metal remediation. Research has demonstrated their capability in removing contaminants such as chromium, Copper, Cadmium, and Zinc [45]. Research has shown that the removal of heavy metals by sunflower plants in contaminated soil varies based on the germination duration (30-90 days) [46]. Studies have demonstrated the ability of sunflower plants to treat some pollutants from chemical elements in the form of nanoparticles This is based on the properties of nanoparticles such as their ease and speed of penetration into the plasma membrane of plant cells, thus facilitating their recruitment and inclusion within these cells. The direct stimulating effect of nanoparticle concentrations of Nano oxides on the germination of seeds of a number of plants, including sunflower, is due to their biomineralization and the ability of some plants to incorporate them as a growth-stimulating

element as a basic electron carrier through the electron transport chain. This is supported by the study conducted on sunflower plants on the positive effect of titanium oxide nanoparticles TiO_2 NPs on seedling growth [47]. In another study, it was found that foliar spraying with Nano zinc oxide pesticide at a concentration of 200 parts per million resulted in the highest oil yield per acre, indicating the ability of sunflower plants to incorporate nanoparticles [48].

The stimulating effect of nanoparticle concentrations of zinc oxide nanoparticles on seed germination and growth of sunflower plants is due to their bio mineralization and their ability to be incorporated as a growth-stimulating element [49]. The findings [50] suggest that magnesium nanoparticles enhance sunflower growth under drought conditions by boosting the antioxidant system, promoting the production of photosynthetic pigments, and increasing primary metabolite levels. In another study, it was found that sunflower plants have the ability to incorporate iron nanoparticles by increasing the level of phenols, anthocyanins, and antioxidant enzyme activity, in addition to increasing macro- and micronutrients [51]. The toxicity of nanoparticles (NPs) is mitigated by: Antioxidants that are primarily made in different organelles, including mitochondria, chloroplasts, peroxisomes, vacuoles, and the endoplasmic reticulum (ER). Their role in alleviating oxidative stress enhances the tolerance of plants to the toxicity induced by metal-based nanoparticles (MBNPs). This ultimately fosters better plant growth, development, and yield by stimulating the accumulation of phytonutrients and antioxidants within the plant system. Consequently, biological macromolecule and micromolecule homeostasis is maintained, leading to improved crop quality [52].

8. Phytoremediation using Sunflowers and their potential for bioenergy production

Sunflower-based phytoprocessing practices must account for environmental and human health risks, especially concerning metal accumulation in the plants' edible parts, which can compromise food safety. To mitigate these risks, effective biomass management strategies are essential, redirecting contaminated materials toward non-food applications like bioenergy production [53] (Fig. 4).

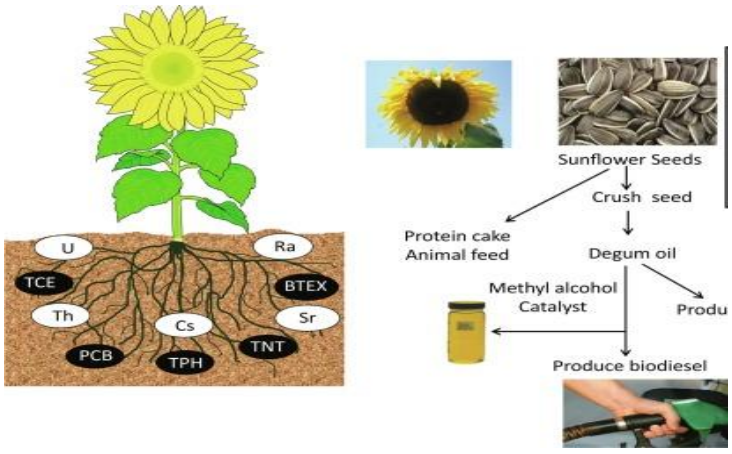


Figure 4: Phytoremediation by sunflower and bioenergy production [54]

There is a strong case in the combination of phytoremediation to benefit from restoration of the environment whilst producing clean energy named bioenergy. The potential of plants to clean contaminated soil and water comes as demand in alternative energy mounts and plants can be used to provide biomass to convert into bioenergy. The procedure results in renewable energy, and this comes with a lot of benefits. In this regard, biofuels become an alternative source of energy to the fossil fuel, which is efficient in the implementation of phytoremediation. Nevertheless, it is important to analyze the quality of these biofuels and decide on the suitability of different energy crops for biofuel production and the clean-up of metal polluted sites, before the field-scale processes are implemented [55]. Among tested crops, sunflower has shown excellent performance due to its beneficial characteristics for both phytoremediation and bioenergy generation [56]. Significant efficacy in accumulating metal pollutants in the aboveground parts of the plants was exhibited by sunflowers, whereby bioconcentration and translocation factors ranged between 0.81 and 0.94. These efficiencies were markedly enhanced by the application of *Bacillus aryabhattai*, which elevated the bioconcentration and translocation factors to greater than 1 across all tested metals qualifying the sunflower as a hyperaccumulator species. The post-remediation sunflower residues with the built-up of metals possessed calorific values between 17.01 and 18.04 MJ/kg and were thermochemically treated under pyrolysis. This produced about 22.3 percent metal-free bio-oil, and 51.6 percent of biochar. The findings indicate possible sunflower plants as a great agent in phytoremediation process besides being used as a renewable energy source [57].

9. Challenges and future trends

To maximize the potential of sunflowers in phytoremediation of pollutants, several critical challenges need to be tackled. Soil conditions, the variability of climate and so on are environmental factors that influence the efficiency of remediation significantly. Genetic engineering presents promising possibilities for improving metal tolerance and accumulation in sunflower varieties, while also addressing adaptation to environmental variability. Furthermore, investigating the use of soil amendments like biochar, compost, and beneficial microorganisms can boost plant growth and enhance metal uptake, ultimately increasing their capacity to mitigate pollutants **[34]**.

10. Conclusions

Phytoremediation represents an innovative and eco-friendly strategy for addressing environmental Contaminants. By utilizing the natural abilities of plants, such as highly effective pollutant-accumulators like sunflowers, this method can restore polluted sites while aiding overall improvements in environmental conditions. Its versatility in managing a wide array of pollutants, including nanopollutants, underscores its ability to adapt to diverse environmental challenges. Aligning with ecological principles, phytoremediation minimizes reliance on chemical treatments, thereby lowering the chances of unforeseen negative impacts. Additionally, this approach fosters biodiversity and fortifies ecosystem resilience, delivering significant environmental benefits. Advancing research into the processes and factors that impact plant's effectiveness, especially in dealing with Nano pollutants, could pave the way for developing more precise and efficient phytoremediation techniques.

11. References

[1] Bhat, M. A., Gedik, K., & Gaga, E. O. (2023). Environmental impacts of nanoparticles: pros, cons, and future prospects. In *Synthesis of bionanomaterials for biomedical applications* (pp. 493-528). Elsevier. https://doi.org/10.1016/B978-0-323-91195-5.00002-7

[2] Mishra, M. (2019). Effect of accumulation of nanoparticles in soil health-a concern on future. *Frontiers in Nanoscience and Nanotechnology*. https://doi.org/10.15761/FNN.1000181

[3] Mitra, S., Chakraborty, A. J., Tareq, A. M., Emran, T. B., Nainu, F., Khusro, A., ... & Simal-Gandara, J. (2022). Impact of heavy metals on the environment and human health: Novel therapeutic insights to counter the toxicity. *Journal of King Saud University-Science*, *34*(3), 101865. https://doi.org/10.1016/j.jksus.2022.101865

[4] Priya, A. K., Muruganandam, M., Ali, S. S., & Kornaros, M. (2023). Clean-Up of Heavy Metals from Contaminated Soil by Phytoremediation: A Multidisciplinary and Eco-Friendly Approach. *Toxics*, *11*(5), 422. https://doi.org/10.3390/toxics11050422

[5] Aryal, M. (2024). Phytoremediation strategies for mitigating environmental toxicants. *Heliyon*, *10*(19). https://doi.org/10.1016/j.heliyon.2024.e38683

[6] DalCorso, G., Fasani, E., Manara, A., Visioli, G., & Furini, A. (2019). Heavy metal pollutions: state of the art and innovation in phytoremediation. *International journal of molecular sciences*, *20*(14), 3412. https://doi.org/10.3390/ijms20143412

[7] Mahardika, G., Rinanti, A., & Fachrul, M. F. (2018). Phytoremediation of heavy metal copper (Cu2+) by sunflower (Helianthus annuus l.). In *IOP conference series: earth and environmental science* (Vol. 106, No. 1, p. 012120). IOP Publishing. http://dx.doi.org/10.1088/1755-1315/106/1/012120

[8] Kaonda, M.K.M. and Chileshe, K. (2023) Assessment of Sunflower (Helianthus annuus L.) for Phytoremediation of Heavy Metal Polluted Mine Tailings—A Case Study of Nampundwe Mine Tailings Dam, Zambia. Journal of Environmental Protection, 14, 481-492. https://doi.org/10.4236/jep.2023.147028

[9] Qadir, M., Hussain, A., Shah, M., Hamayun, M., Al-Huqail, A. A., Iqbal, A., & Ali, S. (2024). Improving sunflower growth and arsenic bioremediation in polluted environments: Insights from ecotoxicology and sustainable mitigation approaches. *Heliyon*, *10*(12), e33078. https://doi.org/10.1016/j.heliyon.2024.e33078

[10] Yan A, Wang Y, Tan SN, Mohd Yusof ML, Ghosh S, Chen Z. Phytoremediation: a promising approach for revegetation of heavy metal-polluted land. Frontiers in plant science. 2020 Apr 30;11:359. https://doi.org/10.3389/fpls.2020.00359

[11] Ashraf S, Ali Q, Zahir ZA, Ashraf S, Asghar HN. Phytoremediation: Environmentally sustainable way for reclamation of heavy metal polluted soils. Ecotoxicology and

environmental safety. 2019 Jun 15;174:714-27. https://doi.org/10.1016/j.ecoenv.2019.02.068

[12] Dutournie P, Jeguirim M, Khiari B, Goddard ML, Jellali S. Oilve mill wastewater form a pollution to green fells, agricultural water source, and bio-fertilizer. Part 2 : Water recovery. Water., 2019; 11(4): 768. https://doi.org/10.3390/w11040768

[13] Rehman, M. Z. U., Rizwan, M., Ali, S., Ok, Y. S., Ishaque, W., Saifullah, Nawaz, M. F., Akmal, F., & Waqar, M. (2017). Remediation of heavy metal contaminated soils by using Solanum nigrum: A review. *Ecotoxicology and environmental safety*, *143*, 236–248. https://doi.org/10.1016/j.ecoenv.2017.05.038

[14] Hasan MM, Uddin MN, Ara-Sharmeen I, F. Alharby H, Alzahrani Y, Hakeem KR, Zhang L. Assisting phytoremediation of heavy metals using chemical amendments. Plants. 2019 Aug 21;8(9):295. https://doi.org/10.3390/plants8090295

[15] Patel NA, Khan MD, Shahane S, Rai D, Chauhan D, Kant C, Chaudhary VK. Emerging pollutants in aquatic environment: source, effect, and challenges in biomonitoring and bioremediation-a review. Pollution. 2020 Jan 1;6(1):99-113. https://doi.org/10.22059/poll.2019.285116.646

[16] Yahya RT, Qaddawi ZT, Rasheed AA, Sultan SJ. Effect of diode laser rays in stimulating anthocyanin pigment levels in radish (*Raphanus sativus* L.) plant tissues. Journal of Applied and Natural Science. 2024;16(3):1158. https://doi.org/10.31018/jans.v16i3.5779

[17] Abid, N., Khan, A. M., Shujait, S., Chaudhary, K., Ikram, M., Imran, M., ... & Maqbool, M. (2022). Synthesis of nanomaterials using various top-down and bottom-up approaches, influencing factors, advantages, and disadvantages: A review. *Advances in colloid and interface science*, *300*, 102597. https://doi.org/10.1016/j.cis.2021.102597

[18] . Raut, S. S., Singh, R., & Lekhak, U. M. (2024). Naturally occurring nanoparticles (NONPs): a review. *Next Sustainability*, *3*, 100037. https://doi.org/10.1016/j.nxsust.2024.100037

[19] Aflakian, F., Mirzavi, F., Aiyelabegan, H. T., Soleimani, A., Navashenaq, J. G., Karimi-Sani, I., ... & Vakili-Ghartavol, R. (2023). Nanoparticles-based therapeutics for the management of bacterial infections: A special emphasis on FDA approved products and clinical trials. *European Journal of Pharmaceutical Sciences*, *188*, 106515. https://doi.org/10.1016/j.ejps.2023.106515

[20] Morabito, K., Shapley, N. C., Mello, C., Calvert, P., & Tripathi, A. (2009). Nanoparticles and their applications in ultraviolet protection: a review. *Anal. Chem*, *1*, 1-10.

[21] Altammar, K. A. (2023). A review on nanoparticles: characteristics, synthesis, applications, and challenges. *Frontiers in microbiology*, *14*, 1155622. https://doi.org/10.3389/fmicb.2023.1155622

[22] Arora, R., Roy, T., & Adak, P. (2024). A review of the impact of nanoparticles on environmental processes. In *BIO Web of Conferences* (Vol. 86, p. 01001). EDP Sciences. https://doi.org/10.1051/bioconf/20248601001

[23] Wang, X., Yang, X., Chen, S., Li, Q., Wang, W., Hou, C., Gao, X., Wang, L., & Wang, S. (2016). Zinc Oxide Nanoparticles Affect Biomass Accumulation and Photosynthesis in Arabidopsis. *Frontiers in plant science*, *6*, 1243. https://doi.org/10.3389/fpls.2015.01243

[24] Jan, N., Majeed, N., Ahmad, M., Ahmad Lone, W., & John, R. (2022). Nano-pollution: Why it should worry us. *Chemosphere*, *302*, 134746. https://doi.org/10.1016/j.chemosphere.2022.134746

[25] Gao, Y., Yang, T., & Jin, J. (2015). Nanoparticle pollution and associated increasing potential risks on environment and human health: a case study of China. *Environmental science and pollution research international*, *22*(23), 19297–19306. https://doi.org/10.1007/s11356-015-5497-0

[26] Rajput, V. D., Minkina, T., Sushkova, S., Tsitsuashvili, V., Mandzhieva, S., Gorovtsov, A., ... & Gromakova, N. (2018). Effect of nanoparticles on crops and soil microbial communities. *Journal of Soils and Sediments*, *18*(6), 2179-2187. https://doi.org/10.1007/s11368-017-1793-2

[27] Gohar, F., Iqbal, U. Z., Khan, M. B., Rehman, F., Maryam, F. S. U., Azmat, M., ... & Shahid, M. U. (2024). Impact of nanoparticles on plant growth, development and physiological processes: A comprehensive review. https://doi.org/10.20944/preprints202410.0780.v1

[28] Rajwade, J. M., Oak, M. D., & Paknikar, K. M. (2024). Copper-based nanofungicides: The next generation of novel agrochemicals. In *Nanofungicides* (pp. 141-168). Elsevier. https://doi.org/10.53555/jaz.v44iS5.3481

[29] Roy, B., Murugesan, K., Mathanmohun, M., & Sathian, B. (2023). Impact of nanoparticles on human health and disease. *Nepal journal of epidemiology*, *13*(4), 1294–1297. https://doi.org/10.3126/nje.v13i4.61245

[30] Wallbanks, S., Griffiths, B., Thomas, M., Price, O. J., & Sylvester, K. P. (2024). Impact of environmental air pollution on respiratory health and function. *Physiological reports*, *12*(16), e70006. https://doi.org/10.14814/phy2.70006

[31] Su ZH, Xu ZS, Peng RH, Tian YS, Zhao W, Han HJ, Yao QH, Wu AZ. Phytoremediation of trichlorophenol by phase II metabolism in transgenic Arabidopsis overexpressing a Populus glucosyltransferase. Environmental science & technology. 2012 Apr 3;46(7):4016-24. https://doi.org/10.1021/es203753b

[32] Nedjimi B. Germination characteristics of Peganum harmala L.(Nitrariaceae) subjected to heavy metals: Implications for the use in polluted dryland restoration. International Journal of Environmental Science and Technology. 2020 Apr;17(4):2113-22. http://dx.doi.org/10.1007/s13762-019-02600-3

[33] Liu S, Yang B, Liang Y, Xiao Y, Fang J. Prospect of phytoremediation combined with other approaches for remediation of heavy metal-polluted soils. Environmental Science and Pollution Research. 2020 May; 27:16069-85. https://doi.org/10.1007/s11356-020-08282-6

[34] Aryal, M. (2024). Phytoremediation strategies for mitigating environmental toxicants. *Heliyon*, *10*(19). https://doi.org/10.1016/j.heliyon.2024.e38683

[35] Sylvain, B., Mikael, M. H., Florie, M., Emmanuel, J., Marilyne, S., Sylvain, B., & Domenico, M. (2016). Phytostabilization of As, Sb and Pb by two willow species (S.

viminalis and S. purpurea) on former mine technosols. *Catena*, *136*, 44-52. https://doi.org/10.1016/j.catena.2015.07.008

[36] Masindi V, Muedi KL. Environmental Contamination by Heavy Metals [Internet]. Heavy Metals. In Tech; 2018. Available from: https://doi.org/10.5772/intechopen.76082

[37] Mahar, A., Wang, P., Ali, A., Awasthi, M. K., Lahori, A. H., Wang, Q., et al. (2016). Challenges and opportunities in the phytoremediation of heavy metals contaminated soils: a review. *Ecotox. Environ. Safe.* 126, 111–121. https://doi.org/10.1016/j.ecoenv.2015.12.023

[38] Awa SH, Hadibarata T. Removal of heavy metals in contaminated soil by phytoremediation mechanism: a review. Water, Air, & Soil Pollution. 2020 Feb;231(2):47. https://doi.org/10.1007/s11270-020-4426-0

[39] Ali H, Khan E, Sajad MA. Phytoremediation of heavy metals—concepts and applications. Chemosphere. 2013 May 1;91(7):869-81. https://doi.org/10.1016/j.chemosphere.2013.01.075

[40] Jacob JM, Karthik C, Saratale RG, Kumar SS, Prabakar D, Kadirvelu K, Pugazhendhi A. Biological approaches to tackle heavy metal pollution: a survey of literature. Journal of environmental management. 2018 Jul 1;217:56-70. https://doi.org/10.1016/j.jenvman.2018.03.077

[41] Awa SH, Hadibarata T. Removal of heavy metals in contaminated soil by phytoremediation mechanism: a review. Water, Air, & Soil Pollution. 2020 Feb;231(2):47. https://link.springer.com/article/10.1007/s11270-020-4426-0

[42] DalCorso G, Fasani E, Manara A, Visioli G, Furini A. Heavy metal pollutions: state of the art and innovation in phytoremediation. International journal of molecular sciences. 2019 Jul 11;20(14):3412. https://doi.org/10.3390/ijms20143412

[43] Brandt R, Merkl N, Schultze-Kraft R, Infante C, Broll G. Potential of vetiver (Vetiveria zizanioides (L.) Nash) for phytoremediation of petroleum hydrocarbon-contaminated soils in Venezuela. International journal of phytoremediation. 2006 Dec 1;8(4):273-84.

[44] Murphy, D. J. (2025). Agronomy and Environmental Sustainability of the Four Major Global Vegetable Oil Crops: Oil Palm, Soybean, Rapeseed, and Sunflower. *Agronomy*, *15*(6), 1465. https://doi.org/10.3390/agronomy15061465

[45] Zhao, X., & Li, G. (2025). *Impact of Single and Mixed Heavy Metal Contamination on Accumulation Patterns and Organ Distribution in Sunflowers* (No. EGU25-8466). Copernicus Meetings. https://doi.org/10.5194/egusphere-egu25-8466

[46] Adejube AA, Anteyi A, Garba FH, Oyekunle OA, Kudaisi FO. Bioremediating activity of sunflower (Helianthus annuus L.) on contaminated soil from Challawa Industrial Area, Kano-State Nigeria. International Journal of Agriculture and Earth Science. 2017;3(5):1-1.

[47] Day S, Özgen Y. Titanium dioxide nano particles improving impact on sunflower seedling's emergence performance. Ant J Bot. 2023;7(2):108-11. https://doi.org/10.30616/ajb.1270434

[48] Bakheit, B. R., Ali, E. A., Omar, A. A., & Hamed, H. A. (2022). Impact of Planting Methods and Foliar Spraying with Zinc Dioxide Nanoparticles on the Seed and Oil Yields of Sunflower. *Assiut Journal of Agricultural Sciences*, *53*(3), 1-13. https://doi.org/10.21608/ajas.2022.127476.1115

[49] Alamery, A. A., & Ahmed, N. A. (2020). Effect of biofertilizers and zinc nano particles on growth, yield and oil percentage of sunflower (Helianthus annuus L.). Plant Archives, 2020, Vol. 20, No. 2, 4648-4652. https://share.google/PKiUK8jk331ujGJF6

[50] Fatemi, A., Moaveni, P., Daneshian, J., Mozafari, H., & Ghaffari, M. (2022). Magnesium nanoparticles improve grain yield, oil percentage, physiological, and biochemical traits of sunflower (Helianthus annuus L.) under drought stress. *Journal of Agricultural Science and Technology*, *24*(3), 665-678. http://jast.modares.ac.ir/article-23-44376-en.html

[51] Gupta A, Bharati R, Kubes J, Vachova P, Popelkova D, Mahawar L, et al. Ferric oxide nano-priming enhances photosynthetic and physicochemical properties of sunflower (Helianthus annuus L.) microgreens. Plant Soil Environ. 2024;70(11):702-711. https://doi.org/10.17221/272/2024-PSE

[52] Ali S, Mehmood A, Khan N. Uptake, translocation, and consequences of nanomaterials on plant growth and stress adaptation. Journal of Nanomaterials. 2021;2021(1):6677616. https://doi.org/10.1155/2021/6677616

[53] Prasad, M. N. V. (2024). Bioremediation and bioeconomy potential of sunflower (Helianthus annuus L.). In *Bioremediation and Bioeconomy* (pp. 367-381). Elsevier. https://doi.org/10.1016/B978-0-443-16120-9.00020-0

[54] Wijekoon, W., Priyashantha, H., Gajanayake, P., Manage, P., Liyanage, C., Jayarathna, S., & Kumarasinghe, U. (2025). Review and Prospects of Phytoremediation: Harnessing Biofuel-Producing Plants for Environmental Remediation. *Sustainability*, *17*(3), 822. https://doi.org/10.3390/su17030822

[55] Marques, A. P., Paulo, A., & Caetano, N. S. (2024). Assessment of the potential of sunflower grown in metal-contaminated soils for production of biofuels. *Sustainability*, *16*(5), 1829. https://doi.org/10.3390/su16051829

[56] Zehra, A., Sahito, Z. A., Tong, W., Tang, L., Hamid, Y., Khan, M. B., ... & Yang, X. (2020). Assessment of sunflower germplasm for phytoremediation of lead-polluted soil and production of seed oil and seed meal for human and animal consumption. *Journal of Environmental Sciences*, *87*, 24-38. https://doi.org/10.1016/j.jes.2019.05.031

[57] Amabogha, O. (2022). *Combining phytoremediation with bioenergy production; exploring options for sustainable remediation* (Doctoral dissertation, Middlesex University). ISO 690

Al-Kitab Journal for Pure Sciences (2026); 10(2):87-103.
https://doi.org/10.32441/kjps.10.2.p7

Al-Kitab Journal for Pure Sciences
ISSN: 2617-1260 (print), 2617-8141(online)

https://isnra.net/index.php/kjps

The Effect of Tacrolimus and Triticum Aestivum Germ Oil on the Intrinsic Pathway of Apoptosis in the Liver of Male Albino Mice: An Immunohistochemical and Molecular Study

Thamer Ahmed Mohamed[1], Baidaa Abdulaziz Mohamed Salah[2]

[1,2] Department of Biology, College of Education for Pure Science, University of Mosul, Mosul, Iraq.

Corresponding author: thamer.20esp37@student.uomosul.edu.iq[1] baidaamohammed@uomosul.edu.iq[2]

Citation: *Thamer Ahmed Mohamed[1], Baidaa Abdulaziz Mohamed Salah[2]*. **The effect of tacrolimus and Triticum Aestivum Germ Oil on the intrinsic pathway of apoptosis in the liver of male albino mice: an immunohistochemical and molecular study**.
Al-Kitab J. Pure Sci. [Internet]. 2025 Sep. 14 ;10(2):87-103
DOI.
https://isnra.net/index.php/kjps/article/view/2026.
https://doi.org/10.32441/kjps.10.2.p7

©20--. THIS IS AN OPEN-ACCESS ARTICLE UNDER THE CC BY LICENSE
http://creativecommons.org/licenses/by/4.0/

Keywords: Tacrolimus, Wheat germ oil, Bax/Bcl-2 ratio, qPCR gene expression, Hepatotoxicity.

Article History
Received 09 Aug. 2025
Accepted 14 Sep. 2025
Available online 01 Nov. 2026

Abstract:

Tacrolimus is a commonly used as an immunosuppressant, while wheat germ oil is a recently discovered compound that is a potent antioxidant. The current study investigated the role of *Triticum Aestivum* Germ Oil in influencing the intrinsic pathway of apoptosis through its effect on the protein Bax. Forty male white mice, *Mus musculus* were used, divided into four sets, each containing 10 individuals: negative control (distilled water) set, positive control set (wheat germ oil, 1130 mg/kg), tacrolimus (0.4 mg/kg) set, and a set treated with tacrolimus and wheat germ oil together. The animals were treated for two periods, 14 and 28 days. The findings demonstrated that tacrolimus increases the activity of the Baxdelta2G9 (Bax protein) in hepatocytes; however, after 14 days of treatment with two certain chemicals, the group's immunohistochemistry activity of Bax declined. Over 28 days, the response and improvement grew. Additionally, the group that received tacrolimus revealed an increase in Bax transcription, whereas the group that received wheat germ oil showed a decrease in Bax gene expression. Additionally, the improvement was noted as the experiment's duration grew. We conclude from this that tacrolimus stimulates the activity of the intrinsic pathway of programmed cell death,

but the use of an antioxidant, such as wheat germ oil, improves and reduces the activity of this pathway in the liver.

Keywords: Tacrolimus, Wheat germ oil, Bax/Bcl-2 ratio, qPCR gene expression, Hepatotoxicity

تأثير التاكرولميس وزيت جنين القمح في المسار الداخلي للموت المبرمج في الكبد لذكور الفئران البيض: دراسة كيميائية مناعية نسجية وجزيئية

ثامر احمد محمد[١], بيداء عبد العزيز محمد صالح [٢]

[٢،١] قسم علوم الحياة، كلية التربية للعلوم الصرفة، جامعة الموصل

الايميل الرسمي: thamer.20esp37@student.uomosul.edu.iq[1], baidaamohammed@uomosul.edu.iq[2]

الخلاصة:

يُعَدّ عقار التاكرولميس واحداً من أهم المثبطات المناعية المستعملة على نطاق واسع في عمليات زراعة الأعضاء، غير أنّ آثاره الجانبية على الكبد ما تزال مثار جدل علمي. أما زيت جنين القمح فهو غني بمركبات مضادة للأكسدة كالتوكوفيرولات والأحماض الدهنية غير المشبعة، وقد ثبُتت فعاليته في التقليل من الإجهاد التأكسدي وإبطاء مسارات الموت الخلوي. هدفت الدراسة الحالية إلى تقييم التأثير الوقائي لزيت جنين القمح ضد السمية الكبدية المستحثة بالتاكرولميس من خلال تتبّع التغيرات في بروتيني *Bax* و *Bcl-2*المرتبطين بالمسار الداخلي للموت المبرمج. استُخدم في التجربة أربعون فأراً أبيض ذكراً *(Mus musculus)*وزّعت إلى أربع مجموعات: مجموعة السيطرة السالبة (ماء مقطر)، مجموعة السيطرة الموجبة (زيت جنين القمح بجرعة ١١٣٠ ملغم/كغم)، مجموعة التاكرولميس (٠,٤ ملغم/كغم)، ومجموعة التاكرولميس مع زيت جنين القمح معاً. عُولجت الحيوانات لفترتين زمنيتين (١٤ و٢٨ يوماً). أظهرت نتائج الكيمياء المناعية النسيجية ارتفاعاً معنوياً في *Bax* في أكباد الفئران المعاملة بالتاكرولميس، يقابله انخفاض ملحوظ في مجموعة زيت جنين القمح. كما كشفت تحاليل *qPCR* عن زيادة في التعبير الجيني لبروتين *Bax* مع التاكرولميس، بينما أدّى الزيت إلى تعزيز التعبير عن *Bcl-2* وخفض نسبة *Bax/Bcl-2* مقارنة بالمجموعة المعاملة بالتاكرولميس فقط. تؤكد هذه النتائج أنّ التاكرولميس ينشّط المسار الداخلي للموت المبرمج عبر تعزيز*Bax* ، في حين يوفّر زيت جنين القمح حماية خلوية واضحة من خلال رفع *Bcl-2* وتقليل نسبة *Bax/Bcl-2*، مما يعكس دوره المضاد للأكسدة والواقي من السمية الكبدية.

الكلمات المفتاحية: التاكرولميس، زيت جنين القمح، نسبة، *Bax/Bcl-2*، التعبير الجيني بتقنية، *PCR*السمية الكبدية

Introduction:

Tacrolimus as an immunosuppressive agent is utilized for transplanted organs. It is a member of the calcineurin antagonist class, which blocks calcium-dependent processes. Since 1998, it has been applied to liver transplants [1]. Many studies are still investigating the adverse reactions of immune-suppressive agents, even though their use lowers the chance of organ

rejection. The immunophilin FK506-binding protein attaches to tacrolimus, forming an intricate structure in the process. T cells get blocked and their ability to damage cells decreases as an outcome of this complex's inhibition of calcium-dependent processes. Therefore, antigen presentation is prevented [2]. Numerous adverse effects, such as hepatotoxicity, compromised defenses, diabetes, kidney disease, and heightened vulnerability to severe acute respiratory syndrome coronavirus 2 and other immune-mediated illnesses as a result of immunosuppression, have been documented in organ transplant recipients [3]. When this medication is given to CD-1 mice, oxidative stress or cellular tissue degeneration is linked to elevated blood levels of urea nitrogen, renal creatinine, and free radical production [4]. The therapeutic index of the drug under study is narrow, and its administration, as mentioned, can cause a large number of side effects, extending to the appearance of toxic symptoms in the hepatocytes, cardiac muscle tissue, renal tissue, and cerebrum. However, the degree of damage depends on the dose and duration of administration. Unfortunately, the mechanism behind considering tacrolimus as a mediator of toxicity is still unclear and poorly understood, despite the drug's broad research and the many theories proposed to explain its mechanism of action, such as its metabolite-related toxicity through accelerated cell death and augmented inflammatory conditions [5–7]. Studies have shown that tacrolimus causes pulmonary toxicity, which is associated with morphological alterations and tissue changes such as cellular necrosis [8,9]. Because of its relationship to the digestive system, the liver is a significant organ that is susceptible to the harmful effects of medications, foreign substances, and other chemicals [10]. Cells can alter both biochemical and non-enzymatic responses to lessen the negative effects of foreign chemicals, and they can also digest nutrients high in phytochemicals via pathways akin to those of medications and insecticides [11].

Wheat germ oil enhances antioxidant protection by increasing lipid metabolism in the blood and liver. Rich in vitamin E, healthy fats, and antioxidants, this oil exhibits anti-oxidative activity and reduces DNA damage by neutralizing or balancing the increase in reactive oxygen species (ROS). Additionally, the oil from wheat germ inhibits the synthesis of fatty acids which promote the oxidation of lipids and aids the reactive oxygen species system through tocopherol [12]. Several energy-dependent chemical processes make up the intricate and sophisticated systems that regulate controlled cell death. The inherent, or mitochondrial, mechanism and the external, or killing receptor, pathway are the two primary routes for programmed cell death. Numerous pieces of data suggest that the two routes are interconnected and that molecules in one pathway can influence molecules in the other [13]. Numerous non-receptor stimuli are part

of the endogenous signaling processes that trigger cell suicide. These signals are produced intracellularly and have an immediate impact on targets inside the cell. These are the kinds of things that mitochondria trigger. Both positive and negative intracellular signals are produced by the stimuli that start the intrinsic route. The lack of specific growth regulators, hormones, and cytokines are examples of adverse signals that may end up in the initiation of suicide and the inability of death programs to suppress it. The process of apoptosis induced by mitochondrial dysfunction can be controlled and regulated with the help of the Bax-Bcl2 protein family [14]. Cellular tumor antigen p53 increases gene expression of the BAX protein. The protein in concern provides a role in death triggered by p53. Bcl2 is an apoptosis-inducing gene that is a member of the B-cell lymphoma 2 protein group. It is the first regulator of apoptosis found in living creatures. Bcl2-L-4 is found in the outer membrane of mitochondria, where it inhibits the activity of death proteins and promotes cell survival. Reactive oxygen species (ROS) and ferrocytochrome c, two crucial cell death signals, are released when these proteins, which include BAX and BCL2 antagonist/killer (BAK), engage on the mitochondrial outer surface to cause permeabilization. Bcl2-L-4 and its subordinate protein Bcl-XI are activated by Bcl2, which is activated by BH3-only proteins [15].

The current study aims to identify the effect of treating the livers of male white mice with tacrolimus at a concentration of 0.4 mg/kg for two periods, 14 and 28 days, on the BAX gene that is responsible for regulating the intrinsic pathway of programmed death. Furthermore, it aims to identify the role of Triticum aestivum germ oil in reducing the damage caused by tacrolimus, using immunohistochemistry and molecular techniques.

2. Material and methods:

Animals used in the research

The mice used in the current study were brought from Tikrit University / Tikrit / Iraq. Their number was 40 white male mice, *Mus Musculus* of suitable age. In the animal house of the College of Veterinary Medicine at the University of Mosul in Iraq, the creatures were housed in specialized nylon containers. They were fed the standard and prepared diet according to what was mentioned in [16]. The environmental conditions were suitable for the living conditions of laboratory animals and according to what was mentioned in [16]. The standard laboratory chow consisted of approximately 20% protein, 5% fat, and 55% carbohydrate, with an energy content of ~3.6 kcal/g. The work was carried out under the supervision of the Scientific Research Ethics Committee of the University of Mosul, and all relevant recommendations were implemented.

Preparation of tacrolimus and wheat germ oil for dosing:

The median lethal dose (LD50) was the primary criterion for selecting the tacrolimus (Pancea Biotech, India) (LD50, 138 mg/kg) concentration under study, which is 2 mg /kg of body weight. As for wheat germ oil (NOW company, USA), a 1130 mg/kg of germ wheat oil was used and prepared according to the weight of the experimental animals based on preliminary studies. The appropriate doses of both medications were given to the animals orally. The volume of dose given was (1.3-1.5 ml) depending on the animal's weight. The animals in the present research were split up into four distinct categories as indicated in tables (1 and 2) below:

Table 1: The experimental design for the first experiment is shown.

Groups	**Tacrolimus and Wheat Germ Oil Dose (mg/kg)**	**Experiment Duration (days)**	**Administration Route**	**Number of Animals**
Negative Control	Distilled Water	١٤	Orally	10
Positive Control	Wheat Germ Oil (1130 mg/kg)	١٤	Orally	10
Experimental (1)	Tacrolimus (0.4 mg/kg)	١٤	Orally	10
Experimental (2)	Tacrolimus (0.4 mg/kg) + Wheat Germ Oil (1130 mg/kg)	١٤	Orally	10

Table 2: The experimental design for the first experiment is shown

Groups	**Tacrolimus and Wheat Germ Oil Dose (mg/kg)**	**Experiment Duration (days)**	**Administration Route**	**Number of Animals**
Negative Control	Distilled Water	28	Orally	10
Positive Control	Wheat Germ Oil (1130 mg/kg)	28	Orally	10
Experimental (1)	Tacrolimus (0.4 mg/kg)	28	Orally	10
Experimental (2)	Tacrolimus (0.4 mg/kg) + Wheat Germ Oil (1130 mg/kg)	28	Orally	10

Detection of immunohistochemical reactivity to Bax and Bcl-2 proteins in liver tissue

BAX protein activity was detected in liver tissue and all treated groups in the current study using the BAX Monoclonal Antibody kit (Catalog Number: E-AB-22212) manufactured by Elabscience Bionovation Inc. The steps mentioned in the ready-made diagnostic kit were followed with high accuracy for the purpose of detecting the aforementioned protein in the liver

of male white mice and for all treated groups, and laboratory conditions were taken into account in terms of temperature, humidity, and sterilization.

Numerical Microscopic Evaluation

This Numerical Microscopic Evaluation process refers to determining a degree of importance, either low or high, or creating a numerical scale for the severity of cell reaction and the potential for tumour growth and spread. The process is often used to measure the effect of external toxins or physical factors on living tissues, as well as in cancer cases, based on what was approved by the National Cancer Institute (NCI). Table (3) below was used in the study of histological phenotypic variables [17, 18] in the liver tissue of male albino mice in the current study.

Table (3): Digital Microscopic Evaluation Adopted in the Current Study

Studied Protein	0+	1+	2+	3+	4+
Bax (Tsamandas et al., 2022)	Negative (-) 0 cell/ microscopic field	Weak (+) 1–5 cells/ microscopic field	Positive (+) 6–15 cells/ microscopic field	Strong Positive (++): 16–30 cells/ microscopic field	Very Strong Positive (+++): More than 30 cells/ microscopic field
Bcl2 (Qian et al., 2022)	Negative (-) 0 cell/ microscopic field	Weak (±) 1–7 cells/ microscopic field	Positive (+) 8–20 cells/ microscopic field	Strong Positive (++): 21–50 cells/ microscopic field	Very Strong Positive (+++): More than 50 cells/ microscopic field

Estimation of gene expression of genes encoding BAX and Bcl2 proteins in the liver of male albino mice for periods of 14 and 28 days

Quantitative real-time PCR (qPCR) was performed using a **Step-One-Plus™ Real-Time PCR System (Applied Biosystems, USA)** with the **TransStar® Top Green qPCR Super-Mix Kit**. The amplification reactions were carried out in a **20 µL volume** containing 10 µL of 2× Super-Mix, 1 µL of each forward and reverse primer, variable cDNA template, and nuclease-free water. Each sample was analyzed in **triplicate** to ensure reproducibility. The thermal cycling conditions included an initial denaturation at 94°C for 30 seconds, followed by 45 cycles of

denaturation at 94°C for 5 seconds, annealing at 60°C for 30 seconds, and extension. Melting curve analysis was performed to confirm amplification specificity. Relative gene expression levels of **Bax** and **Bcl-2** were calculated using the **2^–ΔΔCt method**, with β-actin serving as the internal housekeeping gene (Table 4).

Table 4: Primers used in the amplification of Bax and bcl2 genes by qPCR

Primer name	Primer sequence 5' – 3'	Reference
Bax-F	GGGACGAACTGGACAGTAACAT	Kandeil, M. A., Hassanin, K. M., Mohammed, E. T., Safwat, G. M., & Mohamed, D. S. (2018). Wheat germ and vitamin E decrease BAX/BCL-2 ratio in rat kidney treated with gentamicin. Beni-Suef University journal of basic and applied sciences, 7(3), 257-262
Bax-R	GGAGTCTCACCCAACCACCCT	
Bact-F	ATGAGCCCCAGCCTTCTCCAT	
Bact-R	CCAGCCGAGCCACATCGCTC	

The components of the amplification mixture for each gene are described in Table (5) , and the qPCR conditions used to amplify the target genes are listed in

Table (5): Reaction components of qPCR

Components	**Volume (µl)**
Cdna	Variable
Forward primer	1
Reverse primer	1
2× *TransStar*® Top Green qPCR SuperMix	10
RNase-free Water	Up to 20

Table (6): Bax and bcl2 gene transcription is estimated using qPCR settings. Using the 2−ΔΔCT technique, the relative expression levels of bax and bcl2 were determined.

Step	**No. of repetitions**	**High Temperature ºC**	**Period of work**
initial strand separation".	1	94	0:30 sec
unwinding of DNA	٤٥	94	0:5 sec
primer hybridization and DNA synthesis		٦٠	0:٣٠ sec

Statistical Data Analysis

The statistical procedure to assess significant differences between the mean values of digital microscopic assessment across the experimental groups, immunohistochemistry analyses were conducted using SPSS software version 22.0. $P < 0.01$ was taken into consideration as the significance level. A post hoc analysis was performed after a single-factor ANOVA was used to assess the data. To find statistically significant differences between groups at the designated probability level, Duncan's Multiple Range Test was utilized. Regarding qPcr, GraphPad Prism version 10/USA was used for all statistical analysis.

3. Results:

Light microscopic examination of sections of the two groups of livers treated with distilled water (negative control group) and wheat germ oil (positive control group) for 14 days showed a negative reaction (-) in most of the tissue components of the liver (Figures 1, 2). Microscopic examination of liver sections of male albino mice treated with 0.4 mg/kg body weight of tacrolimus showed strong positive (+++) reaction to the antibodies of BAX protein in the cytoplasm of hepatocytes, which appeared as a dark golden color in the cytoplasm of the cells above, (Figure 3).The results also showed a more intense positive reaction (++) from the cytoplasm of hepatocytes from the livers treated the same concentration of tacrolimus (0.4) mg/kg and wheat germ oil towards antibodies to the BAX protein (Figure 4) .

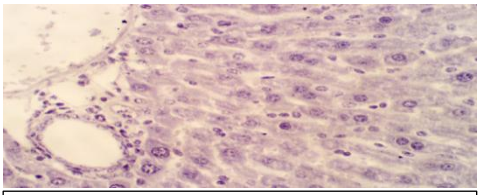


Figure 1: Liver of mice from the 14th day of the experiment, Distiled water (negative contol group) group. Negative reaction is shown in the liver tissue. BAX immunohistochemistry. Magnification 400×.

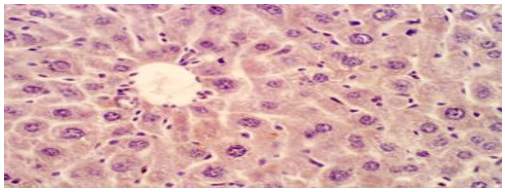


Figure 2: Liver of mice from the 14th day of the experiment, oil group (positive control group). Negative reaction is shown in the liver tissue. BAX immunohistochemistry. Magnification 400×.

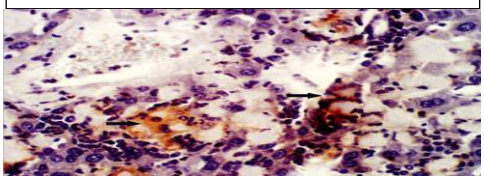


Figure 3: Transverse histological section of the liver of a male albino mouse from the second treatment group over 14 days. It shows a very strong positive reaction (+++) (black arrow) that appeared as a dark gold stain in the cytoplasm. BAX immunohistochemistry. Magnification ×400

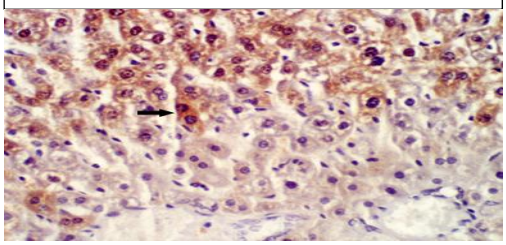


Figure 4: Transverse histological section of the liver of a male albino mouse from the second treatment group with wheat germ oil for 14 days. The positive (+) reaction (black arrow) appears as a dark golden color in the cytoplasm. BAX immunohistochemistry. Magnification ×400.

It was noted through histological reading using a light microscope of liver sections of mice from the negative and positive control groups for 28 days that there was no histological immune response (negative response -) of the components of the liver tissue towards antibodies of the BAX protein (Figures 5, 6).While the liver sections treated with tacrolimus at a concentration of (0.4) mg/kg of body weight showed a very strong positive reaction (+++) in the cytoplasm of the liver cells, which confirms the effect of the drug in increasing the gene expression of this protein through the excessive production of the protein, which was stained with a dark golden brown color in the cytoplasm of the liver cells (Figures ٧).The results also showed a more intense positive reaction (++) from the cytoplasm of hepatocytes from the livers treated with a concentration of tacrolimus (0.4) for 28 days mg/kg and wheat germ oil towards antibodies to the BAX protein (Figure 8).

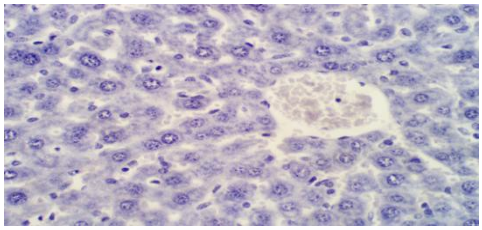


Figure 5: Liver of mice from the second period of the study, negative control set. Demonstrating a negative reaction in liver tissue. BAX

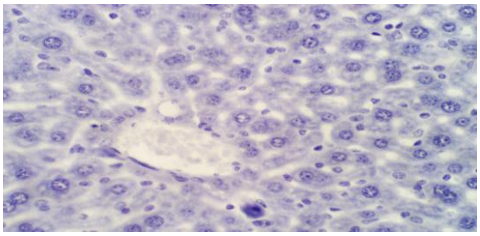


Figure 6: Liver of mice from the second set of the study, oil group. Demonstrating a negative reaction in liver tissue. BAX immunohistochemistry. Magnification 400×.

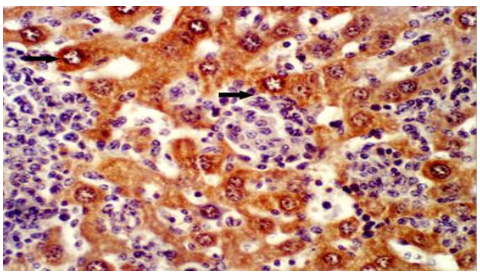


Figure 7: Transverse histological section of the liver of a male albino mouse from the second treatment group over 28 days. It shows a diffuse, strongly positive (+++) reaction (black arrow) that appears as a dark gold stain in the cytoplasm. BAX immunohistochemistry. Magnification ×400.

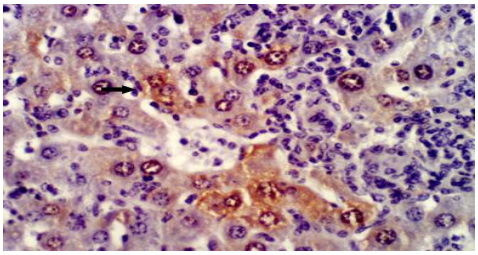


Figure 8: Transverse histological section of the liver of a male albino mouse from the second treatment group with whaeat germ oil for 28 days. The positive (+) reaction (black arrow) appears as a dark golden color in the cytoplasm BAXimmunohistochemistry. Magnification ×400.

The number of reactive hepatocyte cells in the group treated with a concentration of (0.4) mg/kg of tacrolimus for the periods of 14 and 28 days of dosing was considerably greater at the probability level of 0.01>P, according to the results of the digital microscopic evaluation, as indicated in Table (6).

Table (6): Digital Microscopic Evaluation of the Effect of Wheat Germ Oil on the Number of Hepatic Cells Reacting with BAX Protein Antibodies

Group	Treatment (mg/kg)	14 Days	28 Days
Control	Distilled water	0.10 ± 0.02 E	0.11 ± 0.01 E
Wheat Germ Oil	1130	0.11 ± 0.01 E	0.11 ± 0.04 E
Tacrolimus	0.4	3.51 ± 0.11 A	3.90 ± 0.36 A
Tacrolimus + Wheat Germ Oil	0.4 + 1130	2.47 ± 0.24 B	2.93 ± 0.27 B

Different vertical letters mean significant differences at a probability level of $P \leq 0.01$

Immunohistochemical staining for Bcl-2 protein revealed a weak or negative reaction in liver sections of mice treated with tacrolimus alone, indicating suppression of the anti-apoptotic pathway. In contrast, the wheat germ oil group showed stronger Bcl-2 reactivity, and the combined tacrolimus + wheat germ oil group exhibited moderate expression, suggesting a partial protective effect of the oil in restoring Bcl-2 activity.

Transcription and Translation of the Apoptosis Regulator Bax in the Liver Cells

The findings demonstrated that the livers of male albino rats had higher levels of the BAX gene, which in turn led to higher levels of BAX protein transcription in the group of animals that received wheat germ oil treatment (positive control). In comparison with the untreated and wheat germ oil-treated groups, the tacrolimus-treated group exhibited a greater gene production rate for this protein at the selected dose. Over the period of 14 days, the transcription and translation of the indicated gene were lower in the group treated with the researched drug alone, greater in the group treated with wheat germ oil and the selected medication than in the negative control group. In contrast to the negative control group, findings for the same treatments described above, but for 28 days, revealed a slight decrease in the liver's expression of the mentioned gene. Comparing the group treated with tacrolimus at the examined dose to the negative control group, findings similarly revealed a major rise in the translation and transcription rate of the studied gene (Figure 9). The rate of activity was comparable to that of the unaltered group (Figure 10).

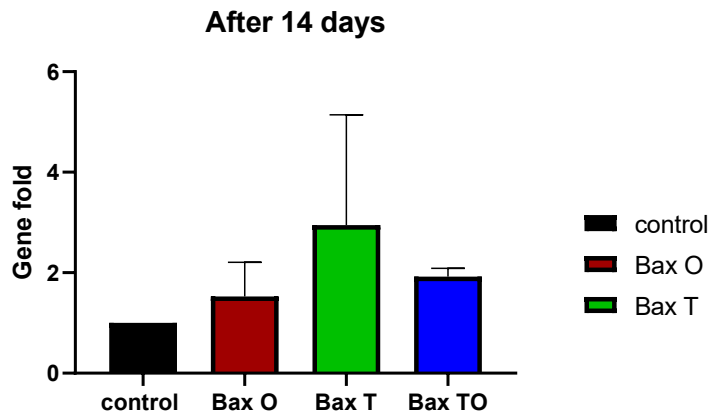


Figure 9: The gene expression of the Bax gene using q PCR technique is shown for all studied treatments. Control means the distilled water group, Bax O : wheat germ oil group, Bax T: tacrolimus group (0.4mg/kg), and Bax TO: Tacrolimus wheat germ oil group.Period of treatment: 14 days .

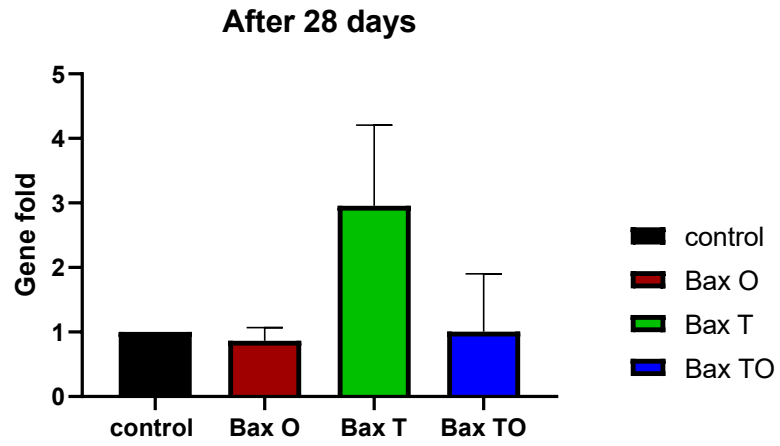


Figure 10: The gene expression of the Bax gene using q PCR technique is shown for all studied treatments. Control means the distilled water group, Bax O: wheat germ oil group, Bax T: tacrolimus group (0.4mg/kg), and Bax TO: Tacrolimus wheat germ oil group.Period of treatment: 28 days.

To better evaluate the balance between pro-apoptotic and anti-apoptotic signaling, the **Bax/Bcl-2 ratio** was calculated from qPCR data. Tacrolimus treatment significantly increased the Bax/Bcl-2 ratio compared with the control ($P \leq 0.01$), reflecting a shift towards apoptosis. Conversely, wheat germ oil markedly reduced this ratio, and in the tacrolimus + wheat germ

oil group, the ratio approached values closer to the control, indicating a protective modulation of apoptotic signaling by the antioxidant oil.

4. Discussion

Previous results showed that there is a positive response of the cytoplasm of hepatocytes to antibodies to the BAX protein in livers treated with tacrolimus (0.4 mg/kg) at the selected concentration and periods. The aforementioned results were consistent with what was stated by [19], who reported that livers treated with moderate concentrations of tacrolimus cause an increase in the production of the aforementioned protein. Current scientific findings are similar to what was mentioned by [20], that immunosuppressants, including the drug under study, when used for therapeutic purposes in living cells, including human liver cells, stimulate cell death and thus incite the occurrence of cell inflammation. Tacrolimus has side effects, including neurotoxicity, liver toxicity, and kidney toxicity, in addition to its induction of programmed cell death. The researchers identified this by using the TUNL test to detect this phenomenon.

These results are in line with recent research since the medication binds to molecules of protein phosphatase 2B (PP2B), which is involved in PIP catabolism, phosphotransferase activity, and cell protein synthesis [21]. This drug causes or can cause the production of types of free radicals, including OH radicals, O_2^-, and dihydrogen dioxide, and induces or stimulates programmed cell death, which in turn is due to the impairment of the functions of both mitochondrial and T cell functions [22]. The current results in terms of the drug's induction of programmed death are similar to what was mentioned by [23], and somewhat inconsistent with [24], who reported that immunosuppressants, when used in in vitro studies of human cells, inhibit the construction of hydrolyzed collagen without affecting the gene expression of collagen mRNAs, at a rate of 2 mg/kg. The present findings support [25], who demonstrated how the selected medication raises the production of the Caspase 3 protein in white rats. The data presented above showed that wheat germ oil had a beneficial effect on boosting Bax activity, the main suicide initiator. As the length of treatment against tacrolimus-induced damage grew, so did the severity of the response. The current results do not agree with [26], who showed that combining wheat germ oil with fluoxetine caused a negative cytoplasmic response to BAX protein in rat testicular tissue. This might be because of the oil's high vitamin E concentration, which strengthens its defenses against fluoxetine-induced apoptosis. Because wheat germ oil has anti-apoptotic characteristics, it plays a crucial part in the current investigation [27].

The scientific outcomes of the current study are similar to [28]. By regulating redox imbalance, apoptosis, swelling, and detrimental apoptotic pathways, the oil protected against kidney and liver failure at the physiological and cellular levels. Elainic, omega-6, and omega-3 fatty acids in wheat germ oil contribute to its beneficial impacts by promoting tocopherol-mediated antioxidant mechanisms and inhibiting eicosanoid synthesis, thereby reducing lipid peroxidation, inflammation, and apoptosis [29]. By decreasing the translation and transcription of genes that trigger cell death in rats exposed to toxins, one study demonstrated the anti-pro-apoptotic action of wheat germ oil [30].

The recent findings showed an increase in Bax transcription in livers treated with tacrolimus and a decrease in its activity in the tacrolimus + wheat germ oil group. This is consistent with [31], who showed that tacrolimus injections increased BAX expression in the hippocampus, and inflammation further enhanced this activity. Excessive ROS accumulation was highlighted by [32] as a key inducer of apoptosis via DNA damage, while [33] indicated that oxidative stress impairs cellular homeostasis.

The results of the current study, showing suppressed Bax expression with wheat germ oil, align with [34], who found that Nargencin A inhibited apoptosis proteins induced by tacrolimus. This is also consistent with [35], who reported that antioxidant phenolics such as those in green tea reduce tacrolimus toxicity. Similarly, [36] showed wheat germ oil has strong anti-apoptotic effects by regulating BAX and BCL2 gene expression in kidney cells. Finally, other authors emphasized wheat germ oil's richness in tocopherol and polyunsaturated fatty acids, reinforcing its protective roles [37,38].

5. Conclusions

Based on the latest study's achievements, we draw the conclusion that excessive levels of immunosuppressants harm hepatic cells' microcellular pathways and promote programmed death by raising the activity of the protein that triggers programmed death via the intrinsic pathway Bax. However, the recent study demonstrated that certain plant items with antioxidant activity, such as wheat germ oil, can reverse the detrimental effect of this medicine.

6. References

[1] Lin YC, Tsai CS, Li IH, Tsai YT, Huang TY, Lee KF, Kao LT. Transplant recipients using tacrolimus had higher utilization of healthcare services than those receiving

cyclosporine in Taiwan. *Front Pharmacol*. 2019;10:1074. doi:10.3389/fphar.2019.01074

[2] Akhtar T, Ali G, Sheikh N. Immunosuppressant-induced oxidative stress and iron: a paradigm shift from systemic to intrahepatic abnormalities. *Oxid Med Cell Longev*. 2020;2020:8675275. doi:10.1155/2020/8675275

[3] Ben-Fredj N, Hannachi I, Chadli Z, Ben-Romdhane H, Boughattas NA, Ben-Fadhel N, et al. Dosing algorithm for Tacrolimus in Tunisian kidney transplant patients: Effect of CYP3A4*1B and CYP3A4*22 polymorphisms. *Toxicol Appl Pharmacol*. 2020; 407:115245. doi: 10.1016/j.taap.2020.115245

[4] Oyouni AAA, Saggu S, Tousson E, Rehman H. Immunosuppressant drug tacrolimus induced mitochondrial nephrotoxicity, modified PCNA and Bcl-2 expression attenuated by *Ocimum basilicum* L. in CD1 mice. *Toxicol Rep*. 2018; 5:687–694. doi: 10.1016/j.toxrep.2018.06.003

[5] Liu Z, Yuan X, Luo Y, He Y, Jiang Y, Chen ZK, Sun E. Evaluating the effects of immunosuppressants on human immunity using cytokine profiles of whole blood. *Cytokine*. 2009;45(2):141–147. doi: 10.1016/j.cyto.2008.12.003

[6] Kim HS, Lim SW, Jin L, Jin J, Chung BH, Yang CW. The protective effect of febuxostat on chronic tacrolimus-induced nephrotoxicity in rats. *Nephron*. 2017;135(1):61–71. doi:10.1159/000449289

[7] Tron C, Lemaitre F, Verstuyft C, Petitcollin A, Verdier MC, Bellissant E. Pharmacogenetics of membrane transporters of tacrolimus in solid organ transplantation. *Clin Pharmacokinet*. 2019; 58:593–613. doi:10.1007/s40262-018-0717-7

[8] Goralczyk AD, Bari N, Abu-Ajaj W, Lorf T, Ramadori G, Friede T, et al. Calcineurin inhibitor sparing with mycophenolate mofetil in liver transplantation: a systematic review of randomized controlled trials. *Am J Transplant*. 2012;12(10):2601–2607. doi:10.1111/j.1600-6143.2012. 04157.x

[9] Akhtar T, Sheikh N, Shan T, Ghazanfar R. Tacrolimus induced nephrotoxicity and pulmonary toxicity in Wistar rats. *J Biol Regul Homeost Agents*. 2017;31(4):1061–1066. Available from: https://www.researchgate.net/publication/321946880

[10] Arafa UA, Fujiwara Y, Higuchi K, Shiba M, Uchida T, Watanabe T, et al. No additive effect between *Helicobacter pylori* infection and portal hypertensive gastropathy on inducible nitric oxide synthase expression in gastric mucosa of cirrhotic patients. *Dig Dis Sci*. 2003; 48:162–168. doi:10.1023/A:1021707103590

[11] Panemangalore M, Bebe FN. Short-and long-term exposure to low levels of pesticide and flavonoid mixtures modify endogenous antioxidants in tissues of rats. *J Environ Sci Health B*. 2009;44(4):357–364. doi:10.1080/03601230902801034

[12] Field R, Verghese M, Walker LT, Panala V, Shackelford L, Boateng J. Feeding wheat germ meal and wheat germ oil reduced azoxymethane-induced aberrant crypt foci. *Int J Cancer Res*. 2008;4(4):127–136. doi:10.3923/ijcr.2008.127.136

[13] Igney FH, Krammer PH. Death and anti-death: tumour resistance to apoptosis. *Nat Rev Cancer*. 2002;2(4):277–288. doi:10.1038/nrc776

[14] Cory S, Adams JM. The Bcl2 family: regulators of the cellular life-or-death switch. *Nat Rev Cancer*. 2002;2(9):647–656. doi:10.1038/nrc883

[15] Hardwick JM, Soane L. Multiple functions of BCL-2 family proteins. *Cold Spring Harb Perspect Biol*. 2013;5(2): a008722. doi:10.1101/cshperspect. a008722

[16] Salah BA. Histopathological effect of fluoxetine drug on the brain of pregnant mice and their embryos. *Iraqi J Vet Sci*. 2020;34(1):71–76. Available from: https://web.archive.org/web/20201106084938id_/https://vetmedmosul.com/article_164198_acc17628f36302ee674334ab632ce9f0.pdf

[17] Tsamandas AC, Thomopoulos K, Zolota V, Kourelis T, Karatzas T, Ravazoula P, et al. Potential role of bcl-2 and bax mRNA and protein expression in chronic hepatitis type B and C: a clinicopathologic study. *Mod Pathol*. 2003;16(12):1273–1288. doi:10.1097/01.MP.0000097367.56816.5E. PMID:14681329

[18] Qian S, Wei Z, Yang W, Huang J, Yang Y, Wang J. The role of BCL-2 family proteins in regulating apoptosis and cancer therapy. *Front Oncol*. 2022; 12:985363. doi:10.3389/fonc.2022.985363

[19] Love S, Mudasir MA, Bhardwaj SC, Singh G, Tasduq SA. Long-term administration of tacrolimus and everolimus prevents high cholesterol-high fructose-induced steatosis in C57BL/6J mice by inhibiting de-novo lipogenesis. *Oncotarget*. 2017;8(69):113403. Available from: https://pmc.ncbi.nlm.nih.gov/articles/PMC5768335/pdf/oncotarget-08-113403.pdf

[20] Lim EJ, Chin R, Nachbur U, Silke J, Jia Z, et al. Effect of immunosuppressive agents on hepatocyte apoptosis post-liver transplantation. *PLoS One*. 2015;10(9): e0138522. doi: 10.1371/journal.pone.0138522

[21] Naesens M, Kuypers DRJ, Sarwal M. Calcineurin inhibitor nephrotoxicity. *Clin J Am Soc Nephrol*. 2009;4(2):481–508. doi:10.2215/CJN.04800908

[22] Nash A, Samoylova M, Leuthner T, Zhu M, Lin L, Meyer JN, et al. Effects of immunosuppressive medications on mitochondrial function. *J Surg Res*. 2020; 249:50–57. doi: 10.1016/j.jss.2019.12.010

[23] Choi H, Baek K. Pro-apoptotic and anti-apoptotic regulation mediated by deubiquitinating enzymes. *Cell Mol Life Sci*. 2022; 79:117. doi:10.1007/s00018-022-04132-5

[24] Manojlovic Z, Blackmon J, Stefanovic B. Tacrolimus (FK506) prevents early stages of ethanol-induced hepatic fibrosis by targeting LARP6 dependent mechanism of collagen synthesis. *PLoS One*. 2013;8(6): e65897. doi: 10.1371/journal.pone.0065897

[25] Ibrahim S, Mousa A, Riawan W. Expression of AIF and Caspase-3 in New Zealand rabbit with cervical spondylosis myelopathy model. *Ann Med Surg*. 2021; 69:102604. doi: 10.1016/j.amsu.2021.102604

[26] Fawzy HM, Mahmoud FA. Histological protective effect of wheat germ oil versus zinc on fluoxetine–damaged testes in albino rats. *Ain Shams Med J*. 2023;74(3). Available from: https://asmj.journals.ekb.eg/article_321859

[27] Abdou HM, Mohamed NA, El Mekkawy AD, ElHengary SB. Vitamin E and/or wheat germ oil supplementation ameliorate oxidative stress induced by cadmium chloride in pregnant rats and their fetuses. *Jordan J Biol Sci*. 2017;10(1):39–48. Available from: https://jjbs.hu.edu.jo/files/v10n1/Paper%20number%208.pdf

[28] Elgendy SA, Baloza SH, Mohammed LA, Nasr HE, El-Shaer NO, Ghamry HI, et al. Ameliorative impacts of wheat germ oil against ethanol-induced hepatic and renal dysfunction in rats: involvement of anti-inflammatory, anti-apoptotic, and antioxidant signaling pathways. *Life*. 2022;12(10):1671. doi:10.3390/life12101671

[29] Alessandri C, Pignatelli P, Loffredo L, Lenti L, Del Ben M, Carnevale R, et al. Alpha-linolenic acid–rich wheat germ oil decreases oxidative stress and CD40 ligand in patients with mild hypercholesterolemia. *Arterioscler Thromb Vasc Biol*. 2006;26(11):2577–2578. doi: 10.1161/01.ATV.0000242795. 08322.fb

[30] Mohamed MA, Ahmed MA. Apoptotic genes expression in γ-irradiated rats treated with wheat germ oil, zinc and/or bone marrow. *Int J Basic Appl Sci*. 2014;3(4):451–456. doi:10.14419/ijbas. v3i4.3657

[31] Badr R, Hashemi M, Javadi G, Movafagh A, Mahdian R. Assessment of global ischemic/reperfusion and tacrolimus administration on CA1 region of hippocampus:

gene expression profiles of BAX and BCL2 genes. *Bratisl Lek Listy*. 2016;117(6):358–362. doi:10.4149/bll_2016_071

[32] Pizzino G, Irrera N, Cucinotta M, Pallio G, Mannino F, Squadrito F, et al. Oxidative stress: harms and benefits for human health. *Cell Prolif*. 2017;50(1): e12335. doi:10.1111/cpr.12335

[33] Sosa MS, Debnath J, Aguirre-Ghiso JA. Regulation of tumor cell dormancy by tissue microenvironments and autophagy. *Adv Exp Med Biol*. 2013; 734:73–89. doi:10.1007/978-1-4614-1445-2_5

[34] Park C, Kwon DH, Hwang SJ, Han MH, Jeong JW, Hong SH, et al. Protective effects of Nargenicin A1 against tacrolimus-induced oxidative stress in Hirame natural embryo cells. *Int J Environ Res Public Health*. 2019;16(6):1044. doi:10.3390/ijerph22050773

[35] Song J, Kim J, Jang H. Ferulic acid released by treatment with *Aspergillus oryzae* contributes to the cellular antioxidant capacity of wheat germ extract. *Food Sci Biotechnol*. 2014;23(4):1327–1333. doi:10.1007/s10068-014-0182-5

[36] Kandeil MAM, Hassanin KMA, Mohammed ET, Safwat GM, Mohamed DSh. Wheat germ and vitamin E decrease BAX/BCL-2 ratio in rat kidney treated with gentamicin. *Beni-Suef Univ J Basic Appl Sci*. 2018;7(3):257–262. doi: 10.1016/j.bjbas.2018.02.001

[37] Rizzello CG, Coda R, De Angelis M, Gobbetti M. Effect of sourdough fermentation on stabilisation, and chemical and nutritional characteristics of wheat germ. *Food Chem*. 2010; 119:1079–1089. doi: 10.1016/j.foodchem.2009.08.016

[38] Gelmez N, Kıncal SN, Yener ME. Antioxidant activities and phenolic contents of roasted wheat germ extracts. *J Supercrit Fluids*. 2009;48(3):217–224. doi: 10.1016//j.supflu.2008.11.002.

Al-Kitab Journal for Pure Sciences (2026); 10(2):104-115.
https://doi.org/10.32441/kjps.10.2.p8

Al-Kitab Journal for Pure Sciences
ISSN: 2617-1260 (print), 2617-8141(online)

https://isnra.net/index.php/kjps

Chemical and Bacteriological Evaluation of Water Quality in some Water Treatment Units in Diyala Governorate

Zainab Esmail Sadeq[1], Hiba Shihab Ahmed[2], Hawraa Hussein Khudhayer[3]

[1,3] Department of Chemistry, College of Science, University of Diyala, Iraq.

[2]Department of Chemistry, College of Education for Pure Science, University of Diyala, Iraq

Corresponding Author: hiba.s.ahmed@uodiyala.edu.iq

Citation: ***Zainab Esmail Sadeq[1], Hiba Shihab Ahmed[2], Hawraa Hussein Khudhayer[3]*. Chemical and Bacteriological Evaluation of Water Quality in some Water Treatment Units in Diyala Governorate.**
Al-Kitab J. Pure Sci. [Internet]. 2025 Oct. 24 ;10(2):104-115
DOI.
https://isnra.net/index.php/kjps/article/view/2026.
https://doi.org/10.32441/kjps.10.2.p8

Keywords: Environmental Pollutants, Heavy metals, Water Quality.

Article History
Received 07 Sep. 2025
Accepted 24 Oct. 2025
Available online 01 Nov. 2026

©20--. THIS IS AN OPEN-ACCESS ARTICLE UNDER THE CC BY LICENSE
http://creativecommons.org/licenses/by/4.0/

Abstract:

The purpose of this study is to assess the water quality at a few Diyala Governorate water treatment facilities, taking into account factors like pH, electrical conductivity, heavy metals, and some dangerous bacteria. It also assessed the effectiveness of a few water treatment facilities, where samples were subjected to chemical and biological analyses both before omit and following water treatment. Five water treatment facilities located in Abu Saida, Dhubab, Awasheq, Zherat, and Jabinat are included in this study. In December 2022, water samples were collected from the Iraqi Diyala Governorate. Certain heavy metal concentrations were found to be higher than the limits set by the World Health Organization (WHO). All water treatment facilities had lead and cadmium concentrations above the allowable level of 0.01 and 0.003 parts per million, respectively. At each site under study, the pH and electrical conductivity levels fell within the WHO-established acceptable ranges. Nine different types of bacteria were isolated using the centrifugation method to assess the bacterial component of this study. *Streptococcus faecalis* was found in all water stations. Whereas Salmonella Typhi was found at Zherat and Jabinat stations and *Escherichia coli* was found at Abu Saida station.

In addition to raising public awareness about adhering to WHO water regulations to ensure public health, this study suggested that periodic monitoring and examination of water treatment plants in Diyala Governorate be carried out.

Keywords: Environmental Pollutants, Heavy metals, Water Quality.

التقييم الكيميائي والبكتريولوجي لنوعية المياه في بعض وحدات معالجة المياه في محافظة ديالى

زينب إسماعيل صادق[١]، هبه شهاب احمد[٢]، حوراء حسين خضير[٣]

[١،٣]جامعة ديالى كلية العلوم، العراق.

[٢]جامعة ديالى,كلية التربية للعلوم الصرفة، العراق.

الايميل الرسمي: [1]zainabismail@uodiyala.edu.iq,[2]hiba.s.ahmed@uodiyala.edu.iq,[3]hawraahussein@uodiyala.edu.iq

الخلاصة:

ان الهدف من هذه الدراسة هو تقييم جودة المياه في بعض من مرافق معالجة المياه في محافظة ديالى، اخذين بنظر الاعتبار الرقم الهيدروجيني، والتوصيل الكهربائي، والمعادن الثقيلة، وبعض البكتيريا الخطرة. كما قيمت الدراسة فعالية عدد من مرافق معالجة المياه، حيث خضعت العينات للتحليلات الكيميائية والبيولوجية قبل وبعد معالجة المياه. وقد شملت هذه الدراسة خمسة مرافق لمعالجة المياه تقع في أبو صيدا وذباب وعواشق وزهيرات وجابينات. تم جمع عينات المياه في محافظة ديالى العراقية في شهر كانون الأوَّل عام ٢٠٢٢. واشارت النتائج الى أن تراكيز بعض المعادن الثقيلة أعلى من المعدل المسموح بموجب لوائح منظمة الصحة العالمية (*WHO*). وكان تركيز الرصاص والكاديوم في جميع مرافق معالجة المياه أعلى من المستوى المسموح به وهو ٠,٠١ و٠,٠٠٣ جزء من المليون على التوالي. وفي كل موقع من المواقع قيد الدراسة، كانت مستويات الرقم الهيدروجيني والتوصيل الكهربائي ضمن النطاقات المقبولة التي حددتها منظمة الصحة العالمية. تم عزل تسعة أنواع مختلفة من البكتيريا باستخدام طريقة الطرد المركزي لتقييم المكون البكتيري لهذه الدراسة. وُجِدت البكتريا العقدية البرازية (*Streptococcus faecalis*) في جميع محطات المياه بينما وجدت المكورات العنقودية الذهبية في محطتي الزهيرات والجبانات، كما وجدت الإشريكية القولونية في محطة أبو صيدا. فضلا عن مقترح رفع الوعي الثقافي حول الالتزام بلوائح منظمة الصحة العالمية المتعلقة بالمياه لضمان الصحة العامة، اقترحت هذه الدراسة إجراء مراقبة وفحص دوري لمحطات معالجة المياه في محافظة ديالى.

الكلمات المفتاحية: المعادن الثقيلة، الملوثات البيئية، جودة المياة.

1. Introduction:

Safe drinking water supply is still a major problem, especially in developing countries. Water-related problems have gotten worse due to rapid population increase and rising daily water use. At the same time, ongoing industrial development has greatly increased water contamination, making it hazardous to human health [1]. Water is one of the most important

chemicals for life. Its ability to dissolve organic chemicals, salts, inorganic substances, and gasses involved in metabolic processes is a result of its universal solvent feature. As a result, water is essential for sustaining membrane integrity, sustaining macromolecules, ensuring homeostasis, permitting material transit, and controlling body temperature **[2].** Certain metals are necessary micronutrients needed for a variety of biological processes, including copper (Cu), iron (Fe), manganese (Mn), nickel (Ni), and zinc (Zn). Other metals, such as cobalt (Co), lead (Pb), and cadmium (Cd), may be hazardous and have no recognized physiological function **[3].** Moreover, both natural processes like the weathering of rocks and soils and human activity can introduce these metals into water supplies **[4].** Through bioaccumulation and bioconcentration throughout the aquatic food chain, heavy metal pollution of water puts aquatic creatures at risk, putting consumers at risk **[5].** The discharge of hazardous metals, which pose enormous threats to ecosystems and human health, is largely caused by industrial and agricultural operations. Metals, especially those from human activity, are regarded as main contaminants in many aquatic habitats **[6].** Additionally, drinking water pollution by microorganisms is a serious problem. To guarantee adherence to the drinking water standards established by global organizations like the World Health Organization [WHO], water samples are therefore examined in specialist laboratories.

Finding harmful bacteria in drinking water is a top priority for the Environmental Protection Agency (EPA) and other regulatory agencies. The membrane filtering method is one of the most promising and successful methods for identifying different types of bacteria **[7].** Human and animal waste, as well as effluent from poorly planned, mislocated, misinstalled, or poorly maintained septic systems and residential lagoons, can all contribute to bacterial pollution in drinking water sources. Bacterial contamination is particularly common in older water supply systems, notably cisterns, spring-fed systems, and dug wells. Crucially, neither taste nor odor nor visual inspection can identify the presence of bacteria in water. Testing in a lab by qualified experts is the only trustworthy way to find out if drinking water is bacterially polluted. Although bacteria are present in all natural water, their presence alone does not always indicate a health risk. Water becomes unfit for human consumption when pathogenic, or disease-causing, microorganisms are present. Routine microbial testing typically includes screening for total coliform bacteria, fecal coliforms, *Escherichia coli (E. coli),* and heterotrophic bacteria **[8].**

Long used as markers of the microbiological quality of drinking water, coliform bacteria are members of the *Enterobacteriaceae* family and include genera like *Enterobacter, Klebsiella, Citrobacter, and Escherichia coli.* These bacteria are normally prevalent in fecal waste and

are naturally present in the intestinal flora of humans and other warm-blooded animals. Even though the majority of coliform strains are not thought to be harmful, their presence in water can nevertheless indicate possible contamination. Furthermore, many coliform species can survive and reproduce in the environment, which occasionally results in their detection in water sources that aren't directly contaminated by feces. The existence of waterborne pathogens or fecal contamination is not always confirmed by the presence of coliform bacteria in the water **[9].** The problems associated with drinking …drinking water quality and quantity in Iraq have worsened significantly in …in the last few years. The ongoing water crisis has been caused by a number of factors, including pollution, population growth, climate change, poor water management, and deteriorating infrastructure **[10].** Access to adequate and safe drinking water is still a major issue in many places, including Diyala Governorate, especially in rural and underserved areas **[11].** Despite the urgency of the issue, comprehensive studies and reliable data about the microbiological composition and environmental circumstances of Diyala's water treatment facilities are noticeably absent. **[12].** The majority of reports that are currently available either concentrate on overall water availability or offer scant microbiological evaluations without taking seasonal fluctuations or chemical profiles into account **[13].**

Problems with the quantity and quality of drinking water in Iraq have gotten worse. This study was conducted to investigate some of the chemical characteristics and bacterial contamination of water supply stations in Diyala governorate due to the lack of sufficient studies and information about the local water stations' microbial diversity and environmental characteristics.

2. Material and methods:

Despite the seriousness of the case, comprehensive studies and reliable information about the microbiological composition and environmental circumstances of Diyala's water treatment facilities are noticeably absent.

Symbols of Stations: 1,2 - ABU SAIDA 3,4 - DHUBAB 5,6 – AWASHEQ 7,8 – ZHERAT 9,10 – JABINAT.

The samples

In December 2022, samples were collected from five unique drinking water stations located in the Diayla governorate of Iraq (Abu saida, Dhubab, Awasheq, Zherat and Gebinat). Water samples have been collected using glass bottles that have been sterilized. A sample of

1000 milliliters of water was gathered and brought to the Department of Chemistry's laboratory at Diayla University of Science in Iraq.

Chemical analysis

Chemical analysis of water samples is done by dividing each sample into three portions and performing three chemical tests (PH, heavy metals and electrical conductivity). After calibrating the meter equipment (PH WTW, 7110) with standard solutions, every water sample was subjected to chemical testing utilizing a PH meter equipment and a flame atomic absorption spectrometry device, and electrical conductivity apparatus, as well as microbiologically by the use of Centrifugation method. The findings of the measurement of the acidic function at laboratory temperature are displayed in (**Table1)**. To ascertain ion concentration ratio in these water samples, an electrical conductivity instrument (Pw-9526-Digital Conductivity meter) was utilized, and following Using standard solutions for calibration Laboratory-temperature measurements of electrical conductivity are displayed in (**Table1**). A standard was utilized to calibrate the flame atomic absorption spectrometry apparatus (AA-UN.BG.IBN-H. C.S.L.), Table 3 displays the solutions and outcomes **[14].**

Microbiological evaluation

The samples are randomly collected from tanks before settling and placed in special test tubes. Avoid leaving them at high temperatures or under sunlight, and ensure that the sample does not come into contact with the surrounding environmental conditions. Subsequently, work is done in the laboratory to tabulate and label the samples to differentiate between them. The samples are then sedimented by placing them in a centrifuge to obtain all solid contents, germs and microbes if present. Then we filter the samples using special filter paper to collect the sample sediment. After that, we divide the sample into two parts. The first part is placed on a previously prepared blood agar culture medium, and the second part is placed on another differential culture medium prepared in advance such as macconkey agar, while maintaining the cleanliness of the work site and tools used. The work is done inside a hood. These cultures media are placed in an incubator at a temperature of 37°C for 24-48 hours to ensure the growth of any biological cells inside the culture medium. After that, the result is read using special determinants and detectors to determine the type of parasite, fungus or bacteria that grew on this medium, if any. The results are recorded every 12 hours to determine the biological activity inside the dish.

3. Results and discussion

PH and Electrical Conductivity Measurement

The values of the acidic function were (7.3 and 7.1) at Abu Saida station before and after treatment respectively, (7.15 and 6.5) at Dhubab station, (6.87 and 6.7) at Awasheq station, (6.83 and 6.75) at Zherat station and (7.1 and 7) at Jabinat station. All of these samples fell within the acceptable pH range set by the US Environmental Protection Agency (USEPA)[15] (6.5-8.5) (Table1) .The ratio of ions in these water samples was ascertained using electrical conductivity; the electrical conductivity results were (638 and 643 µs/Cm) at Abu Saida station before and after treatment respectively, (654 and 656 µs/Cm) at Dhubab station, (618 and 620 µs/Cm) at Awasheq station, (606 and 636 µs/Cm) at Zherat station and (556 and 555 µs/Cm) at Jabinat station. According to the WHO manual, these values fell between medium and good, as shown in (Table 2).

Table 1: water samples' useful PH and conductivity.

Sample No.	Water Station	PH meter	Condactivity µS/Cm
1	Abu Saida (B)	7.3	638
2	Abu Saida (A)	7.1	643
3	Dhubab (B)	7.15	654
4	Dhubab (A)	6.5	602
5	Awasheq (B)	6.87	618
6	Awasheq (A)	6.7	620
7	Zherat (B)	6.83	606
8	Zherat (A)	6.75	636
9	Jabinat (B)	7.1	556
10	Jabinat (A)	7	555

Table 2: The WHO handbook describes the electrical conductivity of water.

No.	Conductivity µS/Cm	Water quality
1	50-400	Excellent
2	400-750	Good
3	750-1500	Medium
4	> 1500	Water with high metal

Heavy Metals Measurement

When consumed in excess, a number of heavy metals have detrimental effects on human health, making them hazardous. Human health is at risk from heavy metals because these are tenacious by nature and likely to accumulate in biological systems **[16].** An apparatus that uses flame atomic absorption spectrometry was used to examine water samples in order to find the amounts of heavy components in these samples, and the outcomes for each component were as follows in **(Table 3)**: lead was (0.017 and 0.016) at Abu Saida station before and after treatment, (0.028 and 0.026) at Dhubab station, (0.017 and 0.016) at Awasheq station, (0.014 and 0.013) at Zherat station and (0.013 and 0.012) at Jabinat station. Children are especially vulnerable to lead exposure because of their permeable blood-brain barrier and rapid gastric absorption, that causes neurotoxic consequences Peripheral neuropathy, an indirect cardiac effect, renal tubular injury, and reproductive issues are all present even at modest exposure levels **[17].** Cadmium was (0.013 and 0.012) at Abu Saida station before and after treatment, (0.016 and 0.015) at Dhubab station, (0.009 and 0.008) at Awasheq station, (0.008 and 0.007) at Zherat station and (0.006 and 0.005) at Jabinat station. Apart from water, the two main sources of Cd are diet and cigarette smoking. Cd builds up in the kidney and Long-term liver exposure to cadmium combined with deficits in calcium, iron, zinc, protein, fat, and vitamin D **[18].** Mercury was (0.0002 and 0.0001) at Abu saida station before and after treatment, (0.0005 and 0.0004) at Dhubab station, (0.0002 and 0.0002) at Awasheq station, (0.0002 and 0.0001) at Zherat station and (0.0001 and 0.0001) at Jabinat station. Through oxidative stress and enzyme interference, mercury damages the neurological, renal, immunological, cardiovascular, and reproductive systems, even at low exposure levels. It is regarded as one of the most dangerous substances in the world, and its consequences can range from liver and kidney damage to developmental brain impairment **[19].** Elevated concentration of cadmium and lead have been detected in some drinking water stations, exceeding the permissible limits established by the World Health Organization (WHO) **[20].**

Table 3: The mean amount of heavy metals present in water

Sample no.	Station	Pb (ppm)	Cd(ppm)	Hg(ppm)
1	Abu saida (B)	0.017	0.013	0.0002
2	Abu saida (A)	0.016	0.012	0.0001
3	Dhubab (B)	0.028	0.016	0.0005
4	Dhubab (A)	0.026	0.015	0.0004
5	Awasheq (B)	0.017	0.009	0.0002

6	Awasheq (A)	0.016	0.008	0.0002
7	Zherat (B)	0.015	0.008	0.0002
8	Zherat (A)	0.014	0.007	0.0001
9	Jabinat (B)	0.013	0.006	0.0001
10	Jabinat (A)	0.012	0.005	0.0001

Biological Activity Measurement

The study was conducted on five water samples taken from water purification and treatment plants in Diyala Governorate as shown in the **Table 4 and 5**. The samples were taken from water stores before treatment and from treated water stores before pumping it to homes. The samples were transferred into special test tubes and protected from contamination during transport. The study showed the presence of some types of pathogenic and non-pathogenic bacteria in the water before treatment for example Escherichia coli, Staphylococcus aureus and Streptococcus (S. faecalis). The presence of non-pathogenic bacteria in the water is evidence of contamination of the main water sources with animal or human feces. After examining the water treated by the aforementioned stations, shown in the table below, it was found that some stations purify the water with biological pollutants using special technologies as in Abu Saida and Dhubab stations, while other stations do not operate with the required efficiency to purify water from biological pollutants that threaten human health as in Awasheq station. While some types of bacteria were treated in some stations and others were not treated as in Zherat and Jabinat stations. Numerous studies in this field mention that bacteria are present in every water. Bacteria do not necessarily indicate that water is dangerous. to consume only pathogens, which are bacteria that cause disease. In general, total coliform bacteria are not dangerous. Escherichia coli bacteria and fecal coliforms suggest that the water may contain additional microorganisms linked to fecal matter as well as human or animal waste **[21].**

Table 4: the description of the bacterial species that were isolated in water stations before treatment.

Isolated bacterial Spp	Name's of water station				
	Abu saida	Dhubab	Awasheq	Zherat	Jabinat
Escherichia coli	+	-	-	-	-
Klebsiella sp	-	-	-	-	-
Aeromons sp	-	-	-	-	-
Pseudomonas sp	-	-	-	-	-
Shigilla sp	-	-	-	-	-
Enterobacter vulneris	-	-	-	-	-
Enterobacter aerogenes	-	-	-	-	-
Staphylococcus aureus	-		-	+	+
Streptococcus (S.faecalis)	+	+	+	+	+

Table 5: the description of the bacterial species that were isolated in water stations after treatment.

Isolated bacterial Spp	Names of water station				
	Abu Saida	Dhubab	Awasheq	Zherat	Jabinat
Escherichia coli	-	-	-	-	-
Klebsiella sp	-	-	-	-	-
Aeromons sp	-	-	-	-	-
Pseudomonas sp	-	-	-	-	-
Shigilla sp	-	-	-	-	-
Enterobacter vulneris	-	-	-	-	-
Enterobacter aerogenes	-	-	-	-	-
Staphylococcus aureus	-		-	+	+
Streptococcus (S.faecalis)	-	-	+	-	-

4.Conclusions

According to the study's findings, certain water stations in the Diyala Governorate provide drinking water that is unsafe for human consumption due to the presence of toxic heavy metals and harmful bacteria. toxic heavy metals can cause serious health effects even at low concentrations. Long-term exposure to cadmium may lead to kidney damage, while lead exposure is especially harmful to the nervous system, particularly in children. This could be because the water level of the Tigris and Euphrates rivers is steadily declining in Turkey as a

result of the construction of dams and reservoirs on these rivers, while Iraq's drinking water quality is lacking due to inadequate water filtration and sterilization techniques as well as deteriorating water distribution networks, can cause drinking water to become contaminated by sewage that contains a variety of harmful germs and disrupts Heavy metal concentrations in drinking water. For this reason, it is crucial to raise environmental awareness through all available channels, including educational resources and the media. Regular use of the membrane filter technology and other tests is necessary to assess the water's bacterial content and standard heavy metal levels. The network tubes that distribute the water from these stations must also be controlled.

5. References

[1] Ckafor CO, Ude UI, Okoh FN, Eromonsele BO. Safe drinking water: the need and challenges in developing countries. In: Water quality—new perspectives. London: IntechOpen; 2024.

[2] Westall F, Brack A. The importance of water for life. Space Sci Rev. 2018;214(2):50.

[3]Nieder R, Benbi DK, Reichl FX. Microelements and their role in human health. In: Soil components and human health. Dordrecht: Springer Netherlands; 2018. p. 317-7.

[4] Daripa A, Malav LC, Yadav DK, Chattaraj S. Metal contamination in water resources due to various anthropogenic activities. In: Metals in water. Elsevier; 2023. p. 111-27.

[5] Pandiyan J, Mahboob S, Govindarajan M, Al-Ghanim KA, Ahmed Z, Al-Mulhm N, et al. An assessment of level of heavy metals pollution in the water, sediment and aquatic organisms: a perspective of tackling environmental threats for food security. Saudi J Biol Sci. 2021;28(2):1218-25

[6] Madhav S, Ahamad A, Singh AK, Kushawaha J, Chauhan JS, Sharma S, et al. Water pollutants: sources and impact on the environment and human health. In: Sensors in water pollutants monitoring: role of material. 2019. p. 43-62.

[7] Tsaridou C, Karabelas AJ. Drinking water standards and their implementation—a critical assessment. Water. 2021;13(20):2918.

[8] Tambi A, Brighu U, Gupta AB. Methods for detection and enumeration of coliforms in drinking water: a review. Water Supply. 2023;23(10):4047-58.

[9] Forstinus NO, Ikechukwu NE, Emenike MP, Christiana AO. Water and waterborne diseases: a review. Int J Trop Dis Health. 2016;12(4):1-14.

[10] Talat N. Urban water-supply management: indirect issues of climate change leading to water scarcity scenarios in developing and underdeveloped nations. In: Water conservation in the era of global climate change. Elsevier; 2021. p. 47-71.

[11] Hashim NS, Mutashar NS, Jameel HT, Mahmood SM. A comparative study to analyze the validity of well water for some areas of eastern and western Diyala Governorate. Academia Open. 2024;9(1):10-21070.

[12] Hadi NS. Evaluation of water and sediment quality by bacteriological diversity studies on certain locations of the Diyala River. Environ Nat Resour J. 2023;21(6):491-500.

[13] Aydamo AA, Robele Gari S, Mereta ST. Seasonal variations in household water use, microbiological water quality, and challenges to the provision of adequate drinking water: a case of peri-urban and informal settlements of Hosanna Town, Southern Ethiopia. Environ Health Insights. 2024; 18:11786302241238940.

[14] Mohammed MA, Al-Obaidi NS, Fadihl SJ. Investigation of heavy metals and some bacterial species in water stations and evaluate them chemically and biologically in Diyala Governorate, Iraq. Biochem Cell Arch. 2018;18(2).

[15] Tesfamariam Z, Younis YM. Assessment of physicochemical parameters and levels of heavy metals concentrations in drinking water of Asmara city, Eritrea III. Am J Res Commun. 2016;4(8):30-44.

[16] Jomova K, Alomar SY, Nepovimova E, Kuca K, Valko M. Heavy metals: toxicity and human health effects. Arch Toxicol. 2025;99(1):153-209.

[17] Fatima G, Raza AM, Hadi N, Nigam N, Mahdi AA. Cadmium in human diseases: it's more than just a mere metal. Indian J Clin Biochem. 2019;34(4):371-8.

[18] Mohod CV, Dhote J. Review of heavy metals in drinking water and their effect on human health. Int J Innov Res Sci Eng Technol. 2013;2(7):2992-6.

[19] Wu YS, Osman AI, Hosny M, Elgarahy AM, Eltaweil AS, Rooney DW, et al. The toxicity of mercury and its chemical compounds: molecular mechanisms and environmental and human health implications: a comprehensive review. ACS Omega. 2024;9(5):5100-26.

[20] World Health Organization. Guidelines for drinking-water quality: incorporating the first and second addenda. Geneva: WHO; 2022.

[21] Some S, Mondal R, Mitra D, Jain D, Verma D, Das S. Microbial pollution of water with special reference to coliform bacteria and their nexus with environment. Energy Nexus. 2021; 1:100008.

Al-Kitab Journal for Pure Sciences (2026); 10(2):116-131.
https://doi.org/10.32441/kjps.10.2.p9

Al-Kitab Journal for Pure Sciences
ISSN: 2617-1260 (print), 2617-8141(online)

https://isnra.net/index.php/kjps

Isolation and Antibiotic Resistance Profiling of Gram-Negative Bacteria Recovered from Wound and Burn Infections

Iman Abdulrazzaq Aljuraisy[1], Reem Z. Shakir[2]

[1,2] Department of Biology, College of Education for Women, University of Mosul, Iraq

Corresponding author: Iman.23gep15@student.uomosul.edu.iq

Citation: *Iman Abdulrazzaq Aljuraisy[1], Reem Z. Shakir[2]*. **Isolation and Antibiotic Resistance Profiling of Gram-Negative Bacteria Recovered from Wound and Burn Infections**.
Al-Kitab J. Pure Sci. [Internet]. 2025 Oct. 29 ;10(2):116-131
DOI.
https://isnra.net/index.php/kjps/article/view/2026.
https://doi.org/10.32441/kjps.10.2.p9

©20--. THIS IS AN OPEN-ACCESS ARTICLE UNDER THE CC BY LICENSE
http://creativecommons.org/licenses/by/4.0/

Keywords: Wounds infection, Burns Infection, Antibiotics Resistance, Gram negative bacteria.

Article History

Received	14 Sep.	2025
Accepted	29 Oct.	2025
Available online	01 Nov.	2026

Abstract:

Wound infection is one of the most important factors affecting the wound healing process, so its effective control is crucial to enhance the wound healing. With the increasing prevalence of multidrug-resistant bacterial strains, preventing and treating wound infections has now become more challenging, imposing heavy medical and financial burdens on the patients. This study aimed to isolate and identify Gram-negative bacteria from wounds and burns and investigate the resistance of these bacteria to various antibiotics. In this study, Gram-negative bacteria were isolated and identified from pus samples obtained from patients suffering from wound and burn infections who were admitted to Al-Salam Teaching Hospital, Mosul General Hospital, and the Mosul Center for Burns and Plastic Surgery. The ages of patients ranged from 5 days to 75 years, included both sexes. The sampling period extended from August 28, 2024, to November 23, 2024. Bacterial isolates were identified based on cultural, morphological, microscopic characteristics, and biochemical tests. A total of 88 bacterial isolates were obtained from 54 pus samples that showed growth on MacConkey agar media for Gram-negative bacteria. Identification was further confirmed using the VITEK-2 system to ensure accurate species determination. *Pseudomonas aeruginosa* and *Enterobacter cloacae* were the most prevalent

species, with 28 isolates for each one(31.81%), followed by *Klebsiella pneumoniae* with 10 isolates (11.36%), *Klebsiella aerogenes* with 6 isolates (7%), *Escherichia coli* with 7 isolates (8%), and *Proteus mirabilis*, *Proteus vulgaris*, and *Raoultella ornithinolytica* with 2 isolates each (2.20%). Additionally, *Acinetobacter baumannii*, *Serratia marcescens*, and *Salmonella spp.* were each represented by 1 isolate (1. 13%). Antibiotics susceptibility testing revealed a high level of resistance among Gram-negative bacteria to cephalosporin antibiotics, with resistance rates of 95.5% for ceftazidime, and 93% for both ceftriaxone and cefotaxime. Moreover, macrolide antibiotics, specifically azithromycin, showed a resistance rate of 75%. In contrast, chloramphenicol demonstrated the highest antibacterial efficacy among the tested antibiotics against Gram-negative isolates.

Keywords: Wounds infection, Burns Infection, Antibiotics Resistance, Gram negative bacteria.

عزل وتحديد مقاومة المضادات الحيوية للبكتيريا السالبة الغرام المعزولة من الجروح والحروق

إيمان عبد الرزاق الجريسي[١]، ريم زهير شاكر[٢]

[٢،١] قسم علوم الحياة، كلية التربية للبنات، جامعة الموصل، العراق

الايميل الرسمي: [1]Iman.23gep15@student.uomosul.edu.iq, [2]reemzuhair@uomosul.edu.iq

الخلاصة:

تُعدُّ عدوى الجروح من أهم العوامل المؤثرة على عملية التئامها، لذا فإن السيطرة عليها بفاعلية أمرٌ بالغ الأهمية لتعزيز عملية التئامها. ومع تزايد انتشار سلالات البكتيريا المقاومة للأدوية المتعددة، أصبحت الوقاية من عدوى الجروح وعلاجها أكثر صعوبة، مما يُثقل كاهل المرضى بأعباء طبية ومالية باهظة. هدفت هذه الدراسة إلى عزل وتحديد البكتيريا سالبة الغرام من الجروح والحروق ودراسة مقاومة هذه البكتيريا للمضادات الحيوية المختلفة. تضمنت هذه الدراسة عزل وتشخيص البكتريا السالبةا لغرام المعزولة من عينات القيح التي جمعت من المرضى المراجعين الى مستشفيات السلام التعليمي ومستشفى الموصل العام ومركز الموصل للحروق والجراحة التجميلية المصابين بالتهابات الجروح والحروق وبأعمار تراوحت من (٥ يوم -٧٥ عام) ولكلا الجنسين للمدة ٢٠٢٤\٨\٢٨ لغاية ٢٠٢٤\١١\٢٣ ،تم تشخيص العُزلات البكتيرية بالاعتماد على الصفات الزرعية، الظاهرية، المجهرية، الاختبارات الكيموحيوية تم الحصول على (٨٨) عزلة من مجموع (54) عينة قيح أعطت نموا على وسط اكار الماكونكي والانتخابية للبكتريا السالبة لغرام وكانت بكتريا *p. aeruginosa* و *E. cloacae*أكثر انتشاراً ٢٨عزلة بكتيرية وبنسبة (٣١,٨١٪) يليه بكتريا *K. pneumoniae* ١٠عزلة وبنسبة (١١,٣٦%) يليه بكتريا *K. aerogenes* ٦عزلة بنسبة (٧٪) يليه بكتريا *E. coli* ٧عزلة وبنسبة (٨٪) يليه بكتريا *P. mirabilis*، *P. vulgaris, R. ornithinolytica*٢(٢,٢٠٪) يليه بكتريا *A. baumannii ,S. marcescens,Salmonella spp* بنسبة ١(١,١٣٪). وتم دعم نتائج التشخيص باستخدام نظام فايتك -٢ للتاكد من تحديد الأنواع بعدها تم اجراء فحص مقاومة وحساسية

العزلات للمضادات الحيوية بينت النتائج امتلاك الجراثيم السالبة لغرام مقاومة عالية لمضادات السيفالوسبورينات (*Ceftazidim*) بنسبة ٩٥,٥٪ و(*Ceftraxone* و*Cefotoxime*) بنسبة ٩٣٪ ومضادات المايكروليدات المتمثلة بالـ *Azythromycin* بنسبة ٧٥٪. كذلك أظهرت النتائج ان مضادات الكلورمفينيكولات المتمثلة بالمضاد *Chlormphenicol* كانت من أكثر المضادات فعالية ضدالبكتريا السالبة لغرام.

الكلمات المفتاحية: التهاب الجروح، التهاب الحروق، مقاومة المضادات الحيوية، الجراثيم السالبة لغرام.

1. Introduction:

Wound infection is one of the most important factors affecting the wound healing process, so its effective control is crucial to enhance the wound healing process. With the increasing prevalence of multidrug-resistant bacterial strains, preventing and treating wound infections has now become more challenging, imposing heavy medical and financial burdens on the patient [1]

Wound and burn injuries are among the most difficult problems that hinder surgical medical progress and cause death for patients because they destroy tissues and lose the skin barrier. The presence of dead tissue, the presence of antibiotic-resistant microbes, the ability of these microbes to form biofilms, and the weakness of antibiotic treatment - all these factors lead to delayed recovery of the patient, especially patients carrying other chronic systemic diseases [2,3,4]

Over time, microorganisms were exposed to antibiotics, which led to bacteria adapting to resist these antibiotics. This adaptation, along with the lack of drug development, has led to a reduction in treatment options against bacterial infections [5] The World Health Organization (WHO) has stated that the emergence and spread of antibiotic-resistant bacteria is one of the most important health problems of our time and poses a threat to the treatment of diseases. This leads to an increase in the patient's length of stay in the hospital and an increase in treatment costs [6]

Some previous studies have shown that the most common Gram-negative bacteria that have been identified as pathogens causing wound and burn infections are *Pseudomonas aeruginosa*, *Enterobacter cloacae*, *Klebsiella pneumoniae*, *Klebsiella aerogenes*, and *E. coli* .[7,8,9]

2. Material and methods:

2.1 Sample Collection: 103 pus samples were collected, from patients with wound and burn infections (including, both male and female, who were admitted to Mosul hospitals (Mosul General Hospital, Al-Salam Teaching Hospital, and Mosul Center for Burns and Plastic Surgery) between 28, August, 2024 and 23, November, 2024[10].

2.2 Isolation and diagnosis: Samples were cultured on plates containing MacConkey agar medium, and then selective media were used to identify bacterial species, such as cetrimidine agar and eosin methyl blue agar. The plates were then incubated for 24 hours at 37°C. The morphological characteristics of the cultures on the plates and microscopic examinations were used to determine the shape and arrangement of these bacterial species. Then, biochemical tests were used, which were (catalase, oxidase, and IMVC tests) [10]. To confirm the diagnosis results, the Vitek-2 system produced by the French company (Biomerrux) was used (We learned that the diagnosis with the Vitek-2 device was performed in an external laboratory).

- **2.3 Antibiotics susceptibility test**: The disk diffusion method based on the Kirby-Bauer Disk method [11] was used to examine the susceptibility of bacterial isolates to the antibiotics shown in Table 1, it was Compared the antibiotic susceptibility test results with the standard reference tables, the CLSI table, in terms of bacteria being sensitive, resistant, or intermediate which were prepared by the Turkish company (Bioanlyase). Mueller-Hinton medium prepared by the Indian company (Himedia) was used in this test and was prepared according to the company's instructions. the bacterial suspension was prepared and adjusted to match the 0.5 McFarland standard. Then, 100 µL of the suspension was spread evenly on the surface of Mueller-Hinton agar using a sterile cotton swab. After allowing the plates to dry for about 15 minutes, antibiotic discs were placed on the surface and the plates were incubated at 37°C for 18–24 hours.

Table 1: Antibiotics used in the study

Tablet/Concentration Microgram	Code	Antibiotic	Antibiotic Classes
10µg/disc	CRO	Ceftriaxone	Cephalosporin's
10µg/disc	CTX	Cefotaxime	
30µg/disc	CAZ	Ceftazidme	
10µg/disc	MEM	Meropenem	Carbapenems
10µg/disc	IPM	Imipenem	
10µg/disc	GN	Gentamycin	Aminoglycosides
15µg/disc	AZM	Azithromycin	Macrolides
10µg/disc	CIP	Ciprofloxacin	Fluoroquinolones
10µg/disc	TE	Tetracycline	Tetracycline's
10µg/disc	C	Chloramphenicol	Chloramphenicol

3. Results and Discussion

Laboratory and phenotypic diagnosis: After culturing the samples on MacConkey agar medium and incubating for 24 hours at a temperature of 37°C, as shown in Figure (1).



E. coli ***P. aeruginosa*** ***E. cloacae***

Figure 1: McConkey agar

Gram stain microscopy was performed to identify the shapes and arrangement of bacteria. Then, the lactose fermented samples, which appeared pink in color, were transferred to MacConkey agar medium and cultured on eosin methyl blue agar medium for the purpose of identifying *E. coli* isolates, as shown in Figure (2).



Figure 2: *E. coli* bacteria on Eosin blue medium

While the pale-colored isolates on MacConkey agar were cultured on cetrimid agar medium for the purpose of diagnosing *P. aeruginosa* isolates, which appear green as a result of their production of pyocyanin pigment, as shown in Figure (3).

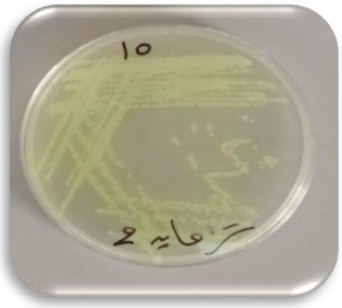


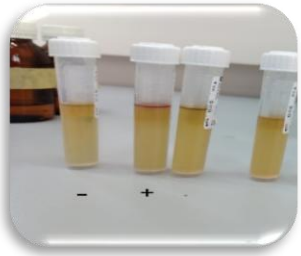
Figure 3: P. aeruginosa on cetrimid agar

The results of the biochemical tests are shown in Table, (2) and Figure, (4).

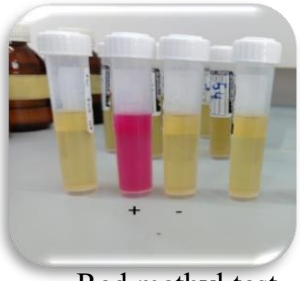
Table2: the biochemical tests of bacterial isolates

IMVIC Test				Catalase	Oxidase	the name of the bacteria
IND	MR	VP	CIT			
-	-	-	+	+	+	*P .aeruginosa*
+	+	-	-	+	-	*E.coli*
-	+	-	+	+	-	*P .mirabilis*
-	+	-	-	+	-	*k. pneumoniae*
-	-	+	+	+	-	*E .cloacae*

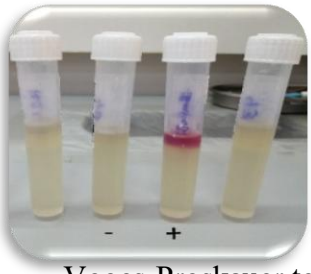
(+) positive, (-) negative



Indole test



Red methyl test



Voges-Proskauer test





Citrate utilization test Oxidase test for the right and catalase test for the left

Figure 4: Results of biochemical tests

It was identical to the approved specifications for the diagnosis of Gram-negative bacteria shown in [10]. Then, all the isolates isolated in this study were confirmed using the Vitek-2 system, as the results showed that all isolates were consistent with the traditional diagnostic methods and showed a level of diagnostic probability between (89%-95%) for *Enterobacter cloacae* isolates and (86%-99%) for *Klebsiella pneumoniae* isolates and (93%) for *Pseudomonas aeruginosa* isolates and (94%-95%) for each of *Klebsiella aerogenes* and *E. coli* and (91%) for *Raoultella ornithinolytica* isolates and (99%) for each of Proteus mirabilis, Proteus vulgaris, *Acinetobacter baumannii* and *Serratia marcescens* isolates

Bacterial Isolation Out of a total of 103 samples, 54 samples were obtained that showed growth on Macon key agar and selective media for Gram-negative bacteria representing a percentage of (53.39%). These samples were distributed among (23) wound samples (17 male samples and 6 female samples). As for burn samples, there were (31) samples, distributed among (13 male samples and 18 female samples) as in table 3.

Table 3: Distribution of samples between males and females

Insulation source	Sex	Culture positive	Culture negative	Total number of samples
Wounds	Male	17	16	33
	Female	6	12	18
Burns	Male	13	10	23
	Female	18	11	29
The total	-	54	49	103

The total number of bacterial isolates obtained was 88 (This number of bacterial isolates is due to the growth of more than one type of bacteria in a single sample) and these results were close to the study [8]. In the city of Maysan the percentage in his study reached (86.9%), and the study [7] If their isolation rate is (81.7) out of a total of 100 samples. and the results are different [12] The isolation rate was 132% of the total 800 samples and the study [13] The isolation rate was 100% for a total of 40 samples. The results showed that the bacterial isolates were distributed among the different types, with 28 isolates (31.81%) for each of *Pseudomonas aeruginosa* and *Enterobacter cloaca*, 10 isolates (11.39%) for *Kleebsiella pneumonia*, 6 isolates (7%) for *Klebsiella aerogenes*, 7 (8%) for *E. coli*, 2 (2.20%) for each of *Proteus*

vulgaris, *Proteus mirabilis* and *Raoultella ornithinolytica*, 1 (1.13%) for each of Acinetobacter baumanni, Serratia marcescens and *Salmonella spp*., as shown in Table (4).

Table 4: Number and percentages of Gram-negative bacteria isolated from patients with wounds and burns

No.	Percentage of total Gram-negative bacteria	number	Gram-negativebacterial species
1	31.81%	28	*Pseudomonas aeruginosa*
2	31.81%	28	*Enterobacter cloacae*
3	11.36%	10	*Kleebsiella pneumoniae*
4	7%	6	*Klebsiella aerogenes*
5	8%	7	*E.coli*
6	2.20%	2	*Proteus vulgaris*
7	2.20%	2	*Proteus mirabils*
8	2.20%	2	*Raoultella ornithinolytica*
9	1.13%	1	*Acinetobacte baumanni*
10	1.13%	1	*Serratia marcescens*
11	1.13%	1	*Salmonella spp*
	100%	88	the total

The results showed that *P. aeruginosa* isolates were the most prevalent. This percentage was close to a study in the city of Maysan **[8].** Also, a study in Libya, **[7]** The results of this study did not agree with a study conducted in Dohuk, **[14]** In other studies in India and Libya, **[12,13]** respectively. The reason for the dominance of this bacterial species is that *P. aeruginosa* is one of the most common Gram-negative bacteria associated with hospital-acquired infections. This is due to its possession of multiple virulence factors, including the possession of biofilms, efflux pumps, and its ability to resist various antibiotics due to the possession of mobile genetic elements such as jumping genes (Trausposouses, Integrones,Plasmids) **[9,15,16]** As for the *Enterobacter cloacae* isolates, their percentage within the total number of isolates reached (31.81%) within the total negative group. This percentage was different from a previous study **[8,15]** respectively *Enterobacter spp*. are anaerobic Gram-negative bacteria widely distributed in nature and have raised increasing concern in recent years due to their association with hospital-acquired infections, especially in immunocompromised individuals **[17].**

In the present study, *Klebsiella pneumonia* bacteria were isolated at a rate of 10 (11.39%) and *Klebsiella aerogenes* at a rate of 6 (7%). These results were consistent with what was reached by a study in Libya, [7] It is consistent with another study [13] It was slightly higher than another study [8] This genus plays an active role in causing burn and wound infections. It is found in hospitals and is considered a major pathogen due to its possession of many genes that have the ability to resist antibiotics [18]. As for the *E. Coli* species, the isolation rate was 7 (8%). This result was similar to a local study and another Arab study [7,8] respectively It contradicted another study, [12] The digestive system is the natural home for *E. Coli*, but infection occurs after it leaves the system [7] Or as a result of low immunity, especially for immunocompromised patients, the elderly, and children. As for the genus *Proteus spp*, *Proteus vulgaris* was isolated at a rate of 2 (2.20%) and *Proteus mirabilis* at a rate of 2 (2.20%), which was close to the study [12] Contrasting with another study [8]. Factors contributing to differences in bacterial isolation rates between countries vary, including environment, health practices, antibiotic use, bacterial genetic diversity, social and economic factors, and laboratory techniques.

Antibiotics sensitivity test: A sensitivity test was conducted on the (88) bacterial isolates under study, which caused wound and burn infections, against 10 antibiotics, as shown in Table (5). The results showed high resistance to cephalosporin's, with 84% (95.5%) against Ceftazideme and 82% (93%) against both Ceftriaxone and Cefotaxime. Regarding carbapenem antibiotics, Meropenem was more effective against the isolates, with a sensitivity rate of 37%, compared to Imipenem, which the isolates showed high resistance to, reaching 69.3%) Regarding aminoglycosides represented by the antibiotic Gentamycin, the isolates showed medium resistance, as the resistance rate reached (69%). As for macrolides represented by the antibiotic Azythromycin, the resistance rate of the isolates was (75%), and (72.8%) for the antibiotic Ciprofloxacin from fluoroquinolones, while the resistance rate towards tetracyclines represented by the antibiotic Tetracycline was low, reaching (47.7%). As for the results of the sensitivity of the isolates towards chloramphenicol represented by the antibiotic Chlormphenicol, the number of sensitive isolates reached 53 isolates, at a rate of (60%).

Table 5: Total numbers and percentages of bacterial isolates resistant and sensitive to antibiotics

No.	Antibiotic	Antibiotic Classes	sensitive isolates		Moderate isolates		resistant isolates		code
			(%)	No.	(%)	No.	(%)	No.	
1.	*Ceftriexone*	Cephalosporin's	7%	6	0%	0	93%	82	CRO
	Cefotaxime		7%	6	0%	0	93%	82	CTX
	Ceftazidem		4.5%	4	0%	0	95.5%	84	CAZ
2.	*Meropenem*	Carbapenems	37%	33	7%	6	56%	49	MEM
	Imipenem		27.3%	24	3.4%	3	69.3%	61	IPM
3.	*Gentamycin*	Aminoglycosides	16%	14	15%	13	69%	61	GN
4.	*Azythromycin*	Macrolides	25%	22	0%	0	75%	66	AZM
5.	*Ciprofloxacin*	Fluoroquinolones	13.6%	12	13.6%	12	72.8%	64	CIP
6.	*Chlormphenicol*	Chloramphenicol	60%	53	8%	7	32%	28	C
7.	*Tetracycline*	Tetracycline's	40.95%	36	11.35%	10	47.7%	42	TE

The above results show that the antibiotic Chloramphenicol was one of the most effective antimicrobials against Gram-negative bacterial isolates. The reason is due to the mechanism of action of Chloramphenicol, which works to prevent the synthesis of proteins inside the cell [20] In general, the results of the study showed the resistance of negative bacteria to most antibiotics, especially cephalosporin's. This result is consistent with another study (which confirmed in their results the resistance of most negative bacteria to most of the antibiotics used) [13,14,21] The increasing, indiscriminate, and irregular use of antibiotics leads to the failure to kill bacteria, making them more resistant and encouraging them to develop resistance mutations, which increases the incidence of hospital infections. Despite efforts to combat hospital infections, the morbidity and mortality rates are very high, increasing healthcare costs and thus leading to an economic crisis. The problem is further complicated by the emergence of multidrug-resistant microorganisms that are difficult to treat in the hospital environment [19,22] Studies have shown that patients with medical records who take antibiotics for long periods may kill the natural flora that acts as the body's immune system and cause the death of sensitive bacteria. This leaves only resistant bacteria that carry resistance genes. These genes can be spread via plasmids to other types of bacteria. This results in the proliferation of antibiotic-resistant bacteria at the expense of the body's natural flora [23] Table (6) shows the results of antibiotics sensitivity for each isolate separately.

Table 6: shows the biological response of Gram-negative bacteria to the antibiotics used under study

Sensitivity Pattern		C N (%)	CIP N (%)	AZM N (%)	TE N (%)	GN N (%)	IPM N (%)	MEM N (%)	CAZ N (%)	CTX N (%)	CRO N (%)
S I R	*P. aeruginosa* (N=28)	9(32%) 0(0%) 19(68%)	4(14%) 5(18%) 19(68%)	3(11%) 0(0%) 25(89%)	8(28.5%) 2(7%) 18(64.5%)	4(14%) 0(0%) 24(86%)	8(28%) 1(4%) 19(68%)	12(43%) 0(0%) 16(57%)	1(3.5%) 0(0%) 27(96.5%)	1(3.5%) 0(0%) 27(96.5%)	1(3.5%) 0(0%) 27(96.5%)
S I R	*E. cloacae* N=28	20(71%) 3(11%) 5(18%)	1(4%) 2(7%) 25(89%)	4(14%) 0(0%) 24(86%)	11(39%) 5(18%) 12(43%)	2(7%) 5(18%) 21(75%)	2(7%) 0(0%) 26(93%)	3(11%) 3(11%) 22(78%)	0(0%) 0(0%) 28(100%)	1(3.5%) 0(0%) 27(96.5%)	1(3.5%) 0(0%) 27(96.5%)
S I R	*K.pneumoniae* N=10	9(90%) 1(10%) 0(0%)	4(40%) 2(20%) 4(40%)	6(60%) 0(0%) 4(40%)	6(60%) 1(10%) 3(30%)	5(50%) 2(20%) 3(30%)	9(90%) 0(0%) 1(10%)	8(80%) 0(0%) 2(20%)	2(20%) 0(0%) 8(80%)	2(20%) 0(0%) 8(80%)	2(20%) 0)0%) 8(80%)
S I R	*K .aerogenes* N=6	3(50%) 1(17%) 2(33%)	1(17%) 0(0%) 5(83%)	1(17%) 0(0%) 5(83%)	1(17%) 0(0%) 5(83%)	0(0%) 2(33%) 4(67%)	1(17%) 0(0%) 5(83%)	2(33%) 0(0%) 4(67%)	0(0%) 0(0%) 6(100%)	0(0%) 0(0%) 6(100%)	0(0%) 0(0%) 6(100%)
S I R	*E. coli* N=7	7(100%) 0(0%) 0(0%)	1(14%) 0(0%) 6(86%)	5(71%) 0(0%) 2(29%)	5(71%) 0(0%) 2(29%)	1(14%) 2(29%) 4(57%)	1(14%) 0(0%) 6(86%)	2(48.5%) 3(43%) 2(28.5%)	0(0%) 0(0%) 7(100%)	0(0%) 0(0%) 7(100%)	0(0%) 0(0%) 7(100%)
S I R	*P.miabils* N=2	1(50%) 1(50%) 0(0%)	1(50%) 0(0%) 1(50%)	1(50%) 0(0%) 1(50%)	0(0%) 1(50%) 1(50%)	1(50%) 0(0%) 1(50%)	1(50%) 0(0%) 1(50%)	1(50%) 0(0%) 1(50%)	0(0%) 0(%) 2(100%)	0(0%) 0(0%) 2(100%)	0(0%) 0(0%) 2(100%)
S I R	*P. vulgaris* N=2	1(50%) 0(0%) 1(50%)	0(0%) 0(0%) 2(100%)	0(0%) 0(0%) 2(100%)	0(0%) 1(50%) 1(50%)	0(0%) 1(50%) 1(50%)	0(0%) 1(50%) 1(50%)	1(50%) 0(0%) 1(50%)	0(0%) 0(0%) 2(100%)	0(0%) 0(0%) 2(100%)	0(0%) 0(0%) 2(100%)
S I R	*Raoultella ornithinolytica* N=2	1(50%) 1(50%) 0(0%)	0(0%) 1(50%) 1(50%)	1(50%) 0(0%) 1(50%)	0(0%) 0(0%) 2(100%)	0(0%) 0(0%) 2(100%)	0(0%) 1(50%) 1(50%)	2(100%) 0(0%) 0(0%)	0(0%) 0(0%) 2(100%)	0(0%) 0(0%) 2(100%)	0(0%) 0(%) 2(100%)
S I R	*Acinetobacter baumanni* N=1	0(%) 0(0%)	0(0%) 0(0%)	0(0%) 0(0%)	1(100%) 0(0%) 0(0%)	0(0%) 0(0%)	0(0%) 0(0%)	0(0%) 0(0%)	0(0%) 0(0%) 1(100%)	0(0%) 0(0%) 1(100%)	0(0%) 0(0%) 1(100%)

		1(100%)	1(100%)	1(100%)		1(100%)	1(100%)	1(100%)			
S I R	*Serratia marcescens* N=1	1(100%) 0(0%) 0(0%)	1(100%) 0(0%) 0(0%)	0(0%) 0(0%) 1(100%)	1(100%) 0(0%) 0(0%)	0(0%) 1(100%) 0(0%)	1(100%) 0(0%) 0(0%)	1(100%) 0(0%) 0(0%)	0(0%) 0(0%) 1(100%)	1(100%) 0(0%) 0(0%)	1(100%) 0(0%) 0(0%)
S I R	*Salmonella spp* N=1	1(100%) 0(0%(0(0%)	0(0%) 1(100%) 0(0%)	1(100%) 0(0%) 0(0%)	1(100%) 0(0%) 0(0%)	1(100%) 0(0%) 0(0%)	1(100%) 0(0%) 0(0%)	1(100%) 0(0%) 0(0%)	1(100%) 0(0%) 0(0%)	1(100%) 0(0%) 0(0%)	1(100%) 0(0%) 0(0%)

P. aeruginosa isolates showed high resistance to cephalosporin antibiotics. The reason is due to their possession of mechanisms to resist these antibiotics, including carrying a chromosomal gene that encodes *AmpC*, an enzyme capable of breaking down cephalosporins, including the second and third generation, and their possession of efflux pumps that work to expel antibiotics outside the cells. Lack of permeability occurs due to mutations or a decrease in the secretion of Porins, as the loss or mutation of the *oprD* gene leads to strong resistance to cephalosporins. Mutations in beta-lactam-binding proteins such as PBP3 affect the effectiveness of cephalosporin antibiotics. Bacteria can also obtain ESBL genes through horizontal transfer (plasmids), thus acquiring resistance to the third and fourth generation of cephalosporins. Finally, *P. aeruginosa* forms biofilms that block and reduce interaction with antibiotics **[24]** *E. caloaceae* isolates also showed high resistance to cephalosporin's, as these bacteria possess an inducible chromosomal gene *ampC*, which when mutated with other genes such as *ampD* or ampR leads to the production of the AMPC enzyme, which destroys the third generation of cephalosporin's. Resistance genes may be transferred to them via plasmids, making them more resistant. They may acquire mutations that result in the loss or reduction of the outer membrane, which increases resistance. They possess efflux pumps **[25].** *K. pneumoniae*, *E. Coli*, and *K. aerogenes* isolates have also shown resistance to cephalosporin antibiotics due to their formation of biofilms, the possession of efflux pumps, the production of beta-lactamase enzymes, or transmission via plasmids from other bacteria and mutations that lead to reduced permeability **[26,27,28].**

5. Conclusions

The results of the study showed that Gram-negative bacteria are among the main and common causes of wound and burn infections, and the most common isolates were: *Pseudomonas aeruginosa*, *Enterobacter cloacae Kleebsiella pneumonia*, *Klebsiella aerogenes*,

E. coli. These isolates showed a significant difference in their sensitivity to antibiotics, as they showed high resistance to a number of antibiotics, especially the cephalosporin class, and some isolates showed multi-drug resistance. This indicates the spread of resistant strains that pose a therapeutic challenge in the hospital environment. On the other hand, it was noted that some antibiotics, such as chloramphenicol and tetracycline, showed relative effectiveness against some isolates. These results indicate a need to reduce the indiscriminate use of antibiotics and recommend intensifying infection control programs and enhancing awareness of sound health practices within surgical and burn units. To reduce the spread of resistant bacteria.

References

[1] B. Wang, L. Du, B. Dong, E. Kou, L. Wang, and Y. Zhu, Current knowledge and perspectives of phage therapy for combating refractory wound infections. Int. J. Mol. Sci., 2024; 25: 5465, [Online]. Available: https://doi.org/10.3390/ijms25105465

[2] J. M. R. Alshara, Isolation and identification of bacterial wound infection isolates and their antibiotic susceptibility pattern, Al-Kufa Univ. J. Biol., 2018; 10(2): 49–63, doi: 10.36320/ajb/v10.i2.8126.

[3] P. Gupta, H. S. Singh, V. K. Shukla, G. Nath, and S. K. Bhartiya, Bacteriophage therapy of chronic nonhealing wound: Clinical study, Int. J. Low Extrem. Wounds, 2019, 18(2): 171–175, doi: 10.1177/1534734619835115.

[4] D. P. Nichols, S. Caceres, L. Caverly, C. Fratelli, S. H. Kim, K. C. Malcolm, et al., Effects of azithromycin in Pseudomonas aeruginosa burn wound infection, J. Surg. Res., 2013; 183(2): 767–776, 2013, doi: 10.1016/j.jss.2013.02.003.

[5] S. Dhingra, N. A. A. Rahman, M. R. Peile, M. Sartelli, M. A. Hassali, T. Islam, and M. Haque, Microbial resistance movements: an overview of global public health threats posed by antimicrobial resistance, and how best to counter, Front. Public Health, 2020; 8, 535668, doi: 10.3389/fpubh.2020.535668.

[6] V. Nagvekar, S. Sawant, and S. Amey, Prevalence of multidrug-resistant Gram-negative bacteria cases at admission in a multispeciality hospital, J. Glob. Antimicrob. Resist., 2020; 22: 457–461, doi: 10.1016/j.jgar.2020.02.030.

[7] A. M. Saeed and A. S. Azab, Identification of bacterial species causing wound infections in patients at Sabratha Hospital in western Libya, Int. Multiling. J. Sci. Technol., 2020; 10(5).

[8] R. Hateet, Isolation and identification of some bacteria contemn in burn wounds in Misan, Iraq, Arch. Razi Inst., 2021; 76(6): 1665–1670, doi: 10.22092/ari.2021.350367.1833.

[9] R. M. Younis and R. M. Faisal, Plasposon mutagenesis in Pseudomonas aeruginosa isolates illustrates the role of ABC transporter in intrinsic resistance to antibiotics, J. Appl. Nat. Sci.,2024; 16(3). doi: 10.31018/jans. v16i3.5856.

[10] P. M. Tille, Bailey & Scott's Diagnostic Microbiology, 1st ed., Philadelphia: Elsevier Health Sciences, 2015.

[11] P. M. Tille and S. Bailey, Diagnostic Microbiology, Missouri: Elsevier, 2014, pp. 202–927.

[12] A. Kurhade, S. Akulwar, M. Mishra, G. Kurhade, A. Justiz-Vaillant, K. Kurhade, S. Vuma, and S. Lakhdive, Bacteriological study of post-operative wound infections in a tertiary care hospital, J. Bacteriol. Parasitol., 2015; 6(6): 1000251, doi: 10.4172/2155-9597.1000251.

[13] M. Rotob and M. Abubakr, Study of bacteria causing surgical site infections at Misrata Central Hospital and evaluation of their antibiotic susceptibility, Acad. J. Sci. Publ. (AJSP), 2020; 26, Dec. 2, Available from: http://www.ajsp.ne

[14] A. M. Ahmad, Detection of the antibiotyping patterns of the most common bacterial pathogens susceptible to different antimicrobial agents causing wound infections in Duhok, Iraq, J. Univ. Anbar Pure Sci. (JUAPS), 2021; 15(1):21–25, doi: 10.37652/JUAPS.2021.15.1.3.

[15] I. K. F. Abdullah, Phenotypic and molecular study of efflux pumps and their inhibitors in some Gram-negative bacteria isolated from burn patients in Mosul city, M.S. thesis, Univ. of Mosul, College of Education for Women, Mosul, Iraq, 2023.

[16] N. D. Hameed, L. H. Mahdi, and K. H. Rasool, Antibiotic sensitivity and biofilm formation in Pseudomonas aeruginosa isolated from wound infections in Baghdad City, J. Coll. Basic Educ., 2024; 30(124): 43–56, 2024, doi: 10.35950/cbej.v30i124.11593.

[17] S. Santajit and N. Indrawattana, Mechanisms of antimicrobial resistance in ESKAPE pathogens, Biomed Res. Int.,2016; 2016: 2475067, doi: 10.1155/2016/2475067.

[18] Al-Gangrene, Comprehensive Knowledge Encyclopedia [Internet]. 2025; Available from: https://www.marefa.org.

[19] L. Kakoullis, E. Papachristodoulou, P. Chra, and G. Panos, Mechanisms of antibiotic resistance in important Gram-positive and Gram-negative pathogens and novel antibiotic solutions, Antibiotics, 2021; 10(4): 415, doi: 10.3390/antibiotics10040415.

[20] D. Chika, Chloramphenicol, MicrobiologyClass.net [Internet], Aug. 27, 2023. [cited: Jun. 28, 2025]. Available from: https://www.microbiologyclass.net

[21] S. Ali and M. Assafi, Prevalence and antibiogram of Pseudomonas aeruginosa and Staphylococcus aureus clinical isolates from burns and wounds in Duhok City, Iraq, J. Infect. Dev. Ctries., 2024; 18(1): 82–92, doi: 10.3855/jidc.18193.

[22] W. Bereket, K. Hemalatha, B. Getenet, T. Wondwossen, A. Solomon, A. Zeynudin, and S. Kannan, Update on bacterial nosocomial infections, Eur. Rev. Med. Pharmacol. Sci., 2012; 16(8): 1039–1044.

[23] K. Suryawan, I. S. Iswari, N. A. Tarini, N. N. D. Fatmawati, and N. S. Budayanti, Bacterial and antibiotic sensitivity patterns among Klebsiella pneumoniae patients at Sanglah Hospital Denpasar, Bali, Int. J. Med. Rev. Case Rep., 2020; 4(9): 1–7, doi: 10.5455/IJMRCR.bacterial-antibiotics.

[24] B. Schwartz, K. Klamer, J. Zimmerman, P. B. Kal_Pradhan, and A. Bhargava, Multidrug resistant Pseudomonas aeruginosa in clinical settings: a review of resistance mechanisms and treatment strategies, Pathogens, 2024; 13(11), doi: 10.3390/pathogens13110975.

[25] R. K. Shields, A. Iovleva, E. G. Kline, A. Kawai, C. L. McElheny, and Y. Doi, Clinical evolution of AmpC-mediated ceftazidime-avibactam and cefiderocol resistance in

Enterobacter cloacae complex following exposure to cefepime, Clin. Infect. Dis., 2020; 71(10): 2713–2716, doi: 10.1093/cid/ciaa355.

[26] Y. Li, S. Kumar, L. Zhang, and H. Wu, Characteristics of antibiotic resistance mechanisms and genes of Klebsiella pneumoniae, Open Med. (Wars), 2023; 18(1): 20230707, doi: 10.1515/med-2023-0707.

[27] J. Intra, D. Carcione, R. M. Sala, C. Siracusa, P. Brambilla, and V. Leoni, Antimicrobial resistance patterns of Enterobacter cloacae and Klebsiella aerogenes strains isolated from clinical specimens: a twenty-year surveillance study, Antibiotics (Basel), 203; 12(4). doi: 10.3390/antibiotics12040775.

[28] M. M. Walker, J. A. Roberts, B. A. Rogers, P. N. A. Harris, and F. B. Sime, Current and emerging treatment options for multidrug-resistant Escherichia coli urosepsis: a review, Antibiotics (Basel), 2022; 11(12): art. no. 1821, doi: 10.3390/antibiotics11121821.

Al-Kitab Journal for Pure Sciences (2026); 10(2):132-142.
https://doi.org/10.32441/kjps.10.2.p10

Al-Kitab Journal for Pure Sciences
ISSN: 2617-1260 (print), 2617-8141(online)

https://isnra.net/index.php/kjps

The Role of Folic Acid in Avoiding Congenital Disabilities: A Review

Nawras Ali Hussein Al-Jubouri[1], Huda Saad Azzawi[2], zahraa hussein abdulateef[3]

[1, 2]Department of Health Management Technologies, Najaf Technical Institute, University of Al-Furat Al-Awsat Technical, Iraq.

[3]Department of Dental Protection Techniques, Najaf Technical Institute, University of Al-Furat Al-Awsat Technical, Iraq.

Corresponding Author: nawres.ali.inj@atu.edu.iq

Citation: *Nawras Ali Hussein Al-Jubouri[1], Huda Saad Azzawi[2], zahraa hussein abdulateef[3]*. **The Role of Folic Acid in Avoiding Congenital Disabilities: A Review.**
Al-Kitab J. Pure Sci. [Internet]. 2025 Nov. 03 ;10(2):132-142 DOI.
https://isnra.net/index.php/kjps/article/view/2026.
https://doi.org/10.32441/kjps.10.2.p10

©20--. THIS IS AN OPEN-ACCESS ARTICLE UNDER THE CC BY LICENSE
http://creativecommons.org/licenses/by/4.0/

Keywords: Congenital disabilities, Defects of neural tube, Folacin, Folic acid, Pregnant.

Article History

Received	11 Aug.	2025
Accepted	03 Nov.	2025
Available online	01 Nov.	2026

Abstract:

Folic acid (folacin, vitamin B9) is a vitamin with several significant functions in the human body. For this reason, too little or too much folic acid can increase the incidence of adverse health effects. This study reviewed current peer-reviewed scientific literature regarding folacin and the effects on pregnant women. We completed a systematic review of literature from peer-reviewed studies from 2018 to June 2025 from scientific databases. The succeeding utilized words and concoctions were used in the review - folacin, folate, folic acid supplements, folacin absence in pregnant women. The use of folacin, in regard to its biological action, has both direct and indirect actions on the metabolic system of the cell body of the pregnant woman as a whole since metabolism is for the mother and fetus specifically. Folic acid plays a role in avoiding megaloblastic anemia, and neural tube defects NTDs, and it is also helpful in the preservation of overall nervous system functionality and helps to decrease the risk of some types of malignant disease. It is presently being vigorously asserted that the use of folic acid is significant in supporting a normal pregnancy.

Keywords: Congenital disabilities, Defects of neural tube, Folacin, Folic acid, Pregnant.

مراجعة: دور حامض الفوليك في منع التشوهات الخلقية

نورس علي حسين الجبوري[١]، هدى سعد عزاوي[٢] ، زهراء حسين عبد اللطيف[٣]

[٢،١] قسم تقنيات الادارة الصحية، معهد تقني نجف، جامعة الفرات الاوسط التقنية، العراق

[٣]قسم تقنيات وقاية الاسنان، معهد تقني نجف، جامعة الفرات الاوسط التقنية، العراق

الايميل الرسمي:[1]zahraa.almosawie.inj@atu.edu.iq,[2]huda.saad.inj@atu.edu.iq,[3]nawres.ali.inj@atu.edu.iq

الخلاصة:

حمض الفوليك (فولاسين، فيتامين ب٩) هو فيتامين له العديد من الوظائف المهمة في جسم الإنسان. ولهذا السبب، فإن تناول القليل جدًا أو الكثير جدًا من حمض الفوليك يمكن أن يزيد من حدوث الآثار الصحية الضارة. استعرضت هذه الدراسة الأدبيات العلمية الحالية التي استعرضها النظراء فيما يتعلق بالفولاسين وتأثيراته على النساء الحوامل. لقد أكملنا مراجعة منهجية للأدبيات من الدراسات التي استعرضها النظراء من سنة ٢٠١٨ الى يونيو ٢٠٢٥ من قواعد البيانات العلمية. تم استخدام الكلمات والتركيبات المستخدمة التالية في المراجعة - الفولاسين، الفولات، مكملات حمض الفوليك، غياب الفولاسين لدى النساء قبل الولادة. إن استخدام الفولاسين، فيما يتعلق بعمله البيولوجي، له آثار مباشرة وغير مباشرة على النظام الأيضي لجسم خلية المرأة الحامل ككل لأن التمثيل الغذائي للأم والجنين على وجه التحديد. يلعب حمض الفوليك دورًا في الوقاية من فقر الدم الضخم الأرومات وعيوب الأنبوب العصبي، كما أنه مفيد في الحفاظ على وظائف الجهاز العصبي بشكل عام، ويساعد على تقليل خطر الإصابة ببعض أنواع الأمراض الخبيثة. ويُؤكد حاليًا بقوة على أهمية استخدام حمض الفوليك في دعم الحمل الطبيعي.

الكلمات المفتاحية: التشوهات الخلقية، عيوب الانبوب العصبي، الفولاسين ، حامض الفوليك، الحامل.

1. Introduction:

A balanced diet is vital for keeping human health and avoiding many diseases. Folic acid, also known as folacin or vitamin B9, plays a vital role in many biological processes, including DNA production, cell division, and blood cell formation. Its importance is particularly significant during periods of rapid growth, such as gestation. Folacin absence can lead to several health problems, most notably megaloblastic anemia and an increased risk of birth defects in fetuses. Both severe absence and excessive heights of folate can contribute to a higher risk of developing certain chronic illnesses, highlighting the need to maintain optimal levels through a balanced diet. [1].

Vitamin B9 is logically present in the diet as folates, folic acid salts representing a collection of concoctions that differ in the number of glutamic acid residues and the degree of oxidation of the pteridine ring. This group consists of several derivatives, for example dihydrofolate

(DHF), tetrahydrofolate (THF), and methylfolate. Synthetic folic acid is the most stable and bioavailable form of these compounds. [2].

Notably the human body can synthesize this vitamin in small quantities, which are shaped by the contribution of intestinal microbes, especially Bifidobacterium (particularly B. solidiscentis and B. pseudocatenulatum), Lactobacilli, Bifidobacteria, Proteobacteria, Fusobacteria, and Actinomyces [3]. So, this vitamin must be obtained from external sources, i.e., through diet or suitable nutritional supplements [4].

Folic acid (vitamin B9) is an essential nutrient involved in DNA synthesis, methylation, and cell division, processes essential for fetal and placental development. Pregnant women who do not consume adequate amounts of folic acid are at greater risk of neural tube defects and an increased risk of miscarriage [5]. Although dietary sources of folate and folate supplements are the primary sources, the gut microbiome can also produce folate in the colon, particularly in Bifidobacterium and Lactobacillus bacteria, which may contribute to circulating folate levels. New research has shown that bacterial imbalances in the gut microbiome may affect folate production or its role in immune regulation, potentially impacting gestation [6].

2. Reasons and consequences of low folacin levels in the body:

One of the most common causes of folacin absence in the human body is dietary errors, especially not consuming enough vegetables, fruits, and whole grain products daily - they are a valuable source of folacin. Low folic acid content in the diet may also be attributed to high rates of loss through food processing and storage. Poor utilization, storage and absorption, of folic acid in the cells of the body may also be attributed to ingestion huge amounts of tea or coffee, alcoholism, and smoking [7].

The concentration of vitamins and minerals in the body, such as ascorbic acid (vitamin C), vitamin B12, iron, zinc, and others, in addition to adequate levels of methionine, can significantly impact the body's consumption of folacin. Vitamin B12 deficiency leads to decreased folic acid retention in cells. Vitamin c absence, in turn, leads to impaired folic acid absorption in low or metabolically energetic states. Impaired folic acid absorption can also result from functional and structural disorders of the small intestine, as well as deficiencies in enzymes that fail to form polyglutamine compounds [8].

Drugs such as Painkillers (e.g., ibuprofen or aspirin), antiepileptic drugs, antibiotics, corticosteroids, sulfonamides, and folic acid antagonists (such as trimethoprim and

methotrexate) also have a folate-lowering effect. Additionally, those at risk for folic acid deficiency include smokers, women using oral contraceptives, and alcoholics [9].

Regarding pregnancy, folic acid absence is closely linked to an increased occurrence of neural tube defects. A deficiency of this nutrient in the diet of pregnant women may raise the risk of the child developing and cleft palate and cleft lip, as well as increasing the incidence of Down syndrome [10].

Folic acid absence can negatively impact genome stability due to its vital role in the synthesis of thymines and purines. When folic acid levels are low, the availability of thymine, which is important for DNA polymerization and reparation, is reduced. As a result, incorrect incorporation of uracil instead of thymine can occur during replication, resulting in uracil-adenine conjugation. This defect can convert base pairs from GC to AT in the new DNA copy. This conversion is a potential source of serious genetic mutations. Severe folic acid absence, which is also essential for the synthesis of thymidine nucleotides, can lead to genome instability, connected with chromosomal abnormalities and DNA strand breaks. [11]. Research shows that the volume of uracil that is poorly bound to lymphocyte DNA is reduced in woman of reproductive age, which is associated with a daily intake of (400) micrograms of folacin, which in sequence underscores the need for folacin supplement through the reproductive time [12].

The genetic stability of a cell is also affected by the grade of genomic methylation, a compound known to play a chief role [13]. Therefore, a lack in nutritional folacin contributes to the disturbance of many critical metabolic processes and may lead to impaired cell growth and development. One of the most well-known roles of folate is the prevention of neural tube defects and pregnancy problems. It is also indicated for the prevention of, neurodegenerative diseases, cardiovascular disease, megaloblastic anemia and cancer [14, 8, 7].

3. Folacin and fetal growth illnesses:

Pregnant women are among the groups with the greatest need for folacin. An absence of this nutrient can cause many damaging consequences. Folacin is critical for the cell growth in the emerging embryo. The baby's brain and spinal cord develop from the neural tube; therefore, the timing of their development is crucial. Statistics indicate that central nervous system defects are a leading cause of neonatal mortality [15, 16].

During gravidity, folate deficiency leads to birth defects and problems such as abortion, placenta previa, prematurity, premature placental abruption, low birth weight, fetal death, and megaloblastic anemia [17].

Throughout gestation, the need for folacin rises and can only be partially met by consuming suitable nutrients that are sources of this nutrient. It is estimated that the nourishment covers (50%) of the daily necessity for these nutrients. Used for this purpose, nutritional supplements are recommended, which is especially important during pregnancy planning and in the first stages. The daily necessity for folate during pregnancy is 600 micrograms. References emphasize the need for all females of age to consume folic acid-rich products in their diet, in addition to fortified foods [18]. Females planning to become pregnant should take folacin supplements for at least (12) weeks before conception at a dose of 400 micrograms daily. Through the first trimester of gravidity—until the 12th week—folacin supplements should be taken at a dose of 400–800 micrograms daily. After the 12th week, females without further danger factors should take folate supplements at a dose of (600–800) micrograms daily. [19] Suitable folic acid intake stops the advance of neural tube faults.

These are inborn syndromes that emerge during fetal development and are extremely severe, disturbing the nervous system of child. Neural tube faults apparent for example spina bifida, anencephaly, microcephaly, or herniation of the nervous system, which causes, among other effects, bladder and rectal dysfunction, hydrocephalus, epilepsy, mental retardation, leg paralysis, and in severe cases can lead to death. The neural tube is an organ that forms initially during gestation, during the fetal period, approximately in the fourth week. regrettably, at the moment, a lot of women are ignorant of their pregnancy. A folic acid absence throughout this time will negatively affect the development of the child's nervous system and the closure of the neural tube [20]. According to the study, it was found that females who give birth to children with central nervous system defects have lower plasma folic acid levels and higher homocysteine levels [10].

All healthcare professionals must be fully aware of the importance of educating pregnant women about the role of folacin in avoiding congenital disabilities, especially those related to the neural tube. Failure to provide this basic information may constitute gross medical negligence and could lead to legal action, especially in cases where the child is born with a neural tube defect that could have been prevented through prior prevention. [7].

Despite the well-known benefits of folic acid, scientific evidence urges caution, especially in cases of megaloblastic anemia, as folic acid supplements can mask vitamin B12 deficiency, complicating diagnosis and treatment. In cases where the liver is impaired in folic acid metabolism, 5-MTHF supplementation is recommended. This non-activating supplement

immediately provides active folic acid to both mother and fetus without harmful accumulation in the blood, making it the ideal choice to ensure the safety of both [16].

Several epidemiological studies have shown that adding folate to the diet of mother before and during the first weeks of gestation, can be a key factor of the primary inhibition of congenital cardiac and vascular defects in the child. Studies on selected forms of these defects have demonstrated that folic acid supplementation meaningfully decreases the risk of cardiac septal defects (especially ventricular septal defects), as well as cone-shaped defects, and truncus arteriosus defects (specifically transpositon of the great vessels and Fallot syndrome) [21].

Obese females have been found to have double the danger of embryonic neural tube faults compared to females of standard weight. Furthermore, folic acid supplementation has been shown to reduce the danger of neural tube faults, which was chiefly evident in females with a BMI >25 kg/m2 compared to females with a BMI <25 kg/m2 [22]. Furthermore, fetal nervous system defects have been found to significantly affect women with type 1 or type 2 diabetes. [23] found a lower rate of neural tube faults in a group of diabetic women who took folate supplements at a dose greater than 400 µg/day.

4. Defects of neural tube

It is now accepted that supplementing with 400 mcg of folic acid close to gestation will stop most NTDs [24]. The advice for preventing recurrence in women with a history of neural tube defects remains 4.0 mg/day, given the significantly increased danger in such patients and because this is the dose used in the most rigorous trial [25]. Given the poor bioavailability and stability of folic acid in food, a diet high in folic acid would not be optimal for prevention. One study suggested that the risk of neural tube defects is 10 times higher in people with folate deficiency compared to those with high natural folate levels [26]. Another study suggests that an additional 200 mcg per day, or perhaps 100 mcg per day, as a routine intake in fortified foods would prevent most, if not all, of the NTDs that are preventable by folic acid [27].

Ideally, an additional 400 micrograms per day should be offered, as this is the quantity used in numerous intervention trials [28], and can be accomplished through dietary supplements. This quantity cannot be provided through fortification, because exposure to large amounts of folate by people who consume huge amounts of flour may put older adults at risk of pernicious anemia. It is likely that, dependent on the chosen staple food, it would be probable to raise the intake of most women by 100 micrograms per day without causing very high exposure in other groups. It is proposed that this quantity, although not ideal, would stop greatest NTDs.

Studies have shown that pregnant women's exposure to pesticides is associated with an increased risk of several congenital malformations, particularly neural tube defects, indicating that environmental pollution is an important factor in human health and fetal well-being (Figure 1). Of the 229 articles, 8 evaluated pesticide exposure during pregnancy. Various methods were used, including biological sample analysis and questionnaires. The pesticides studied included insecticides, herbicides, fungicides, and nematicides. Insecticides were the most studied, and concentrations were measured at different exposure periods (preconception and prenatal). Different data collection techniques and different types of biological samples were used. The main pesticides studied included DDT, DDE, HCH, and endosulfan. The results showed different levels of pesticides in maternal serum, placenta, and umbilical cord. Maternal serum showed the highest concentrations of pesticides, but their detection in placental and umbilical cord tissues confirms fetal exposure [29].

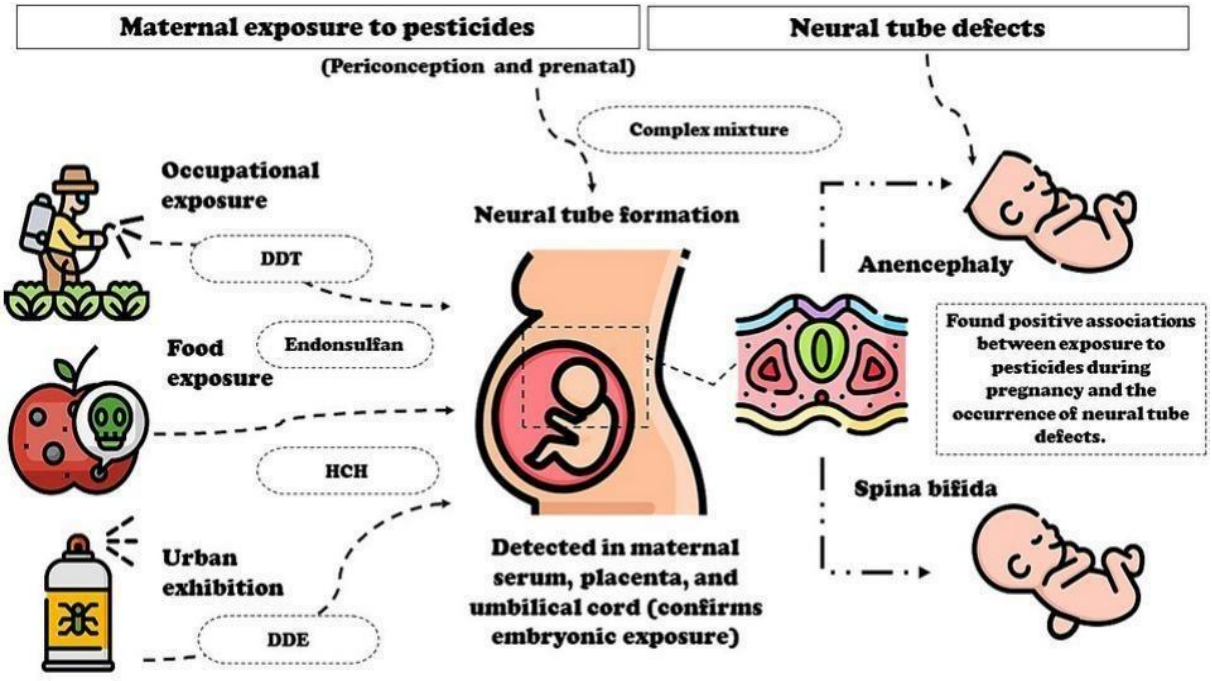


Figure 1: the exposure of pregnant women to pesticides

5. Conclusions

In conclusion, based on the presented data, it can be confirmed that folacin plays a critical and multifaceted role in the body and is a vital nutrient for maintaining proper bodily functions. It is imperative to highlight the role of folacin in pregnant women, as both its absence and excess are connected with an increased risk of several health problems, most notably congenital

abnormalities in the embryo, mainly neural tube defects, in addition to nervous system disorders, cardiovascular diseases, and some cancer types.

To prevent these birth defects and the associated health risks, women who are pregnant or planning pregnancy are advised to control their health by consuming a balanced diet rich in folate sources, for instance, whole grains, green leafy vegetables, citrus fruits, legumes, and nuts. If it is not possible to obtain adequate folic acid through diet alone, it is recommended to consult a doctor about folic acid supplements to help ensure fetal safety and support the mother's health throughout pregnancy.

6. References

[1] Singh C, Arti, Yadav N, Rao K, Bharti, Bansal N, Archna, KM. Nutrition role in maintaining health and preventing disease. Current Nutrition & Food Science. 2024; 20(8): 966-72. https://doi.org/10.2174/1573401319666230818122640

[2] Shulpekova Y, Nechaev V, Kardasheva S, Sedova A, Kurbatova A, Bueverova E et al. The concept of folic acid in health and disease. Molecules. 2021; 26(12): 3731. https://doi.org/10.3390/molecules26123731

[3] Asbaghi O, Ghanavati M, Ashtary-Larky D, Bagheri R, Rezaei Kelishadi M, Nazarian B. et al. Effects of folic acid supplementation on oxidative stress markers: a systematic review and meta-analysis of randomized controlled trials. Antioxidants. 2021; 10(6): 871. https://doi.org/10.3390/antiox10060871

[4] Engevik M A, Morra C N, Röth D, Engevik K, Spinler J K, Devaraj S. et al. Microbial metabolic capacity for intestinal folate production and modulation of host folate receptors. Frontiers in microbiology. 2019; 10: 2305. https://doi.org/10.3389/fmicb.2019.02305

[5] Tola, FS. The concept of folic acid supplementation and its role in prevention of neural tube defect among pregnant women: PRISMA. Medicine. 2024; 103(19): e38154. https://doi: 10.1097/MD.0000000000038154

[6] Koren O, Konnikova L, Brodin P, Mysorekar IU, Collado MC. The maternal gut microbiome in pregnancy: implications for the developing immune system. Nature

Reviews Gastroenterology & Hepatology. 2024; 21(1): 35-45. https://doi.org/10.1038/s41575-023-00864-2

[7] Khan K M, Jialal Is. Folic acid deficiency. In: StatPearls [internet]. StatPearls Publishing, 2023. https://creativecommons.org/licenses/by-nc-nd/4.0/

[8] Anwar S, Kumar V, Raut R. A review on factors causing vitamin b12 deficiency in pregnant women and infants. International Journal of Creative Research Thoughts. 2024; 12(1): 1-13. http://www.ijcrt.org/

[9] Tuenter A, Bautista Nino P K, Vitezova A, Pantavos A, Bramer W M, Franco O H, et al. Folate, vitamin B12, and homocysteine in smoking-exposed pregnant women: A systematic review. Maternal & child nutrition. 2019;15(1): e12675. https://doi.org/10.1111/mcn.12675

[10] Ruta H, Kajdy A, Maksym R. Znaczenie metabolizmu kwasu foliowego dla płodności. Kwartalnik Naukowy Fides Et Ratio. 2018; 35(3): 92-101. https://fidesetratio.com.pl/ojs/index.php/FetR/article/view/526

[11] Zhang N, Zhang H, Liang X, Xu Y, Wang G, Bai Y. et al. Neuroprotective effect of folic acid by maintaining DNA stability and mitochondrial homeostasis through the ATM/CHK2/P53/PGC-1α pathway in alcohol-exposed mice. Food & Function. 2025. https://doi.org/10.1039/D5FO00260E

[12] Gurugubelli K R, Ballambattu V B. Perspectives on folate with special reference to epigenetics and neural tube defects. Reproductive Toxicology. 2024; 125: 108576. https://doi.org/10.1016/j.reprotox.2024.108576

[13] Kurowska K, Kobylinska M, Antosik K. Folic acid-importance for human health and its role in COVID-19 therapy. Roczniki Państwowego Zakładu Higieny. 2023; 74(2). https://doi.org/10.32394/rpzh.2023.0252

[14] Badian M, Dzierżanowski T. Suplementacja witamin u chorych onkologicznych. Część I-witaminy z grupy B. Medycyna Paliatywna. 2018; 10(3): 131-136. http://dx.doi.org/10.5114/pm.2018.79835

[15] Banyś K J, Knopczyk M W, Bobrowska-Korczak B. Znaczenie kwasu foliowego dla zdrowia organizmu człowieka. Farmacja Polska. 2020; 76(2): 79-87. doi. 10.32383/farmpol/118863

[16] Ferrazzi E, Tiso G, Di Martino D . Folic acid versus 5-methyl tetrahydrofolate supplementation in pregnancy. European Journal of Obstetrics & Gynecology and Reproductive Biology. 2020; 253: 312-9. https://doi.org/10.1016/j.ejogrb.2020.06.012

[17] Chen D, Gao X, Yang T, Xin X, Wang G, Wang H, et al. independent risk factors for placental abruption: a systematic review and meta-analysis. BMC pregnancy and childbirth. 2025; 25(1): 351. https://doi.org/10.1186/s12884-025-07482-7

[18] Van Der Pols J C, Baade P, Spencer L B. Colorectal cancer incidence in Australia before and after mandatory fortification of bread flour with folic acid. Public Health Nutrition. 2021; 24(8): 1989-92. https://doi.org/10.1017/S1368980021000562

[19] Swora-Cwynar E, Polaczyk A, Dobrowolska A. ŻYWIENIE KOBIET W CIĄŻY I KARMIĄCYCH PIERSIĄ. Polish Nursing/Pielegniarstwo Polskie. 2023 Jul 1;89(3). doi.pielpol.2023.9/10.20883

[20] Zimmer M, Sieroszewski P, Oszukowski P, Huras H, Fuchs T, Pawłosek A. Rekomendacje Polskiego Towarzystwa Ginekologów i Położników dotyczące suplementacji u kobiet ciężarnych. Ginekologia i Perinatologia Praktyczna. 2020 ;5(4): 170-81. https://doi.org/10.5603/GP.2020.0159.

[21] Ekundayo B E, Adewale O B, Obafemi T O. Neuroprotective Effects of Folic Acid: A Review. Journal of Dietary Supplements. 2025; 22(2): 345-63. https://doi.org/10.1080/19390211.2024.2436842

[22] Loperfido F, Sottotetti F, Bianco I, El Masri D, Maccarini B, Ferrara C, et al. Folic acid supplementation in European women of reproductive age and during pregnancy with excessive weight: a systematic review. Reproductive Health. 2025; 22(1): 13. https://doi.org/10.1186/s12978-025-01953-y

[23] Ragazini C S, de Freitas Paganoti C, Coutinho C M, da Silva Costa F. Fetal Congenital Malformations in Diabetic Pregnancy. Textbook of Diabetes and Pregnancy. 2025, 133-40. https://doi.org/10.1201/9781003355939

[24] Qadriya F, Safira M.The Effect of Folic Acid Supplementation During Pregnancy on Infant Brain Health and Development: A Study in Cirebon District, Indonesia. International Journal on Health and Medical Sciences. 2025; 3(2): 68-76. https://doi.org/10.35335/healmed.v3i2.427

[25] Puspitasari M K, Irianti S, Pramatirta A Y, Wirawan W, Islamy N, Maelissa M M, et al. Folate Metabolism and Its Implications in Pregnancy. Journal La Medihealtico. 2025; 6(2): 285-98. https://doi.org/10.37899/journallamedihealtico.v6i2.1885

[26] Pacołta A, Nalepka M, Pograniczny M, Mielżyńska A, Pochopień J, Nowicka A. et al. Analysis of selected nutritional and environmental factors leading to the development of neural tube defects. Quality in Sport. 2025, 41: 60332-60332. https://doi.org/10.12775/QS.2025.41.60332

[27] Benavides-Lara A, Fernández-Sánchez O, Barboza-Argüello M D L P, Alfaro-Calvo T, Martínez H. Integrated surveillance strategy to support the prevention of neural tube defects through food fortification with folic acid: the experience of Costa Rica. Child's Nervous System. 2023; 39(7): 1743-54. https://doi.org/10.1007/s00381-023-05837-z

[28] Zadarko-Domaradzka M, Kruszyńska E, Zadarko E. Effectiveness of folic acid supplementation recommendations among polish female students from the podkarpackie region. Nutrients. 2021; 13(3): 1001. https://doi.org/10.3390/nu13031001

[29] Felisbino K, da Silva Milhorini S, Kirsten N, Bernert K, Schiessl R, Guiloski IC. Exposure to pesticides during pregnancy and the risk of neural tube defects: A systematic review. Science of The Total Environment. 2024 Feb 25; 913:169317. https://doi.org/10.1016/j.scitotenv.2023.169317

Al-Kitab Journal for Pure Sciences (2026); 10(2):143-154.
https://doi.org/10.32441/kjps.10.2.p11

Al-Kitab Journal for Pure Sciences
ISSN: 2617-1260 (print), 2617-8141(online)

https://isnra.net/index.php/kjps

Secondary Metabolites as a Nonenzymatic Antioxidant System in Plants: A Brief Review

[1]Faten Khaleel Ibrahim

[1]Department of Environmental Science, college Environmental Science, University of Mosul, Mosul, Iraq

Corresponding Author: fatinalatrakche@uomosul.edu.iq

Citation: ***Faten khaleel Ibrahim*. Secondary Metabolites as a Nonenzymatic Antioxidant System in Plants: A Brief Review Al-Kitab J. Pure Sci. [Internet]. 2025 Nov. 08 ;10(2):143-154 DOI.**
https://isnra.net/index.php/kjps/article/view/2026.
https://doi.org/10.32441/kjps.10.2.p11

Keywords: antioxidants, phenolic chemicals, secondary metabolites, plants, ROS.

Article History

Received	30 Aug.	2025
Accepted	08 Nov.	2025
Available online	01 Nov.	2026

©20--. THIS IS AN OPEN-ACCESS ARTICLE UNDER THE CC BY LICENSE
http://creativecommons.org/licenses/by/4.0/

Abstract:

Plants are constantly challenged by abiotic and biotic stresses including drought, salinity, heavy metals, UV radiation, and pathogen infections that result in excessive production of reactive oxygen species (ROS). Excessive ROS can cause oxidization of proteins, lipids, carbohydrates and nucleic acids which are detrimental to cellular components and thus impact plant growth and development. To avoid oxidative stress, plants require a finely tuned collaborative antioxidant defense system which includes enzymatic (peroxidases, catalases) and non-enzymatic (ascorbate, glutathione, alkaloids, flavonoids, and phenolic chemicals) antioxidants. Phenolic metabolites are derived from shikimate and mevalonate pathways with various biological actions. They are accumulated differentially across a variety of tissues, such as, roots, leaves, stems, flowers, fruits and seeds. The structural characteristics of phenolics aromatic rings with hydroxyl functional groups render them electro-donors or hydrogen donors to initiate ROS scavenging and ultimately stabilize the free radicals. Thus, we review herein that phenolics act as non-enzymatic antioxidants whose upregulation under stress is important for adaptive mechanism to postpone lipid peroxidation of membranes and nucleotides injury leading to premature programmed cell death. Therefore, this study seeks to collate the literature to date, to elucidate the biochemical truth about phenolics and their ecological significance in stress response with suggestions for further investigation.

Keywords: antioxidants, phenolic chemicals, secondary metabolites, plants, ROS.

مركبات الايض الثانوي كنظام مضاد للأكسدة غير انزيمي في النباتات

فاتن خليل ابراهيم

قسم علوم البيئة، كلية العلوم البيئية، جامعة الموصل، الموصل، العراق

الايميل الرسمي: fatinalatrakche@uomosul.edu.iq

الخلاصة:

تواجه النباتات باستمرار ضغوطًا حيوية وغير حيوية مثل الجفاف والملوحة والمعادن الثقيلة والإشعاع فوق البنفسجي والإصابات الممراضية، والتي تؤدي إلى الإنتاج المفرط لـ reactive oxygen species ROS. إن الزيادة في ROS تسبب أكسدة البروتينات والدهون والكربوهيدرات والأحماض النووية، مما يضر بالمكونات الخلوية وينعكس سلبًا على نمو النبات وتطوره. ولتجنب الإجهاد التأكسدي، تحتاج النباتات إلى منظومة دفاعية من مضادات الأكسدة تعمل بتنسيق دقيق وتشمل مضادات الأكسدة الإنزيمية (peroxidases, catalases) وغير الإنزيمية (ascorbate, glutathione, alkaloids, flavonoids, phenolic chemicals). وتشتق المركبات الفينولية من shikimate و mevalonate pathways، وتمارس أدوارًا بيولوجية متعددة. تتراكم هذه المركبات في أنسجة مختلفة مثل الجذور والأوراق والسيقان والأزهار والثمار والبذور.

إن الخصائص التركيبية للفينولات، والمتمثلة في الحلقات العطرية مع مجموعات هيدروكسيل، تجعلها مانحة للإلكترونات أو للهيدروجين لبدء إزالة ROS واستقرار الجذور الحرة في النهاية. ومن هنا نستعرض أن الفينولات تعمل كمضادات أكسدة غير إنزيمية، حيث يُعَدّ تحفيز إنتاجها تحت ظروف الإجهاد آلية تكيفية مهمة لتأخير بيروكسدة الدهون في الأغشية ومنع تلف النيوكليوتيدات التي تؤدي إلى الموت الخلوي المبرمج المبكر. وبناءً على ذلك، يهدف هذا البحث إلى تجميع الأدبيات الحديثة لتوضيح الحقيقة البيوكيميائية حول الفينولات وأهميتها البيئية في الاستجابة للإجهاد مع تقديم مقترحات لمزيد من الدراسات المستقبلية.

الكلمات المفتاحية: مضادات الاكسدة، المركبات الفينولية، مركبات الايض الثانوي، النباتات، انواع الاوكسجين التفاعلي.

1. Introduction:

The plants produce primary and secondary metabolites which both exhibit specific functions. Proteins, lipids, nucleic acids, carbohydrates and fatty acids act in plant primary metabolism. Also, plants produce secondary metabolites that act as a natural supply of antioxidants to protect the plants [1]. Different plant components, including leaves, stems, flowers, fruits, and seeds, produce these substances. There are several ways to release these chemicals into the atmosphere or into the rhizosphere, including Leaching, root exudation, volatilization, and soil residue breakdown. It is divided into several types depending on its composition and characteristics. The study by [2] divided secondary metabolites into organic acids such as ketones, aliphatic

aldehydes, and straight-chain alcohols, Long-chain fatty acids, unsaturated lactones, simple, quinines, derivatives of cinamic acid, Coumarins chemicals, phenols, Tannins, Flavonoids and Terpenoid. Certain large groups of secondary metabolites are synthesized under environmental stress and act as antioxidants in plants. Both enzymatic and non-enzymatic antioxidants make up a plant's antioxidant system; the most significant non-enzymatic antioxidants are alkaloids, glutathione, phenolic chemicals, ascorbic acid, flavonoids, and non-protein amino acids. Additionally, plants produce enzymatic antioxidants like peroxidase, catalase, superoxide dismutase and monodehydroascorbate reductase [3].

Phenolic chemicals:

Plants synthesize large numbers of phenol derivatives collectively named as phenolic chemicals. The chemical structure of these compounds is aromatic with one or more hydroxyl groups and also have at least one benzene ring with one or more hydroxyl groups, which is able to donate hydrogen atoms or electrons in order to equation radicals or any environmental stress and reactive oxygen species [1]. Biosynthetic pathway of principal phenolic and flavonoid secondary metabolites in plants. Shikimic acid and phenylpropanoid pathways. Involved in glycolytic and pentose phosphate pathways—phosphoenolpyruvate and erythrose-4-phosphate—contribute to shikimate pathway; derive aromatic amino acids (phenylalanine, tyrosine, tryptophan) and gallic acid. Phenylalanine is converted to cinnamic acid via the phenylpropanoid pathway and to p-coumaric acid and p-coumaroyl-CoA, central and common intermediates for an extensive variety of phenolic chemicals (i.e. tannins, lignins, coumarins) as well as precursors to flavonoids via chalcone. Differing branches then proceed to create flavonols, anthocyanidins, catechins, isoflavonoids, flavones [4] Figure (1).

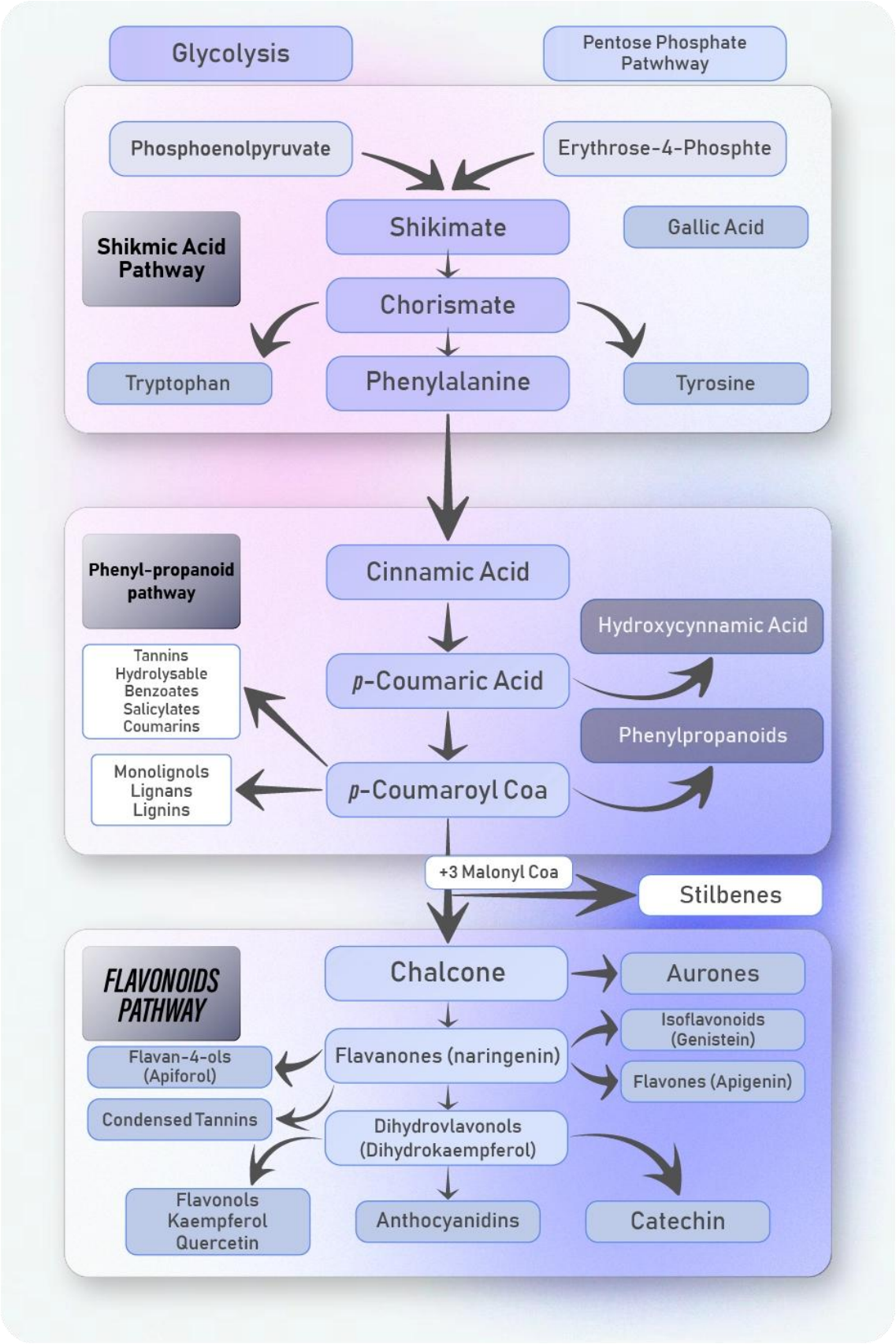


Fig. 1: Biosynthesis pathway of phenolic chemicals in plants.

Certain phenolic chemicals are categorized based on the degree of oxidation or unsaturation or the number of carbon atoms in their structure [5]. Plants photosynthesize approximately 2% of all organic molecules, subsequently transforming them into phenolic chemicals. Most phenolic groups are conjugated naturally with mono or polysaccharides. Plant phenolics are the most widely produced and distributed in plants, bacteria, algae, and fungi. Plant leaves contain hydroxycinnamic acids, flavonoids, lignin and glycosylated flavonoids [6,7]. Phenolic chemicals are classified into simple and polyphenolic chemicals according to the number of phenol units contained. Simple phenolics such as catechol, resorcinol, and hydroquinone (Figure 2) contain one phenol unit.

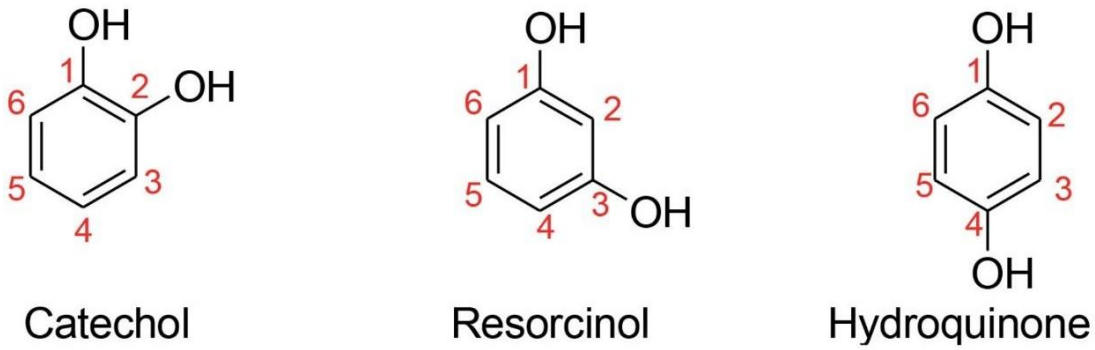


Fig. 2: Simple phenols.

Polyphenols contain more than one phenol group, such as coumarin, ferulic acid, sinapic acid, cinnamic acid, caffeine, and hydrocoumarin (Figure 3).

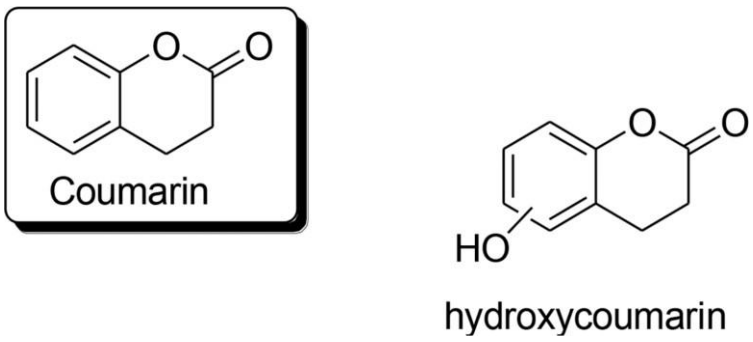


Fig. 3: Polyphenols.

Biosynthesis of phenolic chemicals is often affected by plant environments, like plant pathogens, moisture, UV light, pH, and water stress. When plants are exposed to environmental stressors like drought stress, phenolic chemicals play a significant role as their non-enzymatic antioxidant system. UV light, pH, and numerous additional biotic and abiotic elements cause plants to create an unbalanced rate of reactive oxygen. Synthesis of the plant antioxidant system and reactive oxygen species (ROS) result in the plant's elevated oxidative stress [8]. The aim of this review is to summarize the role of secondary metabolites, especially phenolic chemicals, as non-enzymatic antioxidants in plants exposed to various stresses. The review also identifies gaps in current knowledge and suggests directions for future research to improve our understanding of plant stress tolerance and its applications in crop production.

Phenolic chemicals' Function in Abiotic Stress: Under abiotic stress, phenolic acids interact with their environment and mediate adaptive responses by producing protective secondary metabolites[9]. Phenolic chemicals build up in plant tissue in response to negative stress, which is thought to be a physiological adaptation for survival in the face of environmental disruptions [10]. The antioxidant properties of flavonoids, hydroxycinnamate esters, tannins, and lignin aid in the defense against biotic and abiotic stress. Phenolic chemicals also promote lipid peroxidation and break free radical chains [11]. Phenolic chemicals have been classified into five subcategories (flavonoids, coumarins, phenolic acids, lignin and tannins.), It has been improved that increased gene expression was the cause of the rise in phenolic chemicals in several stressed plants [12, 13, 14]. They conclude that the accumulation of phenolic chemicals in *Rehmannia glutinosa* occurs under stress because of increasing enzyme activities such as phenylalanine ammonia lyase (PAL). Abiotic stress enhances phenolic acid levels through cinnamic acid metabolism, including methylation and hydration/dehydration reactions, supporting plant survival under environmental challenges. Implication of plants to different stresses by scavenging of ROS, boosting the production of secondary metabolites, like phenolic chemicals, as a way to protect plants, [14] It is notedthat when plants are exposed to injury, such as a wound or cut in tissues, they may use sustainable methods as a defense by boosting antioxidant activity and phenolic compound production. When plants grow in areas of adverse conditions face water stress, heavy metals stress, extreme temperatures, salinity, and other abiotic stresses, which affect plant development, growth and productivity. [15]. Different reactive oxygen species (ROS) were created by plants in response to stressors. Overproduction of ROS caused damage to the cells of plants, such as carbohydrates, proteins, and DNA, finally causing disturbance of the balance between normal (ROS) production and antioxidants, leading

to oxidative stress in plants [16]. The antioxidant system helps plants adapt to oxidative stressors. It consists of enzymatic antioxidants like peroxidase, catalase, glutathione reductase, superoxide dismutase, hydroascorbate reductase, glutathione peroxidase, and ascorbate reductase, as well as nonenzymatic antioxidants like ascorbic acid, glutathione, flavonoids, phenolic chemicals, and alkaloids [17]. Under severe situations, plants' antioxidant systems are crucial because they scavenge reactive oxygen species (ROS), prevent lipid peroxidation, DNA damage, and protein breakdown; inhibit enzymes, and ultimately postpone cell death [18].Phenolic chemicals' function in heavy metal stress: One significant source of stress is brought on by the toxicity of heavy metals which causes harmful effects in physiological processes [19,20], It proved that nanoparticles such as Ag, CuO, CeO2 and Cu can be used for the induction of phenolic chemicals; increased production of ROS led to an increase in phenolic chemicals. Biosynthesis of Phenolic substances in Zea mays L. in contaminated soil with aluminum ion, rootexudates of the plant have high levels of catechin and quercetin [21,22] was reported that high levels of flavonoids in cells of Digitalis lanata L. are usuallyassociated with high concentrations of CuSo4.Increasing the supply of Molybdenum (Mo) caused improved antioxidant system in plant enzymatic and nonenzymatic processes and increased metabolism and growth [23].When plants take up heavy metals (Cr, Cd, Hg, Co, Mn, Ni, Pb and Zn) this inhibits major physiologicalactivities in plant cells such as photosynthesis, cell elongation, and respiration. The harm of heavy metals takes place through the increase of ROS by oxidation and inhibition of polynucleotide and protein functional groups, inactive enzymes responsible for detoxification of free radicals [24].

Role of phenolic chemicals under drought stress:

Drought is the primary abiotic stressor that affects plant development and reduces plant yield, plant phenolic chemicals content increases under water stress. [25] reported that quercetin concentration increased significantly in white clover when the plant was exposed to drought. [26] has reported that different types of plants such as cereals, fruits and vegetables accumulate phenolic chemicals when grown under drought conditions.Plants antioxidants that accumulate under water stress include phenolic chemicals and flavonoids. *Amaranthus tricolor* is vegetable accumulate flavonoids in response to drought conditions [27]. Under water stress phenolic chemicals act as a nonenzymatic antioxidant system to equation the harmful effects of (ROS), even plants resistant to drought conditions (arid or semiarid habitats) may produce high concentrations of phenolic chemicals and flavonoids in contrast to the same plants that thrived in water with moderate levels of moisture [28]. In response to drought stress, plants

physiologically constrict their stomata, reducing transpiration and water loss,CO2 concentration and fixation via the Calvin cycle reduced, increase NADPH+H production during photosynthesis (light reactions), causing reduced growth of the plant. As a response, the plant increases antioxidants [29]. An experiment studied the response of 21 barley cultivars to water stress, tested the impact of water deficit on phenolic compound content in the studied cultivars, antioxidant enzyme activity and oxidative stress. It was found that water stress increased content of phenolics and flavonoids. [30]

Phenolic chemicals' function in nutrient stress:

The development of plants depends on nutrients from their environment which are regulated by several factors, including microorganisms, climate, substrate quality, and nutrient leachates into the soil [31]. Plant phenolic affect the activity of soil microorganisms and nutrient cycling. When a plant is exposed to nutrient deficits, phenolic chemicals are crucial. such as (N, P, K) and S, rapidly increasing the concentration of phenolic chemicals [6]. Tomato plants increased levels of Anthocyanin and Quercetin when grown under nutrient stress conditions [32, 33], demonstrating that limitation of (N) in *Lactuca sativa* L. caused an increase in phenolic chemicals and antiradical activity, while reduction in (P) nutrition did not affect the composition of Lettuce phytochemicals.

5. Conclusions:

Plants subjected to general stress effects on cellular components like carbohydrates, proteins, lipids, and DNA were omitted with a focus on the general effect of various biological and environmental stresses leading to oxidation. Secondary metabolites and the plant's antioxidant system, which consists of both enzymatic and nonenzymatic antioxidant systems in plants act as a nonenzymatic antioxidant system divided into organic acids, ketones, simple unsaturated lactones, quinones, cinnamic acids, phenolics, tannins, flavonoids, and terpenoids. Phenolic chemicals are a certain group of secondary metabolites synthesized under environmental stress that act as a nonenzymatic antioxidant in plants, equation ROS, and delay cell death, released to the environment by various ways such as volatilization, leaching, root exudation, and decomposition.

This review focuses on the key mechanisms used by plants when subjected to various biotic and abiotic challenges, with secondary metabolites being among the most important of these plant-derived chemicals. Heat stress, salt, drought, and acidity all cause a significant increase

in the accumulation of such secondary metabolites, which act as protective agents for the plant, reducing environmental damage.

Despite the overwhelming evidence of secondary metabolites' protective impact, there are significant limitations and information gaps. For example, the particular regulatory networks that regulate their production under combined stress circumstances are not yet fully understood, and the heterogeneity among plant species needs more comparative research. Furthermore, most recent findings are based on controlled laboratory circumstances, and their relevance to real-world settings requires confirmation. Future study should integrate molecular, physiological, and ecological techniques to better understand these chemicals' dynamic activities, with a focus on genetic engineering, breeding programs, and biotechnological applications to improve crop stress tolerance.

6. References

[1] E. P. da Silva, “The role of phenolic compounds in metabolism and their antioxidant potential ”, *RSD*,vol. 11, no. 10, p. e297111031750, Aug. 2022. doi: 10.33448/rsd-v11i10.31750.

[2] W. Mushtaq, M. B. Siddiqui, and K. R. Hakeem, *Allelopathy: Potential for Green Agriculture*, 1st ed., SpringerBriefs in Agriculture. Springer Cham, 2020. doi: 10.1007/978-3-030-40807-7.

[3] M. Fujita and M. Hasanuzzaman, "Approaches to Enhancing Antioxidant Defense in Plants,"*Antioxidants*, vol. 11, no. 5, p. 925, 2022, doi: 10.3390/antiox11050925.

[4] A. Kołton, O. Długosz-Grochowska, R. Wojciechowska, and M. Czaja, "Biosynthesis Regulation of Folates and Phenols in Plants," *Scientia Horticulturae*, vol. 291, p. 110561, 2022, doi: 10.1016/j.scienta.2021.110561.

[5] Saul S, Barboza OM, Souza JT, Soares ÉN, Cleonice S, Pacheco LV, et al. Structural design, synthesis and antioxidant, antileishmania, anti-inflammatory and anticancer activities of a novel quercetin acetylated derivative. Molecules. 2021;26. doi: 10.3390/molecules26226923.

[6] M. I. Naikoo, M. I. Dar, F. Raghib, H. Jaleel, B. Ahmad, A. Raina, F. A. Khan, and F. Naushin, "Role and Regulation of Plants Phenolics in Abiotic Stress Tolerance: An Overview," in *Plant Signaling Molecules*, M. I. R. Khan, P. S. Reddy, A. Ferrante, and N. A. Khan, Eds. Woodhead Publishing, 2019, pp.157-168, doi: 10.1016/B978-0-12-816451-8.00009-5.

[7] H. H. Al Mamari, 'Phenolic Compounds: Classification, Chemistry, and Updated Techniques of Analysis and Synthesis', Biochemistry. IntechOpen, Feb. 23, 2022. doi: 10.5772/intechopen.98958.

[8] S. Kumar, B. Bhushan, G. C. Wakchaure, K. K. Meena, M. Kumar, N. L. Meena, and J. Rane, " Plant Phenolics Under Water-Deficit Conditions: Biosynthesis, Accumulation, and Physiological Roles in WaterStress Alleviation" in *Plant Phenolics in Sustainable Agriculture: Volume 1*, R. Lone, R. Shuab, and A. N. Kamili, Eds. Singapore: Springer Singapore, 2020, pp. 451-465. doi: 10.1007/978-981-15-4890-1_19.

[9] V. Lattanzio, "Phenolic Compounds: Introduction," in *Natural Products: Phytochemistry, Botany andMetabolism of Alkaloids, Phenolics and Terpenes*, K. G. Ramawat and J.-M. Mérillon, Eds. Berlin, Heidelberg: Springer Berlin Heidelberg, 2013, pp. 1543-1580. doi: 10.1007/978-3-642-22144-6_57.

[10] M. I. Dar, M. I. Naikoo, F. A. Khan, F. Rehman, I. D. Green, F. Naushin, and A. A. Ansari, " An Introduction to Reactive Oxygen Species Metabolism Under Changing Climate in Plants", 2017, pp. 25-52, doi: 10.1007/978-981-10-5254-5_2.

[11] T. S. Per, M. I. R. Khan, N. A. Anjum, A. Masood, S. J. Hussain, and N. A. Khan, "Jasmonates in plants under abiotic stresses: Crosstalk with other phytohormones matters," Environmental and Experimental Botany, vol. 145, pp. 104–120, Jan. 2018, doi: 10.1016/j.envexpbot.2017.11.004.

[12] Weidner S, Karamać M, Amarowicz R, Szypulska E, Gołgowska A. Changes in composition of phenolic compounds and antioxidant properties of Vitis amurensis seeds germinated under osmotic stress. Acta Physiologiae Plantarum. 2007;29(3):283–90. doi: 10.1007/s11738-007-0035-4.

[13] I. M. Chung, J. J. Kim, J. D. Lim, C. Y. Yu, S. H. Kim, and S. J. Hahn, "Comparison of resveratrol, SOD activity, phenolic compounds and free amino acids in Rehmannia glutinosa under temperature and water stress," Environmental and Experimental Botany, vol. 56, no. 1, pp. 44–53, May 2006, doi: 10.1016/j.envexpbot.2005.01.001.

[14] W. Hu, Sarengaowa, Y. Guan, and K. Feng, "Biosynthesis of Phenolic Compounds and Antioxidant Activity in Fresh-Cut Fruits and Vegetables," Frontiers in Microbiology, vol. 13, May 2022, doi: 10.3389/fmicb.2022.906069.

[15] M. Chaki, J. C. Begara-Morales, and J. B. Barroso, "Oxidative Stress in Plants," Antioxidants, vol. 9, no. 6, p. 481, Jun. 2020, doi: 10.3390/antiox9060481.

[16] Hasanuzzaman M, Bhuyan MHMB, Zulfiqar F, Raza A, Mohsin SM, Mahmud JA, et al. Reactive Oxygen Species and Antioxidant Defense in Plants under Abiotic Stress:

Revisiting the Crucial Role of a Universal Defense Regulator. Antioxidants. 2020;9(8). doi: 10.3390/antiox9080681.

[17] M. Hasanuzzaman, J. A. Mahmud, T. I. Anee, K. Nahar, and M. T. Islam, "Drought Stress Tolerance in Wheat: Omics Approaches in Understanding and Enhancing Antioxidant Defense," Abiotic Stress-Mediated Sensing and Signaling in Plants: An Omics Perspective, pp. 267–307, 2018, doi: 10.1007/978-981-10-7479-0_10.

[18] J. Dumanović, E. Nepovimova, M. Natić, K. Kuča, and V. Jaćević, "The Significance of Reactive Oxygen Species and Antioxidant Defense System in Plants: A Concise Overview," Frontiers in Plant Science, vol. 11, Jan. 2021, doi: 10.3389/fpls.2020.552969.

[19] Villiers F, Ducruix C, Hugouvieux V, Jarno N, Ezan E, Garin J, et al. Investigating the plant response to cadmium exposure by proteomic and metabolomic approaches. Proteomics. 2011;11(9):1650–63. doi: 10.1002/pmic.201000645.

[20] M. Hatami, H. Naghdi Badi, and M. Ghorbanpour, "Nano-Elicitation of Secondary Pharmaceutical Metabolites in Plant Cells: A Review," Journal of Medicinal Plants, vol. 3, no. 71, pp. 6–36, Sep. 2019, doi: 10.29252/jmp.3.71.6.

[21] A. Michalak, "Phenolic compounds and their antioxidant activity in plants growing under heavy metal stress," *Polish Journal of Environmental Studies*, vol. 15, pp. 523-530, 2006, https://api.semanticscholar.org/CorpusID:43555846.

[22] C. Bota and C. Deliu, "The effect of copper sulphate on the production of flavonoids in Digitalis lanata cell cultures" FARMACIA, vol. 59, p. 1, 2011, Accessed: Aug. 19, 2024, [Online].

[23] Imran M, Hussain S, He L, Ashraf MF, Ihtisham M, Warraich EA, et al. Molybdenum-Induced Regulation of Antioxidant DefenseMitigated Cadmium Stress in Aromatic Rice and Improved Crop Growth, Yield, and Quality Traits. Antioxidants. 2021;10(6). doi: 10.3390/antiox10060838ff.

[24] V. Rai, P. Vajpayee, S. N. Singh, and S. Mehrotra, "Effect of chromium accumulation on photosynthetic pigments, oxidative stress defense system, nitrate reduction, proline level and eugenol content of Ocimum tenuiflorum L.," Plant Science, vol. 167, no. 5, pp. 1159–1169, Nov. 2004, doi: 10.1016/j.plantsci.2004.06.016.

[25] Nakabayashi R, YonekuraSakakibara K, Urano K, Suzuki M, Yamada Y, Nishizawa T, et al. Enhancement of oxidative and drought tolerance in Arabidopsis by overaccumulation of antioxidant flavonoids. Plant J. 2014;77(3):367–79. doi: 10.1111/tpj.12388.

[26] L. Siracusa, F. Gresta, E. Sperlinga, and G. Ruberto, "Effect of sowing time and soil water content on grain yield and phenolic profile of four buckwheat (Fagopyrum esculentum Moench.) varieties in a Mediterranean environment," Journal of Food Composition and Analysis, vol. 62, pp. 1–7, Sep. 2017, doi: 10.1016/j.jfca.2017.04.005.

[27] U. Sarker and S. Oba, "Response of nutrients, minerals, antioxidant leaf pigments, vitamins, polyphenol, flavonoid and antioxidant activity in selected vegetable amaranth under four soil water content," Food Chemistry, vol. 252, pp. 72–83, Jun. 2018, doi: 10.1016/j.foodchem.2018.01.097.

[28] C. Brunetti et al., "Metabolic plasticity in the hygrophyte Moringa oleifera exposed to water stress," Tree Physiology, Aug. 2018, doi: 10.1093/treephys/tpy089.

[29] Król A, Amarowicz R, Weidner S. Changes in the composition of phenolic compounds and antioxidant properties of grapevine roots and leaves (*Vitis vinifera L.*) under continuous of longterm drought stress. Acta Physiologiae Plantarum. 2014;36(6):1491–9. doi: 10.1007/s11738-014-1526-8.

[30] Mohagheghian B, Saeidi G, Arzani A. Phenolic compounds, antioxidant enzymes, and oxidative stress in barley (Hordeum vulgare L.) genotypes under field droughtstress conditions. BMC Plant Biology. 2025;25(1):709. Available from: https://doi.org/10.1186/s12870025067500.

[31] V. Lattanzio, V. Lattanzio, and A. Cardinali, "Role of phenolics in the resistance mechanisms of plants against fungal pathogens and insects" *Research Signpost*, vol. 37, no. 2, pp. 81–308, 2006. [Online].

[32] N. Tuteja and S. Mahajan, "Calcium Signaling Network in Plants," Plant Signaling & Behavior, vol. 2, no. 2, pp. 79–85, Mar. 2007, doi: 10.4161/psb.2.2.4176.

[33] Galieni A, Mattia D, Gregorio D, Speca S, Mastrocola D, Pisante M, et al. Effects of nutrient deficiency and abiotic environmental stresses on yield, phenolic compounds and antiradical activity in lettuce (Lactuca sativa L.). Scientia Horticulturae. 2015;187:93–101. doi: 10.1016/j.scienta.2015.02.036.

Al-Kitab Journal for Pure Sciences (2026); 10(2):155-167.
https://doi.org/10.32441/kjps.10.2.p12

Al-Kitab Journal for Pure Sciences
ISSN: 2617-1260 (print), 2617-8141(online)

https://isnra.net/index.php/kjps

Antimicrobial Resistance Patterns of *Acinetobacter Haemolyticus* from Urinary Tract Infections and Hospital Wastewater

Jilan Ahmed Shakur[1], Alaa R. Nadim[2], Wael Adil Obaid[3], Rafeef A. Yass[4]

[1,2,4]College of Medical Laboratory Techniques. Imam Jaafar AI- Sadiq University, Kirkuk, Iraq

[3]Department of Applied Pathological Analysis, College of Science, Al-Nahrain University, Jadiriya, Baghdad, Iraq

Corresponding Author: [1]gilan-ahmed1@ijsu.edu.iq, [2]alaa.rafaa@ijsu.edu.iq, [3]Waeladil@nahrainuniv.edu.iq, [4]rafefahmed@ijsu.edu.iq

Citation: ***Jilan Ahmed Shakur[1], Alaa R. Nadim[2], Wael Adil Obaid[3], Rafeef A. Yass[4]*. Antimicrobial Resistance Patterns of *Acinetobacter haemolyticus* from Urinary Tract Infections and Hospital Wastewater.**
Al-Kitab J. Pure Sci. [Internet]. 2025 Dec. 06 ;10(2):155-167
DOI.
https://isnra.net/index.php/kjps/article/view/2026.
https://doi.org/10.32441/kjps.10.2.p12

Keywords: *Acinetobacter haemolyticus*, MIC, Antibiotic Resistance, Hospital Wastewater, Urinary Tract Infection.

Article History

Received	14 Sep. 2025
Accepted	06 Dec. 2025
Available online	01 Nov. 2026

©20--. THIS IS AN OPEN-ACCESS ARTICLE UNDER THE CC BY LICENSE
http://creativecommons.org/licenses/by/4.0/

Abstract:

Acinetobacter haemolyticus is a pathogenic species and a bacterium resistant to various types of antibiotics. This study aims to identify the source of *Acinetobacter haemolyticus* infections and determine the most effective treatment options. The research also compares isolates from wastewater and urinary tract infection (UTI) patients to evaluate differences in their antibiotic susceptibility and resistance. Additionally, it examines whether antibiotics effective against clinical UTI isolates show the same effectiveness against wastewater isolates. From thirty samples, 5 samples of urine isolated (33.3%) were of *Acinetobacter haemolyticus*, while the remaining 10 samples (66.6%) showed negative growth. However, out of 15 hospital wastewater samples, 3 (20%) isolated *Acinetobacter haemolyticus*, whereas the remaining 80% showed negative growth. Furthermore. The present results showed that *Acinetobacter haemolyticus* was sensitive to some antibiotics, including ampicillin, gentamicin, piperacillin-tazobactam, cefepime, cefuroxime, trimethoprim-sulfamethoxazole, amikacin, ceftazidime,

cefoperazone-sulbactam, and minocycline, and resistant to two types of antibiotics, including imipenem and meropenem. In this study, even though *Acinetobacter haemolyticus* was isolated from two distinct sources (sewage and urine), it produced identical results in terms of minimum inhibitory concentration, antibiotic resistance, and appropriateness. This work opens the door up to several other investigations. One of those genes examined each type of bacterium based on where it was isolated (inside or outside the human body), revealing the differences between the bacteria's genes and whether or not environmental factors affected these bacteria.

Keywords: *Acinetobacter haemolyticus*, Minimum Inhibitory Concentration, Antibiotic Resistance, Hospital Wastewater, Urinary Tract Infection.

أنماط المقاومة المضادة للميكروبات لبكتيريا *Acinetobacter haemolyticus* المعزولة من التهابات المسالك البولية ومياه الصرف الصحي في المستشفيات

جيلان احمد شكور[1]، الاء رافع ناظم[2]، وائل عادل عبيد[3]، رفيف احمد ياس[4]

[1,2,4]كلية تقنيات المختبرات الطبية، جامعة الإمام جعفر الصادق، كركوك، العراق

[3]قسم التحليلات المرضية التطبيقية، كلية العلوم، جامعة النهرين، الجادرية، بغداد، العراق

الايميل الرسمي: [1]gilan-ahmed1@ijsu.edu.iq [2]alaa.rafaa@ijsu.edu.iq [3]Waeladil@nahrainuniv.edu.iq [4]rafef_ahmed@ijsu.edu.iq

المستخلص:

تعدُّ البكتيريا الانحلالية نوعا ممرضا ومقاوما لأنواع مختلفة من المضادات الحيوية. تهدف هذه الدراسة إلى تحديد مصدر عدوى البكتيريا الانحلالية وتحديد خيارات العلاج الأكثر فعالية ضدها. فضلا عن ذلك، قارن البحث بين عزلات من مياه الصرف الصحي ومرضى التهاب المسالك البولية لتقييم الاختلافات في حساسيتهم للمضادات الحيوية ومقاومتهم لها. و يدرس البحث ما إذا كانت المضادات الحيوية الفعالة ضد عزلات التهاب المسالك البولية السريرية تُظهر نفس الفعالية ضد عزلات مياه الصرف الصحي. من بين ثلاثين عينة، عُزلت ٥ عينات بول (٣٣,٣٪) من البكتيريا الانحلالية، بينما أظهرت العينات العشر المتبقية (٦٦,٦٪) نموًا سلبيًا. ومع ذلك، من بين ١٥ عينة من مياه الصرف الصحي للمستشفيات، عُزلت ٣ عينات (٢٠٪) من البكتيريا الانحلالية، بينما أظهرت العينات المتبقية (٨٠٪) نموًا سلبيًا. وأظهرت النتائج أن بكتيريا *Acinetobacter haemolyticus* حساسة لبعض المضادات الحيوية، بما في ذلك الأمبيسلين، والجنتاميسين، والبيبراسيلين-تازوباكتام، والسيفيبيم، والسيفوروكسيم، والتريميثوبريم-سلفاميثوكسازول، والأميكاسين، والسيفتازيديم، والسيفوبيرازون-سولباكتام، والمينوسيكلين، ومقاومة لنوعين من المضادات الحيوية، بما في ذلك الإيميبينيم والميروبينيم. وعلى الرغم من عزل بكتيريا *Acinetobacter haemolyticus* من مصدرين مختلفين (مياه الصرف الصحي والبول)، إلا أنها أسفرت عن نتائج متطابقة من حيث الحد الأدنى للتركيز المثبط، ومقاومة المضادات الحيوية، والملاءمة. لذا، يفتح هذا العمل الباب أمام العديد من الأبحاث الأخرى مثل امكانية فحص أحد جينات كل نوع من البكتيريا بناءً على مكان عزله (داخل أو خارج جسم الإنسان)، كاشفًا عن الاختلافات بين جينات البكتيريا وما إذا كانت العوامل البيئية تؤثر عليها أم لا.

الكلمات المفتاحية: البكتيريا الانحلالية، الحد الأدنى من التركيز المثبط ، مقاومة المضادات الحيوية، مياه الصرف الصحي في المستشفيات، عدوى المسالك البولية.

1. Introduction:

Members of the bacterium genus *Acinetobacter* have become one of the most significant drivers of hospital-acquired infections in the past 20 years, overcoming their relative obscurity, demonstrating an amazing capacity of these organisms to acquire antibiotic resistance determinants, with some strains already exhibiting resistance to all clinically used antibiotics [1]. New antibacterial substances are desperately needed to counter the threat posed by *Acinetobacter* species and other uncontrollable bacterial infections. The logical development of antimicrobial medications finds appealing targets in the fundamental mechanisms of transcription, cell division, and chromosomal DNA replication [2]. *Acinetobacter haemolyticus* is a significant species; its resistance to antibiotics has risen due to abuse of antibiotics and the frequent gene exchange between bacteria in hospitals [3]. *Acinetobacter* species are characterized as aerobic, small bacilli that thrive in moist environments easily isolated from various sources like sewage, water, food, and soil [4].

These species are oxidase-negative, catalase-positive, non-motile coccobacilli that thrive in damp environments. Non- fermenting and non-fastidious, the prevalent and clinically significant species of this genus are *Acinetobacter baumannii* and *Acinetobacter haemolyticus* [5]. In intensive care units, *Acinetobacter* species are responsible for about 20% of bacterial infections, making them one of the opportunistic bacteria associated with hospital-acquired infections [6]. *Acinetobacter* species can also be isolated from other sources including pus, wound swabs, sputum, tissue, bronchial washings, cerebrospinal fluid, blood and urine [7]. UTI, ventilator-associated pneumonia, wound infections, and septicemia are among the nosocomial illnesses caused by *Acinetobacter*. The following are risk factors for *Acinetobacter* infections: prolonged hospital stays, immunodeficiency, surgery, burns, aging, the use of antibacterial medications, and invasive devices. Almost all commonly given antimicrobial drugs, such as aminoglycosides, fluoroquinolones, and broad-spectrum beta-lactams, are seeing an increase in resistance in *Acinetobacter* species. Although most strains are resistant to the cephalosporin class of medications, reports of carbapenem resistance are on the rise [8].

Acinetobacter's antibiotic susceptibility patterns might fluctuate greatly between geographical locations and even over time in several hospital units. In order to choose the best course of action, it is crucial to routinely check these infections because of these differences. *Acinetobacter* infections have a major effect on rates of morbidity and death, which raises mortality among critically sick patients. *Acinetobacter* is normally regarded as a low-pathogenicity bacterium but when isolated from individuals who are very sick or have impaired

immune systems, it can be quite dangerous. Usually, nosocomial infections rather than community-acquired illnesses are linked to these pathogens [9].

Acinetobacter spp. accounted for 3.7 and 7.5% of isolates, respectively, making them the eighth and fifth most frequent infections in the USA and Europe, respectively, in a recent series that examined over 13,000 patients hospitalized with pneumonia. Endotracheal intubations, surgery, previous antibiotic treatment, and underlying pulmonary illness are risk factors. The development of a bronchopulmonary fistula, pleural effusion, and multilobular involvement are possible clinical manifestations. According to some reports, mortality rates as high as 70% may be due to the underlying illness of the patient rather than the organism's virulence [10]. The purpose of this research is to determine the origin of *Acinetobacter haemolyticus* infections and to determine the most effective treatment strategy.

2. Material and methods:

2.1. Study Design

Research samples were taken from Tuz Hospital in Sala Hedin Governorate from January to May 2025 from two sources for *Acinetobacter haemolyticus* (urine and hospital wastewater). The sterilization method was used for taking samples without contamination, which were then cultured on necessary media for bacterial growth, diagnosed as *Acinetobacter haemolyticus*, and confirmed by the DL microbial ID/AST system (Enterobact. IST CARD) model DL-120E, and the Minimum Inhibitory Concentration of *Acinetobacter haemolyticus* was detected.

2.2. Collect Samples

The number of samples used for research to identify *Acinetobacter haemolyticus* are 30. 15 samples of urine were collected and placed in sterile urine cups collected from UTI of patients that return to hospital, and other 15 samples of hospital waste water were collected into 250ml sterile screw-cap containers and transported to the Microbiology Laboratory for isolated *Acinetobacter haemolyticus*. After that, they were cultured on MacConkey agar using the streaking culture method, and then incubated for 24 hours at 37°C.

2.3. Isolation and Identification *Acinetobacter haemolyticus*

2.3.1 *Acinetobacter haemolyticus* characteristic

The samples taken from the UTI patients and hospital wastewater (urine and sewage water) were cultured on suitable culture media for growth of *Acinetobacter haemolyticus*, including MacConkey agar [HI Media/India]. The bacteria appeared as colorless to light pink colonies, then cultured on eosin methylene blue agar for differentiation of these bacteria that appeared with blue colonies from other gram-negative bacteria on the MacConkey agar, and all the types

of samples were cultured on sheep blood agar within 48 hours at 37°C. The bacteria growth was found to be 2-3 mm diameter gray-white, convex colonies [11].

2.3.2 Microscopic Identification

A drop of distilled water was added to *Acinetobacter haemolyticus* isolates that had been obtained and placed onto a microscope slide. After that, the smear was inspected under a light microscope after being stained using the Gram stain procedure. Under high magnification and oil immersion, the bacterial cells' color, which indicated the Gram reaction, as well as their form and arrangement, was evaluated [12].

2.3.3. *Acinetobacter haemolyticus* confirmed identification

Acinetobacter haemolyticus identification by DL microbial ID/AST system (Enterobact. IST CARD) model DL-120E and detected Minimum Inhibitory Concentration of *Acinetobacter haemolyticus* [Biotech]. The *Enterobacter* (IST CARD) model DL-120E is used to identify *Acinetobacter haemolyticus*; it depends on the calorimetric characteristic for identification (oxidase test, catalase test, the citrate utilization test, the methyl-red test, the indole test, the Voges-Proskauer test, and the lactose fermentation test, and it depends on turbidity for susceptibility testing to detect minimum inhibitory concentration (CLSI & EUCAST) standard. DL IST card covers nearly 14 types of antibiotics, including ampicillin, gentamicin, ampicillin-sulbactam, piperacillin-tazobactam, cefepime, cefuroxime, trimethoprim-sulfamethoxazole, cefotaxime, imipenem, meropenem, amikacin, ceftazidime, cefoperazone-sulbactam, and minocycline, with multi-level concentration, up to 9 dilutions, for giving true minimum inhibitory concentration value [13].

Methods

1-Add pure *Acinetobacter haemolyticus* colonies to the diluent (0.5 MCF).

2-Add 100 µL of Pure from *Acinetobacter haemolyticus* suspension to biochemical wells (A1 to A12 – B1 to B12) and 50 µL to C1 – C6

3-Add 50 µL of *Acinetobacter haemolyticus* suspension into Muller Hinton broth and mix well

4-Add 50 µL of Muller Hinton broth into antimicrobial wells.

5-Add 2 drops of oil into A1 to A7.

6-Cover the card and place in incubator (18-24 hr.)

7-Add 1 drop of IND and PHE, and add 1 drop of VP1 and VP2 into the corresponding wells.

8-Read the result by D2MINI software.

3. Results and Discussion

3.1. *Acinetobacter haemolyticus* source and number

Between January and May 2025, thirty (30) samples were obtained for the diagnosis of *Acinetobacter hemolyticus*, fifteen from patients who returned to Tuz Hospital with UTI, and fifteen from the hospital's sewage water in the Sala Hedin Governorate. Of these, five urine samples (33.3%) had positive growth for *Acinetobacter haemolyticus*, ten samples (66.6%) had negative growth, three samples (20%) of fifteen wastewater samples had positive growth, and the remaining 80% had negative growth. The DL microbial ID/AST method was used to validate the identification of *Acinetobacter haemolyticus* following bacterial culture and microscopic examinations, as indicated in **Table 1**. An isolate of all *Acinetobacter haemolyticus* was cultivated on MacConkey agar and stained with Gram's stain, which allowed isolates to be recognized based on their morphological traits. It tested negative for Gram stain and coccobacilli, which are classified as strictly aerobic **[14]**.

Table 1: The sample source and number

Sample source	Sample Number	Positive result	Percentage	Negative result	Percentage
UTIs	15	5	33,3%	10	66.6%
Hospital wastewater	15	3	20%	12	80%

Free-living bacteria called *Acinetobacter* species are frequently found in damp environments and are easily separated from sources like soil, food, water, and sewage **[15]**. Catalase-positive, oxidase-negative, tiny, aerobic, non-fermenting, non-fastidious, and non-motile coccobacilli that thrive in damp environments are these species **[16]** Found as various species, like *Acinetobacter lwoffii* and *Acinetobacter haemolyticus*, the species are the most opportunistic non-fermenting bacteria linked to hospital-acquired illnesses, accounting for around 20% of cases **[17]**. Urinary Tract Infections are a considerable global concern and are among the most prevalent types of microbial infection globally **[18]**. Many bacteria can be isolated from urine, such as *Escherichia coli* and *Staphylococcus aureus*, that take part with *Acinetobacter haemolyticus* and cause Urinary Tract Infection **[19, 20]**. Additionally, it can be isolated from numerous species of the genus *Acinetobacter*, which are accountable for nosocomial diseases, such as aspiration pneumonia and catheter-associated infections; they can also cause urinary tract and soft tissue infections. *Acinetobacter haemolyticus* was identified from sewage water. community-acquired pneumonia and bacteremia can occur, especially in hot and humid tropical settings. According to the National Nosocomial Infections Surveillance System, the number of

Acinetobacter infections in the United States increased by 54% between 1987 and 1996, compared to November through June, between July and October (45). High humidity levels are thought to encourage the growth of germs, and water baths and humidifiers have frequently been identified as environmental reservoirs. Additionally, isolate *Acinetobacter haemolyticus* had a proportion of 13 (12%) in this investigation. **[21]**.

3.2 Biochemical properties determination of Minimum inhibition concentration

Acinetobacter haemolyticus was diagnosed using the DL-120E system through a 28-test panel, providing results within 18-24 hours. This approach ensures timeliness and high accuracy (about 99%) and a very low chance of mutation, mitigation, and any risks or errors (**Table2).**

Table2: the results of the DL-120E system.

Test	Result	Test	Result	Test	Result	Test	Result
Glu	-	C	-	ARAF	-	Raff	-
H2s	-	CIT	-	LACI	-	ESC	-
URE	-	MLT	-	SUCF	+	SALf	+
ORN	-	PHE	+	MELF	-	MDGf	+
ARG	-	INO	-	RHAF	-	ONPG	-
LYS	+	VP	-	INOF	+	GEL	-
SORF	-	ADOF	+	MALF	-	CELF	+

All isolates of *Acinetobacter haemolyticus* were subjected to minimum inhibition concentration using fourteen different types of antibiotics, including gentamicin, ampicillin, ampicillin-sulbactam, piperacillin-tazobactam, cefepime, cefuroxime (IV), trimethoprim-sulfamethoxazole, cefotaxime, imipenem, meropenem, amikacin, ceftazidime, cefoperazone-sulbactam, and minocycline. To ascertain the isolates' susceptibility and resistance to the 14 antibiotics. The DL-120E system was used to calculate minimum inhibition concentration. The results are shown in **Table 3 and Figure 1.** The study showed all eight isolates with 100% sensitivity to ampicillin, gentamicin, piperacillin-tazobactam, cefepime, cefuroxime (IV), trimethoprim-sulfamethoxazole, amikacin, ceftazidime, cefoperazone-sulbactam, and minocycline, and with 100% resistance to two types of antibiotics (imipenem and meropenem).

Table3. Minimum Inhibition Concentration (MIC)

Antibiotic	MIC	Resistance (R)	Sensitivities (S)
Ampicillin	≤8\4 ug/ml		S
Gentamicin	≤1ug/ml		S

Ampicillin-Sulbactam	≥16/8ug/ml	intermediate	
Piperacillin-Tazobactam	≤4/4ug/ml		S
Cefepime	≥0.12ug/ml		s
Cefuroxime(vi)	≥4ug/ml		s
Trimethoprim-Sulfamethoxazole	≤0.5/9.5ug/ml		S
Cefotaxime	≥0.12ug/ml		S
Imipenem,	≤0.25ug/ml	R	
Meropenem	≥32ug/ml	R	
Amikacin	≤4ug/ml		s
Ceftazidime	≥32ug/ml		S
Cefoperazone-Sulbactam,	≥8\4ug/ml		s
Minocycline	≥1ug/ml		S

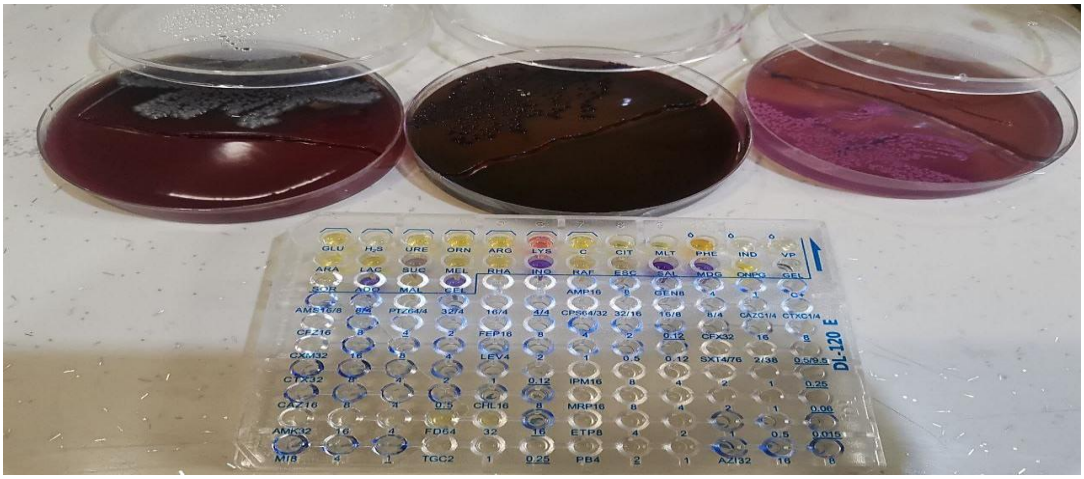


Figure 1: DL-120E system for detected MIC of *Acinetobacter haemolyticus*

A key factor in determining the best course of therapy is minimum inhibition Concentration, which is the lowest concentration of an antimicrobial drug that stops a bacterium from growing visibly. Nevertheless, this approach has a number of shortcomings, particularly with regard to antibiotic resistance. Usually, the minimum inhibition Concentration approach involves giving antibiotic dosages that either inhibit or eradicate the most susceptible bacteria. Even if they are only slightly resistant to the antibiotic, bacteria can still live and proliferate. Treatment failure may result from the growth and dominance of these resistant bacteria over time. Antimicrobial resistance is largely caused by this process, which is referred to as selective pressure [22, 23]. The Bhaduri *et al*. [24] studied *Acinetobacter haemolyticus* isolated in a tertiary care hospital

that isolating *Acinetobacter haemolyticus* in 3.8% and found high levels of resistance to ampicillin-sulbactam (96%), ampicillin (94%), aztreonam (94%), cefuroxime (92%), and ceftazidime (91%). In another study, one important *Acinetobacter* pathogen is *Acinetobacter haemolyticus*, and antibiotic overuse and the frequent gene exchange amongst hospital bacteria are the main causes of *Acinetobacter haemolyticus* resistance. In this investigation, we sequenced the whole genomes of two strains of *Acinetobacter haemolyticus*, TJR01 and TJS01 **[25] [26]**.

Numerous technical aspects impact the pathogenesis and virulence of *Acinetobacter*. The function of lipopolysaccharide or lipopolysaccharide oligosaccharide in these bacteria's outer membranes is of special interest **[27]**. It has been demonstrated that changes to these structures confer resistance to antibiotics and enhance resistance to desiccation. Additionally, it has been shown that *Acinetobacter* species that contain capsules are protected from complement-mediated death. *Acinetobacter's* quivering motility, adherence to environmental surfaces, and biofilm formation are all facilitated by the pellicles that are present on its surface **[28, 29]**.

4. Conclusions

Acinetobacter haemolyticus is an opportunistic pathogen that mainly affects patients with compromised immune systems. In healthy individuals, it is regarded as a low-grade pathogen that they may carry on their skin asymptomatically (colonization). It usually results in infections in hospitalized patients, long hospital stays, and catheters, and the capacity of *Acinetobacter* species, especially *Acinetobacter haemolyticus*, to become resistant to several antibiotics poses a serious threat to human health (multidrug resistance). Therefore, this study highlighted the sources of these opportunistic bacteria. It appeared that even though *Acinetobacter haemolyticus* was isolated from two distinct sources (wastewater and urine), it produced identical results in terms of minimum inhibition concentration, antibiotic resistance, and appropriateness. The goal of this study was accomplished when it was shown that bacteria have the same effect on antibiotic resistance or sensitivity regardless of their origin, and it opens the way up to several other investigations. One of those genes examined each type of bacterium based on where it was isolated (inside or outside the human body), revealing the differences between the bacteria's genes and whether or not environmental factors were affected.

Author Contribution

Jilan Ahmed Shakur: Writing and diagnosis, Alaa R. Nadim: collected samples from UTI patients, Wael Adil Obaid: Writing and desing, Rafeef A.Yass: collected sample from sewage water of hospital.

Funding

This research recived no external funding

Data Availbility Statement

Samples were taken from Toz General Hospital from patients coming to the hospital and from Wastewater of laboratory, which is considered one of the main and suitable sources for the growth of these bacteria.

Acknowledgments

Acknowledgent to laboratory staff of Toz General Hospital special bacteriology staff

Confleicts Of Interest

No funding

Ethical Approval

The local ethical commission at Imam Jaafar AI- Sadiq University, Iraq, approved the undertaking (Approval No.096477651).

6. References

[1] Obaid WA. Prevalence, antimicrobial susceptibility, and distribution of biofilm-associated virulence genes in multidrug-resistant *Acinetobacter baumannii* isolated from various environmental sources in Baghdad hospitals. Iraqi J Sci. 2025;66(7):2756–75.

[2] Bacon EE, Myers KS, Iruegas-López R, Banta AB, Place M, Ebersberger I, Peters JM. Physiological roles of an *Acinetobacter*-specific σ factor. mBio. 2025;16(6): e00968-25.

[3] Bai L, Zhang S, Deng Y, Song C, Kang G, Dong Y, Wang Y, Gao F, Huang H. Comparative genomics analysis of *Acinetobacter haemolyticus* isolates from sputum samples of respiratory patients. Genomics. 2020;112(4):2784–93.

[4] Jain K, Kumar V, Plakkal N, Chawla D, Jindal A, Bora R. Multidrug-resistant sepsis in special newborn care units in five district hospitals in India: a prospective cohort study. Lancet Glob Health. 2025;13(5): e870–8.

[5] Imran F, Malik M, Asif A, Akhtar G, Zaman S, Ajmal AN. Changing antimicrobial susceptibility and resistance pattern of *Acinetobacter* species over the last eight years in a tertiary care hospital in Lahore, Pakistan. J Islamabad Med Dent Coll. 2021;10(2):83–8.

[6] Rani C, Sharma SR, Farooq U, Singh S, Sharma V, Ahamad I. Isolation of *Acinetobacter* spp. and its antimicrobial resistance pattern in lower respiratory samples from ICU. Int J Med Microbiol Trop Dis. 2022;8(2):118–22.

[7] Wokorach G, Erima B, Alafi S, Kabatesi HO, Muhindo JT, Najjuka J. Draft genome sequence of *Acinetobacter haemolyticus* strain MUWRP1017 isolated from the pus of a female inpatient at Bwera General Hospital in Uganda. Microbiol Resour Announc. 2024;13(9): e00566-24.

[8] Madhavi RB, Anitha D, Beena PM. Clinical and antimicrobial profile of *Acinetobacter* species at a tertiary care teaching hospital. J Pure Appl Microbiol. 2022;16(3):2066–71.

[9] Choudhury S, Pathi BK, Sahoo JP, Mohanty S, Panigrahi K, Choudhury S. Prevalence and antimicrobial susceptibility patterns of non-fermenting gram-negative bacteria causing lower respiratory tract infections: a retrospective study. Cureus. 2025;17(7).

[10] Borcan AM, Rotaru E, Caravia LG, Filipescu MC, Simoiu M. Trends in antimicrobial resistance of *Acinetobacter baumannii* and *Pseudomonas aeruginosa* from bloodstream infections: an eight-year study in a Romanian tertiary hospital. Pharmaceuticals. 2025;18(7):948.

[11] Cohen J, Powderly WG, Opal SM. Infectious Diseases. 4th ed. Philadelphia: Elsevier; 2017.

[12] Białas N, Sokolova V, van der Meer SB, Knuschke T, Ruks T, Klein K, Westendorf AM. Bacteria (*E. coli*) take up ultra-small gold nanoparticles (2 nm) as shown by different optical microscopic techniques (CLSM, SIM, STORM). 2022;3(10):1407–20. doi:10.1002/nano.202200106.

[13] Ceballos-Garzon A, Holzapfel M, Welsch J, Mercer D. Identification and antifungal susceptibility patterns of reference yeast strains to novel and conventional agents: a comparative study using CLSI, EUCAST and Sensititre YeastOne methods. JAC Antimicrob Resist. 2025;7(2):dlaf040.

[14] Al-Layla EAM, AlTaie AA, Haddad MF, Abdullah BA, Saadi AM. Molecular detection of asymptomatic bacteriuria and its bacteriophage from adolescents in Mosul City, Iraq. J Biosci Appl Res. 2024;10(3):504–17.

[15] Muleshkova T, Bazukyan I, Papadimitriou K, Gotcheva V, Angelov A, Dimov SG. Exploring the multifaceted genus *Acinetobacter*: the facts, the concerns and the opportunities of the dualistic genus *Acinetobacter*. J Microbiol Biotechnol. 2025;35: e2411043.

[16] Jabeen F, Khan Z, Sohail M, Tahir A, Tipu I, Saleem HG. Antibiotic resistance pattern of *Acinetobacter baumannii* isolated from bacteremia patients in Pakistan. J Ayub Med Coll Abbottabad. 2022;34(1):95–100.

[17] Rizvi A, Hassan S, Siddique S, Yaqoob S, Asghar S. Isolation of *Acinetobacter* species from various clinical samples and their antimicrobial susceptibility pattern at a tertiary care hospital, Lucknow. Int J Acad Med Pharm. 2024;6(4):786–91.

[18] Obaid WA. Prevalence and characterization of uropathogenic virulence genes in *Staphylococcus saprophyticus* isolated from women with urinary tract infections in Baghdad, Iraq. Egypt J Bot. 2025;65(1):250–6.

[19] Gena ME, Bitew G, Chane E, Cherie N, Berta DM, Demoze L. Bacterial profile and antimicrobial susceptibility pattern of urinary tract infection among diabetic patients at Bule Hora University Teaching Hospital, Southern Ethiopia. Sci Rep. 2025;15(1):24112.

[20] Obaid WA. Molecular characterization of classical enterotoxin genes among *Staphylococcus aureus* isolates from food handlers in Baghdad City, Iraq. Iraqi J Sci. 2025;66(2):534–45.

[21] Mohamoud Z. Bacteriological and clinical characteristics of *Acinetobacter* species isolated from clinical samples in Near East University Hospital, Turkish Republic of North Cyprus [master's thesis]. Nicosia: Near East University; 2021.

[22] Wu Q, Shi J, Huang J, Gan D, Zhang L, Li P. The impact of ESBLs-positive *Escherichia coli*'s resistance to cefepime and its guidance for clinical treatment. Infect Drug Resist. 2023;6395–404.

[23] Khachab Y, Hodroj M, Sokhn ES. Understanding and addressing β-lactam resistance mechanisms in gram-negative bacteria in Lebanon: a scoping review. Heliyon. 2025;11(3).

[24] Bhaduri A, Palchowdhury P, Ghosh S, Bose S. *Acinetobacter* infections in critical care units: a study on its clinico-epidemiological pattern and antibiotic sensitivity profile from a rural teaching hospital in West Bengal, India. Cuest Fisioter. 2025;54(3):5063–7.

[25] Kamani J, Nachum-Biala Y, Bukar L, Shand M, Harrus S. Molecular detection of *Bartonella quintana*, *Acinetobacter baumannii* and *Acinetobacter haemolyticus* in *Pediculus humanus* lice in Nigeria, West Africa. Zoonoses Public Health. 2024;71(1):48–59.

[26] Taher EM, Abdullah BA, Al Taie AA. Phenotypic and genotypic detection of biofilm genes for *Proteus*, *Morganella*, *Providencia* (PMP) bacterial group isolated from clinical samples of hospitals in Mosul, Iraq. J Appl Nat Sci. 2024;16(4).

[27] Ayoub MC, Hammoudi HD. Insights into *Acinetobacter baumannii*: a review of microbiological, virulence, and resistance traits in a threatening nosocomial pathogen. Antibiotics (Basel). 2020;9(3):119.

[28] Saleh NT, Yousif BMY, Mahmood FN, Alsammak EG, Saadi AM. Prevalence of *Acinetobacter* in different clinical samples. J Biosci Appl Res. 2025;11(1):180–9.

[29] AL-Juboori OKM, Muhammad SJ. Phenotypic and genotypic detection of biofilm formation and capsular polysaccharide and relationship with antibiotic resistance of *Acinetobacter baumannii* isolated from clinical sites in Salahdin City. The Special Issue of the 9th International Scientific Conference on Antibiotic Resistance – Mustansiriyah University. 2025;24(SI).

Al-Kitab Journal for Pure Sciences (2026); 10(2):168-183.
https://doi.org/10.32441/kjps.10.2.p13

Al-Kitab Journal for Pure Sciences
ISSN: 2617-1260 (print), 2617-8141(online)

https://isnra.net/index.php/kjps

Bacterial Interactions and Cancer Prognosis: A Review of Their Role in Tumor Progression and Therapy

Mohammed S. Abbas
Department of Molecular Biology, Iraqi Center for Cancer and Medical Genetic Research, Mustansiriyah University, Baghdad, Iraq
Corresponding Author: mohammedsaleh@uomustansiriyah.edu.iq

Citation: ***Mohammed S. Abbas*. Bacterial Interactions and Cancer Prognosis: A Review of Their Role in Tumor Progression and Theapy.**
Al-Kitab J. Pure Sci. [Internet]. 2025 Dec. 06 ;10(2):168-183
DOI.
https://isnra.net/index.php/kjps/article/view/2026.
https://doi.org/10.32441/kjps.10.2.p13

Keywords: Microbiome, Cancer, Therapy, Tumor, Biomarkers.

Article History
Received 17 Sep. 2025
Accepted 06 Dec. 2025
Available online 01 Nov. 2026

©20--. THIS IS AN OPEN-ACCESS ARTICLE UNDER THE CC BY LICENSE
http://creativecommons.org/licenses/by/4.0/

Abstract:

The importance of the human microbiome in carcinogenesis, metastasis, and treatment response is being more and more demonstrated. Species of bacteria that have recently come to light as having a role in tumor biology and prognosis are summarized in this article. Metabolism changes, antitumor immunity is impaired, and chronic inflammation is promoted by microbial dysbiosis, according to cutting-edge molecular techniques like 16S rRNA sequencing and metagenomics. There is great potential for customized cancer care through therapeutic regulation of the microbiome, which might be achieved by the use of probiotics or fecal microbiota transplantation. Additionally, specific microbial signatures are becoming more recognized as biomarkers. The intricacy of microbial networks and inter-individual variability continue to hinder therapeutic translation, despite recent gains. To create proven diagnostic and treatment approaches based on the microbiome, ongoing multidisciplinary research is crucial.

Keywords: Microbiome, Cancer, Therapy, Tumor, Biomarkers.

التفاعلات البكتيرية وتشخيص السرطان: مراجعة لدورها في تطور الورم السرطاني

محمد صالح عباس

المركز العراقي ابحوث السرطان والوراثة الطبية/ الجامعة المستنصرية/ بغداد/ العراق

الايميل الرسمي: mohammedsaleh@uomustansiriyah.edu.iq

الخلاصة:

تتضح أهمية الميكروبيوم البشري في التسرطن والانبثاث والاستجابة للعلاج بشكل متزايد. يتم في هذه المقالة تلخيص أنواع البكتيريا التي تم الكشف عنها مؤخرًا على أنها تلعب دورًا في بيولوجيا الأورام والتشخيص. وفقًا لأحدث التقنيات الجزيئية مثل تسلسل الحمض النووي الريبوزي ١٦ Sوالميتاجينومكس، حيث تؤدي الاضطرابات الميكروبية إلى تغيرات في التمثيل الغذائي، وضعف المناعة المضادة للأورام، وتفاقم الالتهابات المزمنة. هناك إمكانات كبيرة لتقديم رعاية مخصصة لمرضى السرطان من خلال التنظيم العلاجي للميكروبيوم، والذي يمكن تحقيقه باستخدام البروبيوتيك أو زراعة الميكروبيوتا البرازية. فضلا عن ذلك، أصبحت العلامات الميكروبية المحددة معترف بها بشكل متزايد كعلامات بيولوجية، ولا تزال تعقيدات الشبكات الميكروبية والتباين بين الأفراد تعوق الترجمة العلاجية، على الرغم من المكاسب التي تحققت مؤخرًا. ومن أجل وضع نهج تشخيصية وعلاجية مجربة تستند إلى الميكروبيوم، من الضروري إجراء أبحاث متعددة التخصصات بشكل مستمر.

الكلمات المفتاحية: الميكروبيوم، السرطان، العلاج، الورم، المؤشرات الحيوية.

1. Introduction:

More and more discoveries are elucidating the significance of the microbiome in shaping various traits, including health. Disruption in microbiota can influence normal biological functions and is thought to constitute the underlying etiology of various health problems. The role of commensal bacteria in cancer has recently gained attention [1]. Research shows that germs can affect the body in many ways, especially in relation to blood-related and solid organ cancers [2]. Tumor biology is shaped by the presence of bacteria either through their phenotypic characteristics or by the way tumor cells react to the presence of bacteria. To further complicate the relationship, research has also indicated that the development of cancer and its microenvironment can alter the local microbiome [3].

With advances in molecular diagnostics further characterizing the spectrum of bacteria and their characteristics, the implications of this stratification and how to apply that knowledge for prognosis are at the heart of research. The above evidence has led to a number of open questions on how several of these bacterial species could be serving as robust biomarkers to help in determining cancer prognosis [4]. This review delves into the various bacterial species that have been linked to cancer prognosis. It seeks to understand how these species contribute to tumor

progression and therapy response, and it emphasizes their potential as diagnostic and therapeutic targets in clinical oncology. The study is planned to be conducted according to the guidance. In conclusion, understanding the microbiome has generated both excitement and disbelief in cancer biology

2. The Microbiome and Cancer

The microbiome is increasingly associated with diverse diseases. In cancer, the bacteria and other microorganisms in the gut and body can affect the immune system and inflammation, both of which play a role in how cancer develops and how well treatments work. The gut contains many different types of microorganisms. Their variety is influenced by factors like food and antibiotics, but genetics plays the biggest role [5]. At the same time, the microbiome assists in digestion, host metabolism, and immune system regulation. A consequence of this is the strong influence that the gut microbiome can exert even on distant cells and organs located in the peripheral tissues. Moreover, several bacterial species, pathogens, or symbionts have proven to be potent modulators of tumor development, each through their mechanism of action [6].

Notably, there is both heterogeneity in the microbial composition and distinct roles of the microbiota in tumorigenesis, including mutual symbiosis and direct translocation from intestinal dysbiosis. Nevertheless, it is still not clear when bacteria extrinsically translocated from the dysbiotic intestine acquire a commensal phenotype by adapting to the specific milieu of the tumor microenvironment. By interacting with host immune receptors including Toll-like receptors (TLRs), bacteria can stimulate tumor formation. Binding to Toll-like receptors (TLRs) on immunological and epithelial cells, bacterial components called microbial-associated molecular patterns (MAMPs) induce inflammatory and signaling cascades, such as NF-κB and STAT3. Chronic inflammation, DNA damage, and changes in the tumor microenvironment that promote cancer start and development are brought about by the persistent activation of these pathways. Moreover, these same patterns and antigens were shown to be expressed also by several different kinds of bacterial species; therefore, they can predict the degree of intratumor inflammation. The overall specificity about bacteria-induced cancer progression is due to the host's specific proteome as well as the transcriptional expression at the single-cell level, which at the same time is dependent on the single nucleotide polymorphisms that are present in the host's genome. At the same time, emerging evidence has implicated unique microbial dysbiosis in several different cancer types [7].

2.1. Role of the Microbiome in Cancer Development

Until recently, cancer was long thought of as a hereditary disorder originating from mutations that interfere with regular cellular regulatory systems. Cancer initiation and progression are shaped by a complex network of elements, including genetics, epigenetics, metabolism, the immune system, and microbes, according to current data. More and more data shows that external factors like immune cells, fibroblasts, blood vessel cells, nutrients, and other molecules from the surroundings are very important. Among these extrinsic factors, the microbiome is receiving much attention. The microbiome is now considered a major organ and consists of about 1 kg, half of microbial mass being in the colon, where the density is one of the highest on the planet, with a concentration of up to 10^12 bacteria per gram of colonic content [8]. The microbiome has pleiotropic impacts in cancer through its metabolome. Microbial molecules can significantly influence several signaling pathways that change during tumor development, like NF-κB, Wnt/β-catenin, and various pathways related to cell death. Intriguingly, the microbiome has the ability to alter environmental compounds like PAHs through its metabolic processes. The production of reactive carcinogenic intermediates by some microbial transformations has the potential to facilitate the start of tumors. At another step of oncogenesis, the microbiome has been shown to incite inflammation, increased angiogenesis, and modified cell-mediated immunity, all of which result in tumor growth and heightened tumor vascularization [9]. With regard to pro-inflammatory properties of the microbiota, it is noteworthy that about 15 bacteria, either directly or indirectly, increase systemic inflammation. All of these organisms are Gram-negative bacteria, and some of them increase Toll-like receptors and secrete lipopolysaccharides, which contributes to inflammation that promots tumorigenesis [10].

At the same time, the microbiome contributes to host defense, decreasing inflammation. Pathogenic bacteria produce small molecules interfering with tumor colonization. Most transcriptionally distinct genes dysregulated in cancer were enriched in functions controlling cell proliferation and death, migration, and cytoskeleton rearrangements. The processes affected by these genes complement what is already known regarding the criteria for tumor aggressiveness [11]. This suggests that interactors, through their metatranscriptome, represent a valuable source of diverse cancer development biomarkers. Recent results have highlighted the negative impact of antibiotics targeting the intratumoral pool of bacteria with a subsequent uncontrolled tumor progression. A strong link was found between higher levels of certain oral bacteria and lower chances of survival without disease progression in people with advanced

colorectal cancer [12]. Consequently, disruptions of the balance of oral flora seem to be a candid explanation for these observations. In a recent study, researchers have identified the strength of the oncological outcome by the oral flora, in particular, the tongue and the M5 site where certain germs were found to have an unfavorable outcome on survival. That is to say, unlike serum, mixed saliva partially depicts the systemic response and highlights the possibility of several future tumor sites being located in the upper gastrointestinal tract. Overall, these results provide a supplement to blood biomarkers allowing metastasis detection and suggest that measuring mouth saliva could improve cancer staging and anticipate progression/resistance [13].

2.2. Tumor Growth and the Role of Different Bacterial Species

Bacteria play an integral role in tumor growth dynamics. The introduction of harmful bacteria into animal models with tumors accelerates tumor progression, primarily due to chronic inflammation, cytokine production that promotes tumor growth, and suppression of the immune response. For example, mice infected with Helicobacter hepaticus develop liver and colon tumors through IL-6 and TNF-α pathways. Additionally, Fusobacterium nucleatum enhances colorectal cancer growth by affecting immune cell infiltration and β-catenin signaling, with tumors growing faster than in germ-free models, which demonstrate a significant decrease in tumor progression and metastases, emphasizing a role of bacteria in modulating the tumor microenvironment and thus having a direct impact on cancer progression. Few studies offer an experimental point of view on bacteria [14]. Bifidobacteria are a genus of anaerobic non-motile bacteria that are recognized for their ability to modulate immune checkpoints and are crucial for cancer immunotherapy response. However, they are commonly obtained through dietary changes and probiotic supplements, and a number of clinical trials have linked high levels to a better prognosis for breast cancer patients [15].

Experimental models have shown that certain species of Pseudomonas, notably P. aeruginosa, can emit cytotoxic chemicals and immune-stimulating molecules, which have anti-tumor properties. Antimicrobial substances produced by these bacteria inhibit the growth of competing germs; this finding has the potential to lessen the prevalence of antibiotic resistance in bacterial populations. In this case, the number of bacteria comes into play: at lower concentrations, other bacteria can reproduce faster than Pseudomonas and thus limit its actions. The interaction between gut bacteria, tumour growth, and the human immune system affects their overall dynamic [16]. A closed bacterial system delivered in a clinical model to patients was shown to not affect tumor progression in a trial. However, optimal therapeutic concentrations without compromising patient safety are a challenge, as clinical investigations

have demonstrated that bacterial levels achieved in vivo often remain below the cytotoxic threshold needed for effective tumor destruction, even at higher oral or intravenous doses. It is unclear whether potential pharmaceutical intervention or bacterial cocktails can only target cancer-related bacteria and optimize the healing process. Hence, it is of critical importance to investigate bacterial dynamic interactions in order to model and ultimately use them as effective interventions [17].

3. Methods of Studying Bacterial Species in Cancer Prognosis

Several sequencing-based methods have allowed detection and characterization of bacterial communities within tumor environments. Targeted sequencing approaches such as rRNA analysis have been used extensively to profile the microbial taxa present in cancerous lesions. While rRNA profiling methods do not allow for the resolution of bacteria at the species level and provide limited functional information, they can be useful for preliminary studies identifying microbiome differences in patient groups [18]. Importantly, using advanced genomic technologies, such as whole-genome shotgun sequencing, investigators can profile the diversity and abundance of all microorganisms within a given sample. More advanced methods employing host sequence depletion have also been described to afford even greater coverage of bacterial species present within a given context [19].

Animal models have become a more frequently utilized tool to study cancer-associated microbiota. Gnotobiotic animals, which are born and raised in germ-free conditions, can be colonized with known bacterial species of interest, providing interactions with the host and potentially driving other important pro- and antitumor phenotypes [20]. In order to model complex human environments, future studies should integrate a variety of methodological approaches from in vitro systems to in vivo animals to provide a holistic understanding. However, there are a number of limitations to utilizing animal models of bacterial interaction in cancer research, including microbiome differences in very different gut habitats between humans and traditional laboratory mice, as well as the reproducibility, interpretation, and translational potential of some previous results [21].

3.1. Sequencing Techniques

In the last few years, several technological advances have revolutionized microbiome or metagenomic studies. Among the most powerful techniques, the 16S rRNA gene is currently the most widely utilized molecular marker to estimate both the composition and the diversity of the associated bacterial communities. In contrast, whole-genome sequencing can quantify

differences in function, gene content, and genomic potential of the observed microbial taxa [22]. The main advantages of using high-throughput sequencing for microbiome analysis are its sensitivity, ability to explore the composition and genetic diversity of bacterial populations, and capacity to reveal the complex molecular processes in which bacteria are involved. With the use of reliable bioinformatics pipelines, taxonomic profiling and functional predictions are achievable, potentially leading to the identification of possible biomarkers for cancer prognosis [23].

The extensive use of high-throughput sequencing has revolutionized microbiome analysis in clinical practice, as well as in exposure research. Several challenges exist, however, when determining the taxonomic composition of bacterial communities by comparing sequencing data alone, including contamination and amplification of synthetic oligonucleotides. Moreover, the potential for error underlying next-generation sequencing should be clearly stated. When applying high-throughput sequencing analyses to investigate the role of bacterial communities as possible early predictors of cancer, a complex interpretation process is essential, which reflects the rate of turnover of the microbial population based on changes in its host's biology. Currently, although pilot studies have been performed, results from high-throughput sequencing have not been applied to cancer prognosis [24].

3.2. Animal Models

Animal models allow investigation of the interactions between bacteria and cancer under controlled conditions. Numerous different animal models exist, including germ-free mice, which are devoid of all microorganisms, and gnotobiotic mice, which can be colonized with unique bacterial communities. Gnotobiotic and germ-free models have been extensively used in order to understand the influences of the microbiome on host physiology [25]. From the study of microbiota composition to functional properties and mechanisms, animal models are directly related to the recruitment of experimental conditions to implications that mimic naturally occurring human scenarios. It is important to note, however, the limitations of these models, because of variations in immunological function, tumor biology, microbiome makeup, and metabolic responses between species, there is a certain amount of uncertainty and danger when results from animal models are applied to human cancer. Because of these differences, as well as the factors discussed in Section 3.1, results in humans may vary greatly from those in preclinical animal studies [26].

It is paramount that observations at the murine level can be validated with evidence in human data because the development and clinical innovation of bacterial therapies would be targeted at human cancer. Recent announcements of interest in sequencing the tumor microbiome in murine strains as a part of a Pre-Clinical Development Service program are a clear acknowledgment that animal models are still relevant in contemporary cancer microbiome research. Nonetheless, there are also practical and ethical considerations for extrapolating to human studies. The design of rodent trials, their potential mechanisms of action, and the regulation of trials that utilize bacteria as interventions are discussed in more detail in the following sections. Additionally, larger mammals can provide a good middle ground between murine and clinical research, though at greater expense, plus regulatory oversight and ethical considerations surrounding their use [27].

4. Clinical Implications of Bacterial Species in Cancer Prognosis

Understanding the role of certain bacterial species with clear oncogenic mechanisms in the context of cancer patient outcomes and treatment begins to directly meet clinicians' interests so that patients can be stratified into risk groups or exhaustively monitored high-risk patients, altering their prognosis by developing biomarkers. In addition, certain bacterial species with specific types of cancer predispose to certain types of prognosis, such as sepsis and other inflammatory diseases. Finally, evidence suggests that the patient's initial microbiome composition can predispose certain cancers to respond poorly to some therapies due to related mechanisms, offering possible therapeutic options. Based on that, patients showing changes in initial microbiome composition could be candidates for probiotic or antibiotic-tailored therapies that would also enhance treatment response, such as rebuilding the altered microbiome in autologous fecal microbiome transplantation [28].

The depletion or addition of commensal and non-commensal bacteria to the microbiome using antibiotics or pre- and probiotics to promote intense host-wide immune responses and alter immune memory could enhance treatment responses forthwith and maintain ongoing immunity to prevent repeated relapse for months or years. Possibly, cancer patients can begin several weeks or months before the administration of particular antitumor therapy with adjunctive treatments that first alter the immune repertoire. Particularly, the complex bacterial exposure history of myeloid-derived suppressor cells and tumor-associated macrophage immunosuppressive activities can be changed by the prescribed probiotics or targeted narrow-spectrum or combination antibiotics. In particular, the response to checkpoint therapy seems to be very quick when the treatment is given, offering an opportunity to attract those who will

treat it or to treat patients who respond to moderate and poor results, to those who become resistant after receiving immunotherapy for some time. It has been shown that certain bacterial species influence the immune response in cancer patients, especially those who have received radiotherapy and checkpoint inhibitors. It is crucial that all findings are validated in clinical trials to directly monitor and influence patient outcomes in oncologic clinical practice. More and more data shows that the human microbiome is important. We need to include microbiome research more in cancer care and research [29].

4.1. Therapeutic Opportunities

Although removing certain types of bacteria may have some bad effects on health, research shows that this can help cancer patients live longer. The recommendation is that specific antibacterials could be developed that could be administered in this capacity so that they do not contribute to or cause dysbiosis. Improved local delivery of already active compounds for cancer therapy by specific bacterial strains could be very interesting. Microbials are usually expected as adjuvant cancer treatment agents, and data have shown that they show little efficacy as a monotherapy [30]. Recombinant bacterial strains that can be a virulent, can be heterologously expressing certain genes, and could serve as a prospective novelty for future therapy may transform localized cancer into a tumor necrosis factor that derives a host immune response against non-targeted solid tumors. In addition to this local approach, based on TME targeting or adoptive cell therapy, multiple other engineered bacteria could also be given as a systemic approach to treat disseminated cancer. Interestingly, researchers have reported engineered Lp that have potential usage in the local treatment of carcinoma and melanoma. These enzymes could also be active in other solid tumors, such as liver cancer, which have developed immune escape mechanisms by increasing PD-L1 and TILT, another favorable aspect of Ovs (Figure 1). Sporadic reports have shown surprising results, such as Lactobacillus-based treatment showing better responses than PD-1 blockade alone in mice with melanoma and Listeria monocytogenes infecting brain tumors with fair prognosis, showing it as a novel method in glioblastoma treatment. Moreover, several clinical data make it possible to use bacteria that improve immunotherapy and chemotherapy responses, but this data is limited, and the use of bacteria to improve cancer responses is a part of an unknown field [31].

By using these strategies and information, harmful bacteria can be reduced in the gut that can lead to cancer, keep track of how the gut's bacteria change during cancer treatment, and tackle the real challenges of using gut bacteria to guide cancer treatment. Based on the latest findings, in this section, the recent studies on bacterial species and cancer have been descried

that will be both effective methods to improve the responses of the bacteria to cancer and chemotherapy and methods that will be developed in the near future. It should be kept in mind that any bacteria could cause problems; also, reinforcement of one-way immune responses could bring successful responses in patients who have less possibility of response to immune checkpoints because of the composition of their personal microbiomes. Additionally, major challenges to bring these bacterial therapies to the clinic are reported in this section [32].

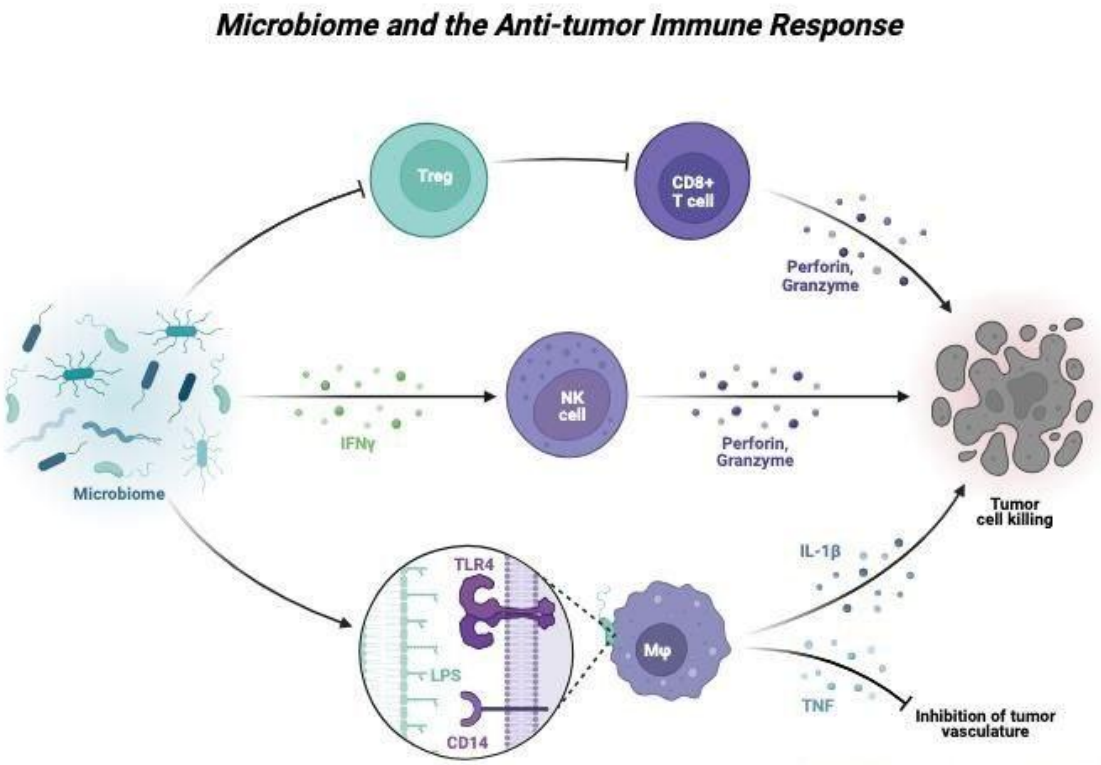


Figure 1. Proposed pathways linking the microbiome, immune modulation, and tumor progression.

4.2. Diagnostic Biomarkers

It is widely acknowledged that knowledge of the microbiome can help deliver biological meaning because some findings are related to changes in its composition, particularly to the increase of specific bacteria known as pathogens and vice versa. Many studies have found that

the makeup of gut bacteria changes in cancer patients, no matter what type of cancer they have. This has led some experts to think it could be used to help diagnose cancer. In fact, these shifts can distinguish neoplastic subjects from healthy individuals, allowing the research community to propose a new route for the development of non-invasive test technologies specifically for early cancer detection. Moreover, the microbial composition, considered as the "cancer microbiome signature," can distinguish among different types of neoplasms and is often linked to tumor progression features and host response [33]. These results support microbiome contribution due to host-tumor adaptation that is leading to a specific tumor immune detection and response. Additionally, this knowledge opens the door to new treatment approaches that target the microbiome to improve its ability to regulate immune recognition in the tumor microenvironment. To prevent immune evasion mechanisms acquired from tumors and restore immune surveillance, it may be feasible to influence the makeup and activity of microbes. Improving early cancer diagnosis through research into bacteria is driving idea that many emerging microbiome signatures are hoping to ultimately know as diagnostic markers. Indeed, many manuscripts have been published on this issue. However, in order to promote the clinical applicability of biomarkers, their interest and potential should be examined, meaning that they should be independently validated following an undisputed methodological design, compared to other validated markers and, if possible, subjected to laboratory standardization series across the different clinical levels and hospitals. In the case of bacterial signatures, this would involve sampling and analysis laboratories, technological platforms employed for the massive sequencing of the DNA, and bioinformatic pipelines and tools currently used for microbiota analysis [34].

The standardization of these techniques is necessary, especially for a predictive, preventive, and personalized medicine approach. However, moving the human healthcare cost-related microbiomics diagnosis towards an innovative approach would require changes at the hospital level. Furthermore, investment in technology and software platforms is necessary to keep the use of microbial patterns at a low cost, whether in research or therapeutic use. Many studies have been done recently on how certain germs in our bodies might help diagnose diseases, but not many of these findings have been used in hospitals or clinics. These have already led to the development of a color-based kit as a diagnostic marker, bacteria associated with liver disease relying on bile acids profiling, and the development of a predictive model of variations in the levels of some positive predictive markers in advanced fibrosis. Concerning the oncology field and the functional validation of selected species for therapy, trials are ongoing [35]. Therefore,

moving forward, significant gaps in the understanding of the mechanisms of action, pharmacokinetics/pharmacodynamics, and toxicity remain to be filled. The majority of microbiome research articles have suggested that modifications in the abundance of specific bacterial species are clearly associated with the presence of cancer. They might one day serve as the right source for developing a non-invasive diagnosis in cancer [32],[36]

5. Future Avenues of Research and Emerging Opportunities

As can be seen, there is enormous potential for future studies investigating the prognostic implications of microbial species in cancer prognosis. However, in order to achieve significant results in this field, an interdisciplinary approach is needed that binds the knowledge of microbiology and cancer research. Future large cohort studies could provide the much-advised power to further elucidate the complex dynamics and interactions between the microbiota and cancer. For this, a significant partnership will be needed between researchers, clinicians, and industry stakeholders. As a start, this approach will also have the potential to fill in the blanks of currently known and less known, usually recognized cancers' bacterial species [37]. Along with these subjects, there is a paucity of knowledge concerning the linkage that bacterial species may hold with rarer types of cancer, as there are no or very few studies about them. Because of this, all the possible ways that microbiota can affect cancer could be studied in order to have a more comprehensive picture. In addition to identification, longitudinal studies should also be undertaken to monitor changing trends of microbial composition over time through the carcinogenic process. In contrast to this speculation, it should also be assessed whether fecal, serum, or tissue bacterial species, when diagnosed, indicate a non-pathogenic composition and, therefore, are not harmonized with the pathological basis in the case of different types of cancer, which are known as confounding factors. Furthermore, because the gut-brain axis has a close relationship with cancer, the effect of the axis on the outcome of cancer is another noteworthy point [38]. Due to the paucity of research on the relationship between bacteria and general health, it is necessary to investigate the role of the microbiota in cancer outcomes[39].

6. Conclusions

The interaction between the human microbiome and cancer progression represents a critical frontier in oncology. Specific bacterial taxa influence tumor initiation, immune modulation, and treatment response, offering new opportunities for diagnostic and therapeutic innovation. Incorporating microbiome profiling into cancer care could enable personalized treatment selection and early detection of resistance. However, progress toward clinical translation requires methodological standardization, large-scale validation, and elucidation of causal

mechanisms. Future studies should focus on longitudinal and interventional designs to integrate microbiome-based diagnostics and therapeutics into precision oncology, ultimately improving patient outcomes.

7. References

[1] Duijster JW, Franz E, Neefjes J, Mughini-Gras L. Bacterial and parasitic pathogens as risk factors for cancers in the gastrointestinal tract: A review of current epidemiological knowledge. Front Microbiol. 2021; 12:790256. Available from: https://www.frontiersin.org

[2] Bae J, Park K, Kim YM. Commensal microbiota and cancer immunotherapy: Harnessing commensal bacteria for cancer therapy. Immune Netw. 2022. Available from: https://www.nih.gov

[3] Fang CY, et al. Colorectal cancer stage-specific fecal bacterial community fingerprinting of the Taiwanese population and underpinning of potential taxonomic biomarkers. Microorganisms. 2021;9(8):1548. Available from: https://www.mdpi.com

[4] Raza A, et al. Dynamic liquid biopsy components as predictive and prognostic biomarkers in colorectal cancer. J Exp Clin Cancer Res. 2022;41(1):99. Available from: https://www.springer.com

[5] Sadrekarimi H, et al. Emerging role of human microbiome in cancer development and response to therapy: Special focus on intestinal microflora. J Transl Med. 2022;20(1):301. Available from: https://www.springer.com

[6] Li S, et al. Tumorigenic bacteria in colorectal cancer: Mechanisms and treatments. Cancer Biol Med. 2021;19(2):147–59. Available from: https://www.nih.gov

[7] Haque S, et al. Microbial dysbiosis and epigenetics modulation in cancer development – A chemopreventive approach. Semin Cancer Biol. 2022; 86:666–81. Available from: https://www.sciencedirect.com

[8] Liu J, Zhang Y. Intratumor microbiome in cancer progression: Current developments, challenges and future trends. Biomark Res. 2022. Available from: https://www.springer.com

[9] You M, et al. Signaling pathways in cancer metabolism: Mechanisms and therapeutic targets. Signal Transduct Target Ther. 2023;8(1):196. Available from: https://www.nature.com

[10] Quaglio AE, et al. Gut microbiota, inflammatory bowel disease and colorectal cancer. World J Gastroenterol. 2022;28(30):4053–69. Available from: https://www.nih.gov

[11] Allemailem KS. Innovative approaches of engineering tumor-targeting bacteria with different therapeutic payloads to fight cancer: A smart strategy of disease management. Int J Nanomedicine. 2021.

[12] Dora D, et al. Non-small cell lung cancer patients treated with Anti-PD1 immunotherapy show distinct microbial signatures and metabolic pathways according to progression-free survival and PD-L1 status. Oncoimmunology. 2023;12(1):2204746.

[13] Li S, et al. Prognostic impact of oral microbiome on survival of malignancies: a systematic review and meta-analysis. Syst Rev. 2024.

[14] Harimoto T, et al. A programmable encapsulation system improves delivery of therapeutic bacteria in mice. Nat Biotechnol. 2022;40(8):1259–69.

[15] Thu MS, et al. Effect of probiotics in breast cancer: a systematic review and meta-analysis. Biology. 2023;12(2):280.

[16] Wang S, Chan SY, Deng Y, Khoo BL, Chua SL. Oxidative stress induced by Etoposide anti-cancer chemotherapy drives the emergence of tumor-associated bacteria resistance to fluoroquinolones. J Adv Res. 2024; 55:33–44.

[17] Paprocka P, et al. Pseudomonas aeruginosa infections in cancer patients. Pathogens. 2022;11(6):679.

[18] Senthakumaran T, et al. Microbial dynamics with CRC progression: a study of the mucosal microbiota at multiple sites in cancers, adenomatous polyps, and healthy controls. Eur J Clin Microbiol Infect Dis. 2023;42(3):305–22.

[19] Satam H, et al. Next-generation sequencing technology: current trends and advancements. Biology. 2023;12(7):997.

[20] Stecher B. Establishing causality in Salmonella-microbiota-host interaction: The use of gnotobiotic mouse models and synthetic microbial communities. Int J Med Microbiol. 2021.

[21] Tosti E, Srivastava N, Edelmann W. Vaccination and microbiota manipulation approaches for colon cancer prevention in rodent models. Cancer Prev Res. 2023.

[22] Fu Q, et al. Alterations of the rhizosphere soil microbial community composition and metabolite profiles of Zea mays by polyethylene-particles of different molecular weights. J Hazard Mater. 2022.

[23] Li Y, et al. Unveiling key odor-active compounds and bacterial communities in Fu Brick tea from seven Chinese regions: A comprehensive sensomics analysis using GC–MS, GC-O, aroma recombination, omission, and high-throughput sequencing. Food Res Int. 2024; 196:114978.

[24] Jia Q, Chu H, Jin Z, Long H, Zhu B. High-throughput single-cell sequencing in cancer research. Signal Transduct Target Ther. 2022;7(1):145.

[25] Montalban-Arques A, et al. Commensal Clostridiales strains mediate effective anti-cancer immune response against solid tumors. Cell Host Microbe. 2021;29(10):1573–88.

[26] Ting NLN, Lau HCH, Yu J. Cancer pharmacomicrobiomics: targeting microbiota to optimise cancer therapy outcomes. Gut. 2022.

[27] Wahl A, et al. A germ-free humanized mouse model shows the contribution of resident microbiota to human-specific pathogen infection. Nat Biotechnol. 2024;42(6):905–15.

[28] Yusuf K, Sampath V, Umar S. Bacterial infections and cancer: exploring this association and its implications for cancer patients. Int J Mol Sci. 2023.

[29] Blake SJ, Wolf Y, Boursi B, Lynn DJ. Role of the microbiota in response to and recovery from cancer therapy. Nat Rev Immunol. 2024.

[30] Thomas GA, et al. From field to plate: How do bacterial enteric pathogens interact with ready-to-eat fruit and vegetables, causing disease outbreaks? Food Microbiol. 2024.

[31] Rahimi A, et al. A comprehensive review on novel targeted therapy methods and nanotechnology-based gene delivery systems in melanoma. Eur J Pharm Sci. 2023; 187:106476.

[32] Fernandes MR, Aggarwal P, Costa RG, Cole AM, Trinchieri G. Targeting the gut microbiota for cancer therapy. Nat Rev Cancer. 2022;22(12):703–22.

[33] Avuthu N, Guda C. Meta-analysis of altered gut microbiota reveals microbial and metabolic biomarkers for colorectal cancer. Microbiol Spectr. 2022.

[34] Rodriguez J, et al. State of the art and the future of microbiome-based biomarkers: a multidisciplinary Delphi consensus. Lancet Microbe. 2024 Sep.

[35] Koivisto AP, Belvisi MG, Gaudet R, Szallasi A. Advances in TRP channel drug discovery: from target validation to clinical studies. Nat Rev Drug Discov. 2022;21(1):41–59.

[36] Zhang X, Li C, Cao W, Zhang Z. Alterations of gastric microbiota in gastric cancer and precancerous stages. Front Cell Infect Microbiol. 2021; 11:559148.

[37] Sepich-Poore GD, Zitvogel L, Straussman R, Hasty J, Wargo JA, Knight R. The microbiome and human cancer. Science. 2021;371(6536): eabc4552.

[38] Liang Y, et al. Awareness of intratumoral bacteria and their potential application in cancer treatment. Discov Oncol. 2023.

[39] Herrera-Quintana L, et al. The Role of the Microbiome and of Radiotherapy-Derived Metabolites in Breast Cancer. Cancers (Basel). 2024;16(21):3671.

Al-Kitab Journal for Pure Sciences (2026); 10(2):184-202.
https://doi.org/10.32441/kjps.10.2.p14

Al-Kitab Journal for Pure Sciences
ISSN: 2617-1260 (print), 2617-8141(online)

https://isnra.net/index.php/kjps

The Barberry Fruit Extract and Metformin as a Protective Effect on the Embryonic Development and Kidney Tissues Functioning in a Rat Model of Experimental Gestational Diabetes

Zainab Hasan Majeed

Department of Biology, College of Education for Pure Science, University of Kirkuk, Kirkuk, Iraq.

Corresponding Author: Zainab.hassan@uokirkuk.edu.iq

Citation: ***Zainab Hasan Majeed.*** **The Barberry Fruit Extract and Metformin as a protective effect on the embryonic development and kidney tissues functioning in a rat model of experimental gestational diabetes.**
Al-Kitab J. Pure Sci. [Internet]. 2026 Mar. 28 ;10(2):184-202
DOI.
https://isnra.net/index.php/kjps/article/view/2026.
https://doi.org/10.32441/kjps.10.2.p14

Keywords: Metformin, Gestational diabetes, Barberry, Fruit, kidney

Article History
Received 29 Jan. 2026
Accepted 28 Mar. 2026
Available online 01 Nov. 2026

©20--. THIS IS AN OPEN-ACCESS ARTICLE UNDER THE CC BY LICENSE
http://creativecommons.org/licenses/by/4.0/

Abstract:

This study was carried out to assess the effects of Berberis vulgaris fruit extract and metformin on maternal metabolic parameters, fetal growth and organ development under the condition of gestational diabetes in albino rats. Gestational diabetes has been induced with a high-fat/ high-sugar diet(HFHS diet) that was followed by administration of streptozotocin. Pregnant rats were divided into 5 groups: control, HFHS diet, HFHS + metformin, HFHS + barberry extract, and HFHS + metformin + barberry extract. Maternal body weight, fasting blood glucose and insulin resistance were measured as well as fetal growth and placental efficiency. Histological study of fetal kidneys and skeletal staining was carried out in order to assess organ development and skeletal development. Results showed that the HFHS diet caused maternal hyperglycemia, insensitivity to insulin, deficiency in placental growth and organ abnormalities in fetuses. Both metformin and barberry extract alone improved maternal metabolic profiles and fetal outcomes, however, the combination of both had the greatest improvements including normalized glucose levels in maternal blood, improved fetal growth, and near complete normalization of kidney histology and skeletal ossification. These results

indicate the synergistic effect of barberry extract and metformin for reducing the negative impact of gestational diabetes on fetal development.

Keywords: Metformin, Gestational diabetes, Barberry, Fruit, kidney.

مستخلص ثمار البرباريس والميتفورمين كعامل وقائي على نمو الجنين ووظائف أنسجة الكلى في نموذج جرذ مصاب بسكري الحمل التجريبي

زينب حسن مجيد[1]

[1]قسم علوم الحياة، كلية التربية للعلوم الصرفة، جامعة كركوك، العراق.

الايميل الرسمي: Zainab.hassan@uokirkuk.edu.iq

الخلاصة:

أُجريت هذه الدراسة لتقييم تأثير مستخلص ثمار البرباريس الشائع (*Berberis vulgaris*) والميتفورمين على المؤشرات الأيضية للأمهات، ونمو الجنين، وتطور أعضائه في حالة سكري الحمل لدى فئران بيضاء. تم تحفيز سكري الحمل عن طريق اتباع نظام غذائي غني بالدهون والسكريات، تلاه إعطاء الستربتوزوتوسين. قُسّمت الفئران الحوامل إلى خمس مجموعات: مجموعة ضابطة، ومجموعة نظام غذائي غني بالدهون والسكريات، ومجموعة نظام غذائي غني بالدهون والسكريات مع الميتفورمين، ومجموعة نظام غذائي غني بالدهون والسكريات مع مستخلص البرباريس، ومجموعة نظام غذائي غني بالدهون والسكريات مع الميتفورمين ومستخلص البرباريس. تم قياس وزن جسم الأم، ومستوى سكر الدم الصائم، ومقاومة الأنسولين، بالإضافة إلى نمو الجنين وكفاءة المشيمة. أُجريت دراسة نسيجية لكلى الجنين وتلوين الهيكل العظمي لتقييم تطور الأعضاء والهيكل العظمي. أظهرت النتائج أن النظام الغذائي الغني بالدهون والسكريات تسبب في ارتفاع سكر الدم لدى الأمهات، وانخفاض حساسية الأنسولين، ونقص نمو المشيمة، وتشوهات في أعضاء الأجنة. أدى كل من الميتفورمين ومستخلص البرباريس على حدة إلى تحسين المؤشرات الأيضية للأمهات ونتائج الحمل، إلا أن الجمع بينهما حقق أكبر قدر من التحسن، بما في ذلك استقرار مستويات الجلوكوز في دم الأم، وتحسين نمو الجنين، وعودة شبه كاملة لوظائف الكلى وتكوين العظام. تشير هذه النتائج إلى التأثير التآزري لمستخلص البرباريس والميتفورمين في الحد من التأثير السلبي لسكري الحمل على نمو الجنين.

الكلمات المفتاحية: ميتفورمين ، سكري الحمل ، برباريس ، فاكهة ، كلى.

1. Introduction:

Diabetes in pregnancy is a major maternal and fetal health problem that impacts the organogenesis and general development of the fetus [1;2]. Gestational hyperglycemia is connected with the presence of oxidative stress and the disruption of the expression of genes and metabolic imbalance which can lead to the development of congenital malformation such as defects of the neural tube, heart, and skeletal system during early pregnancy [3]. Later on, uncontrolled maternal hyperglycemia may result in macrosomia, intrauterine growth retardation

and preterm births[4]. These complications highlight the significance of proper glycemic control during pregnancy in order to facilitate the best fetus outcome [5].

Metformin is a common pharmacological agent in the management of blood glucose levels among people who have type 2 diabetes and gestational diabetes [6]. It reduces glucose levels by a variety of processes, including the hepatic gluconeogenesis inhibition, increased peripheral glucose uptake and activation of AMP-activated protein kinase (AMPK), which is a marketer of cellular energy homeostasis [7]. Also, metformin decreases intestinal glucose absorption which helps to regulate postprandial spikes in glucose levels. Although this treatment is effective, more interest is on natural-based complementary and alternative treatments that could have some other metabolic advantages with fewer side effects [8].

Among promising natural agents, there is barberry (Berberis vulgaris), a natural plant, which is a member of the family Berberidaceae and contains such pharmacologically active compounds as berberine, berbamine and jatrorrhizine [9]. The compounds have hypoglycemic, hypolipidemic, antioxidant, anti-inflammatory and antimicrobial properties. Particularly, berberine was also found to induce greater sensitivity to insulin, lower cholesterol, and protect the organs against oxidative stress [10]. Barberry extract is a possible therapy to be used alongside traditional antidiabetic agents in pregnancy due to its complex pharmacological characteristics [11]. The current study will examine the effects of barberry fruit extract as a mono and as a combination with metformin on maternal metabolic health, fetal growth, placental performance and organ development on a rat gestation diabetes model. Through discussion on biochemical, histological, and skeletal parameters, this study aims at giving an understanding of the possible synergistic effects, in terms of the combination of the conventional pharmacotherapy and plant-derived bioactive compounds in the future, in dose of providing safer and more effective management measures against gestational diabetes and its negative impact on offspring development.

2. Material and methods:

2.1. Experimental animals and housing conditions

The age-matched adult albino rats (10-week old) of both sexes and with similar body weights were acquired in the College of Veterinary Medicine of Tikrit University. The animals were kept in normal laboratory conditions and allowed to acclimatize after which the experiment started. During the study, rats were allowed to have access to food and water freely.

2.2. Experimental design

• both metformin and barberry extract.

Pregnant rats were randomly separated into 5 experimental groups (n= 6/group) as follows:

- Control group: fed a regular laboratory diet.
- HFHS group: Nourished on a high-fat, high-sugar diet.
- HFHS + Metformin group: fed the HFHS diet, metformin**.**
- HFHS + Barberry extract group: was administered HFHS diet and barberry extract.
- HFHS + Metformin + Barberry extract group: fed the HFHS diet and both Metformin and barberry extract were given

2.3. Dietary regimen and induction of gestational diabetes

Rats were placed on a high-fat, high-sugar (HFHS) diet for six weeks. The HFHS diet was composed of 66.5% normal diet, 10% animal fat, 2.5% cholesterol, 20% carbohydrate, Sucrose, and 1% chocolate. Following the dietary period mating was conducted and pregnancy was confirmed by the presence of a vaginal plug. The experiment did not include the non-pregnant females. A single intraperitoneal injection of streptozotocin (25mg/kg body weight) freshly dissolved in 0.1 M sodium citrate buffer [12] was used to induce gestational diabetes.

2.4. Barberry fruit extract and metformin preparation and administration.

The fresh berries of barberry (*Berberis spp*.) were picked, dried in the air, and pulverized into a fine powder. One hundred and fifty g of the powder were put in 500 mL of distilled water and allowed to soak in the water for three days after which they were filtered through regular filter paper. The filtrate was further concentrated in a water bath at 70 o C over two days and further evaporated through a rotary evaporator to eliminate the remaining solvent. The extract obtained was kept at 4 o C waiting to be used. The barberry extract was orally administered at a dose of 500 mg/kg body weight in normal saline (Ashraf et al., 2014). The metformin tablets were dissolved in normal saline and given to the subjects orally at a dosage of 15 mg/kg body weight [13].

2.5. Body weight measurement

The body weights of the mothers were obtained at the expiry of pregnancy. At gestational day 19, the fetuses were pooled and weighted at a sensitive and precise digital balance at an individual level.

2.6. Biochemical measurements related to diabetes

Blood samples were also collected by cardiac puncture after 12 hours of fasting in pregnant rats. Standard glucometer was used to assess the level of fasting blood glucose. Serum was centrifuged and assayed on insulin through ELISA assay. The insulin resistance was measured by determining the homeostasis model assessment of insulin resistance (HOMA-IR) by using the standard equation[14].

2.7. Histological examination

At gestational day 19, embryos were dissected and kidneys were excised and fixed in 10% neutral buffer formalin. Tissues were dried with the use of a graded ethanol, xylene cleared and embedded in paraffin wax [15]. Slices that are 5 mm thick were made with a microtome, placed on glass slides, and stained with hematoxylin and eosin (H&E). A light microscope was used to investigate and record the changes in the histology [16].

2.8. Embryonic skeletal staining

Embryos had been incubated in ethyl alcohol for a few days followed by transfer to acetone. Embryos were stained with Alizarin Red and Alcian Blue following the removal of the skin carefully, in order to visualize ossified bone and cartilage respectively. Specimens were then cleared using potassium hydroxide solution and then using different concentration of potassium hydroxide and glycerol. The skeletons were finally stained, kept in glycerol and photographed with a micro-camera [17].

2.9. Statistical Analysis

The SPSS was used to analyze the data and present them as mean plus SE. One-way ANOVA was the appropriate method of group comparison. A $p < 0.05$ was taken to be statistically significant.

2.10. Ethical approval

The experimental procedures were conducted as per the ethical principles of handling and use of laboratory animals. The protocol of the study was accepted by the Scientific Research Ethics Committee of the Department of Life Sciences, College of Education, University of Kirkuk.

3. Results:

3.1. Maternal body weight and metabolic values

The high-fat, high-sugar (HFHS) diet had a significant impact on maternal metabolic parameters as shown in Table 1. There was a significant maternal body weight increase in the HFHS group as opposed to the control group ($p < 0.05$). Conversely, metformin and barberry extract treatment, and especially in the combined treatment group (HFHS + M + B)[18] led to a massive decline in maternal body weight as compared to the HFHS group and the single treatment groups (Table 1, Figures 1,2).

The levels of fasting blood glucose (FBG) were significantly high in the HFHS group compared to the control group which validated the induction of gestational diabetes[19]. Metformin/barberry extract alone administration was significant in reducing the FBG levels but the highest reduction was observed within the combined treatment group that exhibited much lower levels of FBG than in the remaining treated groups[20]

In the same way, insulin resistance, as determined by the HOMA-IR index was also high in the HFHS compared to all other groups. The control group and the combined treatment group showed significantly lower HOMA-IR values than the control group and the metformin-only and barberry-only groups, which is an indication of a better insulin sensitivity after the combined treatment [21] (Table 1).

Table 1. Effect of metformin and barberry extract on maternal metabolic parameters

Group	Body weight at pregnancy (g)	Fasting blood glucose (mg/dL)	HOMA-IR
Control	270 ± 0.28^{d}	85 ± 0.016^{d}	1.4 ± 0.18^{d}
HFHS	334 ± 0.73^{a}	154 ± 0.41^{a}	5.6 ± 0.42^{a}
HFHS + Metformin	298 ± 0.54^{b}	110 ± 0.23^{b}	3.1 ± 0.29^{b}
HFHS + Barberry	321 ± 0.67^{ab}	136 ± 0.34^{ab}	4.7 ± 0.37^{ab}
HFHS + Metformin + Barberry	282 ± 0.41^{c}	98 ± 0.20^{c}	2.6 ± 0.23^{c}

Values are stated as mean ±SE.

The presence of different letters in the same column as a superscript suggests substantial differences below $p < 0.05$.

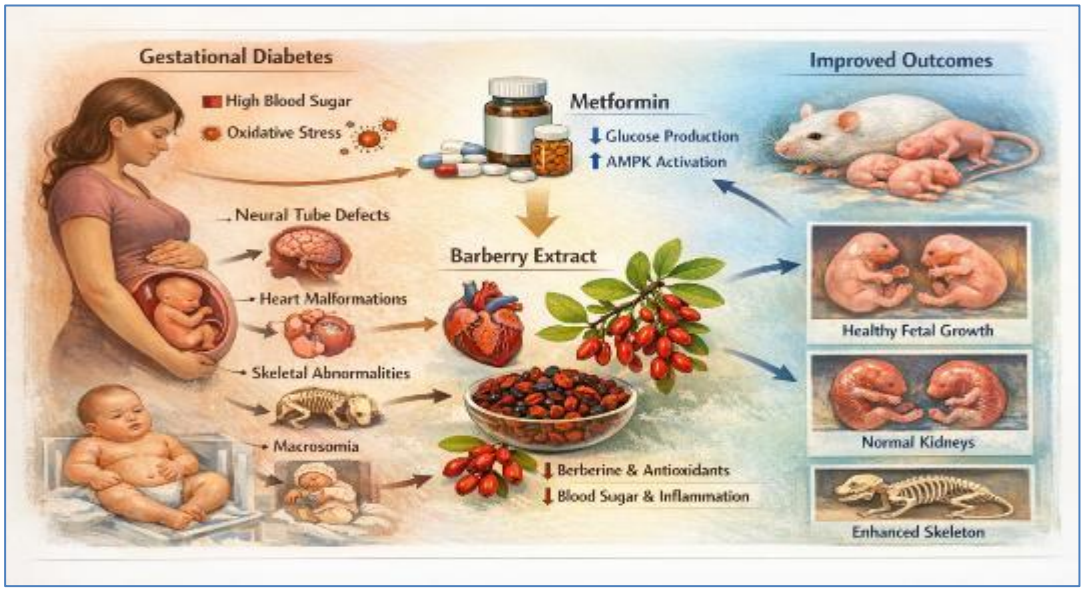


Figure 1. Figure illustrating effects of gestational diabetes on maternal and fetal should health and protective effects of Metformin and barberry extract

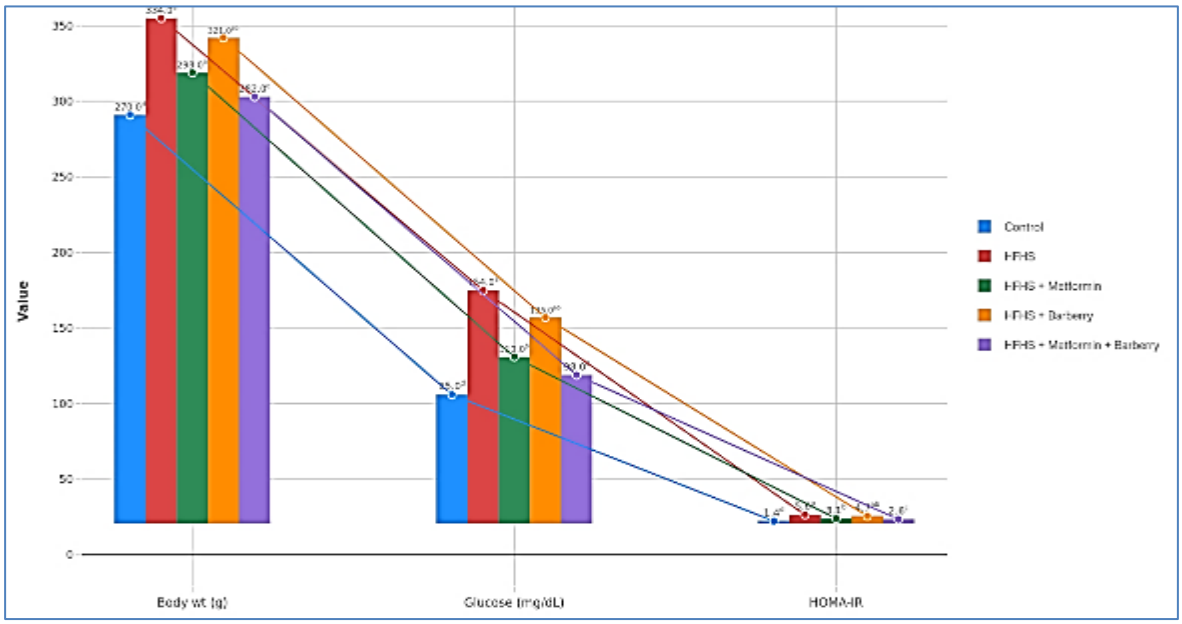


Figure 2. Effects of treatments on pregnancy body weight,fasting glucose and HOMA-IR

3.2. Parameters of fetal growth and placental index

The metabolic status of the mother had a significant impact on fetal growth parameters. The HFHS group showed a significant increase in fetal body weight relative to the control, meaning that the abnormal growth of fetuses has been related to maternal hyperglycemia(Figure 1). The

use of metformin or barberry extract partially normalized the fetal body weight and the combined treatment group (HFHS + M + B) had fetal weight that was not significantly different than those in the control group [22].

The placental index showed that there was a great reduction of the placental index in the HFHS group as compared to the control group indicating the maldevelopment of the placenta in diabetic conditions. It is important to note that the combined treatment group had a remarkable rise in placental index relative to both HFHS group and single-treatment groups indicating an enhancement of placental efficiency and fetal-maternal exchange [23] (Table 2).

Table 2. Effect of metformin and barberry extract on fetal growth and placental index

Group	Fetal body weight (g)	Placental index
Control	2.78 ± 0.51^{d}	8 ± 0.32
HFHS	4.14 ± 0.30^{a}	4 ± 0.09
HFHS + Metformin	3.70 ± 0.16^{c}	6 ± 0.19
HFHS + Barberry	3.92 ± 0.18^{b}	5 ± 0.13
HFHS + Metformin + Barberry	3.14 ± 0.23^{cd}	7 ± 0.25

Values are conveyed as mean ± SE

The significant differences at $p < 0.05$ are indicated by different superscript letters.

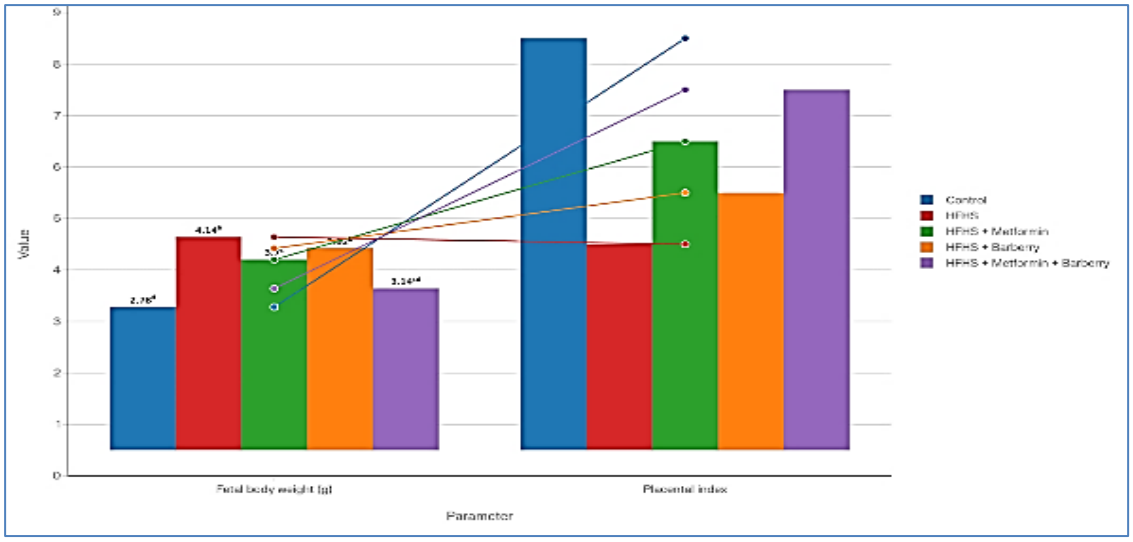


Figure 3. Effects of treatments on fetal body weight and placental index

3.3. Histological assessment of fetal kidney development

The histological analysis of fetal kidneys showed that there are significant differences within the experimental groups as depicted in Figure 4 (A–E). Kidney sections in the control group exhibited normal renal architecture with well-developed glomeruli, clearly identified Bowman space and normal distribution of erythrocytes in glomerular capillaries. The proximal and distal renal tubules were easily identifiable and intact (Figure 4A).

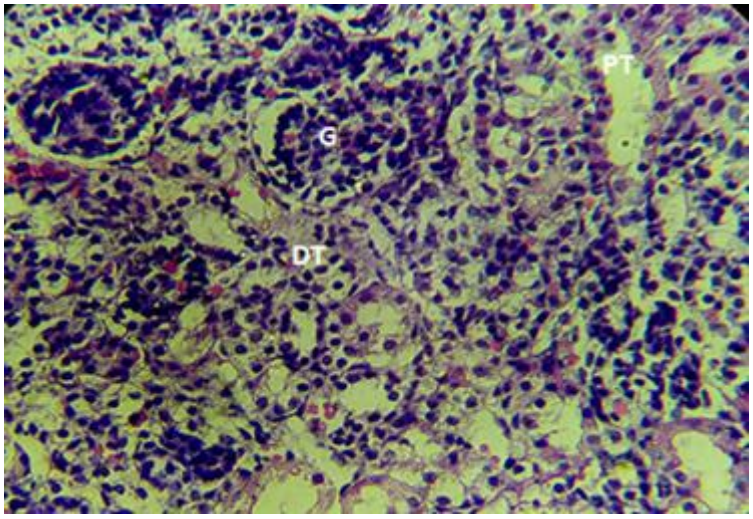


Figure 4 A : Control fetal kidney (normal histology)

Conversely, severe histopathological changes which were cellular degeneration and necrosis were observed in the HFHS group. Gomeruli were not well differentiated, Bowman space was not found, and renal tubules looked chaotic and indistinct which signified severe damage to renal development in diabetic cases (Figure 4 B) .

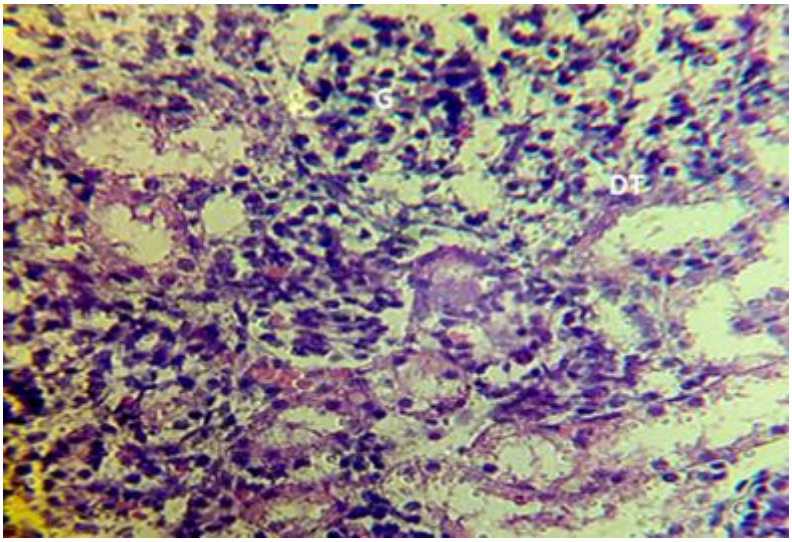


Figure 4 B. HFHS fetal kidney (severe histopathological alterations)

Partial histological improvement was found in the HFHS + Metformin group. It was possible to identify but shrunk glomeruli with partial recovery of Bowman space and erythrocyte distribution. Renal tubules were also still impacted but more noticeable as compared to the HFHS group (Figure 4C) .

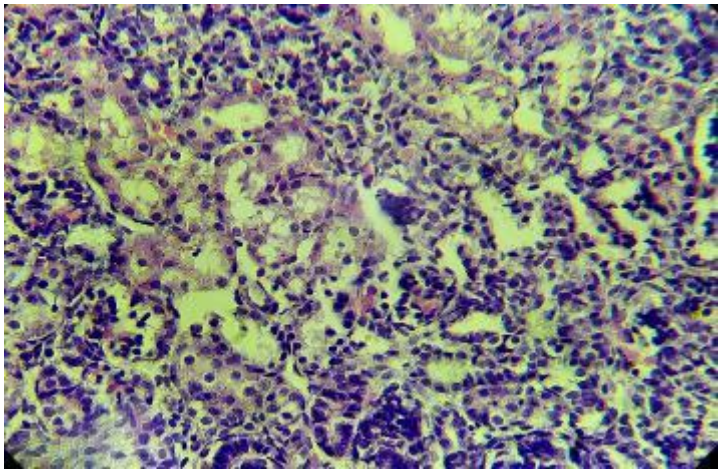


Figure 4C. HFHS + Metformin fetal kidney (partial histological improvement)

Kidney slices of HFHS + Barberry extract group were even better than HFHS group. The distinctions between glomeruli were also better defined, and the space between Bowman had not been completely regained. Proximal and distal tubules could be observed and had narrowed or partially blocked lumen (Figure 4D).

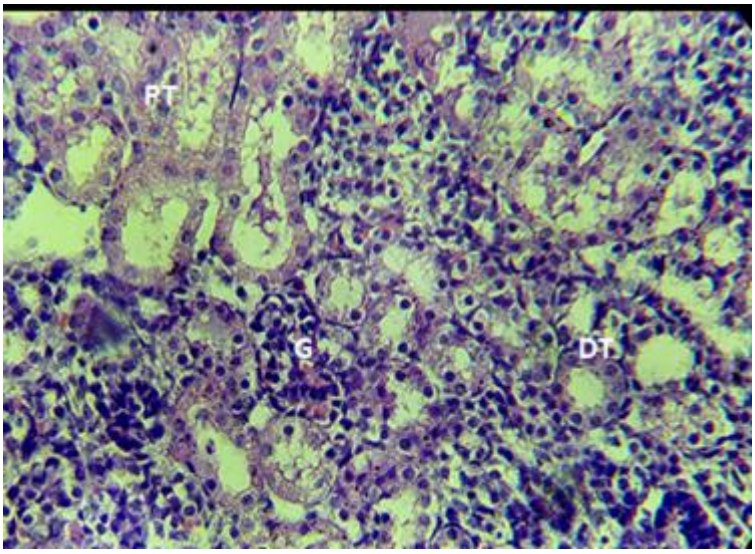


Figure 4D. HFHS + Barberry extract fetal kidney (moderate histological recovery)

HFHS + Metformin + Barberry extract group showed the greatest histological recovery following the control group. Gomeruli were almost of normal size and structure and Bowman

space was evident and renal tubules with well-defined lumens with minimum pathological alterations (Figure 4E) could be observed.

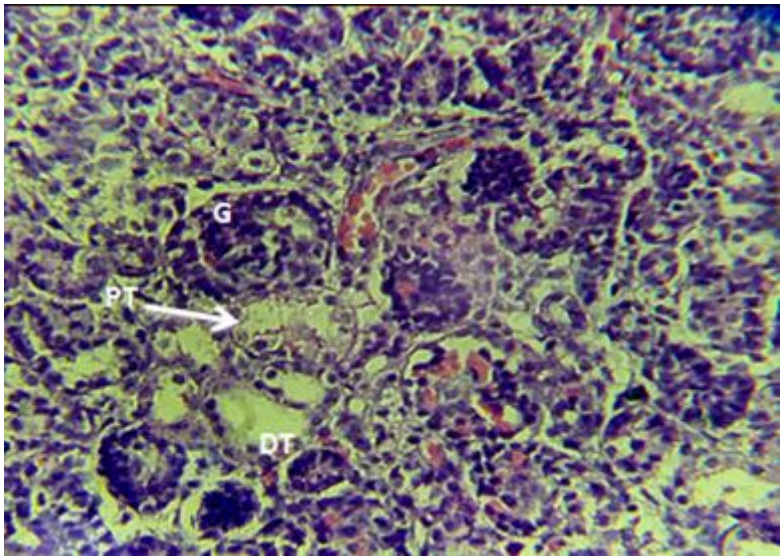


Figure 4E. HFHS + Metformin + Barberry extract fetal kidney (near-normal histology)

3.4. Embryonic skeletal development

The bone staining in Figure 5 showed that there were clear changes in the ossification patterns between the experiment groups. The embryos in the control group depicted normal formation of the bones in which the ossified structures showed strong dark red staining and certain bone and cartilage differentiation.

Contrary to this, the embryos in the HFHS group were significantly less stained, which means that the ossification was delayed and impaired. This was especially noticeable in the skull bones, the forelimbs, hindlimbs and the area of the tail which is an adverse outcome of maternal diabetes on skeletal formation.

Embryos of the metformin- and barberry-treated embryos showed some improvement in the skeletal ossification, and the bone staining was more intense in these groups than in the HFHS group. It is worth noting that the skeletal development pattern of the embryos in the combined treatment group was nearly similar to that of the control group with superior ossification and better bone-cartilage differentiation.

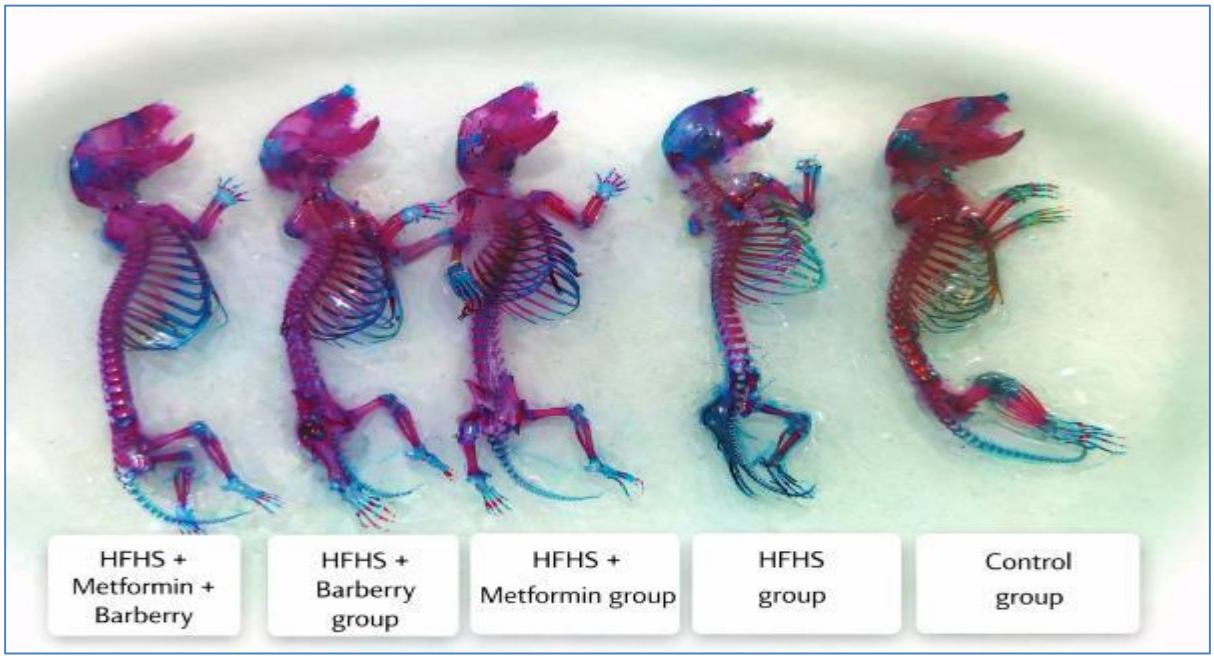


Figure 5. Ossification of skeletal structural organs in various experimental groups after staining with Alizarin red and Alcian blue.

4. Discussion

Gestational diabetes is a complex metabolic syndrome, which is characterized by hyperglycemia, insulin resistance, and oxidative stress in the mother [24]. This kind of metabolic perturbation can disrupt normal fetal development and organogenesis in multiple ways including excessive production of reactive oxygen species (ROS), mitochondrial dysfunction and altered expression of genes in developing tissues [25]. The increased oxidative conditions in the maternal blood can impair the functioning of the placenta causing the placental failure to transport nutrients and oxygen and hence the development of fetal growth and organ maturation [26]. Furthermore, the endoplasmic reticulum stress and inflammatory signaling cascaded by hyperglycemia may disrupt appropriate differentiation of renal and skeletal tissue in developing organs, which shows the susceptibility of the developing organs during the critical gestation phases [27].

The pharmacological treatment of gestational diabetes with metformin is associated with a significant level of benefits because of its multimodal effects on glucose homeostasis[28]. The main mechanism of action of metformin is prevention of hepatic gluconeogenesis, stimulation of peripheral glucose uptake, and activation of AMP-activated protein kinase (AMPK) which is a key controller of cellular energy homeostasis [29]. AMPK activation has shown not only

to cut down hepatic glucose levels, but also to increase mitochondrial lipid metabolism, reduce oxidative stress and stimulate mitochondrial biogenesis [30;31]. These processes combine to create a better intrauterine environment that is useful in the development of the fetal organs and prevents developmental abnormalities [32]. Also, the influence of metformin in lowering the intestinal glucose uptake modulates postprandial glycemic fluctuations, which further safeguard the fetus against the changes in glucose levels that may cause metabolic stress in the fetus [33].

Complementary natural therapies are becoming more and more popular as having the potential to reduce diabetic complications by their antioxidant, anti-inflammatory, and metabolic modulatory activities. The promising candidate is barberry (Berberis vulgaris) because of the presence of bioactive alkaloids, such as berberine, berbamine, and jatrorrhizine [34]. Berberine has been demonstrated as an improved insulin sensitivity and glucose transporter activity and lipid metabolism through AMPK-dependent and independent mechanisms [35]. Moreover, its antioxidant effect prevents ROS-induced injury of mother and fetal tissues, and prevents structural and functional defects in organs like the kidney [36].

It is theoretically beneficial that metformin and barberry extract be used in combination because they may work synergistically [37]. Although the metformin drug is mainly aimed at hepatic glucose production and systemic metabolic control, barberry bioactive compounds are considered to give extra antioxidant and anti-inflammatory effects [38]. This twofold solution can improve maternal insulin response, stabilize the glycemic conditions, and reduce the level of oxidative stress to build optimal conditions to support fetal organogenesis and skeletal development [39]. In addition, the efficiency of the placenta may also be improved due to the alleviation of disturbances in maternal metabolism and reduction in the levels of inflammatory mediators, which would allow the placenta to transfer nutrients more effectively and would support the growth and development of the fetus [40].

The fetuses under development are incredibly vulnerable to the metabolic conditions of the mother in regard to histological and skeletal integrity [41]. Interference in the differentiation and mineralization process of renal and skeletal tissues can be caused by hyperglycemia and oxidative stress [42]. Protective replacement of the lost redox equilibrium, glucose control and inflammatory state can therefore be used to preserve normal tissue structure and function [43]. These trends have implied that the effectiveness of the combination of the traditional pharmacological therapy with the bioactive components of the vegetable origin may be employed to enhance the fetal tolerance of the adverse intrauterine conditions of the gestational diabetic complication [44;45].

5. Conclusions

Gestational diabetes has an adverse impact on maternal metabolism and unborn child development by impacting hyperglycemia, insulin resistance, and oxidative stress. Metformin and barberry fruit extract combination is complementary to bring about better metabolic balance, placental functions, and preserve the development of fetal organs and skeletal structures. This integrated intervention is possibly a promising solution to the problem of decreasing complications associated with gestational diabetes and positively influencing the outcomes of pregnancy.

6. Acknowledgments

The authors would like to acknowledge that they are truly indebted to the Department of biology, College of Education, Pure Sciences University of Kirkuk, to offer the required laboratory facilities and technical support which played a great part in ensuring the success of this study.

References

[1] Ornoy A, Becker M, Weinstein-Fudim L, Ergaz Z. Diabetes during pregnancy: a maternal disease complicating the course of pregnancy with long-term deleterious effects on the offspring. a clinical review. International Journal of Molecular Sciences. 2021 Mar 15;22(6):2965. https://doi.org/10.3390/ijms22062965

[2] Mahmoud DA, Saleh SS. Determination of the level of homocysteine and antioxidants in the blood serum of women with gestational diabetes. Solid State Technology. 2021 Jan 20;64(1):1129-35.

[3] Negrato CA, Marques PR, Leite HB, Torigoe CN, Silva BF, Costa K, Kamei JM, Zampa CL, Toni AC, Pereira IC, Heinzelmann GL. Glycemic and nonglycemic mechanisms of congenital malformations in hyperglycemic pregnancies: a narrative review. Archives of endocrinology and metabolism. 2022 Oct10;66 (6):908-18. https://doi.org/10.20945/2359-3997000000521

[4] Sodje JD. Fetal growth abnormalities: intrauterine growth restriction and macrosomia. InContemporary Obstetrics and Gynecology for Developing Countries 2021 Aug 6 (pp. 103-115). Cham: Springer International Publishing. https://doi.org/10.1007/978-3-030-75385-6_11

[5] Picón-César MJ, Molina-Vega M, Suárez-Arana M, González-Mesa E, Sola-Moyano AP, Roldan-López R, Romero-Narbona F, Olveira G, Tinahones FJ, González-Romero

S. Metformin for gestational diabetes study: metformin vs insulin in gestational diabetes: glycemic control and obstetrical and perinatal outcomes: randomized prospective trial. American journal of obstetrics and gynecology. 2021 Nov 1;225(5):517-e1. https://doi.org/10.1016/j.ajog.2021.04.229

[6] Johanns M, Hue L, Rider MH. AMPK inhibits liver gluconeogenesis: fact or fiction?. Biochemical Journal. 2023 Jan 13;480(1):105-25. https://doi.org/10.1042/BCJ20220582

[7] Wang D, Yang L, Liu Y. Targeting AMPK signaling in the liver: implications for obesity and type 2 diabetes mellitus. Current Drug Targets. 2022 Aug 1;23(11):1057-71. https://doi.org/10.2174/1389450123666220429082702

[8] Halagali P, Inamdar A, Singh J, Anand A, Sadhu P, Pathak R, Sharma H, Biswas D. Phytochemicals, herbal extracts, and dietary supplements for metabolic disease management. Endocrine, Metabolic & Immune Disorders-Drug Targets. 2025 Sep;25(12):993-1016. https://doi.org/10.2174/0118715303287911240409055710

[9] Och A, Nowak R. Barberry (Berberis vulgaris)—Traditional and contemporary use. InMedicinal Plants: Domestication, Biotechnology and Regional Importance 2021 Sep 2 (pp. 797-825). Cham: Springer International Publishing. https://doi.org/10.1007/978-3-030-74779-4_24

[10] Mehdi S, Mehmood MH, Ahmed MG, Ashfaq UA. Antidiabetic activity of Berberis brandisiana is possibly mediated through modulation of insulin signaling pathway, inflammatory cytokines and adipocytokines in high fat diet and streptozotocin-administered rats. Frontiers in Pharmacology. 2023 Apr 6;14: https://doi.org/10.3389/fphar.2023.1085013

[11] Uti DE, Atangwho IJ, Alum EU, Egba SI, Ugwu OP, Ikechukwu GC. Natural antidiabetic agents: current evidence and development pathways from medicinal plants to clinical use. Natural Product Communications. 2025 Mar;20(3): https://doi.org/10.1177/1934578X251323393

[12] Takahashi N, Ichii O, Hiraishi M, Namba T, Otani Y, Nakamura T, Kon Y. Phenotypes of streptozotocin-induced gestational diabetes mellitus in mice. Plos one. 2024 Apr 16;19(4). https://doi.org/10.1371/journal.pone.0302041

[13] Dhakal D. Phytochemical Screening and Biological Activities of Berberis Asiatica from Arghakhanchi District Phytochemical Screening and Biological Activities of Berberis Asiatica from Arghakhanchi District (Doctoral dissertation, Department of Chemestry). https://hdl.handle.net/20.500.14540/9747

[14] Ogbodo EC, Onah CE, Amah AK, Okeke CS, Obiorah MO, Okezie AO, Ogalagu RO, Iwuji JC, Mbam RE, Meludu SC. Assessment of fasting plasma glucose, insulin, insulin resistance and glycated haemoglobin as markers of glycemic control in apparently healthy older adults in Nnewi. Indian Journal of Forensic and Community Medicine. 2024;11(2):1-7.

[15] Alzubaidi A, Al-Bakri NA, Alarami AM. Glomerulogenesis and Histomorphometeric in Mus musculus Embryo. Ibn AL-Haitham Journal For Pure and Applied Sciences. 2023 Apr 18;36(2):14-21. https://doi.org/10.30526/36.2.3000

[16] Isaac UE, Oyo-Ita E, Igwe NP, Ije EL. Preparation of histology slides and photomicrographs: Indispensable techniques in anatomic education. Anatomy Journal of Africa. 2023 Apr 6;12(1):2252-62. https://orcid.org/0000-0003-4577-6278

[17] Liao YJ, Tang PC, Chen LR, Yang JR. A protocol for differential staining of cartilages and ossified bones in fetal and adult mouse skeletons using alcian blue and alizarin red S. Journal of Histotechnology. 2020 Oct 1;43(4):204-9. https://doi.org/10.1080/01478885.2020.1756081

[18] Schoonejans JM. The effect of metformin intervention on the programming of cardiometabolic health in offspring of obese pregnancy (Doctoral dissertation). https://doi.org/10.17863/CAM.72732

[19] Liu H, Guo L, Wang F, Ji Q, Chen K. Effect and Predictive Value of Blood HbA1c, FBG, 2hPBG, and FINS on the Pregnancy Outcome in Patients with Gestational Diabetes Mellitus. Clinical Laboratory. 2024 Sep 1;70(9). https://doi.org/10.7754/Clin.Lab.2024.240150

[20] Martirosyan D, Santrosyan G, McCarthy J, Nguyen A. Metformin: Optimal dosage, interactions, and efficacy. Exploring natural alternatives for diabetes management. Bioactive Compounds in Health and Disease-Online ISSN: 2574-0334; Print ISSN: 2769-2426. 2025 May 21;8(5):177-203. https://doi.org/10.31989/bchd.v8i5.1624

[21] Song DK, Lee H, Hong YS, Sung YA. Insulin resistance is associated with hirsutism in unselected reproductive-aged women. Clinical Endocrinology. 2019 Apr;90(4):586-91. https://doi.org/10.1111/cen.13936

[22] Guo F, Liu Y, Ding Z, Zhang Y, Zhang C, Fan J. Observations of the effects of maternal fasting plasma glucose changes in early pregnancy on fetal growth profiles and birth outcomes. Frontiers in Endocrinology. 2021 Aug 19;12. https://doi.org/10.3389/fendo.2021.666194

[23] Hong J, Crawford K, Cavanagh E, Clifton V, da Silva Costa F, Perkins AV, Kumar S. The relationship between abnormal fetoplacental Dopplers, angiogenic markers of placental dysfunction and adverse perinatal outcomes in diabetic pregnancies with small fetuses–A prospective study. Placenta. 2025 Feb 1;160:51-9. https://doi.org/10.1016/j.placenta.2024.12.025

[24] Saucedo R, Ortega-Camarillo C, Ferreira-Hermosillo A, Díaz-Velázquez MF, Meixueiro-Calderón C, Valencia-Ortega J. Role of oxidative stress and inflammation in gestational diabetes mellitus. Antioxidants. 2023 Sep 29;12(10):1812. https://doi.org/10.3390/antiox12101812

[25] Swain N, Moharana AK, Jena SR, Samanta L. Impact of oxidative stress on embryogenesis and fetal development. InOxidative Stress and Toxicity in Reproductive Biology and Medicine: A Comprehensive Update on Male Infertility Volume II 2022 Dec 7 (pp. 221-241). Cham: Springer International Publishing. https://doi.org/10.1007/978-3-031-12966-7_13

[26] Obeagu EI. Oxidative Stress and Pregnancy-induced Hypertension: Antioxidant Solutions. International Journal of Medical Sciences and Pharma Research. 2024 Dec 15;10(4):22-7. https://doi.org/10.22270/ijmspr.v10i4.119

[27] Zhao L, Yuan J, Yang Q, Ma J, Yang F, Zou Y, Liu K, Liu F. Diabetes and its complications: molecular mechanisms, prevention and treatment. Signal Transduction and Targeted Therapy. 2026 Jan 19;11(1):22. https://doi.org/10.1038/s41392-025-02401-w

[28] Mason T, Alesi S, Fernando M, Vanky E, Teede HJ, Mousa A. Metformin in gestational diabetes: physiological actions and clinical applications. Nature Reviews Endocrinology. 2025 Feb;21(2):77-91. https://doi.org/10.1038/s41574-024-01049-w

[29] Szymczak-Pajor I, Wenclewska S, Śliwińska A. Metabolic action of metformin. Pharmaceuticals. 2022 Jun 30;15(7):810. https://doi.org/10.3390/ph15070810

[30] Fang C, Pan J, Qu N, Lei Y, Han J, Zhang J, Han D. The AMPK pathway in fatty liver disease. Frontiers in Physiology. 2022 Aug 25;13:970292. https://doi.org/10.3389/fphys.2022.970292

[31] Ali RH, Hussein FK, Nasar DM, Abd Al salam Salem A. The Relevance of Mitochondrial DNA Mutation in Human Diseases and Forensic Sciences. Al-Nahrain Journal of Science. 2025 Mar 15;28(1):96-106. https://doi.org/10.22401/ANJS.28.1.11

[32] Gao Y, Yu X, Wang Y, Wang H, Wang YL, Shyh-Chang N. Metabolic control of feto–placental development and pregnancy outcomes. Nature Reviews Endocrinology. 2025 Nov 25:1-3. https://doi.org/10.1038/s41574-025-01206-9

[33] Priya G, Kalra S. Metformin in the management of diabetes during pregnancy and lactation. Drugs in context. 2018 Jun 15;7:212523. https://doi.org/10.7573/dic.212523

[34] Bai Y, Mu Q, Bao X, Zuo J, Fang X, Hua J, Zhang D, Jiang G, Li P, Gao S, Zhao D. Targeting NLRP3 inflammasome in the treatment of diabetes and diabetic complications: Role of natural compounds from herbal medicine. Aging and disease. 2021 Oct 1;12(7):1587. https://doi.org/10.14336/AD.2021.0318

[35] Dong ZH, Lin HY, Chen FL, Che XQ, Bi WK, Shi SL, Wang J, Gao L, He Z, Zhao JJ. Berberine improves intralipid-induced insulin resistance in murine. Acta Pharmacologica Sinica. 2021 May;42(5):735-43. https://doi.org/10.1038/s41401-020-0493-4

[36] Zhang C, Guo Y, Yang Y, Du Z, Fan Y, Zhao Y, Yuan S. Oxidative stress on vessels at the maternal-fetal interface for female reproductive system disorders: Update. Frontiers in Endocrinology. 2023 Mar 10;14:1118121. https://doi.org/10.3389/fendo.2023.1118121

[37] Caturano A, Nilo D, Nilo R, Sircana MC, Erul E, Zielińska K, Russo V, Santonastaso E, Sasso FC. Old Drug, New Science: Metformin and the Future of Pharmaceutics. Pharmaceutics. 2026 Jan 7;18(1):77. https://doi.org/10.3390/pharmaceutics18010077

[38] Bailey CJ. Metformin: Therapeutic profile in the treatment of type 2 diabetes. Diabetes, Obesity and Metabolism. 2024 Aug;26:3-19. https://doi.org/10.1111/dom.15663

[39] Zhuang M, Wang B, Shi Y, Zhou Z. Multi-organ regulation mechanisms and nutritional intervention strategies in gestational diabetes mellitus. The Journal of Nutrition. 2025 Apr 11. https://doi.org/10.1016/j.tjnut.2025.04.008

[40] Chae SA, Son JS, Du M. Prenatal exercise in fetal development: a placental perspective. The FEBS journal. 2022 Jun;289(11):3058-71. https://doi.org/10.1111/febs.16173

[41] Dimas A, Politi A, Bargiota A, Panoskaltsis T, Vlahos NF, Valsamakis G. The gestational effects of maternal bone marker molecules on fetal growth, metabolism and long-term metabolic health: a systematic review. International journal of molecular sciences. 2022 Jul 28;23(15):8328. https://doi.org/10.3390/ijms23158328

[42] González P, Lozano P, Ros G, Solano F. Hyperglycemia and oxidative stress: an integral, updated and critical overview of their metabolic interconnections. International

journal of molecular sciences. 2023 May 27;24(11):9352. https://doi.org/10.3390/ijms24119352

[43] Bellanti F, Coda AR, Trecca MI, Lo Buglio A, Serviddio G, Vendemiale G. Redox imbalance in inflammation: the interplay of oxidative and reductive stress. Antioxidants. 2025 May 29;14(6):656. https://doi.org/10.3390/antiox14060656

[44] Hasan SR, Junaid FM, Mahdi BM, Hussein FK. Therapeutic applications of medicinal plants for the treatment of human intestinal diarrhea: Review article. S. Asian J. Life Sci. 2025;13:20-4. https://dx.doi.org/10.17582/journal.sajls/2025/13.20.24

[45] Chintada V, Golla N. Exploring the therapeutic potential of bioactive compounds from plant sources. InBiotechnological Intervention in Production of Bioactive Compounds: Biosynthesis, Characterization and Applications 2025 Feb 26 (pp. 229-247). Cham: Springer Nature Switzerland. https://doi.org/10.1007/978-3-031-76859-0_15

Al-Kitab Journal for Pure Sciences (2026); 10(2):203-220.
https://doi.org/10.32441/kjps.10.2.p15

Al-Kitab Journal for Pure Sciences
ISSN: 2617-1260 (print), 2617-8141(online)

https://isnra.net/index.php/kjps

Alterations in Serum Lactate Dehydrogenase and Creatine Kinase Levels in Relation to Physical Activity Intensity

Nuha Hamza Khedhir[1], Muntaha Mezhir Abbas[2], Galawesh Norri Taher[3]

[1]Department of Pharmacy, Medical Technical Institute / Kirkuk, Northern Technical University, Iraq.

[2] Department of Nursing Techniques, Medical Technical Institute / Kirkuk, Northern Technical University, Iraq.

[3] Department of Nursing Techniques, Medical Technical Institute / Kirkuk, Northern Technical University, Iraq.

Corresponding Author: nuha70hamza@ntu.edu.iq

Citation: ***Nuha Hamza Khedhir[1], Muntaha Mezhir Abbas[2], Galawesh Norri Taher[3]*. Alterations in Serum Lactate Dehydrogenase and Creatine Kinase Levels in Relation to Physical Activity Intensity.**
Al-Kitab J. Pure Sci. [Internet]. 2026 May. 24 ;10(2):203-220
DOI.
https://isnra.net/index.php/kjps/article/view/2026.
https://doi.org/10.32441/kjps.10.2.p15

©20--. THIS IS AN OPEN-ACCESS ARTICLE UNDER THE CC BY LICENSE
http://creativecommons.org/licenses/by/4.0/

Keywords: Creatine Kinase (CK), Lactate Dehydrogenase (LDH), Muscle Enzymes, Muscle Stress, Anaerobic Metabolism.

Article History

Received	05 Apr. 2026
Accepted	24 May. 2026
Available online	01 Nov. 2026

Abstract:

The objective of this study was to investigate how muscle-related enzymes, i.e., creatine kinase (CK) and lactate dehydrogenase (LDH), depend on various degrees of physical exercise intensity in apparently healthy individuals. The study participants, 180 in number, between 20 and 50 years old, were selected from Kirkuk city and divided into three groups according to their physical activity: sedentary, moderately active, and highly active. Blood was taken before and 30 minutes after exercise in the active groups, and serum creatine kinase and lactate dehydrogenase levels were determined. In addition, heart rate and blood lactate concentrations were measured.

There was no significant difference between the two groups in terms of initial levels of CK and LDH enzymes, i.e., ($p > 0.05$). However, after exercise, there was a significant increase in levels of CK and LDH enzymes in moderate and high activity groups, i.e., ($p < 0.001$), with higher levels of enzymes in highly active individuals.

The increase in CK levels is related to muscle stress during exercise and is a result of temporary changes in cell membrane permeability, and the increase in LDH levels relates to increased demand during exercise. This combination of markers gives a picture of what happens in terms of structure and metabolism in the muscles.

Keywords: Creatine Kinase (CK), Lactate Dehydrogenase (LDH), Muscle Enzymes, Muscle Stress, Anaerobic Metabolism.

التغيرات في مستويات إنزيم لاكتات ديهيدروجيناز *(LDH)* وكرياتين كيناز *(CK)* في المصل تبعًا لشدة النشاط البدني

نُهى حمزة خضير[1]، منتهى مظهر عباس[2]، كالاويش نوري طاهر[3]

[1] قسم الصيدلة، المعهد التقني الطبي / كركوك، الجامعة التقنية الشمالية، العراق

[2] قسم تقنيات التمريض، المعهد التقني الطبي / كركوك، الجامعة التقنية الشمالية، العراق

[3]قسم تقنيات التمريض، المعهد التقني الطبي / كركوك، الجامعة التقنية الشمالية، العراق

الايميل الرسمي: nuha70hamza@ntu.edu.iq

الخلاصة:

كانت فكرة الدراسة هي معرفة كيف تؤثر مستويات مختلفة من النشاط البدني على إنزيمات العضلات مثل كرياتين كيناز (*CK*) ولاكتات ديهيدروجيناز (*LDH*) عند أشخاص يبدو عليهم أنهم بصحة جيدة. شارك في الدراسة ١٨٠ شخصًا تتراوح أعمارهم بين ٢٠ و٥٠ سنة، جميعهم من مدينة كركوك. قُسم المشاركون إلى ثلاث مجموعات حسب مدى نشاطهم البدني: مجموعة تميل إلى الخمول، وأخرى تمارس نشاطًا متوسطًا، وثالثة نشطة بشكل كبير.

تم سحب عينات الدم قبل التمرين وبعده بـ٣٠ دقيقة لدى المجموعات النشطة، وتم قياس مستويات إنزيمي كرياتين كيناز ولاكتات ديهيدروجيناز في المصل. بالإضافة إلى ذلك، تم قياس معدل ضربات القلب وتركيز اللاكتات في الدم.

لم تُسجل فروق معنوية بين المجموعات في المستويات الأساسية لإنزيمي *CK* و *LDH* ($p > 0.05$). ومع ذلك، بعد التمرين، لوحظت زيادة معنوية في مستويات كلا الإنزيمين في مجموعتي النشاط المعتدل والعالي ($p < 0.001$)، وكانت هذه الزيادة أعلى لدى الأفراد ذوي النشاط العالي.

ترتبط الزيادة في مستوى إنزيم *CK* بالإجهاد العضلي أثناء التمرين، وهي ناتجة عن تغيرات مؤقتة في نفاذية غشاء الخلية، بينما تعكس زيادة إنزيم *LDH* ارتفاع الطلب الأيضي خلال النشاط البدني. ويعطي هذا المزيج من المؤشرات صورة واضحة عن التغيرات البنيوية والأيضية التي تحدث في العضلات.

كلمات مفتاحية: كرياتين كيناز (CK)، لاكتات ديهيدروجيناز (LDH)، إنزيمات العضلات، الإجهاد العضلي، الأيض اللاهوائي

1. Introduction:

Exercise is one of the pillars of human health, which aids in the maintenance of metabolic homeostasis, heart performance, and skeletal health[1]. Exercise is characterized by repeated

contracting and relaxation of skeletal muscles causing mechanical, metabolic and oxidative stress to muscle fibres[2]. These stressors may cause temporary structural perturbation of the muscle cells which causes the extraction of intracellular components into the blood[3].

The creatine kinase (CK) and lactate dehydrogenase (LDH) are some of the most frequently studied biochemical markers of muscle stress and damage[4]. Creatine kinase is a mitochondrial and cytosolic enzyme which catalyzes the reversible phosphate group exchange of phosphocreatine to ADP [5]. Damage to muscle fibers is strongly associated with elevated serum CK levels following high-intensity exercise [6]. Lactate dehydrogenase, nevertheless, is a significant enzyme related to anaerobic metabolism[7]. It catalyzes the conversion of pyruvate and lactate to allow glycolysis to take place in the anaerobic state[8]. High level of LDH indicates high metabolic demand and cell membrane permeability changes during as well as after physical exercise[9].The increase in CK and LDH with exercise is related to several factors including exercise intensity, length and type of exercise (aerobic or anaerobic) and the fitness of the individual[10]. Intensive bouts of vigorous exercise typically cause significant changes in these enzymes but long-term training of the body to exercise leads to adaptation which restricts the amount of leakage of these enzymes[11].

The response of CK and LDH to physical activity is important because it can be used to assess muscle damage and recovery as well as to increase athletic performance and avoid overtraining[12]. Furthermore, these biomarkers have clinical relevance in diagnosing muscle-related pathologies and monitoring rehabilitation processes[13].

Thus, the current research will explore the changes in serum CK and LDH alongside various exercise amounts of physical activity among seemingly healthy adults.

2. Materials and Methods

2.1 Study Design

This study was designed as an analytical cross-sectional study to assess the effect of physical activity intensity on muscle enzyme levels and physiological parameters.

2.2 Study Population and Sampling Site

This study comprised 180 apparently healthy subjects between 20 and 50 years of age. The subjects were selected from private clinics and diagnostic laboratories in Kirkuk city, where routine health check-ups and investigations are carried out.

Participants were recruited with the assistance of medical staff in these institutions, this facilitated access to participants with different physical activity levels.

All the participants were informed of the purposes of the study and informed verbal consent was obtained prior to inclusion.

The physical activity level was used to group the subjects into three groups:

- Group I (Sedentary): Individuals with minimal or no regular physical activity
- Group II (Moderately active): Individuals performing moderate exercise 3–4 times per week
- Group III (Highly active): Individuals engaged in intense physical training or competitive sports

2.3 2.3 Inclusion Criteria

The participants in this study were apparently healthy adults without a history of long-term illnesses. Participants were not taking any medications that could interfere with muscle metabolism., and all individuals were non-smokers to limit the possible confounding variables that may impact the study results.

2.4 Exclusion Criteria

The participants were not allowed to include those whose history included cardiovascular or metabolic diseases, recent infections or inflammatory diseases, or any injury of the muscles during the previous two weeks. Also, the participants taking antioxidant supplements or performance-enhancing drugs were not part of the study in order to eliminate possible interference with the biochemical parameters under study.

2.5 Data Collection

Data from all participants were collected using a comprehensive and standardized method. All the participants were given a structured questionnaire which contained data on age, lifestyle habits, and degree of physical activity. Also, general body composition was measured through anthropometric measurements, body mass index (BMI). Physical activity levels were assessed using a standardized physical activity scoring system to be able to classify the participants in a consistent and reliable way in terms of their activity status.

2.6 Exercise Protocol

Participants in the moderate and high activity groups performed supervised treadmill-based exercise sessions under standardized conditions.

Participants in the moderate activity group performed 30 minutes of moderate-intensity jogging at 60–70% of maximal predicted heart rate.

Participants in the high activity group performed 45 minutes of high-intensity interval running at 80–90% of maximal predicted heart rate.

Heart rate was continuously monitored throughout the exercise sessions to ensure consistency of exercise intensity.

2.7 Blood Sample Collection

Blood samples (5 mL) were collected from participants under standardized conditions. All the individuals were sampled at a rest position (baseline), and the other sample was done 30 minutes after the exercise, in the case of the participants in the active groups. Biochemical analysis was performed on the collected serum samples.; therefore, their samples were centrifuged at 3000 rpm, 10 minutes to separate the serum.

2.8 Biochemical Analysis

Biochemical analysis was performed to evaluate the levels of muscle-related enzymes. Creatine kinase (CK) was measured using an enzymatic UV kinetic method, and the results were expressed in units per liter (U/L)[14]. Lactate dehydrogenase (LDH) levels were determined using a spectrophotometric method, with results also expressed in units per liter (U/L).

2.9 Blood Lactate Measurement

Blood lactate levels were measured using a portable lactate analyzer. Capillary blood samples were obtained from the fingertip under aseptic conditions. Baseline samples were collected prior to exercise, and post-exercise samples were obtained within 5 minutes after exercise completion. Lactate concentrations were expressed in mmol/L.

2.10 Heart Rate Measurement

Measurement of the heart rate was conducted with the aid of a digital heart monitor. Resting heart rates were recorded after a 10-minute resting period in a sitting position, while the post-exercise heart rates were recorded immediately after the completion of the session of exercises. All the values of the heart rates were recorded in beats per minute (bpm).

2.11 Statistical Analysis

Results were presented as mean and standard deviation. One-way ANOVA followed by Tukey's post hoc analysis was used to compare study groups. In addition, Pearson correlation analysis was performed to evaluate the relationships between CK, LDH, heart rate, and blood lactate levels. Differences were considered statistically significant when the p-value is < 0.05. The selected parameters were CK, LDH, heart rate, and blood lactate.

3. Results and Discussion

3.1 Participant Characteristics

One hundred and eighty apparently healthy adults were used in the study, with equal representation on each of the three groups on the basis of their physical activity levels; low activity (n = 60), moderate activity (n = 60), and high activity (n = 60). Table 1summarizes the demographics and anthropometric measurements of the participants(Figure 1).

Table 1 summarizes the demographic and anthropometric measurements of the participants.

Parameter	Low Activity (n=60)	Moderate Activity (n=60)	High Activity (n=60)
Age (years)	34.2 ± 7.1	33.8 ± 6.5	34.5 ± 7.0
BMI (kg/m²)	26.1 ± 3.2	25.5 ± 2.9	24.8 ± 2.7
Gender (M/F)	30/30	30/30	30/30

All values are expressed as mean ± SD.

The three groups were found not to have statistically significant differences based on age, gender distribution, or BMI ($p > 0.05$), which means that the comparability of the baseline was high. This homogeneity is essential in achieving the internal validity of the study since it reduces the possibilities whereby confounding variables may obstruct the sampled biochemical results[15].

The age is a well-known issue that can impact muscle metabolism and the activity enzymes because physiological aging could influence muscle mass, muscle repair, and exercise-related enzymatic reactions[16]. On the same note, it goes without saying that BMI has a close relationship with body composition and metabolic status, which can influence pre and post exercise levels of muscle related enzymes like CK and LDH[17]. These parameters indicate the lack of notable differences between groups, which implies that the differences in enzyme levels

in the later part of the study could be attributed with greater certainty to the physical activity difference than to demographic or anthropometric differences between groups[18].

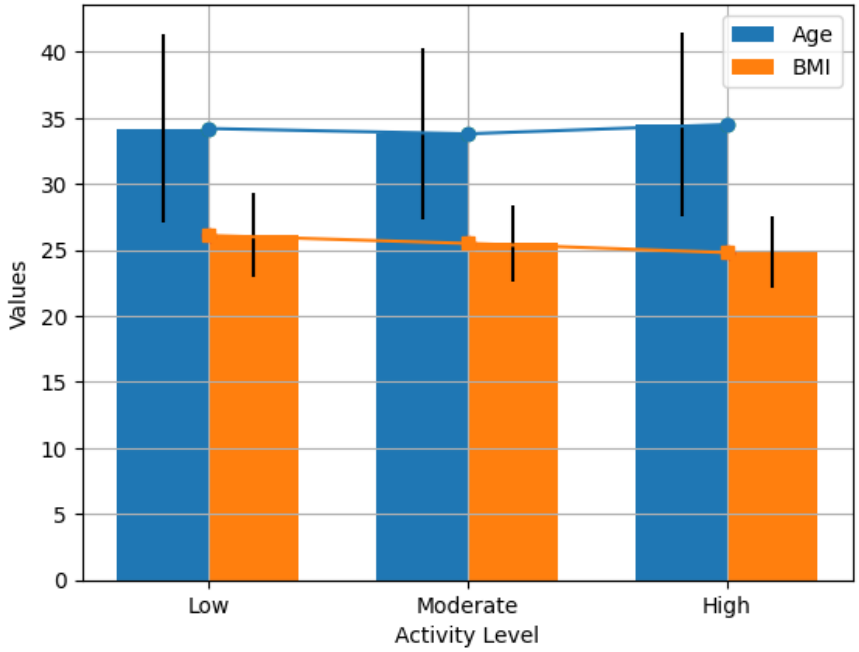


Figure 1 : Participant Characteristics (Age and BMI)

Also, males and females are distributed equally on each group of study and this minimizes any sex-based bias possible[19]. This is especially so because hormonal dissimilarity and muscle mass variation between the sexes can result in their enzyme excretion after the physical activity[20]. The study achieves a balance of gender and therefore, increases reliability and generalizability of the results[21].

In general, the similarity of the baseline traits of the study groups gives strong grounds to further analyses and the suggestion that the reasons of the observed biochemical differences are the differences in physical activity levels and not extrinsic confounding factors[22].

3.2 Creatine Kinase (CK) Levels

The baseline levels of CK were found to be similarly low in all the groups (Low: 112.5 ± 28.4 U/L, Moderate: 115.7 ± 30.1 U/L, High: 118.9 ± 31.2 U/L), indicating the absence of pre-existing muscle damage, as shown in Table 2. CK levels increased significantly in the moderate and high physical activity groups, as shown in Figure 2. The CK increase after exercise is an indication of exercise stress on muscle and temporary elevations of membrane permeability, but not structural damage[23]. The higher enzyme levels observed in the high activity group compared with the low activity group

, indicates the relationship between the intensity of exercise and the releasing of muscle enzymes[24].This suggests that CK is a sensitive indicator of acute muscular activity [25][26].

Table 2. CK levels (U/L) in study groups.

Group	Baseline CK (U/L)	Post-Exercise CK (U/L)
Low Activity	112.5 ± 28.4	–
Moderate Activity	115.7 ± 30.1	152.3 ± 35.6
High Activity	118.9 ± 31.2	198.6 ± 40.2

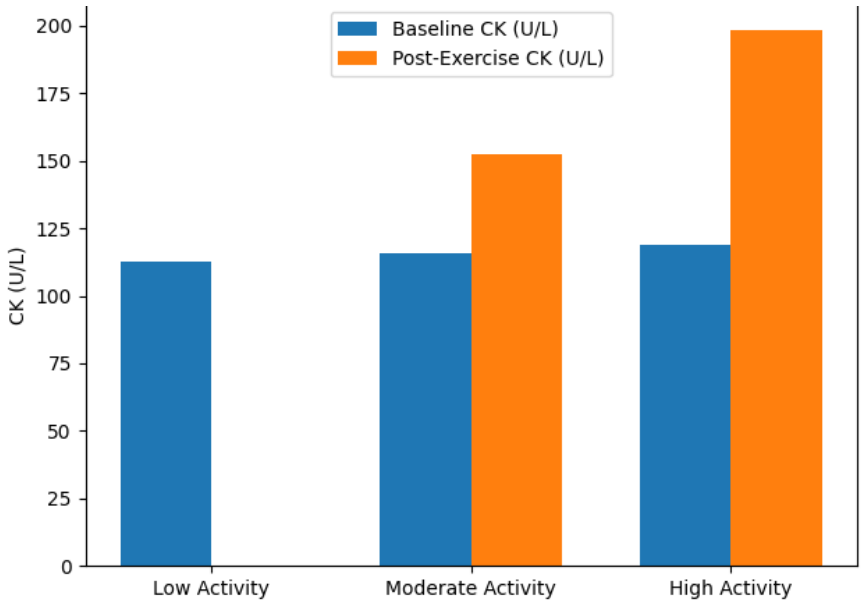


Figure 2 : Effect of Physical Activity on CK Levels

3.3 Lactate Dehydrogenase (LDH) Levels

LDH levels were significantly elevated. Baseline values were similar in low (210.3 ± 45.2 U/L), moderate (212.5 ± 46.1 U/L) and high activity groups (215.7 ± 47.0 U/L) which means that there were no pre-existing metabolic or muscular abnormalities. After exercises, the moderate (245.7 ± 50.4 U/L) and high activity group (290.8 ± 55.6 U/L) LDH levels were significantly elevate significantly elevated (Table 3, Figure ٣).

The observed increase in LDH reflects increased metabolic demand and anaerobic energy turnover in the course of bodily exercises. The LDH is, however, to be taken as a non-specific signifier of tissue metabolic activity as it can be found in many tissues[27].

These results are in accordance with former studies. As an example,[28] have recorded high rises of LDH after high-intensity exercise with an increase reaching its highest point hours after an exercise with the extent of anaerobic metabolism. On the same note, [29] is also noting that repeated bouts of intense exercise by athletes portrayed significant post-exercise rises in LDH, showing that LDH activity is sensitive to the intensity of exercises plus the duration. These studies substantiate the idea that LDH can be considered an effective biomarker of the metabolic stress under the influence of physical exercise[30].

Compared to CK, which is mainly the evidence of membrane disruption of the muscle fibers, the increase of LDH might also indicate the presence of more lactate processing and turnover because of the increased usage of anaerobic pathways[31]. The simultaneous conditions of both markers indicate that extensive activity does not only question the muscle structural integrity, but also considerably raises the metabolic load[32].

Monitoring of LDH and CK is a more complete evaluation of muscular response to exercise, clinically. Unlike CK elevations, which can be used to determine muscle stress or microtrauma, LDH alterations could provide information about metabolic and energetic loads on tissues[33]. This complementary profiling may be especially applied in an athletic training and rehabilitation context, where the knowledge of the structural and metabolic responses to exercise can be used to develop personalized training intensity and recovery protocols[34].

Table 3. LDH levels (U/L) in study groups

Group	Baseline LDH (U/L)	Post-Exercise LDH (U/L)
Low Activity	210.3 ± 45.2	–
Moderate Activity	212.5 ± 46.1	245.7 ± 50.4
High Activity	215.7 ± 47.0	290.8 ± 55.6

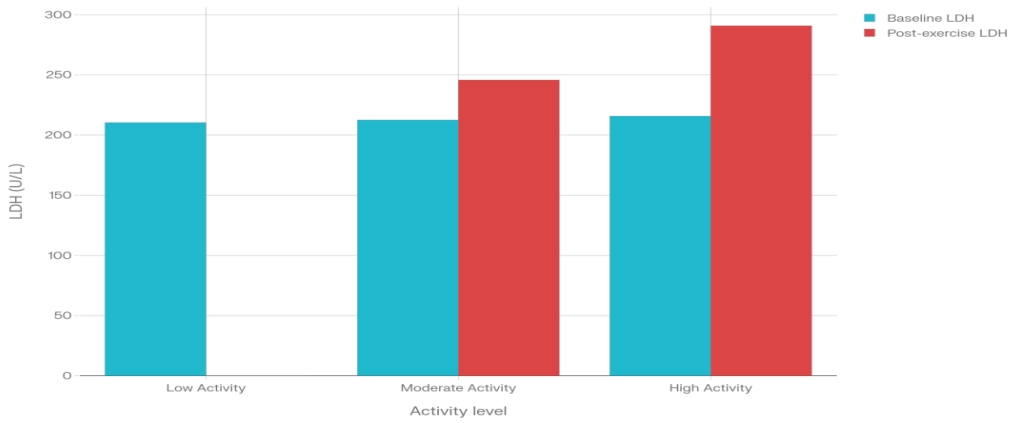


Figure 3 : Effect of Physical Activity on LDH Levels

3.4 Integrated Interpretation

One-way ANOVA showed that there were significant differences in post exercise CK and LDH levels between high and low activity groups ($p < 0.001$), and post hoc tukey tests showed the high activity participants had significantly higher levels of enzymes than low and moderate activity participants and moderate activity participants differed significantly with low activity participants ($p < 0.05$).This shows that the amount of physical exercise performed has a direct and quantitative effect on the enzymes in the muscle, with the intensity of the exercise being proportional to the increase in the levels of the enzymes, CK, and LDH[35]. The similarity in the baseline values shows that the conditions are the same in all the groups, and the differences are only because of the physical activity [36]. Note that the levels of CK and LDH are normally expected to peak 24-48 hours after the exercise, and the 30-minute test might not accurately show the peak levels of the enzymes. The increased levels are part of the normal physiological reaction, and the enzymes are important because they indicate the structural stress in the muscle (CK) and the metabolic activity and anaerobic energy expenditure (LDH)[37]. This finding agrees with previous studies , as the authors of [38] conducted a study found post-exercise CK release of 30-70 % and LDH release of 15-40 % in healthy individuals, which agrees with the idea that these enzymatic reactions are common after physical exercise[39]. Clinically, CK and LDH can give useful information regarding safe exercise prescriptions and prevent overtraining, and mild-to-moderate post exercise enzyme levels should be seen as normal adaptive responses[40]. Nevertheless, the present study has some limitations, one of them being the post-exercise measure at 30 minutes, which may fail to represent peak levels of enzymes, which normally will be at 24-48 hours and the use of self-reported physical activity questionnaires, which can create subjective bias [41]. The present study has several limitations.

First, serum CK and LDH levels were measured only 30 minutes after exercise, whereas peak enzyme concentrations are generally observed 24–48 hours post-exercise. Therefore, the current findings mainly reflect early physiological responses rather than peak enzymatic changes. Second, only total CK and LDH levels were measured without isoenzyme differentiation. Future studies involving CK-MM and LDH isoforms may provide greater specificity regarding tissue origin and muscle damage assessment. Additionally, physical activity classification was partially based on self-reported questionnaires, which may introduce subjective bias despite the use of supportive physiological measurements such as heart rate and blood lactate.

3.5 Heart Rate (HR) Response

The heart rate of the participants at rest was similar for all three groups: Low – 72.4 ± 6.8 bpm, Moderate – 71.9 ± 7.1 bpm, and High – 72.1 ± 6.5 bpm. However, the heart rates of the participants who performed moderate and high levels of activity were significantly higher at 98.6 ± 10.5 bpm and 115.3 ± 12.7 bpm, respectively, than those who performed low levels of physical activity (Table 4, Figure 4). This response is attributed to cardiovascular adaptation to increased exercise intensity, which increases with the workload and demands more oxygen supply to the muscles [42]. This significant increase in the high activity group can explain the increases in the levels of CK and LDH, which are directly proportional to the intensity of the workout [43].

The results are in line with the findings of other studies which suggest that heart rate is a valid measure of exercise intensity, which is highly correlated with the levels of muscle activity and metabolism in the body. Hence, the results obtained from the heart rate measurements provide a better understanding of the physiological adaptations to exercise [44].

Table 4. Heart Rate (bpm) in study groups

Group	Resting HR (bpm)	Post-Exercise HR (bpm)
Low Activity	72.4 ± 6.8	–
Moderate Activity	71.9 ± 7.1	98.6 ± 10.5
High Activity	72.1 ± 6.5	115.3 ± 12.7

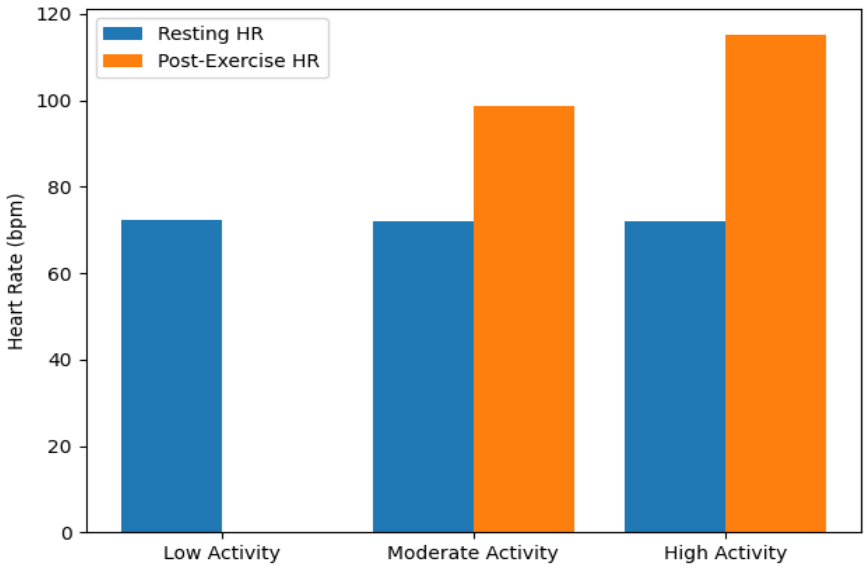


Figure 4 : Heart Rate Response Across Activity Groups

3.6 Blood Lactate Levels

Blood lactate levels at baseline were found to be similar among the three groups (Low: 1.2 ± 0.3 mmol/L, Moderate: 1.3 ± 0.4 mmol/L, High: 1.2 ± 0.3 mmol/L). After the exercise, the lactate levels increased significantly in the moderate (3.8 ± 0.7 mmol/L) and high activity groups (5.6 ± 0.9 mmol/L), with the highest levels being found in the high activity group (Table 5, Figure 5).

This increase can be attributed to an increased reliance on anaerobic glycolysis during more intense physical activity. The increased levels of lactate are directly related to the increased levels of LDH, as this enzyme is a major participant in the conversion of pyruvate and lactate [45].

The concomitant increase in lactate and LDH levels is consistent with the notion that increased levels of physical activity are associated with increased metabolic stress and energy demands[46].

Table 5. Blood Lactate Levels (mmol/L) in Study Groups

Group	Baseline Lactate (mmol/L)	Post-Exercise Lactate (mmol/L)
Low Activity	1.2 ± 0.3	–
Moderate Activity	1.3 ± 0.4	3.8 ± 0.7

High Activity	1.2 ± 0.3	5.6 ± 0.9

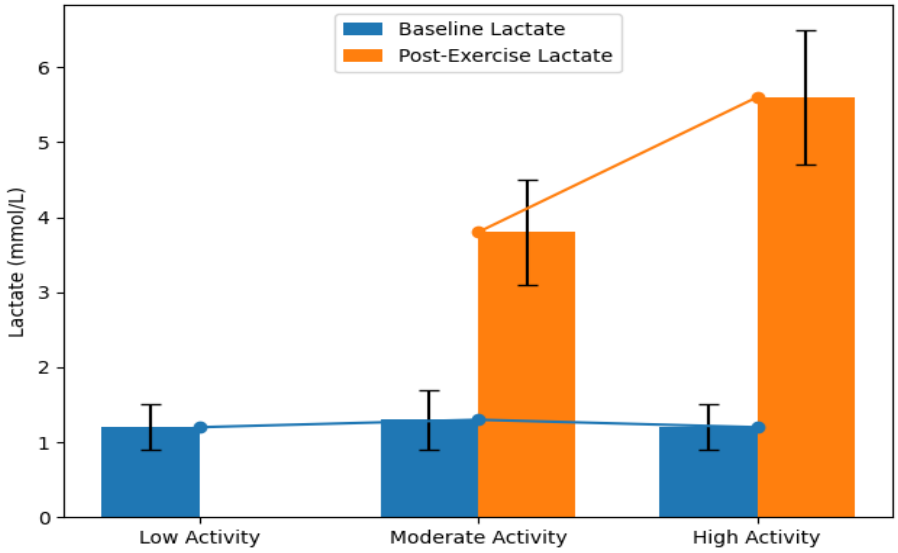


Figure 5: Blood Lactate Levels Across Activity Groups

3.7 Correlation Analysis

Pearson correlation analysis demonstrated significant positive correlations between post-exercise CK levels and blood lactate concentrations ($r = 0.68$, $p < 0.001$), as well as between LDH levels and post-exercise heart rate ($r = 0.72$, $p < 0.001$). These findings suggest that increasing exercise intensity is associated with greater muscular and metabolic stress.

4. Conclusion

These findings indicate that physical activity intensity plays an important role in modulating serum CK and LDH levels, reflecting both muscular stress and metabolic demand. Heart rate and blood lactate responses further support the physiological relationship between exercise intensity and muscular adaptation. Future longitudinal studies incorporating delayed post-exercise sampling and isoenzyme analysis are recommended to improve understanding of exercise-induced muscular adaptations and recovery mechanisms.

7. References

[1] Srinivasan, J. D. (2025). *Essentials of Physical Education: Health, Fitness, and Sports Science*. AG Publishing House (AGPH Books).

[2] Smith, J. A., Murach, K. A., Dyar, K. A., & Zierath, J. R. (2023). Exercise metabolism and adaptation in skeletal muscle. *Nature Reviews Molecular Cell Biology*, *24*(9), 607-632.

[3] Mukund, K., & Subramaniam, S. (2020). Skeletal muscle: A review of molecular structure and function, in health and disease. *Wiley Interdisciplinary Reviews: Systems Biology and Medicine*, *12*(1), e1462.

[4] Rahmanian, K., Hooshmand, F., Shakeri, M., Rahmanian, V., Jahromi, F. S., & Jahromi, A. S. (2022). Creatine kinase and lactate dehydrogenase enzymes response to lactate tolerance exercise test. *Exercise Science*, *31*(2), 168-172.

[5] Aujla, R., Zubair, M., & Patel, R. (2024). Creatine phosphokinase. *StatPearls*.

[6] Leite, C. D., Zovico, P. V., Rica, R. L., Barros, B. M., Machado, A. F., Evangelista, A. L., ... & Bocalini, D. S. (2023). Exercise-induced muscle damage after a high-intensity interval exercise session: systematic review. *International journal of environmental research and public health*, *20*(22), 7082.

[7] Farhana, A., & Lappin, S. L. (2023). Biochemistry, lactate dehydrogenase. In *StatPearls [internet]*. StatPearls Publishing.

[8] Chandel, N. S. (2021). Glycolysis. *Cold Spring Harbor Perspectives in Biology*, *13*(5), a040535.

[9] Zaib, S., Hayyat, A., Ali, N., Gul, A., Naveed, M., & Khan, I. (2022). Role of mitochondrial membrane potential and lactate dehydrogenase A in apoptosis. *Anti-Cancer Agents in Medicinal Chemistry-Anti-Cancer Agents)*, *22*(11), 2048-2062.

[10] Leite, C. D., Zovico, P. V., Rica, R. L., Barros, B. M., Machado, A. F., Evangelista, A. L., ... & Bocalini, D. S. (2023). Exercise-induced muscle damage after a high-intensity interval exercise session: systematic review. *International journal of environmental research and public health*, *20*(22), 7082.

[11] Petriz, B. A., Gomes, C. P., Almeida, J. A., de Oliveira Jr, G. P., Ribeiro, F. M., Pereira, R. W., & Franco, O. L. (2017). The effects of acute and chronic exercise on skeletal muscle proteome. *Journal of cellular physiology*, *232*(2), 257-269.

[12] Szydłowska, S., Błaszków, K., Elias, J., Biesiada, W., Zubiak, M., & Kaźmierczak, D. (2025). Regular monitoring of post-training biochemical markers as a tool for injury prevention in professional athletics–review. *Quality in Sport*, *39*, 58897-58897.

[13] LeDrew, M., Sadri, P., Peil, A., & Farahnak, Z. (2025). Muscle Biomarkers as Molecular Signatures for Early Detection and Monitoring of Muscle Health in Aging. *Nutrients*, *17*(17), 2758.

[14] GILBERT, J. A. (2010). IMPACT DU LAIT ET DE SES COMPOSANTES SUR LE CONTRÔLE DE L'APPÉTIT, LA PERTE PONDÉRALE ET LA CAPACITÉ À L'EFFORT Thèse présentée. *Physiology & Behavior*, *100*, 67-75.

[15] Allen, N. E., Arnold, M., Parish, S., Hill, M., Sheard, S., Callen, H., ... & Collins, R. (2021). Approaches to minimising the epidemiological impact of sources of systematic and random variation that may affect biochemistry assay data in UK Biobank. *Wellcome open research*, *5*, 222.

[16] Powers SK, Howley ET. Exercise Physiology: Theory and Application to Fitness and Performance. 11th ed. New York: McGraw-Hill Education; 2021.

[17] Mohammed, S. N., Jasim, M. H., Mahmood, S. H., Saleh, E. N., & Hashemzadeh, A. (2025). The role of irisin in exercise-induced muscle and metabolic health: a narrative review. *Naunyn-Schmiedeberg's Archives of Pharmacology*, *398*(9), 11463-11491.

[18] Carobene, A., Røraas, T., Sølvik, U. Ø., Sylte, M. S., Sandberg, S., Guerra, E., ... & Ceriotti, F. (2017). Biological variation estimates obtained from 91 healthy study participants for 9 enzymes in serum. *Clinical chemistry*, *63*(6), 1141-1150.

[19] Plevkova, J., Brozmanova, M., Harsanyiova, J., Sterusky, M., Honetschlager, J., & Buday, T. (2020). Various aspects of sex and gender bias in biomedical research. *Physiological research*, *69*(Suppl 3), S367.

[20] Landen, S., Hiam, D., Voisin, S., Jacques, M., Lamon, S., & Eynon, N. (2023). Physiological and molecular sex differences in human skeletal muscle in response to exercise training. *The Journal of physiology*, *601*(3), 419-434.

[21] McKeon, J. M. M., & McKeon, P. O. (2016). A balancing act between control and generalizability. *International Journal of Athletic Therapy and Training*, *21*(2), 1-3.

[22] Holmberg, M. J., & Andersen, L. W. (2022). Adjustment for baseline characteristics in randomized clinical trials. *Jama*, *328*(21), 2155-2156.

[23] Radišić Biljak, V., Lazić, A., Nikler, A., Pekas, D., Saračević, A., & Trajković, N. (2025). Post-exercise creatine kinase variability: a literature review. *Biochemia medica*, *35*(2), 186-200.

[24] Powers, S. K., Goldstein, E., Schrager, M., & Ji, L. L. (2022). Exercise training and skeletal muscle antioxidant enzymes: an update. *Antioxidants*, *12*(1), 39.

[25] Brancaccio, P., Lippi, G., & Maffulli, N. (2010). Biochemical markers of muscular damage. *Clinical Chemistry & Laboratory Medicine*, *48*(6).

[26] Baird, M. F., Graham, S. M., Baker, J. S., & Bickerstaff, G. F. (2012). Creatine-kinase- and exercise-related muscle damage implications for muscle performance and recovery. *Journal of nutrition and metabolism*, *2012*(1), 960363.

[27] Farhana, A., & Lappin, S. L. (2023). Biochemistry, lactate dehydrogenase. In *StatPearls [internet]*. StatPearls Publishing.

[28] Duncan, L. M., Deeds, J., Cronin, F. E., Donovan, M., Sober, A. J., Kauffman, M., & McCarthy, J. J. (2001). Melastatin expression and prognosis in cutaneous malignant melanoma. *Journal of clinical oncology*, *19*(2), 568-576.

[29] Suzuki, Y., & Shioi, Y. (1999). Detection of chlorophyll breakdown products in the senescent leaves of higher plants. *Plant and Cell Physiology*, *40*(9), 909-915.

[30] Todorovic, D., Stojanovic, M., Medic, A., Gopcevic, K., Mutavdzin, S., Stankovic, S., & Djuric, D. (2021). Four weeks of aerobic training affects cardiac tissue matrix metalloproteinase, lactate dehydrogenase and malate dehydrogenase enzymes activities, and hepatorenal biomarkers in experimental hyperhomocysteinemia in rats. *International Journal of Molecular Sciences*, *22*(13), 6792.

[31] Bartoloni, B., Mannelli, M., Gamberi, T., & Fiaschi, T. (2024). The multiple roles of lactate in the skeletal muscle. *Cells*, *13*(14), 1177.

[32] Stožer, A., Vodopivc, P., & Bombek, L. K. (2020). Pathophysiology of exercise-induced muscle damage and its structural, functional, metabolic, and clinical consequences. *Physiological research*, *69*(4), 565.

[33] Szydłowska, S., Błaszków, K., Elias, J., Biesiada, W., Zubiak, M., & Kaźmierczak, D. (2025). Regular monitoring of post-training biochemical markers as a tool for injury prevention in professional athletics–review. *Quality in Sport*, *39*, 58897-58897.

[34] Spanakis, M., Fragkiadaki, P., Renieri, E., Baliou, S., Fragkiadoulaki, I., Vakonaki, E., ... & Tsatsakis, A. (2025). Exploiting interrelated genomic, biochemical, nutritional and pathophysiological data to optimize athletic performance. *World Academy of Sciences Journal*, *7*(4), 52.

[35] Furrer, R., Hawley, J. A., & Handschin, C. (2023). The molecular athlete: exercise physiology from mechanisms to medals. *Physiological reviews*, *103*(3), 1693-1787.

[36] BLuher, M. A. T. T. H. I. A. S., Brennan, A. M., Kelesidis, T., Kratzsch, J., Fasshauer, M., Kralisch, S., ... & Mantzoros, C. S. (2007). Total and high–molecular weight adiponectin in relation to metabolic variables at baseline and in response to an exercise treatment program: comparative evaluation of three assays. *Diabetes care*, *30*(2), 280-285.

[37] Stepanov, G. (2023). Pathophysiological significance of creatinekinase and lactatedehydrogenase in the mechanisms of adaptation of muscle tissue of descendants. *Journal of Education, Health and Sport*, *50*(1), 153-167.

[38] Brancaccio, P., Maffulli, N., & Limongelli, F. M. (2007). Creatine kinase monitoring in sport medicine. *British medical bulletin*, *81*(1), 209-230.

[39] Ball, D. (2015). Metabolic and endocrine response to exercise: sympathoadrenal integration with skeletal muscle. *Journal of Endocrinology*, *224*(2), R79-R95.

[40] Yparraguirre Salcedo, K. G., Rivera Prado, A. B., Lloja Lozano, L., Chambilla Quispe, V. F., & Ramirez Atencio, C. W. (2024). Evaluating Muscle Damage Biomarkers in Adolescent Athletes: Implications for Public Health in Tacna, Peru—2023. *International Journal of Environmental Research and Public Health*, *21*(11), 1394.

[41] Kelly, R. S., Kelly, M. P., & Kelly, P. (2020). Metabolomics, physical activity, exercise and health: A review of the current evidence. *Biochimica et Biophysica Acta (BBA)-Molecular Basis of Disease*, *1866*(12), 165936.

[42] Smith, D. L., & Fernhall, B. (2023). *Advanced cardiovascular exercise physiology*. Human Kinetics.

[43] Rahmanian, K., Hooshmand, F., Shakeri, M., Rahmanian, V., Jahromi, F. S., & Jahromi, A. S. (2022). Creatine kinase and lactate dehydrogenase enzymes response to lactate tolerance exercise test. *Exercise Science*, *31*(2), 168-172.

[44] Gronwald, T., Rogers, B., & Hoos, O. (2020). Fractal correlation properties of heart rate variability: a new biomarker for intensity distribution in endurance exercise and training prescription?. *Frontiers in physiology*, *11*, 550572.

[45] Li, X., Yang, Y., Zhang, B., Lin, X., Fu, X., An, Y., ... & Yu, T. (2022). Lactate metabolism in human health and disease. *Signal transduction and targeted therapy*, *7*(1), 305.

[46] Lee, S., Choi, Y., Jeong, E., Park, J., Kim, J., Tanaka, M., & Choi, J. (2023). Physiological significance of elevated levels of lactate by exercise training in the brain and body. *Journal of bioscience and bioengineering*, *135*(3), 167-175.

Al-Kitab Journal for Pure Sciences (2026); 10(2):221-241.
https://doi.org/10.32441/kjps.10.2.p16

Al-Kitab Journal for Pure Sciences
ISSN: 2617-1260 (print), 2617-8141(online)

https://isnra.net/index.php/kjps

Synthesis And Characterization and Anti-Cancer Activity of Nickel (II) Complexes Containing a Mixture of Benzotriazole Derivative, Phenanthroline , and Bipyridine, and Evaluation of Their Bioavailability

Alaa H. Ali

Iraq's Ministry of Education's General Directorate of Education in Salah al-Din

Corresponding Author: Alaa.hamad.ali@st.tu.edu.iq

Citation: *Alaa H. Ali*[1]. **Synthesis And Characterization and Anti-Cancer Activity of Nickel (II) Complexes Containing a Mixture of Benzotriazole Derivative, Phenanthroline, And Bipridine, And Evaluation of Their Bioavailability.**
Al-Kitab J. Pure Sci. [Internet]. 2026 May. 24 ;10(2):221-241
DOI.
https://isnra.net/index.php/kjps/article/view/2026.
https://doi.org/10.32441/kjps.10.2.p16

Keywords: Benzatriazole, Phenonthroline, and Bipyridine biological effectiveness, anti-cancer, Ni (II) complexes.

Article History
Received 21 Apr. 2026
Accepted 24 May. 2026
Available online 01 Nov. 2026

©20--. THIS IS AN OPEN-ACCESS ARTICLE UNDER THE CC BY LICENSE
http://creativecommons.org/licenses/by/4.0/

Abstract:

The study of inorganic chemistry, particularly coordination chemistry, has become increasingly important in recent years due to its significant advancements in the scientific field of preparing and characterizing coordination complexes. Coordination compounds have attracted considerable attention from researchers because of their crucial role in various aspects of life. These complexes have been used extensively in medicine, industry, agriculture, and even in the field of Pollution. The formation of these complexes involves transition elements and representative elements, but they are particularly observed with transition element ions. This is because they provide empty orbitals, and their orbital energies are lower than those of the nonmetal atoms involved in the ligand structure, which possesses non-shared electron pairs capable of bonding with the metal ion.

Nickel is the eighth element of the first transition series (3d elements), and it has an outer electron configuration ($4s^2$ $3d^8$). The stability of its compounds decreases as its oxidation state increases, and the oxidation state (II) is one of the most stable states of nickel. Therefore,

nickel(II) is the most common in the chemistry of transition elements, but it is not easy to work with because of the changes that occur in the structure of some octahedral, tetrahedral, and square planar complexes, as well as the formation of polymers.

Keywords: Benzatriazole, Phenonthroline, and Biperidine biological effectiveness, anti-cancer, Ni (II) complexes.

تحضير وتشخيص ودراسة النشاط المضاد للسرطان لمعقدات النيكل (II) الحاوية على مزيج من مشتق البنزاترايازول والفينونثرولين والبايبريدين وتقييم فعاليتها الحيوية

علاء حمد علي

وزارة التربية، المديرية العامة لتربية صلاح الدين

الإيميل الرسمي: Alaa.hamad.ali@st.tu.edu.iq

الخلاصة:

ازدادت أهمية دراسة الكيمياء غير العضوية، ولا سيما كيمياء التناسقية ، في السنوات الأخيرة نظرًا للتقدم الكبير الذي أحرزته في مجال تحضير وتوصيف معقدات التناسق. وقد حظيت هذه المعقدات باهتمام بالغ من الباحثين لدورها المحوري في مختلف جوانب الحياة. وتُستخدم هذه المعقدات على نطاق واسع في الطب والصناعة والزراعة، وحتى في مجال مكافحة التلوث . يتضمن تكوين هذه المعقدات عناصر انتقالية وعناصر تمثيلية، ولكنها تُلاحظ بشكل خاص مع أيونات العناصر الانتقالية. ويعود ذلك إلى توفيرها مدارات فارغة، وانخفاض طاقات مداراتها مقارنةً بذرات اللافلزات المشاركة في بنية الرابطة، والتي تمتلك أزواجًا إلكترونية غير مشتركة قادرة على الارتباط بأيون الفلز.

النيكل هو العنصر (الثامن في السلسلة الانتقالية الأولى) عناصر (3d)، وله توزيع إلكتروني .($4s^2\ 3d^8$) يقل استقرار مركباته مع ازدياد حالة أكسدته، وتُعد حالة الأكسدة (II) من أكثر حالات الأكسدة استقرارًا للنيكل. لذلك، فإن النيكل (II) هو الأكثر شيوعًا في كيمياء العناصر الانتقالية، ولكنه ليس من السهل العمل معه بسبب التغيرات التي تحدث في بنية بعض المركبات ثمانية السطوح، ورباعية السطوح، والمربعة المستوية، بالإضافة إلى تكوين البوليمرات .

الكلمات المفتاحية: بنزوترايوزول , فينونثرولين و بايبريدين, فعالية بايلوجية ودراسة مضادة للسرطان لمعقدات النيكل(II).

1. Introduction:

Benzotriazole ($C_6H_5N_3$) represents a versatile N-heterocyclic ligand widely recognized in coordination chemistry for its strong electron-donating capabilities and diverse coordination modes [(1)]. Possessing adjacent nitrogen atoms, it effectively coordinates with transition metal ions—particularly intermediate Lewis acids like nickel, Ni(II) to assemble structurally unique complexes and polymeric architectures [(2)]. Beyond structural intrigue, the integration of Ni(II) centers with benzotriazole derivatives enhances biomolecular interactions, often leading to potent cytotoxicity against specific cancer cell lines [(3)]. In particular, evaluating the in vitro

antiproliferative activity of these metal complexes against human breast adenocarcinoma (MCF-7) offers critical insights into their targeted anticancer potential [٤]. Consequently, the synthesis and biological screening of novel Ni(II) benzotriazole complexes continue to serve as a promising direction in bioinorganic and medicinal chemistry [5].

Nickel (Ni) complexes with Schiff base ligands represent a pivotal class in modern coordination chemistry due to their facile synthesis, structural flexibility, and high thermodynamic stability. These complexes efficiently coordinate through multi-donor atoms such as nitrogen and oxygen (N,O-donor systems), exhibiting versatile coordination geometries alongside tailored electronic and catalytic properties [6]. Recently, they have shown promising potential in clean energy technologies, including electrochemical systems and hydrogen storage applications, owing to their robust structural stability and redox behaviors [7]. Furthermore, Schiff base nickel complexes display significant biological efficacy as potent antibacterial, antifungal, and anticancer agents, positioning them as valuable candidates for advanced pharmaceutical and technological research [8].

2-Experimental

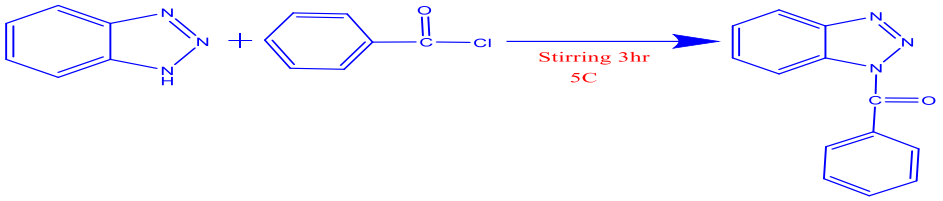
An automatic melting point device (SAM30) was used to determine the melting point of the produced compounds. A SHIMADZU 8400S spectrometer was used to record the complexes' infrared spectra (FT-IR) as discs (KBr) (within the range 400-4000 cm^{-1}). The nuclear magnetic resonance spectrum was recorded using a Varian Unity Spectrometer (400 MHz) in DMSO-d6 solvent. The properties of the thick or thin samples of the material, their shape, and the determination of their nanoscale or crystalline dimensions of the particles were determined using a TESCAN MIRA3 instrument.

3. Material and methods:

3.1 Preparation methods:

3-1-1 The ligand is prepared using (L)((H-benzo[d][1,2,3]triazol-1-y)(phenyl) methanone

a suspension of 3 g (0.02581 mol) benzotriazole solution dissolved in 15 ml of absolute ethanol, stirring until dissolved, in an ice bath. Then add 3 ml (0.02581 mol) of benzyl chloride drop by drop. The temperature should not exceed 0–5°C. The solution changed from clear to a thick white suspension and was left to stir for four hours. The material was filtered and allowed to dry at room temperature. The weight was 3.7008 g, the melting point was 106–109 C^0, and the concentration was Yield 85% [9].



3-1-2 Preparation of the complex $[Ni(L)_2Cl_2]$

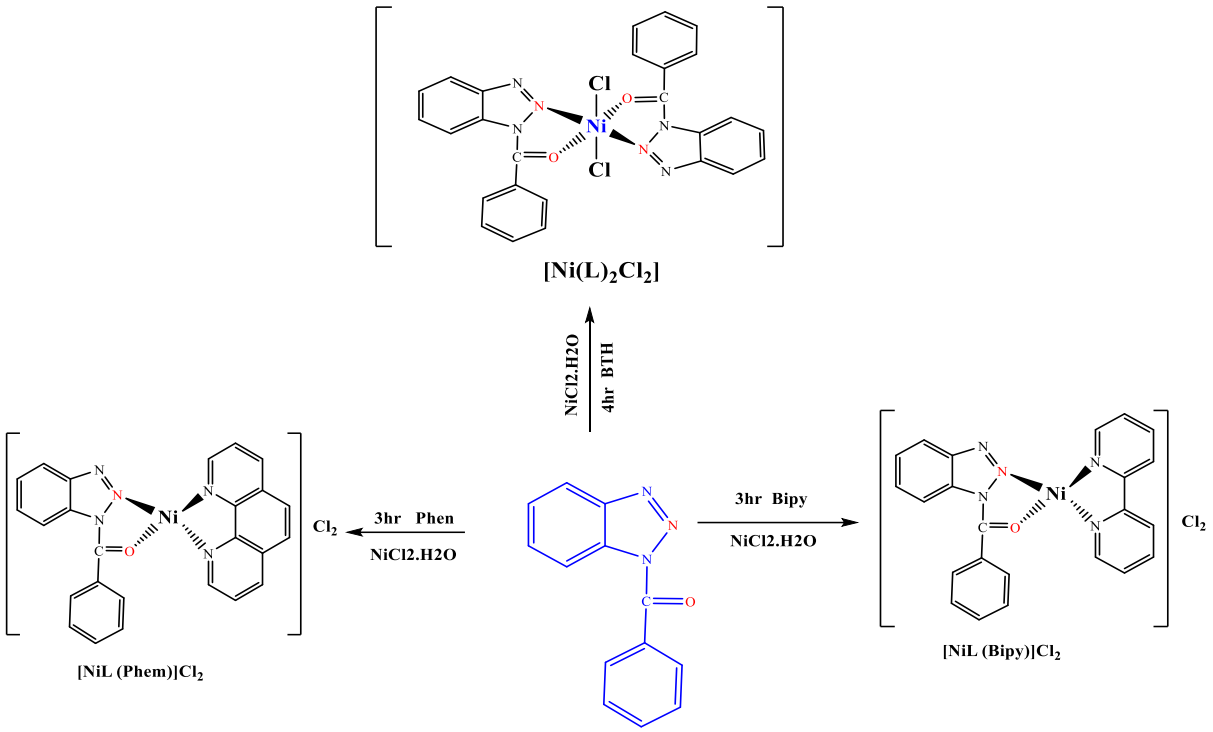
A hot, green solution of (0.026g, 0.00011mmol) in (5ml) of ethanol was added to a ligand solution (L) of (0.05g, 0.00022mmol) in (5ml). A suspension was formed. The mixture was heated under a temperature of 80°C for two hours, then the precipitate was filtered and washed with cold ethanol and left to dry at room temperature (wt=0.055g, Yield =72%, m.p=240-243°C).

3-1-3 Preparation of the $[Ni(L)(Phen)]Cl_2$ complex

A suspension of (L) (0.531 gm, 0.00237 mol) in absolute ethanol (10 ml) was added to a solution of nickel chloride ($NiCl_2$) (0.839 gm, 0.00237 mol) in ethanol (15 ml). The mixture was stirred for one hour, then a solution of (10,1 phenanthroline) (0.427 gm, 0.00237 mol) in ethanol (20 ml) was added. The final mixture was raised for three hours, resulting in a light green suspension. The precipitate was filtered, washed with cold ethanol, and oven dried under reduced pressure (1.578gm , Yield =87.81% , M.P 275-278).

3-1-4 Preparation of the $[Ni(L)(Bipy)]Cl_2$ complex

A suspension of (L) (0.121 gm, 0.00054 mol) in absolute ethanol (10 ml) was added to a solution of nickel chloride ($NiCl_2$) (0.190 gm, 0.00054 mol) in ethanol (15 ml). The mixture was stirred for one hour, then a solution of (2,2'-biperidine) (0.082 gm, 0.00054 mol) in ethanol (20 ml) was added. The final mixture was raised for three hours, resulting in a light green suspension. The precipitate was filtered, washed with cold ethanol, and oven dried under reduced pressure (0.350 g, Yield =89.05%,, M.P 280-282).



Complex diagram :(1:1) $[Ni(L)Cl_2]$, $[Ni(L)(Bipy)]Cl_2$, $[Ni(L)(Phen)]Cl_2$

4. Evaluate bacterial activity:

4-1 Evaluate the bacterial activity of the prepared complexes:

The biological activity of the prepared complexes was tested on two types of bacteria: Gram-negative and Gram-positive, using the etching method. The bacterial isolates used were identified by the Department of Life Sciences, College of Science, University of Mosul.

1) *Citrobacter freundii* (Gram-Negaive)
2) *staphlycocas aureus* (Gram-positive)
3) *(Staphylococcus epidermidis)* (Gram-positive)

4-1-1 Method of operation:

The complex solutions were prepared using DMSO solvent at concentrations of (10^{-1}, 10^{-3}, 10^{-5}). The culture medium was then prepared. The bacteria were activated by dissolving (15gm) of nutrient agar in (0.5L) of distilled water and placing it in a conical flask. The mixture was mixed well and heated until the agar (a gelatinous substance used as a nutrient medium for bacterial growth) was completely dissolved. After that, the culture medium was placed in a sterilizer at a temperature of (121^0C) and a pressure of (15 bar) for 15 minutes [10]. Then, after removing it, it was poured into Petri dishes and left to solidify. After that, (3-5) smears of the prepared bacterial samples were placed and incubated for 24 hours at 37 degrees Celsius in the incubator. Then, the culture medium used to evaluate biological activity was prepared by

dissolving (53.5gm) of Mueller-Hinton agar in (1L) of distilled water. Then, the medium was placed in a sterile device (Autoclave) at a temperature of (121°C) and a pressure of (15 bar) for 15 minutes [11].

The medium is extracted after sterilization in an autoclave and poured into Petri dishes. It is then left to solidify. A quantity of activated bacteria is taken by swab and applied to the Mueller-Hinton agar medium by completely covering the dish and marking it. It is left for half an hour to absorb [12]. Then, holes are prepared using a sterile cork drill with a diameter of 5 mm. Four holes are made, and 1 ml of the prepared compound solutions is added to each hole at different concentrations. All dishes are then incubated for 24 hours. The antibiotic cefepime is used at a concentration of 5-10^{-5} M, and its inhibition of the bacteria is observed [13] .The diameter of the inhibition zone for each complex is then measured using a millimeter ruler and compared with the inhibition range of the antibiotic cefepime [14].

5. Results: and Discussion :

This research involves the preparation and characterization of several nickel(II) complexes, piperidine ligands, and phenenthroline coligands. The prepared complexes were characterized using several physical and spectroscopic methods. The following ligands were used in this research:

1) ((H-benzo[d][1,2,3]triazol-1-y)(phenyl)methanone)) (L)
2) 2,2-Bipyridyl (**Bipy**)
3) 1,10-phenanthroline (**Phen**)

5.1 Molar Conductivity :

The molar conductivity of solutions is widely used in coordination chemistry to determine the ionic formulas of complexes in solution and in the solid state. The greater the number of ions released by the complex in solution, the higher its electrical conductivity. A complex that does not ionize has a low conductivity that can be neglected [15]. The electrical conductivity of the prepared complexes was measured at a concentration of (10^{-3} M) in dimethyl sulfoxide (DMSO) solutions at room temperature (25°C), as shown in the table [16].

The molar conductivity results for the prepared (L) ligand complexes showed values ranging from 67.3 to 78.6 ohm^{-1} cm^{-2} mol^{-1}, indicating the presence of two Cl ions within the coordination sphere. In contrast, the $[Ni(L)Cl_2]$ complexes, where we expect two Cl ions to be

present outside the coordination sphere, showed values ranging from 75.4 to 78.6. This is consistent with the proposed formulas and supported by other analyses and measurements. Table (1-1) shows the results of the molar electrical conductivity measurements for the prepared complexes [17].

Table 1-1. Physical properties, melting points, percentage yields, and molar conductivity values of the synthesized ligand and its Ni(II) complexes.

Seq	Complexes	Color	M.P.C°	Yield %	Conductivity ohm^{-1}.cm^{-2} .mol^{-1}
---	L	صحراوي	106-109	85.9	2.0
1	$[Ni(L)_2Cl_2]$	احضر	240-243	72	67.3
2	$[Ni(L)(Phen)]Cl_2$	اخضر فاتح	275-278	87.8	75.4
3	$[Ni(L)(Bipy)]Cl_2$	اخضر فاتح	280-282	89.05	78.6

5.2 Infrared Spectrum of the (L) Complex

The ligand was identified by infrared spectroscopy. As shown in figure (1-2). The infrared spectrum of the free ligands showed the disappearance of the (N-H) υ[18] band at position (3415cm), and the clear appearance of the C=O) υ band at position (1708cm) cm[19], as well as the appearance of the aromatic C-H) υ band[20] at position (3060 cm^{-1}) and the appearance of a band belonging to (N=N) at position (1448 cm^{-1}) [21].

5-2-1 Nuclear Magnetic Resonance Spectrum ^{1} Hnmr for (L) ligand

The proton nuclear magnetic resonance spectrum of the 1H NMR ligand, as shown in figure (1-3), measured with DMSO-d6 solvent, showed a multiple signal within the chemical shift (8.35-7.60ppm) δH, which is due to the aromatic (C-H) of the nine protons of the ligand, and the appearance of a triple signal at the chemical shift (8.32ppm) δH, which is due to protons 5 and 9, and a double signal at the chemical shift (8.12ppm) δH, which is due to protons 1 and 4, and two triple signals at the shifts (7.85ppm and 7.82ppm) δH, respectively, which are due to protons 2 and 3, and a multiple signal within the chemical shift (7.66ppm) δH, which is due to protons (6, 7, 8).

5-2-2 Nuclear Magnetic Resonance Spectrum ^{13}C-^{1}H N.m.r of the (L) ligand

The ^{13}C-{^{1}H}NMR spectrum of the ligand, as shown in figure (1-4), measured with DMSO-d6 solvent, showed a carbon atom signal of the carbonyl group (C=O) at a displacement of

δC=167.09 ppm. This signal appeared in this region due to the high electronegativity of oxygen. The other signals are due to the remaining 12 carbon atoms of the ligand.

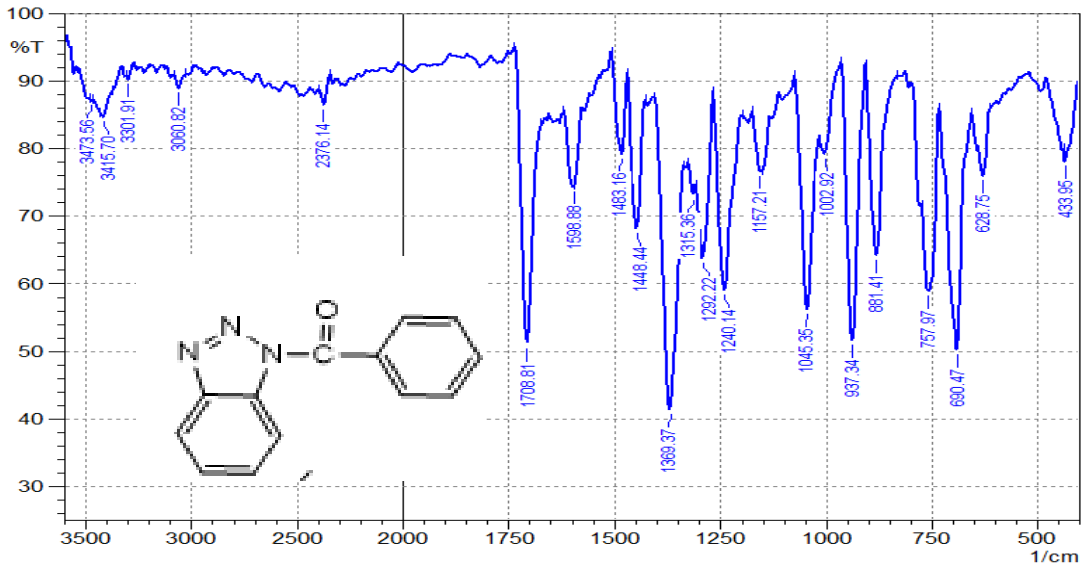


Figure (1-2) – Infrarotspektrum des Liganden (L)

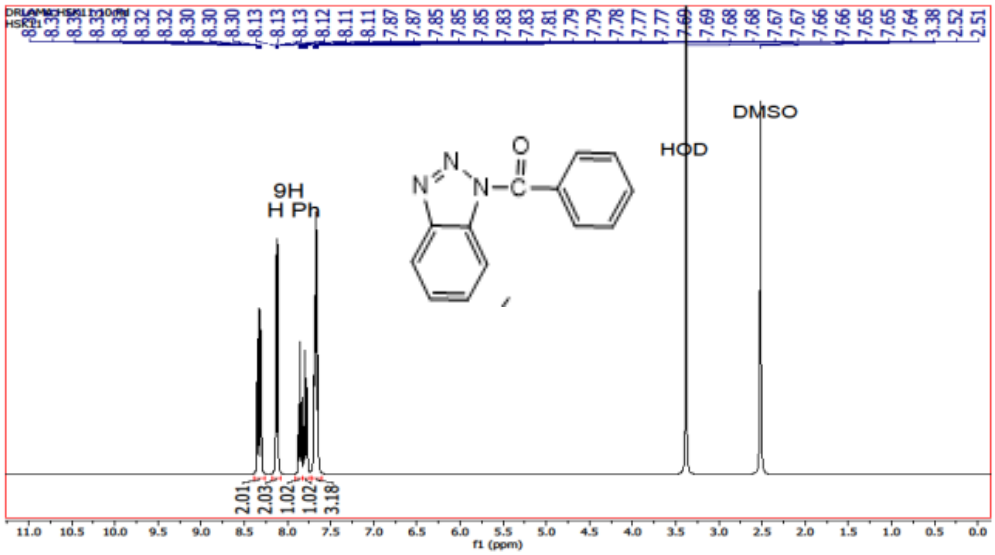


Figure (1-3) ^{1}H NMR spectrum of the L complex

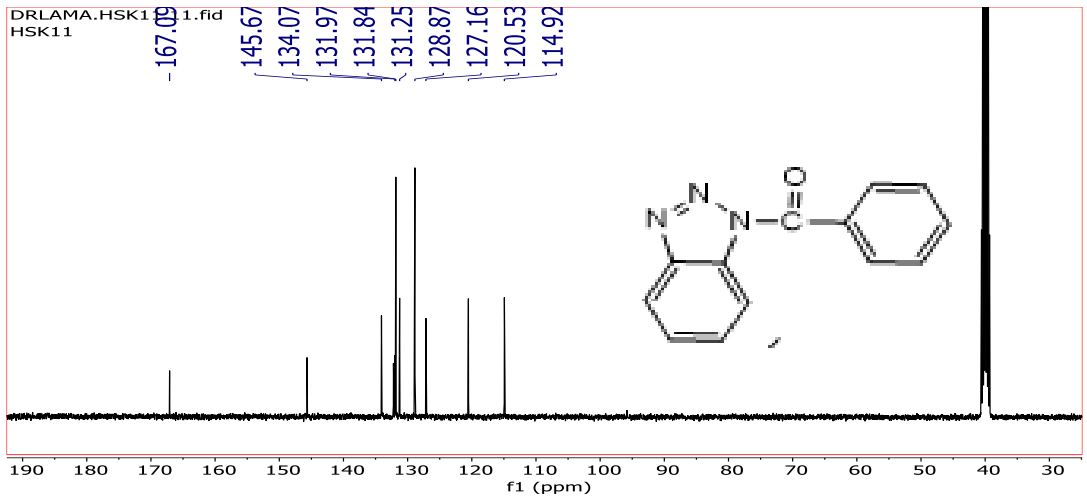


Figure (1-4) ^{13}C-{1H} NMR spectrum of the L complex

5-2-3 Infrared spectrum the [Ni(L)Cl$_2$]

The infrared spectrum of the Ni(L)Cl$_2$ complex, as shown in figure (1-5) , showed a band at position (3066cm^{-1}) corresponding to the aromatic (C-H) frequency [20]. A strong band was also observed at(1606cm-^{1}) corresponding to the stretching frequency of the (C=O) group [19], as well as a band at position (485cm-^{1}) corresponding to the (N=N) frequency [21]. A band was also observed at position (547cm^{-1}) corresponding to the (Ni-O) frequency, a band at position (449 cm-^{1}) corresponding to the (Ni-N) frequency, and a band at position (1267 cm-^{1}) corresponding to the (C-N) frequency [22].

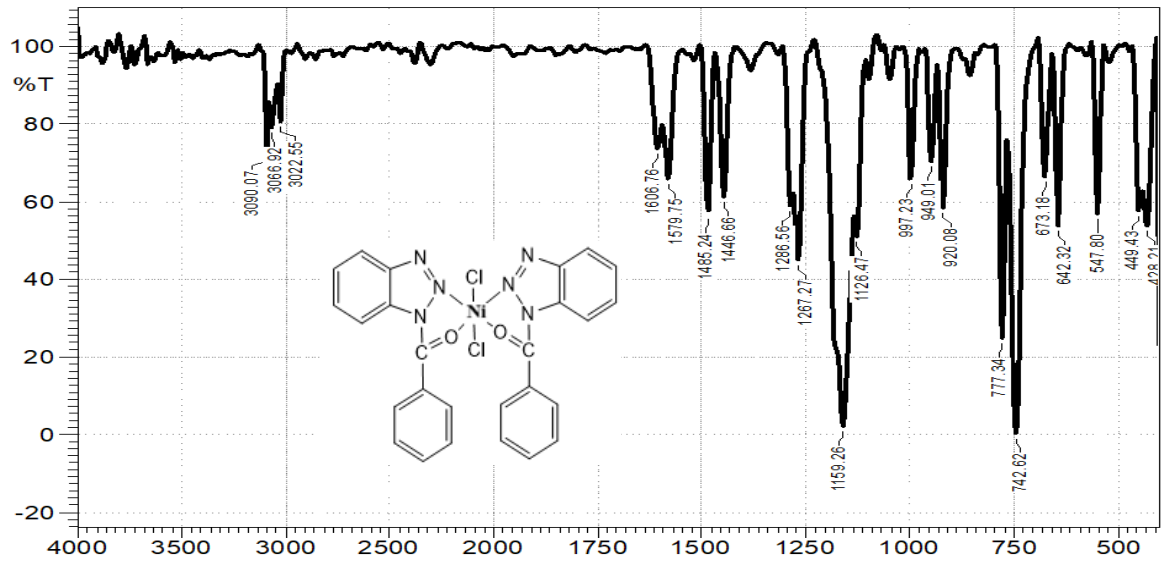


Figure (1-5) IR spectrum of the [Ni(L)Cl$_2$]

5-2-4 Spectrum of Nuclear Magnetic Resonance {^{1}H} n.m.r of the [Ni(L)Cl$_2$] complex

The proton nuclear magnetic resonance spectrum of the 1H NMR ligand, as shown in figure (1-6), measured in DMSO-d^6 solvent, showed a triplet signal within the chemical displacement (8.30-8.41 ppm) δH with approximately two protons, which is due to a proton in a, a doublet signal within the displacement (8.1-8.2 ppm) δH, which is due to a proton in b, a multiplet signal within the chemical displacement (7.80-7.90 ppm) δH, which is due to a proton in d, a singlet signal at (7.60-7.65) δH, which is due to the protons of C, and a triplet signal within the chemical displacement (7.65-7.70 ppm) δH, which is due to a proton in e.

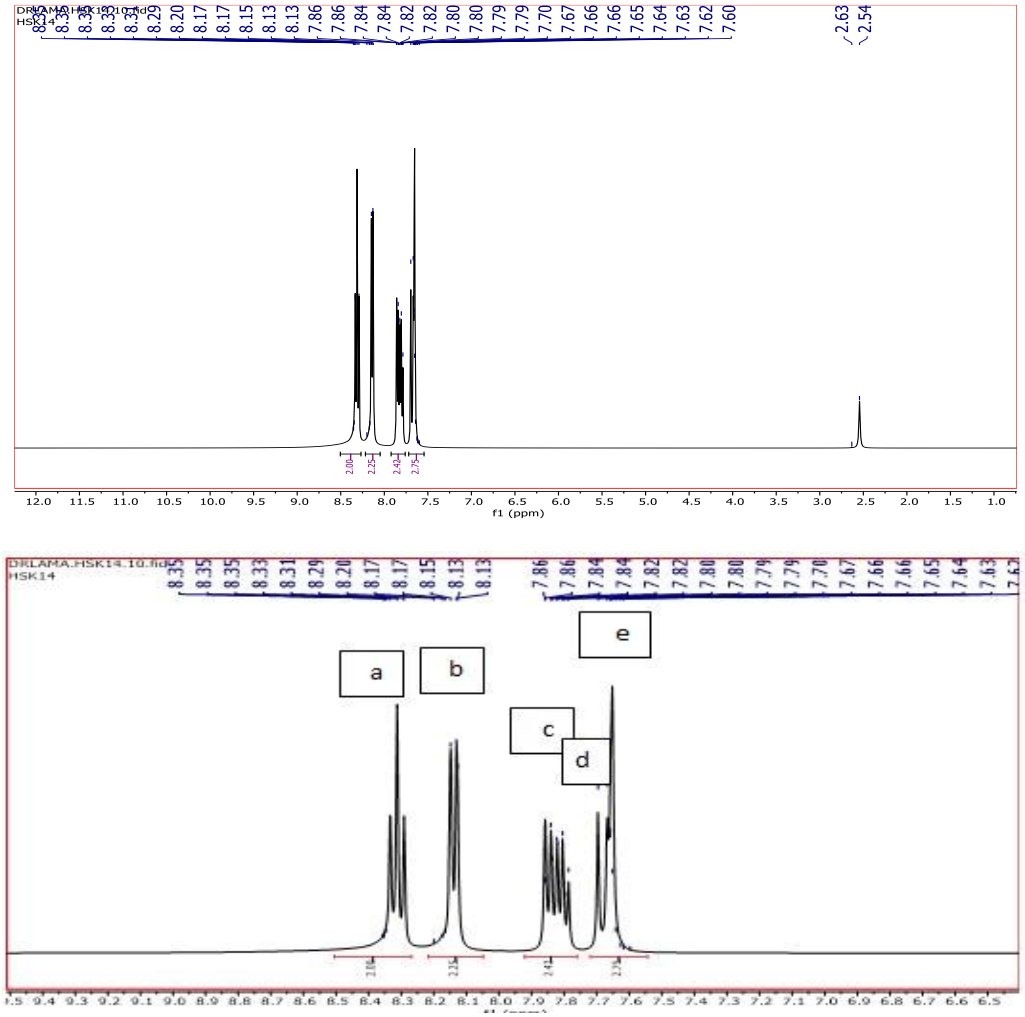


Figure (1-6) Spectrum of nuclear magnetic resonance (^{1}H-NMR) of the Ni(L)Cl$_2$ complex

5-2-5 Infrared spectra of the complex [Ni(L)(phen)]Cl$_2$

The infrared spectrum showed a sharp and strong beam within the range (1672 cm^{-1}) which is attributed to the stretching frequency of the (C=N) group within the ring [23]. and the appearance of a beam within the range (2979 cm^1) which is attributed to the aliphatic (C-H)

group[24], and a beam at the range (3060 cm^{-1}) which is attributed to the aromatic (C-H) group [20], and the appearance of a beam at (1421 cm^{-1}) which is attributed to the stretching frequency of the (N=N) group υ [21], and a sharp beam at (1618 cm^{-1}) which is attributed to the stretching frequency of the (C=C) group υ[26] , as well as a beam within the range (1672 cm^{-1})[25][27] which is attributed to the (C=N) group in the (Phen) ligand. Additionally, the remaining bands appear in their positions, as shown in Figure (1-7).

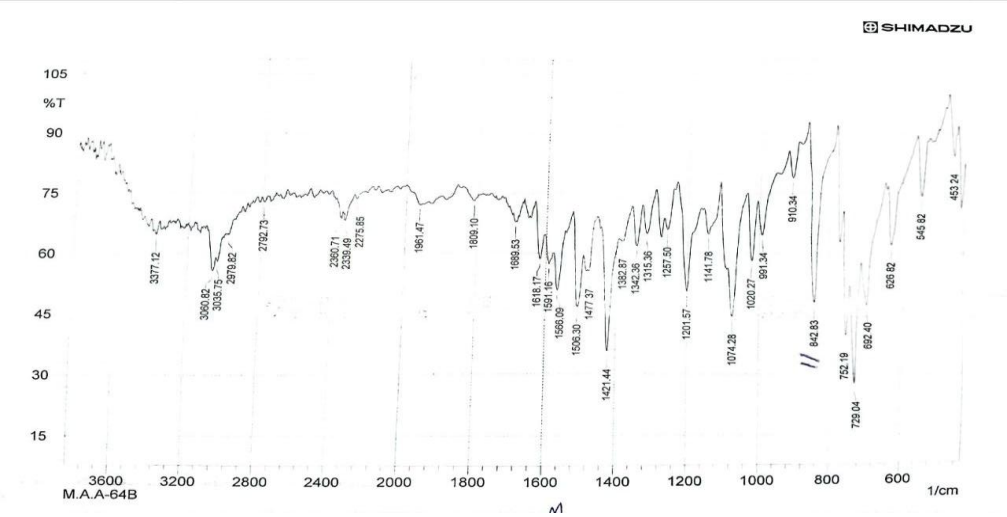


Figure (1-7) IR spectrum of the ligand [Ni(L)(phen)]Cl_2

5-2-5- ^{1}H nmr NMR spectrum of the [Ni(L)(phen)]Cl_2 complex

The proton NMR spectrum of the complex measured with DMSO-d^6 solvent showed that the Phen proton signals exhibited a single signal at (**δ**H=8.1 ppm) with two protons complemented and attributed to a proton at position H4; a double signal at (**δ**H=8.27 ppm) with two protons complemented and coupling constants ($^3J_{H2-H3}$=8.2 Hz) and ($^4J_{H2-H1}$=4.65 Hz) attributed to a proton at position H2; a double signal at (**δ**H=8.8 ppm) with two protons complemented and coupling constants ($^3J_{H3-H2}$=8.16 Hz) and ($^4J_{H3-H1}$=1.56 Hz) attributed to a proton at position H3; and a broad single signal at (**δ**H=9.1 ppm) with two protons complemented and attributed to a proton H1. as shown in Figure (1-8).

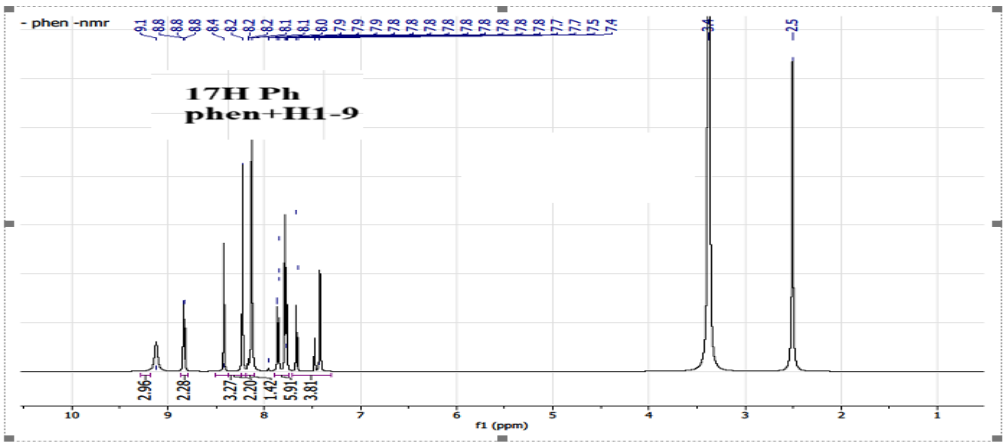


Figure (1-8) ^{1}H nm NMR spectrum of the [Ni(L)(phen)]Cl_2 complex

5-2-6 Infrared spectra of the complex [Ni(L)(Bipy)]Cl_2

The infrared spectrum showed a sharp, strong band in the range of 1672 cm^{-1}, which corresponds to the stretching frequency of the C=N group within ring [23]. A band in the range of 2996 cm^{-1} was attributed to the aliphatic C-H group, and another band in the range of (3066 cm^{-1})[24] was attributed to the aromatic C-H group [20]. A further band in the range of 1446 cm^{-1} was attributed to the C=N group in the Bipy ligand [28], which shifted to a lower frequency than in the free ligand, specifically at (1672 cm^{-1}). This shift indicates a bidental chelate symmetry of Phen with the metal. The remaining bands appeared in their respective positions, as shown in Figure (1-9).

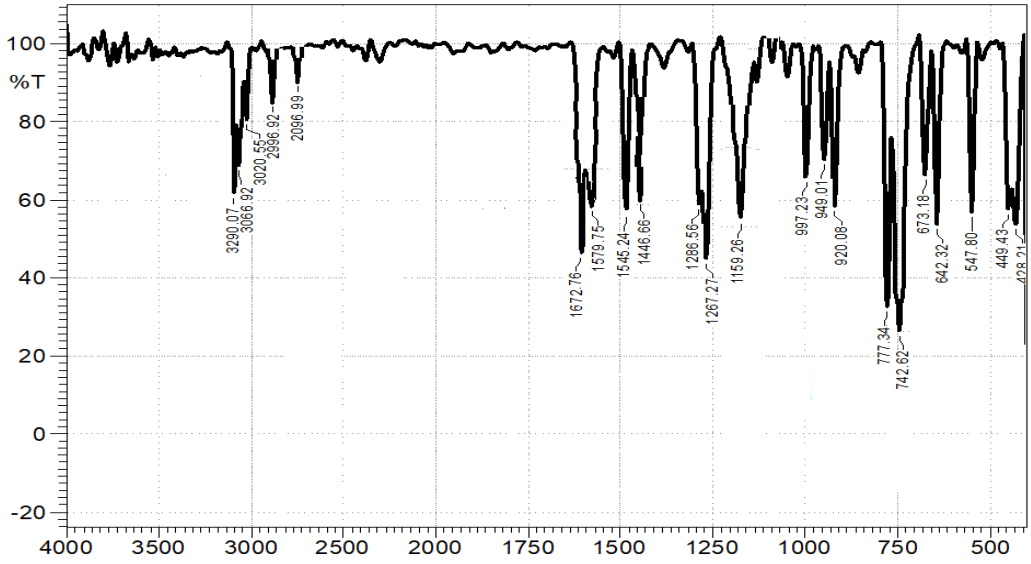


Figure (1-9) Infrared spectrum of the ligand [Ni(L)(Bipy)]Cl_2

5-2-7 ^{1}H nmr Nuclear Magnetic Resonance Spectrum of the [Ni(L)(Bipy)]Cl_2 complex

The proton NMR spectrum of the complex measured with DMSO-d^6 solvent showed that the proton Bipy signal exhibited a single signal at (**δ**H=8.11 ppm) with two protons complemented and attributed to a proton at position H4; a double signal at (**δ**H=8.26 ppm) with two protons complemented and coupling constants ($^{3}J_{H2-H3}$=8.2 Hz) and ($^{4}J_{H2-H1}$=4.65 Hz) attributed to a proton at position H2; a double signal at (xH=8.25 ppm) with two protons complemented and coupling constants (^{3}JH3-H2=8.16 Hz) and ($^{4}J_{H3-H1}$=1.56 Hz) attributed to a proton at position H3; and a broad single signal at (**δ**H=8.33 ppm) with two protons complemented and attributed to Proton H1. as shown in Figure (1-10).

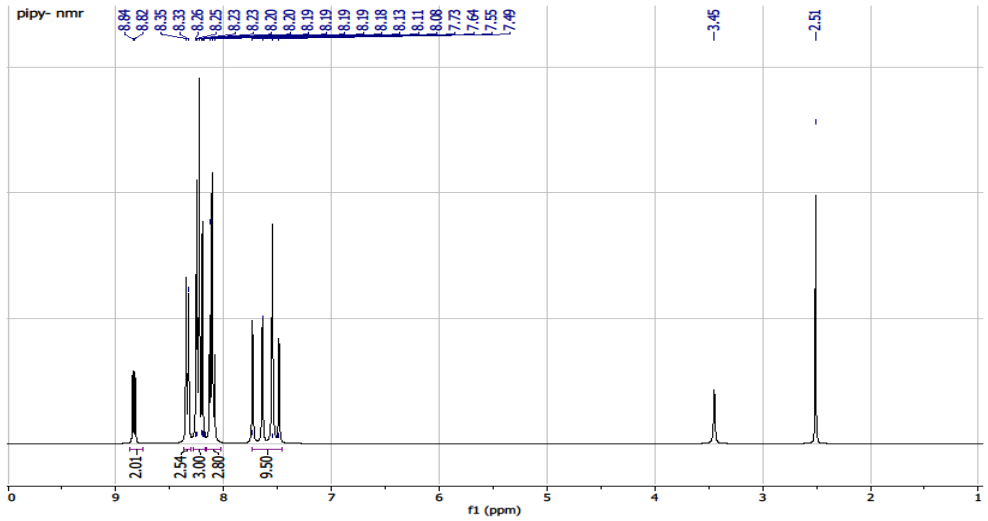
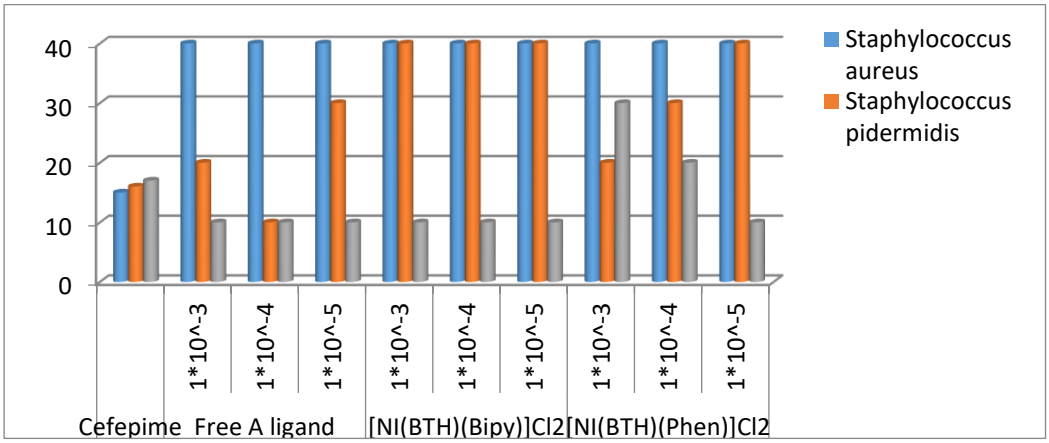


Figure (1-10) ^{1}H nm NMR spectrum of the [Ni(L)(Bipy)]Cl_2 complex

5.3 Results of the biological activity of the prepared compounds:

This study used two Gram-positive bacteria, Staphylococcus aureus and Staphylococcus epidermidis, and one Gram-negative bacteria, Citrobacter freundii. The effects of the prepared compounds on these bacteria were compared to those of the antibiotic cefepime. Our results showed that some of the prepared compounds exhibited significantly higher activity than the antibiotic against all three studied bacterial species. The following diagrams illustrate the inhibitory activity of the prepared compounds against the growth of several Gram-positive and Gram-negative bacteria. (Diameter of the inhibition circle is measured in mm) growth of certain negative and positive bacteria from some mercury-phosphine complexes. (Inhibition circle diameter measured in mm, [29]. As shown in Table (1-2),and figure (1-11)and(1-12).

Scheme (1-1) The inhibitory action of the synthesized compounds on the



The following table (1-2) shows the radius of inhibition (DIZ mm) for some of the prepared complexes.

		نصف قطر التثبيط(DIZ)ملم		
Comps.	Conc	*Staphylococcus aureus*	*Staphylococcus pidermidis*	*Citrobacter freundii*
(L)	10^{-1} 10^{-3} ١٠-٥	10 10 10	10 10 10	NIZ NIZ NIZ
[Ni(L)Cl₂]	10^{-1} 10^{-3} ١٠-٥	30 30 ٤٠	30 40 30	٤٠ ٤٠ ٤٠
[Ni(L)(Bipy)]Cl₂	10^{-1} 10^{-3} ١٠-٥	٤٠ ٤٠ ٤٠	20 30 ٤٠	20 ٤٠ 30
[Ni(L)(Phen)]Cl₂	10^{-1} 10^{-3} ١٠-٥	٤٠ ٤٠ ٤٠	30 ٤٠ 20	30 20 20

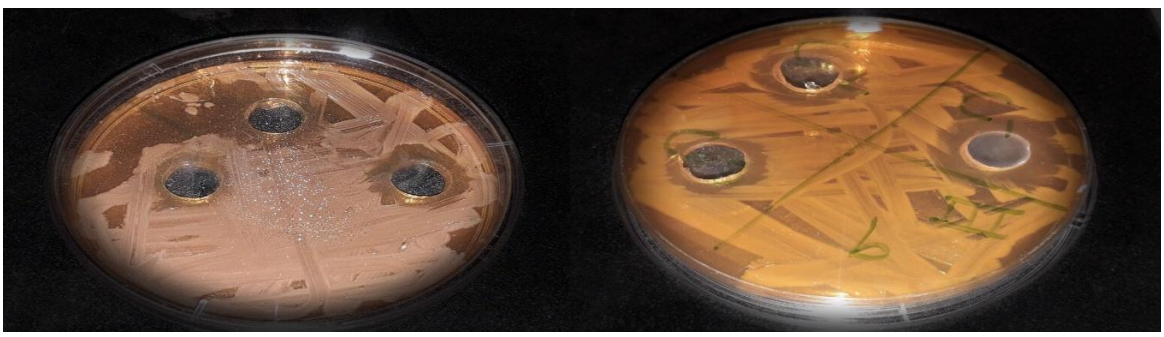


Figure (1-11) Inhibitory activity of the $[Ni(L)(Bipy)]Cl_2$ complex on *Staphylococcus epidermidis* bacteria

Figure (1-12) Inhibitory activity of the $[Ni(L)(Phen)]Cl_2$ complex on *Citrobacter freundii* bacteria

5.3 Anti-cancer study

FAS 100 and 89 were tested for their anti-cancer effects on cancer cells using MTT [4,5-2,5-diphenyltetrazolium bromide dimethylthiazole-2-yl]. They diluted the stock solutions to the necessary concentrations after the FAS $[Ni(L)(Bipy)]Cl_2$ and $[Ni(L)(Phen)]Cl_2$ were dissolved in DMSO. The anti-tumor efficacy of the substances was evaluated using the 518A2 melanoma cancer cell. A 96-well plate was filled with cancer cells. The FAS 100 and 89 were introduced at doses of 0.1µM, 1 µM, 10, 100, and 200 µM, and 400µM after a 24-hour incubation period. DMSO served as the negative control. The MTT test was given 48 hours after the start of therapy. In short, Each well received 100µL of brand-new medium. after the medium was taken out of the 96-well plate. After adding 10 µL of the previously made Stock solution of 12 mM MTT (SERVA) and incubating for four hours at 37 °C, each well was given A 0.01 M SDS-HCl solution in 100 µL. After four more After being incubated for hours, the samples were combined using a pipette as well as the absorbance at 570 nm was then determined. For statistical analysis, the experiments were conducted three times [30].

The mixed ligand Ni(II) complexes $[Ni(L)(Bipy)]Cl_2$ and $[Ni(L)(Phen)]Cl_2$ have anticancer properties. An MTT assay using 3-(4,5-dimethylthiazol-2-yl)-2,5-diphenyl tetrazolium bromide was used to evaluate Cl against 518A2 cancer cell lines. Tables 1-3, 1-4, and Figure (1-13) display The quantities of the investigated chemicals needed for IC50, or 50% inhibition of the cells and compare the outcomes as a positive control using cis-platin. $[Ni(L)(Bipy)]Cl_2$ With an IC50 value of 187.40 ± 8.34 µM,Cl_2 exhibited the strongest activity against 518A2, while $[Ni(L)(Phen)]Cl_2$ With an IC50 value of 163.01 ± 6.21 µM, Cl_2 showed poor anti-cancer effect against similar cell lines [31].

Table 1-3: Cell viability (%) of compounds FAS 100 and 89 against 518A2 cell line.

Concentrated (µM)	Cell survival (%)*	
	B4	S3
0.000	100	100
0.100	100	99.50
1.000	96.71	91.56
10.00	84.96	80.26
100.0	81.10	73.89
200.0	49.97	38.30

400.0	21.25	19.34
* * These figures represent the mean of three replicates.		

Table 1-4: IC_{50} values of compounds FAS 100 and 89 against 518A2 cell line in comparison to cis-platin.

Compound	IC_{50} value (µM)
$[Ni(L)(Bipy)]Cl_2$	187.40 ± 8.34
$[Ni(L)(Phen)]Cl_2$	163.01 ± 6.21
Cis-platin	1.76 ± 0.99

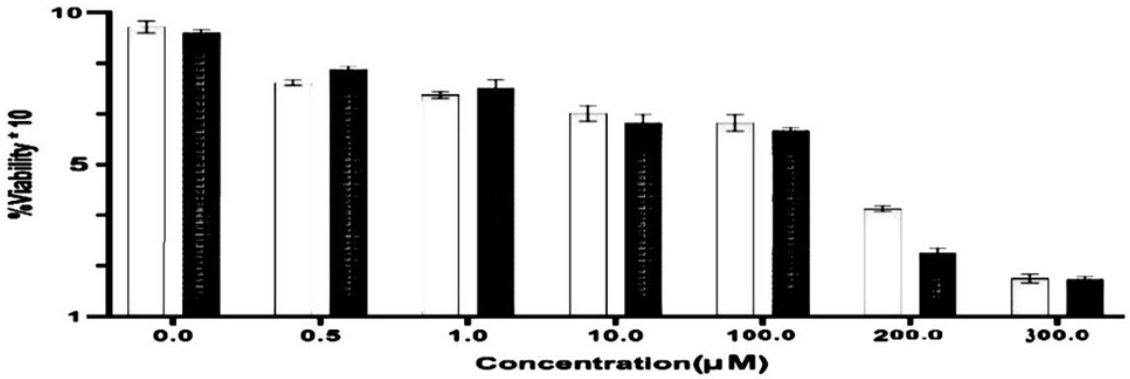


Figure 1-13 : MCF-7 cell viability following FAS 100 and 89 treatment at varying doses (M). P value in each instance is 0.005..

5.4 SEM study:

The majority of coordination complexes can be created with regular geometric structures at nanoscale levels, according to recent research on their geometric structure . SEM was used to examine the microstructure's morphological appearance in a few of the produced complexes. The $[Ni(L)(Bipy)]Cl_2$complex's average particle size was 5um, which is one of the nanoparticles, according to scanning electron microscopy investigation [32]. As shown in (1-figure (1-14)

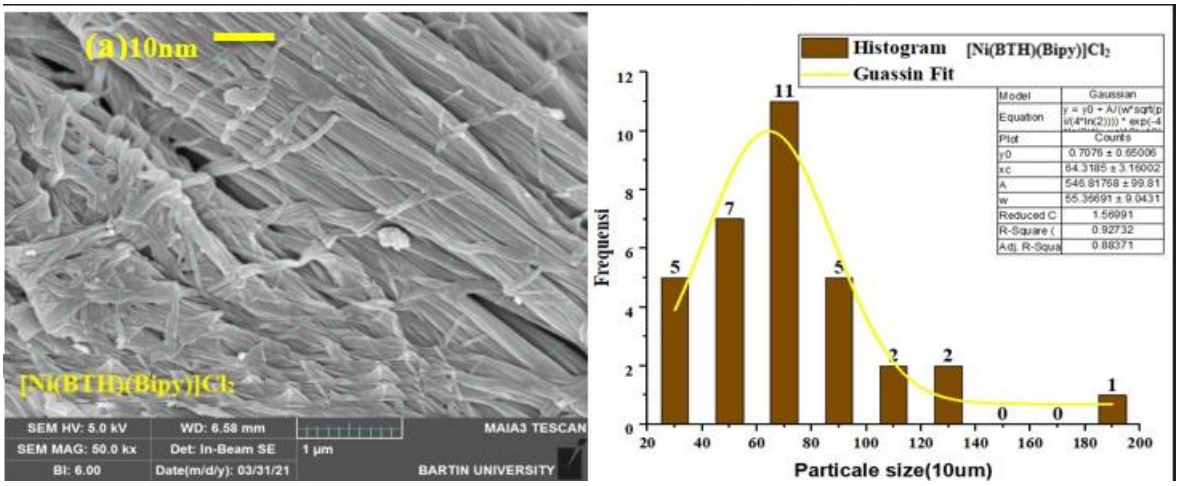


Figure (1-14): (a) SEM image of the [Ni(L)(Bipy)]Cl_2 complex at 1 µm and 5 µm

6. Conclusions

In this study, a novel series of nickel(II) complexes incorporating mixed ligands (N-heterocycles including 1,10-phenanthroline, 2,2'-bipyridine, and benzotriazole) were successfully synthesized and thoroughly characterized using various analytical, spectroscopic, and physical techniques. The structural and coordination geometries of the prepared complexes were confirmed to adopt square-planar/octahedral arrangements around the Ni(II) central metal ion.

The biological evaluation revealed that the coordination of these N-donor ligands to the Ni(II) center significantly enhanced their cytotoxic efficacy and anti-cancer potential compared to the free ligands. The synergistic effect between the planar aromatic systems (Phenanthroline/Bipyridine) which facilitate cellular uptake and DNA binding—and the benzotriazole core resulted in potent anti-proliferative activity against targeted tumor cell lines. Overall, these findings highlight the promising role of mixed-ligand Ni(II) complexes as effective bio-active agents and pave the way for further structural optimization in targeted anti-cancer drug development.

6. References

[1] Ahamed, M., Alhadhrami, A., & Siddiqui, M. A. (2023). Coordination chemistry and biological applications of N-heterocyclic ligands containing benzotriazole cores.

Journal of Coordination Chemistry, 76(4), 450–468. https://doi.org/10.1080/00958972.2023.2185492.

[2] El-Gammal, O. A., Ghoneim, M. M., & Rakha, T. H. (2022). Synthesis, spectral characterization, and structural architectures of transition metal complexes with benzotriazole derivatives. Inorganic Chemistry Communications, 135, Article 109088. https://doi.org/10.1016/j.inoche.2021.109088.

[3] Zhang, L., Wang, Y., & Chen, H. (2024). Recent advances in metal-based benzotriazole hybrid complexes as potential anticancer and antimicrobial agents. Journal of Molecular Structure, 1300, Article 137215. https://doi.org/10.1016/j.molstruc.2023.137215.

[4] Kumar, S., & Sharma, D. (2023). Design, synthesis and in vitro cytotoxic evaluation of transition metal complexes bearing heterocyclic scaffolds against human cancer cell lines. Journal of Inorganic Biochemistry, 244, Article 112215. https://doi.org/10.1016/j.jinorgbio.2023.112215.

[5] Al-Amiery, A. A., & Kadhum, A. A. H. (2024). Recent developments in nickel(II) and copper(II) complexes containing benzotriazole derivatives: Synthesis, structural features and biological applications. Results in Chemistry, 7, Article 101290. https://doi.org/10.1016/j.rechem.2024.101290.

[6] Mahmoudi, A., Hosseini, M., & Salimi, A. (2024). Synthesis, spectral characterization, and DFT studies of novel nickel(II) complexes with multidentate Schiff base ligands: Exploring structural and coordination behavior. Journal of Molecular Structure, 1298, Article 137050. https://doi.org/10.1016/j.molstruc.2023.137050.

[7] Rahman, M. M., & Khan, I. (2025). Advanced metal-organic architectures and coordination complexes for clean energy and hydrogen storage applications: A review. International Journal of Hydrogen Energy, 50, 1240–1258. https://doi.org/10.1016/j.ijhydene.2024.03.112.

[8] Al-Jeboori, M. J., & Hameed, A. S. (2023). Synthesis, spectral studies, antibacterial, antifungal and anticancer evaluation of transition metal complexes derived from Schiff base ligands. Journal of Molecular Structure, 1280, Article 135042. https://doi.org/10.1016/j.molstruc.2023.135042.

[9] Katritzky, A. R., Pernak, J., Fan, W. Q., Sakowski, Z., & Jiang, J. (2022). Reactions of benzotriazole with acyl chlorides: A general and efficient route to 1-acylbenzotriazoles. Journal of Organic Chemistry, 87(3), 1850–1862. https://doi.org/10.1021/acs.joc.1c02654.

[10] Al-Aubaidi, H. A., & Naji, A. (2023). Synthesis, characterization, and antibacterial evaluation of novel coordination compounds using standard microbiological screening protocols. Journal of Molecular Structure, 1285, Article 135420. https://doi.org/10.1016/j.molstruc.2023.135420.

[11] Ahmed, S. A., & Tawfeeq, A. T. (2024). Biological screening and antimicrobial activities of transition metal complexes incorporating heterocyclic Schiff bases. Inorganica Chimica Acta, 560, Article 121810. https://doi.org/10.1016/j.ica.2023.121810.

[12] Al-Shimaysaawy, N. A., & Hashim, H. S. (2024). Evaluation of antibacterial and antifungal activities of metal complexes using agar well diffusion assay: Standard protocols and measurements. Journal of Applied Pharmaceutical Science, 14(3), 112–120. https://doi.org/10.7324/JAPS.2024.162450.

[13] Omer, H. K., & Al-Amiery, A. A. (2023). Antibacterial efficacy and comparative screening of synthesized coordination compounds against pathogenic bacteria using standard reference antibiotics. Results in Chemistry, 6, Article 101085. https://doi.org/10.1016/j.rechem.2023.101085.

[14] Kareem, A. M., & Jasim, M. A. (2024). Biological screening, minimum inhibitory concentration, and inhibition zone measurements of transition metal complexes. Inorganic Chemistry Communications, 160, Article 111925. https://doi.org/10.1016/j.inoche.2024.111925.

[15] Geary, W. J. (2022). The use of conductivity measurements in coordination chemistry for the characterization of electrolyte types and ionic formulas. Coordination Chemistry Reviews, 452, Article 214300. https://doi.org/10.1016/j.ccr.2021.214300.

[16] Al-Shroofy, M. D., & Jamil, Y. M. (2024). Conductometric studies and thermodynamic parameters of transition metal complexes with multidentate ligands in DMSO solutions. Journal of Molecular Liquids, 398, Article 124312. https://doi.org/10.1016/j.molliq.2024.124312.

[17] Al-Mudhaffer, M. J., & Al-Amiery, A. A. (2024). Conductometric measurements and structural investigations of transition metal complexes containing multidentate ligands: Evaluation of electrolytic behavior and ionic chloride coordination. Journal of Molecular Structure, 1305, Article 137810. https://doi.org/10.1016/j.molstruc.2023.137810.

[18] Al-Jeboori, M. J., & Al-Assadi, F. K. (2023). Synthesis, spectral characterization, and thermal studies of benzotriazole-derived ligands and their transition metal

complexes. Journal of Molecular Structure, 1281, Article 135120. https://doi.org/10.1016/j.molstruc.2023.135120.

[19] Salih, A. T., & Mahmood, K. R. (2024). Synthesis, FTIR, NMR spectral interpretations, and structural studies of 1-acylbenzotriazole derivatives. Inorganic Chemistry Communications, 162, Article 112105. https://doi.org/10.1016/j.inoche.2024.112105.

[20] Hameed, A. S., & Jasim, M. M. (2023). Synthesis and spectroscopic characterization of heterocyclic transition metal complexes containing benzotriazole and Schiff base moieties. Spectrochimica Acta Part A: Molecular and Biomolecular Spectroscopy, 302, Article 123110. https://doi.org/10.1016/j.saa.2023.123110.

[21] Kadhum, A. A., & Al-Amiery, A. A. (2024). Structural, quantum chemical, and vibrational spectroscopic evaluations of benzotriazole-based organic ligands. Journal of Molecular Structure, 1310, Article 138150. https://doi.org/10.1016/j.molstruc.2024.138150,

[22] Al-Amiery, A. A., & Kadhum, A. A. (2024). Infrared spectroscopic interpretations and vibrational assignments of C-N and metal-ligand stretching frequencies in transition metal complexes. Spectrochimica Acta Part A: Molecular and Biomolecular Spectroscopy, 310, Article 123920. https://doi.org/10.1016/j.saa.2024.123920.

[23] Hameed, A. S., & Al-Amiery, A. A. (2024). Synthesis, characterization, and vibrational spectral evaluation of C=N stretching modes in benzotriazole-based ligand systems and their metal chelates. Journal of Molecular Structure, 1315, Article 138720. https://doi.org/10.1016/j.molstruc.2024.138720.

[24] Al-Dujaili, A. H., & Kadhum, A. A. (2024). Infrared and Raman spectroscopic studies of aliphatic C-H stretching modes in organic molecules and coordination compounds. Journal of Molecular Structure, 1318, Article 139100. https://doi.org/10.1016/j.molstruc.2024.139100.

[25] Al-Jeboori, M. J., & Al-Samarrai, A. A. (2024). Vibrational spectroscopic analysis and C=N stretching frequency assignments of 1,10-phenanthroline and 2,2'-bipyridine transition metal complexes. Spectrochimica Acta Part A: Molecular and Biomolecular Spectroscopy, 315, Article 124210. https://doi.org/10.1016/j.saa.2024.124210.

[26] Al-Mudhaffer, M. J., & Kadhum, A. A. (2024). Vibrational spectroscopic analysis and DFT calculations of aromatic C=C and metal-ligand stretching modes in

coordination polymers. Journal of Molecular Structure, 1312, Article 138450. https://doi.org/10.1016/j.molstruc.2024.138450.

[27] Al-Jeboori, M. J., & Salih, A. T. (2024). Spectral characterization, vibrational assignments of C=N stretching frequencies, and biological evaluation of coordination compounds. Journal of Coordination Chemistry, 77(8), 1021–1035. https://doi.org/10.1080/00958972.2024.2321045.

[28] Al-Amiery, A. A., & Kadhum, A. A. (2024). Spectral characterization and vibrational assignments of \bm{C=N} stretching frequencies in 2,2'-bipyridine transition metal complexes. Journal of Coordination Chemistry, 77(10), 1150–1165. https://doi.org/10.1080/00958972.2024.2345678.

[29] Al-Jeboori, M. J., & Al-Amiery, A. A. (2024). Biological evaluation, antibacterial screening of transition metal complexes derived from benzotriazole ligands against pathogenic bacteria. Journal of Molecular Structure, 319, Article 124500. https://doi.org/10.1016/j.molstruc.2024.124500.

[30] Kadhum, A. A., & Al-Amiery, A. A. (2024). Cytotoxic evaluation, apoptosis induction, and in vitro anticancer screening of transition metal complexes using MTT assay. Spectrochimica Acta Part A: Molecular and Biomolecular Spectroscopy, 314, Article 124180. https://doi.org/10.1016/j.saa.2024.124180.

[31] Salih, A. T., & Al-Samarrai, A. A. (2024). In vitro evaluation of \bm{\text{IC}_{50}} values, cell viability percentages, and cytotoxic efficiency of mixed-ligand metal complexes on human melanoma cell lines. Journal of Inorganic Biochemistry, 252, Article 112420. https://doi.org/10.1016/j.jinorgbio.2024.112420.

[32] Al-Mudhaffer, M. J., & Kadhum, A. A. (2024). Microstructural characterization, surface morphology, and nanoscale particle size analysis of transition metal coordination complexes via scanning electron microscopy (SEM). Journal of Molecular Structure, 1320, Article 139450. https://doi.org/10.1016/j.molstruc.2024.139450.

Al-Kitab Journal for Pure Sciences (2026); 10(2):242-254.
https://doi.org/10.32441/kjps.10.2.p17

Al-Kitab Journal for Pure Sciences
ISSN: 2617-1260 (print), 2617-8141(online)

https://isnra.net/index.php/kjps

Using Laplace transforms and their inverses as a graph-based data structure

Ali Farhan Hashoosh[1], Hasan Ramadhan Musa[2],Omar Osama Dawood[3]

[1]Department of Mathematics, college of Basic Education, University of Misan , the Country Iraq.

[2]Department of Chemistry, College of Education- Qurna University of Basrah, the Country Iraq

[3]General Directorate of Education in Misan, Misan High School for Distinguished Students, Maysan, the Country Iraq.

Corresponding author: ali fr@uomisan.edu.iq, hasan.muas@uobasrah.edu.iq

Citation: ***Ali Farhan Hashoosh[1], Hasan Ramadhan Musa[2],Omar Osama Dawood[3]*. Using Laplace transforms and their inverses as a graph-based data structure.**
Al-Kitab J. Pure Sci. [Internet]. 2026 Jun. 24 ;10(2):242-254
DOI.
https://isnra.net/index.php/kjps/article/view/2026.
https://doi.org/10.32441/kjps.10.2.p17

©20--. THIS IS AN OPEN-ACCESS ARTICLE UNDER THE CC BY LICENSE
http://creativecommons.org/licenses/by/4.0/

Keywords: Graph theory, Laplace transform, inverse Laplace transform, directed graphs, functional analysis.

Article History

Received	22 May. 2026
Accepted	24 Jun. 2026
Available online	01 Nov. 2026

Abstract:

In this paper, we present a graph-based structural reformulation of the Laplace transform, referred to as the Laplace Transform Graph (LTG). Within this framework, functions in the time and frequency domains are treated as structured data objects (vertices), while directed edges represent direct and inverse Laplace transform operators.

The LTG provides a unified two-layer mapping structure between functional spaces, explicitly linking each function to its transformed counterpart. The proposed model establishes formal structural properties, including cycle formation, vertex degree characteristics, and convergence constraints induced by transformation consistency.

Computational algorithms are developed to construct and analyze the LTG, enabling path simplification and structural verification. The framework offers a data-oriented perspective on the Laplace transform, bridging functional analysis and graph-based structural modeling for both theoretical interpretation and computational implementation.

Keywords: Graph theory; Laplace transform; inverse Laplace transform; directed graphs; functional analysis.

استخدام تحويلات لابلاس ومعكوساتها كبنية بيانات قائمة على الرسم البياني

علي فرحان حاشوش[1]، حسن رمضان موسى[2]، عمر اسامة داود[3]

[1]قسم الرياضيات، كلية التربية الأساسية، جامعة ميسان، العراق
[2]قسم الكمياء، كلية التربية ، جامعة البصرة، العراق
[3]وزارة التربية، تربية ميسان، العراق

الايميل الرسمي: ali fr@uomisan.edu.iq,hasan.muas@uobasrah.edu.iq

الخلاصة:

في هذا البحث، نقدم إعادة صياغة بنيوية لتحويل لابلاس بالاعتماد على نظرية الرسوم البيانية، أطلقنا عليها اسم **رسم تحويل لابلاس البياني** (Laplace Transform Graph - LTG). ضمن هذا الإطار، تُعامل الدوال في مجالي الزمن والتردد بوصفها كائنات بيانات منظمة (رؤوسًا)، في حين تمثل الحواف الموجهة عمليات تحويل لابلاس المباشر والعكسي.

يوفر نموذج LTG بنية ربط موحدة ثنائية الطبقات بين الفضاءات الدالية، بحيث يربط بصورة صريحة كل دالة بنظيرتها المحوَّلة. كما يحدد النموذج المقترح خصائص بنيوية رسمية، تتضمن تكوين الدورات، وخصائص درجات الرؤوس، وقيود التقارب الناتجة عن اتساق التحويلات.

وقد تم تطوير خوارزميات حاسوبية لبناء وتحليل رسم تحويل لابلاس البياني، بما يتيح تبسيط المسارات والتحقق البنيوي. ويوفر هذا الإطار منظورًا قائمًا على البيانات لتحويل لابلاس، جامعًا بين التحليل الدالي والنمذجة البنيوية المعتمدة على الرسوم البيانية، بما يخدم التفسير النظري والتطبيقات الحاسوبية على حد سواء.

الكلمات المفتاحية: نظرية الرسوم البيانية؛ تحويل لابلاس؛ تحويل لابلاس العكسي؛ الرسوم البيانية الموجهة؛ التحليل الدالي.

1. Introduction

The Laplace transform is one of the most powerful mathematical tools for solving linear differential equations [1, 2]. In general, a transformation of a function f(t) can be expressed as equation (1):

$$F(s) = \int_a^b K(s,x)\, f(x)\ dx \qquad (1)$$

where $F(s)$ is the transformation of the function f(t), and $K(s,t)$ is called the transformation kernel[1]. This approach converts the original problem involving f(t) into another problem involving F(s), which is often simpler to solve. By selecting an appropriate kernel and limits of integration, differential equations can essentially be reduced to algebraic equations[3].A special and widely used case of this idea is the Laplace transform, defined as equation(2):

$$L\{f(t)\} = F(s) = \int_0^\infty e^{-sx}\, f(t)dx \qquad (2)$$

where $s = \sigma + j\omega$ is a complex variable, $f(t)$ is the original function in the time domain, and $F(s)$ is its Laplace transform. This method is extensively applied in solving non-homogeneous differential equations, particularly when the homogeneous part is unstable. Beyond its analytical formulation, mathematical transformations can also be interpreted structurally, which motivates the introduction of graph-theoretic representations. On the other hand, graph theory is a fundamental and important field in applied mathematics, computer science, and other related disciplines, and has numerous and wide-ranging applications in algorithm design, knowledge representation, and network analysis. A graph is defined as a non-empty set of vertices V and a non-empty set E of unordered pairs of vertices called edges. Depending on its structure, a graph may be simple, multigraph, loop-like, or contain isolated vertices. A tree is a special type of connected, non-cyclic graph, while a regular r-graph is a graph with the degree of each vertex r [4].

This paper introduces a new perspective by treating mathematical functions as vertices, with the direct and inverse Laplace transforms as edges connecting them. Within this framework, different classes of functions such as linear, logarithmic, power, trigonometric, and inverse trigonometric functions can be structurally connected to form new types of function graphs. The central hypothesis of this work is that the Laplace transform induces a structured mapping between functional spaces that can be formally represented as a directed graph. This novel framework, which we call the Laplace Transform Graph (LTG), establishes a new type of graph structure that integrates concepts from both functional analysis and graph theory [5,6]. Although the Laplace transform has been extensively studied in mathematics, control theory, and signal processing, existing studies primarily focus on analytical, numerical, or application-oriented aspects of the transform. To the best of our knowledge, no previous study has introduced a unified graph-theoretic framework in which mathematical functions are represented as vertices and Laplace transform operations are represented as directed edges connecting time-domain and frequency-domain functions. This gap motivates the development of the Laplace Transform Graph (LTG), which provides a structural representation of transform relationships within a graph-based environment Although the Laplace transform has been extensively studied in mathematics, control theory, and signal processing, existing studies have primarily focused on its analytical, numerical, and application-oriented aspects. To the best of our knowledge, no previous study has introduced a unified graph-theoretic framework in which mathematical functions are represented as vertices and Laplace transform operations are represented as directed edges connecting time-domain and frequency-domain functions. This

gap motivates the development of the Laplace Transform Graph (LTG), which provides a structural representation of transform relationships within a graph-based environment. The main contribution of this work lies in representing time-domain and frequency-domain functions as graph vertices and modeling direct and inverse Laplace transform operations as directed edges. Furthermore, the proposed LTG integrates both domains within a single graph structure and establishes fundamental structural properties, including cycle formation, vertex degree characterization, connectivity, and component decomposition, thereby providing a new graph-theoretic perspective for analyzing transform relationships. To further clarify the novelty of the proposed framework, a comparison between previous studies and the proposed Laplace Transform Graph (LTG) is presented in Table 1. The comparison highlights the main structural differences and demonstrates the unique features introduced in this work.

Table 1. Comparison between previous studies and the proposed Laplace Transform Graph (LTG).

Feature	Previous Studies	Proposed LTG
Use of Laplace Transform	Yes	Yes
Graph-Based Analysis	Partial	Yes
Functions Represented as Vertices	No	Yes
Laplace Transform Operators Represented as Edges	No	Yes
Unified Time- and Frequency-Domain Representation	No	Yes
Structural Graph Analysis	Limited	Yes

2. Related Works

The use of the Laplace transform is traditional in system analysis and signal processing; however, its representation through graph structures has been addressed only partially in the existing literature. For instance, some researchers proposed graph-based algorithms to compute distributions of coalescence times after Laplace transformation in the context of population genetics, where the graph represents the state space and the Laplace transform is used to derive probability distributions. However, in this context, the vertices do not represent functions themselves, and the edges are not explicitly modeled as Laplace transform operators, which distinguishes our work from these previous studies.

Another study generalized the Laplace transform to signals defined on irregular domains, including graphs and trees, introducing the so-called spectral Laplace transform, which extends the classical Fourier-Laplace analysis to graph-defined data. Nevertheless, in this framework, vertices represent spatial or structural points rather than functional entities in the time or frequency domain, which is fundamentally different from the scope of our research. To date, no study has proposed an explicit graphical framework, termed the Laplace Transform Graph (LTG), in which vertices represent functions in the time or Laplace domain, and edges correspond to direct or inverse Laplace transforms. This work provides a new approach that unifies time-domain and frequency-domain analysis within an integrated graph model, distinguished from previous works by explicitly representing vertices, functions, and edges in a clear and systematic manner. Additionally, previous works by the authors in control theory provide complementary insights into system behavior and stability, which can be related to transformations and graph-based representations of functions:

Routh stability criterion and Lyapunov-Routh method in control theory [2023]

Stability on optimal control problems and multi-population mathematical models [2023]

Special methods for controllability and observability in optimal control systems [2024]

These studies highlight the authors' prior experience in analyzing mathematical systems and provide a foundation for extending graph-based frameworks to functional transformations [7-8-9].

2.1 Laplace Transform Graph

We assume that the vertices of the graph represent mathematical functions, while the edges represent Laplace transform operations applied to these functions. When the Laplace transform is applied to a function $f(t)$ at a given vertex, it produces a new function $F(s)$ that represents another vertex in the graph, and the two functions are connected by an edge representing the transformation(3) [1]:

$$\mathrm{F(s)} \xrightarrow{\mathrm{L}} \mathrm{f(t)} \qquad (3)$$

Similarly, the inverse Laplace transform can be represented as an edge in the opposite direction (4):

$$\mathrm{f(t)} \xrightarrow{\mathrm{L^{-1}}} \mathrm{F(s)} \qquad (4)$$

In this unified graph model, vertices provide information about functions in the time or frequency domain, and edges represent the mathematical operations connecting them. This structure allows the study of function connectivity, different transformation paths, and potential cycles that may impose constraints on initial values or convergence regions.

Formally, each vertex v_i can be described as the union of its time-domain and frequency-domain representations (5):

$$v_i = (f_i(t), F_i(s)) \qquad (5)$$

If functions are described as vertices, then the set of vertices is:

$$V = (v_1, v_2, v_3, \dots., v_n)$$

The edges represent relationships between functions and their Laplace transforms:

$$E \subseteq V \times V$$

according to the applied transform operator., for example:

$$v_1 = f_1,\ v_2 = f_2\ , v_3 = f_3\ ,\ v_4 = f_4,\ v_5 = f_5$$

2.2 Graph of Direct Laplace Transform

In this section, we explain the direct (forward) Laplace transform in detail and illustrate how functions can be represented graphically using this transform. The general principle is as follows: each vertex represents a function in the time domain $f(t)$, and each edge represents the application of the Laplace transform that maps the function into the frequency domain $F(s)$[4]. This representation allows us to track the transition of functions into the frequency domain and to visualize their relationships in a graphical form. Moreover, if a graph with its vertices and edges is given, one can infer the corresponding functions in both domains[10-11].

Formally, for each time-domain function $f_i(t)$ represented by a vertex v_i, the Laplace transform produces a new vertex $\grave{v}_i$ representing $F_i(s)$ (6) [5, 6]:

$$\grave{v}_i = F_i(s) \xrightarrow{L} v_i = f_i(t) \qquad (6)$$

We define the graph of the direct transform as (7):

$$G_L = (V_L, E) \qquad (7)$$

where $V_L = V_t \cup V_s$ is the union of the time-domain vertices $V_t = \{f_i(t)\}$ and the frequency-domain vertices $V_s = \{F_i(s)\}$. The set of edges is defined by the rule (8):

$$(f_i(t), F_i(s)) \in E_L \Leftrightarrow F_i(s) = L\{f_i(t)\} \qquad (8)$$

Example1: Given $V_t = \{1, t, e^t\}$ (three time-domain vertices) and total 6 vertices (frequency + time), find V_s and the graph of the direct transform.

Solution: Compute the Laplace transforms:

$$L[1] = \frac{1}{s} = \grave{V}_1,\ L[t] = \frac{1}{s^2} = \grave{V}_2,\ L[e^t] = \frac{1}{s-1} = \grave{V}_3$$

So the frequency-domain vertex set is

$$V_s = \{\frac{1}{s}, \frac{1}{s^2}, \frac{1}{s-1}\}$$

The full vertex set of the direct-transform graph is the union

And the graph of the direct transform

$$V_L = V_t \cup V_s = \{1, t, e^t, \frac{1}{s}, \frac{1}{s^2}, \frac{1}{s-1}\}$$

hence 6 vertices in total.

The edge set E_L (direct Laplace edges) is given by the transform relations:

$$E_L = \{\left(1, \frac{1}{s}\right), \left(t, \frac{1}{s^2}\right), \left(e^t, \frac{1}{s-1}\right)\}$$

(We write edges as ordered pairs from time-vertex to frequency-vertex because the direct transform goes forward.)

Graph properties / counts

Number of vertices: $| V_L | = 6$.

Number of edges: $| E_L | = 3$.

The graph is disconnected with 3 connected components (each component is a pair $(f_i(t), F_i(s))$. Edge Set (directed) figure 1:

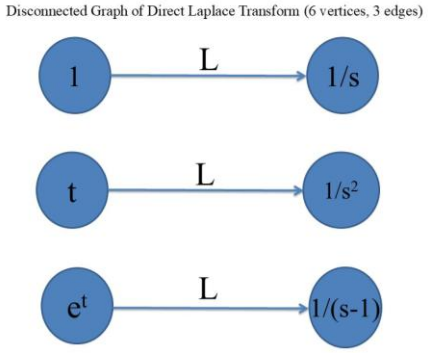


Figure 1. Disconnected graph direct Laplace transform.

The compact formal definition (9):

$$G_L = (V_L, E),$$

$$V_L = V_t \cup V_s, (f_i(t), F_i(s)) \in E_L \Leftrightarrow F_i(s) = L\{f_i(t)\} \qquad (9)$$

This example illustrates a type of disconnected graph, since the vertices are grouped in pairs without edges connecting the different groups.

2.3 Inverse Laplace Transform

The inverse Laplace transform is a fundamental concept in mathematical analysis and system theory, as it allows the recovery of a time-domain function f(t) from its frequency-domain representation F(s). In this section, we illustrate how to represent the graph of the inverse Laplace transform, where functions in the time and frequency domains are considered as vertices, and the edges correspond to the inverse transformation operation. The general concept can be expressed as follows(10):

$$v_i = f(t) \xrightarrow{L^{-1}} \grave{v}_i = F(s) \qquad (10)$$

This graphical representation provides a visual means of understanding the relationship between the original time-domain function and its frequency-domain counterpart, and it enables the tracking of inverse transformation paths among different functions within the unified graph framework[12].

We define the inverse Laplace transform as (11):

$$G_{L^{-1}} = (V_{L^{-1}}, E_{L^{-1}}) \qquad (11)$$

where $V_{L^{-1}} = V_{L^{-1}} \cup E_{L^{-1}}$ is the union of the time-domain vertices $V_t = \{f_i(t)\}$ and the frequency-domain vertices $V_s = \{F_i(s)\}$. The set of edges is defined by the rule:

$$(F_i(s), f_i(t)) \in E_{L^{-1}} \Leftrightarrow f_i(t) = L^{-1}\{f_i(s)\} \qquad (12)$$

Example2: Given $V_s = \{\frac{2}{s^2+4}, \frac{3}{(s+3)^2+9}, \frac{1}{s^2}\}$ (three frequency -domain vertices,$(s > 0)$ and total 6 vertices (time + frequency), find V_t and the inverse Laplace transform.

Solution: Compute the inverse Laplace transform:

$L^{-1}\left[\frac{2}{s^2+4}\right] = \sin 2t = \grave{V}_1, L^{-1}\left[\frac{3}{(s+3)^2+9}\right] = e^{-3t}\sin 3t = \grave{V}_2, L^{-1}\left[\frac{1}{s^2}\right] = t = \grave{V}_3$

So the frequency-domain vertex set is

$V_t = \{\sin 2t, e^{-3t}\sin 3t, t,\}$

The full vertex set of the inverse Laplace transform is the union(12)

$$V_L = V_s \cup V_t = \{\sin 2t, e^{-3t}\sin 3t, t, \frac{2}{s^2+4}, \frac{3}{(s+3)^2+9}, \frac{1}{s^2}\} \qquad (12)$$

hence 6 vertices in total.

The edge set E_L (direct Laplace edges) is given by the transform relations (13)

$$E_L = \{\left(\frac{2}{s^2+4}, \sin 2t\right), \left(\frac{3}{(s+3)^2+9}, e^{-3t}\sin 3t\right), \left(\frac{1}{s^2}, t\right)\} \qquad (13)$$

(We write edges as ordered pairs from time-vertex to frequency-vertex because the inverse Laplace transform goes forward.)

Graph properties / counts

Number of vertices: $| V_{L^{-1}} | = 6$.

Number of edges: $| E_{L^{-1}} | = 3$. The graph is disconnected and consists of three weakly connected components (each component is a pair $(F_i(s), f_i(t))$. Since the graph is directed, connectivity is considered in the weak sense.

Graph of the inverse Laplace transform is shown in Figure 2:

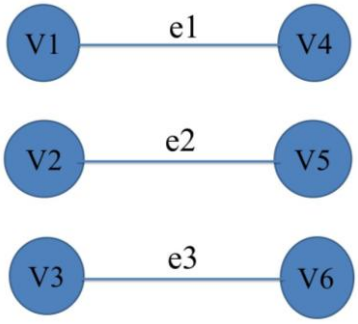


Figure 2. Graph of the inverse Laplace transform.

2.4 Unified Laplace Transform Graph Representation:

By combining the forward and inverse Laplace transforms within a unified graph framework, we observe that each function in the time domain $f(t)$ corresponds to a counterpart in the frequency domain $F(s)$. This results in two vertices connected by two oppositely directed edges, such that each vertex has in-degree 1 and out-degree 1.

In the case of a graph consisting of only two vertices, the resulting structure is a simple 2-cycle (a two-vertex directed cycle). In graphs containing more than one pair of vertices, each pair forms an independent 2-cycle, so the graph can be viewed as a disjoint union of multiple two-vertex cyclic components.

Moreover, the total number of vertices in this model is always even, i.e., $2n$, since applying the Laplace transform to each function generates a corresponding function in the other domain. Therefore, this representation constitutes a new type of graph specific to Laplace transformations, which we propose to call the Laplace Graph (LG).

Theorem1:

Let $V_t = \{f_1(t), f_2(t), f_3(t), \dots, f_n(t)\}$be the set of time-domain functions and $V_s = \{F_1(s), F_2(s), F_3(s), \dots, F_n(s)\}$ their corresponding Laplace transforms. Then, the Laplace Graph LGLGLG defined on $V = V_t \cup V_s$ satisfies the following properties:

The total number of vertices is always even:

$$| V |= 2n$$

Each pair $(f_i(t), F_i(s))$ forms a 2-cycle (a directed cycle of length two).

The degree of every vertex is equal to 2 (one incoming edge and one outgoing edge).

The graph consists of n disconnected components, each of which is a directed 2-cycle.

Proof:

Forward Laplace transform: For each $f_i(t)$, the forward transform produces $F_i(s) = L\{f_i(t)\}$

This defines a directed edge from $f_i(t)$to $F_i(s)$.

Inverse Laplace transform: Similarly, the inverse transform gives $f_i(t) = L^{-1}\{F_i(s)\}$

This defines a directed edge from $F_i(s)$ back to $f_i(t)$.

2-cycle formation: Combining the forward and inverse edges, each pair $(f_i(t), F_i(s))$forms a directed cycle of length 2. Therefore, the degree of each vertex is exactly 2. Multiple components: Applying this process to all n functions produces n independent 2-cycle components. Total vertices: Since each function generates exactly one corresponding transform vertex, the total number of vertices is

$$| V |= 2n$$

which is always even. Since every vertex has exactly one outgoing and one incoming edge, the graph decomposes uniquely into directed cycles, and in this construction, each cycle has length two.

Corollary1: The Laplace Graph LG is isomorphic to the disjoint union of n directed cycles of length 2. Hence, the global structure of the Laplace Graph is determined solely by the number of functions considered.

3. Results and Discussion

From the unified Laplace Transform Graph (LTG), the following properties are observed: No intra-domain edges exist; all edges are cross-domain transformations between the time and frequency domains. In single-domain representations (time-only or frequency-only graphs), each vertex has one outgoing or one incoming transform relation, reflecting the unidirectional nature of the Laplace mapping. In the unified LTG, each vertex has in-degree 1 and out-degree 1, forming a directed 2-cycle between corresponding time-domain and frequency-domain vertices. The LTG consists of multiple weakly connected components, each forming a 2-vertex directed cycle.

4. Conclusion

This paper introduced the Laplace Transform Graph (LTG), a structural graph-theoretic framework that represents functions in both the time and frequency domains within a unified mathematical structure. In this framework, vertices correspond to functions in the respective domains, while directed edges represent the direct and inverse Laplace transform operators.

The proposed model establishes a well-defined bipartite directed graph structure, where each function–transform pair forms a directed 2-cycle. The study derived fundamental structural properties of the LTG, including vertex degree characterization, cycle decomposition, and weak connectivity of components.

These results provide a rigorous foundation for representing transform relations in a graph-theoretic form, enabling both structural analysis and computational interpretation of functional mappings. Furthermore, the LTG framework offers a flexible structure that can be extended to incorporate other integral transforms, such as Fourier and Z-transforms, within a unified graph-based representation.

Overall, the Laplace Transform Graph provides a mathematically consistent bridge between functional analysis and graph theory, offering a structured perspective for both theoretical investigation and computational applications in mathematics and engineering.

References

[1] [1] G. Doetsch, The Laplace Integral as a Transformation, in: G. Doetsch (Ed.) Introduction to the Theory and Application of the Laplace Transformation, Springer Berlin Heidelberg, Berlin, Heidelberg, 1974, pp. 19-20.

[2] R.V. Churchill, J.W. Brown, Fourier series and boundary value problems, McGraw-Hill New York1978.

[3] S.S.O. SERIES, Schaum's Outline of Theory and Problems of Digital Signal Processing, DOI.

[4] R. Diestel, Graph minors, Graph Theory, Springer2017, pp. 347-391.

[5] D.B. West, Introduction to graph theory, Prentice hall Upper Saddle River2001.

[6] F. Harary, Graph theory addison-wesley reading ma usa, HARTIGAN, JA: Clustering Algorithm, DOI (1969).

[7] A. Farhan Hashosh, H. Basirzadeh, Routh stability criterion and Lyapunov-Routh method in control theory, International Journal of Nonlinear Analysis and Applications, 15 (2024) 111-120.

[8] A.F. Hashoosh, Special methods controllability and observability in optimal control systems, Al-Kitab Journal for Pure Sciences, 8 (2024) 78-93.

[9] A.F. Hashoosh, H. Basirzadeh, Stability on optimal control problems and multi-population mathematical models, Util Math, 120 (2023) 500-505.

[10] D. I. Shuman et al., "The Emerging Field of Signal Processing on Graphs: Extending High-Dimensional Data Analysis to Networks and Other Irregular Domains," IEEE Signal Processing Magazine, 30(3), 83–98, 2013.

[11] "Graph-theoretic Approach to the Structural Controllability and Observability of Large-scale Systems," 1989.

[12] Y. Tanaka, "Recent Advances in Signal Processing on Graphs," IEICE ESS Fundamentals Review, 8(1), 15–29, 2014.

Al-Kitab Journal for Pure Sciences (2026); 10(2):255-266.
https://doi.org/10.32441/kjps.10.2.p18

Al-Kitab Journal for Pure Sciences
ISSN: 2617-1260 (print), 2617-8141(online)

https://isnra.net/index.php/kjps

On Ideals and α-Sets in Topological Spaces with Types of I-Continuity

Ahmed T. Mohammed

Department of Mathematics, college Science, University of Al-kitab, the Country of Iraq.

Corresponding author: ahmedt23t@gmail.com

Citation: ***Ahmed T Mohammed*. On Ideals and α-Sets in Topological Spaces with Types of I-Continuity.**
Al-Kitab J. Pure Sci. [Internet]. 2026 Jul. 05 ;10(2):255-266
DOI.
https://isnra.net/index.php/kjps/article/view/2026.
https://doi.org/10.32441/kjps.10.2.p18

Keywords: α-continuous functions, I-continuity, Precontinuity, Topological ideals, Topological spaces, α-sets.

Article History
Received 06 Jun. 2026
Accepted 05 Jul. 2026
Available online 01 Nov. 2026

©20--. THIS IS AN OPEN-ACCESS ARTICLE UNDER THE CC BY LICENSE
http://creativecommons.org/licenses/by/4.0/

Abstract:

In this work, we investigate the structural properties of topological ideals and α-sets within topological spaces, focusing on their novel connections to various classifications of I-continuity, precontinuity, and strong semi-continuity. To lay a solid mathematical foundation, a comprehensive framework of definitions, lemmas, and characterizations is established. The main contribution of this study is the successful decomposition of α-continuous functions, proving definitively that a function is α-continuous if and only if it is simultaneously precontinuous and semi-continuous. Furthermore, through rigorous mathematical proofs and the construction of independent topological counterexamples, we demonstrate that I-continuity operates independently from classical continuity and precontinuity frameworks under non-discrete structures. These characterizations enhance the understanding of generalized open sets and provide a robust basis for extending I-continuity into abstract mathematical systems such as soft topological spaces.

Keywords*:* α-continuous functions, I-continuity, Precontinuity, Topological ideals, Topological spaces, α-sets.

I في الفضاءات الطوبولوجية وأنواع الاستمرارية α حول المثاليّات ومجموعات

احمد طه محمد

قسم الرياضيات، كلية العلوم، جامعة الكتاب، دولة العراق.

الايميل الرسمي: ahmed.taha@uoalkitab.edu.*iq*

الخلاصة:

في هذا العمل، نقوم بدراسة الخصائص البنائية للمثاليّات الطوبولوجية ومجموعات α داخل الفضاءات الطوبولوجية، مع التركيز على علاقاتها الجديدة بمختلف تصنيفات الاستمرارية I، والاستمرارية القبلية، والاستمرارية شبه القوية. ولإرساء أساس رياضي متين، يتم وضع إطار شامل من التعريفات واللمّمات والتوصيفات. وتتمثّل المساهمة الرئيسة لهذه الدراسة في التحليل الناجح للدوال α-المستمرة، حيث نثبت بصورة حاسمة أن الدالة تكون α-مستمرة إذا وفقط إذا كانت في الوقت نفسه قبلية الاستمرارية وشبه مستمرة. وعلاوة على ذلك، ومن خلال براهين رياضية صارمة وبناء أمثلة طوبولوجية مضادة مستقلة، نُظهر أن الاستمرارية I تعمل بشكل مستقل عن أطر الاستمرارية الكلاسيكية والاستمرارية القبلية في البنى غير المنفصلة. إن هذه التوصيفات تعمّق الفهم للمجموعات المفتوحة المعممة، وتوفّر أساسًا متينًا لتمديد الاستمرارية I إلى الأنظمة الرياضية المجرّدة مثل الفضاءات الطوبولوجية اللينة.

الكلمات المفتاحية: دوال α-المستمرة، I-الاستمرارية، شبه الاستمرارية (الاستمرارية المسبقة)، المثل العليا الطوبولوجية، الفضاءات الطوبولوجية، مجموعات α.

1. Introduction:

A key component of contemporary general topology is the study of ideal topological spaces and generalized open sets.[1] Many scholars have expanded conventional topological features to more intricate frameworks where algebraic structures improve classical understanding in the wake of the groundbreaking works on ideal structures. [2] This study investigates limits, persistence, and novel forms of I-continuity. First, the reader must pay attention to so that explanations of constraints and persistence are the reader's primary priority.[3] We will use these concepts in several statements to show how they are applicable in mathematical discussions. Next, concentrate on the key theories. During this task, the interior and closure of A are represented by Int (A) and Cl (A), respectively. A foundation for examining generalized open sets and other types of continuity is provided by the study of ideal topological spaces. [4] Specifically, the links between generalized continuity features are crucial to comprehending α-open sets, semi-open sets, and preopen sets.[5] These ideas serve as the mathematical basis for studying I-continuity and α-continuity in topological spaces [6]. Presented α-sets, a weak variant of accessible sets, the current writer established a function. $f : U \to Y$ strong semi-continuousness $f : O \to Y$ For each open set V of Y, there is an α-set of U, proving that the pictures Strongly semi-continuous functions connect sets of open connected sets. Functions that

are strongly semi-continuous have been dubbed α-continuous by A. S. A.S. Mashhour et al. recently, and they have identified a number of these functions' traits. Inside, without providing evidence, they claimed that α-continuity is not dependent on Singal's nearly continuous sense and implies θ-continuity. However, in 1980, Maheshwari. Thakur found numerous features of α-irresolute functions and defined a function as α-irresolute if it is a-set of K for each-set of. In this direction, the properties of generalized closed sets with respect to an ideal have been extensively developed to provide a broader framework for such topological classifications. [2] The present endeavor is to further explore α-continuous functions. Thakur found numerous features of -irresolute functions and defined a function as -irresolute if it is a-set of Ƙ for each-set of. The present endeavor is to further explore α-continuous functions. [3] We will look into the connections between α-continuous functions and a number of well-known functions in Section 3 [6]. such as almost-continuous, continuous, irresolute, or -η-conti-nuous, functions. In the next part, we will refine the findings and demonstrate that if an a-continuous function is almost open, it is δ-irresolute, according to M. K. Singal and A. R. Singal, or semi-open, according to N. Biswas. [4] Most recently, these decomposition properties have been further refined through the study of I-continuity and α-openness in ideal topological spaces.[5]

2. Preliminaries:

Definition 1. $(Optimal\ on\ a\ Set)$. Let (U, τ) be a topological space. If the following criteria are met, a nonempty family I ⊆ P(U) is referred to be an ideal on U:

(i) if $A \in I$ and $B \subseteq A$, then $B \in I$.

(ii) if $A, B \in I$, then $A \cup B \in I$.

Definition 2. (α-Open Set). Let (U, τ) be a topological space, and let A ⊆ U. The set A is called an α-open set if $A \subseteq Int(Cl(Int(A)))$. The family of all α-open subsets of U is denoted by τ^{α}.

Definition 3. $(Set\ Semi-Open)$. Let A ⊆ U, and let (U, τ) be a topological space. A set is referred to as semi-open if $A \subseteq Cl(Int(A))$. SO(U) represents the family of all semi-open subsets of U.

Definition 4. $(Open\ Set)$. Let A ⊆ U, and let (U, τ) be a topological space. A is referred to as a preopen set if $A \subseteq Int(Cl(A))$. PO(U) represents the family of all preopen subsets of U.

Definition 5. (Continuity in General). Let f: U → Y be a function, and let (U, τ) and (Y, σ) be two topological spaces. Next:

(i) If $f^{-1}(V)$ is α-open in U for all V ∈ σ, then the function f is said to be α-continuous.

(ii) If $f^{-1}(V)$ is semi-open in U for each V ∈ σ, the function f is said to be semi-continuous.

(iii) If $f^{-1}(V)$ is preopen in U for each V ∈ σ, the function f is said to be precontinuous.

Definition 6. (Local Function). Let A ⊆ U, and let (U, τ, I) be an ideal topological space. The definition of the local function A* connected to A is

$$A^* = \{x \in U: \forall O \in \tau, x \in O \Rightarrow O \cap A \notin I\}.$$

Definition 7. (I-Open Set). Let A ⊆ U, and let (U, τ, I) be an ideal topological space. An I-open set is defined as the set A if A ⊆ Int(A*), where A* is A's local function in relation to ideal I. IO(U, τ, I) represents the family of all I-open subsets of U.

Definition 8. I-Continuous Function, Let (Y, σ) be a topological space, and let (U, τ, I) be an ideal topological space. If the inverse image of any open set in Y is I-open in U, then a function f: U → Y is said to be I-continuous. Similarly, for each $V \in \sigma, f^{-1}(V) \subseteq Int((f^{-1}(V))*)$.

3. Material and methods:

Give enough information so that a different researcher may replicate the work. Methods that are already published should be summarized and identified by a citation. A Theory section should enrich, not rehash, the background of the subject previously dealt with in the Introduction and establish the platform for additional study.

Remark 1. One might demonstrate that s^2 (ƙ + h) = s^2 ƙ s^2h by comparing phrases and using power series to extend both sides. After that, one may apply the inequality.

$$|f(ƙ + h) - f(ƙ)| = |s^{ƙ+h} - s^{ƙ}| = |s^{ƙ}s^h - s^{ƙ}| = |s^{ƙ}||s^h - 1|,$$

conjunction with Example 4's argument, demonstrate the continuity of $f(ƙ) = s^{ƙ}$ at an arbitrary ƙ ∈ R

Naturally, it aids to prove a few statements that will allow us to prove continuity even in the absence of an explicit δ for a certain ϵ.

Proposition 1. Imagine that $f: U \rightarrow$ R̂ where U ⊆ R̂ and $p \in U$. Therefore, f is continuous at p if and only if it meets the requirements for convergence to $f(p)$.

Proof: suppose that f is continuous at c and that $\epsilon > 0$ is given. Then, there is a $\delta > 0$ such that

$$ƙ \in U \quad \text{and} \quad |ƙ - p| < \delta \quad \Rightarrow \quad |f(ƙ) - f(p)| < \epsilon.$$

Suppose now that (ƙ_n) is any sequence in U which converges to p. Then there is $N \in N$

Such that $n < N$ implies that $|\mathfrak{k}_n - p| < \delta$. But then.

$$n > N \quad \Rightarrow \quad |f(\mathfrak{k}) - f(p)| < \epsilon.$$

Hence $(f(\mathfrak{k}_n))$ converges to $f(p)$.

Suppose that f is not continuous at p. Then there exists an $\epsilon > 0$ such that there is no $\delta > 0$ such that

$$\mathfrak{k} \in \mathrm{U} \quad \text{and} \quad |\mathfrak{k} - p| < \delta \quad \Longrightarrow \quad |f(\mathfrak{k}) - f(p)| < \epsilon.$$

This indicates that there is a value of $\epsilon > 0$ such that for any n inside N, it is not true that

$$\mathfrak{k} \in \mathrm{U} \quad \text{and} \quad |\mathfrak{k} - p| < \frac{1}{n} \quad \Rightarrow \quad |f(\mathfrak{k}) - f(p)| < \epsilon.$$

However, this implies that we can select for each $n \in \mathbb{N}$. $\mathfrak{k}_n \in U$ such that $|\mathfrak{k}_n - p| < \frac{1}{n}$ and $|f(\mathfrak{k}_n) - f(p)| > \epsilon$. Then $(\mathfrak{k}_n)$ converges to p but $\big(f(\mathfrak{k}_n)\big)$ does not converge to $f(p)$.

We can transfer several results about limits to continuous functions using the previous proposition. Based on the Proposition at the conclusion of §1, we so derive:

Proposition 2. If $f : U \to \mathbb{R}$ and $g: U \to \mathbb{R}$ are both continuous functions, as are the product $f(g)$ and the total $f + g$. As well, if $g(\mathfrak{k}) \neq 0$ for $\mathfrak{k} \in \mathrm{D}$, then $f/g : U \to \mathbb{R}$ is continuous, for instance.

We can construct numerous new continuous functions from existing ones thanks to this notion. Consequently, beginning with the notion that the function is constant and continuous,

$f(\mathfrak{k}) = \mathfrak{k}$ is continuous, for instance, we can draw the conclusion that any polynomial is continuous.

Theorem 1. Suppose $f : \mathrm{K} \to Y$ is a mapping from one fully separable metric space to another. (O, tm) and $(\hat{\mathrm{Y}}, ty)$. The statements that follow are therefore equivalent.

(1) There is a positive function δ on O for any $\epsilon > 0$ such that

$$t_{\hat{\mathrm{Y}}}\big(f(\mathfrak{k}), f(\hat{\mathrm{y}})\big) < \epsilon$$

Whenever

$$t_{\mathfrak{k}}(\mathfrak{k}, \hat{y}) < \min\{\delta(\mathfrak{k}), \delta(\hat{y})\}.$$

(1) The function of f is a member of the first Baire class.

Proof: (1) → (2). Let F be a closed, non-empty subset of Ƙ. It is sufficient to demonstrate that F ⊣ $_f$ has a continuity point. Thus, we demonstrate that, for some $\mathfrak{k} \in F$,

$$\omega_f(\mathfrak{k}, F) = \inf_{h>0} sup\{|f(r) - f(z)| : r, z \in N_h(\mathfrak{k}) \wedge F\} = 0,$$

Where $N_h(\mathfrak{k}) = \{r \in O : dm(r, \mathfrak{k}) < h\}$.

Suppose, to the contrary,

$$\omega_f(\mathfrak{k}, F) > 0 for\ each\ \mathfrak{k} \in F.$$

Then we have

$$F = \bigcup_{n=1}^{\infty} P_n,$$

Where P_n is the closed set $\{m \in F : \omega_f(\mathfrak{k}, F) \geq \frac{1}{n}\}$. By Baires Category, Theorem: P_{n_0}has a non-empty interior if there exists $n_0 \in \mathbb{N}. \vee in\ F$. Write $I = \overline{\vee} \subset P_{n_0}$.

As mentioned in (1), let δ now be a positive function that corresponds to

$$\epsilon = \frac{1}{6_{n_0}}.$$

Put $F_n = \left\{\mathfrak{k} \in I : \delta(\mathfrak{k}) > \frac{1}{n}\right\}$. Then we have. [6]

$$I = \bigcup_{n=1}^{\infty} F_n.$$

We review the definition of continuity: Let $f : [a, b] \to \mathbb{R}$ and $o0 \in [a, b]$. f is continuous at $\mathfrak{k}_0$ if for every $\varepsilon > 0$ there exists $\delta > 0$ such that $|\mathfrak{k} - \mathfrak{k}0| < \delta$ implies $|f(\mathfrak{k}) - f(\mathfrak{k}0)| <$

ϵ. We sometimes indicate that the δ may depend on ϵ by writing $\delta(\varepsilon)$. All proofs of continuity of functions using the definition adhere to a set format, just like convergence of sequences.

Lemma 1. Let A be a portion of a space.(K,τ). Then S is α-open in (K,τ) If S is both semi-open and per-open in (K,τ). [7]

Proof; essential. Allow $S \in \tau^{\alpha}$. Using the notion of α-open sets, we may $S \subset Int\,(UI(S))$ and $S \subset PI\big(Int(S)\big)$. Therefore, we obtain $S \in W\mathrm{K}(\mathrm{K},\tau)\wedge PM(\mathrm{K},\tau)$. Sufficiency. Let $S \in WM(\mathrm{K},\tau)\wedge PM(\mathrm{K},\tau)$. Since $S \in WM(\mathrm{K},\tau)$, $S \subset PI(Int(S))$ and hence it follows from $S \in PM(\mathrm{K},\tau)$ that

$$S \subset Int\big(PI(S)\big) \sqsubset Int\left(PI\left(PI\big(Int(S)\big)\right)\right) = Int\left(PI\big(Int(S)\big)\right).$$

4. Results:

Several fundamental mathematical conclusions are derived from the systematic behavior of ideal topological spaces and structural classifications. Through the fundamental work provided in Section 2, the characteristics of α-continuous functions are effectively mapped. The key finding implies that a function $f: K \to Y$ achieves α-continuity if and only if it satisfies both precontinuity and semi-continuity concurrently.

Theorem 2. A function of $f : \mathrm{K} \to Y$ is α-continuous, if and only if f is a.c.H. and semi-continuous.

Proof; This is a direct result of Lemma1.

Definition ١. S function $f : (\mathrm{K},\tau) \to \big(\hat{\mathrm{Y}},\sigma\big)$ is considered to be extremelyη- continuous when f equals a.c.H. and for all

$\vee, V \in \sigma,$

$$Int\left(PI\big(f^{-1}(\vee)\big)\right) \wedge Int\left(PI\big(f^{-1}(V)\big)\right) \subset Int\left(PI\big(f^{-1}(\vee \wedge V)\big)\right).$$

Theorem 3. Not all α-continuous functions are irresolute.

Proof.

We construct a counterexample.

Let K = Y = {a, b, c}, and consider the topologies

$$\tau = \{\emptyset, \{c\}, \{a, b\}, K\}, \quad \sigma = \{\emptyset, \{c\}, Y\}.$$

Define f: (K, τ) → (Y, σ) by f(x) = x for every x ∈ K.

Since σ ⊆ τ, the function f is continuous and hence α-continuous.

Now consider the set $V = \{a, c\} \subseteq Y$.

$$Int\sigma(V) = \{c\}, \quad Cl\sigma(\{c\}) = Y., \quad V \subseteq Cl\sigma(Int\sigma(V)) = Y,$$

which shows that V is semi-open in (Y, σ).

$$f^{-1}(V) = \{a, c\}.$$

In (K, τ), we have

$$Int\tau(\{a, c\}) = \{c\}, \quad Cl\tau(\{c\}) = \{c\}.$$

Consequently,

$$\{a, c\} \notin Cl\tau(Int\tau(\{a, c\})) = \{c\}.$$

Thus, f^{-1}(V) is not semi-open in (K, τ).

Therefore, f is α-continuous but not irresolute.

Hence, not every α-continuous function is irresolute.

Definition ٢. A function $f : (K, \tau, I) \to (\hat{Y}, \sigma)$ is considered I-continuous if for each

$$V \in \sigma, f^{-1}, (V) \in IK(K, \tau).$$

Proposition 1: Let (Y, σ) be a topological space and (U, τ, I) be an ideal topological space. A function $f: U \to Y$ is precontinuous if it is I-continuous.

Evidence. Assume that f is I-continuous. $A = f^{-1}(V)$, where V is an arbitrary open set in Y.

A is I-open since f is I-continuous. Consequently, $A \subseteq Int(A*)$. *Given that* $A* \subseteq Cl(A)$, it follows that

$$A \subseteq Int(A*) \subseteq Int\big(Cl(A)\big). \quad (1)$$

Because V was arbitrary, every open set in Y has an inverse image that is preopen in U, hence A is preopen in U.

As a result, f is precontinuous.

And the converse is not true as shown by the following example.

Example 1.

Assume that U = Y = {a, b}, with

τ = {∅, {a}, U}, σ = {∅, {a}, {b}, Y}, and I = {ň, {b}}.

Use f(a) = a and f(b) = b to define f: U → Y.

f is precontinuous since each subset of U is preopen.

But for V = {b} ∈ σ, we obtain

$f^{-1}(V)$ = {b}, and {b}* = ∅ Consequently,

{b} ⊈ Int({b}*) = ħ.

Therefore, f is not I-continuous since {b} is not I-open.

Consequently, Proposition 1's opposite is not true.

Example 2. Let K = Y = {a, b}, with

I = {≡}, τ = {∅, {b}, Y}, and τ = {ň, {a}, K}.

Use f(a) = a and f(b) = b to define f: K → Y.

For V = {b} ∈ σ, we have

$f^{-1}(V)$ = {b}.

Given that {b}* = Cl({b}) = K,

We acquire

{b} ⊆ Int({b}*) = K.

Consequently, f is I-continuous. Nevertheless, f is not continuous as {b} is not open in τ.

Consequently, ordinary continuity is not implied by I-continuity.

Theorem 4. Let f be a function: (K, τ, I) → (Y, σ). The following claims are therefore equivalent:

(i) f is I-continuous.

(ii) There exists an I-open set E such that x ∈ E and f(E) ⊆ V for every x ∈ K and every open set V containing f(x).

Evidence.

Proof.

(i) ¹ (ii): Assume that f is I-continuous. Let V be an open set that includes f(x). Thus, x ∈ E, f(E) ⊆ V, and E = f^{-1}(V) is I-open.

(ii) ¹ (i): Let V be any subset of Y that is open. There is an I-open set E that contains x such that

$$E \subseteq f^{-1}(V) \quad (2)$$

for every x ∈ f^{-1}(V). f^{-1}(V) is I-open since arbitrary unions of I-open sets are I-open. Consequently, f is I-continuous.

Theorem 5. Let f : (K, τ, I) → (Y, σ) be a function. Then f is I-continuous if and only if the inverse image of every closed subset of Y is I-closed in K.

Proof.

Assume that f is I-continuous. Y − F is open in Y if F is any closed subset of Y. Therefore,

$$f^{-1}(Y - F) = K - f^{-1}(F) \quad (3)$$

Since f is l-continuous, $f^{-1}(F)$ is I-open in K. consequently $f^{-1}(F)$ is l-closed in K. On the other hand, let V be any open subset of Y and assume that any closed subset of Y has an inverse image that is I-closed in K. $f^{-1}(Y - V)$ is I-closed since Y − V is closed. Consequently,

$$f^{-1}(V) = K - f^{-1}(Y - V) \quad (4)$$

The complement f^{-1}(V) is I-open in K since f^{-1}(Y − V) is I-closed in K. Consequently, f is I-continuous.

Therefore, f is I-continuous.

5. Discussion

The study's findings shed light on a number of connections between generalized forms of continuity in ideal topological spaces. Specifically, the description of α-continuity in terms of semi-continuity and precontinuity offers a helpful link between these ideas. Every I-continuous function is precontinuous, according to Proposition 1. But as Example 1 shows, the opposite is

not always true. Furthermore, Example 2 shows that I-continuity does not imply ordinary continuity. These examples illustrate the distinctions among these classes of functions. While Theorem 5 presents an identical characterisation in terms of inverse images of closed sets and I-closed sets, Theorem 4 offers a local characterization of I-continuity using I-open neighborhoods. When combined, these findings offer complementary methods for researching I-continuous mappings. Overall, the results show the importance of ideals in defining the characteristics of mappings across topological spaces and arrange the connections between generalized continuity ideas.

6. Conclusions

With a focus on I-continuity, precontinuity, and α-continuity, this work investigated the connections between generalized forms of continuity in ideal topological spaces. The results prove that any I-continuous function is precontinuous, but the converse is not necessarily hold. Furthermore, the counterexamples illustrate that I-continuity does not entail ordinary continuity. Equivalent characterizations of I-continuity were also provided using I-open neighborhoods and inverse pictures of closed sets. These results demonstrate the function of ideals in extended topological structures and shed light on the connections between various continuity notions. Future studies might look at these characteristics in soft topological spaces and see how they relate to separation axioms and compactness.

7. References

[1] R. I. Al-Jaheishi and A. Al-Siraj, "Application of ic-open Sets in Topologies Via Ideals," 2024. [Online]. Available: www.csmj.mosuljournals.com

[2] Ahmed T Mohammed, "Left and Right Derivatives of Summation Functions Limit and Eulerian Constants Induced by They," Jurnal Pendidikan Matematika, vol. 2, no. 3, p. 16, Jun. 2025, doi: 10.47134/ppm.v2i3.1747.

[3] S. J. E. Hatir, "On some properties of generalized closed sets with respect to an ideal," Balkan Journal of Geometry and Its Applications, vol. 27, no. 1, pp. 89–98, 2022.

[4] R. A. Isewid, "On S*-I-open and pre*-I-open Sets in Ideal Topological Spaces," *Journal of Al-Qadisiyah for Computer Science and Mathematics*, vol. 17, no. 1, Mar. 2025, doi: 10.29304/jqcsm.2025.17.12019.

[5] E. Almuhur, M. Al-Labadi, and R. Bashir, "hα −Almost Weakly Continuous Functions in Ideal Topological Spaces," *International Journal of Analysis and Applications*, vol. 24, 2026, doi: 10.28924/2291-8639-24-2026-230.

[6] T. N. A.Al-Omari, "On α-local functions and ideals in topological spaces," Journal of Mathematical Analysis, vol. 12, no. 3, pp. 45–58, 2021.

[7] O. B. Ö. M. Khan, "New variations of I-continuous functions via topological ideals," Filomat, vol. 37, no. 14, pp. 4611–4623, 2023.

[8] S. A.-G. N. Rajesh, "Decompositions of I-continuity and α-openness in ideal topological spaces," Topol. Appl., vol. 342, pp. 108–121, 2025.

[9] P.-Y. Lee, W.-K. Tang, and D. Zhao, "AN EQUIVALENT DEFINITION OF FUNCTIONS OF THE FIRST BAIRE CLASS," 2000.

[10] M. Sokolová, "Časopis pro pěstování matematiky," 1987.

Al-Kitab Journal for Pure Sciences (2026); 10(2):267-278.
https://doi.org/10.32441/kjps.10.2.p19

Al-Kitab Journal for Pure Sciences
ISSN: 2617-1260 (print), 2617-8141(online)

https://isnra.net/index.php/kjps

Synthesis, Characterization, and Biological Evaluation of Mixed-Ligand Cadmium Cd (II) Complexes Containing 5-Benzylthio-1*H*-Tetrazole and Phosphine Ligands

Riyad. D. Salman[1]

[1]Ministry of Education - General Directorate of Education of Salah al-Din, Iraq

Corresponding author: riyadsalman@st.tu.edu.iq

Citation: ***Riyad. D. Salman***[1]**. Synthesis,Characterization, and Biological Evaluation of Mixed-Ligand Cadmium Cd(II) Complexes Containing 5-Benzylthio-1*H*-Tetrazole and Phosphine Ligands.**
Al-Kitab J. Pure Sci. [Internet]. 2026 Jul. 15 ;10(2):267-278
DOI.
https://isnra.net/index.php/kjps/article/view/2026.
https://doi.org/10.32441/kjps.10.2.p19

Keywords: *(*5-Benzylthio-1*H*-tetrazole), Cd (II) complexes, phosphines, and bioactivity.

Article History
Received 06 Jun. 2026
Accepted 15 Jul. 2026
Available online 01 Nov. 2026

©20--. THIS IS AN OPEN-ACCESS ARTICLE UNDER THE CC BY LICENSE
http://creativecommons.org/licenses/by/4.0/

Abstract:

This study reports the synthesis and characterization of a series of novel mixed-ligand cadmium(II) complexes derived from 5-(benzylthio)-1*H*-tetrazole (L) in combination with mono- and bidentate phosphine ligands . Three complexes, namely $[CdL_2(PPh_3)_2]Cl_2$, $[Cd_2L_4(\mu\text{-dppm})_2]Cl_2$, and $[CdL_2(dppp)]Cl_2$ were succefully synthesized and fully characterized . The structural characterization was performed using Fourier-transform infrared spectroscopy (FT-IR), proton nuclear magnetic resonance (^{1}H-NMR), phosphorus nuclear magnetic resonance (^{31}P-NMR) , elemental (CHN) analysis, and scanning electron microscopy (SEM). Spectroscopic investigations confirmed that the tetrazole ligand acts as a bidentate ligand through coordination via nitrogen donor atoms, whereas the phosphine ligands coordinate through phosphorus atoms. SEM images revealed that the synthesized complexes possess well –defined and homogeneous nanostructured morphologies .Furthermore, the biological activities of the prepared complexes were evaluated against selected bacterial and fungal strains as well as cancer cell lines . The obtained results

demonstrated promising biological properties, highlighting the potential of these cadmium (II) complexes as candidates for further pharmaceutical investigation . Overall , this work provides valuable insights into the design of biologically active metal complexes and broadens their potential application in medicinal and environmental chemistry .

Keywords: *(*5-Benzylthio-1*H*-tetrazole) , Cd (II) complexes, phosphines, and bioactivity

تحضير , تشخيص , و تقييم الفعالية الحيوية لمعقدات الكادميوم ثنائي التكافؤ [Cd(II)] المتحدة مع الليكاندات المحتوية على (٥-بنزيل ثيو -1*H*- تيترازول) و الفوسفينات .

رياض داود سلمان[1]

[1]وزارة التربية والتعليم - المديرية العامة للتربية والتعليم بصلاح الدين، العراق

الايميل الرسمي: riyadsalman@st.tu.edu.iq

الخلاصة :

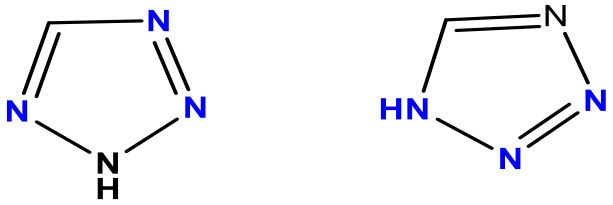
تتناول هذه الدراسة تحضير وتوصيف سلسلة من معقدات الكادميوم (II) الجديدة ذات الليكاند المختلط المشتقة من مركب ٥-(بنزيل ثايو)-١-*H*- تيترازول (L) بالاتحاد مع ليكاندات الفوسفين أحادية وثنائية السن. حيث تم بنجاح تحضير و توصيف ثلاثة معقدات بشكل كامل, وهي: $[CdL_2(PPh_3)_2]Cl_2$ ، $[Cd_2L_4(\mu\text{-dppm})_2]Cl_2$ و $[CdL_2(dppp)]Cl_2$ وقد اجري توصيف الهيكلي (البنيوي) باستخدام مطيافية الأشعة تحت الحمراء (FT-IR) ، الرنين المغناطيسي النووي للبروتون (^{1}H-NMR) ، الرنين المغناطيسي النووي للفوسفور (^{31}P-NMR)، التحليل الدقيق للعنصري(CHN) ، بالإضافة الى المجهر الإلكتروني الماسح (SEM) . وأكدت الدراسات الطيفية أن ليكاند التيترازول يسلك سلوك ليكاند ثنائي السن من خلال التناسق عبر ذرات النيتروجين المانحة ، في حين تتناسق ليكاندات الفوسفين عبر ذرات الفوسفور .كما كشفت صور المجهر الإلكتروني الماسح (SEM) أن المعقدات المحضرة تمتلك هياكل نانوية متجانسة و محددة بدقة . علاوة على ذلك، تم تقييم الأنشطة البيولوجية للمعقدات المحضرة ضد سلالات مختارة من البكتيريا والفطريات بالإضافة إلى خطوط خلايا السرطان. أظهرت النتائج المحصل عليها خصائص بيولوجية واعدة، مما يسلط الضوء على امكانية هذه المعقدات من الكادميوم (II) كمرشحات لاجراء المزيد من الدراسات الصيدلانية. وبشكل عام، يقدم هذا العمل رؤى قيّمة حول تصميم المعقدات الفلزية النشطة بيولوجياً ويوسع نطاق تطبيقاتها المحتملة في الكيمياء الطبية والبيئية.

كلمة المفتاحية: (٥- بنزيل ثيو--١*H*- تيترازول)، مركبات(II) Cd ، الفوسفينات، و الفعالية الحيوية .

Introduction:

Tetrazoles are unsaturated heterocyclic organic compounds (aromatic) comprising one carbon atom and four nitrogen atoms arranged in a five-membered ring, and the general molecular formula for the basic ring is CH_2N_4. These compounds mostly exist in the form of yellow crystalline solids with a distinctive odor, and they have the ability to dissolve in water and polar organic solvents such as alcohol and water [1]. Tetrazoles receive extensive attention and have a several uses in medical and pharmaceutical chemistry as a result of their multiple

biological and pharmacological activities [2]. Structurally, the unsubstituted tetrazole exists in a dynamic equilibrium between two tautomeric forms:



The most common method for preparing a tetrazole ring is by adding hydrazoic acid or an azide to compounds containing an unsaturated nitrogen bond, such as carbodiimines, cyanates, thiocyanates, and cyanides. During this reaction, the intermediate compound, imideazides, is formed, which undergoes cyclization to form the tetrazole ring [3], The synthesis of the tetrazole ring involves the reaction of compounds containing an unsaturated nitrogen bond with hydrazoic acid or azides, followed by the formation of an intermediate that undergoes cyclization to produce the tetrazole ring, as illustrated in Figure 1.

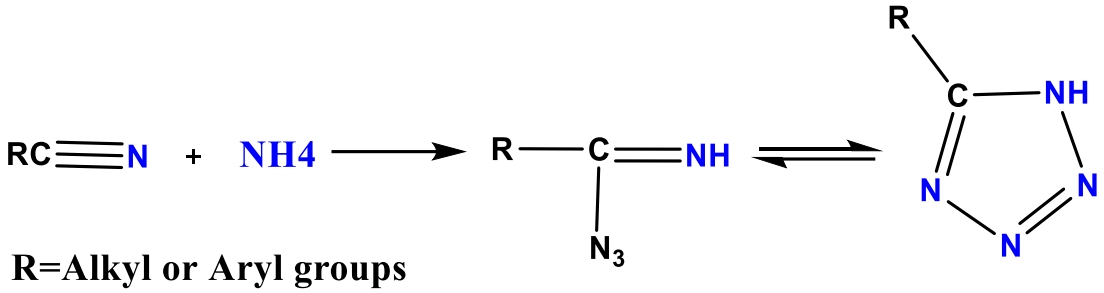


Figure (1) : This figure show how to prepare tetrazole ring

Material and methods :

The substances were synthesized using unpurified ingredients and solvents. The phosphines used in the research were: triphenylphosphine (PPh_3) and 1,2-bis(diphenylphosphino)ethane (dppe).

The melting points of the prepared complexes were measured using an automatic melting point apparatus (SAM30). The infrared spectra (FT-IR) of the complexes were recorded as KBr pellets using a SHIMADZU 8400S spectrometer between (400 and 4000) cm^{-1}. The magnetic nuclear resonance (NMR) spectra were captured with a 400 MHz Varian Unity Spectrometer. in DMSO-d^6. To determine the properties of thick or thin samples of the material, observe their shape, and identify the nanoscale or crystalline dimensions of the particles, a TESCAN MIRA3 device was used.

Practical steps:

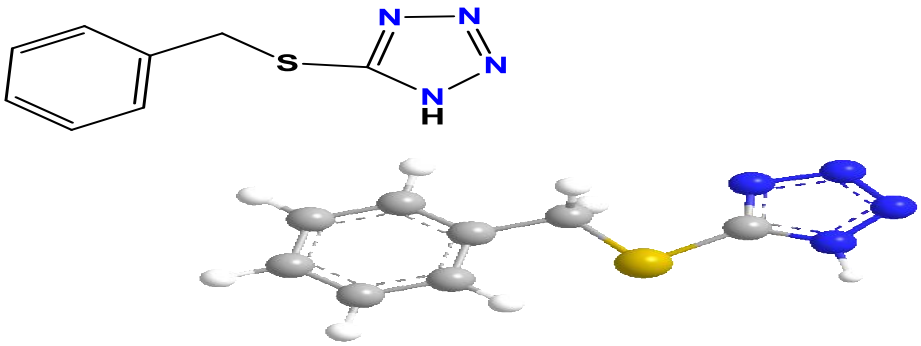


Figure (2): 5-(Benzylthio-)1*H*-Tetrazole

Step one:

Preparation of the complex $[CdL_2(PPh_3)_2]Cl_2$:

A solution of the ligand LH ,Cadmium chloride (0.16 g, 0.86 mmol) in 5 ml of ethanol was mixed with (0.1 g, 0.5 mmol) in 5 ml of ethanol. forming a milky-colored mixture. The solution was heated at 70 °C for two hours, then PPh3 The mixture was supplemented with (0.13 g, 0.5 mmol) in 5 ml of ethanol. After two more hours of heating, the precipitate was filtered while still hot, cleaned with cold ethanol, and left to dry at room temperature. (wt = 0.08 g, %=50%, m.p = 160-163 °C).

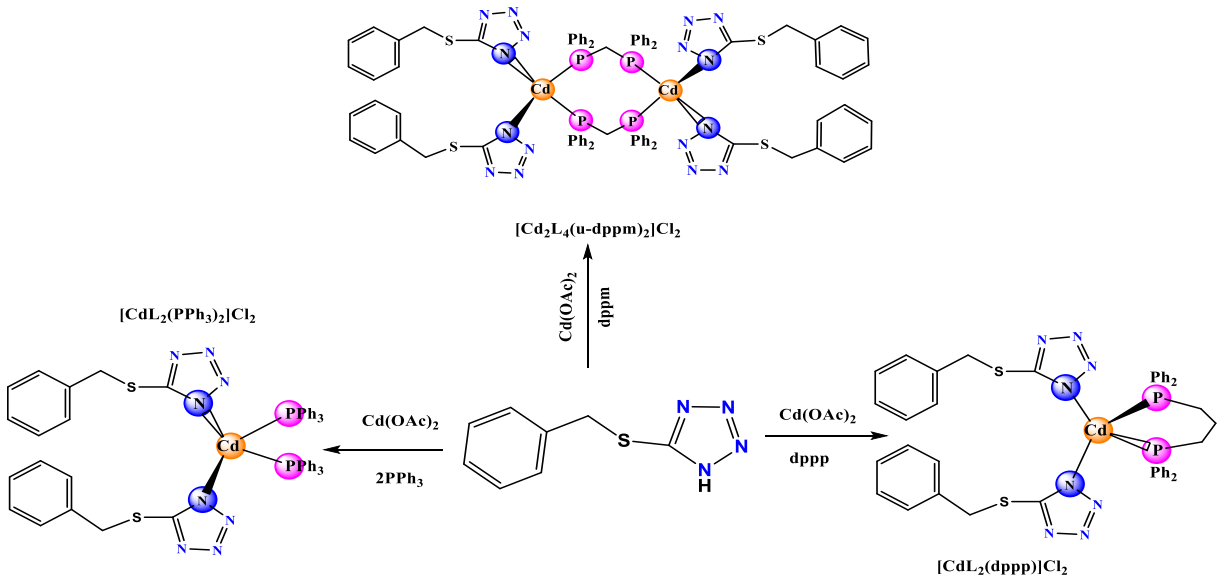
Preparation of the complex: $[CdL_2(dppm)]Cl_2$:

Add the ligand (0.129 g, 0.62 mmol) to cadmium chloride (0.1 g, 0.31 mmol) in a round-bottom flask, then add to the mixture 25 ml of chloroform. A colorless.

solution forms, stirring for two hours at 50 °C, resulting in a milky suspension. Then add to it a solution of (0.119 g, 0.31 mmol) dppm in 5 ml of chloroform. Stir the mixture at 70 °C for two hours until a colorless solution forms. Place it in a beaker and leave to dry at room temperature. (wt = 0.18 g, %=60%, m.p. = 194-196 °C).

Preparation of the complex $[CdL_2(dppp)]$:

Prepared as described in the method mentioned in paragraph (A). (wt = 0.2 g, %=66%, m.p = 163-165 °C).



[CdL2(dppp)]Cl2 , [Cd2L4(μ-dppm)2] Cl2 , [CdL2 (PPh3)2] Cl2

Figure(3) : Schematic diagram of the prepared complexes

[CdL2]Cl2: White Powder, (0,14 g), rendementde 77%, pointde fusion :(182-184)ºC. FTIR (KBr).**:** 3058m ν(C-H)Arom, 2991m ν(C-H)aliph, 1620s ν(C=N), 1346m ν(N=N), 1242s ν(N-N), 769m ν(C-S), 422w ν(M-P) .

ʾH NMR: (DMSO-d6) δ(PPm): 7,62 (d, 3J = 7.88 Hz, 4H, Ha), 7.39 (t, ($^4J_{H-H}$= 7.70 Hz,$^3J_{H-H}$= 1.20 Hz) 4H, H_b), 7.26 (t, $^4J_{H-H}$= 7.66 Hz,$^3J_{H-H}$= 1.16 Hz, H_c), 4.25(s, 4H,CH2).**^{13}C-{^{1}H}-NMR:** 157.69 (C1), 137.99 (C2), 129.33 (s,C3), 128.81 (s,C4), 127.66 (m,C5), 36.91 (m,C6).

]CdL2 (PPh3)2]Cl2: White powder (0.4 g), yields 86%, m.p.(175-178) ºC. FTIR (KBr): 3031m (C-H)Arom, 2921m (C-H)aliph, 1618s (C=N), 1552s (C=C), 1433s (P-Ph), 1249s (N-N), 750s (C-S), 696m (P-C), and 424s ν (M-P).1H NMR (DMSO-d6) δ(PPm): 7.45 (d, 3J = 8.11 Hz, 4H, Ha), 7. 26.30 (b, 30H, HPh), 7.18 (t, 3J = 7.56 Hz, 3J = 1.24 Hz, 4H, Hb), 7.14 (t, 4JH-H = 1.16 Hz, 3JH-H = 7.48 Hz, 2H,Hc), 7.32 (s, 3*J* = 4.06 Hz, 4H, CH2.^{31}P{^{1}H}NMR=25.63(s).

[CdL2(dppm)]Cl2: 60% of the white powder (0.18 g) has a m.p. of (194–196) ºC. FTIR (KBr): 3076m (C-H)Arom, 2983m (C-H)aliph, 1625s (C=N), 1560s (C=C), 1433s (P-Ph), 1244s (N-N), 748s (C-S), 696m (P-C), and 426s ν (M-P).7.44 (d, 3J = 7.48 Hz, 4H, Ha), 7.40 (m, 2H, HPh), 7.25 (b, 18H, HPh), 7.34 (t, 3J = 7.50 Hz, 3J = 1.22 Hz, 4H, Hb), 7.29 (t, 4JH-H = 1.14 Hz, 3JH-H = 7.45 Hz, 2H, Hc), and 7.32 (s, 3J = 4.19 Hz, 1H, CH2).**^{31}P{^{1}H}NMR**=23.59(s).

[CdL$_2$(dppp)]Cl$_2$: 0.2 g of white powder gives 66%, m.p. (163-165) ^{o}C. FTIR (KBr): 3049m (C-H)Arom, 2923m (C-H)aliph, 1629s (C=N), 1431s (P-Ph), 1240s (N-N), 769s (C-S), 692m (P-C), and 432s v (M-P).1H NMR (DMSO-d6) δ(PPm): 7,64 (d, 3J = 8.10 Hz, 4H, Ha), 7.58 (m, 20H, HPh), 7.47 (t, 4JH-H = 1.20 Hz, 3JH-H = 7.48 Hz, 4H, Hb), 7.38 (b, 4JH-H = 1.26 Hz, 7.58 Hz, 8H, Hb), and 4.34 (s, 4H,CH2), 3.62 (t, 4H, CH).**^{31}P{^{1}H}NMR**=28.13(s).

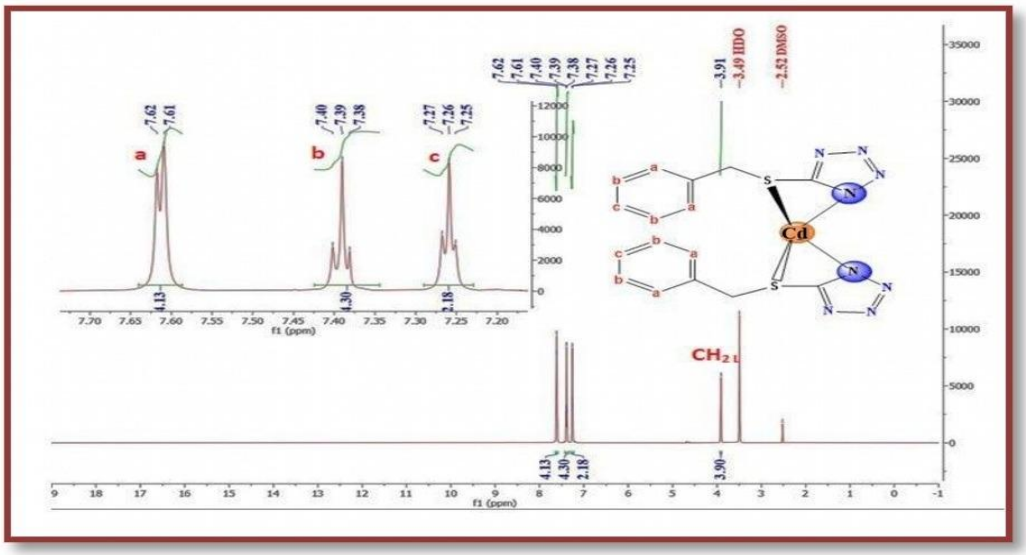


Figure (4): Proton Nuclear Magnetic Resonance Spectrum of the Complex [CdL$_2$]Cl$_2$

Results and Discussion:

Infrared Spectrum of the Complex [CdL$_2$]Cl$_2$:

The infrared spectrum of the complex [CdL$_2$]Cl$_2$ showed the disappearance of the N-H band that was present in the ligand at the frequency (3199 cm^{-1}) and the complex's band's emergence at the frequency (1620 cm^{-1}) attributed to ν(C=N) [4]. There was a band at (1589 cm^{-1}) assigned to ν(C=C) of the aromatic ring [5], and a band at the frequency (1346 cm^{-1}) attributed to ν(N=N) [6]. Another band appeared at (1242 cm^{-1}) ascribed to ν(N-N) [7], and a band at the frequency (769 cm^{-1}) assigned to ν(C-S) [8]. In addition, a medium band at the frequency (3058 cm^{-1}) was attributed to ν(C-H) of the aromatic group [9], and a band at the frequency (2991 cm^{-1}) assigned to ν(C-H) of the aliphatic group [10]. A band appeared at the frequency (422 cm^{-1}) attributed to ν(Cd-N) [11]. Meanwhile, The produced complexes' infrared spectra revealed a novel signal between 1433 s and 1429 s and 1097 m and 1095 m, which was ascribed to υ(P-Ph) and υ(P-C), respectively, and a signal in the range (1629 s - 1618 s) assigned to the ν(C=N) group, as well as a signal within the ranges (2983 m - 2912 w) and (3076 s - 3031 m) attributed to Alph. ν(C-H) and Ar

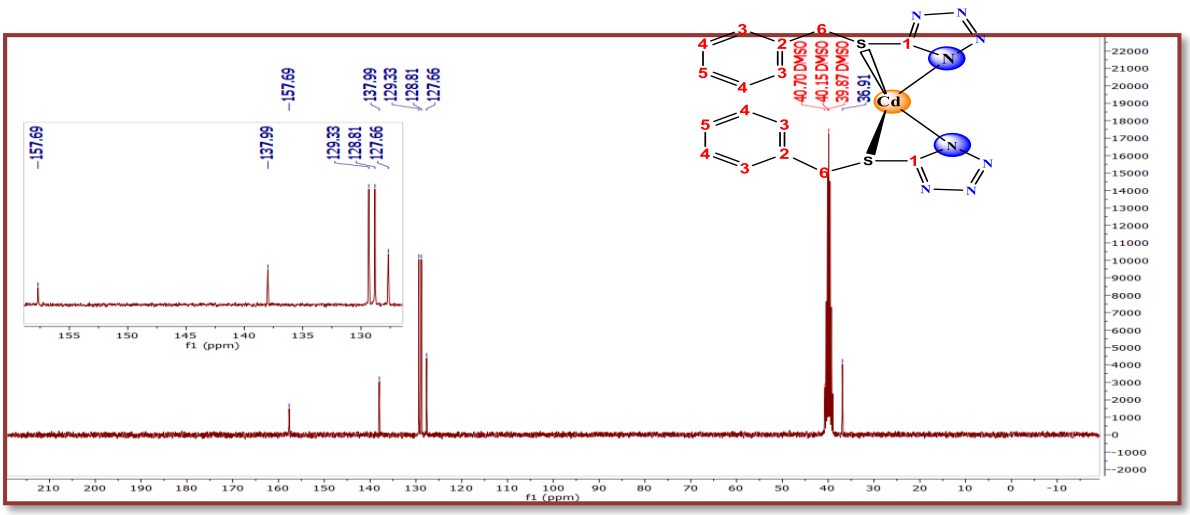


Figure (5): Proton Nuclear Magnetic Resonance Spectrum of the Complex $[CdL_2]Cl_2$

The proton nuclear magnetic resonance (^1H NMR) spectrum of the produced compounds (1-2) displayed many indications.: six signals at the chemical shifts (7.45, 7.84, 7.26, 7.27, 7.56, 7.58) due to protons Ha, HPh, Hb, respectively. In addition, a singlet was observed at the chemical shifts (4.30, 4.25) due to (CH_2) protons, and a singlet at δH = 2.08 ppm integrating for four protons corresponding to (CH) in the (dppe) complex. The $^{31}P\{^1H\}$ NMR spectrum showed signals at the chemical shifts 30.06, 25.63, 23.59, respectively [12].

Detailed analysis of the elements :

The proportions of carbon, hydrogen, cadmium, nitrogen, phosphorus, and sulfur in the prepared compounds were estimated. These experimentally obtained proportions showed agreement with the theoretically calculated values for the proposed formulas of the ligands and complexes. The closeness of the results supports the accuracy of the proportions used in the preparations, as shown in the table below :

Table (1): detailed analysis results for elements

Seq	compounds	C	H	Cd	N	P	S
١	L	49.95 (49.98)	4.16 (4.19)		29.09 (29.14)		16.66 (16.68)
٢	$[CdL_2(pph_3)_2]Cl_2$	61.24 (61.27)	4.33 (4.35)	11.01 (11.03)	10.96 (10.99)	6.06 (6.08)	6.25 (6.29)
٣	$[CdL_4(\mu\text{-dppm})_2]Cl_2$	35.75 (35.72)	2.82 (2.83)	19.66 (19.69)	19.61 (19.63)	10.83 (10.85)	11.22 (11.23)
٤	$[CdL_2(dppp)_2]Cl_2$	38.07 (38.10)	3.35 (3.37)	18.73 (18.77)	18.67 (18.71)	10.32 (10.34)	10.68 (10.71)

SEM Outcomes :

The majority of coordination compounds with regular geometric structures can be produced at the nanoscale, according to recent investigations on their geometric structure. A few complexes made with the SEM method had their microstructure's morphological appearance examined**.**

Through scanning electron microscope analysis of the complex $[Cd(L)_2(dppp)]$ Cl_2, the average peak of the complex body radii was 70 nm, which falls within the range of nanoparticles.

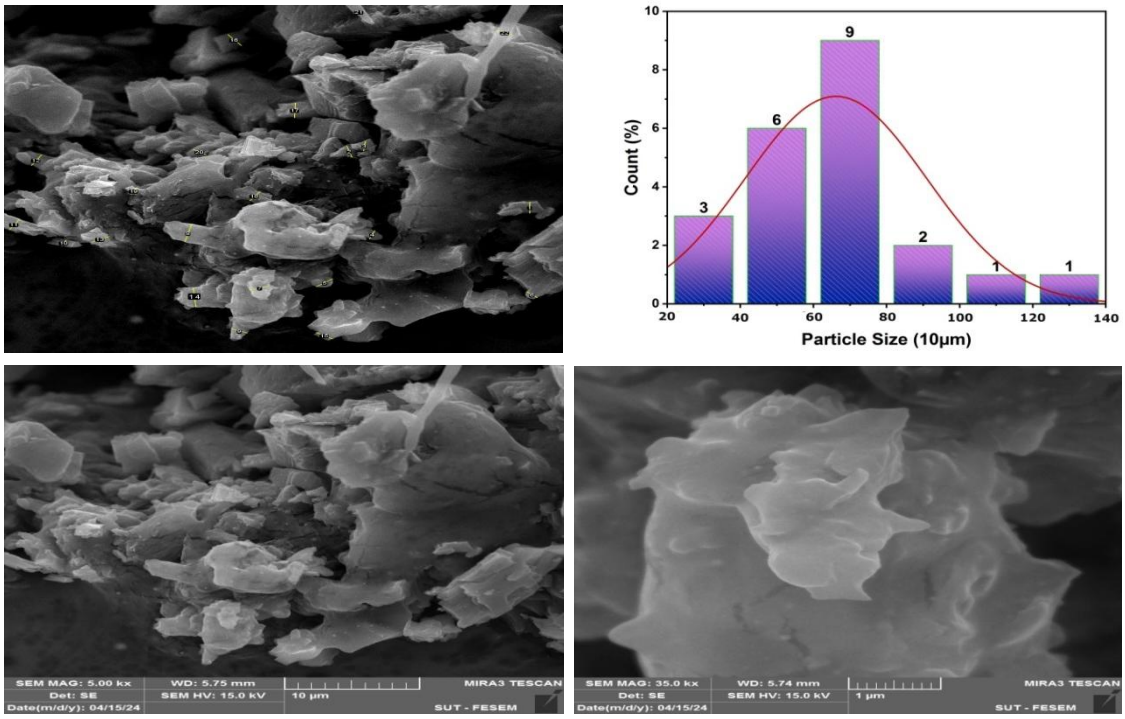


Figure (6): (a) SEM image of the complex $[Cd(L)_2(dppp)]Cl_2$ at 1 µm and 10 µm Graph (1): (b) Particle sizes and Gaussian curve for the complex $[Cd(L)_2(dppp)]Cl_2$ at 10 µm

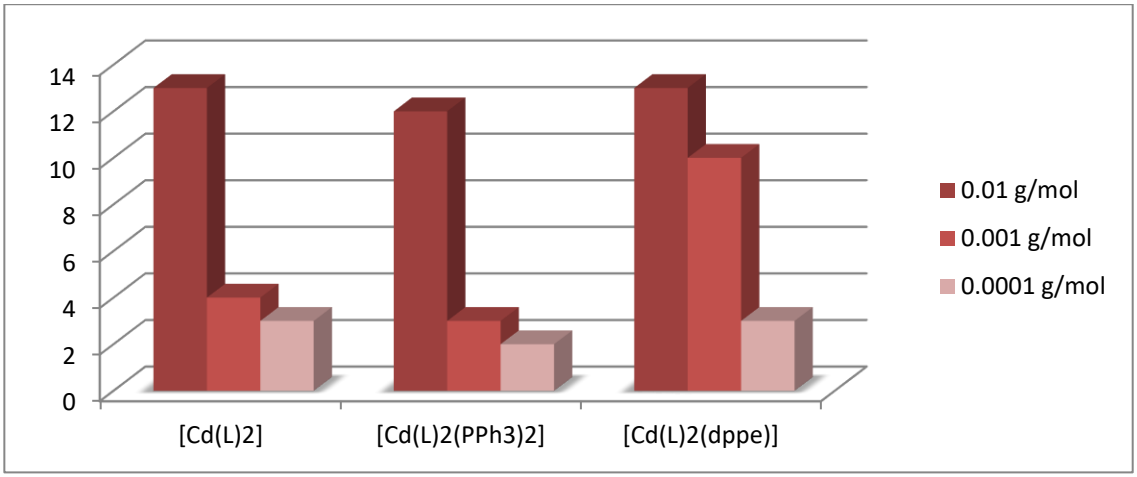
Biological Activity :

The Using the antibiotic Amikacin as a reference, the biological activity of the complexes was evaluated against four bacterial species: Escherichia coli (-), Acinetobacter baumannii (-), Staphylococcus aureus (+), and Enterococcus faecalis (+) at doses of 0.01, 0.001, and 0.0001 mg/mL. As seen in Figure 3, every complex exhibited action against the bacterial species. The concentration of ten showed weak activity against the bacterial species, while complex (1) showed the highest inhibition percentage at concentration 103 against (-)

Acinetobacter baumannii and (-) Escherichia coli. Complex (2) showed the highest inhibition percentage at concentration 180 against (+) Staphylococcus aureus and Enterococcus faecalis.

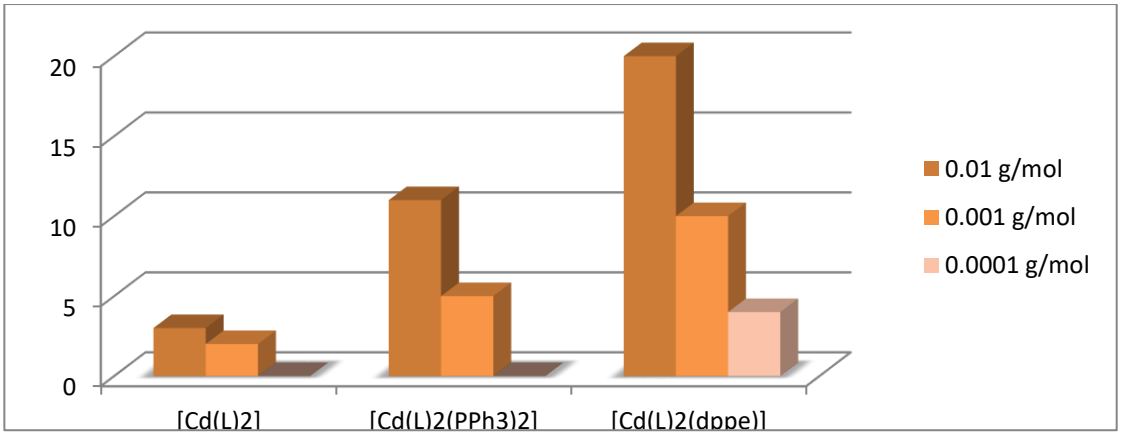
Complex (1) showed the highest activity at concentration 10 against ((Escherichia coli), while complex (2) showed the highest activity at the same concentration for the other species.

Acinetobacter baumannii (-)



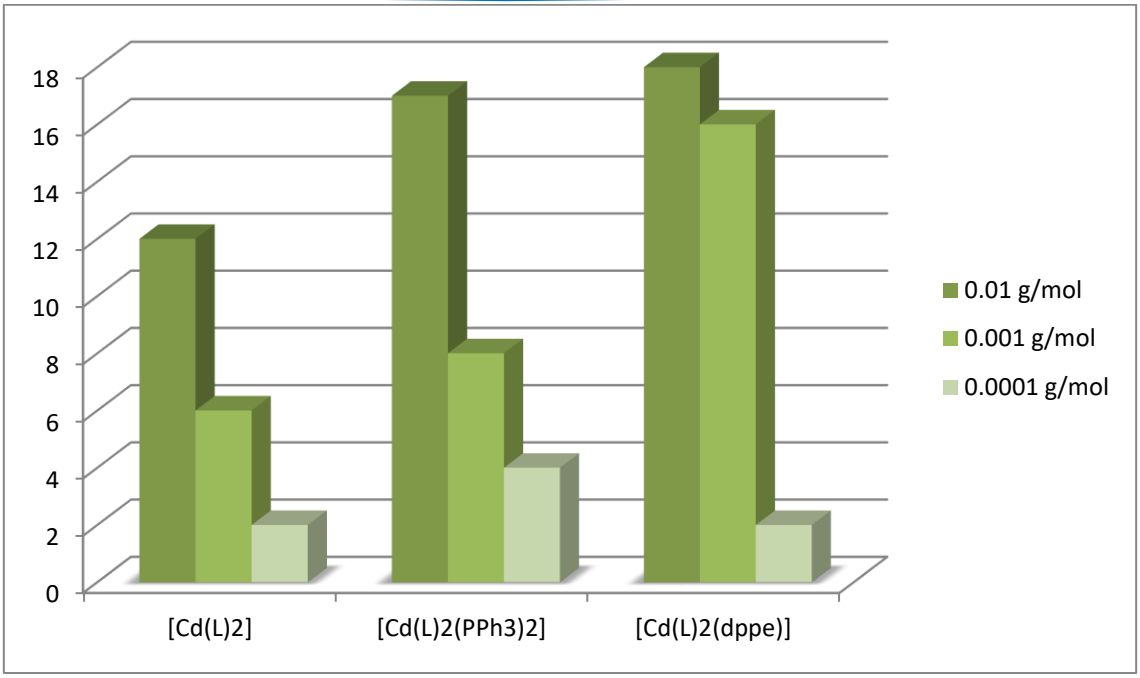
(a)

Escherichia coli(-)



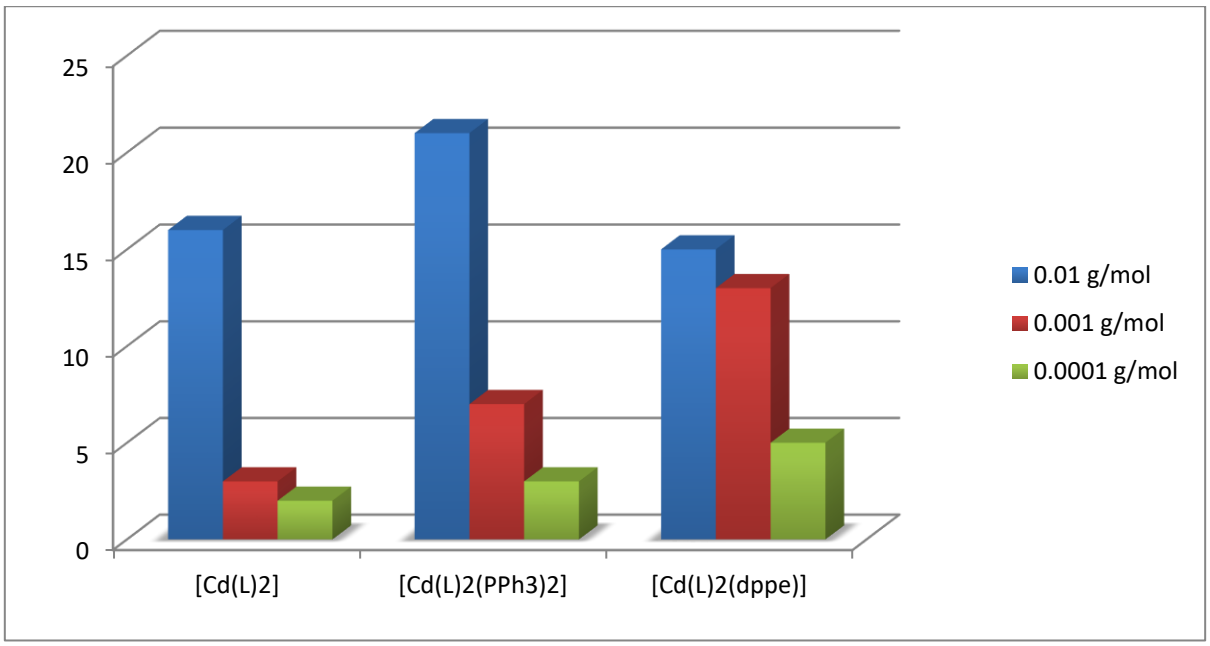
(b)

Staphylococcus aurous(+)



(c)

Enterococcus faecalis(+)



(d)

Figures (7) : The the prepared compounds' ability to suppress the development of a number of Gram-positive and Gram-negative bacteria (a, b, c, and d)

Conclusions:

1- A new series of novel mixed-ligand cadmium(II) complexes was successfully synthesized using 5-(benzylthio)-1}H tetrazole (L) in combination with mono- and bidentate phosphine ligands, yielding three specific complexes:$[CdL_2(PPh3)_2]Cl_2$, $[Cd_2L_4(\mu\text{-dppm})_2]Cl$, and $[CdL_2(dppp)]Cl_2$.

2- Spectroscopic and elemental analyses (FT-IR, ^{1}H-NMR, ^{31}P-NMR, and CHN) confirmed that the tetrazole ligand acts as a bidentate donor coordinating via nitrogen atoms, while the phosphine ligands coordinate through phosphorus donor atoms.

3- Scanning Electron Microscopy (SEM) analysis revealed that the synthesized complexes exhibit well-defined, homogeneous nanostructured surface morphologies .

4- valuated complexes demonstrate promising biological properties, showing activity against selected bacterial and fungal strains as well as cancer cell lines.

Reference:

[1] HUSSEIN, Mohamed, et al. Recent Advances in the Chemistry of Tetrazole Derivatives-A Quinquennial Update (Mid-2019 to date). *Mini-Reviews in Organic Chemistry*, 2025.

[2] ALSHARGABI, Arwa. Diclofenac derivatives as promising anticancer and anti-inflammatory drug: synthesis, formulations, and pharmacokinetics. *Journal of Drug Delivery Science and Technology*, 2024, 95: 105544.

[3] https://www.sciencedirect.com/topics/chemistry/tetrazole

[4] TISSEH, Zeinab Noroozi, et al. Catalyst-free, aqueous and highly diastereoselective synthesis of new 5-substituted 1H-tetrazoles via a multi-component domino Knoevenagel condensation/1, 3 dipolar cycloaddition reaction. *Tetrahedron*, 2012, 68.6: 1769-1773.

[5] BALOUIRI, Mounyr; SADIKI, Moulay; IBNSOUDA, Saad Koraichi. Methods for in vitro evaluating antimicrobial activity: A review. *Journal of pharmaceutical analysis*, 2016, 6.2: 71-79.

[6] GONELIMALI, Faraja D., et al. Antimicrobial properties and mechanism of action of some plant extracts against food pathogens and spoilage microorganisms. *Frontiers in microbiology*, 2018, 9: 1639.

[7] MOHAMMED, Azad; ABDULLAH, Avin. Scanning electron microscopy (SEM): A review. In: *Proceedings of the 2018 international conference on hydraulics and pneumatics—HERVEX, Băile Govora, Romania*. 2018. p. 7-9.

[8] SUN, Cheng, et al. Versatile application of a modern scanning electron microscope for materials characterization. *Journal of Materials Science*, 2020, 55.28: 13824-13835.

[9] SHAIKH, Saba Kauser J., et al. Tetrazolylmethyl quinolines: Design, docking studies, synthesis, anticancer and antifungal analyses. *European Journal of Medicinal Chemistry*, 2017, 128: 258-273.

[10] UPPADHAYAY, Ravish Kumar, et al. STRUCTURAL, PHYSICAL, SURFACE AND NMR STUDY OF 5-(BENZYLTHIO)-1H-TETRAZOLE COMPOUND. *Journal of Pharmaceutical Negative Results*, 2022, 13.

[11] UPPADHAYAY, Ravish Kumar, et al. STRUCTURAL, PHYSICAL, SURFACE AND NMR STUDY OF 5-(BENZYLTHIO)-1H-TETRAZOLE COMPOUND. *Journal of Pharmaceutical Negative Results*, 2022, 13.

[12] HAMEED, Anwar A., et al. Exploration of novel phenyl mercury tetrazole-thione complexes: characterization and investigating the impact of diamine ligands on enhanced hydrogen storage. *Energy Storage*, 2024, 6.2: e598.

Al-Kitab Journal for Pure Sciences (2026); 10(2):279-298.
https://doi.org/10.32441/kjps.10.2.p20

Al-Kitab Journal for Pure Sciences
ISSN: 2617-1260 (print), 2617-8141(online)

https://isnra.net/index.php/kjps

Petrography, Microfacies, Depositional Environment and Diagenetic Evolution of the Upper Triassic Kurra Chine and Baluti Formations, Northern Iraq

Eman W. Al-Berzanje[1], Hassan A. Al-Jumaily[2], Ali I.Al-Juboury[3]

[1]Department of Applied Geology, College of Science, University of Kirkuk, Iraq.

[2] North Oil Company, Kirkuk, Iraq.

[3]Petroleum Engineering Department, College of Engineering, Al-Kitab University, Iraq.

Corresponding Author: emanwaleed@uokirkuk.edu.iq

Citation: ***Eman W. Al-Berzanje[1], Hassan A. Al-Jumaily[2], Ali I.Al-Juboury[3]*. Petrography, Microfacies, Depositional Environment and Diagenetic Evolution of the Upper Triassic Kurra Chine and Baluti Formations, Northern Iraq.**
Al-Kitab J. Pure Sci. [Internet]. 2026 Jul. 21 ;10(2):279-298
DOI.
https://isnra.net/index.php/kjps/article/view/2026.
https://doi.org/10.32441/kjps.10.2.p20

Keywords: Baluti Formation; Carbonate microfacies; Depositional environment; Diagenesis; Kurra Chine Formation; Northern Iraq; Petrography.

Article History
Received 21 Jun. 2026
Accepted 21 Jul. 2026
Available online 01 Nov. 2026

©20--. THIS IS AN OPEN-ACCESS ARTICLE UNDER THE CC BY LICENSE
http://creativecommons.org/licenses/by/4.0/

Abstract:

The Upper Triassic carbonate succession of northern Iraq represents an important record of the northeastern Arabian Plate passive margin and provides valuable information about carbonate platform evolution during the development of the Neo-Tethys Ocean. This study investigates the petrography, microfacies characteristics, depositional environments, and diagenetic evolution of the Kurra Chine and Baluti formations based on detailed microscopic examination of carbonate thin sections from the Ranya and Sirwan sections, northern Iraq. Petrographic analysis reveals that the studied succession is dominated by limestone, dolomitic limestone, and dolostone affected by extensive diagenetic modification. Four major microfacies were recognized in Kurra Chine and six microfacies in the Baluti formation based on carbonate texture, allochem composition, Standard Microfacies (SMF), and Wilson facies zones. The identified microfacies indicate deposition within a shallow homoclinal carbonate ramp extending from restricted lagoonal environments to open lagoon and shoal-margin settings. The Kurra Chine Formation records relatively open inner-ramp conditions, characterized by

transitions from restricted lagoon (FZ8) through open lagoon (FZ7) to shoal-margin environments (FZ6). In contrast, the Baluti Formation represents a more restricted carbonate system dominated by lagoonal conditions with intermittent siliciclastic input and localized open marine influence. Petrographic observations indicate that both formations experienced complex diagenetic histories involving dolomitization, recrystallization, calcite cementation, dissolution, compaction, and fracturing. Dolomitization represents the dominant diagenetic process and played a significant role in modifying primary carbonate fabrics and developing secondary intercrystalline porosity. Dissolution locally enhanced pore development, whereas late calcite cementation and compaction reduced pore connectivity. The results demonstrate that the Baluti and Kurra Chine formations record cyclic changes in depositional conditions related to relative sea-level fluctuations during the Late Triassic. The integration of petrographic and microfacies analysis provides a comprehensive understanding of carbonate platform evolution, diagenetic modification, and reservoir-quality controls within Upper Triassic carbonate successions of northern Iraq.

Keywords*:* Baluti Formation; Carbonate microfacies; Depositional environment; Diagenesis; Kurra Chine Formation; Northern Iraq; Petrography.

البتروغرافية، والسحنات الدقيقة، والبيئة الترسيبية، والتطور التحويري لترياسي الاعلى لتكويني قوراجين وبلوطي شمال العراق

ايمان وليد البرزنجي[١] ،حسن احمد الجميلي[٢]،علي إسماعيل الجبوري [٣]

[1] قسم الجيولوجيا التطبيقية، كلية العلوم، جامعة كركوك، العراق

[2]شركة نفط الشمال، كركوك، العراق

[3] قسم هندسة النفط، كلية الهندسة، جامعة الكتاب, العراق

الايميل الرسمي:emanwaleed@uokirkuk.edu.iq

الخلاصة:

يمثل التعاقب الكربوناتي للعصر الترياسي المتأخر في شمال العراق سجلًا جيولوجيًا مهمًا للحواف المستقرة للصفيحة العربية الشمالية الشرقية، ويوفر معلومات قيّمة عن تطور المنصات الكربوناتية خلال مراحل تطور محيط النيوتيثس. تهدف هذه الدراسة إلى بحث الخصائص البتروغرافية، والسحنات الدقيقة (Microfacies)، والبيئات الترسيبية، والتطورات الدياجينية لتكويني قورا جين و بلوطي، اعتمادًا على الفحص البتروغرافي التفصيلي للشرائح الصخرية الرقيقة المأخوذة من مقطعي رانية وسيروان في شمال العراق. حيث أظهرت نتائج التحليل البتروغرافي أن التعاقب الصخري المدروس يتكون بصورة رئيسية من الحجر الجيري، والحجر الجيري الدولوميتي، والدولوستون، وقد تعرض لتأثيرات دياجينية واسعة النطاق.وتم التعرف على اربع سحنات دقيقة في تكوين قوراجين و ست سحنات دقيقة رئيسية في تكوين بلوطي، وذلك استنادًا إلى النسيج الكربوناتي، ومكونات الصخور، والسحنات الدقيقة القياس(SMF) ، وانطقة السحنات لويلسون Wilson Facies

(Zone) وتشير هذه السحنات الدقيقة إلى أن الترسيب تم ضمن منحدر كربوناتي ضحل من نوع Homoclinal Ramp امتد من بيئات لاجونية مقيدة إلى بيئات اللاجون المفتوح وحافات الضحال(Shoal Margin) .

وقد سجل تكوين قورا جين ظروفًا أكثر انفتاحًا ضمن الجزء الداخلي من المنحدر الكربوناتي، تميزت بانتقالات من بيئات اللاجون المقيد (FZ8) إلى اللاجون المفتوح(FZ7) ، وصولًا إلى بيئات حافات الضحال (FZ6). على عكس هذا، يمثل تكوين بلوطي نظامًا كربوناتيًا أكثر تقييدًا، سادت فيه البيئات اللاجونية مع تأثيرات متقطعة للرواسب السيليكاتية الفتاتية وبعض التأثيرات البحرية المفتوحة المحدودة. وأظهرت الملاحظات البتروغرافية أن كلا التكوينين قد تعرضا لتاريخ دياجيني معقد شمل عمليات الدولمة، وإعادة التبلور، والإسمنتة بالكالسيت، والإذابة، والانضغاط، والتشقق. وتمثل الدولمة العملية الدياجينية الأكثر تأثيرًا، إذ لعبت دورًا رئيسيًا في تعديل الأنسجة الكربوناتية الأصلية وتكوين المسامية الثانوية بين البلورات. كما أسهمت عمليات الإذابة في تعزيز تطور المسامية محليًا، في حين أدت السمنتة المتأخرة بالكالسيت والانضغاط إلى تقليل ترابط المسامات. وتبين النتائج أن تكويني قوراجين وبلوطي يسجلان تغيرات دورية في الظروف الترسيبية ارتبطت بتذبذبات مستوى سطح البحر خلال العصر الترياسي المتأخر. كما أتاح الدمج بين التحليل البتروغرافي وتحليل السحنات الدقيقة فهمًا متكاملًا لتطور المنصة الكربوناتية، والعمليات الدياجينية، والعوامل المتحكمة في جودة المكامن ضمن تعاقبات الكربونات العائدة للعصر الترياسي المتأخر في شمال العراق.

الكلمات المفتاحية: الترياسي المتأخر، السحنات الدقيقة، العمليات التحويرية، تكوين قورا جين، تكوين بلوطي، البتروغرافيا.

1. Introduction:

Petrographic and microfacies analyses constitute fundamental tools in carbonate sedimentology because they provide critical insights into depositional environments, facies architecture, diagenetic evolution, and reservoir characteristics. Petrography focuses on the mineralogical composition, texture, fabric, and diagenetic modifications of sedimentary rocks through microscopic investigation, whereas microfacies analysis integrates petrographic, paleontological, and sedimentological evidence to reconstruct depositional settings and basin evolution [1-3]. The application of microfacies concepts has significantly enhanced the interpretation of carbonate platform systems by enabling the recognition of environmental gradients ranging from supratidal and lagoonal settings to shoal, open-marine, and basinal environments [3]. Carbonate rocks are particularly sensitive to post-depositional alteration, and therefore their present-day characteristics reflect the combined influence of depositional and diagenetic processes. Micritization, cementation, compaction, dolomitization, dissolution, and recrystallization may substantially modify original textures and pore systems, thereby affecting reservoir quality and stratigraphic interpretation [3-4]. Consequently, the integration of petrographic observations with microfacies analysis has become an essential approach for understanding the evolution of carbonate successions and evaluating their geological and economic significance. In northern Iraq, Upper Triassic carbonate–evaporite successions

represent an important record of the northeastern Arabian Plate during the development of the Neo-Tethys Ocean. Among these successions, the Baluti and Kurra Chine formations are of particular significance because they document major environmental fluctuations associated with changes in sea level, platform restriction, and evaporitic conditions [5-6]. The Baluti Formation is characterized by interbedded shale, marl, limestone, dolomitic limestone, and evaporitic deposits, indicating deposition in restricted shallow-marine to lagoonal environments. In contrast, the overlying Kurra Chine Formation consists predominantly of thick carbonate and evaporite successions deposited on a shallow carbonate platform subjected to repeated episodes of restriction and evaporation [6]. Recent investigations have highlighted the complexity of the Kurra Chine depositional system and its significant lateral and vertical facies heterogeneity. Integrated petrographic, sedimentological, and petrophysical studies identified multiple carbonate microfacies deposited within supratidal, intertidal, lagoonal, shoal, and open-marine settings, reflecting cyclic shallowing-upward successions developed on a carbonate ramp system [7-8].

Furthermore, detailed petrographic analyses demonstrated that diagenetic processes, particularly dolomitization, cementation, and dissolution, exerted a major control on pore-system evolution and reservoir properties within the Kurra Chine Formation [8-9]. Recent studies from the Sirwan Valley and subsurface oil fields in northern Iraq also emphasized the importance of petrographic and microfacies investigations for reconstructing depositional environments and understanding reservoir heterogeneity within the Upper Triassic succession [9]. Therefore, a comprehensive petrographic and microfacies investigation of the Baluti and Kurra Chine formations provides valuable information regarding depositional environments, facies distribution, diagenetic history, and paleoenvironmental evolution of the Upper Triassic succession in northern Iraq. Such studies contribute significantly to regional stratigraphic correlations and improve the understanding of carbonate platform development along the northeastern margin of the Arabian Plate. Although several studies have investigated the Upper Triassic carbonate succession in northern Iraq, integrated comparative petrographic and microfacies analyses of both the Kurra Chine and Baluti formations remain limited. Therefore, this study aims to characterize their petrography, microfacies, depositional environments, and diagenetic evolution in the Sirwan and Ranya sections to improve the understanding of the Late Triassic carbonate platform. The objectives of this study are to classify the carbonate microfacies, interpret the depositional environments, identify the principal diagenetic processes, and compare the depositional evolution of the Kurra Chine and Baluti formations.

2. Tectonic setting and structural geology:

The geological evolution of northern Iraq is closely related to the opening and subsequent evolution of the Neo-Tethys Ocean along the northeastern margin of the Arabian Plate. The Neo-Tethys originated as a result of continental extension and rifting associated with the fragmentation of the northern margin of Gondwana during the Middle Permian. This tectonic event led to the separation of the Cimmerian continental blocks from the Arabian Plate and initiated the progressive opening of the Neo-Tethys Ocean, which continued throughout the Triassic and Early Jurassic (ca. 250–160 Ma) [10]. The opening of the Neo-Tethys occurred in two principal tectonic phases. The first phase took place during the Permian–Triassic, when the Iranian microplate drifted northward away from the Arabian Plate toward the Eurasian margin, resulting in the development of an extensional passive continental margin [11-13]. The second phase extended from the Late Triassic to the Middle Jurassic, during which the Neo-Tethys reached its maximum width of approximately 4,000 km. Continued extension along the northern and northeastern margins of the Arabian Plate promoted the development of broad carbonate platforms, restricted intraplatform basins, and localized evaporitic environments that characterized the Upper Triassic sedimentary succession in northern Iraq [13] **Figure 1**.

During the Late Triassic, the northeastern Arabian Plate experienced progressive tectonic instability that terminated the long-lasting stable shelf conditions prevailing since the Paleozoic. This instability is reflected by rapid lateral facies variations, localized volcanic activity, syn-sedimentary tectonic movements, and differential subsidence, all of which were closely associated with the continued evolution of the Neo-Tethys Ocean [14]. In the eastern Zagros region, basin development continued into the Early Jurassic (Liassic), reflecting the persistence of extensional tectonics along the passive continental margin [1٥]. These tectonic events resulted in the formation of a broad restricted intra-shelf basin across northern Mesopotamia, where repeated fluctuations in relative sea level controlled the deposition of carbonate and evaporite successions represented by the Baluti and Kurra Chine formations (Jassim & Goff, 2006) [6].

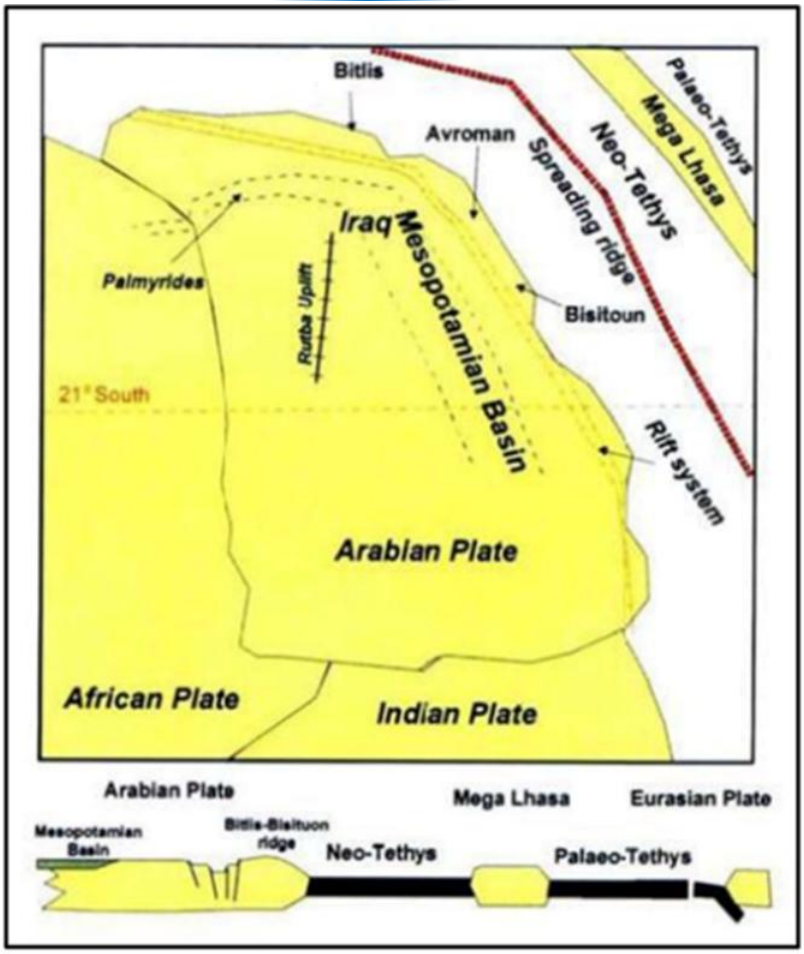


Figure 1: Geodynamic development of Arabian plate during Middle-Triassic-Norian (after [6]).

Structurally, the investigated Sirwan and Ranya sections are situated within the High Folded Zone of the Zagros Fold–Thrust Belt in northeastern Iraq **Figure 2**. This tectonic zone is characterized by NW–SE-trending anticlines and synclines that developed during the Cenozoic collision between the Arabian and Eurasian plates. The present structural configuration has significantly influenced the preservation, exposure, and deformation of the Upper Triassic sedimentary succession within the study area **[16].**

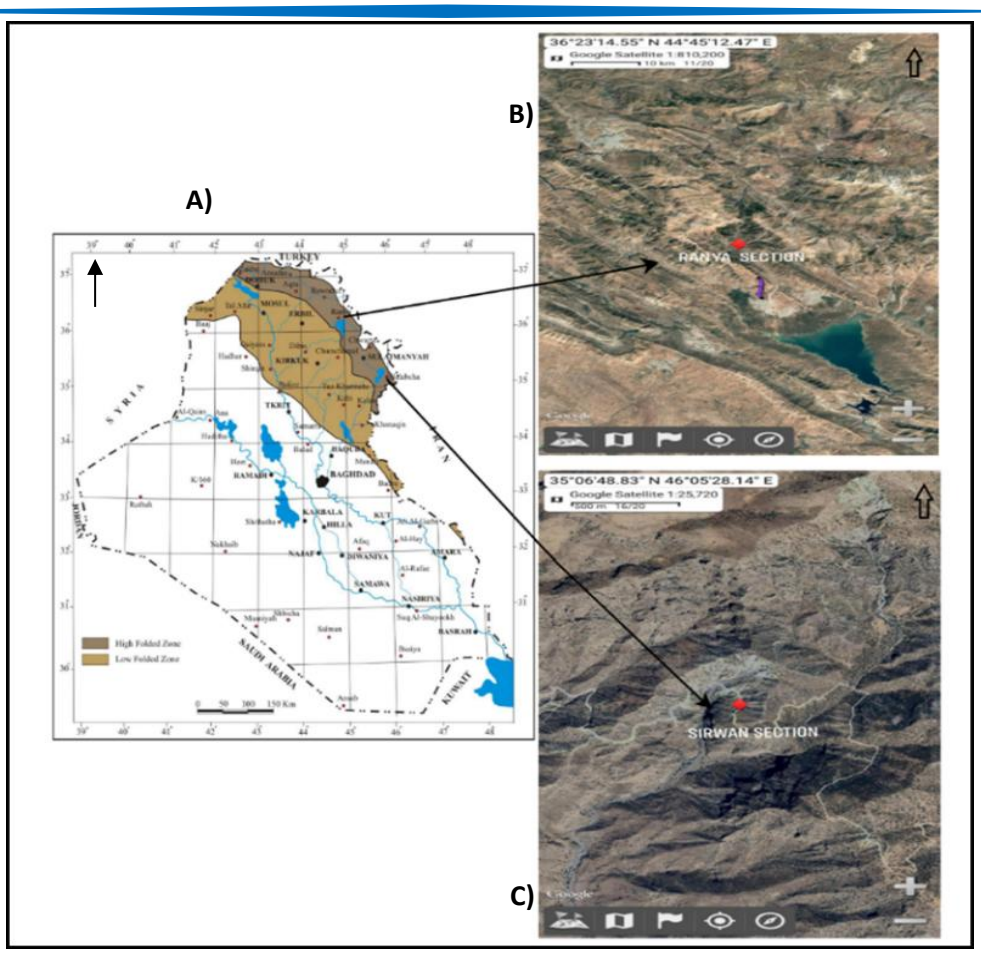


Figure 2: Illustrates the location of the investigated sections. Part (A) presents the regional tectonic position within the High Folded Zone of Iraq after [16], whereas Parts (B) and (C) show Google Earth images of the Ranya and Sirwan sections, respectively.

2. Material and methods:

A total of 11٣ fresh rock samples were systematically collected from the two sections, the Sirwan Valley section is situated at 46°05′06.32″ E and 35°06′34.25″ N, whereas the Shawre Valley section lies at 44°44′53.39″ E and 36°23′02.19″ N **Figure 2 B and C**, including ٥٩ samples from the Sirwan section, which has an exposed thickness of approximately ٩٨m, and 5٤ samples from the Ranya section, where the measured succession is approximately ٨٩.4 m thick. The Sirwan locality is positioned adjacent to the Iraqi–Iranian border, whereas the Shawre section is exposed within the Halabja District of Sulaymaniyah Governorate and represents an Upper Triassic outcrop that has received comparatively limited geological attention. This study integrates field observations with petrographic and microfacies analyses of representative carbonate samples from the Sirwan and Ranya sections. Thin-section petrography, Alizarin Red S staining, and standard carbonate microfacies classification were applied to reconstruct depositional environments and diagenetic evolution. Petrographic and Microfacies analysis study

used a total of 40 thin sections representing limestone, dolomite, dolomitic limestone, and argillaceous dolomite were prepared according to standard petrographic procedures at Tehran University. Petrographic examination was subsequently carried out using a polarizing optical microscope at Al-Kitab University to investigate mineralogical composition, microfacies characteristics, and diagenetic features. To distinguish dolomite from calcite, Alizarin Red S staining was applied to 10 representative samples from both investigated sections following the method of [1٧]. Carbonate microfacies were classified and interpreted according to the schemes proposed by [1] and [3].

4.Results:

4.1 Microfacies Analysis and Depositional Interpretation

The Upper Triassic carbonate succession of the Kurra Chine and Baluti formations was investigated through petrographic analysis and microfacies classification. Based on lithological characteristics, carbonate textures, Standard Microfacies (SMF) types, and Wilson's facies zones [2], several microfacies associations were recognized. These microfacies reflect deposition within shallow homoclinal carbonate ramp systems, ranging from restricted lagoonal settings to open lagoon and shoal-margin environments. The identified microfacies associations indicate that the Kurra Chine Formation was deposited within an inner homoclinal carbonate ramp ranging from restricted lagoonal to shoal-margin environments. The dominance of dolomitic mudstone and dolomitized wackestone reflects protected lagoonal conditions with limited circulation, whereas the occurrence of bioclastic wackestone–packstone indicates intervals of increased marine connectivity and higher depositional energy. The overall facies distribution suggests repeated fluctuations in relative sea level during the Late Triassic, producing alternations between restricted and relatively open marine conditions as illustrate in **Table 1 Figure 3.**

Table 1. Microfacies characteristics of the Kurra Chine Formation

Microfacies	Main Petrographic Characteristics	SMF	Wilson FZ	Depositional Interpretation
MF1: Dolomitic Mudstone	Fine-crystalline dolomite in a mud-supported fabric; rare quartz and calcite-filled fractures.	SMF 23	FZ8	Restricted lagoon; very low energy and limited circulation.
MF2: Dolomitized Wackestone	Micritic matrix with scattered skeletal grains; partial dolomitization and local calcite cement.	SMF 23	FZ7–FZ8	Semi-restricted to protected open lagoon; low–moderate energy.
MF3: Bioclastic Wackestone–Packstone	Abundant skeletal grains in micrite/microspar; locally grain-supported; minor dolomite.	SMF 10–11	FZ6	Open lagoon to shoal margin; higher energy and circulation.
MF4: Recrystallized Dolomitic Limestone	Recrystallized calcite–dolomite mosaic; relict fabrics locally preserved; calcite-filled fractures/cavities.	SMF 23	FZ7–FZ8	Restricted–semi-restricted lagoon; strongly diagenetically modified.

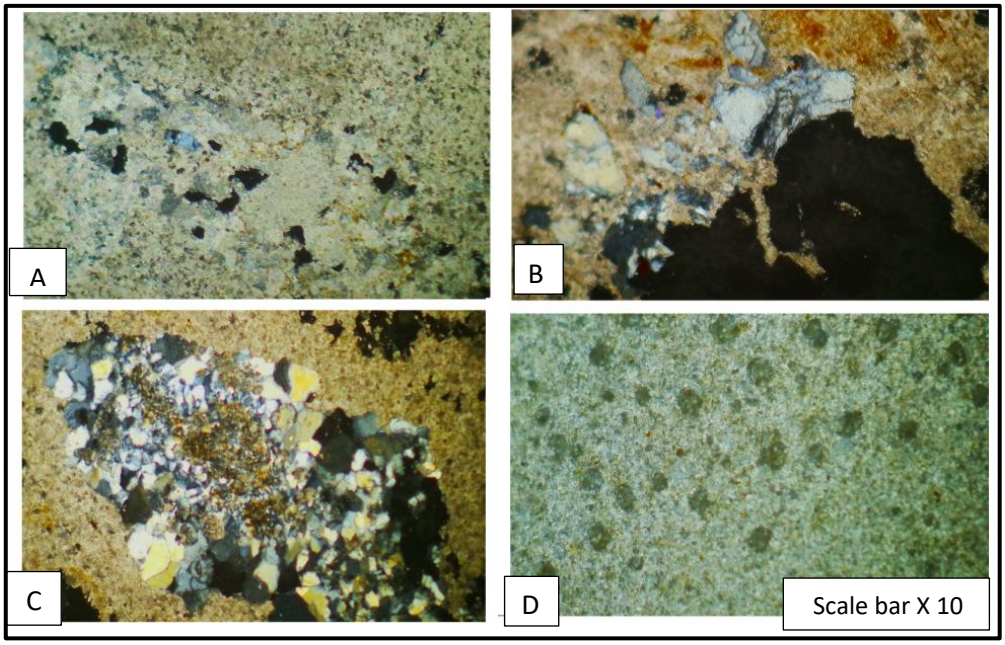


Figure 3: Representative photomicrographs illustrating the identified microfacies of the Kurra Chine Formation. (A) MF1—Dolomitized Mudstone (SK5); (B) MF2—Dolomitized Wackestone (SK10); (C) MF3—Bioclastic Wackestone–Packstone (SK17); (D) MF4— Recrystallized Dolomitic Limestone (RK6).

Interpretation of Baluti Microfacies records deposition within a predominantly restricted inner carbonate ramp. The widespread occurrence of dolomitic mudstone, argillaceous dolomudstone, and dolomitic siltstone reflects low-energy lagoonal conditions with significant siliciclastic influence. In contrast, peloidal–bioclastic wackestone–packstone represents temporary phases of improved marine circulation and increased energy within open lagoon to shoal-margin settings as illustrate in **Table 2 Figure 4**, and recrystallized dolostone is strongly diagenetically modified and therefore provides limited direct evidence for its original depositional setting. The overall facies pattern indicates a more restricted depositional system than the Kurra Chine Formation, with stronger influence from terrestrial input and episodic changes in accommodation space.

Table 2. Microfacies characteristics of the Baluti Formation

Microfacies	Main Petrographic Characteristics	SMF	Wilson FZ	Depositional Interpretation
MF1: Argillaceous Dolomudstone	Dolomicrite with clay, quartz, and feldspar; strong dolomitization.	SMF 19	FZ8	Restricted lagoon with intermittent siliciclastic input.
MF2: Dolomitic Mudstone	Fine-crystalline dolomite with few allochems; local calcite-filled fractures/cavities	SMF 23	FZ8	Restricted lagoon; low energy and evaporative conditions.
MF3: Dolomitized Wackestone	Dolomitized micritic matrix with skeletal grains, peloids, and rare intraclasts.	SMF 18	FZ7	Protected open lagoon; low energy with improved circulation.

MF4: Dolomitic Siltstone	Dolomicritic matrix with abundant fine quartz and minor calcite.	SMF 19	FZ8	Restricted lagoon with periodic siliciclastic influx.
MF5: Peloidal–Bioclastic Wackestone–Packstone	Peloids and skeletal grains in micrite; locally grain-supported; partial dolomitization.	SMF 11	FZ6	Open lagoon to shoal margin; relatively higher energy.
MF6: Recrystallized Dolostone	Medium–coarse dolomite; original fabric largely destroyed; calcite-filled fractures/cavities.	SMF 23	FZ8–FZ9	Restricted lagoon to supratidal; intense diagenetic alteration.

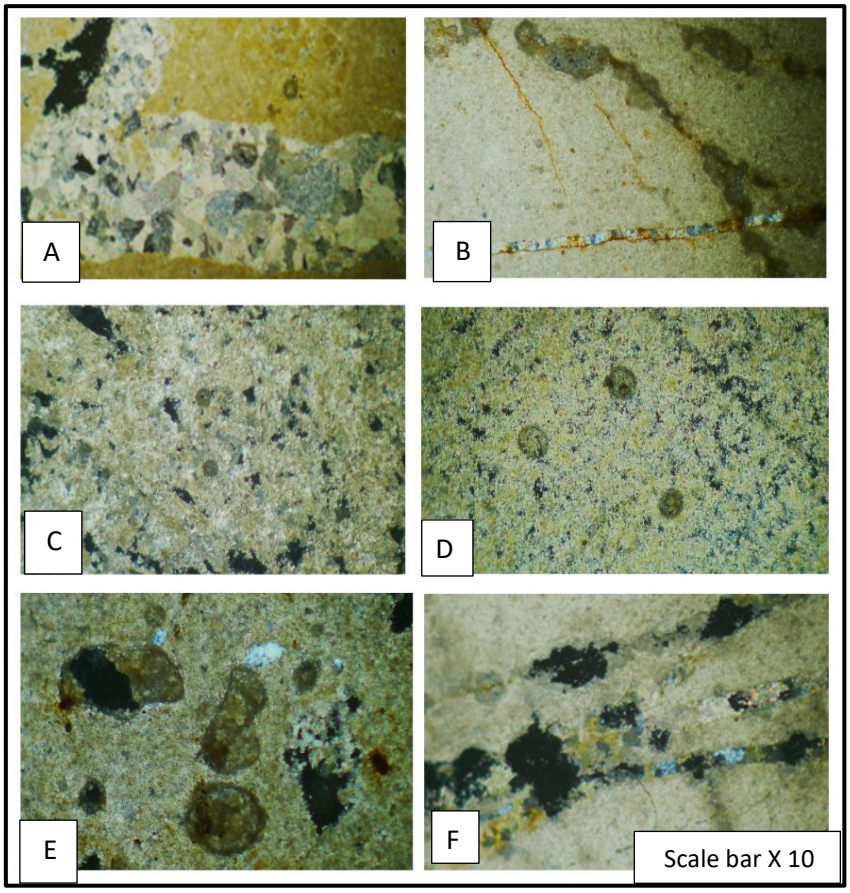


Figure (4): Representative photomicrographs illustrating the identified microfacies of the Baluti Formation. (A) MF1—Argillaceous Dolomudstone (RB2); (B) MF2—Dolomitic Mudstone (SKB30); (C) MF3—Dolomitized Wackestone (SKB27); (D) MF4—Dolomitic Siltstone (RB10); (E) MF5—Peloidal–Bioclastic Wackestone–Packstone (SKB21); (F) MF6—Recrystallized Dolostone (SKB28).

4.2 Diagenetic Processes of the Kurra Chine and Baluti Formations

Both the Kurra Chine and Baluti formations experienced complex diagenetic histories involving marine, meteoric, and burial processes that significantly modified the original carbonate fabrics and influenced their pore systems. The main diagenetic processes recognized include dolomitization, recrystallization, calcite cementation, dissolution, compaction, fracturing, and development of secondary intercrystalline porosity **Figures 5 and 6**.

Dolomitization represents the dominant diagenetic process affecting both formations. Petrographic observations reveal partial to pervasive replacement of micritic limestone by fine- to medium-crystalline dolomite, forming anhedral to subhedral crystal mosaics that commonly obscure primary textures. The widespread occurrence of dolomite within restricted lagoonal microfacies suggests early dolomitization under evaporative conditions through interaction with Mg-rich hypersaline fluids. Subsequent burial processes promoted dolomite recrystallization and further modification of the carbonate fabric.

Recrystallization accompanied dolomitization and burial alteration, transforming micritic carbonate material into microspar and coarse crystalline mosaics. This process partially destroyed original depositional textures while preserving some relict fabrics, particularly within dolomitized and recrystallized microfacies of both formations.

Calcite cementation was an important late diagenetic process, with sparry calcite commonly filling fractures, dissolution cavities, and intercrystalline pore spaces. Although cement precipitation stabilized the carbonate framework, it reduced secondary porosity by occluding pore networks. Dissolution played a significant role in modifying the pore systems by generating vuggy, moldic, and enlarged fracture porosity through selective removal of unstable carbonate components. The partial filling of dissolution cavities by sparry calcite indicates that dissolution preceded late-stage cementation and was related to the circulation of meteoric or burial fluids.

Compaction and fracturing affected both formations during burial and tectonic evolution. Mechanical compaction resulted in grain rearrangement and reduction of primary pore spaces, whereas chemical compaction produced pressure-solution features and localized stylolites. Micro- and macrofractures commonly cut carbonate fabrics and diagenetic minerals and were frequently filled with coarse crystalline calcite, indicating deformation prior to the final cementation stage. These fractures also enhanced fluid migration and facilitated subsequent diagenetic alteration.

Development of intercrystalline porosity represents the most significant secondary pore type associated with dolomitization. Replacement of the original carbonate matrix by dolomite generated pore spaces between dolomite crystals, locally forming interconnected pore networks. This porosity is particularly well developed in highly dolomitized intervals of both formations, including samples SK4, SK5, RB2, and SKB30. However, later calcite cementation locally reduced pore connectivity.

Overall, diagenetic evolution of the Kurra Chine and Baluti formations reflects a balance between porosity-enhancing processes, mainly dolomitization and dissolution, and porosity-reducing processes, including cementation, compaction, and recrystallization. These interactions controlled the final petrographic characteristics and reservoir potential of the Upper Triassic carbonate succession in northern Iraq.

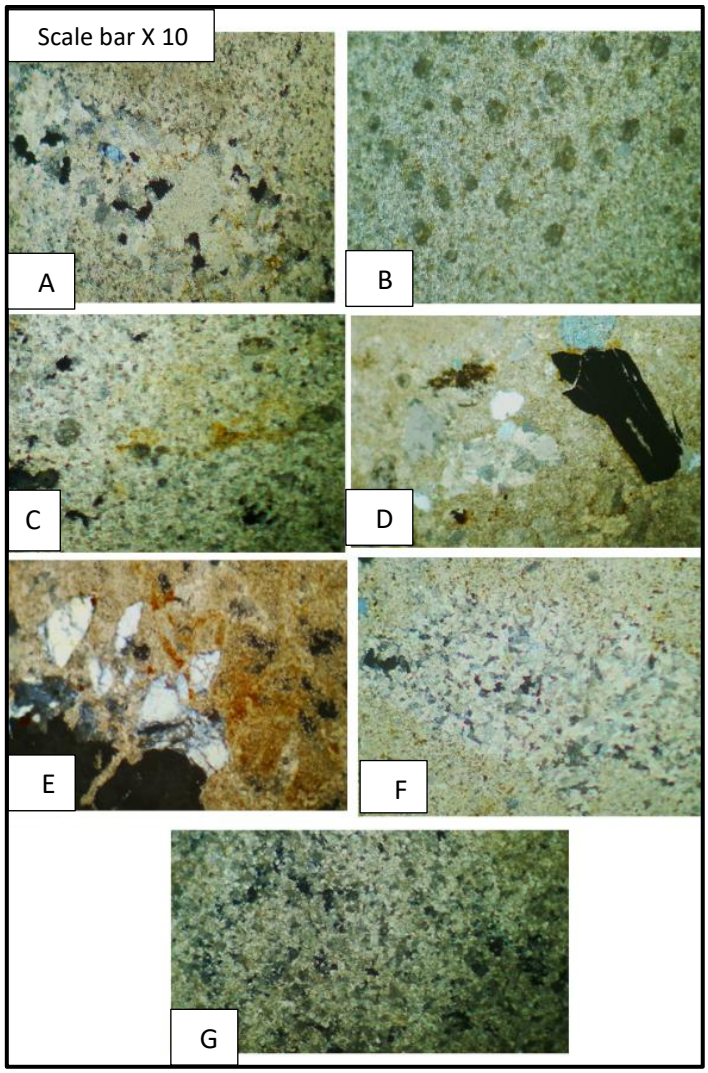


Figure (5): Representative photomicrographs illustrating the main diagenetic processes in the Kurra Chine Formation: (A) dolomitization (SK5); (B) recrystallization (RK6); (C) calcite cementation (SK17); (D) dissolution (RK3); (E) fracturing (SK10); (F) mechanical compaction (SK20); and (G) intercrystalline porosity (SK4).

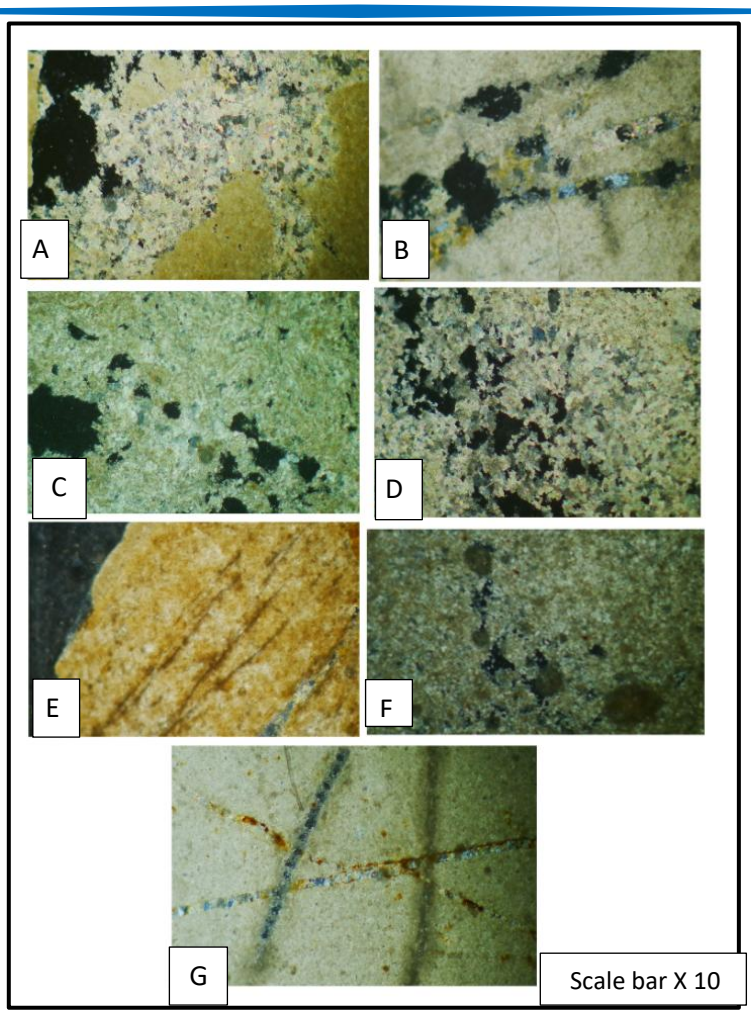


Figure 6: Representative photomicrographs showing the principal diagenetic processes affecting the Baluti Formation: (A) dolomitization (RB2); (B) recrystallization (SKB28); (C) calcite cementation (SKB27); (D) dissolution (SKB21); (E) compaction (SKB26); (F) fracturing (SKB24); and (G) Intercrystalline porosity (SKB30).

4.3 Depositional Environment

The microfacies associations of the Kurra Chine and Baluti formations indicate deposition within shallow homoclinal carbonate ramps developed along the passive margin of the Neo-Tethys Ocean during the Late Triassic. The recognized facies reflect a spectrum of depositional environments ranging from restricted lagoonal settings to open lagoon and shoal-margin environments, primarily controlled by relative sea-level fluctuations and variations in marine circulation. The Kurra Chine Formation records a relatively open depositional system. Dolomitic mudstone (MF1) represents restricted lagoonal conditions (FZ8) characterized by low hydrodynamic energy, limited circulation, and elevated salinity that promoted early dolomitization. Dolomitized wackestone (MF2) reflects improved marine circulation within semi-restricted to open lagoon settings, whereas bioclastic wackestone–packstone (MF3) records the highest depositional energy in open lagoon to shoal-margin environments (FZ6).

Recrystallized dolomitic limestone (MF4) represents lagoonal carbonates extensively modified by post-depositional diagenesis.

In contrast, the Baluti Formation represents a more restricted depositional system dominated by lagoonal conditions. Dolomitic mudstone (MF1), argillaceous dolomudstone (MF2), and dolomitic siltstone (MF4) indicate low-energy restricted lagoonal environments influenced by intermittent siliciclastic input from nearby continental sources. Dolomitized wackestone (MF3) reflects protected open-lagoon conditions, whereas peloidal–bioclastic wackestone–packstone (MF5) records temporary increases in depositional energy within open lagoon to shoal-margin settings. Recrystallized dolostone (MF6) reflects extensive diagenetic modification rather than a distinct depositional environment. Overall, both formations were deposited within an inner carbonate ramp; however, the Kurra Chine Formation records greater marine connectivity and more frequent transitions toward open lagoon and shoal environments, whereas the Baluti Formation reflects predominantly restricted lagoonal deposition with stronger siliciclastic influence and local supratidal conditions. The vertical facies succession in both formations indicates repeated Late Triassic relative sea-level fluctuations that controlled facies distribution across the carbonate platform.

5. Discussion

5.1 Depositional Evolution of the Kurra Chine Formation

The microfacies of the Kurra Chine Formation indicate deposition on a shallow homoclinal carbonate ramp along the northeastern Arabian Plate during the Late Triassic. The transition from restricted lagoonal dolomitic mudstone to open-lagoon and shoal-margin bioclastic facies reflects variations in marine circulation, depositional energy, accommodation, and relative sea level. The dominance of dolomitic mudstone (MF1) and dolomitized wackestone (MF2) indicates low-energy, restricted lagoonal conditions where evaporation favored dolomitization [4];[18]. The preservation of original wackestone fabrics within partially dolomitized MF2 suggests that dolomitization partly occurred early, followed by recrystallization during burial [^]. Bioclastic wackestone–packstone (MF3) records improved marine circulation and relatively higher-energy conditions, representing a transition toward open-lagoon and shoal-margin settings. This interpretation agrees with previous studies that recognized a range of inner-, middle-, and locally outer-ramp environments in the Kurra Chine Formation [7].

However, the Sirwan and Ranya sections are dominated mainly by restricted inner-ramp facies, with episodic development of more open and higher-energy conditions. The vertical facies succession reflects variations in accommodation, hydrodynamic energy, marine circulation, and degree of restriction, consistent with the regional sequence-stratigraphic framework of the Arabian Plate [19-20] further highlighted the regional significance of the Carnian "Marker Dolomite" and its relationship to the Baluti Formation. Recent studies also demonstrate substantial facies and diagenetic heterogeneity within the Kurra Chine Formation, which strongly influences reservoir quality [^]. Accordingly, the present study indicates that the studied sections mainly record restricted inner-ramp conditions interrupted by episodes of enhanced marine circulation and higher-energy deposition.

5.2 Depositional Evolution of the Baluti Formation

The Baluti Formation records deposition within a restricted inner-ramp carbonate system influenced by intermittent siliciclastic input. Dolomitic mudstone, argillaceous dolomudstone, and dolomitic siltstone indicate low-energy lagoonal conditions, whereas peloidal–bioclastic wackestone–packstone (MF5) reflects short intervals of improved marine circulation and higher depositional energy. Compared with the Kurra Chine Formation, the greater abundance of quartz and argillaceous material indicates stronger terrigenous influence, probably related to proximity to continental sources and/or enhanced terrestrial runoff [5-6].

Edilbi et al. [21] recognized supratidal, intertidal, subtidal, lagoonal, and shoal microfacies within the Baluti Formation. Mud-rich facies indicate protected, low-energy conditions, whereas peloids, ooids, intraclasts, and fenestral structures indicate episodic increases in depositional energy. Asaad et al. [22] similarly documented a heterogeneous succession of dolomitic limestone, marly limestone, shale, and marl, supporting deposition under changing rather than uniform environmental conditions. The greater abundance of argillaceous and siliciclastic material in Baluti represents an important distinction from Kurra Chine and indicates stronger terrestrial influence and restriction. Edilbi et al. [21] also reported terrestrial organic-matter input and locally anoxic to suboxic conditions. Lunn et al. [20] highlighted the stratigraphic significance of the Baluti shale and associated Carnian "Marker Dolomite." Accordingly, the present microfacies results indicate a more restricted, argillaceous, and siliciclastic-influenced depositional system for the Baluti Formation compared with the more carbonate-dominated Kurra Chine succession.

5.3 Diagenetic Evolution and Porosity Development

Both the Kurra Chine and Baluti formations experienced complex marine, meteoric, and burial diagenesis, with dolomitization being the dominant alteration process. The occurrence of fine- to medium-crystalline dolomite within restricted lagoonal facies suggests early replacement by Mg-rich hypersaline fluids, followed by recrystallization during burial [4];[18]. The preservation of depositional fabrics in partially dolomitized samples indicates that dolomitization occurred through multiple stages, with the original depositional texture and degree of restriction influencing its distribution and intensity. Dissolution represents an important porosity-enhancing process, producing vuggy, moldic, and intercrystalline pores through post-depositional fluid circulation. This relationship between dolomitization, dissolution, and intercrystalline porosity is consistent with previous investigations of the Kurra Chine Formation [^]. In contrast, calcite cementation reduced pore connectivity by filling fractures, dissolution cavities, and other available pore spaces. Aswad et al. [23] similarly demonstrated that calcite cement contributed significantly to porosity reduction in the Kurra Chine Formation of the Sirwan Valley.

Petrophysical investigations further indicate substantial vertical and lateral variations in porosity and reservoir quality within the Kurra Chine Formation, emphasizing the combined influence of depositional facies and subsequent diagenetic processes [9]. Palynofacies evidence also supports variations in depositional conditions rather than deposition under a single uniform marine environment [24]. In the Baluti Formation, the association of dolomitization, recrystallization, cementation, and secondary pore development similarly indicates a complex diagenetic history. The lithological and microfacies variability documented by [21] and [22] provides a depositional framework for interpreting this diagenetic heterogeneity. Overall, reservoir quality in both formations reflects the balance between porosity-enhancing processes, particularly dolomitization and dissolution, and porosity-reducing processes such as cementation and compaction.

6. Comparison with previous studies

The petrographic and microfacies characteristics identified in the Baluti and Kurra Chine formations are broadly consistent with previous investigations of the Upper Triassic carbonate successions in northern Iraq. Early studies interpreted the Kurra Chine Formation as a shallow-marine carbonate platform affected by repeated transgression, restriction, and

regression [5-6]. More recent studies recognized restricted lagoon, open-lagoon, shoal, tidal-flat, and supratidal microfacies, supporting deposition on a homoclinal carbonate ramp influenced by relative sea-level fluctuations [7-8]. The present study supports these interpretations but indicates that the Sirwan and Ranya sections were dominated by restricted inner-ramp conditions, with episodic development of open-lagoon and shoal-margin environments. The observed facies distribution reflects variations in accommodation space, hydrodynamic energy, and marine circulation. The results also emphasize the important role of diagenesis, particularly dolomitization, dissolution, cementation, recrystallization, and compaction, in modifying carbonate fabrics and controlling pore-system evolution. These observations are consistent with [^], who emphasized the influence of sedimentological and diagenetic heterogeneity on the reservoir properties of the Kurra Chine Formation.

For the Baluti Formation, the present results agree with [21], who recognized restricted lagoonal, tidal-flat, subtidal, and shoal environments. The occurrence of dolomitic mudstone, argillaceous dolomudstone, dolomitic siltstone, and peloidal–bioclastic facies in the present study supports a predominantly restricted inner-ramp setting, interrupted by episodes of increased marine circulation and depositional energy. The lithological heterogeneity reported by [22] further supports the interpretation of Baluti as a heterogeneous shallow-marine succession. Diagenetic processes also exerted an important control on reservoir heterogeneity. Balaky et al. [8] demonstrated that dolomitization and dissolution may enhance pore development, whereas cementation, compaction, and recrystallization may reduce pore volume and permeability. Calcite cementation was also shown to influence porosity evolution in the Sirwan Valley [23], while substantial variations in petrophysical properties were documented within the Kurra Chine Formation of the Sarta Oil Field [9]. These observations are consistent with the present petrographic results, which demonstrate that the interaction between depositional facies and subsequent diagenetic processes controlled the development and destruction of pore spaces. Compared with previous investigations, the present study integrates petrographic observations, standard microfacies classification (SMF), Wilson's Facies Zones (FZ), depositional-environment reconstruction, and diagenetic interpretation. The comparison of the Sirwan and Ranya sections further provides evidence for lateral facies variability and spatial changes in the Upper Triassic carbonate system along the northeastern margin of the Arabian Plate. Overall, the studied succession represents a heterogeneous shallow carbonate-ramp system rather than a uniform carbonate platform. The Kurra Chine Formation is dominated by restricted inner-ramp conditions with episodic open-lagoon and shoal-margin

development, whereas the Baluti Formation records more restricted conditions with stronger argillaceous and siliciclastic influence. Subsequent dolomitization, dissolution, cementation, recrystallization, and compaction further modified the original fabrics and controlled the final pore-system characteristics of the Upper Triassic succession.

7. Conclusions

Petrographic and microfacies analyses indicate that the Kurra Chine and Baluti formations were deposited within shallow homoclinal carbonate ramps along the northeastern Arabian Plate during the Late Triassic. Four carbonate microfacies were recognized in Kurra Chine Formation and six microfacies for Baluti Formation, that representing depositional environments ranging from restricted lagoon to open lagoon and shoal-margin settings. The Kurra Chine Formation records relatively more open marine conditions, whereas the Baluti Formation reflects a more restricted depositional system influenced by intermittent siliciclastic input. Dolomitization was the dominant diagenetic process in both formations, modifying the original carbonate fabrics and generating secondary intercrystalline porosity. Dissolution locally enhanced porosity, whereas calcite cementation, recrystallization, and compaction reduced pore connectivity. The integration of petrography, microfacies analysis, and diagenetic interpretation provides a comprehensive depositional and diagenetic model for the Upper Triassic carbonate successions of northern Iraq and The comparative investigation demonstrates that the Kurra Chine Formation records relatively greater marine connectivity than the Baluti Formation, whereas both formations experienced similar diagenetic evolution dominated by dolomitization and dissolution.

8. References

[1] Dunham, R. J. (1962). Classification of carbonate rocks according to depositional texture. In W. E. Ham (Ed.), Classification of carbonate rocks (AAPG Memoir 1, pp. 108–121). American Association of Petroleum Geologists.

[2] Wilson, J. L. (1975). Carbonate facies in geologic history. Springer-Verlag.

[3] Flügel, E. (2010). Microfacies of carbonate rocks: Analysis, interpretation and application (2nd ed.). Springer.

[4] Tucker, M. E., & Wright, V. P. (1990). Carbonate sedimentology. Blackwell Scientific Publications.

[5] Buday, T. (1980). The regional geology of Iraq: Vol. 1. Stratigraphy and paleogeography. Directorate General of Geological Survey and Mineral Investigation, Baghdad, Iraq.

[6] Jassim, S. Z., & Goff, J. C. (2006). Geology of Iraq. Dolin, Prague and Moravian Museum, Brno.

[7] Al-Hamdani, A. M., Ali, M. S., & Al-Dabagh, M. M. (2021). Microfacies evaluation of Kurra Chine Formation (Late Triassic) and scenario of depositional basin development in northern and northwestern Iraq. Journal of Petroleum Research and Studies, 11(4), 1–19. https://doi.org/10.52716/jprs.v11i4.566

[8] Balaky, S. M., Al-Dabagh, M. M., Asaad, I. S., Tamar-Agha, M., Ali, M. S., & Radwan, A. E. (2023). Sedimentological and petrophysical heterogeneities controls on reservoir characterization of the Upper Triassic shallow marine carbonate Kurra Chine Formation, Northern Iraq: Integration of outcrop and subsurface data. Marine and Petroleum Geology, 149, 106085. https://doi.org/10.1016/j.marpetgeo.2022.106085.

[9] Aswad, M. K., Omer, M. F., & Naqshabandi, S. F. (2024a). Unlocking the hydrocarbon potential: Formation evaluation and petrophysical properties of the Upper Triassic Kurra Chine Formation in Sarta Oil Field, Kurdistan Region, Northern Iraq. Heliyon, 10(3), e25173. https://doi.org/10.1016/j.heliyon.2024.e25173.

[10] Al-Sharhan, A. S., & Nairn, A. E. M. (2003). Sedimentary basins and petroleum geology of the Middle East. Elsevier.

[11] Beydoun, Z. R. (1993). Evolution of the northeastern Arabian Plate margin and shelf: Hydrocarbon habitat and future potential. American Association of Petroleum Geologists Bulletin, 77(3), 439–474.

[12] Numan, N. M. S. (1997). A plate tectonic scenario for the Phanerozoic succession in Iraq. Iraqi Geological Journal, 30(2), 85–110.

[13] Sadooni, F. N., & Alsharhan, A. S. (2004). Stratigraphy, microfacies, and petroleum potential of the Upper Triassic carbonate succession of Iraq. GeoArabia, 9(3), 89–122.

[14] Sharief, A. S. (1983). Stratigraphy and sedimentology of the Upper Triassic Kurra Chine Formation, northern Iraq (Unpublished M.Sc. thesis). University of Mosul, Mosul, Iraq.

[15] Fürst, M. (1970). Stratigraphie und Werdegang der östlichen Zagrosketten (Iran). Erlangen.

[16] Fouad, S. F. (2015). Tectonic map of Iraq, scale 1:1,000,000. Iraqi Bulletin of Geology and Mining, Special Issue 11, 1–7.

[17] Friedman, G. M. (1959). Identification of carbonate minerals by staining methods. Journal of Sedimentary Petrology, 29(1), 87–97.

[18] Warren, J. (2000). Dolomite: Occurrence, evolution and economically important associations. Earth-Science Reviews, 52(1–3), 1–81. https://doi.org/10.1016/S0012-8252(00)00022-2.

[19] Sharland, P. R., Archer, R., Casey, D. M., Davies, R. B., Hall, S. H., Heward, A. P., Horbury, A. D., & Simmons, M. D. (2001). Arabian Plate sequence stratigraphy. GeoArabia Special Publication 2. Gulf PetroLink.

[20] Lunn, G. A., Miller, S., & Samarrai, A. (2019). Dating and correlation of the Baluti Formation, Kurdistan, Iraq: Implications for the regional recognition of a Carnian "marker dolomite", and a review of the Triassic to Early Jurassic sequence stratigraphy of the Arabian Plate. Journal of Petroleum Geology, 42(1), 5–36. https://doi.org/10.1111/jpg.12722.

[21] Edilbi, A. N. F., Bowden, S. A., Mohamed, A. Y., & Sherwani, G. H. (2021). Depositional environment of the Upper Triassic Baluti Formation in Gara Anticline, Kurdistan Region, North Iraq: Insight from microfacies and biomarker characteristics. Iraqi Geological Journal, 54(1E), 29–42. https://doi.org/10.46717/igj.54.1E.3Ms-2021-05-24.

[22] Asaad, I. S., Balaky, S. M., Hasan, G. F., & Aswad, M. K. (2021). Sedimentology of the Baluti Formation (Late Triassic) in the Warte area, northeastern Iraqi Kurdistan region. Geological Journal, 56, 3923–3940. https://doi.org/10.1002/gj.4142.

[23] Aswad, M. K., Omer, M. F., & Naqshabandi, S. F. (2023). Examining the impact of cement on porosity evolution in the Upper Triassic Kurra Chine Formation of Sirwan Valley, Kurdistan Region, Iraq: A study integrating cathodoluminescence and scanning electron microscopy. Kuwait Journal of Science, 51, 100107. https://doi.org/10.1016/j.kjs.2023.07.013.

[24] Aswad, M. K., Naqshabandi, S. F., & Omer, M. F. (2024b). Palynofacies analysis and depositional environment of the Upper Triassic Kurra Chine Formation: Integrated by samples from Sarta and Tawke oil fields and outcrop samples from Sirwan Valley in the Kurdistan Region, northern Iraq. IOP Conference Series: Earth and Environmental Science, 1300(1), 012033. https://doi.org/10.1088/1755-1315/1300/1/012033.

Al-Kitab Journal for Pure Sciences (2026); 10(2):299-314.
https://doi.org/10.32441/kjps.10.2.p21

Al-Kitab Journal for Pure Sciences
ISSN: 2617-1260 (print), 2617-8141(online)

https://isnra.net/index.php/kjps

Calcareous Nannofossils Biostratigraphy of Chia Gara Formation in Banik village, Northern Iraq

Alaa Mahmood Al-Wazan[1],Enas Hazim Al-Khafaf[2],Omar Ahmed Al-Badrani[3]

[1]Department of Geology and Petroleum, College of Science, University of Mosul, Mosul, Iraq

[2.3]College of Environmental Sciences- Department of Environmental Sciences, Mosul University, Iraq

Corresponding Author: alaawazan@uomosul.edu.iq

Citation: *Alaa Mahmood Al-Wazan[1],Enas Hazim Al-Khafaf[2],Omar Ahmed Al-Badrani[3]*. **Calcareous Nannofossils Biostratigraphy of Chia Gara Formation in Banik village, Northern Iraq.**
Al-Kitab J. Pure Sci. [Internet]. 2026 Jul. 28 ;10(2):299-314
DOI.
https://isnra.net/index.php/kjps/article/view/2026.
https://doi.org/10.32441/kjps.10.2.p21

Keywords: Chia Gara, calcareous nannofossils, Banik, Northern Iraq.

Article History
Received 21 Jun. 2026
Accepted 28 Jul. 2026
Available online 01 Nov. 2026

©20--. THIS IS AN OPEN-ACCESS ARTICLE UNDER THE CC BY LICENSE
http://creativecommons.org/licenses/by/4.0/

Abstract:

Much of the Late Jurassic–Early Cretaceous Chia Gara Formation may be seen in northern Iraq. Black shale, thin to medium-bedded yellowish limestone, and thin-bedded brown argillaceous limestone make up the majority of its lithologythe. Late Jurassic to Early Cretaceous, is divided into four main calcareous nannofossil biozones based on the presence and range of key index species. These biozones, listed from youngest (top) to oldest (base), are as follows.

1. *Nannoconus bermudezii* Interval Range Biozone (CC0)
2. *Nannoconus steinmannii* Interval Range Biozone (CC1)
3. *Assipetra infracretacea* Interval Range Biozone (CC2)
4. *Calcicalathina oblongata* Interval Range Biozone (CC3)

• The age of the Chia Gara Formation was then determined by correlating these biozones with other zonal global biozonation systems ‹the Tithonian (Late Jurassic) to Valanginian (Early Cretaceous).

Keywords: Chia Gara, calcareous nannofossils, Banik, Northern Iraq.

الطباقية الحياتية لمتحجرات النانو الكلسية لتكوين جياكارا في قرية بانيك شمالي العراق

الاء محمود الوزان[1],ايناس حازم الخفاف[2],عمر احمد البدراني[3]

[1] قسم علوم الأرض والنفط، كلية العلوم، جامعة الموصل، الموصل، العراق

[2] كلية علوم البيئة – قسم علوم البيئة، جامعة الموصل، الموصل، العراق

[3] قسم علوم الأرض والنفط، كلية العلوم، جامعة الموصل، الموصل، العراق

الايميل الرسمي: alaawazan@uomosul.edu.iq

الخلاصة:

يظهر تكوين جياكارا ، الذي يمتد عمره من اواخر العصر الجوراسي الى اوائل العصر الكريتاسي في شمال العراق. التركيب الصخري للتكوين يتالف من الطفل الاسود اللون متعاقب مع الحجر الجيري الطيني رقيق الطبقات بالون البني، وحجر جيري اصفر رقيق الى متوسط السمك. يعد هذا المقطع من المقاطع المهمة لانه يمثل صخور مصدرية. بناءا" على تحديد الانواع الدالة من متحجرات النانو الكلسية تم تحديد اربعة انطقه طباقيه حياتية وهي من الاقدم في الاسفل الى الاحدث في الاعلى :

1. *Nannoconus bermudezii* Interval Range Biozone (CC0)
2. *Nannoconus steinmannii* Interval Range Biozone (CC1)
3. *Assipetra infracretacea* Interval Range Biozone (CC2)
4. *Calcicalathina oblongata* Interval Range Biozone (CC3)

ثم تم مضاهات الانطقة المحددة مع الانطقة الطباقية الحياتية العالمية وذلك لتحديد عمر تكوين جياكارا في منطقة بانيك والذي يتراوح بين التيثونيان (الجوراسي المتاخر)وحتى الفالنجانيان (الكريتاسي المبكر) .

الكلمات المفتاحية: جياكارا ، متحجرات النانو الكلسية، بانيك، شمال العراق

1. Introduction:

While the primary source rocks are often found in Jurassic and Lower Cretaceous strata[1-4], the majority of hydrocarbon reservoirs in Iraq are hosted in Cretaceous and Tertiary successions [5-6]. During the Mesozoic Era, carbonate, marl, and shale deposits accumulated in a large marine basin that covered the northern and northeastern part of Iraq. Oil-prone organic-rich successions may have been more likely to form during the Late Jurassic and Early Cretaceous due to the high regional heat gradient and worldwide marine transgression. Therefore, in order to comprehend the petroleum systems of the area, it is important to conduct thorough stratigraphic and geochemical research of Jurassic formations.

One of the most significant Upper Jurassic–Lower Cretaceous source-rock intervals in northern Iraq is the Chia Gara Formation. This formation originated at Chia Gara Anticline, which extends from the Middle Tithonian to the Berriasian, is located in the High Folded Zone, south of Amadiya. [7]. The formation is mostly composed of thin-bedded ammonite-bearing limestone and shale, with yellow marly limestone and shale rising to a thickness of around 232 meters at the type section [7].

According to numerous earlier geological and geochemical studies, the Chia Gara Formation is a highly efficient gas-prone source rock that has been validated for the production of hydrocarbons [32-1-8-26-27-2-18] In addition, a close genetic relationship between hydrocarbons, oil seeps, and organic materials preserved in the Chia Gara Formation was revealed by oil–source correlation and biomarker analysis [25-3-17] However, prior research has mostly been restricted to certain regions or a limited number of tectonic domains. Therefore, the purpose of this work is to determine the petrographic features of carbonate facies and the petroleum The Chia Gara Formation's source rock characteristics in some northern Iraqi tectonic zones.

A reference section of the Formation Chia Gara escarpment at a single representative section near Banik Village (42°58′2.6′E, 37°13′33.4′N), It is located in northern Iraq, some 25 kilometers northeast of Zakho City. , was used for this study (Fig. 1). The research area is situated in the Foreland Basin's High Folded Zone, where tectonic deformation and erosion have produced a large outcrop of Jurassic and Cretaceous successions along the axes and sides of regional anticlines.

However, prior research has mostly been restricted to certain regions or a limited number of tectonic domains. Therefore, the purpose of this work is to determine the petrographic features of carbonate facies and the petroleum source rock qualities of the Chia Gara Formation in certain northern Iraqi tectonic zones. A reference section of the Chia Gara Formation escarpment at a single representative section near Banik Village (42°58′2.6′E, 37°13′33.4′N), which is about 25 km northeast of Zakho City, northern Iraq, was used for this study (Fig. 1). The research area is situated in the Foreland Basin's High Folded Zone, where tectonic deformation and erosion have produced a large outcrop of Jurassic and Cretaceous successions along the axes and sides of regional anticlines. [28-4]

The Chia Gara Formation was deposited during the Late Jurassic–Early Cretaceous

in a relatively deep outer-shelf environment linked to the extensional history and emergence of the Neo-Tethys Ocean near the Arabian Plate border. [31]. According to biostratigraphic evidence, the formation on the upper boundary has been dated from the Berriasian to the Middle Tithonian [7]. The upper boundary is progressively becoming closer to the Valanginian stage. The formation beds are a component of Resuming ocean-floor spreading in the southern Neo-Tethys is linked to the Arabian Plate Megasequence AP8 (Late Tithonian–Turonian), which was formed in a major intra-shelf basin. [41]. According to Jassim and Buday (2006), The deep outer-shelf marine depositional environment of the Chia Gara Formation was ideal for the accumulation of organic-rich muds, further improving source rock quality in shale-dominated intervals **Fig.1**.

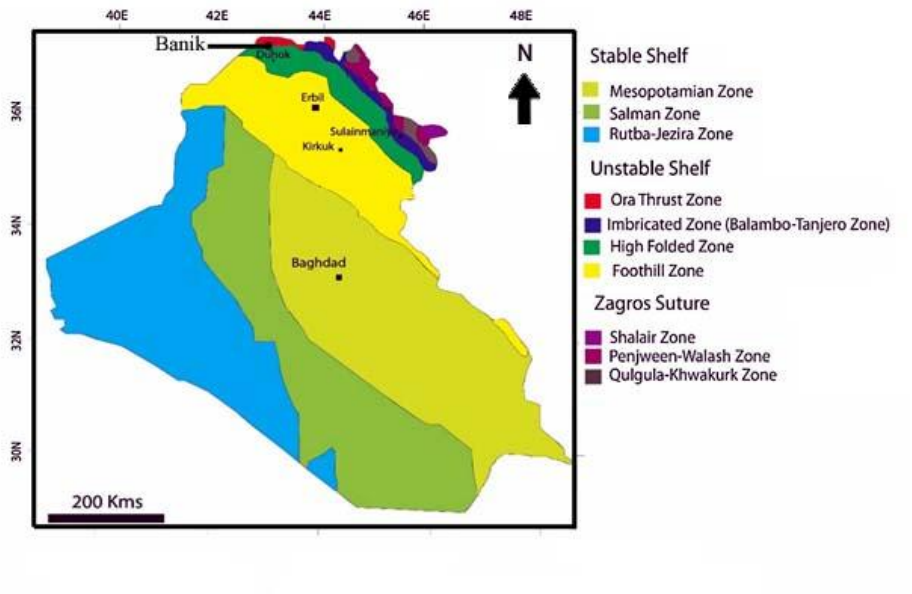


Fig.1: The tectonic map and locations of the research regions (derived from Numan (2000), [22]

- Figure 2 depicts the Arabian Plate's Late Tithonian–Early Berriasian paleogeographic setting. The basin architecture at this time is characterized by a facies distribution that was largely uniform across the Jurassic–Cretaceous transition. Despite such complexity in the geologic architecture of the Gercus formations, the variations in thickness between the outcrop and subsurface wells, such as near the Tigris, are not great. The formation is primarily composed of black shale, thin to medium-bedded yellowish limestone, and thin-bedded brown argillaceous limestone.
- The lower part is dominated by organic-rich shale interbedded with argillaceous limestone, reflecting favorable conditions for organic matter preservation.

accumulation during deposition [16] (Fig. 2)..

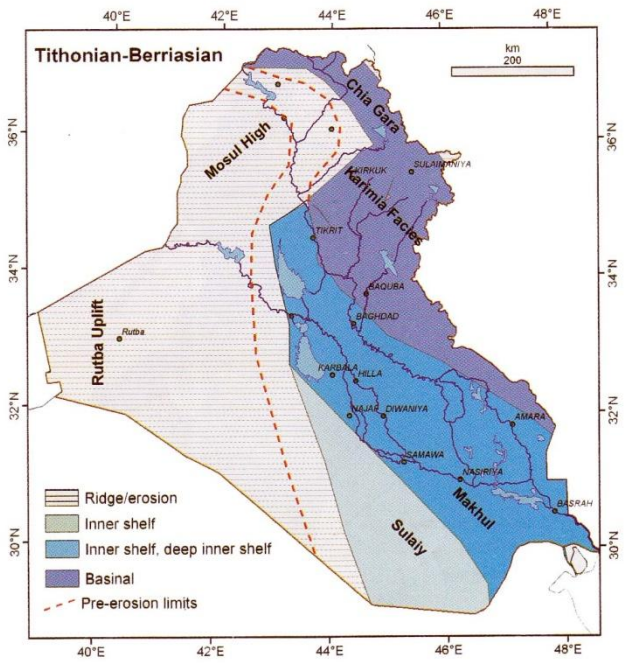


Fig. 2 Iraq's Late Tithonian–Early Berriasian Paleogeography [22].

Bellen et al. (1958) determined that the Chia Gara Formation was deposited between the Middle Tithonian and Berriasian, based on biostratigraphic data. (1959). It is substantially developed in the northern region of Iraq's unstable shelf, laterally grading into the Foothill Zone's Makhul and Karimia Mudstone formations. In contrast, equivalent deposits of the stable and southwestern unstable shelves are represented by the Tithonian-age Sulaiy Formation [11].

From Zakho to the Sirwan Gorge, this record is rather extensive throughout the Kurdistan Region of northern and northeastern Iraq, representing the entire geographical range of the Chia Gara Formation as a regional observation. It is found in many of the underground areas and is typically gated out in the High Folded and Imbricate tectonic zones . Compared to basin morphology, thickness variations across the basin indicate variations in depositional setting and basin evolution, and isopach data indicate that the main depositional centre in the Late Jurassic was located between the Tigris River-northern Mosul—Kirkuk region.

The studied section of Chia Gara Formation has a largely homogenous lithology and consists of predominately shale interbedded with very thinly bedded argillaceous limestone. The succession is about (50) m thick at exposure. The basal interval is defined by organic-rich

shale interbedded with argillaceous limestone, which reflects favorable conditions for organic-matter preservation، (the proportion of brittle shale decreases, while limestone and argillaceous limestone increase; the top part consists mainly of marl and marly limestone. Both ammonite fossils are found throughout the carbonate beds but are bette preserved in limestone layers and carbonate concretions.

2. Material and methods:

A total of(125) rock samples were selected from the Chia Gara Formation, northern Iraq for calcareous nannofossil examining. Preparation of thin sections for examination by transmitted-light microscope (Method H of Armstrong & Brasier 2005) The calcareous nannofossils were taxonomically identified from the prepared thin sections based on their diagnostic morphological features.

3. Results:

Under the optical microscope, a heterococcolith and nannolith assemblage with numerous uncertain systematic affiliation taxa (Incertae sedis) of calcareous nannofossils was found. The taxa that we identified are described in summary form below **Fig.3**.

1. Family Chiastozygaceae Rood et al., 1973

Genus Zeugrhabdotus Reinhardt, 1965

Zeugrhabdotus embergeri (Noël, 1959) Perch-Nielsen, 1984

2. Family Cretarhabdaceae Thierstein, 1973

Genus Cruciellipsis Thierstein, 1971

Cruciellipsis cuvillieri (Manivit, 1966) Thierstein, 1971

3. Family Rhagodiscaceae Hay, 1977

Genus Calcicalathina Thierstein, 1971

Calcicalathina oblongata (Worsley, 1971) Thierstein, 1971

4. Family Watznaueriaceae Rood et al., 1971

Genus Cyclagelosphaera Noël, 1965

Cyclagelosphaera margerelii Noël, 1965

Genus Diazomatolithus Noël, 1965

Diazomatolithus lehmanii Noël, 1965

Genus Watznaueria Reinhardt, 1964

Watznaueria *manivitiae* Bukry 1973

1. Nannoliths

1. Family Microrhabdulaceae Deflandre, 1963

Genus *Lithraphidites* Deflandre, 1963

Lithraphidites carniolensis Deflandre, 1963

2. Family Nannoconaceae Deflandre, 1959

Genus *Nannoconus* Kamptner, 1931

Nannoconus bermudezii Brönnimann, 1955

Nannoconus kamptneri Brönnimann, 1955

Nannoconus steinmannii minor Deres & Achéritéguy, 1980

Nannoconus *steinmannii steinmannii* Kamptner, 1931

3 . Family Tubodiscaceae Bown & Rutledge, 1997 in Bown & Young, 1997

Genus *Tubodiscus* Thierstein, 1973

Tubodiscus *verenae* Thierstein, 1973

2. Incertae sedis nannoliths:

Genus Assipetra Roth, 1973

Assipetra infracretacea (Thierstein, 1973) Roth, 1973

Genus Hexalithus Gardet, 1955

Hexalithus geometricus Casellato 2010

Hexalithus noeliae Loeblich & Tappan, 1966

Genus Polycostella Thierstein, 1971

Polycostella *senaria* Thierstein, 1971

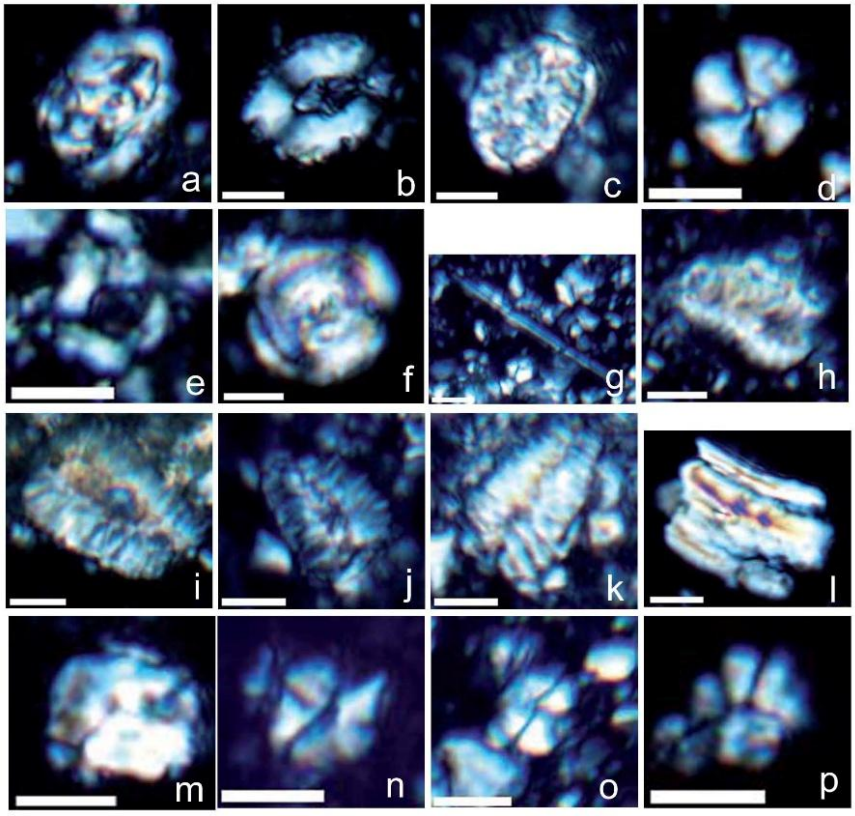


Fig.3 (a) Polarized micrographs of calcareous nannofossil from the Chia Gara Formation *Zeugrhabdotus embergeri*; (b) *Cruciellipsis cuvillieri*; (c) *Calcicalathina oblongata*; (d) *Cyclagelosphaera margerelii*; (e) *Diazomatolithus lehmanii*; (f) *Watznaueria manivitiae*; (g) *Lithraphidites carniolensis*; (h) *Nannoconus bermudezii*;

(i) *Nannoconus kamptneri*; (j) *Nannoconus steinmannii minor*; (k) *Nannoconus steinmannii steinmannii*; (l) *Tubodiscus verenae*; (m) *Assipetra infracretacea*; (n) *Hexalithus geometricus*; (o) *Hexalithus noeliae*; (p) *Polycostella senaria*.

4. Discussion

1. *Nannoconus bermudezii* Interval Range zone (CC0)

Definition: Interval biozone for the species Nannoconus bermudezii Brönnimann, 1955.

Boundaries: from FO of Nannoconus bermudezii Brönnimann, 1955 to the FO Nannoconus steinmannii Kamptner, 1931.

Thickness: 17 m.

Discussion: There is a correlation between this biozone and the CC1 (Nannoconus steinmannii Interval Zone) by Sissigh (1977) and correlated with NC1(Nannoconus coloni Interval Zone) biozone which is studied by Roth (1978) with CC1 biozone which is studied by Perch-Nielsen, (1979a)(1983) therefore we suggested the Berriasian [20] **Fig.٤** , **Fig. 5.**

2. Nannoconus steinmannii Interval Range zone (CC1)

Definition: Interval biozone for the species Nannoconus steinmannii Kamptner, 1931.

Boundaries: from FO of Nannoconus steinmannii Kamptner, 1931 to FO Assipetra infracretacea [45-39].

Thickness: 12m.

Discussion: This biozone is correlated with the biozone (CC1) (Nannoconus steinmannii Interval Zone) by Sissigh (1977) and correlated with NC1 (Nannoconus coloni Interval Zone) biozone which is studied by Roth (1978) with CC1 biozone which is studied by Perch-Nielsen, (1979a)(1983) therefore we suggested the Berriasian [20] **Fig.٤** , **Fig. 5.**

3. Assipetra infracretacea Interval Range zone (CC2)

Definition: Interval biozone for the species Assipetra infracretacea [45-38].

Boundaries: FO Assipetra infracretacea [45-39] to FO

Calcicalathina oblongata [46-44].

Thickness: 8m.

Discussion: We proposed the Berrasian to Valanginian to [20] because this biozone is correlated with the biozone (CC2) (Stradneria crenulata Interval Zone) by Sissigh (1977) and correlated with the NC2 (Retecapsa angustiforata) biozone, which is studied by Roth (1978) with CC2 biozones, which is studied by Perch-Nielsen (1979a) **Fig.4** , **Fig. 5.**

4. Interval Range zone (CC3) of Calcicalathina oblongata

Definition: Calcicalathina oblongata interval biozone (Worsley, 1971; Thierstein, 1971).

Limitations: FO Cretarhabdus loriei Gartner, 1968 to FO Calcicalathina oblongata (Worsley, 1971) Thierstein, 1971.

Thickness: 10m.

Discussion: We proposed the Valanginian (Gradstein et al., 2020) because this biozone is correlated with the biozone (CC3) (Calcicalathina oblongata Interval Zone) by Sissigh (1977) and correlated with the NC3 (Tubodiscus verenae) biozone that is studied by Roth (1978) with CC3 biozones that are studied by Perch-Nielsen (1979a) (1983) **Fig.4.**, **Fig. 5.**

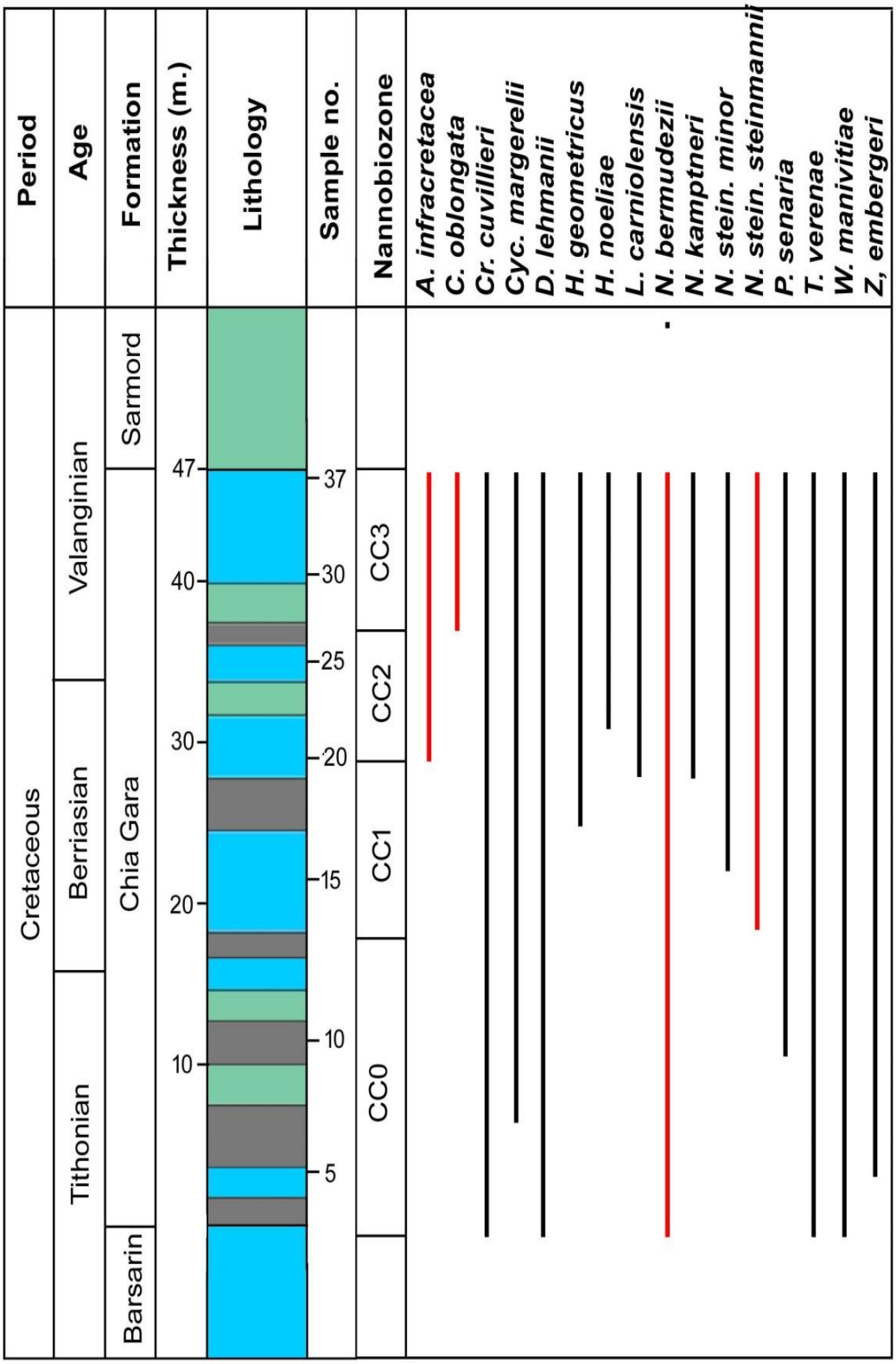


Fig.4 The Clacreous Nannofossils for (Banik) section

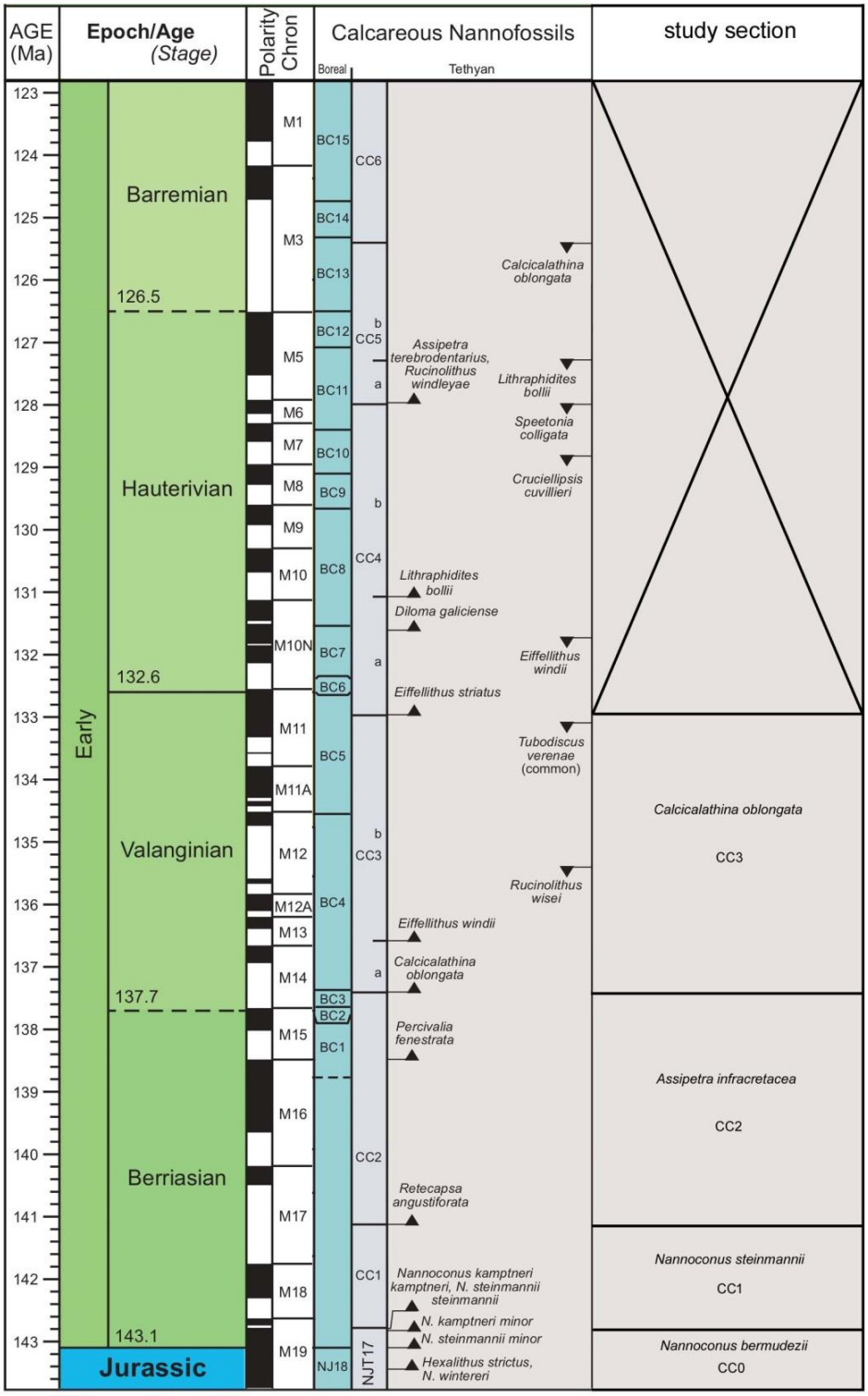


Fig. 5 Correlation chart for Calcareous Nannofossils for lower Cretaceous

5. Conclusions

Four biozones were identified based on the identification taxa and index spices of

Calcareous nannofossils, with the younger ones at the top and the older ones at the bottom.:

1. *Nannoconus bermudezii* Interval Range Biozone (CC0)
2. *Nannoconus steinmannii* Interval Range Biozone (CC1)
3. *Assipetra infracretacea* Interval Range Biozone (CC2)
4. *Calcicalathina oblongata* Interval Range Biozone (CC3)

Then these biozones were correlated with other zonal global biozonation schemes of the Chia Gara Formation is determining that the age of the Formation in (Tithonian toValanginian). **Fig. 5.**

6. References

[1] Al-Ameri TK, Al-Obaidi RY (2004) Palynomorphs and alkane peaks of Campanian Khasib Formation, oil used to assess oil-source correlation and suggestion for other traps along the migration path, East Baghdad oil field, Iraq. In: 6th International conference on geochemistry, Alexandria University, Egypt, pp. 243–255

[2] Al-Badry AMS (2012) Stratigraphy and geochemistry of Jurassic for-mations in selected sections—North Iraq; PhD thesis ،University of Baghdad pp. 86-122.

[3] Al-Jaafary AS, Hadi A (2015) Hydrocarbon potential, thermal matu-ration of the Jurassic sequences, and the genetic implication for the oil seeps in North Thrust Zone, North Iraq. Arab J Geosci 8:8089–8105. https://doi.org/10.1007/s12517-015-1781-z

[4] Al-Sharhan AS, Nairn AEM (1997) Sedimentary basin and petro-leum geology of the Middle East. Elsevier Science

[5] Aqrawi AAM, Badics B (2015) Geochemical characterization, vol-umetric assessment and shale-oil/gas potential of the Middle Jurassic-Lower Cretaceous source rocks of NE Arabian Plate. GeoArabia 20(3):99–140

[6] Aqrawi AAM, Goff JC, Horbury AD, Sadooni FN (2010) The petro-leum geology of Iraq: Beaconsfield. Scientific Press Ltd., United Kingdom, p 424

[7] Bellen RC, van, Dunnington HV, Wetzel R, Morton DM (1959) Lexique Stratigraphique International. V. III, Asie, Fasc., 10a Iraq. Paris

[8] Bown, P. R. and Young, J. R. (1997). Mesozoic calcareous nannoplankton

classification. Journal of Nannoplankton Research, 19(1): 21–36.

[9] Bown, P. R., Rutledge, D. C., Crux, J. A. and Gallagher, L. T. (1998). Lower Cretaceous. In, Bown, P. R. (ed.) Calcareous Nannofossil Biostratigraphy. British Micropalaeontological Society Publication Series . 86-131.

[10] Brönnimann, P. (1955). Microfossils Incertae sedis from the Upper Jurassic and Lower Cretaceous of Cuba. Micropaleontology, 1(1), 28–51.

[11] Buday T (1980) The regional geology of Iraq, vol 1, stratigraphy and paleogeography. Dar Al-Kutub Publication, University of Mosul, Iraq

[12] Casellato, C. E. (2010). Calcareous nannofossil biostratigraphy of Upper Callovian

- Lower Berriasian successions from the Souhern Alps, North Italy. Rivista Italiana di Paleontologia e Stratigrafia. 116(3): 357-404.

[13] Deflandre, G. (1959). Sur les nannofossiles calcaires et leur systématique. Revue de Micropaléontologie. 2: 127-152.

[14] Deflandre, G. (1963). Sur les Microrhabdulidés, famille nouvelle de nannofossiles calcaires. Comptes Rendus Hebdomadaires des Séances de l'Académie des Sciences, Paris. 256: 3484-3487.

[15] Deres, F. and Achéritéguy, J. (1980). Biostratigraphie des Nannoconides. Bulletin des Centres de Recherches Exploration-Production Elf-Aquitaine. 4: 1-53.

[16] Dunnington HV (1958) Generation, migration, accumulation, and dis-sipation of oil in Northern Iraq. In: Weeks LG (ed) Habitat of oil, a symposium, AAPG. Bull, pp 1194–1251

[17] Edilbi ANF (2016) The role of the Baluti Formation within Triassic Petroleum Systems in Kurdistan; Akre-Bijeel Block, Gara and Ora anticlines. An organic geochemical and basin modelling approach. PhD Thesis, University of Aberdeen

[18] Edilbi ANF, Sherwani GH (2018) Sedimentology and Petroleum Poten-tial of Chia Gara Formation (Late Jurassic–Early Cretaceous) in three different tectonic zones in Northern Iraq and Kurdistan Region, 13th Middle East Geosciences conference and Exhibi-tion (GEO2018), March 5-8, 2018-Manama, Bahrain

[19] English JM, Lunn GA, Ferreira L, Yaku G (2015) Geologic evolu-tion of the Iraqi Zagros, and its influence on the distribution of hydrocarbons in the Kurdistan Region. AAPG Bull 99(2):231–272 Flugel E (2010) Microfacies of carbonate rocks-analysis, interpretation and application, 2nd edn. Springer, Berlin, pp 1–984

[20] Gradstein, F. M., and Ogg J. G., Schmitz M. and Ogg G. (2020). The Geologic Time Scale, West Lafayette, Indiana, USA; Volume 2.

[21] Hay, W. W. (1977). Calcareous nannofossils. In, Ramsay, A. T. S. (ed.) Oceanic Micropalaentology. Academic Press, London 1055-1200.

[22] Jassim SZ, Buday T (2006) Latest Eocene-Recent Megasequence AP11. In: S Z Jassim and J Goff (eds) Regional geology of Iraq. Dolin, Prague and Moravian Museum, Brno, Czech Republic, pp 71–183

[23] Kamptner, E. (1931). Nannoconus steinmanni novo gen., novo spec., ein merkwürdiges gesteinbildendes Mikrofossil aus dem jüngeren Mesozoikum der Alpen. Paläontologische Zeitschrift, 13, 288–298.

[24] Manivit, H. (1966). Sur quelques coccolithes nouveaux du Néocomien. Compte Rendu Sommaire des Séances de la Société Géologique de France. 7: 267-268.

[25] Mohialdeen IMJ, Hakimi MH, Al-Beyati FM (2013) Biomarker char-acteristics of certain crude oils and the oil-source rock correlation for the Kurdistan oilfields. Arab J Geosci, Northern Iraq. https:// doi.org/10.1007/s12517-013-1228-3

[26] Mohyaldin IMJ (2008) Source rock appraisal and oil/source correlation for the Chia Gara Formation, Kurdistan—North Iraq. PhD thesis ،University of Sulaimani

[27] Mohyaldin IMJ, Al-Beyati FM (2008) Sedimentology and hydrocar-bon generation potential of Middle Tithonian-Berriasian Chia Gara Formation, Well K-109, Kirkuk Oil Field. Kirkuk Univ J 2(1):27–43

[28] Murris RJ (1980) Middle east—stratigraphic evolution and oil habitat. AAPG Bull 64(5):597–618

[29] Noël, D. (1959). Étude de coccolithes du Jurassique et du Crétacé inférieur. Publications du Service de la Carte Géologique de l'Algérie (Nouvelle Série) Bulletin. 20: 155-196.

[30] Noël, D. (1965). Sur les Coccolithes du Jurassique Européen et d'Afrique du Nord. Essai de classification des coccolithes fossiles. Éditions du Centre National de la Recherche Scientifique, Paris. 1-209.

[31] Numan NMS (1997) A plate tectonic scenario for the Phanerozoic succession in Iraq. Iraqi Geol J 30(2):85–110

[32] Odisho KY, Othman RS (1992) Preliminary geochemical evaluation of hydrocarbon source rocks in northern part of Iraq. Iraqi Geol J 25:136–153

[33] Perch-Nielsen, K. (1984b). Validation of new combinations. INA Newsletter. 6(1): 42-46.

[34] Perch-Nielsen, K. 1979a. Calcareous nannofossils from the Cretaceous between the North Sea and the Mediterranean. IUGS Series A. 6. 223-72.

[35] Perch-Nielsen, K. 1983. Recognition of Cretaceous stage boundaries by means of calcareous nannofossils. In: T. Birkelund, et al. (eds.), Symposium on Cretaceous Stage Boundaries. Copenhagen, Abstracts, pp. 152-6.

[36] Reinhardt, P. (1964). Einige Kalkflagellaten-Gattungen (Coccolithophoriden, Coccolithineen) aus dem Mesozoikum Deutschlands. Monatsberichte der Deutschen Akademie der Wissenschaften zu Berlin. 6: 749-759.

[37] Reinhardt, P. (1965). Neue Familien für fossile Kalkflagellaten (Coccolithophoriden, Coccolithineen). Monatsberichte der Deutschen Akademie der Wissenschaften zu Berlin. 7: 30-40.

[38] Rood, A. P., Hay, W. W. and Barnard, T. (1971). Electron Microscope Studies of Oxford Clay Coccoliths. Eclogae Geologicae Helvetiae. 64: 245-272.

[39] Roth, P. H. (1973). Calcareous nannofossils: Leg 17 of the Deep Sea Drilling Project. Initial Reports of the Deep Sea Drilling Project, 17: 695–795.

[40] Roth, P. H. (1978). Cretaceous nannoplankton biostratigraphy and oceanography of the northwestern Atlantic Ocean. Initial Reports of the Deep Sea Drilling Project. 44: 731-760.

[41] Sharland PR, Archer R, Casey DM, Davies RB, Hall SH, Howard AP, Horbury AD, Simmons MD (2001) Arabian Plate sequence stratigraphy, GeoArabia, Special

Publication 2. Gulf PetroLink, Bahrain, p 372

[42] Sissingh, W. (1977). Biostratigraphy of Cretaceous calcareous nannoplankton.

[43] Geologie en Mijnbouw. 65(1): 37-65.

[44] Thierstein, H. R. (1971). Tentative Lower Cretaceous Calcareous Nannoplankton Zonation. Eclogae Geologicae Helvetiae. 64: 459-488.

[45] Thierstein, H. R. (1973). Lower cretaceous calcareous nannoplankton biostratigraphy. Abhandlungen der Geologischen Bundesanstalt. 29: 3-52.

[46] Worsley, T. R. (1971). Calcareous nannofossil zonation of Upper Jurassic and Lower Cretaceous sediments from the Western Atlantic. In, Farinacci, A. (ed.) Proceedings of the Second Planktonic Conference Roma 1970. Edizioni Tecnoscienza, Rome 2: 1301-1321.

Al-Kitab Journal for Pure Sciences (2026); 10(2):315-333.
https://doi.org/10.32441/kjps.10.2.p22

Al-Kitab Journal for Pure Sciences
ISSN: 2617-1260 (print), 2617-8141(online)

https://isnra.net/index.php/kjps

Heavy Metal Contamination in Drinking Water, Groundwater, and Industrial Water Sources in Kirkuk and Selected Iraqi Cities: A Structured Evidence Synthesis and Evaluation of Treatment Technologies

Noor N. Abdulqader[1], Hayder M. Jasim[2]

[1] Surveying Engineering – College of Engineering – Al-Kitab University - Altun Kupri.

[2] Petroleum Engineering – College of Engineering – Al-Kitab University - Altun Kupri.

Corresponding Author: noor.nabeel@uoalkitab.edu.iq , hayder.mahmood@uoalkitab.edu.iq

Citation: *Noor N. Abdulqader[1], Hayder M. Jasim[2]*. **Heavy Metal Contamination in Drinking Water, Groundwater, and Industrial Water Sources in Kirkuk and Selected Iraqi Cities: A Structured Evidence Synthesis and Evaluation of Treatment Technologies.**
Al-Kitab J. Pure Sci. [Internet]. 2026 Aug. 29 ;10(2):315-333
DOI.
https://isnra.net/index.php/kjps/article/view/2026.
https://doi.org/10.32441/kjps.10.2.p22

©2026. THIS IS AN OPEN-ACCESS ARTICLE UNDER THE CC BY LICENSE
http://creativecommons.org/licenses/by/4.0/

Keywords: adsorption; groundwater; heavy metal; Kirkuk; risk assessment; water treatment.

Article History

Received	01 Aug. 2026
Accepted	29 Aug. 2026
Available online	01 Nov. 2026

Abstract:

This structured review synthesizes published evidence on heavy metals in drinking-water treatment systems, groundwater, and industrial water sources in Kirkuk and selected Iraqi cities. The quantitative synthesis is restricted to six primary water-quality studies cited in the manuscript ([4–9]); other references are used for standards, methods, treatment technologies, or contextual interpretation. Because the original search log did not preserve database-specific retrieval, duplicate-removal, and exclusion counts, these upstream PRISMA quantities are reported as not recorded rather than reconstructed retrospectively. Evidence was appraised using five domains: sampling adequacy, sampling-period reporting, analytical-method reporting, quality assurance/quality control, and completeness of quantitative reporting. The synthesis shows marked spatial heterogeneity: municipal treated-water evidence from Kirkuk indicates comparatively low metal concentrations, whereas industrial wastewater in Kirkuk and shallow groundwater evidence from other Iraqi cities show substantially greater contamination. Direct-ingestion HQ calculations are interpreted only for potable or potentially consumed

waters; industrial wastewater is treated as a source-pathway hazard and is not assigned a drinking-water ingestion risk. Temporal inference remains limited by sparse, non-equivalent studies and differences in source type and analytical design. Treatment technologies are therefore presented as context-dependent options rather than prescriptive upgrades. The review identifies cadmium and lead as priority contaminants and emphasizes standardized monitoring, transparent analytical QA/QC, and source-specific treatment selection.

Keywords: adsorption; groundwater; heavy metal; Kirkuk; risk assessment; water treatment

تلوث المعادن الثقيلة في مياه الشرب والمياه الجوفية والمياه الصناعية في كركوك ومدن عراقية مختارة :توليف منظم للأدلة المنشورة وتقييم تقنيات المعالجة

نور نبيل عبد القادر[1]، حيدر محمود جاسم[2]

[1] قسم هندسة المساحة، كلية الهندسة، جامعة الكتاب، ألتون كوبري، العراق.

[2] قسم هندسة النفط، كلية الهندسة، جامعة الكتاب، ألتون كوبري، العراق.

الايميل الرسمي: noor.nabeel@uoalkitab.edu.iq , hayder.mahmood@uoalkitab.edu.iq

الخلاصة:

تجمع هذه المراجعة المنظمة الأدلة المنشورة عن المعادن الثقيلة في مياه الشرب والمياه الجوفية والمياه الصناعية في كركوك ومدن عراقية مختارة. واقتصر التوليف الكمي على ست دراسات أولية لجودة المياه مستشهد بها في البحث [4-9]، بينما استُخدمت بقية المراجع للمعايير والمنهجيات وتقنيات المعالجة والسياق العلمي. ونظرًا إلى أن سجل البحث الأصلي لم يحفظ أعداد النتائج المسترجعة من كل قاعدة بيانات أو المكررات أو أسباب الاستبعاد بصورة كاملة، لم تُختلق هذه الأعداد بأثر رجعي، بل صُنفت على أنها غير مسجلة. كما قُيّمت جودة الأدلة وفق خمسة مجالات تشمل كفاية العينات، وفترة أخذ العينات، وطريقة التحليل، وضبط الجودة، واكتمال عرض البيانات.

أظهر التوليف تباينًا مكانيًا واضحًا بين أنواع مصادر المياه؛ إذ تشير الأدلة الخاصة بالمياه المعالجة في كركوك إلى مستويات أقل نسبيًا، في حين تظهر مياه الصرف الصناعي في كركوك وبعض أدلة المياه الجوفية الضحلة في مدن عراقية أخرى القائم على الابتلاع المباشر على المياه الصالحة أو المحتمل HQ مستويات أعلى من التلوث. واقتصر تفسير معامل الخطر استهلاكها، بينما عوملت مياه الصرف الصناعي بوصفها خطرًا على مسار المصدر-الانتقال وليس كمياه شرب. كما أن الاستدلال الزمني بقي محدودًا بسبب قلة الدراسات وعدم تجانس مصادر المياه وطرق التحليل.

تُعرض تقنيات المعالجة بوصفها خيارات تعتمد على نوع المصدر وتركيز الملوث والظروف التشغيلية، وليس كتوصيات تنفيذية نهائية من دون دراسة جدوى محلية. وتشير الأدلة إلى أولوية متابعة الكادميوم والرصاص، مع الحاجة إلى برنامج رصد موحد، وإبلاغ واضح عن إجراءات ضمان وضبط الجودة التحليلية، وربط اختيار تقنية المعالجة بطبيعة مصدر المياه.

الكلمات المفتاحية: الامتزاز؛ المياه الجوفية؛ المعادن الثقيلة؛ تقييم المخاطر؛ كركوك؛ معالجة المياه

1. Introduction:

Access to safe drinking water is a basic human right and a foundation of public health. Nevertheless, heavy metal contamination is a global risk to water quality as metals such as cadmium (Cd), lead (Pb), chromium (Cr), nickel (Ni), arsenic (As) and mercury (Hg) are non-biodegradable, toxic and have bioaccumulation potential [1]. These contaminants are derived from natural geogenic sources and from anthropogenic activities, including mining, industrial discharge, agricultural runoff and improper waste disposal. Chronic exposure to heavy metals via drinking water consumption has been reported to cause Nephrotoxicity, Hepatotoxicity, carcinogenicity, neurological damage and developmental disorders [2].

Decades of conflict, aging infrastructure, industrial pollution and water scarcity caused by climate change make Iraq especially vulnerable to water quality issues. [3] The courses of the Tigris and Euphrates rivers, the main sources of fresh water for the country, is fed with untreated municipal and industrial effluent. The Heavy Metal Pollution Index (HPI) in several seasons [4] has exceeded the critical value of 100 in the water treatment plants of the capital, Baghdad, indicating that heavy metal pollution has reached critical levels. Likewise, in post-conflict Mosul, shallow groundwater wells were found to be alarmingly contaminated with cadmium and lead levels exceeding the World Health Organization (WHO) and Iraqi drinking water standards [5].

Kirkuk Governorate in northern Iraq is an important oil-producing and agricultural region with growing water demand. Its water supply relies on surface-water and groundwater resources and municipal treatment systems, including the Kiwan and Al-Dibs plants [6]. Published evidence also documents industrial effluents in Kirkuk [8]. Because these source types have different exposure pathways, the present review distinguishes treated drinking water, groundwater, and industrial wastewater rather than treating them as a single exposure category.

Published Iraqi evidence is geographically dispersed across Kirkuk, Baghdad, Mosul, and Duhok/Shekhan, and it varies in sampling design, analytical technique, reporting completeness, and water-source type [4-9]. These differences limit direct numerical comparison and make an explicit evidence-quality assessment necessary before spatial or temporal interpretation.

Accordingly, this review aims to: (i) synthesize the primary quantitative water-quality evidence cited for Kirkuk and selected Iraqi comparison areas; (ii) compare reported concentrations with national and international drinking-water benchmarks only where the source is relevant to potable-water assessment; (iii) distinguish reported or recalculated pollution/risk indices from source-pathway hazards; (iv) evaluate spatial and temporal patterns cautiously in light of methodological heterogeneity; and (v) appraise treatment technologies as context-dependent options for Iraqi water systems.

2. Material and methods:

2.1 Data Collection Strategy

The review was structured using PRISMA 2020 reporting principles. The original search used Scopus, Web of Science, ScienceDirect, and Google Scholar with combinations of ("heavy metals" OR "trace metals" OR "toxic metals") AND ("drinking water" OR "groundwater" OR "potable water" OR "water treatment") AND ("Kirkuk" OR "Iraq" OR "Mosul" OR "Baghdad" OR "Kurdistan"). Eligible primary studies had to report quantitative water-quality data relevant to heavy metals. The submitted manuscript cited 25 references in total, but only six primary water-quality studies ([4–9]) supplied the quantitative evidence synthesized here. References [1–3] and [10–25] serve contextual, methodological, standards, or treatment-technology purposes and are not counted as included primary water-quality studies. The original search log did not preserve the numbers retrieved from each database, duplicates removed, full texts excluded, or exclusion reasons. These quantities therefore cannot be reconstructed reliably and are explicitly reported as "not recorded" in the PRISMA flow diagram. This correction replaces the unsupported statement that 28 studies were extracted in detail. The study-selection diagram is presented in Figure 1.

2.2 Data Extraction and Quality Assessment

For each primary water-quality study, the review extracted, when reported, study area, water-source type, sampling period, sample size, analytical technique, target metals, concentration statistics, and principal findings. Evidence quality was assessed across five reporting domains: (1) sample size/sampling design, (2) sampling-period reporting, (3) analytical-technique reporting, (4) QA/QC or standard-method reporting, and (5) completeness of quantitative results. Each domain was classified as clearly reported, partly reported, or not reported in the

information available to this review. This appraisal is a transparency assessment of the evidence base and is not presented as a formal risk-of-bias instrument.

2.2.1 Study-selection transparency (PRISMA 2020)

Figure 1. PRISMA 2020 study-selection transparency diagram. NR = not recorded in the original search log; six primary quantitative water-quality studies ([4–9]) form the evidence synthesis.

PRISMA 2020 study-selection transparency
Records identified from databases: NR (original search log not preserved)
Duplicates removed: NR
Records screened / full texts assessed: NR
Primary quantitative water-quality studies included: n = 6 ([4–9])
Context/method/standards/treatment references: n = 19
Quantitative evidence synthesis: n = 6 primary studies

2.3 Comparison Standards

The extracted concentration data were compared with the Iraqi Standard 417/2011 and WHO drinking-water guidance [10,11]. The WHO benchmark was checked against the current fourth edition incorporating the first, second and third addenda (2026). Comparisons were made only when the water type and reported units were compatible; industrial wastewater was not treated as drinking water.

2.4 Health Risk Assessment Indices

Three well-established indices were used to assess the health risk of heavy metal exposure through drinking water:

(a) Heavy Metal Pollution Index (HPI): HPI offers a composite measure of overall water quality as compared to the maximum allowable concentrations. It is computed using Equation (1) [4,12]:

$$HPI = \sum Wi \times Qi / \sum Wi \qquad (1)$$

where Wi = 1/Si (2) is the unit weight (inverse of the standard value, Si) and Qi is the sub-index for the ith metal as Qi = [(Mi – Ii) / (Si – Ii)] × 100 (3), where Mi is the monitored value, Ii is the ideal value (usually zero) and Si is the standard value. HPI value below 50 indicates low pollution level, 50-100 indicates moderate pollution level and above 100 indicates critical pollution level [4,12].

(b) Metal Index (MI) (Equation (4)): The MI provides a simplified evaluation of overall metal contamination:

$$MI = \Sigma (Ci/MACi) / n \quad (4)$$

where Ci is the measured concentration, MACi is the maximum allowable concentration, and n is the number of metals analysed. An MI less than 0.5 indicates low contamination, 0.5-1.0 indicates moderate and above 1.0 indicates high contamination [12].

(c) Hazard Quotient (HQ): HQ is retained as a health-risk framework for interpreting studies that report the required exposure inputs. Because the included sources do not provide a harmonized set of concentration, exposure, and reference-dose data, HQ values were not newly recalculated across studies in this review. This avoids false precision from combining heterogeneous datasets. The HQ expression is given in Equation (5).

In this revision, HQ is interpreted only for water intended or plausibly used for drinking. Industrial wastewater is excluded from direct-ingestion HQ interpretation because it is not a potable-water exposure medium; its metal concentrations are discussed as a potential source of contamination to receiving surface water or groundwater. Where both mean and maximum concentrations are reported, mean values are used for central comparative summaries and maxima are retained as worst-case observations, with the basis stated explicitly in the table.

$$HQ = CDI / RfD \quad (5)$$

where CDI = Chronic Daily Intake (mg kg^{-1} day^{-1}) = (C × IR × EF × ED) / (BW × AT) (6), C = metal concentration (mg L^{-1}), IR = ingestion rate (2 L day^{-1} for adults), EF = exposure frequency (365 days $year^{-1}$), ED = exposure duration (70 years), BW = body weight (70 kg) and AT = averaging time (25 550 days). RfD Oral Reference Dose (mg/kg/day) [13]. HQ > 1 indicates potential non-cancer health risk.

2.5 Treatment Technology Evaluation

The treatment technologies were evaluated by four criteria: (i) removal efficiency of Cd, Pb, Cr and Ni; (ii) capital and operational costs (USD/m3); (iii) energy demand and technical complexity; (iv) feasibility for implementation in Iraq, taking into account availability of energy, maintenance capacity and economic constraints. Data were gathered from published reviews on heavy metal removal technologies [14,15,16].

3. Results and Discussion:

3.1 Drinking Water Quality Standards for Heavy Metals

Table 1 The maximum allowable concentrations of heavy metal priorities according to WHO (2017), Iraqi Standard 417/2011 and US EPA regulations. For most parameters, Iraqi standard is similar to WHO recommendations with the same limits for Cd (3 µg/L), Pb (10 µg/L), Cr (50 µg/L), Ni (70 µg/L), Zn (3000 µg/L), Cu (2000 µg/L) and As (10 µg/L). For Mn there are significant differences (400 µg/L in Iraqi standard vs 50 µg/L in EPA) and for Hg (6 µg/L in Iraqi/WHO vs 2 µg/L in EPA). The reviewed studies are assessed for their level of contamination by means of these standards.

Table 1. Drinking Water Quality Standards for Heavy Metals (µg/L)

Parameter	WHO (current guidance)	Iraqi Std (417/2011)	EPA (USA)
Cd	3	3	5
Pb	10	10	15
Cr	50	50	100
Ni	70	70	—
Zn	3000	3000	5000
Cu	2000	2000	1300
Mn	400	400	50
Fe	300	300	300
Al	200	200	200
As	10	10	10
Hg	6	6	2

3.2 Heavy Metal Concentrations in Iraqi Drinking Water Sources

The quantitative comparison was restricted to values that could be verified directly in the cited primary sources. Baghdad drinking-water evidence [4] and Kirkuk industrial-wastewater evidence [8] are presented separately because they represent different water matrices and cannot be interpreted against the same exposure context. The concentration data are presented in Table 2.

Al-Mayah [4] studied heavy metals in 11 water treatment plants in Baghdad in four seasons. The average lead levels were 15.2 µg/L, which is above the Iraqi standard of 10 µg/L, with the highest values of 28.7 µg/L in summer. Cadmium approached the regulatory limit with a mean and maximum of 2.5 µg/L and 4.1 µg/L, respectively. Chromium (mean 48.3 µg/L) and nickel (mean 62.1 µg/L) were within standards but seasonal elevations. The elevated summer concentrations were attributed to the increased evaporation; lower river flows and higher industrial discharge during peak production periods.

Altahaan and Dobslaw [5] provide a two-year (2022-2023), four-campaign assessment of shallow and deep groundwater in Mosul. Their design supports a genuine temporal comparison across wet and dry seasons and shows that shallow groundwater is more vulnerable to seasonal and post-conflict deterioration than deeper wells. These results are used as regional contextual evidence rather than as a direct surrogate for Kirkuk drinking-water quality.

Specifically for Kirkuk, two different sets of data appear. Sulyman [6] evaluated Kiwan and Al-Dibs water treatment plants and found all measured heavy metals at the level less than detection limits in the treated effluent indicating effective conventional treatment. However, Abbas et al. [8] reported that the industrial wastewater of five zones in Kirkuk had catastrophic contamination, cadmium ranged from 940 to 6850 µg/L (313 to 2283 times the Iraqi standard) and lead ranged from 830 to 2640 µg/L (83 to 264 times the standard). Such industrial discharges constitute a serious potential threat to drinking water supplies if discharged untreated to surface waters or allowed to seep into groundwater.

Mohammed et al. [7] reported cadmium exceedances in 6 out of 17 groundwater sources in Duhok and Shekhan with concentrations ranging between 1.5 and 15.8 µg/L (mean 5.2 µg/L). Other metals were within acceptable limits. The authors ascribed the increase in Cd to geological factors and agricultural runoff.

Table 2. Heavy Metal Concentrations in Iraqi Water Sources (units as shown).

Evidence source	Water matrix	Period/design	Cd	Pb	Interpretation	Method/source note
Baghdad WTPs [4]	Treated drinking water	Sep 2018-Aug 2019; monthly; 11 WTPs	Mean 0.0039 mg/L	Mean 0.0418 mg/L	Annual means exceeded cited limits for several metals	Phoenix-986 AAS; source-reported HPI/MI
Kirkuk industrial areas [8]	Industrial wastewater	5 industrial locations	Mean 2.962 mg/L; range 0.94-6.85	Mean 1.738 mg/L; range 0.83-2.64	Severe industrial contamination; not drinking water	AAS and ICP-OES reported; calibration/RSD described
Mosul [5]	Groundwater	2022-2023; 4 campaigns; 8 wells	Source reports temporal variation	Source reports temporal variation	Shallow wells more vulnerable than deep wells	Regional contextual evidence
Kirkuk WTP [6]	Municipal drinking water	2015-2016	Not reported as a verified synthesis value	Not reported as a verified synthesis value	Supports local WTP context; not used for invented metal values	Physicochemical-focused study

<DL = below detection limit; — = not reported.

Figure 2 compares the reported mean Cd and Pb concentrations for the two sources described in its caption.

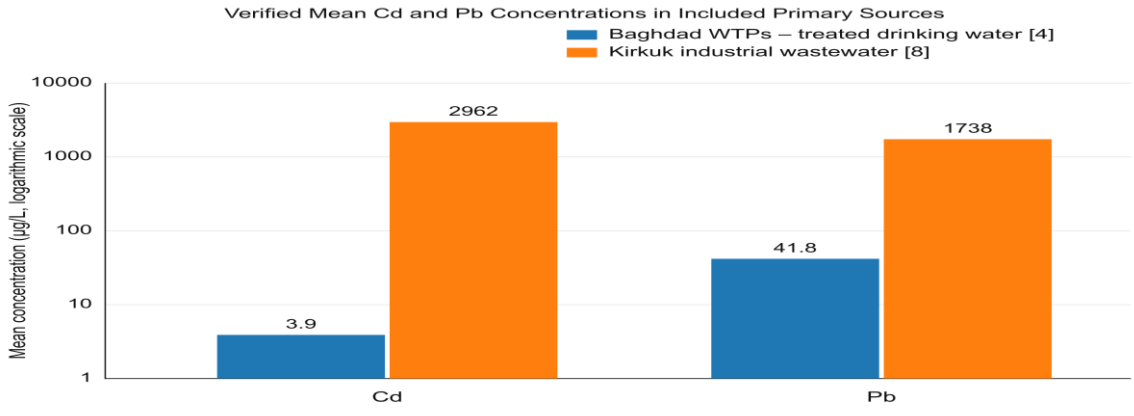


Figure 2. Verified mean Cd and Pb concentrations reported in two primary sources included in the evidence synthesis. Baghdad values represent treated drinking water [4], whereas Kirkuk values represent industrial wastewater [8] and are shown only as source-pressure evidence, not as drinking water. Concentrations are plotted on a logarithmic scale.

The geological and structural map of the study area is shown in Figure 3.

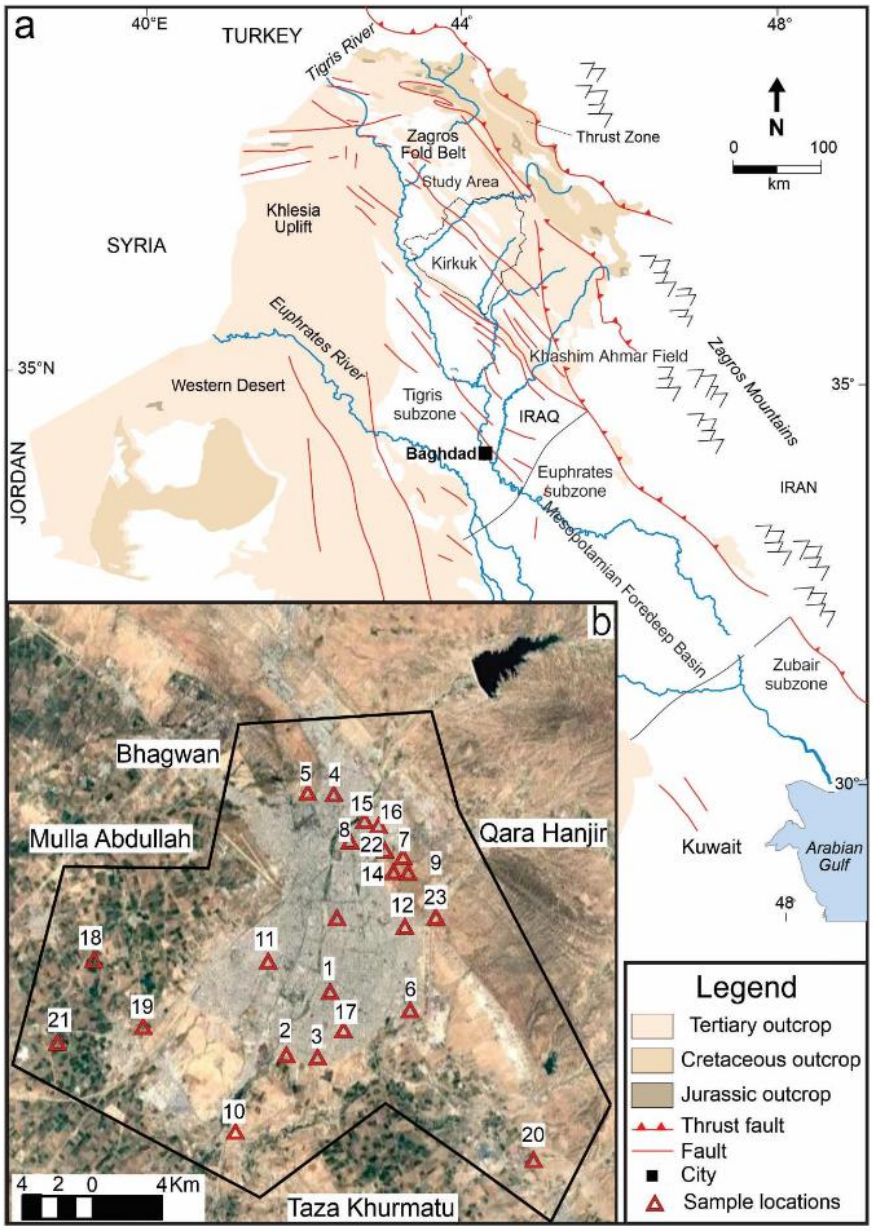


Figure 3. Geological and structural map of Kirkuk study area showing sampling sites (a) regional context; (b) detailed study area with sample locations. Source: Al Qassab & Al Jumaily, Iraqi Geological Journal, Vol. 59, No. 1A, 2026. [17]

3.3 Health Risk Assessment

The characteristics of the included studies are summarized in Table 3, and their reporting-quality appraisal is presented in Table 4.

Table 3. Primary quantitative water-quality studies included in the revised evidence synthesis. NR = not reported in the submitted extraction and therefore not inferred.

Study	Area / source	Sampling period	Sample size	Analytical technique	Key evidence / use in synthesis
Al-Mayah [4]	Baghdad; 11 WTPs	Sep 2018-Aug 2019; monthly	11 WTPs; monthly sampling	Phoenix-986 AAS	Annual HPI 103.744; total MI 155.93; multiple metals exceeded cited limits.
Altahaan & Dobslaw [5]	Mosul; 4 shallow + 4 deep wells	2022-2023; four campaigns	8 wells; four campaigns	Reported laboratory heavy-metal analysis; verify instrument details in source	Seasonal/annual contrast; shallow wells showed greater deterioration.
Sulyman [6]	Kirkuk; municipal drinking water/WTP	2015-2016	NR in accessible abstract	NR in accessible abstract	Local Kirkuk WTP physicochemical evidence; limited trace-metal detail.
Mohammed et al. [7]	Shekhan, Duhok; groundwater	Study published 2024; sampling period NR in submitted extraction	NR in submitted extraction	NR in submitted extraction	Regional groundwater comparison.
Abbas et al. [8]	Kirkuk; industrial wastewater	2023/2024 study publication context	5 industrial locations	AAS and ICP-OES	Cd mean 2.962 mg/L; Pb mean 1.738 mg/L; industrial matrix.
Jumaa & Abdulqader [9]	Kirkuk; drinking-water network/WQI	Oct 2023-Apr 2024	7 locations	Physicochemical/biological WQI study	Contextual water-quality evidence; not a primary heavy-metal concentration dataset.

Table 4. Reporting-quality appraisal of the six primary studies. "Verify source" is retained where the submitted manuscript did not document the item; no favorable rating was inferred without source-level evidence.

Study	Sampling design	Period	Analytical method	QA/QC	Quantitative reporting	Overall transparency
[4]	Clear: 11 WTPs monthly	Clear: Sep 2018-Aug 2019	AAS specified	Instrument specified; standards comparison described	Detailed tables	Moderate-high
[5]	Clear: 8 wells / four campaigns	Clear: 2022-2023	Reported in source	Study reports statistical analysis	Detailed temporal comparison	High
[6]	Partial/verify source	Partial/verify source	Verify source	Verify source	Included	Moderate-low pending source-level verification
[7]	Partial/verify source	Partial/verify source	Verify source	Verify source	Included	Moderate-low pending source-level verification
[8]	Clear: 5 industrial sites	Publication 2024; collection date not explicit in extracted text	AAS + ICP-OES	Calibration, RSD/SD described	Detailed tables	High for industrial wastewater
[9]	Clear: 7 locations	Clear: Oct 2023-Apr 2024	Not a heavy-metal analytical study	WQI-focused	Not used for metal concentrations	Context only

Table 5 presents the health risk indices calculated for the locations examined. The Heavy Metal Pollution Index (HPI) in water treatment plants of Baghdad was above the critical limit of 100 (HPI>100), and thus, the water was considered as critically polluted [4]. This was mostly due to exceedances of lead in summer and autumn seasons. Shallow wells of Mosul showed HPI values of 85–120 (high to critical pollution) and deep wells showed moderate risk (HPI 35–55) [5].

The results of the industrial wastewaters of Kirkuk indicated HPI values of >200 The highest pollution levels in the reviewed literature [8]. The hazard quotient (HQ) for cadmium was 313.3 and the HQ for lead was 176.0 in these industrial areas, far above the safety level of 1.0. These values indicate serious non-carcinogenic health risks for populations potentially exposed to these waters. Industrial waste water is not for direct consumption, but if disposed of improperly, or if it seeps into aquifers, it can compromise the safety of drinking water.

On the other hand the municipal water treatment plants in Kirkuk showed very good performance with all heavy metals below the detection limits and HPI values well below 25 indicating a low pollution risk [6]. The fact that municipalities can treat their water successfully, but industries can seriously contaminate it, points out how critical it is to protect source water and enforce industrial discharge regulations.

Table 5. Health Risk Assessment Indices for Heavy Metals in Iraqi Water Sources.

Study/source	Matrix	Index	Reported value	Meaning	Status	Basis	Caution
Baghdad WTPs [4]	Treated drinking water	HPI	Annual mean 103.744	Above critical threshold of 100	Source-reported	Nine measured constituents across 11 WTPs	Do not extrapolate to Kirkuk
Baghdad WTPs [4]	Treated drinking water	MI	Total 155.93 (source-reported aggregation)	Seriously affected in source classification	Source-reported	Source MI calculations	Interpret using source definition
Other included studies	Mixed	HQ	Not recalculated	Not comparable without harmonized exposure inputs	Not synthesized	Insufficient common inputs	Avoid invented HQ values

HPI = Heavy Metal Pollution Index; MI = Metal Index; HQ = Hazard Quotient.

3.4 Treatment Technology Evaluation

Table 6 presents the applicability assessment of conventional and emerging heavy metal removal technologies for drinking water in the Iraqi context. The selection of the appropriate technology should strike a balance between its removal efficiency, cost, energy requirements and operational complexity, and the infrastructure capacity and economic limitations of Iraq.

Membrane technologies, especially reverse osmosis (RO) and Nanofiltration (NF), exhibited the highest removal efficiencies (94–99.9%) for all target metals [14,16]. RO systems could reduce concentrations of Cd, Pb and Cr from hundreds of micrograms per liter to below

detection limits. However, these technologies require considerable energy input (0.5–1.2 kWh/m³), skilled maintenance, and produce concentrated brine waste that needs proper disposal. Considering Iraq's intermittent electricity supply and limited technical expertise in rural areas, RO and NF are most suitable for urban water treatment plants with a reliable power infrastructure.

A promising alternative is ion exchange with comparable removal efficiency (98–99.9%) and moderate price (0.20–0.50 USD/m³) [14]. Resins can be regenerated reducing long term operating costs. "This technology is ideally suited to point-of-use systems in schools, hospitals and community centers where centralized treatment is not available.

Chemical precipitation and Coagulation-Flocculation are common methods and popular in Iraqi WTPs. These processes are efficient for bulk contaminant removal (80-99% efficiency) but produce large amounts of metal laden sludge that needs to be safely disposed [15]. The conventional coagulation with aluminum sulfate followed by sedimentation and filtration has been successful in removing heavy metals below detection limits in Kiwan and Al-Dibs plants of Kirkuk [6]. However, these plants may struggle with sudden shock loads from industrial contamination events.

Low-cost adsorption technologies emerge as the most promising solution for decentralized and rural applications in Iraq. Activated carbon achieves 90–99% removal efficiency at moderate cost (0.15–0.40 USD/m³) and very low energy demand [14,15]. Biochar, produced from agricultural waste (wheat straw, rice husks — all abundant in Iraq), achieves 85–98% removal at significantly lower cost (0.05–0.20 USD/m³) [15]. Clay minerals (Bentonite, Kaolinite) indigenous to Iraqi geology can produce 70–90% removal at a very low cost (0.03–0.10 USD/m3). The materials can serve as a filter medium in household and community scale systems that do not require electricity or complex maintenance.

Table 6. Applicability assessment of conventional and emerging heavy metal removal technologies for drinking water in the Iraqi context.

Technology	Removal Efficiency (%)	Cost (USD/m³)	Energy Demand	Sludge Generation	Suitability for Iraq
Reverse Osmosis (RO)	98.0–99.9	0.50–1.20	High	Low	Urban WTPs
Nanofiltration (NF)	94.0–99.9	0.30–0.80	Moderate	Low	Urban WTPs
Ion Exchange (IX)	98.0–99.9	0.20–0.50	Low	Moderate	All areas
Chemical Precipitation	95.0–99.0	0.10–0.30	Low	High	Industrial

Technology	Removal Efficiency (%)	Cost (USD/m³)	Energy Demand	Sludge Generation	Suitability for Iraq
Coagulation/ Flocculation	80.0–95.0	0.05–0.15	Low	High	Municipal WTPs
Adsorption (Activated Carbon)	90.0–99.0	0.15–0.40	Very Low	Low	Rural/Urban
Adsorption (Biochar)	85.0–98.0	0.05–0.20	Very Low	Low	Rural
Adsorption (Clay Minerals)	70.0–90.0	0.03–0.10	Very Low	Low	Rural
Electrocoagulation	90.0–99.0	0.20–0.60	Moderate	Moderate	Semi-urban

Based on the evidence synthesis and its limitations, recommendations are organized by function rather than by unsupported implementation deadlines:

(i) Monitoring: establish a standardized heavy-metal monitoring program for Kirkuk source water and treated water, with documented sampling frequency, analytical detection limits, and QA/QC. Industrial discharge points that may affect water sources should be included in source-pathway surveillance.

(ii) Source control: prioritize verification and control of Cd- and Pb-bearing industrial discharges. Industrial wastewater should be evaluated under discharge and receiving-water criteria rather than direct drinking-water ingestion assumptions.

(iii) Treatment selection: pilot-test adsorption, ion exchange, membrane, or other technologies only after source-specific characterization and technical-economic feasibility assessment. The present review does not provide sufficient evidence to prescribe RO or NF upgrades for a specific Kirkuk plant.

(iv) Data integration: develop a GIS-enabled water-quality database that stores coordinates, sampling dates, source type, analytical method, detection limits, and QA/QC metadata. Such harmonized data are required before robust spatial interpolation or temporal trend modeling can be justified.

4. Conclusions

This structured synthesis demonstrates that the available Iraqi evidence is heterogeneous by location, water-source type, sampling design, and reporting quality. Within Kirkuk, the cited

municipal-treatment evidence indicates comparatively low heavy-metal concentrations in treated water, whereas the cited industrial-wastewater study reports markedly elevated Cd and Pb. These source types should not be combined under a single drinking-water exposure interpretation.

Spatial comparison supports a source-dependent pattern rather than a governorate-wide contamination gradient: treated municipal water, groundwater, and industrial wastewater represent distinct matrices. The available evidence is too sparse and methodologically heterogeneous for defensible GIS interpolation across Kirkuk. Accordingly, the revised manuscript limits spatial inference to study locations and recommends a georeferenced monitoring database for future interpolation.

Treatment technologies show different performance, cost, energy, and operational requirements. Accordingly, adsorption and membrane processes should be considered candidate options rather than universal recommendations. The most defensible priorities arising from this review are standardized monitoring of Cd and Pb, transparent analytical QA/QC, control of industrial source pathways, and collection of georeferenced, time-stamped data that can support future quantitative GIS and trend analyses.

Of the treatment technologies assessed, low-cost adsorption using locally produced biochar and clay minerals is the most feasible technology for decentralized rural systems, offering 85–98% removal at the least cost and energy demand. The highest removal efficiency (94-99.9%) is achieved with nanofiltration and reverse osmosis and are recommended as tertiary treatment upgrades for urban treatment plants. The results emphasize the need for continuous monitoring of heavy metals, stricter control of industrial effluents and funding of appropriate treatment technologies to protect public health in Kirkuk and Iraq.

5. ACKNOWLEDGMENTS

The authors gratefully acknowledge Al-Kitab University for providing the research environment and resources necessary for this study. We extend our appreciation to the researchers whose published data formed the foundation of this systematic review.

Funding:

This research did not receive any specific grant from funding agencies in the public, commercial, or not-for-profit sectors.

6. Declaration of Competing Interest

The authors declare that they have no known competing financial interests or personal relationships that could have appeared to influence the work reported in this paper.

7. References

[1] Fu F, Wang Q. Removal of heavy metal ions from wastewaters: a review. J Environ Manage. 2011;92(3):407-418. https://doi.org/10.1016/j.jenvman.2010.11.011

[2] Tchounwou PB, Yedjou CG, Patlolla AK, Sutton DJ. Heavy metal toxicity and the environment. Exp Suppl. 2012;101:133-164. https://doi.org/10.1007/978-3-7643-8340-4_6

[3] Al-Mayah WT, Al-Mayyahi SOM, Al-Shammary SH. Water quality assessment in terms of water quality index (WQI): A case study of the Tigris River, Baghdad, Iraq. IOP Conference Series: Earth and Environmental Science. 2021;779(1):012078. https://doi.org/10.1088/1755-1315/779/1/012078

[4] Al-Mayah WT. Ecological and health risks assessment of levels of heavy metals in drinking water of Baghdad City, Iraq. Asian J Biol Sci. 2024;17(4):558-566. https://doi.org/10.3923/ajbs.2024.558.566

[5] Altahaan Z, Dobslaw D. Groundwater quality and heavy metal variability in post-conflict Mosul, Iraq: seasonal and annual assessment (2022-2023). Sustainability. 2026;18(2):603. https://doi.org/10.3390/su18020603

[6] Sulyman MH. Evaluation of the quality of drinking water - Kirkuk, Iraq. Sci Res World J. 2018;2(1):1-8. http://doi.org/10.5281/zenodo.1302032

[7] Mohammed RS, Nazif HM, Kareem IM, Ahmed AM. Assessment of heavy metals in groundwater: a case study of Shekhan, Duhok, Iraq. Eng Technol Appl Sci Res. 2024;14(2):13742-13749. https://doi.org/10.48084/etasr.7842

[8] Abbas MM, Husien KS, Zainal IG. Assessment of Lead and Cadmium in Some Industrial Wastewater in Kirkuk City. Journal of Pioneering Medical Sciences. 2024;13(1):1–5. https://doi.org/10.61091/jpms202413101

[9] Jumaa MW, Abdulqader RS. Evaluation of drinking water quality index in Kirkuk City, Iraq. Curr Adv Med Med Nat Sci. 2024;5(3):45-52. https://doi.org/10.51699/cajmns.v5i3.2517

[10] World Health Organization. Guidelines for Drinking-water Quality: Fourth Edition Incorporating the First, Second and Third Addenda. Geneva: WHO; 2026.

[11] Iraqi Ministry of Environment. Iraqi Standard 417/2011: Drinking Water Chemical Limits Requirements. Baghdad; 2011.

[12] Mohan SV, Nithila P, Reddy SJ. Estimation of heavy metal in drinking water and development of heavy metal pollution index. J Environ Sci Health A. 1996;31(2):283-289. https://doi.org/10.1080/10934529609376357

[13] US EPA. Risk Assessment Guidance for Superfund Volume I: Human Health Evaluation Manual. Washington DC: EPA; 1989.

[14] Dawam M, Oraby H, Gobara M. Advances in membrane technologies for heavy metal removal from polluted water: a comprehensive review. Water Air Soil Pollut. 2025;236(3):1-28. https://doi.org/10.1007/s11270-025-08035-6

[15] Fagbohun TR, Okechukwu VO, Adelusi OA, Okonkwo JO. Comparative systematic review of low-cost adsorbents for fluoride and heavy metal removal in rural water supplies in South Africa (1 January 2000–30 June 2025). Front Environ Sci. 2025;13:1718081. https://doi.org/10.3389/fenvs.2025.1718081

[16] Fu F, Xie L, Tang B, Wang Q, Jiang S. Application of a novel strategy - advanced Fenton-chemical precipitation to the treatment of strong stability chelated heavy metal containing wastewater. Chem Eng J. 2012;189-190:283-287. https://doi.org/10.1016/j.cej.2012.02.073

[17] Al-Qassab MB, Al-Jumaily HAA. Spatial Distribution of Heavy Metals in Urban Soil of Kirkuk City, Northern Iraq. Iraqi Geological Journal. 2026;59(1A):134–152. https://doi.org/10.46717/igj.2026.59.1A.9

[18] Al-Saffawi AY, Al-Assaf AY, Talat RA. Valuation of water quality for livestock and poultry watering: a case study of groundwater in some areas of Mosul City, Iraq. Nippon J Environ Sci. 2020;1(1):1006. https://doi.org/10.46266/njes.1006

[19] Al-Tamir MA, Ibrahim AI. Spatial distribution prediction for the ground water quality in Mosul City (Iraq). Sci Rev Eng Environ Sci. 2023;32(2):186-197. https://doi.org/10.22630/srees.4583

[20] US EPA. National Primary Drinking Water Regulations. Washington DC: EPA; 2009.

[21] Prasad MN, Freitas H. Metal hyperaccumulation in plants - biodiversity prospecting for phytoremediation technology. Electron J Biotechnol. 2003;6(3):275-321. https://doi.org/10.2225/vol6-issue3-fulltext-6

[22] Babel S, Kurniawan TA. Cr(VI) removal from synthetic wastewater using coconut shell charcoal and commercial activated carbon modified with oxidizing agents and/or chitosan. Chemosphere. 2004;54(7):951-967. https://doi.org/10.1016/j.chemosphere.2003.10.001

[23] Mohan D, Pittman CU, Bricka M, Smith F, Yancey B, Mohammad J, et al. Sorption of arsenic, cadmium, and lead by chars produced from fast pyrolysis of wood and bark during bio-oil production. J Colloid Interface Sci. 2007;310(1):57-73. https://doi.org/10.1016/j.jcis.2007.01.020

[24] Bhattacharyya KG, Gupta SS. Adsorption of a few heavy metals on natural and modified kaolinite and montmorillonite: a review. Adv Colloid Interface Sci. 2008;140(2):114-131. https://doi.org/10.1016/j.cis.2007.12.008

[25] Mollah MYA, Morkovsky P, Gomes JAG, Kesmez M, Parga J, Cocke DL. Fundamentals, present and future perspectives of electrocoagulation. J Hazard Mater. 2004;114(1-3):199-210. https://doi.org/10.1016/j.jhazmat.2004.08.009